

DANUBE ADRIA ASSOCIATION FOR AUTOMATION & MANUFACTURING  
DAAAM International Vienna  
DAAAM Baltic



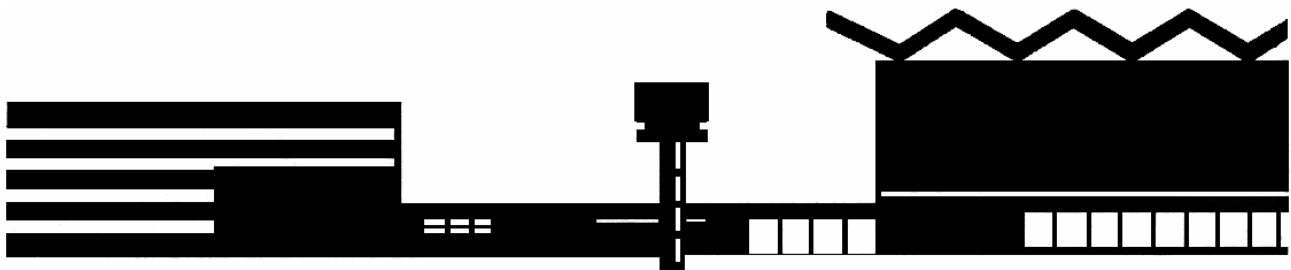
# PROCEEDINGS

OF THE 8<sup>TH</sup> INTERNATIONAL CONFERENCE OF DAAAM BALTIC  
INDUSTRIAL ENGINEERING  
19-21<sup>ST</sup> APRIL 2012, TALLINN, ESTONIA

**ORGANIZED UNDER THE AUSPICES  
OF DAAAM INTERNATIONAL VIENNA**

in co-operation with:  
**BALTECH Consortium**  
**Estonian Academy of Sciences**  
**Federation of Estonian Engineering Industry**  
**Association of Estonian Mechanical Engineers**

EDITED BY  
T. OTTO



TALLINN UNIVERSITY OF TECHNOLOGY

The Chairman of DAAAM Baltic Scientific Committee expresses special personal thanks to Professor Branko Katalinic for encouraging to organise and for advising during the organisation of the conference. Also special thanks for the support during the organising the conference to the following persons: A. Hermaste, K. Karjust, E. Jürves, R. Kulbas, I. Veldi, M. Randmaa, A. Napp.

#### **EDITORS' NOTE**

This publication was reproduced by the photo process, using the soft copies supplied by their authors. The editor and the DAAAM Baltic are not responsible either for the statements or for the opinion expressed in this publication.

#### **Copyright: Tallinn University of Technology, 2012**

Abstracting and non-profit use of the material is permitted with credit to the source. Libraries are permitted to photocopy for private use of patrons. Instructors are permitted to photocopy isolated articles for non-commercial classroom use without fee. After this work has been published by the DAAAM Baltic, the authors have right to republish it, in whole or part, in any publication of which they are an author or editor, and to make other personal use of the work. Any republication, referencing, or personal use of the work must explicitly identify prior publication in the *Proceedings of 8th International Conference of DAAAM Baltic INDUSTRIAL ENGINEERING, Editor T.Otto, 19–21 April 2012, Tallinn, Estonia*, including page numbers.

#### **Proceedings of 8th International Conference of DAAAM Baltic INDUSTRIAL ENGINEERING**

**Editor T. Otto**

**19–21 April 2012, Tallinn, Estonia**

ISBN 978-9949-23-265-9

Layout & Design copyright: B. Katalinic, R. Kyttner, T. Otto

Additional copies can be obtained from the publisher:

DAAAM Baltic, Tallinn University of Technology, Ehitajate tee 5, 19086 Tallinn  
Estonia

Phone: +372 620 3257

Fax: +372 620 3250

E-mail: daaam@ttu.ee



## Foreword

Over the past years, DAAAM-Baltic has been an international forum for researchers and engineers to present their research results in the areas of industrial engineering, manufacturing and automation. It provides an avenue for discussion and exchange of new ideas addressing new techniques and methods for product development and manufacturing engineering.

This DAAAM-Baltic-2012 conference in the DAAAM-Baltic Conference series will continue the mission of the DAAAM, which is to give for young and active scientists of the Baltic Sea region an opportunity to introduce their works and find partners.

The main idea of starting DAAAM-Baltic meetings was to organize regional conferences of DAAAM International events (DAAAM – Danube-Adrian Association for Automation & Manufacturing). DAAAM International is association for international scientific and academic cooperation in the fields of intelligent automation and modern production. DAAAM-Baltic is organized in Estonia every second year. Estonia has been represented as a member of International DAAAM Committee since 1994. In year 2012 we have 8th Conference of DAAAM-Baltic and 16 years of history of publishing the Proceedings. The Proceedings of DAAAM-Baltic are included in Web of Science of Thomson Reuters.

The Conference addresses the issues of managing globalization in the internet age. Its scope ranges from design engineering, production engineering, production management, materials engineering to mechatronics and system engineering, with an emphasis on innovative practices, to ensure that the focus of the conference is on learning, networking and generating new ideas. We emphasize importance of European initiatives towards Factories of the Future and technology platform Manufuture, and hope to give our contribution by bringing scientists, entrepreneurs and industry specialists together for exchange of future visions based on scientific research and case studies.

In 2012 we received about two hundred proposals from 16 countries. Over a hundred participants from 12 countries take part in the Conference. All proposals have been carefully selected and full texts of presentations peer-reviewed to address key topics of the conference. 130 papers were selected to present orally. Part of proposals were rejected on the grounds of either not being appropriate for the areas that DAAAM-Baltic covers or being of rather narrow and specialized nature.

We wish to thank all authors, referees, members of the Organizing Committee and Program Committee, as well as supportive organizations for their efforts which made this conference possible. DAAAM-Baltic would not be possible without contributions from members of the scientific community of the Baltic-Sea region.

We look forward to a very exciting and stimulating conference, and hope that you will join us in next DAAAM-Baltic in 2014.

Tallinn; April 2012

Tauno Otto

Chairman of the Scientific Committee DAAAM-Baltic 2012

## Steering Committee

Tauno Otto - *chair*

Kristo Karjust

Rein Küttner

Aadu Paist

Leo Mõtus

Mart Tamre

Renno Veinthal

## International Program Committee

M.Airila (FIN)

J.Balic (SLV)

F.Boór (HUN)

S.Bockus (LIT)

J.Brnić (CRO)

M.Eerme (EST)

L.Hagman (SWE)

H.Jähn (GER)

T.Karaulova (EST)

B.Katalinic (AUT)

T.Kjellberg (SWE)

P.Kulu (EST)

P.Kuosmanen (FIN)

J.Lavrentjev (EST)

I.Liiv (EST)

V.Mironov (LAT)

J.Martikainen (FIN)

S.Ottosson (SWE)

J.-G.Persson (SWE)

D.Polize (SUI)

P.Pukk (SWE)

V.Reedik (EST)

J.Riives (EST)

A.Schulz (LAT)

F.Sergejev (EST)

A.Siirde (EST)

M.Veveris (UK)

A.Voet (BEL)

A.Zawada-Tomkiewicz (POL)



## CONTENTS

<b>I DESIGN ENGINEERING .....</b>	<b>13</b>
<b>Aarnio, A., Kananen, E., Keltto, V., Vartiainen, V-M, Kiviluoma, P., Kuosmanen, P.</b> Device for branch volume measurement.....	15
<b>Boyko, A.</b> Influence of boiler damages on life time of tank wagons .....	21
<b>Dubovska, R.</b> The quality control of machining process with CAD/CAM systems support.....	27
<b>Enache, I.C., Simion, I. &amp; Bogza, A.M.</b> Influence of shape product design in the manufacturing process.....	33
<b>Gonca, V., Shvabs, J., Noskovs, S.</b> Projecting elastomeric shock absorbers with moving side stop .....	39
<b>Goremikins, V., Rocens, K., Serdjuks, D.</b> Cable truss analyses for prestressed suspension bridge .....	45
<b>Gruescu, C. A., Vela, I.</b> Optimising the regulating system of supercharged diesel engines.....	51
<b>Nad, M., Cicmancova, L.</b> The effect of the shape parameters on modal properties of ultrasonic horn design for ultrasonic assisted machining .....	57
<b>Nánási, T.</b> Extreme modal patterns of vibrating two-span beams .....	63
<b>Nastac, S., Anghelache, D., Stanciu, M. &amp; Curtu, I.</b> On acoustic panels with high performances for pollutant individual working place insulation .....	69
<b>Pabut, O., Allikas, G., Herranen, H., Talalaev, R. &amp; Vene, K.</b> Model validation and structural analysis of a small wind turbine blade .....	74
<b>Polukoshko, S., Gonca, V.</b> Dynamics of gravity feeder for prismatic workpieces .....	80
<b>Potirniche, A., Nastac, S., Leopa, A., Debeleac, C. &amp; Capatana, G.</b> On Unitary Rheological Approach of Vibration Isolation Passive Devices .....	87
<b>Rimašauskas, M., Rimašauskienė, R.</b> Investigation of the membranes permeability of the flow control device based on piezo actuator .....	92
<b>Sonk, K., Hermaste, A., Sarkans, M.</b> Functional requirements as a company and process modeling tool .....	98
<b>Zaharia, S.M., Martinescu, I. &amp; Morariu, C.O.</b> Statistical processing of accelerated life data with two stresses using monte carlo simulation method .....	104
<b>Widmaier, T., Kontio, J., Juhanko, J. &amp; Kuosmanen, P.</b> Collaborative design process of a configurable product .....	110

<b>II PRODUCTION ENGINEERING.....</b>	<b>117</b>
<b>Bolanča Mirković, I., Majnarić, I., &amp; Bolanča, S.</b> Recycling optimisation of the electrophotographic prints.....	119
<b>Brutans, V., Torims, T., Kumermanis M., Rosado Castellano, P., Torres, R., Gutierrez Rubert S. C.</b> High speed milling impact to the 3D surface roughness parameters .....	125
<b>Caramidaru, V. D., Vela, I., Tufoi, M. &amp; Gruescu, C. A.</b> Researches regarding the noise and vibrations of metal toothed wheel gears after applying a fluoropolymer dispersion of xylan 1052.....	129
<b>Grinevich, I., Mozga, N.</b> The calculations of nutdrivers electricity consumption when assembling fixed threaded joints .....	134
<b>Gutakovskis, V., Pikurs, G., Brutāns, V., Ratkus, A., Bunga, G.</b> An experimental study of the cutting forces in the metal cutting process .....	140
<b>Ilves, R., Olt. J., Mikita.V. &amp; Küüt. A.</b> The development of an additional fuel supply system to an internal combustion engine .....	146
<b>Kiitam, A. &amp; Tammaru, T.</b> Impact of application of excellence models on organizational performance .....	152
<b>Koštál, P., Delgado Sobrino, D. R. &amp; Velíšek, K.</b> The laboratory of drawing less manufacturing.....	158
<b>Kristjuhan, K., Metsla, E. &amp; Ling,H.</b> Quality of management practices and application of complex automated systems .....	163
<b>Lemmik, R., Karjust, K.</b> Interoperability between different interest groups - Practice Portal case study .....	169
<b>Leopa, A., Nastac, S., Debeleac, C., Capatana, G., Potarniche, A.</b> Identification of parameters characterizing the nonlinear behavior of viscoelastic systems on dynamic loadings.....	175
<b>Madisoo, M., Maksarov, V., Olt, J.</b> Increasing the efficiency of external turning by using the multiple layer construction of the cutting tool holder.....	181
<b>Menind, A., Križan, P., Šooš, L., Matúš, M., Kers, J.</b> Optimal conditions for valuation of wood waste by briquetting .....	187
<b>Pompurová, A., Bílik, J. &amp; Ridzoň, M.</b> The increasing lifetime of forming tools .....	193
<b>Põdra, P. &amp; Laaneots, R.</b> Uncertainty focused strength analysis model .....	198
<b>Pullinen, T., Sievänen, S., Schiestl, M., Kiviluoma, P. &amp; Kuosmanen, P.</b> Development of patternless sand mold milling machine .....	204
<b>Pääsuke, K., Pohlak, M.</b> The technology for low-volume manufacturing of fenders for an advanced light electric vehicle .....	210
<b>Radelja, H., Hasković, D., Šikulec, L., Plančak, M., Kršulja, M. &amp; Car, Z.</b> Concept for online web machine tool control based on open source .....	216
<b>Ratkus, A., Torims, T.</b> Research on the bucket bore renewal technologies .....	222

<b>Simson, K., Kübarsepp, T., Uljas, H., Leito, I., Karotamm, L., Karilaid, M., Metssalu, M., Parker, M.</b>	
The impact of metrology in industrial sector in Estonia .....	227
<b>Takala, M., Helkiö, H., Sundholm, J., Kiviluoma, P. &amp; Kuosmanen, P.</b>	
Ink-jet printing of pharmaceuticals .....	233
<b>Zarins, M., Torims, T. &amp; Vilcans, J.</b>	
Diagnostic of drum type wood shredder machines .....	240
<b>Zawada-Tomkiewicz, A.</b>	
Micro-machining process and its effectiveness .....	244
<b>III MECHATRONICS AND SYSTEM ENGINEERING.....</b>	<b>249</b>
<b>Aleksandrov, D., Penkov, I.</b>	
Optimal gap distance between rotors of mini quadrotor helicopter .....	251
<b>Aruväli, T., Serg, R. &amp; Otto, T.</b>	
Machinery utilization monitoring and pause identification prototype model design.....	256
<b>Aryassov, G., Zhigailov, S., Zinovjev, E.</b>	
Development of movement algorithms of the robot-manipulator .....	262
<b>Astapov, S., Preden, J. S., Aruväli, T. &amp; Gordon, B.</b>	
Production machinery utilization monitoring based on acoustic and vibration signal analysis .....	268
<b>Gheorghe, G. I., Badita L.L.</b>	
Micro/nanorobotics in technological micro/nanoprocessing and micro/nanosystems engineering .....	274
<b>Gheorghe, Gh. I. &amp; Despa, V.</b>	
Micro-technologies and special materials for the development of mechatronic micro-nano systems for ultra precise measurement processes .....	280
<b>Gheorghe, I. Gh., Istrateanu, S.</b>	
Adaptronic microtechnologies regarding mechatronic nanometric micro-nanosystems for micro-nanodisplacements and micro-nanopositioning.....	286
<b>Hiiemaa, M., Tamre, M.</b>	
Low Speed Motion Feedback for the Unmanned Ground Vehicle .....	293
<b>Hudjakov, R., Tamre, R.</b>	
Comparison of aerial imagery and satellite imagery for autonomous vehicle path planning ..	301
<b>Iruikwu, D. O., Isomaa, J. M., Korkkolainen, P., Kiviluoma, P., Calonius, Olof &amp; Kuosmanen, P.</b>	
Dynamic loading system for air bearing testing .....	309
<b>Körbe, K., Kuhi, K. &amp; Koppel, O.</b>	
Measuring temperature and water content in road structures with sensor equipped rfid tags...	315
<b>Lapkovskis, V., Mironovs, V.</b>	
Single-stage electromagnetic elevator modelling in femm software.....	321
<b>Olaru, S., Filipescu, E., Niculescu, C. &amp; Salistean, A.</b>	
3D fit garment simulation based on 3d body scanner anthropometric data .....	326
<b>Petritshenko, A., Sell, R.</b>	
Wheel motion resistance and soil thrust traction of mobile robot.....	332

<b>Pölder, A., Juurma, M., Tamre, M.</b> Automatic products identification method .....	338
<b>Sell, R., Aryassov, G., Petritshenko, A., Kaeeli, M.</b> Kinematics and dynamics of configurable wheel-leg .....	345
<b>Shvarts, D., Tamre, M.</b> Local and global descriptors for place recognition in robotics .....	351
<b>Tiidemann, M., Kalja, A., Tiidemann, T., Tyugu, E.</b> Using software with AI elements for conceptual design of machine elements.....	357
<b>Tiimus, K., Tamre, M.</b> Camera gimbal performance improvement with mechanical gyroscopes on a multi rotor VTOL platform.....	361
<b>Väljaots, E., Sell, R.</b> Dynamic motion energy efficiency measurement of ground vehicles .....	367
<b>Verheecke, W., Van Dyck, M., Vogeler, F., Voet, A., Valkenaers, H.</b> Optimizing aerosol jet printing of silver interconnects on polyimide film for embedded electronics applications .....	373
<b>Winter, E., Dahl, J., Nordling, K., Kiviluoma, P., Kuosmanen, P &amp; Praks, J.</b> Development of tracking system for satellite ground station .....	380
<b>IV PRODUCTION MANAGEMENT .....</b>	<b>387</b>
<b>Aan, A., Heinloo, M., Aarend, E., Mikita, V.</b> Analysis of four-stroke cycle internal combustion v-engine in mathcad environment.....	389
<b>Babalová, E., Taraba, B. &amp; Duehring, S.</b> Computer modelling methodology for laser cutting process supported with experiment on stainless steel plate .....	395
<b>Bashkite, V., Durmanenko, D., Karaulova, T.</b> Life cycle extension for used vehicles and reduction their environmental impact .....	401
<b>Bercu, A., Roman, A.</b> The impact of human resource professional development on the smes performance. Evolutions and challenges. ....	407
<b>Broum, T., Gorner, T., Kleinova, J. &amp; Simon, M.</b> Increasing the value of ergonomic design of workplace in compliance with limit costs .....	413
<b>Cambal, M., Caganova, D., Sujanova, J.</b> Corporate culture influence on industrial enterprise performance .....	419
<b>Čechová, L., Horejc, J.</b> Risk in PLM – Planning .....	424
<b>Cigjnik, M., Úradníček, J. &amp; Valčuha, Š.</b> The problem of optimal selection partners in distributed manufacturing systems.....	430
<b>Delgado Sobrino, D. R., Košťál, P., Velíšek, K.</b> Contributions to the design and analysis of the material flow at an intelligent manufacturing cell.....	436
<b>Dvorak, J., Hosnedl, S.</b> Cost prediction of designed technical product using similarity based reasoning.....	442
<b>Fera, M., Macchiaroli, R., Miranda, S.</b> Cost analysis in small wind projects .....	448

<b>Gabriš, P., Pavlenda, P. &amp; Malá, J.</b> Knowledge Management Maturity Aspects in Industrial Enterprises .....	454
<b>Grossschmidt, G., Harf, M.</b> Multi-pole modeling and intelligent simulation of technical chain systems .....	458
<b>Holecek, J., Caganova, D. &amp; Cambal, M.</b> Employee stability in the automotive company .....	472
<b>Kartus, R. &amp; Kukrus, A.</b> Innovation, product development and patents at universities. ....	477
<b>Katalinic, B., Kukushkin, I. K., Cesarec, P &amp; Kettler, R.</b> Hybrid control structure and scheduling of bionic assembly system .....	483
<b>Kerak, P., Holubek, R. &amp; Košťál, P.</b> Novel trends in the intelligent manufacturing systems .....	490
<b>Kulderknup, E.</b> Modelling of symmetry measurement uncertainty using monte-carlo method .....	496
<b>Källo, R., Eerme, M., Reedik, V.</b> Ways of increasing synergy in engineering design teamwork .....	500
<b>Küttner, R.</b> Multistage manufacturing planning .....	506
<b>Lavin, J &amp; Randmaa, M.</b> Relationships between business objectives and the actual outcome of the business.....	512
<b>Lõun, K., Riives, J. &amp; Otto, T.</b> Workplace performance and capability optimization in the integrated manufacturing .....	518
<b>Maceika, A., Zabelavičienė, I.</b> Innovative knowledge: the importance and functionality in the present and future enterprises.....	524
<b>Maceika, A., Zabelavičienė, I.</b> The creativity of innovation team.....	530
<b>Makraiova, J., Caganova, D. &amp; Cambal, M.</b> A proposal to improve adaptation control system within automotive enterprises .....	536
<b>Maleki, M., Liiv, I., Shevtshenko, E, Cruz-Machado, V.</b> Classification of supply chain practices according to customer values in automotive industry .....	542
<b>Randmaa, M., Howard, T.J. &amp; Otto, T.</b> From product centred design to value centred design: understanding the value-system .....	548
<b>Riives, J., Karjust, K., Lavin, J., Koov, K.</b> Software development platform for integrated manufacturing engineering system .....	555
<b>Riives, J., Lavin, J., Karjust, K., Koov, K.</b> Offer management in the networking manufacturing .....	561
<b>Sahno, J., Opik, R., Kostina, M., Paavel, M., Shevtshenko, E., Wang, Y.</b> Knowledge management framework for production route selection in manufacturing enterprises.....	567
<b>Snatkin, A., Karjust, K., Eiskop, T.</b> Real time production monitoring system in SME .....	573
<b>Stan, L. &amp; Mărăscu - Klein, V.</b> Techniques to reduce costs sustainable quality in the industrial companies .....	579

<b>Stan, L., Mărăscu - Klein V., Neagoe, L. &amp; Tecău, A.</b> Kpi performance indicators for evaluating employees on industrial production lines.....	585
<b>Talalaev, R., Veinthal, R., Laansoo, A., Sarkans, M.</b> Methodology for configuration of robot welding cell for SMEs under conditions of small and medium sized production using MIG/MAG process.....	591
<b>Taucean, I.M.</b> Production planning with the support of the megatrends and gigatrends.....	597
<b>Tähemaa, T., Temerbulatova, A., Karjust, K.</b> Lean product development in estonian smes.....	603
<b>V MATERIALS ENGINEERING .....</b>	<b>609</b>
<b>Boiko, I., Filipov, A.</b> Research on welding of stainless steel vacuum chamber components.....	611
<b>Chachula, M., Koleňák, R. &amp; Koleňáková, M.</b> Study of properties of lead-free solder type au-20sn at ultrasound assistance.....	616
<b>Juhani, K., Pirso, J., Viljus, M., Letunoviš, S.,Tarraste, M.</b> Abrasive impact wear of WC-Co and TiC-NiMo cermets .....	621
<b>Kaps, T., Kers, J., Reiska, R., Kallavus, U., Luga, Ü.</b> Development of emulsion and impregnation technology for wood bioprotection.....	627
<b>Karjust, K., Pohlak, M., Majak, J.</b> Adhesion process optimization in reinforced composites .....	633
<b>Katsich, C., Zikin, A., Badisch, E.</b> Wear protection of highly loaded components: Advantages of plasma transferred arc welding as hardfacing technology.....	639
<b>Kommel, L., Metsvahi, R., Mihhaltsekov, M.</b> Production technology elaboration and characterization of al-cnt and al-b4c composites .....	645
<b>Kommel, L., Metsvahi, R., Viljus, M., Kimmari, E., Kolju, K., Traksmäa, R.</b> Design of superhard c-bc2n-precipitates in b4c/al-composites through shs and heat treatment .....	651
<b>Krasnikovs, A., Zaharevskis, V., Kononova, O., Lasis, V., Galushchak, A. &amp; Zaleskis, E.</b> Fiber concrete properties control by fibers motion investigation in fresh concrete during casting.....	657
<b>Kängsepp, K., Larnøy, E., Kers, J. &amp; Meier, P.</b> Leachability of wood protection agents from impregnated pine wood.....	663
<b>Leemet, T., Hokka, M., Kuokkala, V.-T., Olt, J.</b> Behavior of ti-15-3 alloy at a wide range of strain rates and temperatures.....	668
<b>Lübert, L., Treu, A., Kers, J., Meier, P.</b> Potential eco-friendly wood protection systems used in royal process.....	674
<b>Lille, H., Kõo, J., Ryabchikov, A., Reitsnik, R., Veinthal, R., Mikli, V. &amp; Sergejev, F.</b> Comparison of values of residual stresses determined by various methods in hard nickel coatings prepared by brush-plating in sulfate solution.....	680
<b>Mironovs, V., Lisicins, M., Boiko, I., Zemchenkova, V.</b> Manufacturing of cellular structures of the perforated steel tape.....	688

<b>Okipnyi, I., Maruschak, P., Soroachak, A. &amp; Sergejev, F.</b> Measurement of deformation hardening of heat-resistant steel of the wwer-type reactor .....	694
<b>Parker, M., Pokatilov, A., Raba, K., Kübarsepp, T.</b> Accurate measurements of electrical conductivity of metals in the range from 2 MS/m to 14 MS/m .....	700
<b>Piirlaid, M., Kers, J., Rohumaa, A.</b> Effect of birch veneer processing factors on adhesive bond shear strength.....	705
<b>Pirso, J., Juhani, K., Viljus, M., Letunovitš, S.</b> Two-body abrasive wear of WC-Co hardmetals in wet and dry environments .....	711
<b>Sepper, S., Peetsalu, P., Mikli, V., Saarna, M.</b> The effect of substrate microstructure on morphology of zinc coatings .....	717
<b>Sergejev, F., Petrov, M. &amp; Kübarsepp, J.</b> Determination of the mechanical properties of carbide composites by spherical indentation ..	723
<b>Shirokova, V., Laas, T., Väli, B., Priimets, J., Ainsaar, A., Demina, E. V., Pimenov, V. N., Maslyayev, S.A., Gribkov, V. A., Dubrovsky, A. V., Scholz, M.</b> Sensitivity of tungsten and tungsten doped with $La_2O_3$ to deuterium plasma processing .....	729
<b>Siim, K., Kask, R., Lille, H., &amp; Täkker, E.</b> Study of physical and mechanical properties of birch plywood depending on moisture content .....	735
<b>Stanciu, M. D., Curtu, I., Cosereanu, C., Lica, D., Nastac, S.</b> Research regarding acoustical properties of recycled composites .....	741
<b>Terciu, O. M., Curtu, I. &amp; Teodorescu-Draghicescu, H.</b> Effect of wood particle size on tensile strength in case of polymeric composites .....	747
<b>Umalas, M., Reedo, V., Lõhmus, A., Hussainova, I.</b> Solution based processing for nanocarbides.....	753
<b>Velsker, T.</b> Design of glass canopy panel .....	759
<b>Voltsihhin, N., Cura, M.E., Hussainova, I., Hannula, S-P.</b> Sintering routes for zirconia doped hardmetals.....	765
<b>Voltsihhin, N., Cura, M.E. , Hussainova, I., Hannula, S-P.</b> Effect of carbon content on sinterability and properties of $ZrO_2$ doped wc-cermets .....	771
<b>Zikin, A., Yung, D., Hussaionova, I. &amp; Ilo, S.</b> Chemical pre-treatment of mechanically milled recycled hardmetal powders .....	777
<b>Yung, D., Kollo, L., Hussaionova, I., &amp; Zikin, A.</b> Reactive sintering of zirconium carbide based systems .....	783





# I DESIGN ENGINEERING



## DEVICE FOR BRANCH VOLUME DISTRIBUTION MEASUREMENT

**Aarnio, A.; Kananen, E.; Keltto, V.; Vartiainen, V-M; Laasasenaho, J.; Kiviluoma, P.  
& Kuosmanen, P.**

**Abstract:** *The volume and cross-sectional area of tree as a function of its length can be estimated by mathematical taper curve models which often exclude branches. To include branches into new whole tree volume models representative measurement data is required. Currently the data is acquired by manual measurements.*

*This study presents an automated measuring device based on Archimedes' principle which will offer fast and accurate method to measure the volume distribution of irregular shaped objects such as branches.*

*This study shows that measuring with this device is faster than manual measuring and the results are promising. The device is a potential platform for diversity of volume measurements and it could define global standards for cross-sectional area and volume measuring in forest research.*

*Key words: irregular volume measurement, immersion, cross-sectional area, Archimedes' principle*

### 1. INTRODUCTION

The dimensions and volume of a standing tree can be estimated by mathematical models [1,2]. These models are being used for example to estimate the amount and quality of the biomass in the forest and to determine the optimal log length (bucking) of the trees. Most of the current models take into account only the stem volume and diameters, but there is a growing interest to include also the branch volume into the

models. The amount and type of branches affects to the distribution of tree's biomass and on the tree's effect as a carbon sink. The type, size, amount and placement of branches affects also to the quality of the saw timber and to the distribution of the stem volume (known as taper curve).

The standard method so far to obtain accurate branch volume information in research work is manual measurement, which is time-consuming and inaccurate. Measuring a branch can take up to several hours. In manual measurement branches are divided into segments which are limited between two branching points as shown in Figure 1.

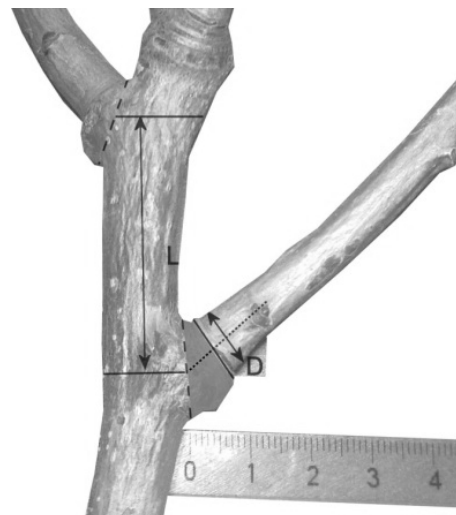


Fig. 1. Branch segment and measuring points.

From each segment, several measurements are taken: segment length (L), maximum and minimum diameter (D) as close as possible to the beginning, the middle and the end of the segment. From these values

the volume of the branch segment can be estimated with Newton's equation

$$V = \frac{1}{6(g_b + 4g_m + g_e)l} \quad (1)$$

where  $g_b$  is cross-sectional area in the beginning of the segment,  $g_m$  in the middle,  $g_e$  in the end and  $l$  is the length of the segment.

Immersion in the water has been used to estimate the total wood volume both in forest industry [3] and in forest research [4]. In this research also the distribution of the volume is measured.

This study presents an automated measuring device that speeds up the measurement process, facilitates the data gathering by instantaneously saving and visualizing the branch volume distribution and it also removes some of the possible error sources of the manual measurements. As a result, large amounts of representative branch volume information can be collected. Combining this with other information such as branch type and distance from the ground a new, branch-including tree model could be created.

The purpose of this study is to verify if the manual measurement method can be replaced with automated measuring device. Determining factors are most importantly precision and accuracy, but also measurement speed and usability of the device.

## 2. METHODS

### 2.1. Measuring device

The branch volume distribution measuring device is shown in Figure 2. The main structure of the device is a crane mounted to a supporting frame. A winch is mounted to the crane and winch cable runs through two pulley wheels. The height and the reach of the crane arm can be adjusted for fluid containers of different sizes. A force sensor is attached to the mounting bracket which is attached to the winch cable. The immersion depth is determined by the

distance sensor mounted to the crane arm. It measures the distance between the crane arm and the force sensor mounting bracket. Support stand is attached to the force sensor during measurement. It consists of a threaded rod and a bottom plate of known dimensions. Fluid tank is located under the crane arm and it is positioned in a way that the support stand is located at the centre of the tank.

This first generation device is designed for branches up to 1.4 m and 3.4 kg. Longer and heavier branches can be measured in pieces.

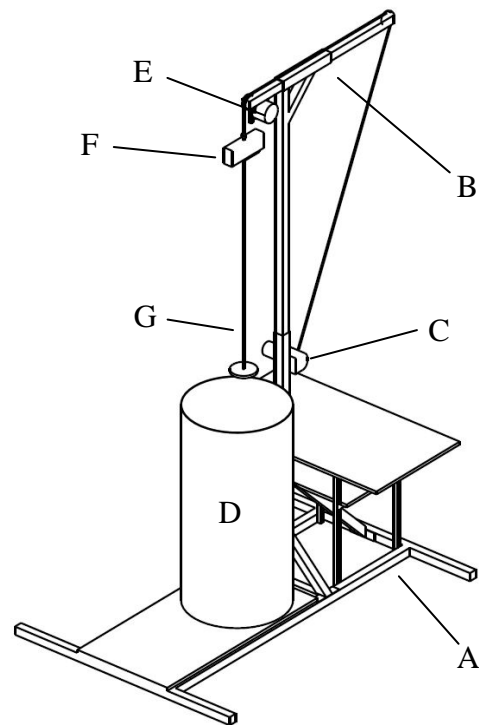


Fig. 2. Measurement device consisting of frame (A), crane (B), winch (C), fluid container (D), distance sensor (E), force sensor mounting bracket (F) and support stand (G).

### 2.2. Immersion method

When an object is immersed it displaces fluid and causes an upwards force called buoyancy. The force is defined by Archimedes' law

$$F = V\rho g \quad (2)$$

where  $V$  is the volume of displaced fluid,  $\rho$  is the density of the fluid,  $g$  is standard gravity and  $F$  is the buoyancy. When measuring the volume as a function of branch's length, equation (2) becomes

$$F(x) = V(x)\rho g \quad (3)$$

where  $V(x)$  is the volume of displaced fluid as a function of immersion depth and  $F(x)$  is the buoyancy caused by the displaced fluid. Volume of the displaced fluid equals the volume of immersed object. When the density of fluid and the buoyancy is known the volume of immersed object can be calculated.

The device measures the objects according to the functional model shown in Figure 3.

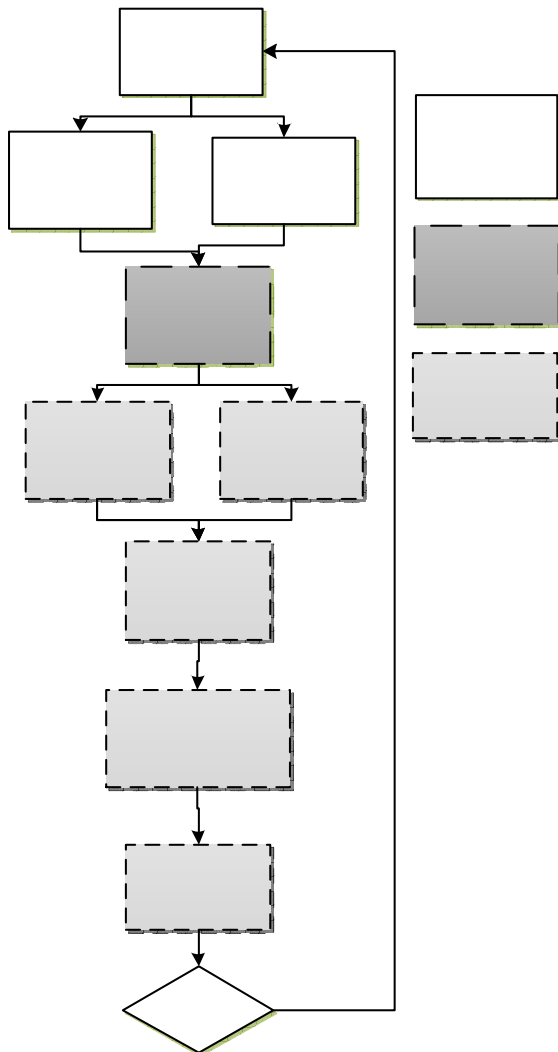


Fig. 3. Functional model of the wood volume distribution measuring device.

In the branch measurements, the base of the measured branch was set on top of the support stand's bottom plate and sub branches were folded to align with the main branch. Branches were attached to the support stand with a thin steel wire to keep them stationary during the measurement and to minimize the momentum caused by buoyancy. Branch prepared for the measurement is shown in Figure 4.



Fig. 4. Branch attached to the support stand

After fastening of the branch the support stand was attached to the force sensor and immersed into the fluid tank. While immersing, the immersion depth and the weight of the branch were measured using 20 Hz sample rate. Immersions were done both by hand and by using the winch.

Total volumes of the branches were also measured by a static immersion using a precision scale. In this study this is considered to be the most accurate method to measure the total branch volumes.

### 2.3. Materials

Measurement and data acquisition components used in measurements are shown in Table 1. In this study two aspen (*Populus tremula*) specimens and a reference object of known volume and shape were measured. The reference object is shown in Figure 5. Water was used as

the fluid into which the immersions were made.

Force sensor	Tedea Hunleight 1022 (5 kg)
Force sensor amplifier	CLIP IG AE 301
Distance sensor	UniMeasure JX-PA-80
Measurement card	National Instruments NI USB-6009
Precision scale	Precisa XB 620M

Table 1. Data acquisition instruments.



Fig. 5. Reference object.

### 3. RESULTS

As the viscosity of water creates a drag force in vertically moving branch, the measurement was done in both lowering and lifting directions. In this way the combined data of these two directions cancel the effects of the additional, opposite forces.

Volume of a steel wire which was used to attach the branch was neglected. Volume of the measurement platform was known so its volume was compensated for the final measurement data.

The measurement data from all repetitions of each branch was placed in one table. The processed data is presented in a graphical form in Figures 6 and 7, the volume of the immersed branch as a function of immersing depth. A polynomial fit of fourth order was determined. The volumes of both branches measured in the conventional way were also included in the

charts. As it is seen, the variation of values is significant in a single point. The initial branch weight in the beginning of the immersion is determined by averaging multiple points in the beginning of each measurement repetition.

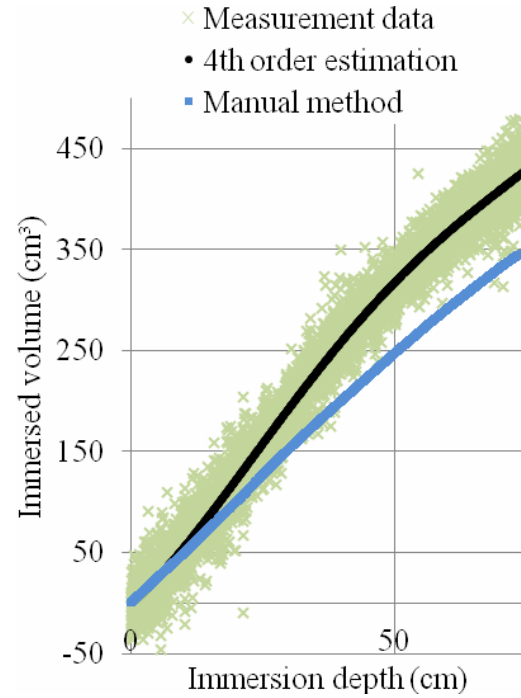


Fig. 6. Branch #1.

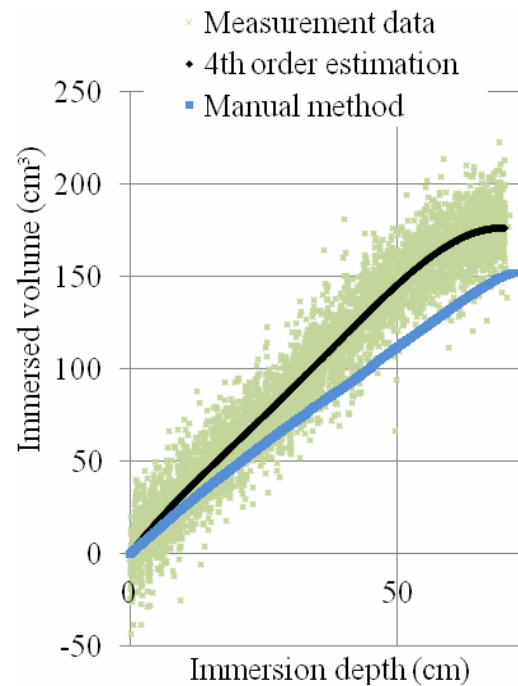


Fig.7. Branch #2.

The total volumes of branches are calculated from equations of the fourth-order polynomial fits shown in Figures 7 and 8. The volumes defined in three different methods are shown in Table 2.

	Method	Volume (cm <sup>3</sup> )
Branch #1	Device	426
	Manual	347
	Precision scale	399
Branch #2	Device	176
	Manual	152
	Precision scale	179

Table 2. Total volume of branch #1 and #2 defined by different methods.

In addition to the branches, the reference object was measured and the data was processed as with the branches. Measured volume and accurate known volume of this reference object is illustrated in Figure 8.

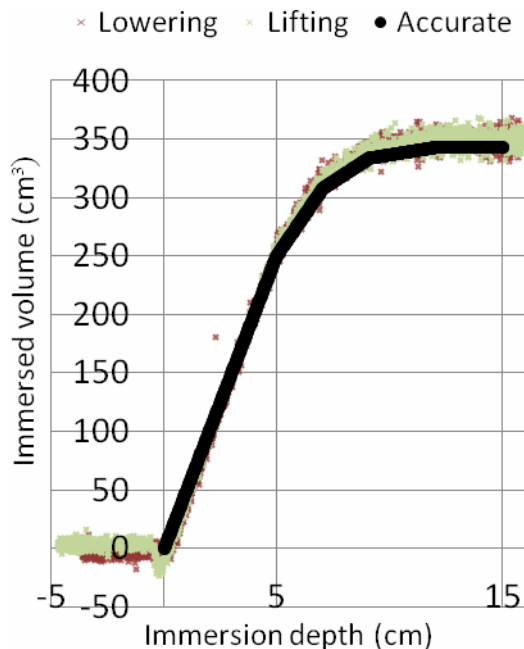


Fig. 8. Reference object.

The theoretical maximum error for the measured weight due to the inaccuracies of measurement system is 2 grams in force transducer, 4.5 grams in force sensor amplifier and 3.865 grams in measurement

card. Total error is 10.365 grams. Theoretical maximum error in distance measurement is 5 mm in distance sensor and 4 mm in measurement card, being 9 mm in total. Observed deviation in static measurement was 4 mm for distance and 11 grams for weight. In dynamic branch measurement the observed weight deviation was 30 grams.

#### 4. CONCLUSION

The device works as expected and the results prove that the branch volume can be measured by buoyancy. The automated measurement process removes routine work and is at least twice as fast as the manual method. The device produces results that are close to the accuracy scale volume which is considered as the best estimation of the total volume. Therefore the results obtained by the device can be considered more accurate than the ones obtained by the manual method. Also the reference object measurements prove that valid data can be obtained.

With the branch specimens, difference between manually and automatically measured volumes is surprisingly large. This may be caused by the fact that manual measurement doesn't take all of the branch specialities into account. For example, in each branching point there is a base enlargement which is difficult to measure and to predict (grey branch area in figure 1). Also the cross-sectional area and the shape of the stem are difficult to estimate with limited amount of measurements. Furthermore, the length of the branch in manual and automated measurement isn't exactly the same as can be seen in Figure 8. This is because in manual measurement the segment lengths are added up instead of measuring the total length of the branch. Also manual measurement takes into account the changes of directions in different sections whereas the device measures the length only in the direction of immersion.

The results are interesting, but they are based on only two specimens of single tree species. Larger amount of both manual and automated measurements on many different species would be required to have statistically valid comparison of these two methods.

There are two main reasons for the variation in the measurement data. First is the lack of signal filtering. Second and greater reason for the variation is the changes in the lowering speed and mechanical vibrations of the lowering system. This is supported by the fact that the lowering done by hand produced a lot less variation in the measurement data than the lowering by winch.

Based on the results, several improvements can be suggested in order to achieve better measurement accuracy. These include the stabilization of the lowering process, improving sensor accuracy and the use of signal filtering.

The device can also be used to determine the cross-sectional area of a branch as a function of the immersing depth as well as the total density of the branch. By combining data from several different measurements the volume distribution of other tree parts such as bark and leaves can be distinguished. The device can be used for various shapes and a wide range of materials and it can be scaled to measure different sizes of objects by changing the force sensor to the suitable range.

## 5. REFERENCES

1. Laasasenaho, J. 1982. Taper curve and volume functions for pine, spruce and birch. *Communicationes Instituti Forestalis Fenniae* 108. 74 p.
  2. Zianis, D., Muukkonen, P., Mäkipää, R. & Mencuccini, M. 2005. Biomass and stem volume equations for tree species in Europe. *Silva Fennica Monographs* 4. 63 p.
  3. Wood logs imported to Finland. Measuring Instruction. Forest Industries Association's standard, 2007, (in Finnish) [WWW]
- [http://www.idanmetsatieto.info/fi/document.t.cfm?doc=show&doc\\_id=1277](http://www.idanmetsatieto.info/fi/document.t.cfm?doc=show&doc_id=1277) (8.3.12).
4. Williamson, G, B & Wiemann, M, C. Measuring wood specific gravity...Correctly. *American Journal of Botany* 97(3): 519–524. 2010.

## CORRESPONDING ADDRESS

Panu Kiviluoma, D.Sc. (Tech.), Post-doc researcher  
Aalto University School of Engineering  
Department of Engineering Design and Production  
P.O.Box 14100, 00076 Aalto, Finland  
Phone: +358 9 470 23558,  
E-mail: [panu.kiviluoma@aalto.fi](mailto:panu.kiviluoma@aalto.fi)  
<http://edp.aalto.fi/en/>

## 6. ADDITIONAL DATA ABOUT AUTHORS

Aarnio, Aleks, B.Sc. (Tech)  
Phone: +358 40 838 4856  
E-mail: [aleksi.aarnio@aalto.fi](mailto:aleksi.aarnio@aalto.fi)

Keltto, Ville  
Phone: +358 50 343 5721  
E-mail: [ville.keltto@aalto.fi](mailto:ville.keltto@aalto.fi)

Vartiainen, Vesa, B.Sc. (Tech)  
Phone: +358 44 364 1000  
E-mail: [vesa-matti.vartiainen@aalto.fi](mailto:vesa-matti.vartiainen@aalto.fi)

Kuosmanen, Petri, D.Sc. (Tech.), Professor  
Phone: +358 9 470 23544  
E-mail: [petri.kuosmanen@aalto.fi](mailto:petri.kuosmanen@aalto.fi)

Kananen, Eero, B.Sc.  
Phone: +358 40 586 2850  
E-mail: [eero.kananen@helsinki.fi](mailto:eero.kananen@helsinki.fi)

Laasasenaho, Jouko, D.Sc., Professor Emeritus  
Phone: +358 40 5066 055  
E-mail: [jouko.laasasenaho@helsinki.fi](mailto:jouko.laasasenaho@helsinki.fi)  
Department of Forest Sciences  
University of Helsinki



## INFLUENCE OF BARREL DAMAGES ON LIFE TIME OF TANK WAGON

Boyko, A.

**Abstract:** *Analysis of damages of such elements of barrel where fatigued cracks appear during the barrel exploitation time was performed. Normative calculations which confirmed sufficient strength of the barrel were implemented. To substantiate heightened level of stresses in local areas of the barrel the additional calculations were performed in accordance with elaborated modes of loading. During CAE simulation the risky levels of stresses in mentioned areas without damages, with damages and repaired damages were obtained as a result of simulation. Recommendations for preparing and counting of results of calculating models in areas of damages and concentrators of stresses are given. The changes in resource of barrel of tank car, depending on the type of damage and variants of damage repair, were defined.*

**Key words:** *Railway tank wagon, barrel damages, SW Simulation, stress-strain analysis, life time.*

### 1. INTRODUCTION

From all variety of railway tank wagons let consider the tank wagons which are used for transportation of liquid and highly dangerous goods. To strength of barrels of tank wagons increased demands are being made towards their strength on stages of designing, testing and technical examination. The barrels which being put into operation have strength reserves necessary in accordance with the "Norms ..." [1] during service term which being set by manufacturer. However during operation before the service term end the

fatigued cracks of the barrel elements appear. In conditions of Latvian railway the main damages of the barrels of oil tank wagons and their quantity (Fig. 1.) are: cracks of welding seams of shaped pads – 50%, barrel damages in area of supports – 30%, damages of welding seams of the barrel – 15%, unfastening of shaped pads – 5%.

Distribution of damages tallies with statistical data of tank wagons for transporting of liquefied hydrocarbon gases (LHCG) which given in the work [2]. Considerable damaging of welding seams of the barrel is due to higher level of pressure in the barrel in comparison with oil tank wagons (Fig. 2).

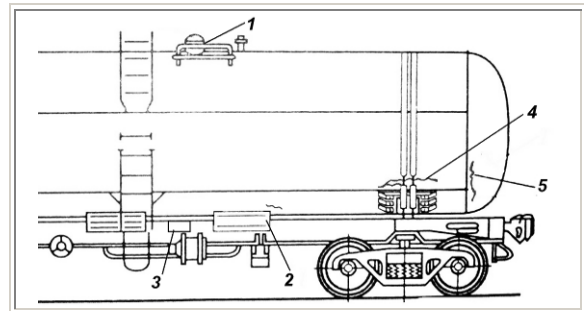


Fig. 1. Areas of damages of barrel of tank wagon: 1-welding seams of manhole hatch, 2-welding seams of shaped pads, 3-welding seams of discharging device, 4-welding seams of the barrel shell near supports, 5-welding seams of dome

As causes of such quantity of damages, possible, are the following: constructive concentration of stresses and concentration of stresses in welding seams, defects of welding seams, uneven wear of the structure elements, high longitudinal forces

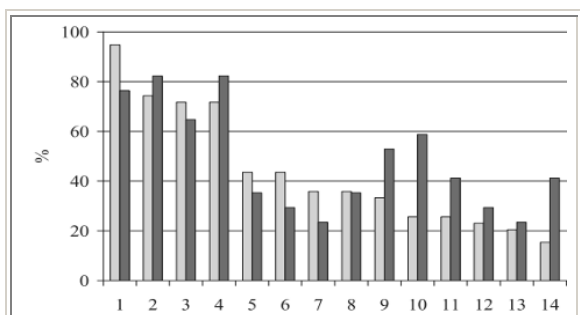


Fig. 2. Statistical data about damaging of tank wagons 903P and 15-1407 accordingly: 1-cracks of welding seams of shaped pads, 5-damage of support, 10-defects of the barrel welding seams, 13-unfastening of shaped pads, 14-unfastening of retaining bands. The rest points don't shown as they concern the wagon frame

during shunting works with heightened speeds and emergency situations (emergency braking, collisions between wagons and with obstacles), longitudinal forces of hydraulic stroke of the cargo.

To define causes of the barrel damages before end of set service term it is necessary to evaluate values and character of the acting loads.

## 2. LOADS AND MODES WHICH LEAD TO DAMAGES

### 2.1. Normative calculation

To evaluate influence of loads to stressed state of areas where damages occur, calculation of strength of barrel of loaded tank wagon of model 15-II863 done for modes of loading which prescribed in the "Norms ..." [1]: 1st (extraordinary mode), 3rd (operation mode), testing pressure, vacuum acting per pressure of the safety valve in the empty barrel. To estimate contribution of horizontal and vertical forces into the barrel stressed state additionally calculations of strength under acting of vertical dynamic forces and horizontal forces of hydraulic stroke were carried out.

The barrel is made from steel BcT3 (yield strength  $\sigma_T=245$  MPa, breaking point

$\sigma_B=390$  MPa [1]). In result of analysis of the stressed state the loads which cause the highest stresses were defined: in the areas 1, 3 – load from testing pressure and load of the 1st mode, in the area 2 – loads of the 1st mode and from hydraulic stroke of the cargo, in the area 4 – loads of the 1st mode, in the area 5 – loads of the 1st mode and load from testing pressure. The loads enumerated in order of their significance. Values of amplitudes of dynamic stresses in whole range of loads from empty condition till extraordinary loads were defined (Fig. 3).

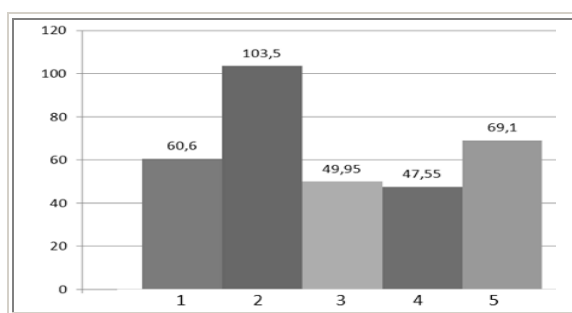


Fig. 3. Amplitudes of equivalent stresses of barrel of wagon 15-II863 in areas No. 1-5 (Fig. 1)

Higher amplitudes arise in the barrel shell – area of shaped pads 2 and in welding seams of the barrel dome – area 5. Amplitudes for the area 4 are minimal, but during operation in 30% of cases there arise cracks and deformations.

As per the normative calculations the barrel strength is in accordance with condition of sufficient strength (Table 1.).

No. of area, name	Stress, MPa	
	Modes	
	1st	3rd
2 Pads	208	99
5 Dome	146	89
4 Supports	101	60

Table 1. Maximum stresses under first and third modes of loading

Arising of damages in operation, possible, is caused by such fact that the normative calculations don't take into account character and values of the barrel loads in

full, or don't take into account character of the loads damaging effect in one or another area of the barrel. Therefore models for evaluation of the stressed state in local areas No. 2, 4, 5 (Fig. 1) where the barrel damages arise were developed. Simulation of damages (defects) of the barrel for these areas was implemented.

## 2.2. CAE simulation

For creation of model of the barrel and models of damages the AutoCad program was used. The strength calculations were made using FEM programme SolidWorks Simulation. Since the design and loads acting are symmetrical calculations of the barrel damages were made on  $\frac{1}{4}$  part of the model (Fig. 4.). To cutting edges of the model border boundary conditions Symmetry were put.

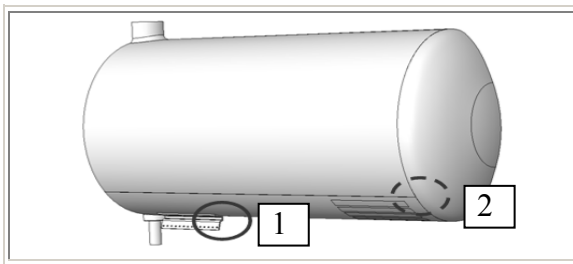


Fig. 4. Calculating model  $\frac{1}{4}$  of barrel: 1- welding seams of shaped pads, 2-T-joint of the barrel seams

Due to curved surface of the structure the finite elements of the second kind (Mesh quality-High) were used, mesher type – Standard – this mesher is faster, Automatic transition – On. Small surfaces of cracks and concentrators of stresses in the area being analysed are divided by smaller mesh by hand, using Mesh Control, finite element size is 6 mm in zone 1 (Fig.4.) and in zone 3 (Fig.1.). The defect dimensions should be larger than the mesh value of inaccuracy in this area for one-layer dividing. In areas of cracks and in transitional areas equal dimensions of the mesh for inner and outer walls of the barrel (element) were set, that furthers formation of finite elements with regular shape.

Number of elements in FE model is about 464052. After developing of model quality of the mesh being verified numerically (Mesh properties) per quantity of elements with irregular shape and visually.

Strength of the barrel is evaluated per equivalent stresses. Results are counted at distance 20-25 mm from concentrators of stresses using strain gauges with base 10-20 mm for environmental tests of wagons. Dimension of finite elements in these areas should correspond with dimensions of the strain gauges.

## 2.3. Simulation of damages of the area of shaped pads (pads)

As per results of the normative calculation without damages of the barrel strength in area of pads is sufficient. During operation cracks arise in this area: 1 – in transversal welding seam of the pads, 2 – in the barrel shell (Fig. 5). Simulation of more frequent damage No. 1 was implemented.

The created detailed model of pad is welded to the barrel shell not by whole contact area (as it is taken in the normative calculation), but by perimeter, longitudinal and transversal welding seams and seams in cuts of the pad middle part (Fig. 5.). Variants calculations of the pad strength for transversal seam in manufacturer's, repairs' performances and with crack on whole width of the pad (Figures 6, 8, 10.) were executed.

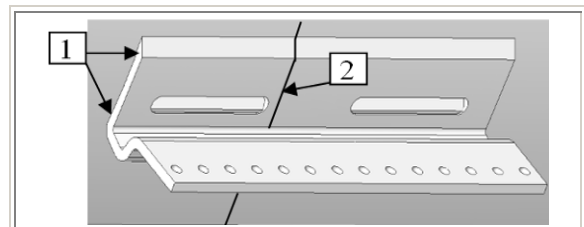


Fig. 5. Model of pad. Scheme of pads' cracks: 1-in transversal seam, 2-in the barrel shell

From results of the calculations defined that in case of manufacturer's performance of the transversal welding seam (Fig. 6, length about 100 mm) stresses reach

65MPa, and 96MPa in joint with the longitudinal seam (Fig. 7).

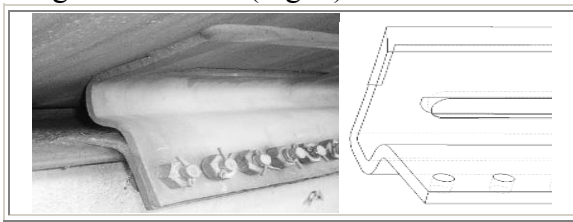


Fig. 6. Manufacturer's performance of transversal seam of the pad on wagon and in the model

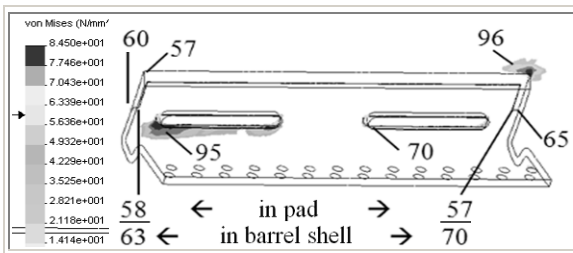


Fig. 7. Stresses of the pad, MPa (seams in manufacturer's performance)

When the transversal seam in repairs' performance has length equal to width of the pad (Fig. 8), stresses in the welding seam grow by 2.1 times and reach 145 MPa, and 93 MPa in joint with the longitudinal seam (Fig. 9). In end of welding seam (concentrator of stresses), when the seam length is maximal, stresses reach 240-400 MPa, that exceeds yield strength and limit strength of the material, and corroborate arising of cracks.

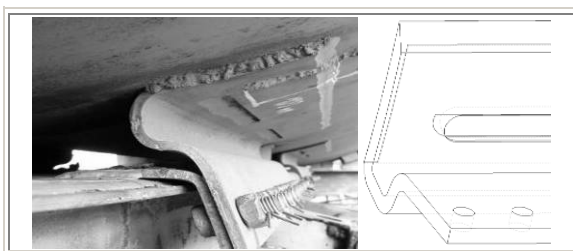


Fig. 8. Repaired transversal seam of the pad on wagon and in the model

In case of crack in transversal seam (Fig. 10), stresses in ends of longitudinal seam reach 57MPa and 95MPa (Fig. 11). Stresses in welding seams in cuts of middle part of the pads reach 77MPa and 101MPa. Crack in transversal seam not lead to growing of stresses in longitudinal seam,

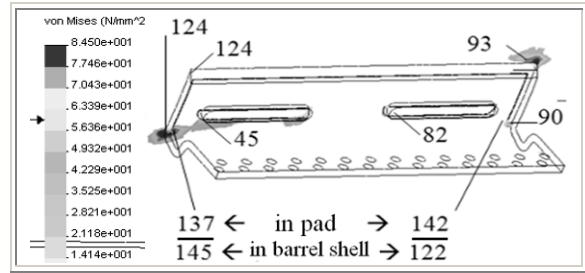


Fig. 9. Stresses of the pad, MPa (length of seams – as far as the pad width)

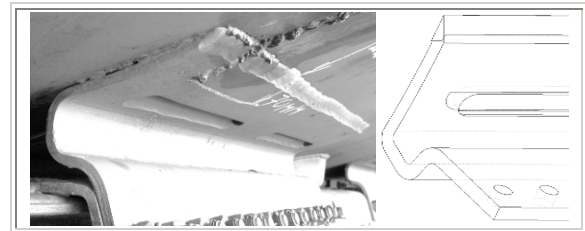


Fig. 10. Crack in transversal seam of the pad on wagon and in the model

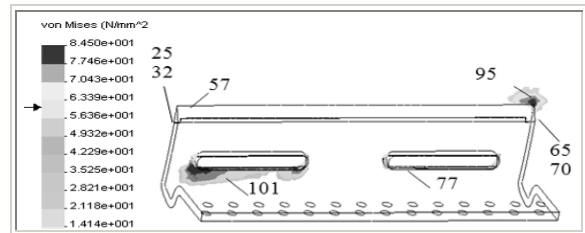


Fig. 11. Stresses of the pad, MPa (seams with cracks)

but in welding seams in cuts of the pads stresses have grew by 9% in comparison with stresses in case of manufacturer's performance of the transversal seam.

During repair it is necessary to control length of transversal seam which should be in limits from 100 mm till ~140 mm (till line of projection of longitudinal seams in cuts of middle part of the pad to line of the transversal seam).

#### 2.4. Simulation of damages of the area of supports

In accordance with results of the normative calculation (Table 1) the barrel strength in area of pads is sufficient. During operation cracks arise in this area: in horizontal welding seam of the barrel shell near supports (area 4 – Fig. 1), in vertical seam of dome near supports (area 5 – Fig. 1).

Uneven sagging and wear of the supports, which made from wood, lead to the barrel leaning on the upper supports. Results of simulation of such case are shown on Fig. 12, and in Table 2.

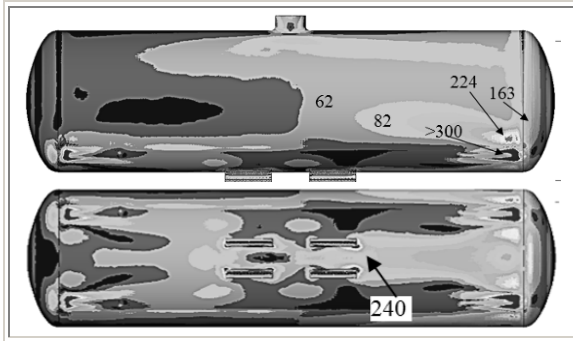


Fig. 12. Equivalent stresses when the barrel leans on upper supports

Stresses in area of the barrel shell are higher than yield strength of the material, which leads to arising of the barrel shell deformations and welding seams' cracks in areas No. 4, No. 5 (Fig. 1) during operation.

No. of area, name	Stress, MPa; 1st / 3rd mode		
	By Norms	Sagging of supports	Increase
2 Pads	208 \ 99	240 \ 110	32 \ 11
5 Dome	146 \ 89	163 \ 103	17 \ 14
4 Supports	101 \ 60	224 \ 130	123 \ 70

Table 2. Evaluation of the central supports sagging influence to the barrel stressed state

During repair it is necessary to control if the supports fit closely to the barrel shell. For calculations of the barrel it is necessary to take into account uneven leaning on supports.

### 3. ESTIMATION OF THE BARREL LIFETIME

Let implement calculating estimate of remaining lifetime for the barrel per two criteria [3]: 1 – per destruction from single blow (extraordinary loads); 2 – per accumulation of residual deformations.

#### 3.1. Estimation of lifetime till single fracturing blow

Mathematical expectation of quantity of blows  $\bar{n}$  till arising of bearing elements damages being defined by approximate relation:

$$\bar{n} \approx \frac{1}{p}, \quad (1)$$

where  $p$  – probability of such blow, in the time of which stresses in some bearing element will exceed the breaking point.

When the longitudinal forces distribution function  $P$  is known, then this probability

$$p = 1 - P_i, \quad (2)$$

where  $P_i$  – value of distribution function for such values of forces when the acting stresses not more than permissible level.

As quantity of longitudinal blows per year is known it is possible to evaluate lifetime approximately per this criterion.

As per the normative calculations, the highest stresses in the barrels are in seams of welding of pads to the barrel shell (area 2, Fig. 1) – 208 MPa from longitudinal load 2.5 MN. Parameter of Rayleigh distribution for this point is:  $S = (208 \times 0.88) / 2.5 = 73.21$  MPa.

Breaking point of heavy-plate steel BCт3 is 390 MPa and includes 5.327 scale parameters. Probability of this level exceeding is  $p = 1 - 0.999999$ , and mathematical expectation of quantity of blows till damaging level will reach 1000000, and as the quantity of compression blows per year is 7500, it corresponds to 193 years of operation.

In calculation for additional modes – in case of enlarged length of transversal seam of pads and in case of the barrel leaning on the upper supports mode, – stresses in pads will grow up to 240 MPa. In such case lifetime will sink till 5.66 years, and it confirms possibility of non-permissible cracks (damages) arising in pads of 30% wagons in operation between major repairs of the wagons (8 years).



### 3.2. Estimation of lifetime per low-cyclic fatigue

Average time till accumulation of plastic yield when crack in a bearing element arises can be defined from the formula below:

$$\bar{T} = \frac{\sigma_{-1}^m N_0}{n_g 2^{\frac{m}{2}} \Gamma\left(\frac{m}{2} + 1\right) S^m}, \quad (3)$$

where  $G_{-1}$  – fatigue endurance limit on base  $N_0=10^6$  cycles (taken per the fatigue curve on base 80000 cycles as 140 MPa);  $m$  – slope of the S-N-curve (for the carbon steel  $m=3.33$ );  $n_g$  – quantity of compression loads during one year of operation;  $\Gamma(\dots)$  – gamma-function.

As per the normative calculation the higher stresses in area of seams of the pads are 208 MPa. Lifetime per criterion of low-cyclic fatigue will be 19 years. In mode of the barrel leaning on the upper supports and in case of enlarged length of transversal seam of pads the lifetime in area of the pads is  $T_{240} = 12$  years. In the barrel shell in area of supports  $T_{224} = 15$  years. The calculation estimation of the remaining lifetime confirms possibility of fatigue cracks arising between major repairs of wagons in areas of pads and supports (Table 3.).

No. of area, name	Lifetime per low-cyclic fatigue, years		
	By Norms	Sagging of supports	Decrease
2 Pads	19	12	7
5 Dome	63	43	20
4 Supports	214	15	199

Table 3. Evaluation of the central supports sagging influence to the barrel remaining lifetime

### 4. CONCLUSION

From statistical data and calculations follows, that there are two areas which are subject to larger damages: cracks of welding seams of shaped pads and cracks

of barrel in area of supports. Main loads and elements of the barrel which limit lifetime of tank wagon were defined on base of results of normative calculations and new-worked out modes of loading. Measures for lifetime increasing are elaborated and proposed. Recommendations for preparing of simulation of damages with small dimensions by means of CAE are given.

### 5. REFERENCES

1. *Normi dlya raschyeta i proyektirovaniya vagonov, zhyelyeznih dorog MPS kolyei 1520 mm (nesamohodnih)*, 1<sup>st</sup> and 2<sup>nd</sup> Revising and Supplements, VNIIV-VNIIZhT, Moscow, 1996. (in Russian)
2. Bityutskiy, N. A. The analysis of operational dependability of specialized tank-cars to transport condensed hydrocarbon gases. In *Transport Urala*, 2010, 4 (27), 67-71. (in Russian)
3. Vuchetich, I. I., Derkach, B. A., Kachnov, F. D. Otsyenka ostatochnogo ryesoorsa groozovih vagonov zhyelyeznih dorog. In *Vyestnik VNIIZhT*, 2008, 2, 14-18. (in Russian)

### 6. ACKNOWLEDGEMENTS

This work has been supported by the European Social Fund within the project «Support for the implementation of doctoral studies at Riga Technical University».

### 7. ADDITIONAL DATA ABOUT AUTHOR

Dr.sc.ing. Alexander Boiko  
 RTU, Institute of Mechanics  
 Ezermalas 6k, LV-1006, Riga, Latvia  
 Phone +371 67089396  
 E-mail: [boyko\\_af@yahoo.com](mailto:boyko_af@yahoo.com).  
 Baltic Testing Centre Ltd.  
 Phone +371 67801732  
 E-mail: [btc@btcentr.com](mailto:btc@btcentr.com)

## THE QUALITY CONTROL OF MACHINING PROCESS WITH CAD/CAM SYSTEMS SUPPORT

Dubovská, R.

**Abstract:** *The aim of this paper was to study the simulation process of components in the CAD/CAM system CATIA. This process is important to enter the manufacturing process of various precision components of complex shape designed for automotive and aerospace industry. Each machining technology must be supported by selection of the relevant cutting tools and cutting materials, design of equipment and machinery suitable for innovative machining technology, which benefits must always be continuous reduction in production time and mechanical machining time in each operation, subject to the quality and accuracy of the product. Production. Improvement of production quality is defined by characteristic features. The production process quality and final product milling are influenced by determination of optimal cutting conditions in milling.*

*Key words: Quality Control, Machining process, CAD/CAM, Production Processes, Quality*

### 1. INTRODUCTION

One of the management strategies for business in the market is a strategy of continuous improvement of production quality through the implementation of quality processes of machining and continuous improvement [1].

Great importance to all new technologies, materials, machinery, progressive methods and information tools that enable more efficient use of starting materials, produce a more cost effective, fast enough to

produce reliable and quality products and above all succeed in the market in an increasingly challenging competitive environment. Today's trend component is machining in one setup, with minimal clamping. This is achieved by the time reduction of the final machining, while eliminating inaccuracies caused by manual switching of the workpiece. Introduction of computer graphics allows a computer to create pieces, handle and examine them. Universal application of computer aided systems brings significant benefits. CAM systems are used for the preparation of data and then creation of NC programs for manufacturing components [8].

The production process quality and final product machining are influenced by determination of optimal cutting conditions in milling. We can define cutting conditions in consideration of the workpiece material. Then we can choose optimal type of cutting tool with the proper cutting material and tool geometry by pursuant to optimal type of machining in 3D CAD/CAM system CATIA V5 NC MANUFACTURING surroundings [2].

CATIA V5 is one of the higher CAD/CAM systems, because in addition to modeling and offers technical documentation and production assembly kits, assemblies and design areas of thin metal sheets, different strength analysis, as well as simulate turning, milling moulds, drilling etc. 3D model created from CAD part of CATIA is then inserted to a process of simulation, where is generated NC code for the various systems, CNC machining centers [6].

Machining of various components of complex shape, using milling, drilling

holes and so on, it is possible to implement more gripping and carrying out each operation machining on various machine tools. By automating the production process of such components can be performed all the operations to a minimum number of clamping in more axial CNC machining center. The CAD Support/CAM system makes faster the entire production process, and what is particularly important in those parts of complex shape [10].

For finishing machining of hard materials such as hardened steel was previously a problem due to the high temperature process of cutting, high cutting parameters and non adequate system machine-tool-workpiece-fixture. The replacement of grinding by the turning tools with coated cemented carbide and ceramic cutting inserts and automated production process with the support of CAE systems to achieve the desired quality of machined surface in a shorter manufacturing time and improved accuracy of production [7].

## 2. MACHINING PROCESS

High-speed machining is applied with significantly higher cutting speeds the relatively small cross sections cut. High-speed machining technology is realized with extremely hard and heat-resistant cutting tools. Temperature in the cutting zone and chip creation approaches the melting temperature of workpiece. Chip in the transition shear plane shear increases across its cross-section of a sudden its temperature, turn red and soften hardened steel scrap and thus reduce its downforce on the front of the instrument.

Chips from the contact zone quickly and leaves no time to pass heat tool or workpiece. This minimizes heat transfer into the tool and workpiece, and most of the resulting heat goes with chips. All this despite an overall increase in heat reduce tool wear. As a result of cutting forces decreasing and reduce heat transfer into the workpiece and increases machining accuracy.

Design tools for machining long been a criterion for the interaction of creative abilities of designers, material specialists, engineering and manufacturing engineers in practice. New materials and new technologies require the use of a new generation of tools. New materials and new technologies require the usage of a new generation of cutting tools [12].

The choice of cutting tools must comply with changes in production such as new construction materials, increasing accuracy requirements, progress in the production of CNC machine tools and application of new technologies [5].

### 2.1 Technological aspect for dry and hard machining technology

The aim aside to dry (dry cutting), the elimination or minimization of the quantity used cutting fluid and thus reduce the cost of their purchase, maintenance and disposal and also to supporting acts such as: wet degreasing workpieces and chips, or spinning them. The latest experience aside and know that some machined materials using certain cutting materials is prepared in the dry without the use of cutting fluids (e.g. machining gray cast iron by carbides K10 to K40), respectively machining with cutting ceramics.

A newly designed tool (using CAD/CAM techniques) must not only have superior technical specifications, but also possibility of wide application in accordance with market needs and users [11].

The suitable cutting tool materials for dry machining are fine HW, HT, CC, BN, DP. Widespread application of dry machining is becoming more hard machining hardened steel with a hardness of 45÷65 HRC. Among the machined materials that can be machined under drought include: aluminum and its alloys using diamond-coated HC, respectively in the production industry and using the tools of polycrystalline diamond. Dry machining can be done only where there is no guarantee that the machine tool to achieve the same surface quality and mechanical



piece that also time is the same as for cooling.

Hard machining is motivated by a desire to replace the finishing grinding hardened and hard materials, machining tool with defined geometry and the cutting tools for turning, boring, milling, but gradually and with reaming, drilling sporadically, respectively in planetary milling threading. This is a working material hardness of 45÷65 HRC hardened steel, cemented and hardened steel, hardened cast iron, Ti - alloys, Co - alloy (Stellite).

Suitable hardness range of workpiece materials for hard machining is on Fig.3. Hard machining is classified as high-speed machining, although the cutting speed  $v_c = 100$  to  $150$  m/min, cut in small cross sections ( $p = 0.15$  to  $0.25$  mm,  $f = 0.05$  to  $0.2$  mm). Material removal rate is higher than in grinding time and reduces -  $t_{AS}$ . We can use cutting fluid, when apply mixed hard turning cutting ceramics ( $Al_2O_3 + TiC$ ) coated with waste, or the PCBN, as equivalent cutting materials for hard machining, and cooling may be also used.

Hard machining technology can be applied by the using cutting materials, based on polycrystalline cubical boron nitride (BN), a mixed cutting ceramics (CM), for helical milling of monolithic ultra-fine grain EN-ISO-K10/K20, coated with hard coatings. On Fig. 2 see the extent of hardness of workpiece materials suitable for hard machining applications [10].

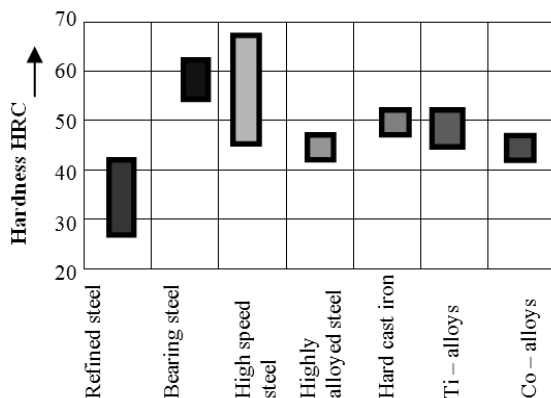


**Fig. 1.** Rockwell hardness HRC of selected metallic materials - suitable for application of the hard machining technology [10].



**Fig. 2.** Hard milling technological process of hardened abrasion-resistant sheet HARDOX 500,  $46 \div 50$  HRC [10].

### 3. CAD/CAM SYSTEM CATIA V5

Emergence of new technologies used in the automotive industry is the customer's satisfaction with the services and become more closely linked to technical and software equipment partner [3].

The creation of NC programs use elements of ISO programming in combination with 3D graphics support, as in CAD/CAM systems. This method of programming CNC machines essentially reduces editing time [9].

The graphical creation of models with components using 3D system CATIA V5 which is implemented using the main Start menu, where they are located SKETCHER subsections, which is 2D creation of sketches and shapes, serving as a basis for later create 3D models in other parts of the product such as CATIA V5 DESIGN PART, Generative SHAPE DESIGN, SHEET METAL DESIGN, Wireframe and Surface Design, etc. The main basics of using CATIA V5, is the proper use and therefore the transition from 2D plane in the first dimensional space, but not least the construction site. In order to establish a complex and multiple mounting kit, create a flawless technical drawings, it is important to know appropriate to set up different models of machine parts, which form the basis for further work and subsequent CAD and CAM systems team. The advantage of the underlying

modeling and creating sketches lies in simplifying the control itself, ie used all the features and icons are mostly single-level, resulting in a much better insight into the work itself, unlike some other CAD systems. After creating 2D sketches through the "Exit Workbench" get into 3D environments such as PART, SHAPE DESIGN, etc.. In fact the 3D environment, then use the appropriate functions, depending on the type and the shape of the future model components to create the final PART or part of the product, if you worked for in subsection ASSEMBLY DESIGN. CATIA V5R advantage is its transparency, icons are placed directly on the sides of the active desktop, or you can activate them via the main menu View-Toolbars. This structure of the system is necessary in view of the scope and job opportunities CATIA. Modeling procedure itself is clearly stated in the so-called working application tree, which is always on the left side of the active desktop.

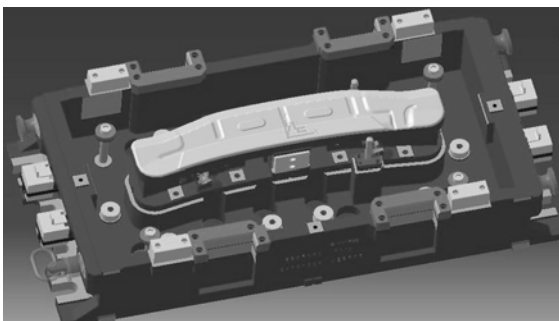


**Fig.3.** Overall view on a product designed and connected together in ASSEMBLY DESIGN modul of CATIA V5 [9].

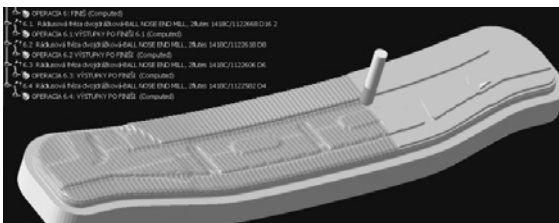


**Fig.4.** Simulation process of Milling edges technology in CAM interface of CATIA V5-NC Manufacturing (milling) [9].

#### 4. THE QUALITY OF CAM PROCESS

Individual acts necessary for the design of machining on CNC machining

centers in the CAD/CAM system CATIA V5 R20 Machining modul are as follows:

- Determine appropriate and Geometric BODY SET for parts and semi-on working tree. Create a 3D model parts.
- Create a blank with those allowances which will be model.
- Go to the machine mode of CAD/CAM system CATIA V5.
- Parameter setting tool, which will perform roughing model.
- Define the machining operations, which are determined semi-alone model, the machining allowance, tolerance, sliding, speed and infeed machine tool path.
- Set parameters of other instruments which will perform profiling.
- Define the machining operations, which also set aside all the parameters.
- Running simulations of machining, simulation output control machining (can see on Fig. 4, 5, 6).
- NC code in the form of ISO, as appropriate CNC machine and control system [5].

After creating a technological process of production, the choice of an appropriate strategy roughing and finishing the functional areas of the drawing tool milling tools to select suitable material, geometry and cutting plate holder. Then determine the optimum cutting parameters for each roughing and finishing hard milling (feed, cutting speed). Model created with the tool, along with intermediate put into the environment module of CATIA V5 NC Manufacturing in the work of the tree PRODUCT LIST. Creation of the production process is at the top of the tree under the name PROCESS LIST. Process through the menu is listed in NC Manufacturing module design type CNC machine tool. Then we determine the zero point of the workpiece coordinate system of the machine, the type of post-processors to generate NC code for FANUC. Through Auxiliary operations generate optimal shape and material, tool holders, cutting plates and determine the strategy

(Fig.3) of whole process of production using Machining milling operations. Using the tool path replay and simulate the process of routing module Generating NC code then generates the NC program in ISO format (G and M codes), using a memory card, transferred to a control system for CNC machine tool.

## 5. THE SIMULATION PRODUCTION PROCESS IN CATIA & RESULTS

NC code in CATIA V5 is implemented through function Generative NC code [4]. When activated, this icon to formation of the NC program from the active machining process, which was designed in the previous steps.

Before the act of generating NC code necessary to determine the correct data on the method of machining, tool and defining its holder. The generated NC code can be further edited on a computer or directly to the CNC machining center, the second option is not desirable in terms of production efficiency. A necessary early step is to delete the generated NC code, therefore, since these data are set in the CNC machining centers and the abolition of numbering lines. It is important to change the file to NC code program without an extension, was known to process CNC machining center. The last stage is to upload NC code for portable media and injected into a CNC machining center, which operate codes directly from portable media due to lack of internal memory machining center [5].

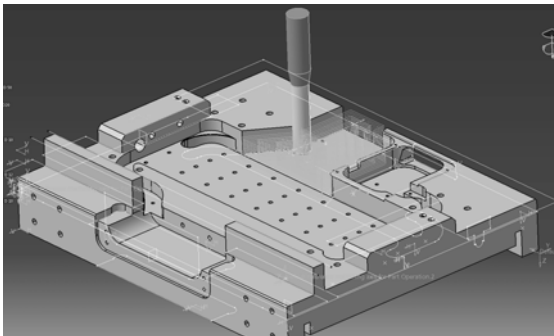


**Fig. 5.** Prismatic machining process on the selected component in CAD/CAM [6].

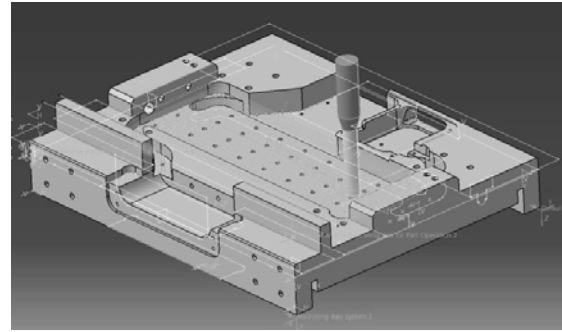


**Fig. 6.** The simulation of prismatic machining process simulation in the CAM interface of CATIA V5 R20 [6].

Prismatic machining model components were carried out on a vertical machining center.

Machine parameters: Workbench 700x450 mm, Table load max 300 kg, Max. spindle speed 10 000 rev/min, spindle taper SK40  
Workspace: X-axis (610mm), Y-axis (460mm), Z-axis (480 mm)

Shifts: Rapid X/Y = 36 m/min rapid traverse Z = 24 m/min

Roughing:  $n=1490$  min,  $f=1700$  mm/min,  $a_p=0.8$  mm.

Finishing:  $n=2900$  min,  $f=2300$  mm/min,  $a_p=0.15$  mm.

Workpiece material: tool steel TOOLOX 44 with 45 HRC [5, 6].

After clamping the stock was vice settings planes and other corrections that are needed to start machining. Milling model was used cylindrical roughing cutter with a diameter of 32 mm carbide insert, stem diameter of 32 mm radius of curvature of 2 mm. Profiling model has been implemented cylindrical cutter with a diameter of 16 mm, 16 mm shank diameter of 2 mm radius. The additional material from the milled grooves was used spherical cutter with a diameter of 6 mm. Milling was carried out without cooling the emulsion as a medium for removing chips was used compressed air [5, 6].

## 6. CONCLUSION

The advantage of dealing with the issue of creating NC code in the CAD/CAM system CATIA model for machining on a vertical milling machine tool system is that

the creation of the NC program for a relatively short period of time due to the complexity of the shape components utilized milling. Facility these systems is sufficiently rapid generation of NC code and its easy adaptation to a suitable form for the CNC machining center. Using the systems with CNC machining center in practice reduces the risk of errors arising during operation models.

## 7. ADDITIONAL DATA ABOUT AUTHORS

- 1) Rozmarina Dubovska, Prof. Ing. DrSc. Professor of the University of Hradec Kralove, Director of the department of technical subjects
- 2) The quality control of machining process with CAD/CAM system support
- 3) Full Address of all authors: (Professor / prof. Ing. DrSc. / Namesti Svobody 301, 500 03 Hradec Kralove, Czech republic / rozmarin-dubovska@uhk.cz / www.uhk.cz
- 4) Corresponding Author: (Rozmarina Dubovska, Namesti Svobody 301, 500 03 Hradec Kralove, Czech republic)

## 8. REFERENCES

- [1] Jambor, J. *Analysis of the results of audits of quality management system – sales service of cars*, Quality Innovation Prosperity, Kosice 2010, Vol.XIV/1-2, ISSN 1335-1745, **8**,1-8.
- [2] Jambor, J., Majerik, J. *Hard Die & Mould Milling Process with CAD/CAM system CATIA V5R18 Support*, Annals of DAAAM for 2009 & Proceedings of the 20th International DAAAM World Symposium, Vienna, 25-28th November 2009, ACV, ISSN 1726-9679, ISBN 978-3-901509-70-4, **2**, 1465-1466.
- [3] Lechan, P., Jambor, J. *SEAT Service quality management system*, International scientific conference of Vehicles - New trends in construction and exploitation automobiles, Slovak University of Agriculture, ISBN 978-80-8069-942-0, Nitra 2007, **5**, 119-123.
- [4] Majerik, J., Bajcik, S. Jambor. J. *Automation of the Production Process for Metallic Flexible Diaphragm with CAD/CAM system Catia V5R19 Support*, Annals of DAAAM for 2010&Proceedings of the 21st International DAAAM World Symposium, Zadar, 20-23rd October 2010, ISSN 1726-9679, ISBN 978-3-901509-73-5, **2**, 0623-0624.
- [5] Majerik, J., Danisova, N. *Automation & Simulation of Milling Process with CAD/CAM system CATIA V5R19 support*. AI Magazine – Automotive Journal, Vol.II, No.4, ISSN 1337-7612, 2009, **3**,20-22,
- [6] Majerik, J., Jambor, J. *Prismatic milling simulation process and CNC programming in the CAD/CAM system CATIA V5R20*. Annals of DAAAM for 2011&Proceedings of the 22nd International Wold Symposium, Vienna, 23-26th November 2011, ACV, ISSN 1726-9679, ISBN 978-3-901509-70-4, **2**, 1465-1466.
- [7] Majerik, J., Jambor, J. *Automation of hard turning process with FANUC MANUAL GUIDEi support and CNC programme generation*, Proceedings in Manufacturing systems, Bucharest 2010, Vol. 5, ISSN 2067-9238, **4**, 281-284.
- [8] Majerik, J., Jambor, J. *Technological aspects of manufacturing process programming with CAD/CAM system CATIA V5R20 support*, Proceedings in Manufacturing systems, Bucharest 2011, Vol. 6, Issue 3, ISSN 2067-9238, **6**, 141-146.
- [9] Majerik, J., Baska, I. *Automation of milling process in CNC system FANUC*, It CAD, 03/2010, ISSN1802-0011, **2**, 16-17.
- [10] Majerik, J., Šandora, J. *The new progressive cutting tools and machining technology methods*, ISBN 978-80-8075-515-7, EAN 9788080755 157, 2012.
- [11] Majerik, J., Šandora, J. *Cutting tools for machining-the new trends*, Mechanical engineering Journal, ISSN1335-2938, Vol. XIII., No.3, 2009, **2**, 30-31.
- [12] Majerik, J., Šandora, J. *Drilling and milling tool-new trends*, Mechanical engineering Journal, ISSN1335-2938, Vol. XIII., No.4, 2009, **2**, 82-83.

## INFLUENCE OF SHAPE PRODUCT DESIGN IN THE MANUFACTURING PROCESS

Enache, I.C.; Simion, I. & Bogza, A.M.

**Abstract:** *Paper shows how much renewing design products influence the manufacturing process. The variety of products, low manufacturing cost and high quality of products describes the market situation today and for that the competition in marketplaces requires quickly renew existing products and develop new ones. Product design has a direct effect on the cost of a product and plays an important role in the production process. There are many articles that treat this subject putting the question " How much a new product design changes the manufacturing process and the cost? ". In this purpose we give an example to illustrate it and to put in evidence the changes made in the production process.*

*Key words: design, manufacturing process, flexibility, cutting die.*

### 1. INTRODUCTION

Design is integrated in product and is not only an aesthetics element attached.

The process engineering is connected with product design. Production is a process whereby raw material is converted into semi finished products and thereby adds to the value of utility of products, which can be measured as the difference between the value of inputs and value of outputs [1].

The main objective of production is to produce the goods and services demanded by the customers in the most efficient and economical way. Market interest for firms and companies is maintained by launching new products. The change level depends on the modification and transformation scale,

being placed on a product after studies, research and design activities [2].

The manufacturing infrastructure required to support production: function support, manufacturing planning and control systems, manufacturing system engineering, quality assurance and control, clerical procedures, work structuring and organizational structure [3].

Production process converts a set of inputs into a set of desired outputs.

### 2. PRODUCT DESIGN

Engineering design is the result of someone trying to do a task more quickly or efficiently. Design activity occurs over a period of time and requires a step-by-step methodology [4].

Industrial design is a creative activity of aesthetic and useful products which can be applied at different levels:

Surface Design - involves the coverage with ornaments, textures, decorative elements etc.

Shape product design - involves changing outside design of an existing product or one passed to a new product and that interior mechanism remains the same.

Product design - involves product conception along with the technical design. In this Process are involved all firms departments.

Radical design - involves a radical conception, a break with tradition.

Radical design products present a greater risk than the traditional ones, because users may prefer traditional products and in this context the financial risk is high.

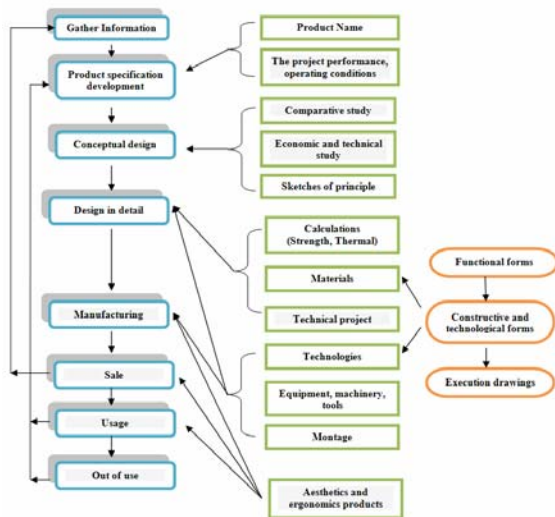


Fig. 1. Product design

Different disciplines start communicating and collaborating with each other to optimize their sub-component design considering the whole system design requirements [4].

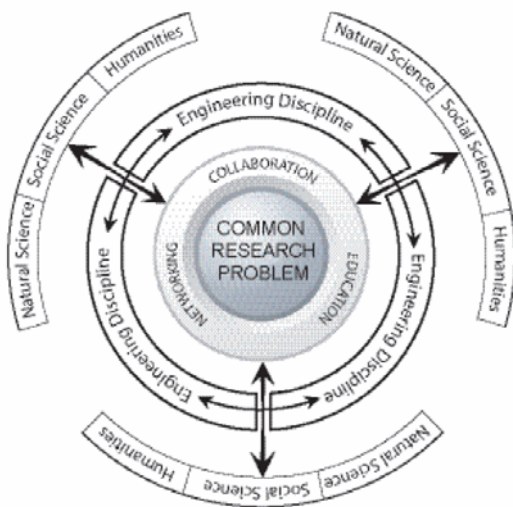


Fig. 2. Interdisciplinary Research Process

Market study of a product is directly influenced by marketing this. The conception in detail is characterized besides specific calculations and materials by functional and constructive-technological forms studied in detail. An important role in designing and manufacturing industrial products, they have the materials that represent about 50% of the total cost of a product.

They have a significant contribution in technical and aesthetic success of products. Because the product design is dictated by the market demand, in 2011, with the expansion of marketplace, ARCTIC received orders for a new product with new design, and therefore had to bring some changes to the tools of the line to process outer cabinet door. It is an important decision and therefore the company pays the effort, time, energy and attention in order to get the best results. To achieve this objective it took to change some active parts of drawing press of the line OLMA according to the new design of cabinet door.

### 3. SHEET METAL ROLL RECEPTION

One of the raw materials used in the manufacturing of refrigerators is the sheet metal cold or hot roll with different concentration in carbon. At the reception of raw materials is preparing a checklist of quality that is achieved by following four steps:

Step1: Identification of the product and the provider is done by: product and supplier identification, identification data sheet, documents that accompany the product, the certificate of conformity, test certificate, the reception data sheet for raw materials.

Step 2: Check delivery. Personnel in charge checking the way it was transported, packaging integrity and check that it has appropriate label. If these conditions were not respected is announced the responsible, is mentioned in the transport document the findings and photos will be made for their support.

This step follow some characteristics which must respect a limit allowed under the technical documentation:

- C1 (aspect);
  - C2 (dimension);
  - C3 (tensile strength);
  - C4 (elongation on break)
- Step 3: Presentation of results.



If at least one control characteristic does not fall within the tolerance field, the check is repeated with a new sample.

If the result is accepted, the personnel stick the green label and announce the staff that the cargo is received. In case the result is not accepted, a red label is stuck and is called the personnel of the department purchases and the provider. Denied receiving material is stored in a place specially designed and marked. Following the results obtained at the reception, raw materials are recorded in a database according to their use.

Step 4: The sheet metal rolls are arranged by category in the warehouse.

#### 4. CUTTING SHEET

From the warehouse the sheet metal roll is transported to GABELLA line, which cuts the board to the desired format (length parameter is determining) depending on the final product design.

Sheet metal is placed on drum machine where it is caught and fixed. After fixing and catching sheet metal, will be entered the following data into numerically controlled machine: thickness and length, smoothing parameters and the number of the sheet metal which should be cut.

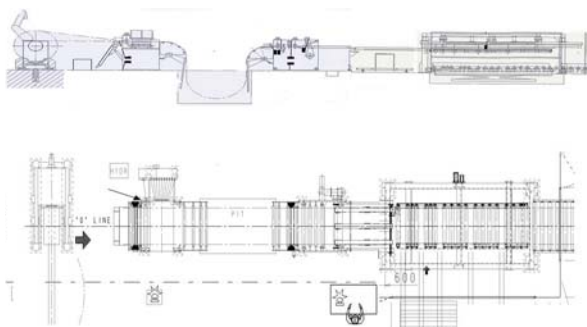


Fig. 3. Layout of the line GABELLA

During all this process the raw material passes through three steps.

Step 1: Sheet metal passes through a roller system in order to remove all existing deformations.

Step 2: Cutting sheet metal to desired length.

Step 3: represents the end of the whole process where already the cut sheet metal is run-off on a band carrier and placed on special supports.

After all this debited sheet metal it is transported to the processing lines or stored in specially designed shelves. On the production lines we encountered two sheet metal processing machines, which perform the following operations: stamping, bending, cupping, all depending on the product design. Because the heading and end of roll has small defects due of transport, they are cut to a certain size and used to the parts without commercial aspects of the refrigerators.

#### 5. FLOW SHEET METAL PROCESSING

Line processes are designed to produce a large volume of a standardized product for mass production. They are also known as flow shops, flow lines, or assembly lines. With line processes the product that is produced is made in high volume with little or no customization [5].

A process flowchart is used for viewing the sequence of steps involved in producing the product, and the flow of the product through the process. It is useful for seeing the totality of the operation and for identifying potential problem areas.

The debited sheet metal is taken from warehouse and is distributed at processing lines OLMA and BERETA, where cabinet and door are machined for refrigerators.

- BERETA line. On this line are produced 3400 lateral panels per day, the time between two parts is 30 seconds. The sheet metal bending is done with two bars. Also on this line is produced a certain range of doors.

- OLMA line. On this line the sheet metal bending is done with rollers. Compared with BERETA, the line produced 1800 lateral panels per day; the time between two parts is 20 seconds. Like in the case of BERETA line and here is produced a range of doors and the upper part of cabinet from

0.4 sheet metal, with a production of 4800 parts per day.

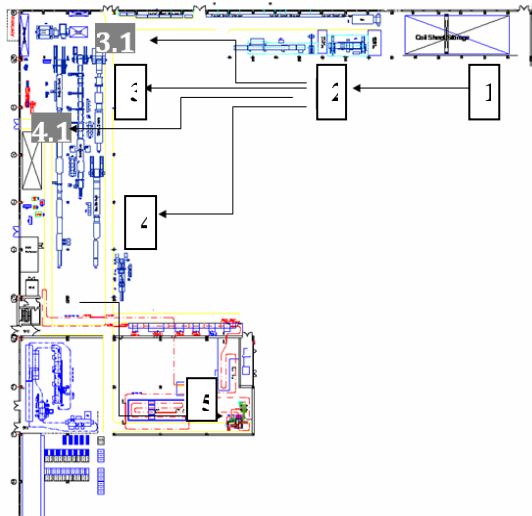


Fig. 4. Flow sheet metal processing

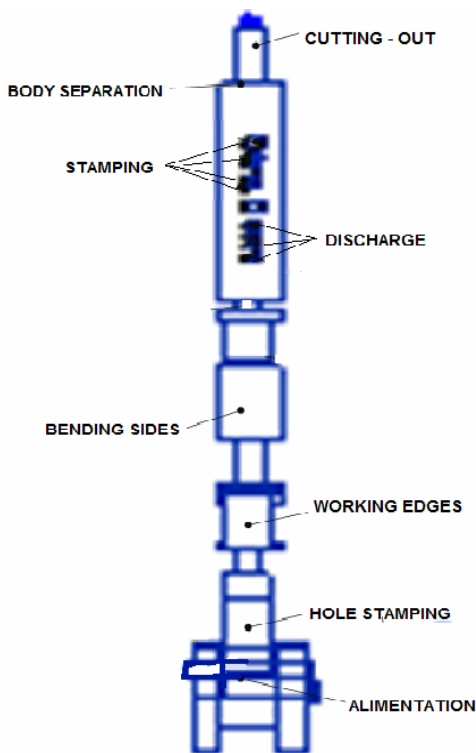


Fig. 5. Layout and manufacturing flow

1. Sheet metal rolls warehouse;
2. GABELLA line;
3. OLMA processing line doors;
- 3.1. BERETTA processing line doors;
4. Processing line OLMA lateral panels
- 4.1. Processing line BERETTA
5. Electrostatic painting plant WAGNER / LEC

## 6. NEW DESIGN CHANGES

The request was to realize the new model GRAM/AMICA. For this it was necessary to modify the active parts of bending die display from existing OLMA line, according to the new design of door.

To process OLMA door, cupping is done by means of cutting bending die.

This process is necessary to achieve a cutting on the cabinet door surface for positioning the electronic display that shows the working parameters of the cooling device, respectively, the temperature in freezer and cooler.

Cutting and cupping for display door is performed through some dies by bending die.

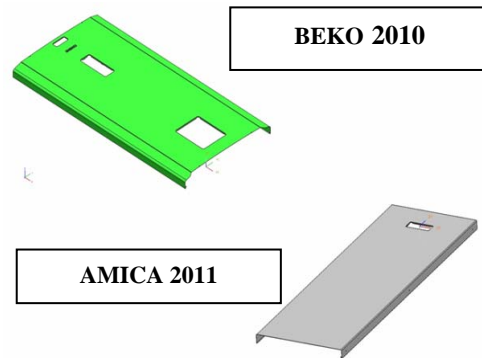


Fig. 6. The new design of door

The request for change was proposed of the department Tools Manufacturing and Design Department to be designed and executed, according to the procedure of execution tools. Following the design of new bending die, the clamping system and other elements have not been modified.

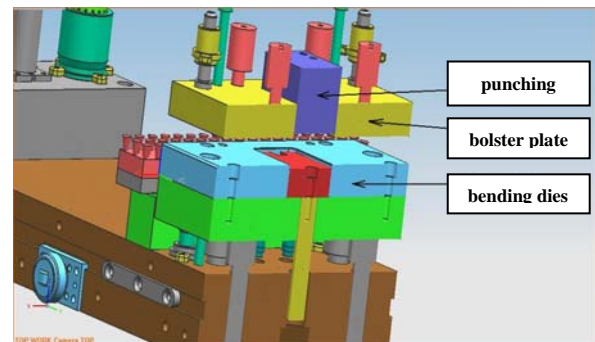


Fig. 7. Cutting die changes



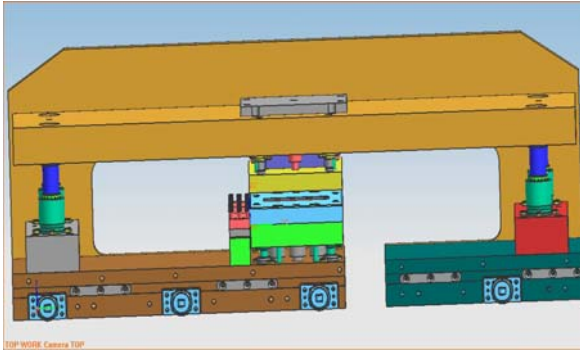


Fig. 8. Cutting die

The only changes that were made to give the new shape of display are: punching, bolster plate and bending dies. To execute correctly the modified parts and to avoid trouble in assembling the new die was taken into account the some necessary data that are listed in the tables below.

MATERIAL THICKNESS (mm)	MANUFACTURING TOLERANCE (mm)	
	T <sub>pl</sub>	T <sub>p</sub>
0.3	0.015	0.010
0.5	0.020	0.010
0.8	0.020	0.012
1.0	0.025	0.015
1.5	0.030	0.020
2.0	0.040	0.020
2.5	0.050	0.030
3.0	0.060	0.030
4.0	0.080	0.040
5.0	0.100	0.050
6.0	0.120	0.060
8.0	0.160	0.080
10.0	0.200	0.100
12.0	0.240	0.120

Table 1. Tolerances in execute punching and active plates

### 6.1. Conditions that must be fulfilled by cutting die

Produce the piece by cold plastic deformation consist of transforming the initial shape of the black piece in a geometric shape corresponding to the proposed design configuration

Cutting die are complex tools, which often perform one operation or one type of piece in a certain range of production [6].

Designing cutting die involves generally to satisfy certain conditions, as follows:

- High accuracy of the machined parts;
- Cost as low as possible;

- Execution as easy is possible in a time as low;

- High reliability in operation.

Establishing the optimal technological process requires fulfillment of all conditions mentioned earlier depending on the size and production volume proposed.

In conclusion, optimal selection of constructive solutions is related to the series of manufacture which will be determined depending on the type of technological process.

In the work piece machining by cold plastic deformation it is taken into account the production time depending on the number of parts and tool waiting time between two or more uses.

Adapting cutting die to the new conditions created by modifying the geometric shape or degree of complexity of a piece is achieved by reassembling the appropriate elements imposed by the geometrical shape of the active parties.

The degree of complexity of a cutting die depends of the size and configuration parts as well the shape of the blank.

Their rigidity is not affected by the system assembly and fixation of various elements because they are provided with safety systems against disassembling.

In this way is ensured a appropriate stability of exploitation conditions of cutting die with modular elements required by the parts manufacturing process. The use of modular tools is recommended when the pieces have high dimensional and shape variations and production knows a continuous fluctuation due to the assimilation of new products or modernization of production.

In the design phase of active elements it started from the size of bolster plate and punching, taking into account the fundamental sketch of the tool.

After performing calculations of strength are determinate the conditions to assembly the elements.

Execution of final dimensions of the active elements is closely in line with the overall tool.

## 6.2. Principles of designing cutting and forming die

Designing cutting dies is based on shape and size of workpieces, being in close contact with the production volume required.

When designing punches and dies should had assured technical conditions referring to manufacturing parts precision, possibility of easily realise the all components parts or the adaptation of technological forms, high productivity, low cost, durability and high reliability in operation.

In terms of functional mode the active parts, punching and bolster plate, must have the following conditions:

- To ensure proper positioning of the punching in relation to the active area of the bolster plate;
- The construction of the two elements must be rigid and to provide stability in operation;
- To allow the adoption of reciprocal positioning and fixing the active elements, according to the conditions imposed by the scheme of cutting the workpiece
- To allow large possibilities to assemble on the supports of punching and bolster plate elements for positioning, for stop, driving and fixing of the workpiece;
- To create favorable conditions for removing the waste material from the blanking and the elimination of this or of the piece trough bolster plate of the cutting die;
- The fits that are between body-punch and the bore of the bolster plate and punching shall be provided with processing possibilities of tolerances;
- Dimensions of the support for bolster plate and punchings have to be chosen so as to allow active elements assembly which included cross-section in a range of values determined by the group dimensions of the parts belonging to a geometric families;
- The supports of bolster plate and punching must provide opportunities for quick installation and disassembling of active elements and their own weight have to be reduced.

## 7. CONCLUSION

Given the new aesthetic design data for a refrigerator we will expose all the transformation processes of raw materials starting from delivery to the end of manufacturing process. Renewing product design influence some devices of line production, but not the factory layouts because a new one can be expensive and cause disruption as it is installed.

The layout consists of blocks for different departments and areas. The plan it is used as a guide to show precisely where everything goes. We will see in the same time that manufacturing process is similar to a chain composed of interconnected and well defined cells. The problem that designers must solve in this case is to redesign an existing product to satisfy the new market requirements.

## 11. REFERENCES

- [1] Procesul de Productie si Organizarea lui [WWW] <http://www.svedu.ro/curs/ei/c8.html>(17.02.2012);
- [2] Dumitru M, *Design Industrial, Designul Formei*, Bren, Bucuresti, 2009;
- [3] Geiskopf F., Goepf V., Kiefer F., Caillaud E., *A problem driven approach to interface manufacturing strategy analysis and manufacturing system design*, Computers & Industrial Engineering, 2009, 355–367; vol 57
- [4] Ertas A., *Prevention through design: Transdisciplinary Process*, Transdisciplinary Journal of Engineering and Science. Vol. 1, No: 1, pp. 30-48; 2010
- [5] Engineering Design Process <http://iisme.org/etp/HS%20Engineering-%20Engineering.pdf> (24.02.2012);
- [6] Constantin D., Ionel G., Gheorghe B., Militaru C., Visan A., Popescu C., *Stante si matrite din elemente modulate*, Ed. Tehnica, Bucuresti, 1980.

## PROJECTING ELASTOMERIC SHOCK ABSORBERS WITH MOVING SIDE STOP

Gonca, V.; Shvab, J.; & Noskov, S.

**Abstract:** *In the design of Vibration isolator it is often necessary to ensure a reduction (or increase) of the value of frequency  $\eta_r$ , that requires the ability to calculate the stiffness characteristics of elastomeric Vibration isolator in the low finite and medium finite deformations. A similar problem arises in the design and calculation of equiprevent rubber-metal compensating devices, which find application in various fields of engineering and construction industries, effectively replacing the hydro- pneumatic - spring compensating devices, working under axial stress-strain. In this case, the stiffness characteristic of "force – settlement"  $P = P(\Delta)$ , even for small finite deformations, will be non-linear (or piecewise linear). In this title proposed a method for determination of rigidity dependence "Force - Settlement" for shock-absorbing elements with absolutely rigid moving (parallel to the vertical axis  $z$ ) vertical side stops being under pressure, and it is taken into account low compressibility of material of rubber layers. Received solutions can be used to find the dependence „force - settlement” of cylindrical shock absorbers, as well as in projecting such shock absorbers.*

**Keywords:** *rubber, shock-absorber, weak compressibility, side stops, stiffnes.*

### 1. INTRODUCTION

To reduce the harmfulness of vibrations in engineering structures are widely used rubber-metal vibration isolators of different geometry, with unquestionable advantages<sup>[2]</sup> compared to vibration isolators made from other materials. In the theory of isolation of vibrations attenuation coefficient transfers power from the source of vibration through the vibration isolators on the base is introduced for the frequency  $\eta > 2^{0.5} \eta_r$ , where  $\eta_r$  – mass's resonance frequency of vibration source<sup>[1]</sup>:

$$\eta_r = \frac{(c/M)^{0.5}}{2\pi} \quad (1)$$

where:  $c$  - stiffness of vibration isolator;  $M$  - mass of vibrating mechanism.

The main task in the design of elements of vibration isolator is to provide basic reduction of the resonance frequency below  $\eta_r$  frequency range of vibroactive disturbing forces. At the same time static and dynamic displacements of vibration source do not shall to exceed the permissible values.

For below resonance modes:

$$\eta_r = \frac{(g/\Delta_0)^{0.5}}{2\pi} \quad (2)$$

where:  $g$  - acceleration of gravity;  
 $\Delta_0$  – static settlement of the elastic elements of vibration isolator, if we assume that the stiffness of vibration isolator does not depends on the frequency and the load value.

From (2) yields, that only for small deformations increase of permissible settlement  $/\Delta_0/$  decreases the fundamental

frequency  $\eta_r$  (since there is a linear relationship for the rigidity characteristics of the "force - settlement") of elastomeric isolator<sup>[1,3]</sup>. For large deformations stiffening dependence "force - settlement" of elastomeric vibration isolator has significantly non-linear behavior of the hard type<sup>[4]</sup> and from (2) yields, that frequency  $\eta_r$  can grow again. For elastomeric vibration isolators minimum attainable frequency  $\eta_r$ , depending on the physical and mechanical properties of elastomeric material, is<sup>[2]</sup>: 8 Hz - for unreinforced elastomers, 5 Hz - for rubber-metal elements working under compression, 3 Hz - for rubber-metal elements working under a shift loading. In the design of Vibration isolators is often necessary to ensure a reduction (or increase) of the value of frequency  $\eta_r$ , that requires the ability to calculate the stiffness characteristics of elastomeric Vibration isolator in the low finite and medium finite deformations. A similar problem arises in the design and calculation of equiproportional rubber-metal compensating devices, which find application in various fields of engineering and construction industries. In this case, the stiffness characteristic of "force - settlement"  $P = P(\Delta)$ , even for small finite deformations, will be non-linear (or piecewise linear). To solve this problem for the function  $P = P(\Delta)$ , in the general case, it is necessary to design shock absorber that ensures the condition:

$$\frac{dP(\Delta)}{d\Delta} \cdot \frac{1}{P(\Delta)} = f(P(\Delta)) \quad (3)$$

For the special case  $f(P(\Delta)) = \text{const} = C$ , then from equation (3) we obtain the solution for  $P(\Delta)$ :

$$P(\Delta) = B \cdot \exp(C \cdot \Delta) \quad (4)$$

The constant of integration B is determined from additional conditions. For example, if shock absorber is multi-layered, an additional condition can be minimization of weight of elastomeric material, providing the required initial settlement  $\Delta_0$  of shock absorber. In this case, from (4):

$$B = P(\Delta_0) \cdot \exp(-C \cdot \Delta_0) \quad (5)$$

and to write down the shock absorber stiffness characteristics  $P(\Delta)$ :

$$P(\Delta) = P(\Delta_0) \cdot \exp[C(\Delta - \Delta_0)] \quad (6)$$

will provide the desired balance between rigidity and the level of shock absorber loading.

If constant  $C = \rho^2/g$  (where:  $\rho$  - the natural frequency of equipment that is equipped with the projected shock absorber;  $g$  - acceleration of gravity), equation (6) describes the stiffness characteristics  $P(\Delta)$ , which provides a description of equiproportional characteristic of compensative shock absorber. It can be several design solutions. In<sup>[1, 4]</sup> for one of the features (cylindrical shock absorbers with fixed absolutely rigid side stops) the technique of calculation of such shocks absorbers is described.

## 2. PROBLEM DESCRIPTION

In this paper we propose a design of shock absorber with rigid side boards, which can move parallel to the direction of the applied compressing force. Since due to lateral movement of stops changes free surface of elastomeric layer in a shock absorber, the stiffness of shock absorber changes. In contrast to the shock absorbers with fixed side stops (fixed stops help to implement only the increase of stiffness in the process of loading), the moving side stops make it possible to increase or decrease stiffness (from initial stiffness) in the process of loading. Stiffness of shock absorber can vary from the hard shock (free lateral surface of the elastomeric layer of shock absorber is zero, the precipitation is only due to the weak compressibility of the elastomer) to the stiffness of the shock absorber with no side stops (height of the free elastomeric layer of a shock absorber is the height of the elastomeric layer). Then it can be three cases of moving of side supports.

In the first case, the side stops are moving at the time when the shock absorber is not loaded (fig.1).

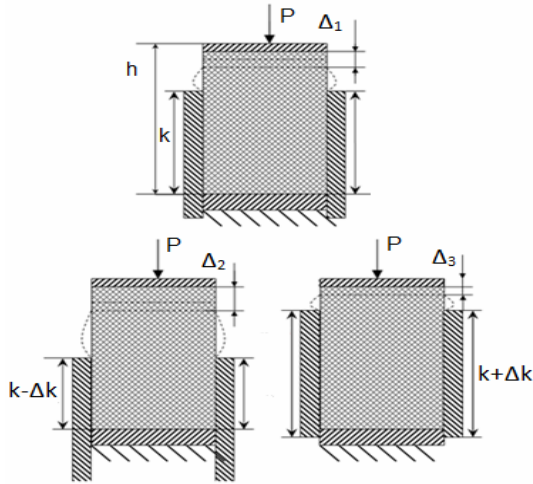


Fig. 1. Shock absorber with moving side stops

In this case we obtain a linear stiffness characteristic “force-settlement” (fig. 2).

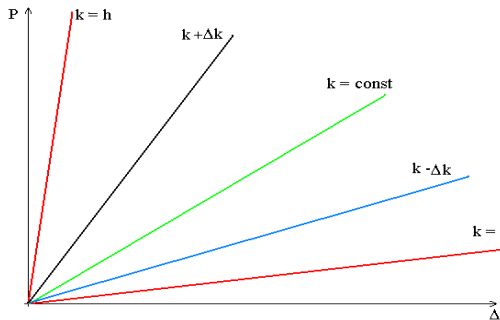


Fig. 2. Dependence “force – settlement” for shock absorber with moving side stops. First case.

In the second case side stops are moving step by step depending on the loading of the shock absorber (fig. 3).

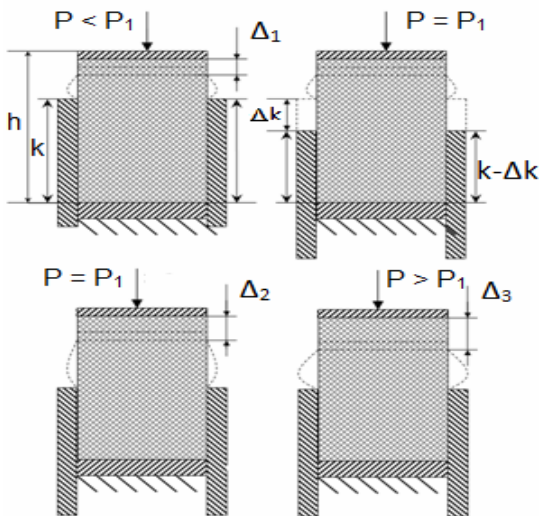


Fig. 3. Shock absorber with moving side stops. Side stops moving “step by step”.

In this case, a piecewise nonlinear stiffness characteristics “force-settlement” (fig.4) “jumps” along the axis of settlement corresponding to the change of height of the side stops in time. At this point force is constant, but by decreasing the free surface of the elastomeric layer settlement increases.

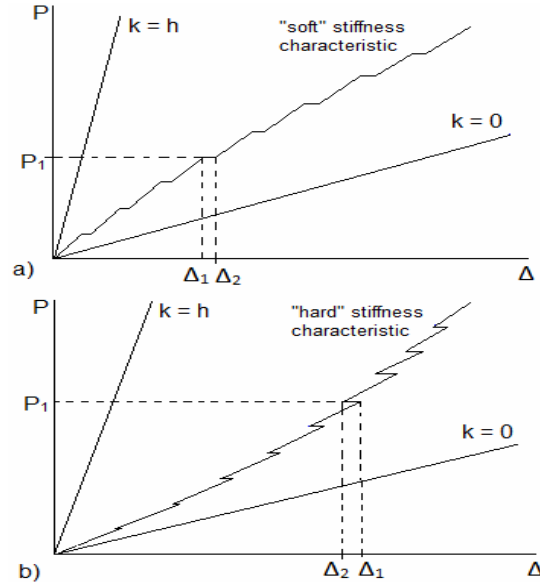


Fig.4. Dependence “force – settlement” for shock absorber with moving side stops. Second case, (a) – “soft” stiffness characteristic, (b) – “hard” stiffness characteristic

In third case, the height of the side stops does not change continuously, depending on the load (fig. 5)

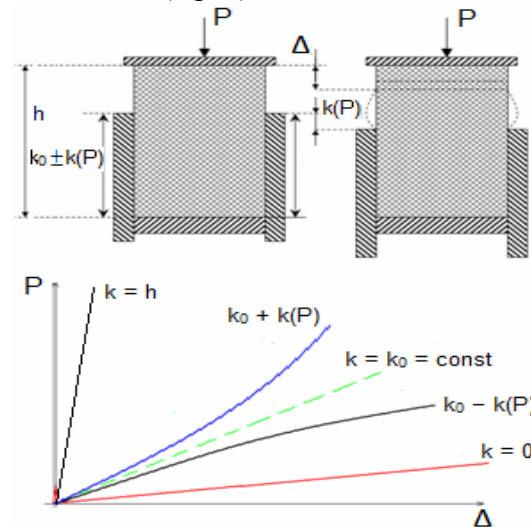


Fig.5 Dependence “force – settlement” for shock absorber with moving side stops. Third case.

### 3. SOLUTION

To obtain the analytic dependence of P ( $\Delta$ ) "force-settlement" for small finite strains (up to 10% - 15%) shock absorber divided into two parts: Part I ( $(h - k(P)) \leq z \leq h$ ), we have an axisymmetric compression. In Part II ( $0 \leq z \leq (h - k(P))$ ) volume compression. The solution we obtain taking into account the weak compressibility of the elastomer.

For the first part of shock absorber the dependence of the "force - settlement" P( $\Delta$ ) in the light of weak compressibility of rubber, we find using the principle of minimum total potential energy of deformation  $U(u_1, w_1)$  [1,2]:

$$U(u_1, w_1) = J(u_1, w_1) - P\Delta_1 \quad (7)$$

where:

$$J = 2\pi G \int_{\frac{h}{2}}^{\frac{h}{2}} \int_0^b \left[ \left( \frac{\partial u}{\partial r} \right)^2 + \left( \frac{u}{r} \right)^2 + \left( \frac{\partial w}{\partial r} \right)^2 + \frac{1}{2} \left( \left( \frac{\partial u}{\partial z} \right) + \left( \frac{\partial w}{\partial r} \right) \right)^2 + \frac{3\mu}{1+\mu} s \left( \left( \frac{\partial u}{\partial r} \right) + \frac{u}{r} + \left( \frac{\partial w}{\partial z} \right) - \frac{9\mu(1-2\mu)}{4(1+\mu)^2} s^2 \right) r dr dz \quad (8)$$

Where: G - is modulus of rigidity,  $\mu$  - is Poisson's ratio.

Choosing the displacement functions  $u_1(r, z)$ ,  $w_1(r, z)$ , respectively, along the axes r and z:

$$u_1 = A_1 r \left(1 - \frac{z}{h}\right) \left(1 - \frac{z}{h^*}\right), \quad h^* = h - k(P)$$

$$w_1 = -\frac{3\Delta_1}{2h^* \left(1 + 2\frac{h}{h^*}\right)} \left(z - \frac{z^2(h+h^*)}{hh^*}\right) + \frac{z^3}{3hh^*} - \frac{4h^{*2}}{3h} \quad (9)$$

that satisfy the geometric boundary conditions:

$$\begin{aligned} u_1(r, h) &= 0, & u_1(r, h-k(P)) &= 0 \\ w_1(r, h) &= -\Delta_1, & & \\ w_1(r, h-k(P)) &= 0 & & \end{aligned} \quad (10)$$

From the principle of minimizing the functional  $U(u_1, w_1)$  the dependence of the "force - settlement" P( $\Delta_1$ ):

$$\Delta_1 = \frac{P \cdot (h - k(P))}{\pi b^2 G} \left[ 1.8 + \frac{1.2 + 1.5\alpha^2}{\left(1 + 3\frac{1-2\mu}{2\mu}\alpha^2\right)} \right]^{-1}, \quad \alpha = b/(h - k(P)) \quad (11)$$

For the second part of the shock absorber, assuming that the mobility of the side constraint is absolutely rigid, the dependence of the force - of sediment P ( $\Delta_{II}$ ), without taking into account the frictional forces on the contact surface elastomer - metal, defined as in the case volumetric compression [1]:

$$\Delta_{II} = \frac{3Ph}{2\pi b^2 G} \cdot \frac{(1-2\mu)}{(1+\mu)} \quad (12)$$

For all the shock absorber dependence "force - settlement" P ( $\Delta$ ), with (9) and (10) takes the form:

$$\Delta = \Delta_1 + \Delta_{II} \quad (13)$$

When using the dependences (9) - (13), note that they are obtained for small finite deformations, when:

$$0 \leq \Delta_1 / (h - k(P)) \leq 0,1 \div 0,15 \quad (14)$$

The thickness of a free (without side boards) elastomeric layer  $h_0$  ( $P = 0$ ) in the process of loading can vary:

$$0 \leq h_0(P=0) = h - k(P=0) \leq h \quad (15)$$

Based on the requirements of exploitation the shock absorber can vary the thickness of the elastomeric layer is free depending on the size of loading, or can be given any requirement to change the stiffness characteristics of the shock absorber. For the two algorithms condition of smallness of final deformation must be satisfied (11). The most simple to constructing dependence of "force - settlement", If you specify the intervals for changing the load P and the thickness of the free layer of elastomeric shock absorber. In this case,

the algorithm for constructing the function  $P(\Delta)$  will be the following. Let the interval values of the compressive of force  $P$  is split into  $N$  (not necessarily equal) intervals and set requirements for the change in the thickness of the free elastomeric layer, that is a function  $k(P)$  for each interval of the force  $P$ . For  $i$ -th interval:

$$P_{i-1} \leq P_i \leq P_{i-1} + P_i^* \quad (16)$$

Where:  $P_i^*$ - step of force  $P$  (if these steps are the same,  $P_i^* = P / N$ )

The thickness of the free (without side boards) elastomeric layer to the  $i$ -th interval of loading takes values:

$$\begin{aligned} h_{i-1}(P = P_{i-1}) \leq h(P = P_i) = h(P = P_{i-1}) \\ - k(P = P_i) \leq h \end{aligned} \quad (17)$$

The total settlement  $\Delta_{\Sigma i}$  shock absorber on the  $i$ -th step of loading is given by:

$$\begin{aligned} \Delta_{\Sigma i} = \Delta_{\Sigma(i-1)} + (\Delta_I (h_0 - k_i(P_i), P_i^*) + \\ \Delta_{II} (k_i(P_i), P_i^*)) \end{aligned} \quad (18)$$

where the values of  $\Delta_I ((h_0 - k_i(P_i), P_i^*))$  and  $\Delta_{II} (k_i(P_i), P_i^*)$  calculated by formulas (11) and (12) and substituting the values of the required thickness of the free elastomeric layer is at each stage of loading. From (8) - (14) that if  $k(P = P_i)$  is negative, the thickness of the elastomeric layer is free to grow and shock absorber stiffness will decrease, that is dependence of the force - settlement be precipitate a "soft" type. For positive values of  $k(P = P_i)$  elastomeric layer thickness of free will decrease and damping increases, that is dependence of the force - settlement be precipitate a "hard" type.

## 4. EXPERIMENT

### 4.1 Description

As an example, consider a step change in stiffness of the shock absorber. Parameters of the shock absorber:  $b = 18$  mm,  $h = 40$  mm,  $\mu = 0.493$ ,  $G = 5.2 \cdot 10^5$  N/m<sup>2</sup>.

A cylindrical rubber shock absorber loaded

with an axial compressive force and the height of the side stop has changed "step by step", step size is 6.5 mm. The experiment was performed on the test machine Zwick/Roell Z150.

### 4.2 Experimental Results

The results obtained in the experiment are shown in Table 1.

Force, N	k, mm	Stiffness, N/mm
0 - 20	0	39.24
20 - 40	6.5	46.46
40 - 60	13	56.65
60 - 80	19.5	70.22
80 - 100	26	101.76
100 - 120	32.5	152.72
120 - 140	37	332.40

Table 1. The dependence of the stiffness of rubber shock absorber on the height of the side stops. The experimental results.

### 4.3 Analytical Solution

The analytical solution consider using formula (13). The calculation was made using "MathCad" software. We have two analytical solutions. In first solution (solution "a") rubber is considered as weakly compressible material. Results are shown in Table 2.

Force, N	k, mm	Stiffness, N/mm
0 - 20	0	39.41
20 - 40	6.5	46.67
40 - 60	13	57.23
60 - 80	19.5	71.19
80 - 100	26	103.46
100 - 120	32.5	154.8
120 - 140	37	338.05

Table 2. The dependence of the stiffness of rubber shock absorber on the height of the side stops. Analytical solution "a".

In second analytical solution (solution "b"), rubber is considered as non - compressible material and in formula (13) we use Poisson's ratio  $\mu = 0.5$ . Results are shown in Table 3.

Force, N	k, mm	Stiffness, N/mm
----------	-------	-----------------



0 - 20	0	39.43
20 - 40	6.5	47.09
40 - 60	13	58.43
60 - 80	19.5	76.96
80 - 100	26	112.69
100 - 120	32.5	210.36
120 - 140	37	529.91

Table 3. The dependence of the stiffness of rubber shock absorber on the height of the side stops. Analytical solution “b”.

#### 4.4 Comparison of Results

Force, N	Error $\epsilon$ , % (solution “a”)	Error $\epsilon$ , % (solution “b”)
0 - 20	0.43	0.48
20 - 40	0.45	1.36
40 - 60	1.02	3.14
60 - 80	1.38	9.60
80 - 100	1.67	10.74
100 - 120	1.36	37.74
120 - 140	1.70	59.42

Table 4. Comparison of both obtained results - experimental and analytical.

Then we compare the results obtained analytically with the results obtained during the experiment and calculate the error. Results are shown in Table 4.

#### 5. CONCLUSION

In this title proposed a method for determination of rigidity dependence "Force - Settlement" for shock-absorbing elements with absolutely rigid moving (parallel to the vertical axis z) vertical side stops being under pressure. It's also taken into account low compressibility of material of rubber layers. Received solutions can be used to find the dependence „force - settlement” for cylindrical shock absorbers, as well as in projecting such shock absorbers. You can design a shock absorber with a given non-linear („hard” or „soft”) stiffness characteristics. As an example, considered the technique of constructing a rubber shock absorber with variable stiffness (the first example of a “soft” stiffness, the second with “hard” stiffness). The height of the side stops depends on the applied force, and changes “step by step”. As can

be seen from a comparison of the results (Table 4.) neglecting the weak compressibility of rubber leads to a large error when the thickness of rubber decreases.

#### 7. ACKNOWLEDGMENTS

This work has been supported by the European Social Fund within the Project Nr.

2009/0201/1DP/1.1.1.2.0/09/APIA/VIAA/112 “Nanotechnological research of the mechanical element surface and internal structure in mechanical engineering”.

This work has been supported by the European Social Fund within the project «Support for the implementation of doctoral studies at Riga Technical University».

#### 8. REFERENCES

- [1] Lavendel E.E. *Calculation of rubber products*. Машиностроение, Moscow, 1976.
- [2] Lyapunov V.T., Lavendel E.E., Schlyapochnikov S.A. *Rubber vibration isolators*. L., Судостроение, 1988.
- [3] Lavendel E.E., Dymnikov S.I., Pavlovskis A.A., Sniegs M.I. *Applied methods of calculating the product of highly elastic materials*. Zinatne, Riga, 1980.
- [4] Gonca V., Švabs J. *Projecting Elastomeric Shock Absorbers with Variable Stiffness* In Journal of Vibroengineering. - Vol.12, Issue 3. (2010) pp 347-354.

#### 6. ADDITIONAL DATA ABOUT AUTHORS

V. Gonca, J. Shvab, S. Noskov;  
Riga Technical University, Ezermalas 6,  
LV-1006, Riga, Latvia  
e-mails: Vladimirs.Gonca@rtu.lv,  
Jurijs.Svabs@rtu.lv,  
Stanislavs.Noskovs@rtu.lv  
Phone: +371-67089473



## CABLE TRUSS ANALYSES FOR PRESTRESSED SUSPENSION BRIDGE

Goremikins, V.; Rocens, K. & Serdjuks, D.

**Abstract:** *At the present moment a suspension bridge is the most suitable type for very long-span bridges. Increased deformability is one of the basic disadvantages of suspension bridges. Usage of prestressed suspension bridge with cable truss is a method of fixing the problem of increased deformability. A prestressed suspension bridge with cable truss with the cross web and span of 200 m was considered as an object of investigations. It was shown, that usage of cable truss for prestressed suspension bridge allows reducing the vertical displacements up to 16% in comparison with the single cable. Applying of structure with four stabilization cables instead of structure with two stabilization cables allow to reduce difference of displacements in transverse direction by 24%.*

*Key words: long span bridge, physical model, kinematic displacements.*

### 1. INTRODUCTION

At the present moment a suspension bridge is the most suitable type for very long-span bridges [1]. So long spans can be achieved because main load carrying cables are subjected to tension and distribution of normal stresses are close to uniform [2].

Increased deformability is one of the basic disadvantages of suspension bridges [3]. Increased deformability is conditioned by appearance of elastic and non-straining (kinematic) displacements. The elastic displacements are caused by large tensile inner forces. Kinematic displacements are caused by initial parabolic shape change, resulting from non-symmetrical or local

loads [4]. Serviceability limit state is dominating for suspension cable structures. The problem of increased kinematic displacements can be solved by increasing the relation of dead weight to imposed load, which is achieved by adding of cantledge [5]. But this method causes the increase of material consumption.

Usage of prestressed cable truss is another method of fixing the problem of shape change under the action of unsymmetrical load [6 – 9]. Usage of prestressed cable truss allows the development of bridges without stiffness girder, but overall bridge rigidity will be ensured by prestressing of stabilization cable [10]. The deck can be made of light composite materials.

Smaller displacements can be achieved if we replace a single cable with a cable truss with a cross web, in case of non-symmetrical load (Fig.1) [11].

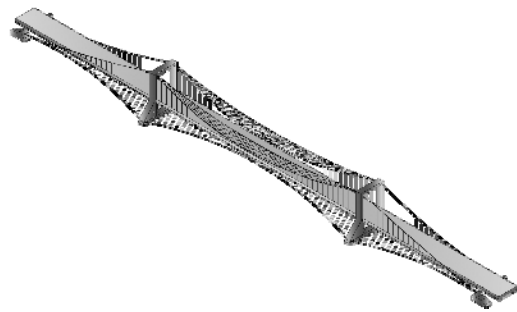


Fig. 1. Prestressed suspension bridge with cable truss load carrying structure

The other problem of suspension bridges is non-uniform displacements, in the case when the load is applied to the half of suspension bridge in transversal direction. The problem can be fixed by the rational placement of stabilization cables [12].

A prestressed suspension bridge with span

of 200 m was considered as an object of investigations.

The aim of this study is to develop rational structure of cable truss for prestressed suspension bridge when load is applied to half of span and to compare it with the single cable. Achieved results should be checked on the physical models. Rational placement of stabilization cables also should be obtained.

## 2. APPROACH TO THE SOLUTION OF THE PROBLEM

### 2.1. Design model

The prestressed suspension bridge with span of 200 m was chosen as an object of investigations. Bridge pylon height is equal to 21 m. Bridge has two lines in each direction and two pedestrian lines. Bridge main load caring structure is made from cable trusses. Deck is connected to cables by suspensions and is made from pultrusion composite trussed beam with step 5 m, pultrusion composite beams with height 300 cm and step 1 m and composite pultrusion plank with height 40 mm [13-15]. The bridge is characterized with reduced dead weight of the deck in comparison with existing structures [16]. It was assumed that deck do not have stiffness in longitudinal direction. The bridge is loaded by the load model LM:1 (according to Eurocode 1) [17].

Design scheme of investigation object is shown on the Fig. 2.

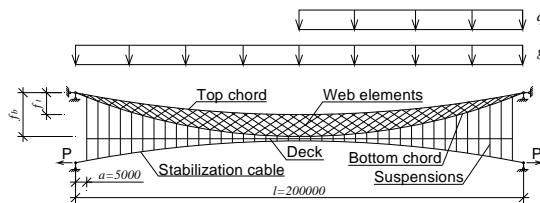


Fig.2. Design scheme of cable truss.  $q$  – imposed load;  $g$  – dead load;  $f_b$  – bottom chord camber,  $f_t$  – top chord camber.

The structural material is pretensioned steel rope [18, 19] with modulus of elasticity 167000 MPa and rope grade 1960 MPa.

The dead load, applied to the structure is 51.1kN/m, imposed load is 82.2 kN/m. The load is applied to the deck.

### 2.2. Design method

The vertical displacement under the action of load applied to half of span was considered as criteria of rationality of cable truss structure. Rational structure of cable truss is defined by rational relation of top and bottom chord cambers, rational slope of web elements, rational number of web elements inclined to the center of cable truss, rational distribution of material consumption among bottom cord, top chord and web elements.

The slope of each web element is expressed by the distance from the pylon to the connection of web element with the top chord. The distance from the pylon to the connection of web element with the top chord for any web element can be expressed by dependency depending on the distance from the pylon to the connection of the same element with bottom chord (Fig. 3).

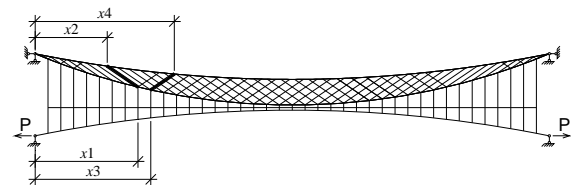


Fig. 3. Position of web elements.  $x_2$  and  $x_4$  – distance from the pylon to the connection of web element and top cord;  $x_1$  and  $x_3$  – distance from the pylon to the connection of web element and bottom cord

Rational characteristics of cable truss was found by enumeration of possible variants [20] using cycles in the FEM software ANSYS 12 environment. Enumeration was realized in three steps, at each step finding optimal field, then increasing precision by 10 times and finding new optimal field. Cable truss is modelled by two node link type compression less finite elements (LINK10 in ANSYS). The analysis type is geometrically nonlinear static including large deflection effects, because suspension

cable structures are characterized with large deflections before stabilization.

### 3. RATIONAL STRUCTURE OF CABLE TRUSS

Rational characteristics of cable truss for prestressed suspension bridge, when load is applied to half of span, were found. Rational relation of top chord camber and bottom chord camber:  $f_t/f_b=0.71$ . Rational relation of bottom chord material consumption and material consumption of whole truss:  $g_b/g=0.6$ . Rational relation of web elements material consumption and material consumption of whole truss:  $g_w/g=0.05$ . Rational number of web elements inclined to the center of cable truss is achieved removing element from 5 to 11 from both sides.

Rational slope of web elements inclined to the edges of cable truss is expressed by rational value of distance  $x_2$  of each web element depending on the distance  $x_1$  and is expressed in the form of polynomial equation (1).

$$x_2 = -6.783 \cdot 10^{-4} \cdot x_1^2 + 0.8182 \cdot x_1 - 2.108, \quad (1)$$

Position of web elements inclined to the center of cable truss was founded by mirroring elements inclined to the edges of cable truss.

### 4. COMPARISON OF CABLE TRUSS WITH SINGLE CABLE FOR PRESTRESSED SUSPENSION BRIDGE

The vertical displacements when the load is applied to half of span for suspension bridge with cable truss are by 49% smaller than displacements when load is applied for full span, so the case of half span loading is more important for suspension bridges. The vertical displacements of suspension bridge with cable truss and single cable were compared. Shape of displacements in non-symmetrical loading case is shown on the Fig. 4. Total

displacements are calculated as sum of upwards and downwards displacements. The displacements of prestressed suspension bridge in case if load is applied to half of span are shown in Table 1. The difference between displacements upwards of prestressed suspension bridge with single cable and cable truss is 34%, the difference between displacements downwards is 8% and difference between total displacements is 16%.



Fig. 4. Shape of displacements when load is applied to half of span

Structure type	Displacement direction		Total, m
	Downwards, m	Upwards, m	
Single cable	0.6684	0.3039	0.9723
Cable truss	0.6157	0.1995	0.8152

Table 1. Displacements of prestressed suspension bridge with single cable and cable truss when load is applied to half of span

### 5. EVALUATION OF RATIONAL POSITION OF STABILIZATION CABLES.

The difference of displacements of left and right side of the bridge, when only half of bridge is loaded in transversal direction, is equal to 0.3565 m, or 1/51 of bridge span in transversal direction, or slope  $1.12^\circ$  for considered bridge.

Different variants of stabilization cable placement and connection with the deck were analyzed, such as structure with one chord and diagonal suspensions, two chords and vertical and diagonal crossing suspensions, with inclined and crossing suspensions, with three chords and vertical suspensions, with three chords and inclined and crossing suspensions and with four

chords and inclined and crossing suspensions. The material consumption of suspensions was constant in all variants. The analyses were done analytically using FEM program LIRA 9.6. Only transversal scheme was analyzed to simplify calculations. Elements of structure were modeled with geometrically nonlinear arbitrary 3D bar (cable) finite element (FE310 in LIRA). It was assumed, that the material of the deck is steel with dimensions 20 x 10 cm and modulus of elasticity 206000 MPa. The suspensions are made from steel cables with diameter 3 cm and modulus of elasticity 167000 MPa. The load is applied only to one side of the deck and is equal to 283 kN. The construction is initially prestressed. The design scheme is shown on Fig. 5 (a). Rational from the point of view of displacements are structure with four bottom chords and inclined and crossing suspensions (Fig. 5 (b)).

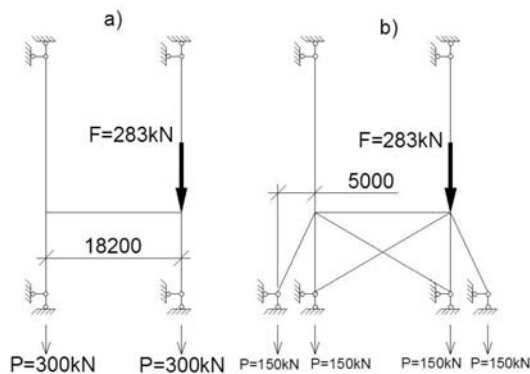


Fig. 5. Design scheme of the bridge in transversal direction. (a)- structure with two bottom chords and vertical suspensions; (b) – structure with four bottom chords and inclined and crossing suspensions

Applying of structure with four bottom chords and inclined and crossing suspensions instead of structure with two bottom chords and vertical suspensions for transversal construction of suspension bridge allow to reduce difference of displacements in transverse direction by 24 % or by 0.085 m.

## 6. PHYSICAL MODEL TESTING

Two small scale physical models of prestressed suspension bridge were constructed to confirm advantages of the cable truss in comparison with the single cable from the point of view of vertical displacements minimization.

The span of the models is equal to 2.1 m. Top chord camber is equal to 22 centimeters. The deck is connected to main load carrying structure by suspensions in 15 points (Fig. 6).

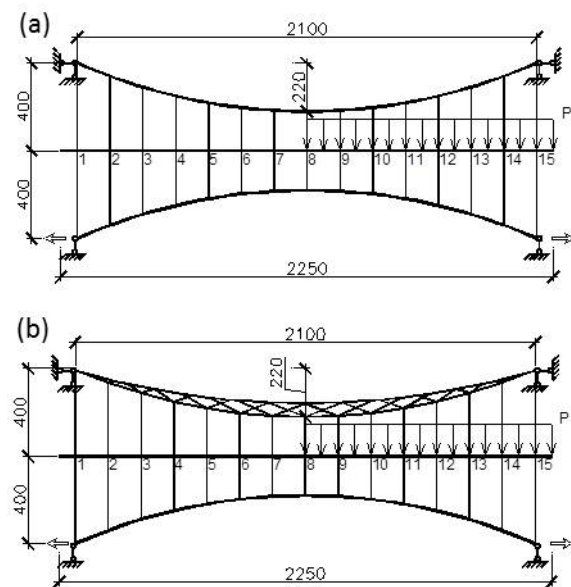


Fig. 6. Schemes of the physical models of prestressed suspension bridges. (a) – scheme of the model with single cable; (b) – scheme of the model with cable truss

The elements of the physical models are made from steel cables. Two types of cables are used: 6x7+WSC (wire steel core) and 6x19+WSC. Tensile strength of wires for both cables is 1770 MPa. The modulus of elasticity was experimentally obtained and is 60000 MPa. The diameter of single cable and stabilization cable is 10 mm and 8 mm, respectively. The diameter of bottom chord, top chord and wed elements of cable truss is 8 mm, 5.5 mm and 2 mm, respectively. The diameters of elements are specially selected to produce the same material consumption single cable and cable truss physical models.

The prestressing was organized in stabilization cable and is equal to 348 MPa. The load was applied to half of models span. The models were loaded up to load 1495 kg with step 155 kg. The displacements of physical models when load is applied to half of span are shown in Table 2.

Structure type	Displacement direction		Total, mm
	Downwards, mm	Upwards, mm	
Single cable	23.81	13.83	37.64
Cable truss	21.04	11.61	32.65

Table 2. Displacements of physical models of prestressed suspension bridge with single cable and cable truss when load is applied to half of span

The experimental results shown, that replacing single cable with cable truss with cross web allows to decrease vertical displacements of prestressed suspension bridge model upwards by 16% and downwards by 12%. Total displacements can be reduced by 13%.

## 7. CONCLUSIONS

Rational structure of the cable truss for prestressed suspension bridge with span 200 m was developed. The vertical displacement was considered as criteria of rationality of cable truss structure. Rational relation of top chord camber and bottom chord camber is equal to 0.71, rational relation of bottom chord material consumption and material consumption of whole truss is equal to 0.6 and rational relation of web elements material consumption and material consumption of whole truss is equal to 0.05. It was stated, that usage of cable truss with the cross web for prestressed cable truss instead of single cable allows to reduce vertical displacements upwards by 34%, downwards by 8% and total displacements

by 16% in the case when load is applied to half of span.

The results were verified on the small scale physical models of prestressed suspension bridges with single cable and cable truss. Model testing results indicate, that usage of cable truss with the cross web for prestressed suspension bridge instead of single cable allows to reduce vertical displacements upwards by 16%, downwards by 12% and total displacements by 13% in case when load is applied to half of span.

Applying of structure with four bottom chords and inclined and crossing suspensions instead of structure with two bottom chords and vertical suspensions for transversal construction of suspension bridge allow to reduce difference of displacements in transverse direction by 24% in case when only half of bridge is loaded.

## 8. ACKNOWLEDGMENTS

This work has been supported by the European Social Fund within the project "Support for the implementation of doctoral studies at Riga Technical University".

## 9. REFERENCES

1. Chen, W.F., Duan, L. *Bridge Engineering Handbook*. CRC Press LLC, New York, 2000.
2. Juozapaitis, A., Idnurm, S., Kaklauskas, G., Idnurm, J., Gribniak V. Non-linear analysis of suspension bridges with flexible and rigid cables. *Journal of Civil Engineering and Management*, 2010, **16(1)**, 149-154.
3. Walther, R., Houriet, B., Isler, W., Moia, P., Klein, J.F. *Cable Stayed Bridges*. Second edition. Thomas Telford, London, 1999.
4. Juozapaitis, A., Norkus, A. Displacement analysis of asymmetrically loaded cable. *Journal of Civil Engineering and Management*, 2004, **10(4)**, 277-284.

5. Strasky, J. *Stress Ribbon and Cable Supported Pedestrian Bridge*. Thomas Telford Publishing, London, 2005.
6. Serdjuks, D., Rocens, K. Decrease the Displacements of a Composite Saddle-Shaped Cable Roof. *Mechanics of Composite Materials*, 2004, **40(5)**, 675-684.
7. Mihajlov, V. *Prestressed Combined and Cable Structures*. ACB, Moscow, 2002 (in Russian).
8. Tibert, G. 1999. *Numerical Analyses of Cable Roof Structures*. KTH TS-Hogskoletryckeriet, Stockholm, 1999.
9. Kachurin, V., Bragin, A., Erunov, B. *Design of suspension and cable stayed bridges*. Transport, Moscow, 1971 (in Russian).
10. Kirsanov, M. *Suspension Structures with Increased Stiffness*. Strojizdat, Moscow, 1973.
11. Goremikins, V., Rocens, K., Serdjuks, D. Rational Structure of Cable Truss. *World Academy of Science, Engineering and Technology. Special Journal Issues*, 2011, **0076**, 571-578.
12. Goremikins, V., Rocens, K., Serdjuks, D. Cable truss analysis for suspension bridge. *Proc. of Engineering for Rural Development*, 2012 (accepted paper).
13. Goremikins, V., Serdjuks, D. Rational Structure of Trussed Beam. *Proc. of the 10th International Conference "Modern Building Materials, Structures and Techniques" Vilnius, Lithuania*, 2010, 613–618.
14. Goremikins, V., Rocens, K., Serdjuks, D. Rational Large Span Structure of Composite Pultrusion Trussed Beam. *Scientific Journal of RTU. 2. series., Construction Science*, 2010, **11**, 26-31.
15. Goremikins, V., Rocens, K., Serdjuks, D. Rational Structure of Composite Trussed Beam. *Proc. of the 16th International Conference "Mechanics of Composite Materials" Riga, Latvia*, 2010, 75.
16. Bahtin, S., Ovchinnikov, I., Inamov, R. *Suspension and Cable Stayed Bridges*. Saratov State Technical University, Saratov, 1999.
17. *Eurocode 1: Actions on structures. Part 2: Traffic loads on bridges*. Brussels, 2004.
18. *Eurocode 3: Design of steel structures. Part 1-11: Design of structures with tensile components*. Brussels, 2007.
19. Feyrer, K. *Wire Ropes*. Springer-Verlag Berlin Heidelberg, Berlin, 2007.
20. Sliseris, J., Rocens, K. Rational structure of panel with curved plywood ribs. *Proc. of "International Conference on Building Science and Engineering", Venice, Italy*, 2011, **0076**, 317-323.

## 10. ADDITIONAL DATA ABOUT AUTHORS

**Vadims Goremikins**, Researcher, M.sc.ing., Institute of structural Engineering and reconstruction, Riga Technical University. Azenes Str.16, LV-1048, Latvia  
Phone: 00371 29231772;  
E-mail: goremikin@inbox.lv.

**Kārlis Rocēns**, Professor, Dr.Habil.sc.ing., Institute of structural Engineering and reconstruction, Riga Technical University. Azenes Str.16, LV-1048, Latvia  
E-mail: rocensk@latnet.lv .

**Dmitrijs Serdjuks**, Associated Professor, Dr.sc.ing., Institute of structural Engineering and reconstruction, Riga Technical University. Azenes Str.16, LV-1048, Latvia.  
E-mail: dmitrijs@bf.rtu.lv.

## OPTIMISING THE REGULATING SYSTEM OF SUPERCHARGED DIESEL ENGINES

Gruescu, C., A.; Vela, I.; Caramidaru, V. D.

**Abstract:** *Increasing the performances of supercharged Diesel engines and reducing their specific fuel consumption and environment pollution suppose not only the application of some efficient constructive solutions, but also the improvement of their control and adjustment, otherwise the above goals cannot be reached. The present paper forwards an original concept and several solutions related to the optimisation of the regulating system's characteristics with the PGAV governor for supercharged Diesel engines equipping diesel-electric locomotives or variable-pitch propeller ships. In this respect we presented the calculus algorithm and computer software used for the numerical simulation of the PGAV Woodward governor with the purpose of determining an optimised governor characteristic.*

*Key words: Diesel engine, Woodward governor, optimizing characteristics*

### 1. INTRODUCTION

The regulating system optimisation supposes determining the governor characteristics that should ensure the supercharged Diesel engines operation on its optimal drive characteristic  $P=f(n')$ , power depending on speed, where we obtain the engine's optimal functioning, on all speed steps, as well as the minimum specific fuel consumption.

For optimising the regulating system of supercharged Diesel engines we need to know exactly: the governor characteristic  $T=f(n)$ , the governor travel depending on speed and the fuel limiter characteristic  $T=f(p_{lim})$ , the governor travel

depending on supercharging pressure, as well as, the levers system characteristic  $R=f(T)$ , the engine injection pumps rack travel depending on the governor travel.

The practical establishment of the governor characteristic  $T=f(n)$  is essential in the optimising process of the regulating system, since the engine's propulsion characteristic, in steady state operation, depends on this characteristic.

The governor fuel limiter characteristic  $T=f(p_{lim})$  is decisive during the accelerating process of any variable-speed supercharged Diesel engine and the dynamic performances of such engines depend on this characteristic.

The characteristic  $R=f(T)$  of the levers system between governor and engine is particularly important in the optimisation process of the regulating system since through this system the main adjusting parameters are correlated.

In the adjusting system of variable-speed supercharged Diesel engine for locomotives or ships we encounter a PGAV or PGEV Woodward governor. The PGAV Woodward governors, in present-day construction, is described by a "two-slope" characteristic as seen in Fig.1 [5], still up-to-date, which generates a similar characteristic  $P=f(n')$ , power depending on speed, of the Diesel engine overlaps over the propulsion characteristic of the engine only in maximum four points, resulting thus surcharge and undercharge areas. The surcharge areas generate an incomplete combustion in the engine, resulting in the increase of the specific fuel consumption and of environment pollution as well as in the reduction of the engine life span.



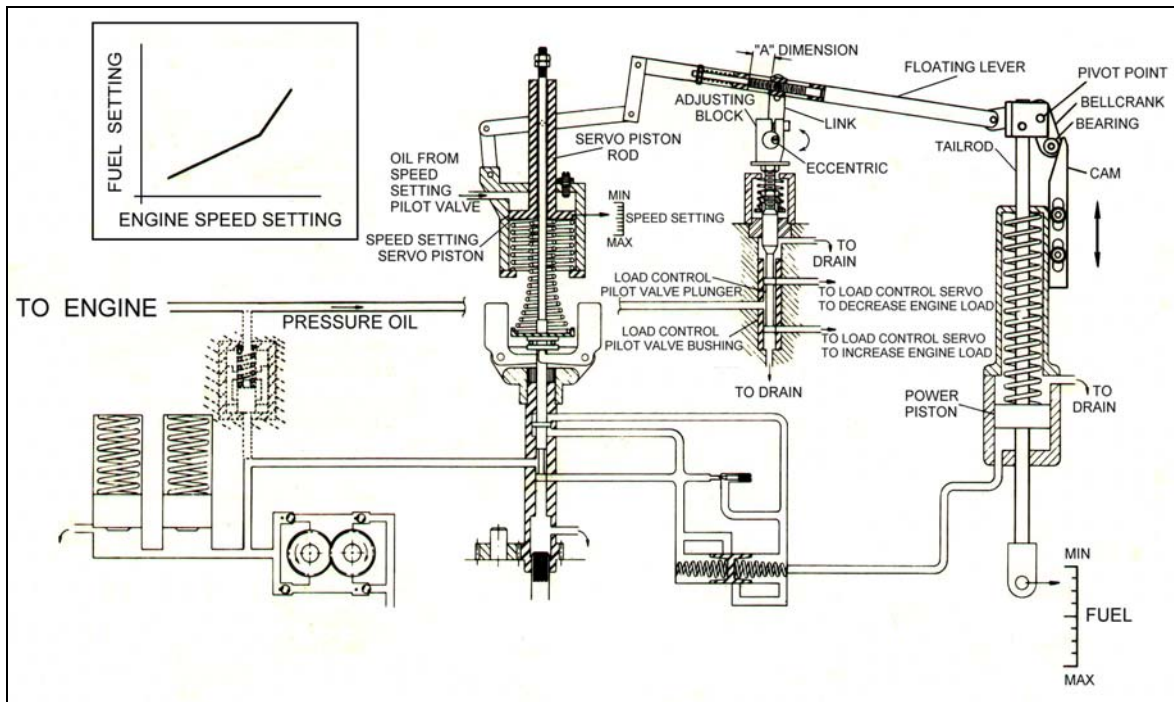


Fig.1. Schematic of PG Governor with “two-slope” Load Control

## 2. NUMERICAL SIMULATION OF THE PGAV WOODWARD GOVERNOR OPERATION

In order to improve the PGAV governor characteristic in Fig.1, schematically presented in Fig.2, the author conceived a numerical simulation computer software using the Visual Fox Pro programming language.

The aim of the numerical simulation software is to determine the cam profile from the levers mechanism of the governor (Fig.1), which decisively contributes to the reaching of the desired governor characteristic  $T=f(n)$ .

This is done by imitating, by means of mathematical relations, the actual position occupied, in balance state, by each element of the mechanism, for a chosen number of speed steps within the governor adjusting range. In this respect, when determining the calculus algorithm for the mechanism in Fig.2, we take into account the fact that the joint point A follows the movement of the servo-speed piston rod through  $S=f(n)$  relation, experimentally determined, whereas the joint point E strictly follows the movement of the power

piston tail rod (T), calculated with  $T=f(n^2)$  or  $T=f(n^3)$  relation [1], the governor travel depending on the governor speed.

The imitation of the balance operation of the mechanism in Fig.2, during simulation is performed by maintaining constant the lever  $l_3$  length and the fixed position of joint O. The joint O connects the lever  $l_3$  and the eccentric, fixed in the adjusting block of the load control pilot valve plunger (s. Fig.1).

In order to determine the calculation algorithm necessary for the elaboration of the numerical simulation software, the mechanism in Fig.2 has been transposed in a conveniently chosen system of co-ordinates.

From the ABCOA quadrilateral (Fig.2) we determine the angle  $\varphi_2$ , knowing the  $l_1$ ,  $l_2$ ,  $l_3$  and  $l_4$  lengths (from the governor construction) and partially the calculated value of  $\varphi_1$  angle.

The angle  $\varphi_2$  represents the momentary tilt of the floating lever BD, in relation to the  $Ox_r$  axis represented by the straight line  $\Delta$ .

The initial value of the  $\varphi_1$  angle, for each position of the mechanism, in the numerical simulation process is determined



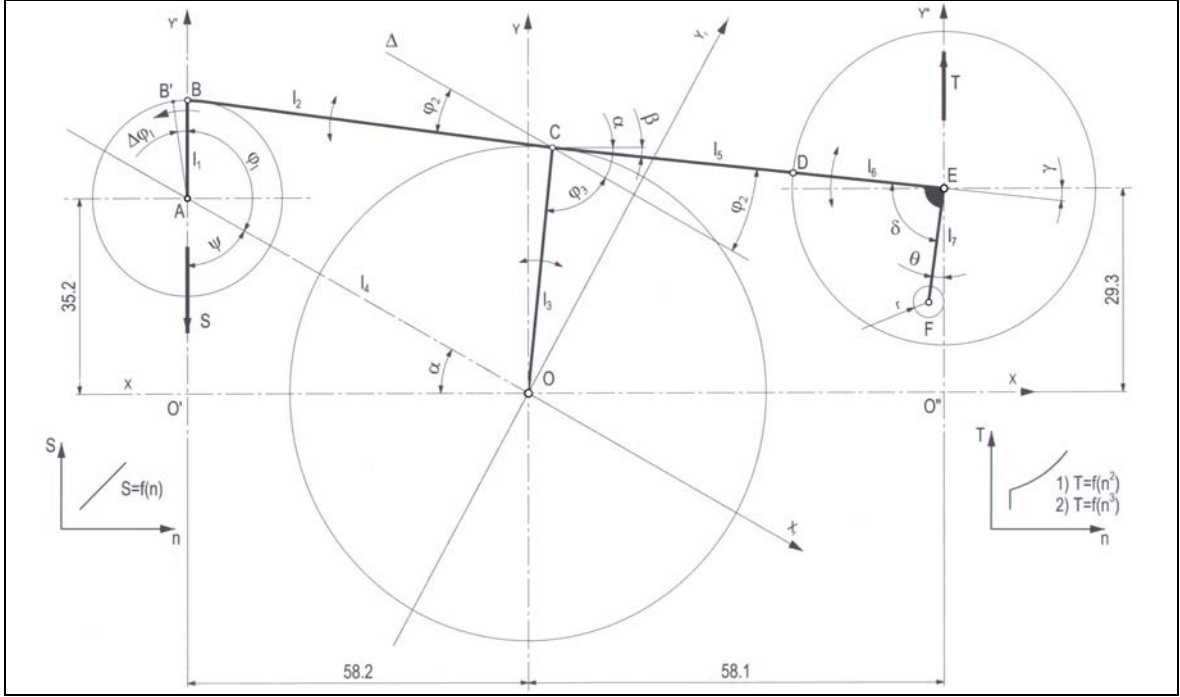


Fig. 2. Schematic of PGAV Governor levers mechanis

with the equation (1):

$$\varphi_1 = 180^\circ - \psi \quad (1)$$

The angles  $\varphi_1$ ,  $\alpha$  as well as the  $l_4$  length are determined from  $\Delta AOO'$  (Fig.2)

$$\psi = 90^\circ - \alpha \quad (2)$$

$$\alpha = \arctg \frac{O'A}{O'O} \quad (3)$$

$$l_4 = OA = \sqrt{O'A^2 + O'O^2} \quad (4)$$

$$O'A = 35,2 - S \quad (5)$$

where:  $S$  – represents the translation travel of the joint point  $A$ , performed for each speed step within the considered adjusting range, calculated with the formula deduced by the author [1].

By projecting the outline  $ABCOA$  on the axes of co-ordinates, we obtain:

$$\begin{cases} l_3 \cdot \cos \varphi_3 = l_4 + l_1 \cdot \cos \varphi_1 - l_2 \cdot \cos \varphi_2 \\ l_3 \cdot \sin \varphi_3 = l_1 \cdot \sin \varphi_1 + l_2 \cdot \sin \varphi_2 \end{cases} \quad (6)$$

We eliminate the angle  $\varphi_3$  from the equations (6) by rising to square power and addition and then by substituting:

$$\begin{aligned} a &= l_4 + l_1 \cdot \cos \varphi_1; & b &= l_1 \cdot \sin \varphi_1; \\ c &= \frac{l_3^2 - a^2 - b^2 - l_2^2}{2 \cdot a \cdot l_2}; & d &= \frac{b}{a}; \end{aligned}$$

we obtain eq. (7):

$$d \cdot \sin \varphi_2 - \cos \varphi_2 = c \quad (7)$$

Substituting in eq.(7)  $\sin^2 \varphi_2 = 1 - \cos^2 \varphi_2$ , we obtain eq.(8) with the solutions (9):

$$(1 + d^2) \cos^2 \varphi_2 + 2c \cdot \cos \varphi_2 + c^2 - d^2 = 0 \quad (8)$$

$$\varphi_2', \varphi_2'' = \arccos \frac{-c \pm \sqrt{c^2 - (1 + d^2)(c^2 - d^2)}}{1 + d^2} \quad (9)$$

We select the smaller value of the angle  $\varphi_2$ . We may determine the co-ordinates of the joint point  $B(x_B, y_B)$ , returning to the  $xO'y$  system of co-ordinates axes as follows:

$$\begin{cases} x_B = 0 \\ y_B = (35,2 - S) + l_1 \end{cases} \quad (10)$$

We intersect the straight line eq.(12), crossing the joint point  $B$ , with the tilt  $\beta$  eq.(11), with the circle eq.(13) having the center in  $E$  and the radius  $l_6$ :

$$\beta = \alpha - \varphi_2 \quad (11)$$

$$y_D - y_B = -tg\beta \cdot (x_D - x_B); \quad -tg\beta = m \quad (12)$$

$$(x_D - x_E)^2 + (y_D - y_E)^2 = l_6^2 \quad (13)$$

where:  $y_E = 29,3 + T$

and  $T$  – represents the governor tail rod travel corresponding to each speed step.

From the intersection of the straight line eq.(12) with the circle eq.(13) there results the eq.(14):

$$p \cdot x_D^2 - q \cdot x_D + rr = 0 \quad (14) \quad \text{where:}$$

$$\begin{cases} p = 1 + m^2 \\ q = 2(x_E + m \cdot y_B + m^2 x_B - m \cdot y_E) \\ rr = y_B^2 + x_E^2 + 2 \cdot m \cdot x_B y_B + m^2 x_B^2 \\ - 2 \cdot y_E y_B - 2 \cdot m \cdot y_E x_B + y_E^2 - \ell_6^2 \\ dd = q^2 - 4 \cdot p \cdot rr \end{cases}$$

with the solutions (15)

$$x_D' = \frac{q + \sqrt{dd}}{2 \cdot p} ; \quad x_D'' = \frac{q - \sqrt{dd}}{2 \cdot p} \quad (15)$$

We select the smaller value of the abscissa  $x_D$ . The ordinate  $y_D$  is determined by the condition that the distance between joints B and D be equal with  $\ell_2 + \ell_5 = BD$ :

$$y_D = y_B + \sqrt{(\ell_2 + \ell_5)^2 - (x_D - x_B)^2} \quad (16)$$

Practically we start from the initial value of the angle  $\varphi_1$ , determined with the equation (1), adding for each step a calculated  $\Delta\varphi_1$  angle and then we resume calculation from the equation (1), in which the angle  $\varphi_1$  becomes  $(\varphi_1 + \Delta\varphi_1)$ , as far as the equation (16). The return to the  $xO'y'$  system of co-ordinates is made with the equations (17):

$$\begin{cases} x_B = -\ell_1 \cdot \sin \Delta\varphi_1 \\ y_B = 35,2 - S + \ell_1 \cdot \cos \Delta\varphi_1 \end{cases} \quad (17)$$

where  $\Delta\varphi_1$  represents the angle obtained with the help of the numerical simulation, which correspond to the condition imposed

by equation(16). Knowing the co-ordinates of joints D( $x_D, y_D$ ) and E( $x_E, y_E$ ), we determine the tilt  $\gamma$  of straight line DE ( $\ell_6$ ) in respect to the O''x axis, with the eq.(18):

$$\gamma = \arctg \frac{y_E - y_D}{x_E - x_D} \quad (18)$$

The angle  $\delta$  is known, and thus the tilt  $\theta$  of the straight line EF, in respect to O''y'' axis of the  $xO''y''$  system will be:

$$\theta = |\delta - (90^\circ - \gamma)| \quad (19)$$

With the calculated values of the  $\theta$  angle we calculate the co-ordinates of joint F( $x_F, y_F$ ) which represents the pivot point of the bellcrank DEF roller  $r$ :

$$\begin{cases} x_F = x_E + \ell_7 \cdot \sin \theta \\ y_F = y_E - \ell_7 \cdot \cos \theta \end{cases} \quad (20)$$

The numerical simulation software calculate and display, for each speed step („N” in Tab.1), S(Sx)-travel, T(Tx)-travel and the co-ordinates of the bellcrank D,E,F joints (XD,YD,YE,XF and YF in Tab.1),  $X_E = ct.$  (s. Fig.2). The results are synthetized in Table 1.

The co-ordinates of point F( $X_F, Y_F$ ) (s. Table 1) were used to process the cam profile on a numerical control machine and also for the graphic plotting of the cam profile, the objective aimed by the computer numerical simulation.

Table. 1

Step	Sx	Tx	XD	YD	YE	XF	YF	N
1	2.24	3.65	92.68	37.20	32.95	116.96	20.27	361.60
2	2.24	6.31	92.67	39.83	35.61	116.94	22.93	361.60
3	3.56	7.02	92.68	40.55	36.32	116.94	23.63	406.80
4	4.88	7.81	92.37	39.96	37.11	116.92	24.42	452.00
5	6.20	8.68	92.37	39.80	37.98	116.94	25.30	497.20
6	7.51	9.64	92.32	39.87	38.94	117.41	26.29	542.40
7	8.83	10.68	92.30	39.94	39.98	117.92	27.38	587.60
8	10.15	11.80	92.32	40.04	41.10	118.46	28.58	632.80
9	11.47	13.01	92.40	40.14	42.31	119.03	29.90	678.00
10	12.79	14.29	92.53	40.27	43.59	119.63	31.34	723.20
11	14.11	15.67	92.73	40.43	44.97	120.25	32.90	768.40
12	15.43	17.12	93.01	40.64	46.42	120.89	34.58	813.60
13	16.74	18.66	93.37	40.88	47.96	121.55	36.39	858.80
14	18.06	20.28	93.81	41.21	49.58	122.20	38.33	904.00
15	19.38	21.99	94.34	41.59	51.29	122.85	40.41	949.20
16	20.70	23.77	94.99	42.04	53.07	123.52	42.62	994.40

### 3. CHARACTERISTICS OPTIMISING

#### 3.1 The Governor Characteristic

Using the simulation software in a concrete application we determine the cam profile which can generate a governor characteristic of second square grade  $T=f(n^2)$ , compatible with a propeller curve  $P=f(n^{3.3})$  of the engine.

The cam profile generated through numerical simulation is plotted in Fig.3 by a continuous line along with the cam profile in the existing solution, drawn by the dot-dash line tilted at  $74^\circ$ .

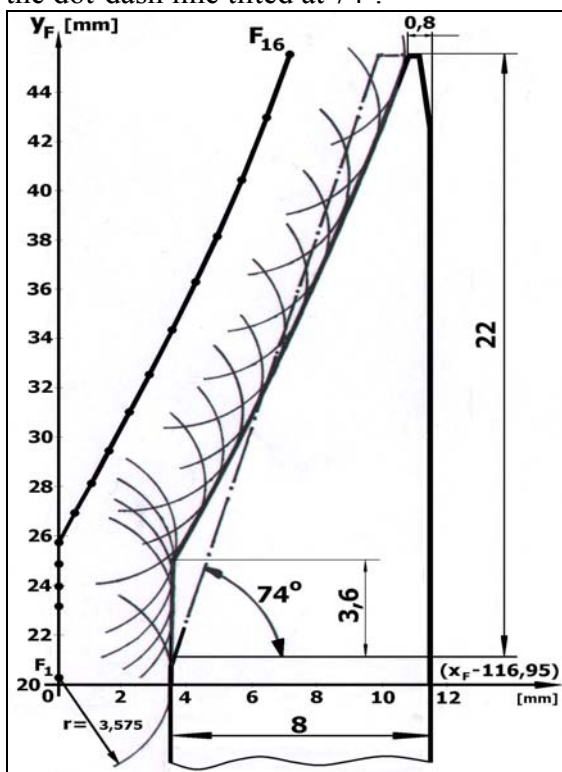


Fig.3. Cam profile

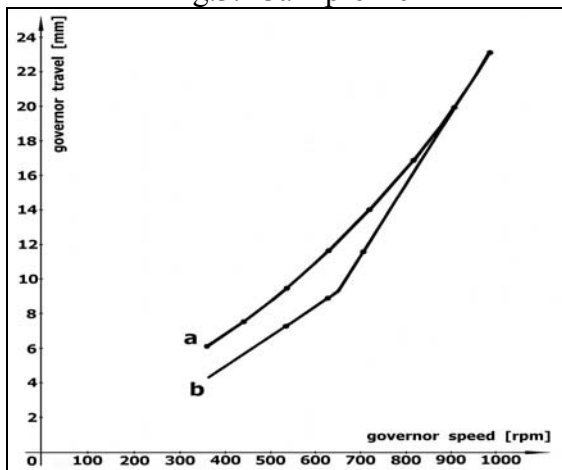


Fig.4. Governor characteristics

Fig.4 shows the plotting of the correspondent characteristics obtained: a – the optimised governor characteristic reached by simulation; b – the governor characteristic in the existing cam solution [4]. Thus, theoretically, the engine running on the optimal characteristic is achieved, as we have reached the set goal, i.e. obtaining of the governor characteristic  $T=f(n^2)$ .

#### 3.2 The Levers System Characteristic

We must find what kind of characteristic is transmitted from governor to engine by the levers system. In this respect it is necessary to determine the characteristic of this system  $R=f(T)$  (Fig.5) for which the author forwards an original concept in the paper [3]. An accurate transmission is reached when this characteristic exhibits a straight-line shape.

For an optimal adjustment of the engine it is important to know not only the shape of this characteristic, but also the concrete values of the rack travel (R) which will be realized at the engine in correlation with the governor travel (T).

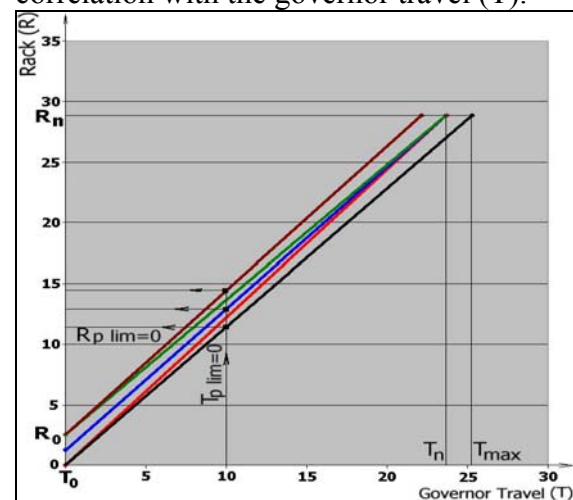


Fig.5. Typical characteristics  $R=f(T)$

From this characteristic, the system designing engineer can find if the regulating parameters adopted in the calculus are reached and, if not, he can intervene in the levers system adjustment in order to modify the characteristic, as shown in Fig.5 so that the optimal solution could be found.

### 3.3 The Fuel Limiter Characteristic

By optimising the fuel limiter characteristic, shown in Fig.6, we aim at matching this characteristic with the supercharging characteristic of the Diesel engine so that, during the accelerating process, an optimal air to fuel ratio be obtained in view of reaching a complete combustion in the engine. The travel difference, realized between the supercharging and limiting characteristics, indirectly expresses the excess fuel fed to the engine in the accelerating process.

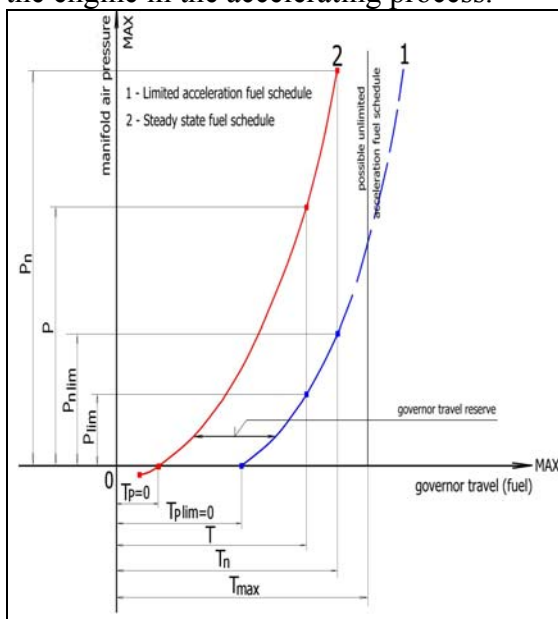


Fig.6. Typical fuel schedule curve

The amount of the “governor travel reserve” is very important since it serves to decide the duration and quality of the engine accelerating process. An excessively low “reserve” will lead to a difficulty and defective acceleration of the engine. An excessively high “reserve” will generate a delayed acceleration with smoke emission at exhaust, increased fuel consumption and pollution.

When practically realising the optimal “reserve”, an important part is played by the establishment and realization of the correlation between adjusting parameters  $R_{P_{lim=0}}$  and  $T_{P_{lim=0}}$  from the levers system characteristic  $R=f(T)$  (s. Fig.5) as well as by the establishment of an adequate value for the  $p_{n_{lim}}$  (s. Fig.6).

### 4. CONCLUSIONS

The numerical computer simulation, using the original concept forwarded in this paper, allows the determination of the optimal characteristic of the PGAV Woodward governor.

The solution obtained from the numerical simulation is applicable for all PGAV governors equipping variable-speed supercharged Diesel engines for diesel-electric locomotives or for variable-pitch propeller ships. Thus, the engine operation is assured and guaranteed on the optimal propulsion characteristic where obvious, the minimal specific fuel consumption and the smallest environment pollution are reached. Practically, the original constructive solution, presented in this paper, was successfully tested on our Woodward governor stand and on engine.

### 5. REFERENCES

- [1] Gruescu, C. A., Regulating System Calculus for Supercharged Diesel Engines of Variable Speeds, *Doctor Report*, “Eftimie Murgu” University of Resita 2011
- [2] Gruescu, C. A., Kinematic Calculus of the Governor from the Regulating System Structure of a Supercharged Diesel Engine, *Doctor Report*, “Eftimie Murgu” University of Resita, 2012.
- [3] Gruescu, C. A., Calculus of the Levers System between Governor and Engine, *Doctor Report*, “Eftimie Murgu” University of Resita, 2012.
- [4] Woodward Governor Company, Load Control Schedule, TSP 403 SH 436
- [5] Woodward Governor Company, Two-Slope Load Control for PG Governors, Bulletin 36607, 1982.

### 6. ADDITIONAL DATA

Author: Gruescu Constantin Andrei  
 “Eftimie Murgu” University of Resita  
 Piata Traian Vuia, nr.1-4, 320085 Resita  
 Romania, tel:+40255210227, www.uem.ro  
 e-mail: andy\_gruescu@yahoo.com

## THE EFFECT OF THE SHAPE PARAMETERS ON MODAL PROPERTIES OF ULTRASONIC HORN DESIGN FOR ULTRASONIC ASSISTED MACHINING

Nad, M.; Cicmancova, L.

**Abstract:** *In many machining processes, the positive effects of ultrasound are applied. Ultrasonic horn is an important element of the ultrasonic excitation system. The role of horn is the transfer of ultrasonic vibration energy from ultrasonic transducer to the tool cutting edge interacting with the workpiece (ultrasonic assisted machining-UAM). The UAM system performance depends on well-designed ultrasonic horn. The most important aspects of horn design are a horn resonant frequency, amplification factor and the determination of horn resonant wavelength - usually integer multiple of half wavelength. The effect of geometrical parameters of different horn shapes (cylindrical, tapered, exponential) on horn dynamical properties is presented in this paper. The horn modal properties are determined using finite element method (FEM) design procedures. Key words: vibration, ultrasonic assisted machining, ultrasonic horn, finite element method, modal properties*

### 1. INTRODUCTION

Ultrasonic vibrations have been harnessed with considerable benefits for a variety of industrial applications. These applications include the automotive, food preparation, medical, textile and material joining and mainly applications in manufacturing industries.

The remarkable advantages are obtained by application of ultrasonic phenomenon in field of the machining of materials. The using of the ultrasonic vibration energy provides two different approaches to machining process. The first approach is

based on application of ultrasonic transducer which is utilised indirectly to propel abrasive particles suspended in slurry at the work surface causing slow erosion. This principle of the machining is called as „ultrasonic machining (USM)“. The second approach is based on the transfer of the ultrasonic vibrations directly on the cutting tool, respectively directly to a cutting process. The second approach is known under term of „ultrasonic assisted machining (UAM)“. The advantages of this possibility, which is referred to subsequently as ultrasonic cutting/machining, are not obvious, because normally machine tool vibration has to be vigorously suppressed in the most cases [1]. The principle of UAM can be applied to different machining technologies, like a turning, grinding, boring, milling and others. The repetitive high-frequency vibro-impact mode brings some unique properties and improvements into metal cutting process [1], [2], [7], where the interaction between workpiece and the cutting tool is transformed into a micro-vibro-impact process.

In the ultrasonic machining systems, the electromechanical transducer acts as the source of mechanical oscillations, transforming the electrical power received from the generator into mechanical vibrations. The electromechanical transducers are based on the principle utilizing magnetostriction or piezoelectric effects. The electromechanical ultrasonic transducers generate the vibration with resonant frequency  $f_{res} \approx 20$  kHz and more. However, the amplitude of the resulting ultrasonic vibrations is inadequate for realization of the cutting process. To



overcome this problem, a wave-guide focusing device known as a horn (also known as concentrator or tool holder) is fitted onto the end of the transducer. The horn transfers the longitudinal ultrasonic waves from the transducer end to the toe end with attached the cutting tool. The cutting performance of ultrasonic machining equipment primarily depends on the well-taken design of the sonotrode [5]. It amplifies the input amplitude of vibrations so that at the output end the amplitude is sufficiently large to required machining process.

Positive results [3] in machining processes of hardly machinable materials (hard, soft, brittle and ductile materials) are obtained by using ultrasonic assisted machining. These positive results could not be achieved using conventional machining processes. The benefits of ultrasound applications in machining are related to a reduction in cutting forces, improved machined surface quality, reduction of tool wear and the resulting increasing his life cycle, etc.

In the present paper, a finite element method (FEM) design procedure was used to the study and to determine of modal properties of considered ultrasonic horns. The main aim of this paper is to present generally valid results leading to the geometrical design of sonotrode with effective dynamical properties.

## 2. ULTRASONIC HORN DESIGN

The ultrasonic horn is used as an element that serves to transfer of the vibration energy from the transducer towards to the tool interacting with workpiece. The principal function of the horn is to amplify the amplitude of ultrasonic vibration of the tool to the level required to the effective machining. It does so by being in resonance with the transducer. The horn design and its manufacture of require special attention. Incorrectly designed horn will impair machining performance and can lead to the destruction of the vibration system and cause considerable damage to

the generator. Generally, the horns are made of metals that have high fatigue strengths and low acoustic losses. To the most often used metals to the horn manufacturing are monel, titanium, stainless steel, heat treated steel and aluminium.

The most important aspect of horn design is a horn resonant frequency and determination of the correct horn resonant wavelength, which should be usually integer multiple of the half wavelength of the system. The resonant frequency can be determined analytically (simple geometrical shape) or numerically (complicated geometrical shape). The required performance of ultrasonic horn is assessed by an amplification factor

$$\mathfrak{G} = \left| \frac{A_2}{A_1} \right|, \quad (1)$$

where  $A_1$ , resp.  $A_2$  - amplitude of input end, resp. output end of horn. The fundamental horn design requirement is  $\mathfrak{G} > 1$ .

### 2.1 Mathematical model of vibrating horn

We suppose that a horn is made of isotropic material (Young's modulus -  $E$ , density -  $\rho$ , Poisson's ratio -  $\nu$ ).

The governing equation of longitudinally free vibrating ultrasonic horn with variable circular cross-section can be expressed in following form

$$\frac{\partial^2 u(x,t)}{\partial t^2} = \frac{c_p^2}{S(x)} \frac{\partial}{\partial x} \left[ S(x) \frac{\partial u(x,t)}{\partial x} \right] = 0, \quad (2)$$

where  $x$  - coordinate,  $u(x, t)$  - longitudinal displacement of cross-section,  $c_p = \sqrt{E/\rho}$  - velocity of the longitudinal elastic waves propagation in horn material,  $S(x) = S_0 f(x)$  - circular cross-section at coordinate  $x$ ,  $f(x)$  - function defining the cross-section change in longitudinal  $x$  direction,  $S_0$  - circular cross-section at coordinate  $x = 0$ .

Generally, the solution of equation of motion (2) can be supposed in the form

$$u(x,t) = U(x)e^{i\omega_0 t}. \quad (3)$$

The following non-dimensional quantities are introduced:

- dimensionless coordinate

$$\xi = \frac{x}{l_0}; \quad \xi \in \langle 0; 1 \rangle, \quad (4)$$

- dimensionless longitudinal displacement

$$\bar{U}(\xi) = \frac{U(\xi)}{l_0}. \quad (5)$$

After substituting (3)-(5), the equation (2) as the following form

$$\frac{1}{f(\xi)} \frac{d}{d\xi} \left[ f(\xi) \frac{d\bar{U}(\xi)}{d\xi} \right] + \beta^2 \bar{U}(\xi) = 0. \quad (6)$$

The frequency parameter  $\beta$  is defined by

$$\beta = \frac{\omega_0}{c_p} l_0, \quad (7)$$

where  $\omega_0$  - natural angular frequency,  $l_0$  - length of horn.

For the cylindrical shape of ultrasonic horn  $f(\xi) = \text{const.}$ , the equation

$$\frac{d^2 \bar{U}(\xi)}{d\xi^2} + \beta^2 \bar{U}(\xi) = 0, \quad (8)$$

has the solution in the form

$$\bar{U}(\xi) = A \cos(\beta \xi) + B \sin(\beta \xi), \quad (9)$$

The integration constants  $A$ ,  $B$  can be determined by boundary conditions [6]. The boundary conditions for free vibration of horn are supposed (free edge on both sides of the horn) [7] in the form

$$\left. \frac{d\bar{U}(\xi)}{d\xi} \right|_{\xi=0} = 0, \quad \left. \frac{d\bar{U}(\xi)}{d\xi} \right|_{\xi=1} = 0. \quad (10)$$

Introducing (9) into boundary conditions given by (10), the following modal parameters of horn vibration are determined:

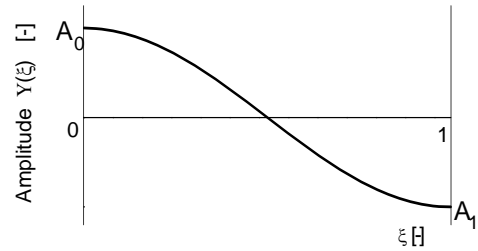
- natural frequency of the  $k^{\text{th}}$  mode shape

$$f_{0k} = \frac{k}{2l_0} \sqrt{\frac{E}{\rho}}, \quad k = 1, 2, \dots, \quad (11)$$

- wave length of the  $k^{\text{th}}$  mode shape

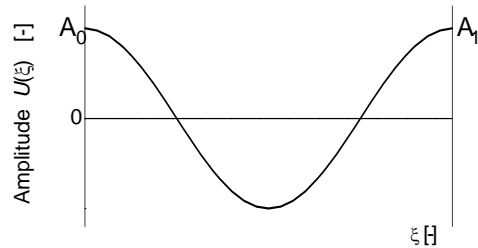
$$\lambda_k = \frac{2\pi}{\beta_k} = \frac{2}{k}, \quad k = 1, 2, \dots \quad (12)$$

To the horn shape design only two cases are used. i.e. for  $k=1$  so-called “half wave” shape and  $k=2$  “wave” shape (see Fig. 1).



$$\lambda_1 = 2, \quad f_{01} = \frac{1}{2l_0} \sqrt{\frac{E}{\rho}}, \quad \vartheta_1 = 1$$

$\lambda/2$  - „half wave” shape



$$\lambda_2 = 1, \quad f_{02} = \frac{1}{l_0} \sqrt{\frac{E}{\rho}}, \quad \vartheta_2 = 1$$

$\lambda$  - „wave” shape

Fig. 1. Modal shapes of horn vibration

The analytical calculation of the resonant length and resonant frequency for the cylindrical shape of ultrasonic horn is simply problem. To the determination of modal properties for more complicated geometrical horn shapes, the numerical simulation [4] is better to use.

## 2.2 FE modelling of horn vibration

The effects of variations in design variables on the modal properties (modal shapes, natural frequencies) in typical geometries of horns used for UAM is analysed by finite element method. The FEM modelling was done using the software package ANSYS.

The basic dynamic FEM equation of motion for free vibration of horn suitable to horn modal properties can be generally expressed as

$$\mathbf{M}\ddot{\mathbf{u}} + \mathbf{K}\mathbf{u} = \mathbf{0}, \quad (13)$$

where  $\mathbf{M}$ , resp.  $\mathbf{K}$  - mass matrix, resp. stiffness matrix,  $\ddot{\mathbf{u}}$ , resp.  $\mathbf{u}$  - vector of node acceleration, resp. node displacement.

The modal properties of horn are determined by the solution of eigenvalue problem

$$(\mathbf{K} - \omega_i^2 \mathbf{M})\boldsymbol{\phi}_i = \mathbf{0}, \quad (14)$$

where  $\boldsymbol{\phi}_i$  -  $i^{\text{th}}$  mode shape,  $\omega_i$  - natural angular frequency of  $i^{\text{th}}$  mode shape.

The horns can be manufactured in various shapes and dimensions. They are primarily of circular cross-section and the most common shapes are cylindrical, tapered and exponential (see. Table 1).

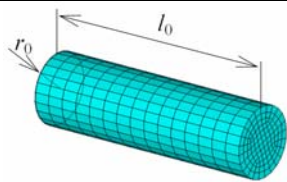
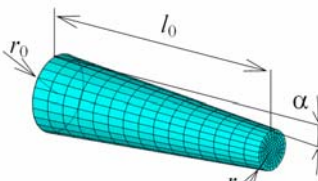
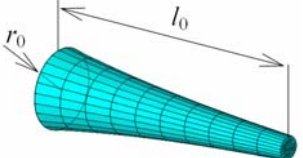
<b>Cylindrical</b>	
slenderness ratio	$\delta = 2r_0/l_0$
shape parameter	---
shape function	$f(\xi) = 1$
<b>Tapered</b>	
slenderness ratio	$\delta = 2r_0/l_0$
shape parameter	$\alpha \in \langle 0^\circ; 15^\circ \rangle$
shape function	$f(\xi) = [1 - (1 - 2\delta^{-1} \tan \alpha)\xi]^2$
<b>Tapered</b>	
slenderness ratio	$\delta = 2r_0/l_0$
shape parameter	$a \in \langle 0,1; 0,9 \rangle$
shape function	$f(\xi) = a^{2\xi}$

Table 1. Geometrical parameters of horn shapes

In the Table 1, the parameter  $r_0$  is radius of input end of horn and  $l_0$  is length of horn,  $\alpha$  is incline angle of tapered horn shape and  $a$  is exponential base function.

The finite element models of considered shapes of ultrasonic horns, which are created by ANSYS code are shown in Table 1. The type of finite element is SOLID45.

### 3. ANALYSIS AND RESULTS

The numerical simulation to determine the modal properties of considered ultrasonic horn shapes are performed. The shapes used to the horn model creation and horn parameters are shown in Table 1. The steel as a horn material is used to numerical simulation ( $E = 210$  GPa,  $\rho = 7800$  kgm<sup>-3</sup>,  $\nu = 0,3$ ).

In the following, the non-dimensional natural frequencies for different geometrical shapes of horn are defined as

$$\theta_i = \frac{f_i}{f_{0i,cyl}}, \quad (15)$$

where  $f_i$  -  $i^{\text{th}}$  natural frequency of analysed horn,  $f_{0i,cyl}$  -  $i^{\text{th}}$  natural frequency of cylindrical horn. Both frequencies are considered for the same slenderness ratio.

Then the value of resonant frequency of corresponding geometrical horn shape is determined using following equation

$$f_i = \theta_i f_{0i,cyl}. \quad (16)$$

#### Cylindrical horn shape.

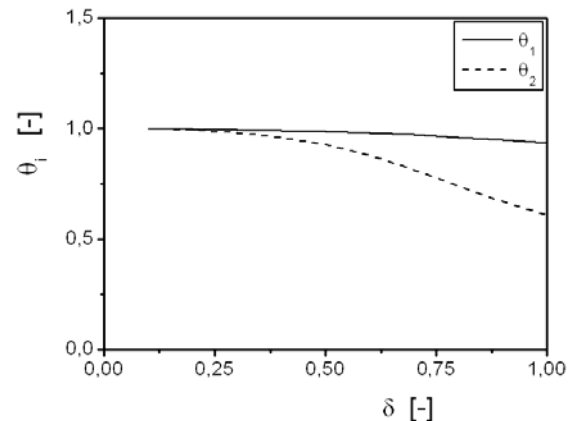


Fig. 2. Dependency of  $\theta$  vs. slenderness ratio  $\delta$  for cylindrical horn shape



**Tapered horn shape.**

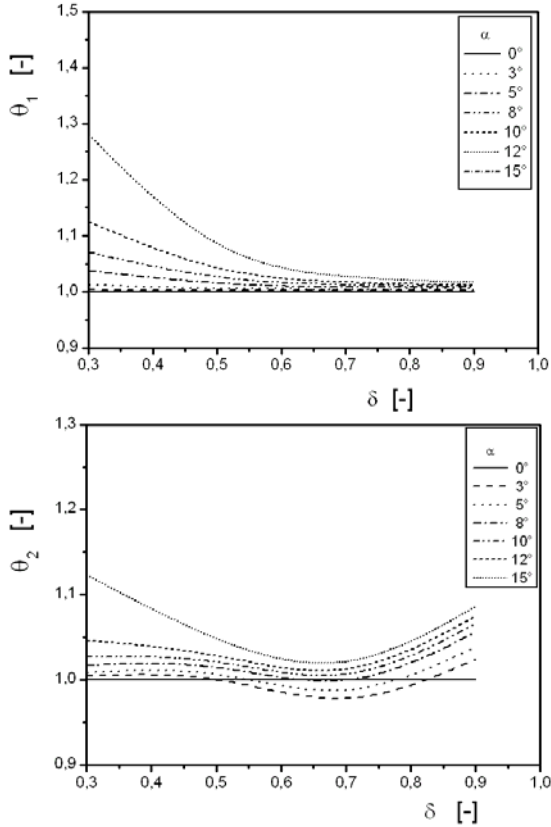


Fig. 3. Dependency of  $\theta_1$  (resp.  $\theta_2$ ) vs. slenderness for different incline angles

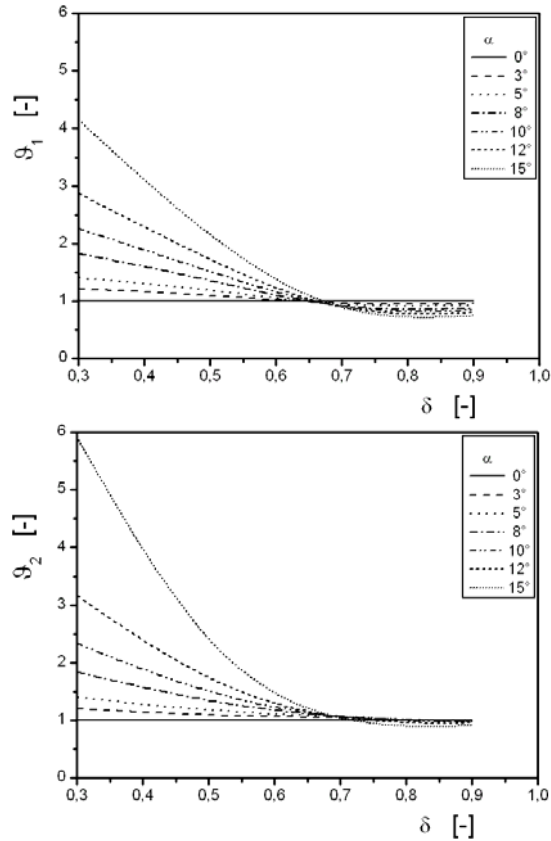


Fig. 4. Dependency of  $\vartheta_1$  (resp.  $\vartheta_2$ ) vs. slenderness for different incline angles

**Exponential horn shape.**

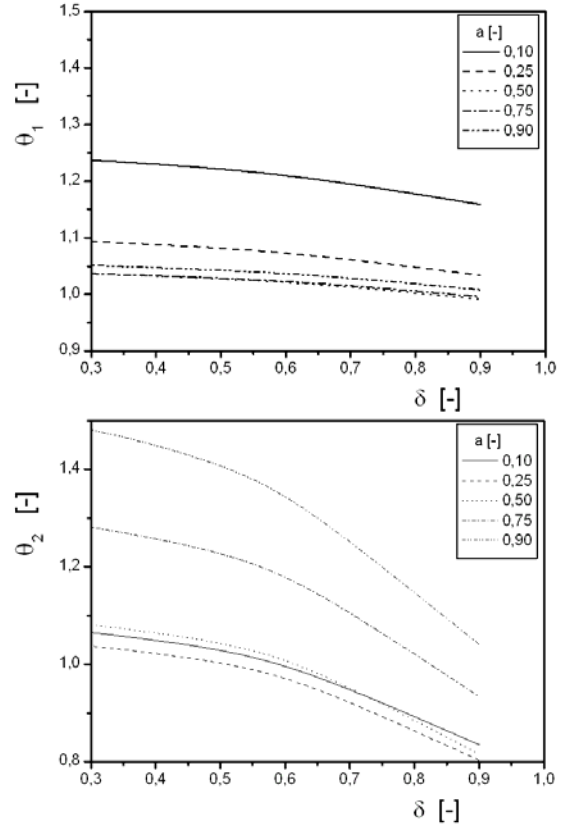


Fig. 5. Dependency of  $\theta_1$  (resp.  $\theta_2$ ) vs. slenderness for different exponential bases

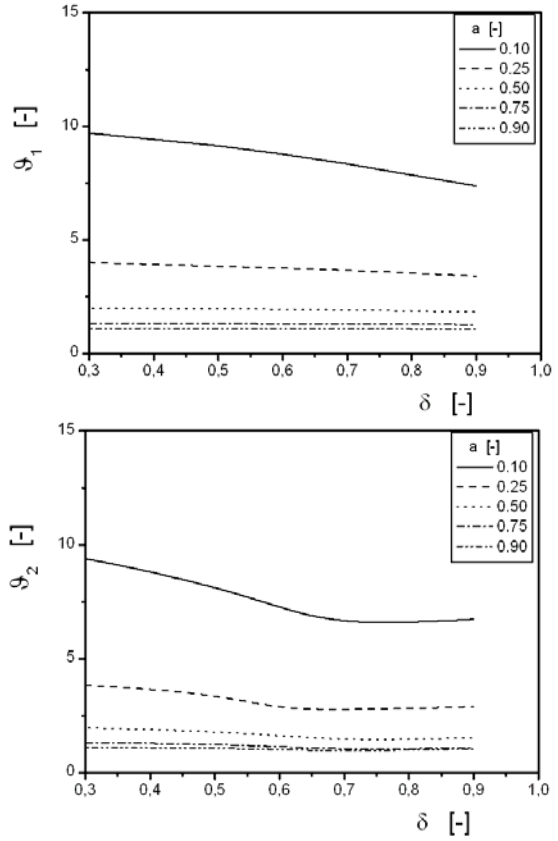


Fig. 6. Dependency of  $\vartheta_1$  (resp.  $\vartheta_2$ ) vs. slenderness for different exponential bases

#### 4. CONCLUSIONS

A general procedure for design of high-frequency ultrasonic horn for ultrasonic manufacturing technologies is presented in this paper. By use of wave theories for longitudinal vibration of rod and FEM analysis, the effect of horn geometrical shape for ultrasonic manufacturing technologies is analysed. The different geometrical horn shapes (cylindrical, tapered and exponential) were considered. The effects of horn shape parameters such as a slenderness ratio  $\delta$ , incline angle  $\alpha$ , base of exponential function  $a$  on natural frequencies had been analysed.

The results presented in this paper give the possibilities to design of ultrasonic horn with required dynamical properties. Using Eq. (16), the required value of resonant frequency is determined. Note that the fundamental requirements required for the application of considered ultrasonic horns - resonance frequency have to be more than 20 kHz and amplification factor is  $\mathfrak{g} > 1$ .

#### 5. ACKNOWLEDGEMENT

This work has been supported by VEGA grants No. 1/0389/11.

#### 6. REFERENCES

1. Astashev, V.K., Babitski, V.I. *Ultrasonic Processes and Machines-Dynamics, Control and Applications*, Springer - Verlag Berlin Heidelberg, 2007.
2. Amini, S., Soleimanimehr, H., Nategh, M.J., Abudollah, A., Sadeghi, M.H., *FEM analysis of ultrasonic-vibration-assisted turning and the vibratory tool*, Journal of Materials Processing Technology, 2008, **201**, pp. 43–47.
3. Babitsky, V.I., Kalashnikov, A.N., Meadows, A., Wijesundara, A.A.H.P. *Ultrasonically assisted turning of aviation materials*. Journal of Materials Processing Technology, 2003, **132**, 157-167.
4. Dekys, V., Saga, M., Zmindak, M. *Dynamics and Reliability of Mechanical Systems*. VTS University of Zilina, Zilina, 2004. (in slovak)
5. Nánási, T. *The effect of non-conservative load on the stability limits of compressed beams*. Acta Mechanica Slovaca, 2007, **11**, No. 4-A, 311-316. (in slovak)
6. Nánási, T. *Boundary conditions and vibration of slender beams*. In: Proc. of National Conf. with Inter. Participation - Engineering Mechanics 2007, Svratka, Czech Republic, 1-8.
7. Seah, K. H. W., Wong, Y. S., Lee, L. C. *Design of tool holders for ultrasonic machining using FEM*. Journal of Materials Processing Technology, 1993, **37**, 801-816.

#### 7. ADDITIONAL DATA ABOUT AUTHORS

Milan Nad, Assoc. Prof., PhD.  
Slovak University of Technology  
Faculty of Materials Science and Technology  
Department of Applied Mechanics UVSM  
Paulinska 16  
917 24 Trnava  
Slovak Republic  
e-mail: [milan.nad@stuba.sk](mailto:milan.nad@stuba.sk)

Lenka Cicmancova, MSc. (Eng.).  
Slovak University of Technology  
Faculty of Materials Science and Technology  
Department of Applied Mechanics UVSM  
Paulinska 16  
917 24 Trnava  
Slovak Republic  
e-mail: [lenka.cicmancova@stuba.sk](mailto:lenka.cicmancova@stuba.sk)

## EXTREME MODAL PATTERNS OF VIBRATING TWO-SPAN BEAMS

Nánási T.

**Abstract:** *Vibration confinement known in technical literature also under the term of vibration localization is a consequence of slight disorder in nominally periodic structure possibly leading to radical changes of the dynamic characteristics of structures. The ultimate effect of localization is the partial absence of vibration in some areas of the structure while in complementary parts high levels of vibration may occur. The aim of the paper is to develop efficient analytical and numerical tools enabling the clarification of those conditions which lead to substantial separation of dynamically active and passive regimes. Two-span beams of various boundary conditions have been chosen as suitable mathematical model due to its relative simplicity and assumed ability to properly represent the phenomena under the study.*

*Key words: mechanical vibration, modal confinement, mode localization, dynamical response, semi-exact solution*

### 1. INTRODUCTION

Periodic structures are widely used in industries due to their inherent advantages with respect to dynamical properties and due to the relatively easy manufacturing process. The analysis of turbomachinery bladed-disk, multi-span beams or rib-stiffened plates is simple when perfect periodicity is enforced [1-9]. However, in practice the cyclic symmetry of these structures is inevitably destroyed by random imperfections resulted from manufacturing tolerance, material irregularity or in-service damage [2-7]. Small irregularities or deviations are referred to as mistuning. Periodic struc-

tures with weak internal coupling have demonstrated high sensitivity with respect to such mistuning, which may lead to a well-known phenomenon called vibration localization or vibration confinement [10-13]. Many studies [3,7,9,12] have shown that even a small degree of mistuning can have a dramatic effect on the vibratory behavior of periodic structures. A single blade or a few blades of the mistuned structure may experience vibration response amplitudes and local stresses that are excessively high compared to those of the corresponding regular structure and as such may lead to fatigue failure or at least to undesired increase of dynamical load of the structure. [1,4,8,9]. Subsequently it has been realized, that mode confinement can be present in weak or in strong form even in case of non-periodic structures. Ideal model for the study of the phenomenon is the two-span beam, dealt with in some detail for example in papers [14-16]. Langley presented in [14] an excellent study of the phenomenon using wave approach with the main conclusions, that both the global and local modes can occur over the whole frequency range and that the localization is in every case restricted by precisely defined finite upper and lower bounds, depending only on the reflection coefficient of inter-span coupling element. However, the wave approach required to abandon the influence of evanescent waves, what is fully justified only for high frequency response. Another study [15] analysed the phenomenon using the so called characteristic graph based on wave numbers of individual spans, which gives efficient overall insight to the distribution of natural frequencies due to the extremely

useful ability to capture in single graph the spectrum of all possible configurations. In general, the results of both papers are in good agreement except for one minor detail. Among others, in sharp contradiction to results of Langley, authors of paper [15] concluded the existence of infinite localization for certain, though very specific configurations.

The aim of the presented paper is to estimate the conditions for eventual mode localization by virtue of exact analytical computation including the evanescent components, which have been fully neglected in previous studies. New results presented in this paper stem from the detailed computation of localization metrics along the curves of characteristic graph for various end configurations (pinned-pinned, clamped-clamped and simple supported-free). As an alternative to laborious numerical computation of exact coupled nonlinear equations a semi-exact computational method is proposed, which allows derive an explicit formula relating the wave numbers. This approximation is based on partial neglecting the evanescent waves and suffers from significant errors only in case of low frequencies. When approximated wave number relations are substituted to the exact frequency equations, an explicit semi-exact relation for the amplitude ratio is obtained. Our results fully confirm the conclusions of Langley [14] in the high frequency domain.

## 2. GOVERNING EQUATIONS

Let us consider two-span beam with simply supported extreme ends. The left span in coordinates ( $0 \leq x_1 \leq l_1$ ) and the right span in coordinates ( $l_1 \leq x_2 \leq l_1+l_2$ ) are coupled by rotational spring  $K_R$  (Fig. 1).

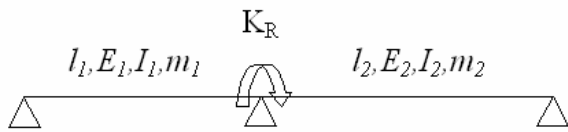


Fig. 1. Simply supported two-span beam with rotational coupling stiffness

Governing equations for bending vibration of each subsystem under Euler-Bernoulli framework are of the form

$$\begin{aligned} E_1 I_1 \frac{d^4 y_1(x_1)}{dx_1^4} - \omega^2 m_1 y_1(x_1) &= 0, \\ E_2 I_2 \frac{d^4 y_2(x_2)}{dx_2^4} - \omega^2 m_2 y_2(x_2) &= 0 \end{aligned} \quad (1)$$

Trivial boundary conditions reflect the zero displacements at  $x_1 = 0$ ,  $x_1 = l_1$ ,  $x_2 = l_1$  and  $x_2 = l_1+l_2$  as well as zero bending moments at the ultimate simple supports

$$\begin{aligned} y_1(0) = 0, \frac{d^2 y_1(0)}{dx_1^2} = 0, y_1(l_1) = 0, \\ y_2(l_2) = 0, y_2(l_1+l_2) = 0, \frac{d^2 y_2(l_1+l_2)}{dx_2^2} = 0 \end{aligned} \quad (2)$$

with  $x_l = 0$  at the left support, while the continuity conditions are of the form

$$\begin{aligned} \frac{dy_1(l_1)}{dx_1} = \frac{dy_2(l_1)}{dx_2}, \\ E_1 I_1 \frac{d^2 y_1(l_1)}{dx_1^2} - E_2 I_2 \frac{d^2 y_2(l_2)}{dx_2^2} + K_R \frac{dy_2(l_2)}{dx_2} = 0 \end{aligned} \quad (3)$$

Substitution of the general solution

$$\begin{aligned} y_i(x_i) = A_i \sin(\lambda_i x_i) + B_i \cos(\lambda_i x_i) + \\ + C_i \sinh(\lambda_i x_i) + D_i \cosh(\lambda_i x_i) \quad i = 1, 2 \end{aligned} \quad (4)$$

into boundary conditions immediately gives the relations

$$\begin{aligned} B_1 = D_1 = 0, \quad C_1 = -A_1 \sin(\lambda_1 l_1) / \sinh(\lambda_1 l_1), \\ B_2 = -A_2 \sin(\lambda_2 (l_1 + l_2)) / \cos(\lambda_2 (l_1 + l_2)), \\ C_2 = -A_2 \frac{\cosh(\lambda_2 (l_1 + l_2)) \sin(\lambda_2 l_2)}{\cos(\lambda_2 (l_1 + l_2)) \sinh(\lambda_2 l_2)}, \\ D_2 = A_2 \frac{\sinh(\lambda_2 (l_1 + l_2)) \sin(\lambda_2 l_2)}{\cos(\lambda_2 (l_1 + l_2)) \sinh(\lambda_1 l_1)}, \end{aligned} \quad (5)$$

so that for the trivial standard cases conditioned by restrictions  $\cos(\beta_1 + \beta_2) \neq 0$  and  $\sin(\beta_1 + \beta_2) \neq 0$  the mode shapes are of the form

$$\begin{aligned} y_1(x) = A_1 \left( \sin(\beta_1 \frac{x}{l_1}) - \frac{\sin \beta_1}{\sinh \beta_1} \sinh(\beta_1 \frac{x}{l_1}) \right) \\ y_2(x) = \frac{A_2}{\cos(\beta_1 + \beta_2)} \left( \sin(\beta_2 \frac{x}{l_2} - \beta_1 - \beta_2) - \right. \\ \left. - \frac{\sin \beta_2}{\sinh \beta_2} \sinh(\beta_2 \frac{x}{l_2} - \beta_1 - \beta_2) \right) \end{aligned} \quad (6)$$

Finally, both continuity conditions (3) relate the remaining two independent unknown

coefficients  $A_1, A_2$  for the standard case  $\cos(\beta_1 + \beta_2) \neq 0$  by equations

$$\begin{bmatrix} \lambda_1 \Theta(\beta_1) \cos(\beta_1 + \beta_2) & -\lambda_2 \Theta(\beta_2) \\ -2E_1 I_1 \lambda_1^2 \sin(\beta_1) \cos(\beta_1 + \beta_2) & a_{22} \end{bmatrix} \begin{bmatrix} A_1 \\ A_2 \end{bmatrix} = \begin{bmatrix} 0 \\ 0 \end{bmatrix} \quad (7)$$

with  $a_{22} = -2E_2 I_2 \lambda_2^2 \sin(\beta_2) + K_R \lambda_2 \Theta(\beta_2)$  and

$$\beta_1 = \lambda_1 l_1 = \sqrt{\alpha} (m_1 / E_1 I_1)^{1/4} l_1, \quad \beta_2 = \lambda_2 l_2 = \sqrt{\alpha} (m_2 / E_2 I_2)^{1/4} l_2$$

$$\begin{aligned} \Theta(\beta) &= \cos(\beta) - \frac{\cosh(\beta)}{\sinh(\beta)} \sin(\beta), \\ \Theta_1 &= \Theta_1(\beta_1), \quad \Theta_2 = \Theta_2(\beta_2) \\ \Psi_1(\beta_1, \beta_2) &= -\sin(\beta_1) + \frac{\cosh(\beta_2)}{\sinh(\beta_2)} \cos(\beta_1) \\ \Psi_2(\beta_1, \beta_2) &= \cos(\beta_1) - \frac{\cosh(\beta_2)}{\sinh(\beta_2)} \sin(\beta_1). \end{aligned} \quad (8)$$

### 3. CHARACTERISTIC GRAPH

Resulting frequency equation for the standard case follows directly from Eq. (7) and can be written in form

$$K_R \Theta(\beta_1) \Theta(\beta_2) - 2(E_2 I_2 / l_2) \beta_2 \Theta(\beta_1) \sin \beta_2 - 2(E_1 I_1 / l_1) \beta_1 \Theta(\beta_2) \sin \beta_1 = 0 \quad (9)$$

in which  $\beta_1, \beta_2$  are non-dimensional wave numbers conveniently used instead of unknown natural frequency  $\omega$ . Nondimensional wave numbers are coupled by relations

$$\beta_2 = \alpha \beta_1, \quad \alpha = \frac{l_2}{l_1} \left( \frac{m_2 E_1 I_1}{m_1 E_2 I_2} \right)^{1/4}. \quad (10)$$

The parameter  $\alpha$  is the measure of the differences in the geometrical and material properties of the two subsystems. It is called the ‘‘structural parameter’’ in [15], as explicit specification of numerical values assigned to parameters  $m_i, E_i, l_i$  and  $I_i$  at each span leads to unique value of  $\alpha$  characterizing the selected system configuration. For homogeneous subsystems, i.e. subsystems with identical material properties and identical cross-sections the variation in  $\alpha$  reduces to the variation of the ratio of subsystems lengths, as  $\alpha = l_2 / l_1$  according to Eq. (10).

Traditionally the frequency equation is presented in terms of unknown frequency  $\omega$ , however, the form (9) written in terms of wave numbers  $\beta_1, \beta_2 = \alpha \beta_1$  is extremely

useful in giving systematic overall insight to the distribution of natural frequencies for any configuration of the subsystems.

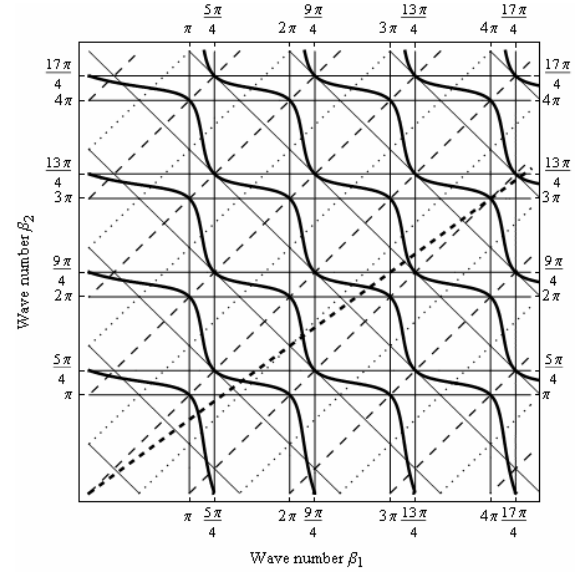


Fig. 2. Characteristic graph of the two-span system for  $K_R = 0$

Solutions of the frequency equation (9) for arbitrary configuration of the homogeneous system are presented in Fig. 2 as characteristic lines  $\beta_2 = f(\beta_1)$  for the rotational stiffness of  $K_R = 0$ . Characteristic lines fall apart into branches, corresponding to the first, second, etc. natural frequency. Particular system is characterized by fixed parameter  $\alpha$ , so the eigenvalues of the two-span beam are given as points of intersection of the structural line  $\beta_2 = \alpha \beta_1$  (thick dashed line) with characteristic lines  $\beta_2 = \varphi(\beta_1)$ , representing the solutions of the frequency equation Eq. (12), visualized by thick full line. Here the structural parameter for particular configuration is arbitrarily chosen as  $\alpha = 13/17$ . It is of value, that characteristic lines give the overall picture of the distribution of natural frequencies for any configuration obtained visually for the structural line  $\beta_2 = \alpha \beta_1$  running at angle  $\arctg(\beta_2 / \beta_1)$  from the horizontal. Remarkable feature of the characteristic graph is its high regularity. Thin horizontal and verticals  $\beta_1 = k\pi$  and  $\beta_1 = (m + 1/4)\pi$  create cells to which the pairs  $(\beta_1, \beta_2)$  as solutions  $\beta_2 = f(\beta_1)$  of frequency

equation 12) are mapped. The complicating factor is, that the condition  $\cos(\beta_1 + \beta_2) \neq 0$  is violated along subdiagonal lines  $\beta_1 + \beta_2 = (1+2k)\pi/2$ , which at points  $((m_1 + 1/4)\pi, (m_2 + 1/4)\pi)$  exclude specific discrete locations from the characteristic graph  $\beta_2 = f(\beta_1)$ , as at these locations the mode shapes given by (6) corresponding to the standard case  $\cos(\beta_1 + \beta_2) \neq 0$  are invalid and therefore the special case  $\cos(\beta_1 + \beta_2) = 0$  has to be solved separately. Dashed thin diagonal lines  $\beta_2 - \beta_1 = k\pi$  correspond to nonlocalization points according to [15] and the points of intersections of the dotted thin diagonal lines relating the wave numbers by relation  $\beta_2 - \beta_1 = (k+1/2)\pi$  with the characteristic graph correspond to modes with maximum amount of localization according to [15].

The influence of coupling realized by rotational spring  $K_R$  is presented on Fig. 3 for several values of non-dimensional spring constants  $K_R = 0, 10, 50, 100$ . Increase of stiffness of coupling gives rise to increase of eigenfrequencies, however, the characteristic lines  $\beta_2 = f(\beta_1, K_R)$  have the remarkable feature of remaining to be confined in rectangular blocks, as it is obvious from Fig. 3. Extremely high values of coupling stiffness tend to transform the

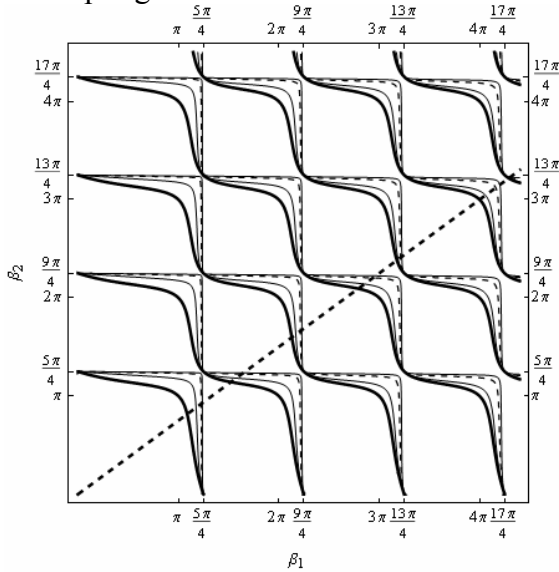


Fig. 3. Characteristic graph of the two-span system for  $K_R = 0$  (thick full line),  $K_R = 10$  (thin full line),  $K_R = 50$  (thin dashed line) and  $K_R = 100$  (another thin full line)

structure to one with almost double eigenfrequencies, what is in accordance with the intuitive understanding, that in this limiting case the left and the right span tend to vibrate independently much the same as in the case of a pair of pinned-clamped and clamped-pinned beam. This extreme case of  $K_R \rightarrow \infty$  together with extremely high values of  $K_R$  is in the literature referred as the case of weak coupling.

To estimate the conditions of localization it is necessary to compute the ratios of amplitudes in the left and the right span along the lines  $\beta_2 = f(\beta_1, K_R)$ .

#### 4. METRICS FOR ASSESMENT OF LOCALIZATION

From Eqs (6-7) it is obvious, that eventual mode localization is manifested in extend of the decline of the ratio of amplitudes of individual spans, say  $A_2/A_1$ , from value 1, and also that the liberty of disregarding the signs of amplitudes can be taken. For the direct ratio of  $A_1, A_2$  we have from the first equation of the system (7) the relation holds

$$\begin{aligned} \frac{A_2}{A_1} &= \frac{\lambda_1 \Theta_1}{\lambda_2 \Theta_2} \cos(\beta_1 + \beta_2) = \\ &= \left( \frac{m_1 E_2 I_2}{m_2 E_1 I_1} \right)^{1/4} \frac{\Theta_1}{\Theta_2} \cos(\beta_1 + \beta_2) \end{aligned} \quad (11)$$

When the spans differ only in their lengths, which is the most common case, and is referred to as a homogeneous system, then the above ratio is further simplified into

$$\frac{A_2}{A_1} = \frac{\Theta_1}{\Theta_2} \cos(\beta_1 + \beta_2) = \frac{\Theta(\beta_1)}{\Theta(\beta_2)} \cos(\beta_1 + \beta_2) \quad (12)$$

Thus, the amplitude ratio for homogeneous system in the standard case is directly proportional to the ratio of functions  $\Theta(\dots)$  evaluated at wave numbers corresponding exactly to the eigensolution.

The metrics for assessment of the degree of mode confinement is in literature subject of discussion, see [2-3]. It can be selected arbitrarily as some function of modal amplitudes  $A_1, A_2$  of subsystems, which enables to compare properly the vibration levels. In

[14-15] the logarithm of the ratio of the mean squared free vibration amplitudes in subsystems was used, here for simplicity the direct amplitude ratio  $\rho$  and the scaled amplitude ratio  $\eta$  are used, being defined by following relations:

$$\rho = \left| \frac{A_2}{A_1} \right| = \left| \frac{\theta(\beta_1)}{\theta(\beta_2)} \cos(\beta_1 + \beta_2) \right|, \quad (13)$$

$$\eta = \frac{\text{Min}(|\theta(\beta_1)|, |\theta(\beta_2)|)}{\text{Max}(|\theta(\beta_1)|, |\theta(\beta_2)|)}.$$

The values of the scaled ratio  $\eta$  are restricted to interval  $(0,1)$  with understanding, that  $\eta = 1.0$  corresponds to the absence of any localization, while higher degree of localization is indicated by smaller values of  $\eta$ . The values of the direct amplitude ratio  $\rho$  are difficult to interpret graphically, as high degree of confinement corresponds to both the extremely high and extremely low numerical values, however, for nonlocalization here we have also  $\rho = 1.0$ . Figures. 5 and 6 show the dependence of localization factors  $\rho$  and  $\eta$  on the structural characteristics  $\alpha = \beta_2/\beta_1$  for the case of strongly coupled subsystems. The full range of possible values of the structural parameter  $\alpha \in (0, \infty)$  is transformed to corresponding angle with more convenient range of possible values restricted to finite interval  $(0, \pi/2)$ . Due to evident symmetry of the problem the pre-presented of results in Fig 6 is restricted to the half-interval  $(0, \pi/4)$ .

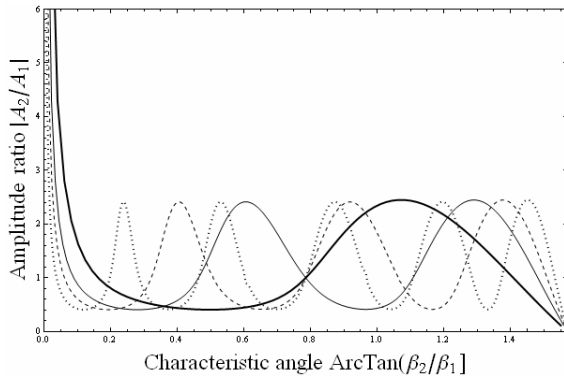


Fig. 4. Amplitude ratio  $\rho$  for the first four eigenmodes

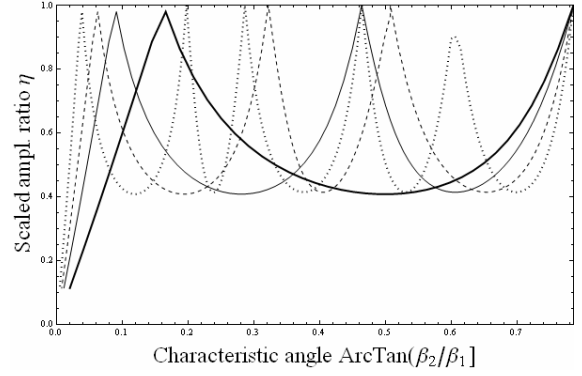


Fig. 5. Scaled amplitude ratio  $\eta$  for the first four eigenmodes

## 5. SEMI-EXACT FORMULATION

The frequency equation (9) can be transformed to shear trigonometric form under the assumption  $\tanh(\beta_i) \approx 1$  valid with high precision for second and higher modes. After rather lengthy calculations an explicit relation between the wave numbers is obtained in the form

$$\beta_2 = \varphi(\beta_1, \kappa, e_{21}) = k\pi - \text{arctg}\left(\frac{p}{q}\right),$$

$$p = \kappa \cos \beta_1 - (\kappa + 2\beta_1) \sin \beta_1$$

$$q = (\kappa + 2\beta_1(e_{21} + 1)) \sin \beta_1 - (\kappa + 2\beta_1 e_{21}) \cos \beta_1 \quad (13)$$

$$\kappa = \frac{K_R I_1}{E_1 I_1}, \quad e_{21} = \frac{E_2 I_2}{E_1 I_1}, \quad k = 1, 2, \dots$$

The existence of explicit relation  $\beta_2 = \varphi(\beta_1, \kappa, e_{21})$  allows immediate computation of the estimate of the amplitude ratio for given configuration of the boundary conditions without the need of performing tedious numerical calculations of the exact amplitude ratio along the numerically accessible wave coordinates  $(\beta_1, \beta_2)$ . Similar relations can be derived for other combinations of boundary conditions at extreme ends of the two-span beam. Numerous tests have been undertaken to show the efficiency of the semi-exact approach for wave numbers of ranks higher than 2.

## 12. CONCLUSION

Presented analysis and numerical results allow to assess the degree of vibration localization for arbitrary configuration of subsystems of two-span beams by collecting and visualization of the data structure  $\alpha, \beta_1, \beta_2, K_R, \rho$  or  $\eta$  in systematic manner. Phenomenon of localization manifests highly regular pattern when the results are presented and interpreted in terms of wave numbers.

## 11. REFERENCES

- [1] Fang, X., Tang, J., Jordan, E. and Murphy, K.D. Crack induced vibration localization in simplified bladed-disk structures. *J. of Sound and Vibration*, 2006, **291**, 395-418.
- [2] Yoo, H.H., Kim, J.Y. and Inman, D.J. Vibration localization of simplified mistuned cyclic structures undertaking external harmonic force. *J. of Sound and Vibration*, 2003, **261**, 859-870.
- [3] Pierre, C., Castanier, M.P. and Chen, W.J. Wave localization in multi-coupled periodic structures: applications to truss beams. *ASME Appl. Mech. Review* 1996 **49**, 65-86.
- [4] Nad, M. Modal properties of a cracked beam. In *Engineering Mechanics 2007*. UTAM, Prague, 2007, 1-8.
- [5] Nad, M. Modal properties of cantilever beam with pre-stressed core. In *Noise and Vibration in Practice*. Bratislava, 2008, 71-74.
- [6] Tang, J. and Wang, K.W. Vibration delocalization of nearly periodic structures using coupled piezoelectric networks, *J. of Vibration and Acoustics*, 2003, **125**, 95-108.
- [7] Chen, W. and Xie, C. Vibration localization in plates rib-stiffened in two orthogonal directions. 2005, **280**, 235-262.
- [8] Sága, M., Žmindák, M., Dekýš, V., Sapietová, A. and Segľa, Š. *Selected methods of the analysis and synthesis of*

*mechanical systems (In Slovak)*. VTS ŽU, Žilina, 2009.

- [9] Nad, M. *Modification of Modal Characteristics of Vibrating Structural Elements*. Scientific Monographs Hochschule Anhalt, Köthen, 2010.
- [10] Hodges, C.H. Confinement of vibrations by structural irregularity. *J. of Sound and Vibration*, 1982, **82**, 414-424.
- [11] Bendiksen, O.O. Localization phenomena in structural dynamics. *Chaos, Solitons and Fractals*, 2000, **11**, 1621-1660.
- [12] Pierre, C. and Dowell, E.H. Localization of vibrations by structural irregularity. *J. of Sound and Vibration*, 1987, **114**, 549-564
- [13] Shahruz, S.M. Elimination of vibration localization: a mathematical justification. *J. of Sound and Vibration*, 2005, **283**, 449-458.
- [14] Langley, R.S.: Mode localization up to high frequencies in coupled one-dimensional subsystems. *J. of Sound and Vibration*, 1995, **185**, 79-91.
- [15] Kim, D.O. and Lee, I.W. Mode localization in simply supported two-span beams of arbitrary span lengths. *J. of Sound and Vibration*, 1998, **213**, 952-961.
- [16] Issa, J., Mukherjee, R., Diaz, A.R. and Shaw, S.W.: Modal disparity and its experimental verification. *J. of Sound and Vibration*, 2008, **311**, 1465-1475.

## ACKNOWLEDGEMENTS

The support given by the VEGA grant Nr. 1/0389/11 from the Ministry of Education of the Slovak Republic is highly acknowledged.

## CORRESPONDING ADDRESS

Tibor Nánási, MSc.(Eng.), PhD.  
Faculty of Materials Science and  
Technology in Trnava,  
Pavlínska 16  
917 24 Trnava, Slovakia.  
E-mail: tibor.nanasi@stuba.sk



## ON ACOUSTIC PANELS WITH HIGH PERFORMANCES FOR POLLUTANT INDIVIDUAL WORKING PLACE INSULATION

Nastac, S.; Anghelache, D.; Stanciu, M. & Curtu, I.

**Abstract:** *This paper deals with noise protection and the practical means to achieve this purpose. Individual working places, especially for construction machines with intensive and random dynamical working cycle require proper noise insulation because of the high level of acoustical pollution. The authors propose a feasible acoustic panel solution based on composites core thus that it will be assure proper noise isolation level for large area of applications in respect with the noise emissions characteristics and the spatial distribution and acoustic sensitivity of the receivers. The basic idea of this study combines selective quantitative and qualitative characteristics of a group of materials such as metal sheets, elastomers and textiles to obtain a proper performance of the panel ensemble.*

*Key words: acoustics, panels, insulation, performances.*

### 1. INTRODUCTION

Basic idea of this analysis starts from the practical necessity of noise insulation at working places denoted by intensive acoustical pollution. Taking into account the large and various range of noise characteristics of the usual technological equipments results a strength requirement of proper noise insulation solutions which can provides relative high performances for a large frequency domain. Low frequencies due to the structural vibrations will combines with medium and high frequencies due to the various types of mechanical parts and ensembles having dynamic behaviour. Besides these one can

have the hydraulic and/or pneumatic driving systems, the certain types of fans, the electrical or thermal engines, the different types of handlers and hand tools, etc. All of these equipments and systems lead to an apparent random noise which can affect a certain working place.

In such conditions a proper technical solution for noise insulation has to provide a constant value of acoustical absorption coefficient for how many frequency domains. Whereas single materials which supply this requirement is very difficult to obtain, a composite which combines a various frequency characteristics can assure easily such as conditions.

The authors proposed and analyzed some composites of metal, rubber and textile sheets with different number of layers and different thicknesses. Optimum ratio between acoustical insulation performances and weight of used material was mainly taken into account.

### 2. MATERIALS CHARACTERISTICS

Appropriate combinations of insulation materials supposes a mixture of vibration isolation and acoustic absorption thus that low frequencies isolation and medium-high frequencies absorption will provides a large characteristic regardless the pollutant sources type.

Vibration isolation performances were characterized by damping coefficient. Instrumental analysis of vibration isolation composites were performed using Oberst Beam Method (OBM), the well known experimental method for damping loss factor evaluation [1...7].

In respect with the initial hypothesis it was adopted four types of composite plates. Damping materials were rubber sheets with 2, 3 and 4 mm thickness, and synthetic felt ingrained with latex. Basic material for the entire set of combinations was a metal sheet with 1 mm thickness [8].

In Fig.1 were depicted the comparative diagrams of damping loss factor for the proposed composites together with the basic case (e.g. 1 mm thick metal sheet).

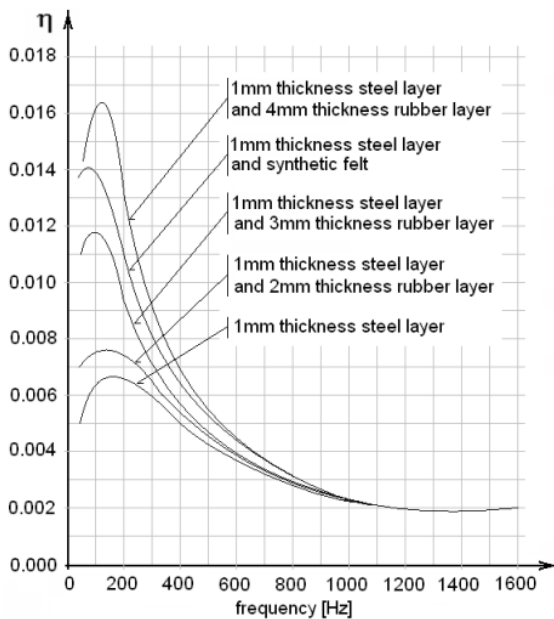


Fig. 1. Damping loss factor for vibration isolation composites (reproduced from [8])

Noise insulation supposes an appropriate mixture of materials thus that the relative acoustical absorption coefficient acquires high values for medium and high frequencies.

The previous studies [8...10] and the authors analyses developed both on computational models, and on experimental tests reveals that acoustical absorption parameter increase in respect with noise frequency. In the same time, the noise absorption efficiency of the porous materials grows up for the high frequencies. This last conclusion also results from an analytical approach [8].

Practical set of tested materials for noise insulation contains both simple layer, and complex structure with multiple layers from different materials.

Basic materials were textile sheet - *intersin* (6 mm thick), synthetic rubber sheet - *intex* (13 mm thick) and wasted textiles composite sheet - *tefo* (6 mm thick). Complex composite material (*netrom*) contains multiple layers of synthetic skin against textile layer ingrained with synthetic rubber.

Samples of these materials were tested with the help of Kundt method based on the stationary waves approach. In Fig.2 were depicted the acoustical absorption characteristics for the four combinations of materials previously described.

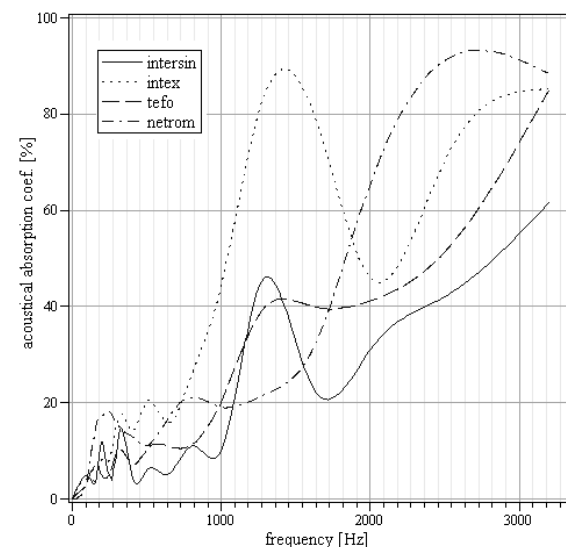


Fig. 2. Relative acoustical absorption for different materials

Comparative analysis of the diagrams in Fig.2 denotes differences between the four types of composites. Also, it reveals low acoustical absorption efficacy for frequency values between 100 and 1000 Hz, while that for frequency values over than 1000 Hz the acoustical absorption coefficient acquire high values. All the composites have a roughly the same characteristics, but the peaks are different for each type.

In respect of the number of identical layers, for the same material or composite the acoustical absorption coefficient acquires high values for high frequencies domain. For frequency values over than 1kHz the acoustical absorption increase up to double

value comparative with single layer case. Low frequencies range (under the 250 Hz) does not acquire influences in respect with the number of layers.

### 3. EXPERIMENTAL TESTS RESULTS

The practical utilization of the composite panels for reducing the technological noise at working area imposes a lot of instrumental tests and analysis thus that the Regulations requirements for each application type can be accomplish.

If the vibration isolation also benefits from an additional technical means such as the passive or active dampers embedded on the pollutant sources, the noise insulation have to be taken into account for each case. Following this idea, it was supposed three types of technological equipments from different category to verify the efficacy of the proposed noise insulation solutions. Hereby it were considered two types of equipments which are affected by different dynamic loads during the working cycle (*MMT45* low capacity wheel loader and *S1201* excavator) and one equipment which uses vibrations into its working cycle (*CVA10* vibratory compactor).

It was evaluated the average acoustical absorption coefficient in respect with frequency for each equipment using the expression

$$\alpha_{av} = \frac{\sum \alpha_i S_i}{S} \quad (1)$$

where  $\alpha_i$  denotes the acoustical absorption coefficient for each surface  $S_i$ , with total surface of the protection area denoted by  $S$ . For basic unprotected surface (thin metallic sheet) and for glass area (windows) was adopted the acoustical absorption coefficients as follows:  $\alpha_{base} = 0.08$ , respectively  $\alpha_{glass} = 0.33$ .

Global evaluation of noise insulation performances contains also the other two parameters. The first is noise total level reduction  $\Delta L$  evaluated with the expression

$$\Delta L = 10 \lg \frac{A}{A_0}, [\text{dB}] \quad (2)$$

where  $A$  and  $A_0$  denote equivalent areas of acoustical absorption after, respectively before the noise insulation treatment application.

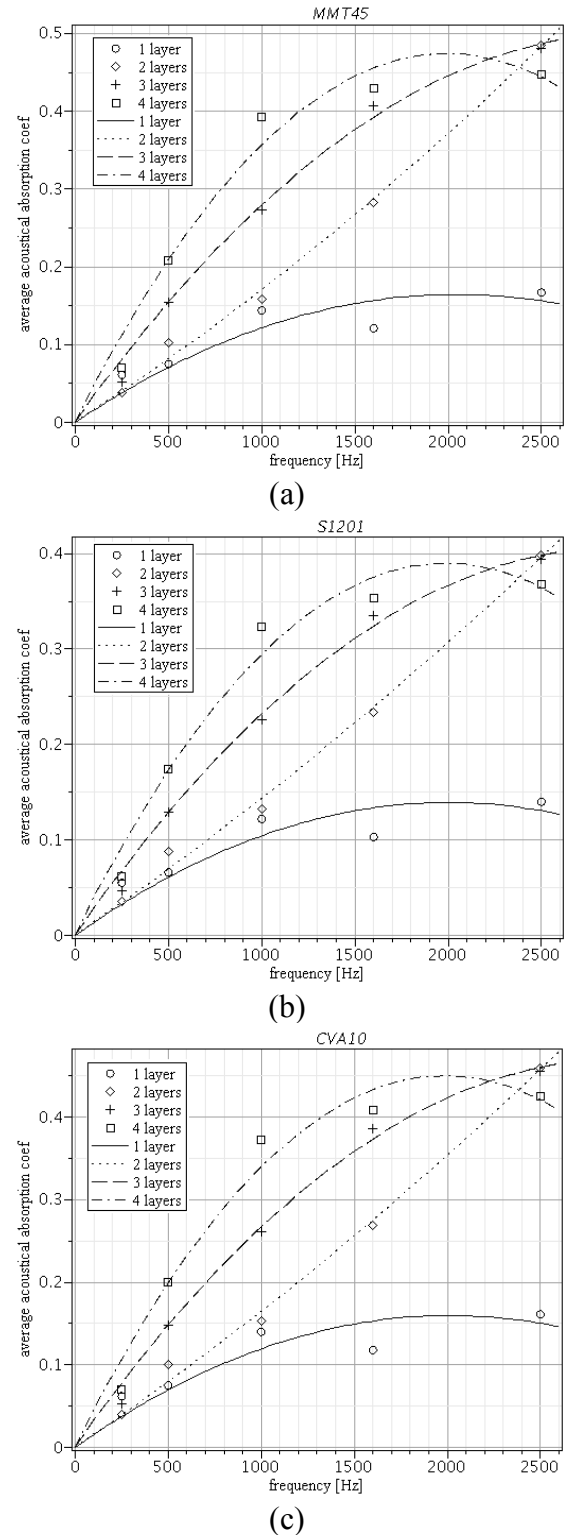


Fig. 3. Parametrical diagrams of average acoustical absorption coefficient in respect with frequency and number of layers

The second is the absorption constant  $R$  evaluated based on the average acoustical absorption coefficient  $\alpha_{av}$  with expression

$$R = \frac{\alpha_{av} S}{1 - \alpha_{av}} \quad (3)$$

Diagrams depicted in Fig.3 present the characteristics of the average acoustical absorption coefficient  $\alpha_{av}$  in respect with frequency. The analysis was made with variable number of identical protective layers from single to fourfold.

Analysis of these parametrical graphs reveals a relative similar shape but quantitative differences. The acoustical absorption performances widely increase between single and double layers cases, but roughly maintain at the same values for elder layers number.

In Fig.4 it was presented a comparative analysis between protected and different types of unprotected areas of working domain. First and second situations suppose relative close values for total protection area; last situation have a quarter less value than other two. The glass area of the second situation is half of its corresponding total surface; this case supposes a less noise protected surface (38%). In the same time the noise protected surface of the last situation exceeds half of its total surface. But it provides a relative high unprotected area (24%). First situation corresponds to a balanced case, with relative close values of protected and glass surfaces, with low value of unprotected area (17%). It had to be mentioned that full noise protected surfaces provide between double and three times value of acoustical absorption coefficient than the glass area.

Taking into account the percentage values in Fig.4 and the previous suppositions, a global comparative quantitative analysis between diagrams in Fig.3 reveals the major influences both of the unprotected surface percentage, and of the glass surface percentage, in respect with the total protection area. Balanced solutions can assure better protection than an extremely closed approach of the working area, especially when it is required windows.

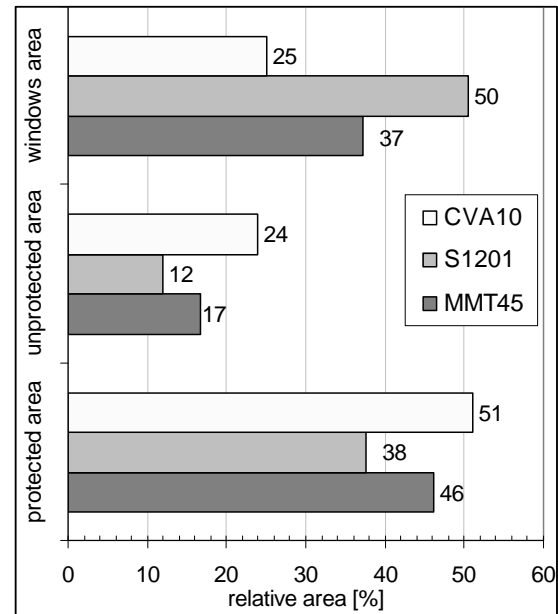


Fig. 4. Comparative analysis regarding the protection components of working domain

#### 4. CONCLUSION

The complexity of vibration and noise insulation at the working places comes from the strength necessity of human operator protection assurance. European and National Regulations stipulations contain acceptable limit values both for vibration and noise exposure.

In order to frame into the normal state of noise exposure it is imperative to use acoustic barriers and vibration isolation systems. Frequency range of technological equipments includes medium and high values. In the same time, structural vibration leads to a background noise with low and very low frequencies. This structural noise can affect both inside and outside the noisy structure.

The analyses briefly presented into this paper show the suiting capability of the some regular materials, for simple or complex composite utilization, to assure high performance regarding noise absorption.

Future studies follow the requirement of quantitative reducing of basic materials both through the layers thickness decreasing, and through an appropriate combination into the final composites.

## 5. REFERENCES

- [1] Wojtowicki, J.L., Jaouen, L., Panneton, R. New approach for the measurement of damping properties of materials using the Oberst beam, *Rev. Sci. Instrum.* **75**, 2569 (2004).
- [2] Xu, Y., Nashif, A. Measurement, Analysis and Modeling of the Dynamic Properties of Materials, *Sound and Vibration/July 1996*, pp.20-23.
- [3] Malogi, D., Gupta, A., Kathawate, G.R. Center Impedance Method for Damping Measurement, *Advances in Acoustics and Vibration*, Hindawi Publishing Corp., In Volume 2009, Article ID 319538, 7 pp., doi:10.1155/2009/319538.
- [4] Deverge M., Jaouen, L. A review of experimental methods for the elastic and damping characterizations of acoustical porous materials, *The Proceedings of The 33rd International Congress and Exposition on Noise Control Engineering - InterNoise 2004*, Prague, Czech Republic, August 22-25, 2004.
- [5] Koruk, H., Sanliturk, K.Y., On Measuring Dynamic Properties of Damping Materials Using Oberst Beam Method, ESDA 2010-24452, *The Proceedings of the ASME 2010 10th Biennial Conference on Engineering Systems Design and Analysis - ESDA2010*, July 12-14, 2010, Istanbul, Turkey.
- [6] Erdoğan, G., Bayraktar, F., Sanliturk, K.Y., Measurement of Dynamic Properties of Materials, *The Proceedings of The 32nd International Congress and Exposition on Noise Control Engineering - InterNoise 2003*, Seogwipo, Korea, August 25-28, 2003.
- [7] Jaouen, L., Renault, A., Deverge, M. Elastic and damping characterizations of acoustical porous materials: Available experimental methods and applications to a melamine foam, *Applied Acoustics* **69** (2008) 1129–1140.
- [8] Bratu, P. *Indoor Acoustics for Constructions and Machineries*, Impuls Publishing House, 2002.
- [9] Anghelache, D., Nastac, S. Noise and Vibration Protective Solutions Analysis for Technological Equipments, *The Annals of "Dunarea de Jos" University of Galati*, Fascicle XIV Mechanical Engineering, vol.1, 2010, pp.81-86.
- [10] Anghelache, D. About phonic isolation of the mobile equipment cabin, *The Annals of "Dunarea de Jos" University of Galati*, Fascicle XIV Mechanical Engineering, vol.1, 2008.

## 6. ADDITIONAL DATA

Corresponding author:

*Silviu NASTAC*

"Dunarea de Jos" University of Galati  
Engineering Faculty in Braila

Complex Measurements and Virtual

Instrumentation Laboratory

Calea Calarasilor 29,

810017 Braila

Romania

email: snastac@ugal.ro

Authors:

*Diana ANGHELACHE*

"Dunarea de Jos" University of Galati  
Engineering Faculty in Braila

Research Center for Mechanics of

Machines and Technological Equipments

Calea Calarasilor 29,

810017 Braila

Romania

email: danghelache@ugal.ro

*Mariana STANCIU*

"Transilvania" University of Brasov

Romania

email: mariana.stanciu@unitbv.ro

*Ioan CURTU*

"Transilvania" University of Brasov

Romania

email: curtuioan@yahoo.com

## MODEL VALIDATION AND STRUCTURAL ANALYSIS OF A SMALL WIND TURBINE BLADE

Pabut, O.; Allikas, G.; Herranen, H.; Talalaev, R. & Vene, K.

**Abstract:** *The goal of this study was to develop and validate a simplified finite element analysis (FEA) model for a glass fibre reinforced plastic (GFRP) wind turbine blade. A 3D virtual model of the blade was built up in ANSYS Workbench software with corresponding load cases and boundary conditions. Data for the FEA was obtained from tensile tests of GFRP laminates. Experimental validation of the virtual model was performed on manufactured blade subject via bending tests and modal analysis.*

*Key words: wind turbine blade, GFRP, finite element analysis, modal analysis*

### 1. INTRODUCTION

One of the most important components of a wind energy converter is the rotor together with blades. Structural design and performance analysis of wind turbine blade is an important part of the design theory and application of wind turbines [1-2]. Manufacturing costs of a small horizontal axis wind turbine (SHAWT) blade can reach about 20% of the turbine productions costs. Therefore, possible profits resulting from a better structural model and use of suitable composite materials refer to a need of multi-criteria optimization and refined modeling techniques [3]. These statements are furthermore reinforced by the fact that for a cost effective wind turbine solution, the blades must achieve a very long operating life of 20-30 years [4].

For SHAWT blades, only few full scale blades are normally physically tested during the design process as a confirmation of general structural integrity. By utilizing

computational technology and various design approaches, information from these tests can be taken into account in a rational way in order to speed up the design process and increase structural reliability of blades [5].

In this paper, validation of a full scale single layer lay-up SHAWT blade 3D FEA model is performed. The virtual model is validated through experimental bending test and modal analysis. The proposed model allows effective consideration of GFRP material properties, large dimensions of the structure and rapidly changing geometrical variables [6-7].

### 2. PROBLEM FORMULATION

#### 2.1 Blade structure

The SHAWT blade subjected to analysis consist of three main structural components that are presented in the Figure 1.

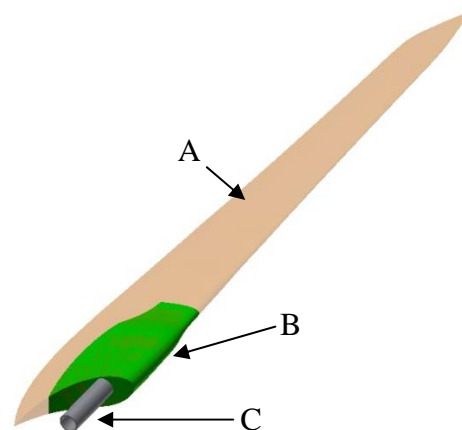


Fig. 1. GFRP blade: geometrical layout

GFRP skin material is denoted by A, resin based connection part by B and metallic root tube by C. The blade has an overall

length of 2850 mm and a maximum width, at the widest chord length, of 465 mm.

The manufacture skin laminate consists of following E-Glass fiber materials:

- one layer of Gelcoat GS with 0,4 mm thickness.
- one layer of 600 g/m<sup>2</sup> Chopped Strand Mat (CSM) with 2 mm thickness;
- four layers of 600 g/m<sup>2</sup> balanced stitched biaxial roving mat 0°/90° with 4×0,5 mm thickness.

The fibers were impregnated via hand lay-up with polyester resin (413-568). This resulted in a 4,4 mm thick shell structure, after being post-cured at a room temperature. The skin in this case is the main load bearing element as it is subjected to aerodynamic thrust loads.

The connection part B consists only of polyester resin which is formed in a separate mold. It is mainly used as a load transferring unit from the skin to the root tube element. The root tube C is made of conventional S355 steel and acts as a fixing unit.

## 2.2 Goals of model validation

In order to achieve preliminary safety of the blade structure, it has to possess properties that do not lead to catastrophic failures under ultimate loads. Therefore, it becomes necessary to be able to predict following properties of the blade: maximum allowed loads, bending stiffness and natural frequencies [8, 9].

The natural frequencies are important as the blade is of an elastic structure and the load on it is of stress alternation and random variability. This could lead to coupling modes and often to direct malignant structure damage and failure [9].

## 3. EXPERIMENTAL STUDY

### 3.1 Stiffness and strength analysis

For an experimental study, the blade subjects were manufactured according to previously mentioned parameters. Stiffness and strength analysis was performed in a

manner where calibrated weights were attached to a designated point at the blade tip. The deformation was acquired with a laser measurement device as a vertical tip displacement from initial position. The test was carried out until a full loss of blade structural integrity occurred. Results of the experimental test are presented in Table 1. The applied force is weighed against vertical deformation of the blade tip.

Nr.	Load [kg]	Load [N]	Def. [mm]
1	20	196,2	86
2	25	245,3	116
3	30	294,3	141
4	35	343,4	169
5	40	392,4	196
6	45	441,5	234
7	50	490,5	261
8	55	539,6	293
9	60	588,6	322
10	65	637,7	364
11	70	686,7	402
12	75	735,8	483
13	80	784,8	failure

Table 1. Experimental results of the stiffness and strength analysis



Fig. 2. Broken test subject

At a load of 784,8 N the test specimen experienced a full loss of structural integrity as the bottom side of the skin collapsed under compressive load (Figure 2). Also opening of the two skin halves due to shear forces was noted during the failure incident.



### 3.2 Modal analysis

The experimental modal analysis was performed in a form of calibrated impulse hammer (Model AU01) test. The test specimen was mounted with soft restraints. Predefined measurement points were excited to acquire the frequency response functions (FRF). Results were recorded with SigLab Model 20-22A.



Fig. 3. Experimental modal analysis

The measurement data was processed in STAR Modal software. The obtained FRFs were iteratively curve fitted with polynomial method to identify the modal parameters (Figure 4). Results of first five natural frequencies are presented in Table 2.

Mode	Frequency, Hz
1	16,6
2	46,8
3	82,1
4	95,4
5	125,7

Table 2. Results of experimental analysis

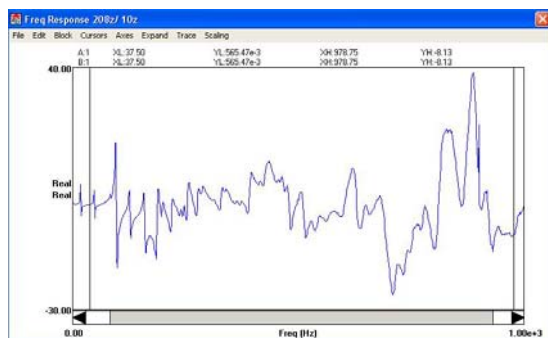


Fig 4. FRF of a 10<sup>th</sup> measurement point

### 4.1 FEA model

ANSYS Workbench software was utilized for numerical analysis. For the skin hexahedral shell elements (SHELL181) with four nodes were considered. These are well-suited for linear, large rotation, and/or large strain nonlinear applications [10]. Due to the complex and irregular geometry solid tetrahedral (SOLID187) elements were considered for the connection part. The root tube was meshed with solid hexahedral (SOLID186) elements. Three different element side lengths were considered according to the general importance of the objects. Skin was meshed with 10 mm element side length, connection part with 20 mm side length and root tube with 6 mm side length (Figure 5).

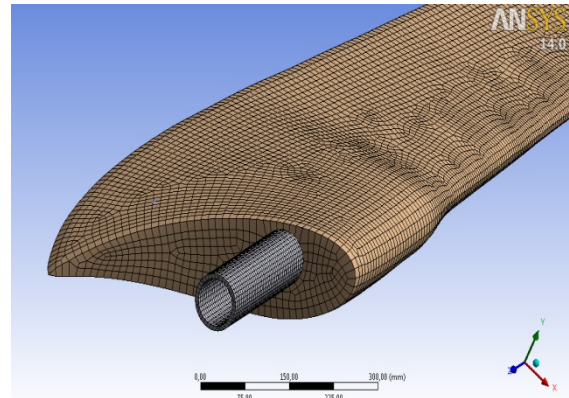


Fig. 5. Mesh for FEA

For the connector and root tube linear isotropic material models were used (defined by elastic modulus  $E$  and Poisson's ratio  $\nu$ ). Linear orthotropic material model was used to define the skin properties (defined by elastic modulus  $E$ , Poisson's ratio  $\nu$  and shear modulus  $G$ ). The skin lay-up was depicted as one layer to simplify the model and reduce calculation time. Properties of the 4,4 mm layer were determined via tensile test with a servo hydraulic test machine Instron 8800. Material properties were calculated according to methods mentioned in previous studies [11].

**E-Glass singel layer lay-up, GPa**



$E_x$	14500
$E_y$	14500
$E_z$	1800
$\nu_{xy}$	0.11
$\nu_{yz}$	0.30
$\nu_{xz}$	0.30
$G_{xy}$	2800
$G_{yz}$	1500
$G_{xz}$	1500

Table 3. Mechanical properties of GFRP laminate

#### 4.2 Stiffness and strength analysis

Boundary conditions for the strength and stiffness analysis were selected according to the test setup. The principle scheme of the stiffness and strength analysis is presented in the Figure 6.

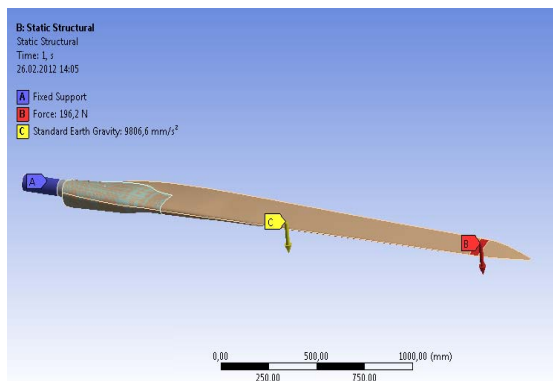


Fig. 6. Boundary conditions for the stiffness and strength analysis

In Figure 6 the fixed support of the root tube is denoted by A. The tube is supported along 200 mm area, starting from the free end of the tube. Acting force is denoted by B and applied to a 50 mm area, measured 2675 mm from the free end of the root tube. Standard earth gravity ( $9,806 \text{ m/s}^2$ ) is denoted by C.

During the simulation force magnitude was incrementally raised to generate a force-displacement curve. Due to the relatively large deformations compared to the initial bounding box, ANSYS large deformation mode was used. This enabled to include non-linear material effects and utilized multiple time step iterations in order to achieve a more refined solution. However,

it must be noted that the usage of large deformation mode increases considerably calculation time and effort.

Results of the stiffness and strength analysis are presented in Table 4. The applied force is weighed against resulting vertical deformation of the blade tip and maximum stress on the skin. Each load case can be traced by corresponding number.

Nr.	Load [N]	Stress [MPa]	Def. [mm]
1	196,2	33	86
2	245,3	40	107
3	294,3	46	128
4	343,4	53	149
5	392,4	60	171
6	441,5	66	195
7	490,5	73	220
8	539,6	79	248
9	588,6	89	285
10	637,7	139	337
11	686,7	221	410
12	735,8	336	503
13	784,8	447	607

Table 4. FEA results of the strength and stiffness analysis

#### 4.3 Modal analysis

The essence of modal analysis is solving the vector of the modal equations with a finite number of degrees of freedom under the non-damping and non-external load condition. The impact of structural damping to the modal frequency and the vibration mode is so small that it is ignored [9].

Modal analysis with two different sets of boundary condition was carried out. Firstly, a free body analysis without supporting fixtures was conducted. This method allows to discard the stiffness of restraints and therefore exhibits fewer degrees of uncertainty.

Secondly, a fixed body analysis was carried out to predict the natural frequencies of the blade in its working position. In this configuration the end of

the root tube had all degrees of freedom removed (Figure 7).

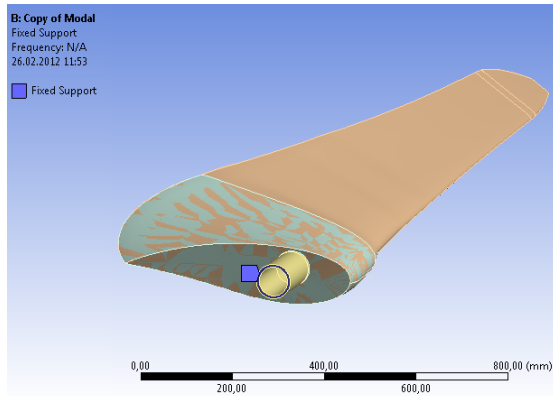


Fig. 7. Boundary conditions for fixed body modal analysis

Results of the modal analysis are presented in Table 5. It has to be noted that for a free body analysis the first six natural frequency modes are always 0. These represent the unfixed 6 degrees of freedom of a rigid body.

Free body anal.		Fixed body anal.	
Mode	Freq., Hz	Mode	Freq., Hz
1	0,0	1	7,2
2	0,0	2	21,4
3	0,7E-03	3	27,1
4	0,9E-03	4	54,8
5	0,2E-02	5	77,3
6	0,2E-02		
7	15,5		
8	43,2		
9	78,2		
10	82,3		
11	91,1		

Table 5. FEA results of the modal analysis

For the fixed body analysis the first natural mode is found at 8,3 Hz. It is a bending mode of the blade tip and is depicted in Figure 8.

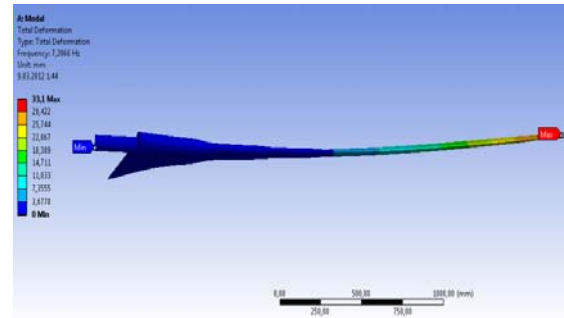


Fig. 8. First natural mode of the blade

## 5. RESULTS

The obtained FEA deformations are in good correlations with the experimental results. The maximum difference of 16,8% occurs during load case 6 (Figure 9). The stress figures predict structural failure of the blade already at load case 12, as the obtained stress is above the yield strength of the skin element ( $R_m=250$  MPa). This can be explained by a rapid change of the blade geometry that leads to a singularity effect which results in a higher stress concentration factor.

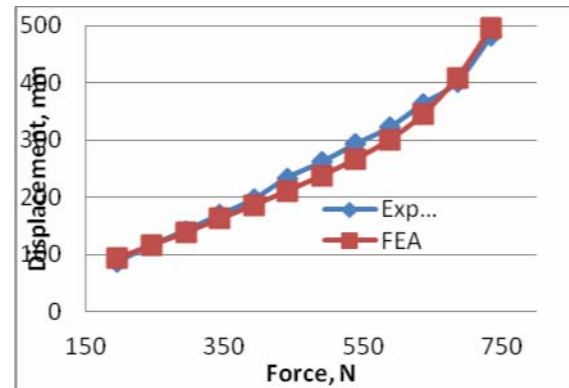


Fig. 9. Deformation comparison of FEA and experimental analysis

The obtained FEA modal frequencies provide satisfactory correlation of the result for first three frequencies with a differences of 7%, 8% and 5% respectively. However, for higher frequencies the deviation also increases. This can be explained by the fact that higher frequencies are more influenced by structural deviations. In current study the higher frequencies are not of concern as their influence for structural vibrations is

relatively low and usually for turbine blades only first and second natural frequencies are of interest. Therefore, in general it can be concluded that the FEA model is validated against experimental results.

## 6. CONCLUSION

FEA model validation of a single layer lay-up GFRP wind turbine blade has been performed. Experimental bending test and modal analysis have confirmed the results achieved in the ANSYS model. It can be concluded that:

- a) Simplified representation of the skin layout in FEA can be used to study the stiffness, and strength characteristic of the blade.
- b) Simplified representation is suitable to study the lower natural frequencies of the blade.

In future studies different connections interfaces have to be examined in greater detail. It is planned to develop design principles for the root tube-resin and skin-glue interfaces. Also a study of fatigue properties of the blade shall be carried out.

## 7. REFERENCES

- [1] Song, F., Ni, Y., Tan, Z. Optimization Design, Modeling and Dynamic Analysis for Composite Wind Turbine Blade. *International Workshop on Automobile, Power and Energy Engineering*, 2011, **16**, 369–375.
- [2] Ronold, K.O., Cristensen, C.J. Optimization of a Design Code for Wind-Turbine Rotor Blades in Fatigue. *Engineering Structures*, 2001, **23(8)**, 993-1004.
- [3] Jureczko, M., Pawlak, M., Mezyk, A. Optimization of a Wind Turbine Blades. *2005 Int. For. on the Adv. in Mat. Proc. Tech*, 2005, **167(2-3)**, 463-471.
- [4] Kong, C., Kim, T., Han, D., Sugiyama Y. Investigation of Fatigue Life for a Medium Scale Composite Wind Turbine Blade. *The Third Int. Conf. on Fat. of Comp.*, 2006, **28(10)**, 1382-88.
- [5] Toft, H.S., Sorensen, J.D. Reliability-based Design of Wind Turbine Blades. *Structural Safety*, 2011, **33(6)**, 333-342.
- [6] Pohlak, M., Majak, J., Küttner, R. Multicriteria Optimization of Large Composite Parts. *Composite Structures*, 2010, **92**, 2146-152.
- [7] Kers, J., Majak, J. Modeling a New Composite From a Recycled GFRP. *Mechanics of Composite Materials*, 2008, **44(6)**, 623 - 632.
- [8] Chen, C.P., Kam, T.Y. Failure Analysis of Small Composite Sandwich Turbine Subjected to Extreme Wind Load. *The Proc. of the 20<sup>th</sup> East Asia-Pacific Conf. on Str. Eng. and Const.*, 2011, **14**, 1973-981.
- [9] Yanbin, C., Lei, S., Feng, Z. Modal Analysis of Wind Turbine Blade Made of Composite Laminated Parts. *Pow. and En. Eng. Conf., 2010 Asia-Pacific*, 2010, 1-4.
- [10] ANSYS, Inc. *ANSYS 14.0, Manual*, 2011
- [11] Herranen, H., Pabut, O., Eerme, M., Majak, J., Kers, J., Saarna, M., Allikas, G., Aruniit, A. Design and Testing of Sandwich Structures with Different Core Materials. *Jour. of Mat. Scn. of Kaun. Un. Of Tech*, 2011, **17(3)**, 276-281.

## 8. ADDITIONAL DATA ABOUT AUTHORS

MSc. Ott Pabut  
TUT, Department of Machinery  
Ehitajate tee 5, 19086 Tallinn, Estonia  
Phone: 372+51 644 57,  
E-mail: [ottpabut@hotmail.com](mailto:ottpabut@hotmail.com)  
<http://www.ttu.ee>

## DYNAMICS OF GRAVITY FEEDER FOR PRISMATIC WORKPIECES

Polukoshko, S.; Gonca, V.

**Abstract:** *Feeders are mechanisms of the single-piece feeding for the forced moving of the oriented workpieces. In this work the vertical gravity-impact feeder for moving of the prismatic or plane details is presented. The parts move on inclined guiding plates, free fall and collide with the down plates, the impact phenomena may be used both for decreasing of velocity and for the orientation of the tracking work pieces (lateral reversing). System of equations of plane motion of detail, including stages of sliding on the slope guideway, free flight, impact and motion to the next guideway, are written down. System of equations is solved numerically with help of MathCAD program.*

*Key words: forced motion, oblique impact, dry friction, unilateral constraint.*

### 1. INTRODUCTION

Widely used types of technological transport are various kind conveyors, descents, bunkers, feeders. Feeders are a various kind of loading - unloading devices which serves for parts giving in the focused position on the conveyors, or to the processing equipment [1], [2], [3]. In this paper the vertical mechanical feeder with gravitational method of transportation is considered; devices of this kind serve for transportation of light workpieces with small speed of sliding (Fig. 1). The impact phenomenon can be used in feeders both for decreasing of speed of transported details, and for their orientation – turn by the opposite side. The feeder represents a vertical tray with plates attached to walls;

the angle of plate slope to horizon can be regulated (adjusted). The part begins motion on a plate surface when the plate angle of slope to horizon becomes more than angle of a friction. For proper orientation of the parts the guide groove is made in a plate, so part motion on a plate is considered to be plane.

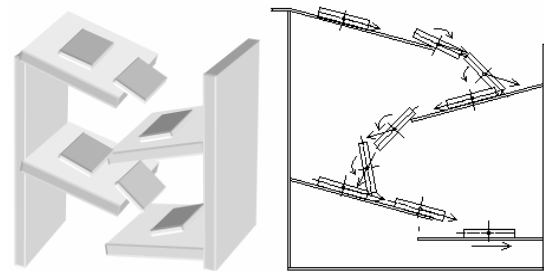


Fig. 1. Model of a gravitational feeder and the scheme of part motion

The part slides on an inclined plate, freely falls on the downstream plate, during the impact with down plate part can change position, turning (upside down) over an underside. The number of plates depends on height to which it is necessary to transfer details, the inclination of plates and distance between them depends on allowable velocity of parts motion and necessity to turn a part. The scheme of movement of flat section of a detail on the guide is shown in Fig.1.

### 2. ANALYTICAL MODEL

Workpieces, moving on the feeder plate, is considered as perfectly rigid body which motion is interrupted by collisions with surface of fixed perfectly rigid plate. Such problems concern the section of mechanics

studying dynamics of systems with unilateral constraints [4], [5], [6], [7]. The most actual here is modelling and the analysis of the impact phenomenon [8], [5], [19]. In this work impact is modelled as perfectly rigid body impact; the classical theory of impact in a combination with Rauss hypothesis is used for the solution, taking into account a friction at impact in accordance with the Coulomb law. For impact parameters obtaining the general equations of dynamics are drawn up, and the time of impact is divided into two phases –at the end of the first phase normal velocity of contact point of a body is equal to zero, this gives the additional equation for definition of unknown parameters. For the description of the collision process the impact impulse is used. Total impulses of normal reaction in the first and second phases are connected by relation:  $S_{IIN} = RS_{IN}$ , where  $R$  is coefficient of restitution; total impulses of friction forces at sliding are  $S_{IF} = -fS_{IN}$ ,  $S_{IIF} = -fS_{IIN}$ , where  $f$  is friction factor. As it is shown in [8] at plane impact of a body against a fixed obstacle, depending on initial conditions of impact and inertial properties of a body there can be seven qualitatively different cases of impact: 1) full sliding of a body in one direction, generated by pre-impact body motion; 2) the same, generated by pre-impact a body location; 3) non-sliding in a contact point; 4) full sliding at first in one, and then in an opposite direction with a backspacing in the second phase of impact; 5) the same, with a backspacing in the first phase of impact; 6) the sliding termination in the second phase of blow; 7) the same, in the first phase of blow. The second and third cases of impact occur when the contact point has only normal to a surface of impact velocity, that in this case of parts motion is excluded. Impact is considered as perfectly inelastic, i.e. coefficient of restitution  $R=0$ , so the fourth and sixth cases of impact are also not considered. In this work the equations of dynamics for cases 1, 5, 7 of impact are taken as in [8] and do not cited here.

### 3. DYNAMICS EQUATIONS

When body moves on feeder guide plates five stages of motion are differed:

1) Sliding on an inclined plane – translatory motion, 2) planar motion – sliding with rotation in the presence of unilateral constraint, 3) free motion of a body under gravity, 4) collision with an inclined plane, 5) planar motion – sliding with rotation till contact with a plane. Peculiar feature of writing of the equations of dynamics and definition of parameters of movement in is using own coordinates system for each stage of motion, drawing up the formulas of coordinates transform and projection components of velocities transformation from one system into another. Final values of parameters of motion at each stage are initial one in new system of coordinates for a following stage of motion.

1) Translation motion - sliding on an inclined plane (Fig. 2).

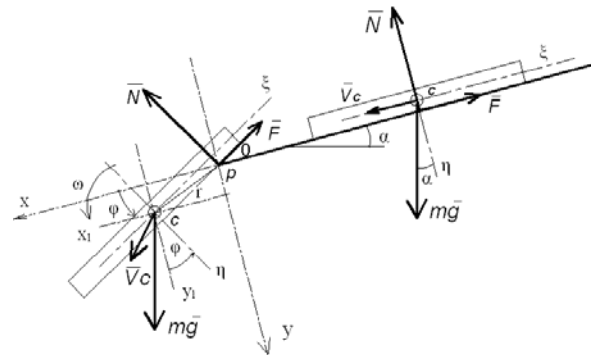


Fig.2. the first and the second stages of motion

Coordinate – an axis  $x$ , the equation of motion at the first stage at continuous movement:

$$\ddot{x}_c = g(\sin(\alpha) - f \cos(\alpha)), \quad (1)$$

velocity and time:

$$v = \sqrt{2gL(\sin(\alpha) - f \cos(\alpha))},$$

$$T = \sqrt{\frac{2L}{g(\sin(\alpha) - f \cos(\alpha))}},$$

where  $\alpha$  – a plane slope angle to horizon,  $c$  – mass centre of a body,  $f$  – friction factor (rest and sliding are provided identical).

2) Planar motion - rotation round point P with sliding till separation from surface (fig. 2). Constraint in a point of contact P of a part and a plate is unilateral; reaction force in a contact point is subject to the law of a dry friction, i.e. the Coulomb law:

$$F = -fN \frac{v_p}{|v_p|} \text{ at } v_p \neq 0,$$

$$|F| \leq fN \text{ at } v_p = 0, N \geq 0$$

$N$  - normal force of reaction,  $F$  - tangent force of reaction.

Coordinates systems (Fig. 2):  $xoy$  - fixed rectangular Cartesian coordinates system, the origin of coordinates - plate edge,  $x_1cy_1$  - passing through the mass centre Cartesian system of the coordinates parallel  $xoy$ ,  $\xi c\eta$  - the rectangular system of coordinates rigidly connected with a body, polar coordinates:  $r$ -radius vector, from point P to point  $c$ , and  $\varphi$  - rotation angle of a body,

$$r = r(t), \varphi = \varphi(t),$$

$$x = r \cos(\varphi), y = r \sin(\varphi).$$

The equations of motion:

$$\begin{cases} r\ddot{\varphi} + 2\dot{r}\dot{\varphi} = -\frac{N}{m} + g \cos(\alpha + \varphi) \\ \ddot{r} - r\dot{\varphi}^2 = -\frac{F}{m} + g \sin(\alpha + \varphi) \\ J\ddot{\varphi} = Nr \end{cases} \quad (2)$$

Angular velocity and angular acceleration of a body:

$$\dot{\varphi} = \omega, \ddot{\varphi} = \varepsilon,$$

radial and tangential velocities of the mass centre:

$$v_{cr} = \dot{r}, v_{c\varphi} = r\dot{\varphi}.$$

Initial conditions of the second stage:

$$\omega_0 = 0, v_0 = v_r = v, r_0 = 0, \varphi_0 = 0,$$

$$N_0 = mg \cos(\alpha),$$

final parameters of the second stage:

$$\omega_1, \varphi_1, r_1, \dot{r}_1.$$

The end of stage - equality to zero of normal reaction  $N_1 \leq 0$ , or equality of mass center coordinate to the distance from the mass center to detail edge  $r_1 = a/2$ .

Initial conditions of the third stage:

$$x_{c0} = r_1 \cos(\varphi_1), y_{c0} = r_1 \sin(\varphi_1),$$

$$\omega_0 = \omega_1,$$

$$\dot{x}_{c0} = \dot{r}_1 \cos(\varphi_1) - r_1 \dot{\varphi}_1 \sin(\varphi_1),$$

$$\dot{y}_{c0} = \dot{r}_1 \sin(\varphi_1) - r_1 \dot{\varphi}_1 \cos(\varphi_1).$$

3) Free movement of a body in the field of gravity (Fig. 3).

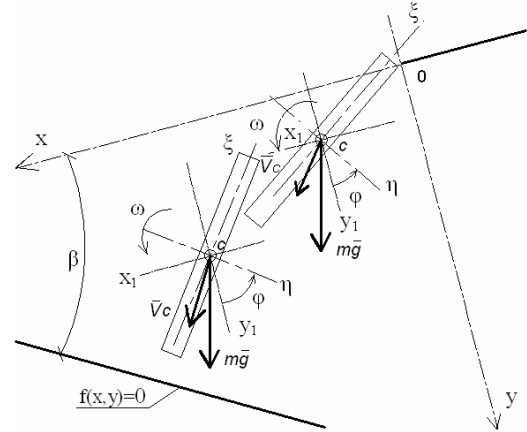


Fig.3. The third stage of motion of body

Cartesian coordinates  $xoy$  are used:

$$\begin{cases} \ddot{x}_c = g \sin(\alpha) \\ \ddot{y}_c = g \cos(\alpha) \\ J\ddot{\varphi} = 0 \end{cases} \quad (3)$$

The equation of the lower plate in coordinates  $xoy$ :  $f(x,y)=0$ , or in the intercept form of the equation of a straight line:

$$\frac{x}{d} + \frac{y}{b} = 1,$$

where  $d$  and  $b$  - the intercepts, cut by the lower plate on axes  $x$  and  $y$ .

Coordinates of a point of collision  $K$ :

$$x_K = x_c + \frac{a}{2} \cos(\varphi), y_K = y_c + \frac{a}{2} \sin(\varphi).$$

Definition of a point of impact and the impact moment - fulfilling of a condition of unilateral constraint:

$$\frac{x_K}{d} + \frac{y_K}{b} \geq 1.$$

Normal and tangent to a plane velocity of contact point at the beginning of impact:

$$\dot{x}_K = \dot{x}_c - \omega_1 \frac{a}{2} \sin(\varphi),$$

$$\dot{y}_K = \dot{y}_c + \omega_1 \frac{a}{2} \cos(\varphi), \omega_1 = \omega_0,$$

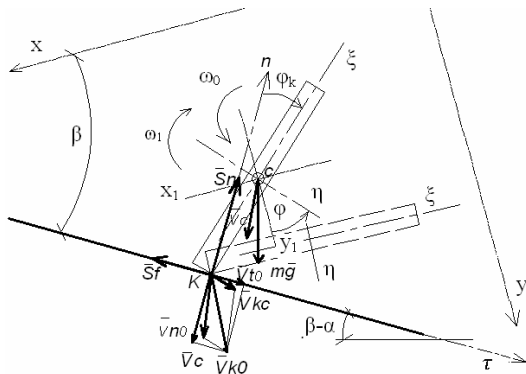
$$v_{Kn} = \dot{x}_K \sin(\beta) + \dot{y}_K \cos(\beta),$$

$$v_{Kt} = -\dot{x}_K \cos(\beta) + \dot{y}_K \sin(\beta),$$

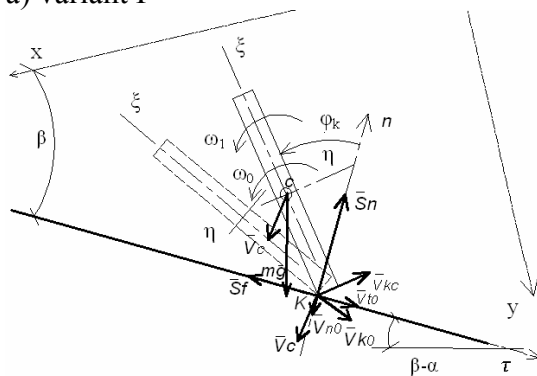
$$v_{Kn} = \dot{x}_c \sin(\beta) + \dot{y}_c \cos(\beta) + \omega_1 \frac{a}{2} \cos(\alpha + \beta)$$

$$v_{Kt} = -\dot{x}_c \cos(\beta) + \dot{y}_c \sin(\beta) + \omega_1 \frac{a}{2} \sin(\alpha + \beta)$$

4) Body impact about the fixed surface of the lower plate (fig. 4), coordinates - a normal and a tangent to a plate, the beginning of coordinates – in a point of collision K:  $nK\tau$ , coordinates of a body during blow don't change, post-impact velocities are defined from the general equations of dynamics for impact [8].



a) variant I



b) variant II

Fig.4. The fourth and fifth stages of motion

The angle between direction of axis  $\xi$  of plates and a normal to a plate:

$$\varphi_K = \beta + \varphi - \frac{\pi}{2}.$$

Angle between a direction of pre-impact velocity and a normal to a plate:

$$\theta = \arctan\left(\frac{v_{Kt}}{v_{Kn}}\right).$$

5) Post-impact motion (Fig. 4) – plane motion with sliding on a plate without

separation under condition of perfectly nonelastic impact. Movement of a body after impact is described by the differential equations in a projection to axes  $\tau$  and  $n$ , with the initial conditions received at the previous stage of calculation – angular velocity, mass center velocity and dynamic reaction in the collision point.

#### 4. NUMERICAL EXAMPLES

The example of the numerical solution of this problem for parts transportation on two guide plates is resulted bellow. Part has following parameters: mass  $m=0.3$  kg, length of 0.1 m, the moment of inertia in respect to an axis passing through the mass centre  $J_c = 2.5 \cdot 10^{-4}$  kgm<sup>2</sup>. Two variants of part motion are considered – feed-moving from one plate to another without turning of a part and feed-moving with reversing. For this purpose different ways of plates locations are used:

1) in the first variant following parameters are accepted: angles of guide plate inclination  $\alpha = 15^\circ$ ,  $\beta = 30^\circ$ , the equation of a surface of the lower plate in axes  $xy$ , passing through the edge of first the plates:

$$\frac{x}{0.347} + \frac{y}{0.2} = 1.$$

2) in the second variant angles of slope of the upper and lower guide plates are  $\alpha = 10^\circ$ ,  $\beta = 35^\circ$ , the equation of a surface of the lower plate in axes  $xy$ :

$$\frac{x}{0.428} + \frac{y}{0.3} = 1.$$

The sliding friction and statical friction factor are assumed identical and equal  $f=0.15$ , coefficient of restitution of normal reaction in impact point is accepted zero.

Part movement begins with continuous sliding on the top plate, calculation is executed in program MathCAD, and calculation results are presented in table 1.

As it is shown in table, in the first case angular velocity changes a sign after impact, the velocity of body in contact with surface point, also changes a sign, after impact the body lies down on a plate by the same side; in the second case the velocities



don't change the direction, and after impact the body lies down on a plate by reverse side.

Parameter	unit	case 1	case 2
		$\alpha=15^\circ$ $\beta=30^\circ$	$\alpha=10^\circ$ $\beta=35^\circ$
The first stage -slipping			
$t$	$s$	0.423	0.887
$v_0$	$m/s$	0.473	0.226
The second stage – plane motion till release			
$r_0$	$m$	0	0
$\varphi_0$	$rad$	0	0
$v_{r0}$	$m/s$	0.473	0.226
$v_{\varphi 0}$	$m/s$	0	0
$\omega_0$	$s^{-1}$	0	0
$t$	$s$	0.879	1.169
$r$	$m$	0.5	0.35
$\varphi$	$deg$	$15.18^\circ$	$45.15^\circ$
$v_{r1}$	$m/s$	0.746	0.527
$v_{\varphi 1}$	$m/s$	0.271	0.269
$\omega_1$	$s^{-1}$	5.490	7.637
The third stage – free plane motion			
$x_{c0}$	$m$	0.049	0.032
$y_{c0}$	$m$	0.012	0.015
$v_{xc0}$	$m/s$	0.653	0.363
$v_{yc0}$	$m/s$	0.461	0.467
$\omega_0$	$s^{-1}$	5.490	7.637
$t$	$s$	0.821	1.417
$x_{c1}$	$m$	0.111	0.101
$y_{c1}$	$m$	0.082	0.178
$\varphi_1$	$deg$	$41.02^\circ$	$87.15^\circ$
$v_{xc1}$	$m/s$	0.862	0.605
$v_{yc1}$	$m/s$	1.239	1.837
The fourth stage – collision with an inclined plane- impact			
$\varphi_K$	$deg$	$18.97^\circ$	$32.14^\circ$
$\tau_{c0}$	$m$	0,016	-0.027
$n_{c0}$	$m$	0,047	0.042
$v_{cr0}$	$m/s$	-0.127	0.558
$v_{cn0}$	$m/s$	-1.504	-1.852
$v_{K\tau 0}$	$m/s$	0.133	0.881
$v_{Kn0}$	$m/s$	-1.593	-1.649
<b>impact type</b>		5	1
$v_{cr1}$	$m/s$	0.043	0.408
$v_{cn1}$	$m/s$	-0,188	-0.851
$\omega_1$	$s^{-1}$	-11.722	31.972

$v_{K\tau 1}$	$m/s$	-0,508	0.408
$v_{Kn1}$	$m/s$	0	0
The fifth stage – planar motion before contact with plane			
$t$	$s$	0.868	0.031
$\omega_1$	$s^{-1}$	-18.837	34.50
$v_{cr1}$	$m/s$	0.284	0.527
$v_{cn1}$	$m/s$	-0.876	-1.072

Table 1. The parameters of the body motion along the feeder guide plates

Plots of dependence of some parameters of motion from time for the first variant are shown in Fig. 5-7

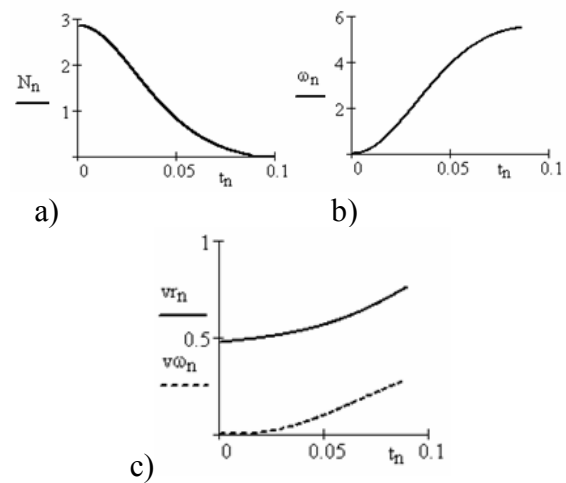


Fig.5. Motion in the second stage. Plots of dependence on time: a)  $N=N(t)$ , b)  $\omega=\omega(t)$  c)  $v_{cr}=v_{cr}(t)$  and  $v_{c\omega}=v_{c\omega}(t)$

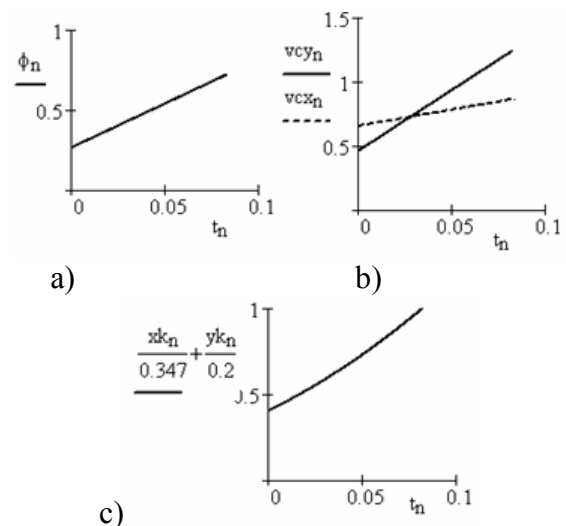


Fig. 6. Motion in the third stage. Plots of dependence on time: a)  $\varphi=\varphi(t)$ , b)  $v_{xc}=v_{xc}(t)$ ,  $v_{yc}=v_{yc}(t)$ , c) constraint function  $x_k/0.347+y_k/0.2=1$

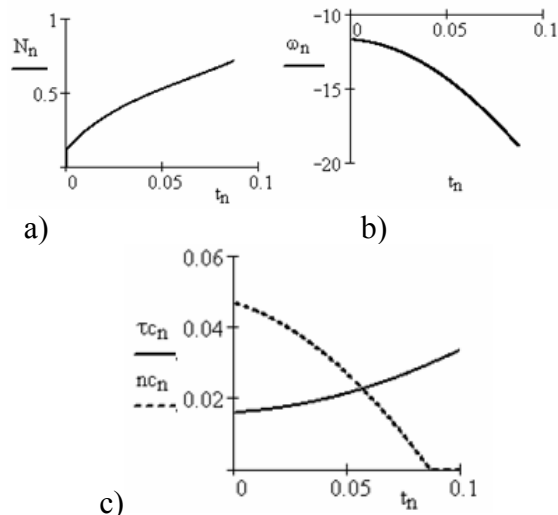


Fig. 7. Motion in the fifth stage. Plots of dependence on time: a)  $N=N(t)$ , b)  $\omega=\omega(t)$  c)  $\tau_c=\tau_c(t)$ ,  $n_c=n_c(t)$

## 5. CONCLUSION

In this paper the the variant of gravity-operated feeder is presented and dynamics of workpieces motion in this device is investigated. The dynamic equations are written down for each stage of motion with using eigensystem of coordinates for every type of motion and development of formulas for coordinates conversion and velocity projections transform from one coordinate system into another. The conditions of turning of part as a result of its collision with rigid guide plate are found: in order to a body turned over it is necessary, that angular speed must not change a direction after impact and, in addition, to be sufficient for body rotation in necessary direction. At inclination of plate from left to right downward, positive initial angular velocity and positive initial angle between surface normal and part  $\varphi_k$  - greater, than inclination angle of plate to horizon - angular velocity after impact remains positive and perfectly inelastic impact will be of the 1-st type (with complete sliding in one direction to the right downward); a negative initial angle between normal to the surface and a part results in reversing of rotation, here perfectly inelastic impact occurs of the 5-th type (with the complete sliding and

changing of sliding direction). The changing of this angle is possible by the increase of angular velocity of free motion or by increasing of time of free motion. There is a parameters domain of initial angle ( $0 \leq \varphi_k \leq \beta - \alpha$ ), in which the impact may be 7-th type with stopping of sliding and angular velocity reversing. The numeral examples of workpiece motion are given; equations of motion are solved with help of MATHCAD program.

## 6. REFERENCES

1. Akella S., Huang W., Lynch K. and Mason M. Parts feeding on a conveyor with a one joint robot. *Algorithmica*, 26(3): 313–344, 2000.
2. Berretty Robert-Paul, Goldberg Ken, Cheung Lawrence, Overmars Mark H., Smith Gordon, van der Stappen A. Frank. Trap Design for Vibratory Bowl Feeders. <http://ford.ieor.berkeley.edu/~goldberg/pubs/pdf/trap.pdf>.
3. Moll M., Erdmann M. A., Fearing R., Goldberg. Orienting Micro-Scale Parts with Squeeze and Roll Primitives. <http://www.ieor.berkeley.edu/~goldberg/pubs/moll-micromanip.pdf>
4. Deriabin M.V., Kozlov V.V. On the theory of systems with unilateral constraints. *App. Math. and Mech.*, 1995, V.59, 4, 531-539.
5. Ivanov A.P. *Dynamics of system with mechanical collision*. IPE, Moscow, 1997. (in Russian)
6. Markeev, A. P. Dynamics of a rigid body that collides with a rigid surface. *Nonlinear dynamics*, 2008, V.4, 1, 1-38.
7. Rozenblat G.M. On motion without separation of solid on a plane. *Reports of Rus.Acad.of Sc.* 2007, v.416, 5, 622-624.
8. Viba J.A. *Optimisation and synthesis of vibro-impact machines*. Zinatne, Riga, 1988. (in Russian)
9. Lapshin V.V., A body plane collision with a rough surface. *Inst.App.Math.*, [http://www.keldysh.ru/papers/2001/prep10/prep2001\\_10.html](http://www.keldysh.ru/papers/2001/prep10/prep2001_10.html)

## **ADDITIONAL DATA ABOUT AUTHORS**

Polukoshko, S.; Gonca, V.  
Dynamic of gravity feeder for prismatic  
workpieces

Svetlana Polukoshko, leading researcher,  
Dr. Sc.ing. Engineering Research Institute  
“VSRC”, Ventspils University College  
Address: 101a Inzenieru Street, Ventspils,  
LV-3601, Latvia, Fax +37163629600  
Phone: +371-29294968  
<http://www.venta.lv/>  
E-mail: [pol.svet@inbox.lv](mailto:pol.svet@inbox.lv)

Vladimirs Gonca, professor, Dr. sc .ing.  
Riga Technical University, Institute of  
Mechanics, Address: 6 Ezermalas Street,  
Riga, LV-1006, Latvia,  
Phone: +371-29274953  
<http://www.rtu.lv/>  
E-mail: [vladimirs.gonca@rtu.lv](mailto:vladimirs.gonca@rtu.lv)

Corresponding Author:  
Svetlana Polukoshko  
E-mail: [pol.svet@inbox.lv](mailto:pol.svet@inbox.lv)

## ON UNITARY RHEOLOGICAL APPROACH OF VIBRATION ISOLATION PASSIVE DEVICES

Potirniche, A.; Nastac, S.; Leopa, A.; Debeleac, C. & Capatana, G.

**Abstract:** *This paper deals with advanced simulation methods of passive devices intended for vibration isolation of different dynamic sensitive technical systems. This study supposes an elastomeric material used for isolator core. Various rheological models are used to simulate the overall behaviour of the vibration isolator under different dynamic loads. A finite element method provide better tool with the main condition that suppose an appropriate constitutive law for base material. The authors propose and underlie a unitary rheological model useful both for lumped, and for continuous mass computational models. The main advantage of this model results from the easiness of simulation of different basic rheological behaviors for a single serviceable implementation. It is provided both individual and comparative survey of various dynamical situations.*  
*Key words: vibration, isolation, rheology, performances, computational dynamics.*

### 1. INTRODUCTION

Rheological computational simulation of behaviour of different materials requires dedicated numerical approaches for each single case or category of analysis. During the simulation it is very difficult to significant change the numerical model because of the different constitutive differential equations. Hereby, one model means one application.

The main purpose of this study was to formulate a unitary model which will be able to provide different types of known rheological models behaviour with the help of only a few basic settings.

Thus the model tuning and usage become as simple as the basic characteristics input. The major utilization of this complex new approach frames the area of computational dynamics regarding vibration mitigation and passive isolation of dynamic actions. In order to simulate different cases of shock, vibration and seismic actions against structures the authors was developed a numerical implementation of this model into Matlab set of applications. It had to be mentioned that the entire analysis exclusively treats the elastic model with viscous damping.

### 2. MODEL FORMULATION

Such as a briefly description of this complex model in terms of well known classical rheological formulations this computational approach are based on Voigt-Kelvin model succeeded by a Zenner model, and the entire ensemble installed in derivation with a Maxwell model [1...6].

In Fig.1 could be found the simplified schematic diagram according to the basic representation rules for rheological models. Thus the  $k_i$  suggests the elastic components, while the  $c_i$  means the damping elements. Maxwell type part contains the succession of  $k_1$  and  $c_1$ . Voigt-Kelvin part contains a derivation between  $k_4$  and  $c_4$ . Last part, means Zenner model, contains  $k_2$ ,  $k_3$  and  $c_3$  basic elements.

The notations  $F_{ex}$  and  $x(t)$  on the Fig.1 denotes the external dynamic excitation, respectively the variable independent coordinate (single direction displacement). Main hypothesis of this study supposes a linear behaviour of each element [7...10].

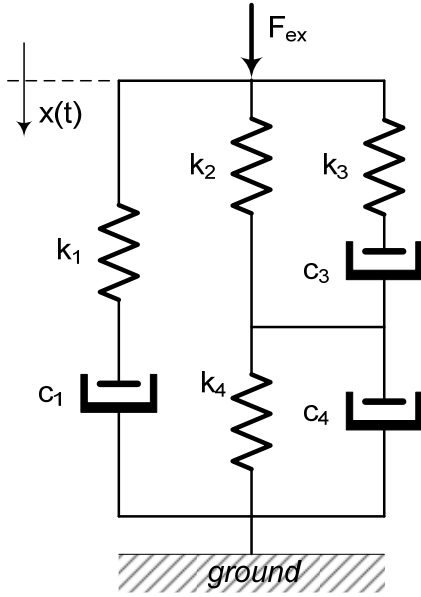


Fig. 1. Complex unitary rheological model with linear viscous and elastic behaviour

Using usual methods results the constitutive differential equation of this model as follows

$$\begin{aligned}
 & F(k_1 k_2 k_3 + k_1 k_3 k_4) + \\
 & \dot{F} \left( k_1 k_3 c_4 + k_1 k_4 c_3 + k_1 k_2 c_3 + \right. \\
 & \quad \left. + k_1 k_3 c_3 + k_3 k_4 c_1 + k_2 k_3 c_1 \right) + \\
 & \ddot{F} \left( k_1 c_3 c_4 + k_3 c_1 c_4 + k_4 c_1 c_3 + \right. \\
 & \quad \left. + k_2 c_1 c_3 + k_3 c_1 c_3 \right) + \\
 & \ddot{F} (c_1 c_3 c_4) = \\
 & x (k_1 k_2 k_3 k_4) + \\
 & \dot{x} \left( k_1 k_3 k_4 c_1 + k_1 k_2 k_3 c_1 + k_1 k_2 k_4 c_3 + \right. \\
 & \quad \left. + k_1 k_3 k_4 c_3 + k_1 k_2 k_3 c_4 + k_2 k_3 k_4 c_1 \right) + \\
 & \ddot{x} \left( k_1 k_3 c_1 c_4 + k_1 k_4 c_1 c_3 + k_1 k_2 c_1 c_3 + \right. \\
 & \quad \left. + k_1 k_3 c_1 c_3 + k_1 k_2 c_3 c_4 + k_1 k_3 c_3 c_4 + \right. \\
 & \quad \left. + k_2 k_4 c_1 c_3 + k_3 k_4 c_1 c_3 + k_2 k_3 c_1 c_4 \right) + \\
 & \ddot{x} (k_1 c_1 c_3 c_4 + k_2 c_1 c_3 c_4 + k_3 c_1 c_3 c_4)
 \end{aligned} \tag{1}$$

where  $F$  denotes the external dynamic excitation and  $x$  is the linear deformation (independent coordinate), both in respect with time  $t$ . Terms grouping in Eqn.(1) was performed according to the derivative order of each variable.

High order derivative terms in Eqn.(1) supply the model capacity to dignify the various and intensive dynamic actions and their structural effects inside the simulated part. Also it enable the dynamic effects

analysis about the entire ensemble base structure - isolator - super structure. Short impulsive actions (like mechanical shocks, detonations, burst actions, etc.) have to be simulated precisely otherwise their high order derivatives become null and the dynamic capacity of the model could be affected.

### 3. COMPUTATIONAL ANALYSIS

The constitutive equation - Eqn.(1) - enables both dynamic and kinematical inputs in order to evaluate the behaviour of the model. Thus if the input forces are known then results displacement response of the system. Also dynamic response can be evaluates for known displacement laws. Classical signals in evaluation of the model responses (e.g. pulse, step, ramp, harmonic, random) can be successfully used taking into account the analytic formulation of constitutive law. Computational approach of model behaviour requires continuous functions because of two main reasons as follows: null division avoidance and realistic simulation.

The authors evaluated a large area of theoretical and computational responses. In this paper two groups of diagrams were presented as follows: phase domain response (see Fig.2) and hysteretic response (see Fig.3).

Each case supposes five types of dynamic inputs (known external forces at input) as follows: (a) unitary input; (b) continuous pulse signal; (c) un-recurrent signal; (d) recurrent signal; (e) harmonic shape excitation. Actually, these signals represent transient or almost harmonic signals, which allow evaluating of quasi-static flowing, weight, step, and harmonic responses.

The input signals for cases (b)...(d) was based on the continuous pulse signal generated with the expression

$$S(t) = A_s \exp \left[ \left( \frac{\delta}{2} - t_0 \right) (t - t_0)^2 \right] \tag{2}$$

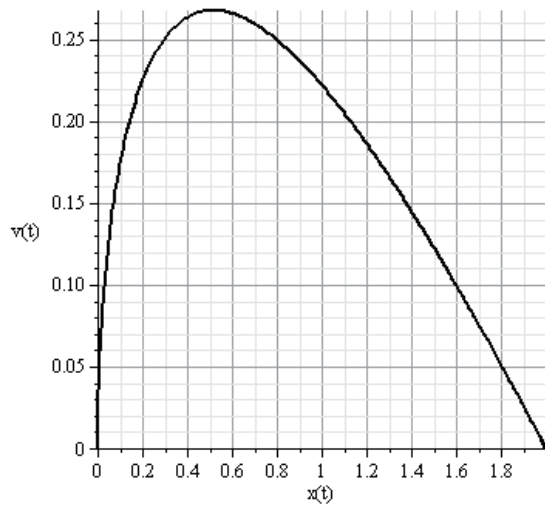
where  $S(t)$  denotes input signal;  $A_s$  is the excitation magnitude;  $\delta$  denotes the total

time period of pulse signal - pulse base time;  $t_0$  is the moment of time for maximum value of step magnitude ( $S = A_s$ ) - pulse central time.

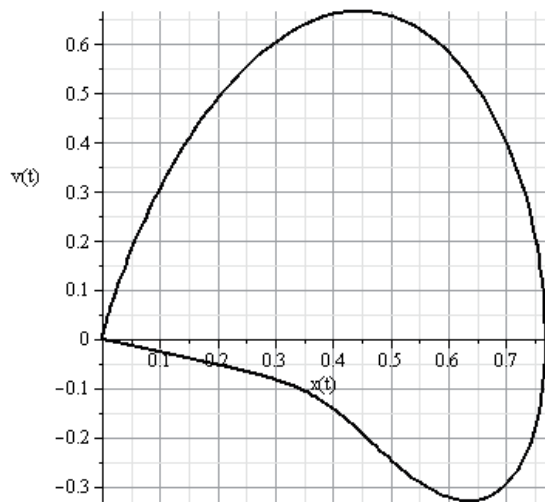
Hereby, the un-recurrent signal (c) means two identical pulse signals with pulse central time having the same value with their base time. This signal can be easily assimilated with a continuous realistic singular step input.

Also, the recurrent signal (d) denotes two identical singular step signals (means un-recurrent signal) which appear delayed between them. Delay time have to be greater than fourfold of pulse base time.

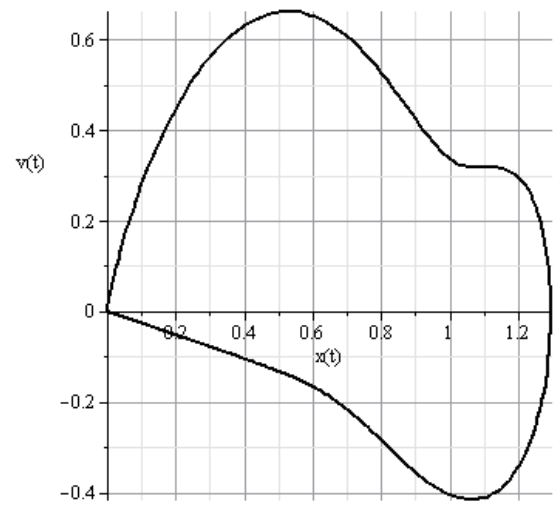
Diagrams depicted in Fig.2 show the displacement versus velocity phase domain response in respect with the five types of inputs previously presented.



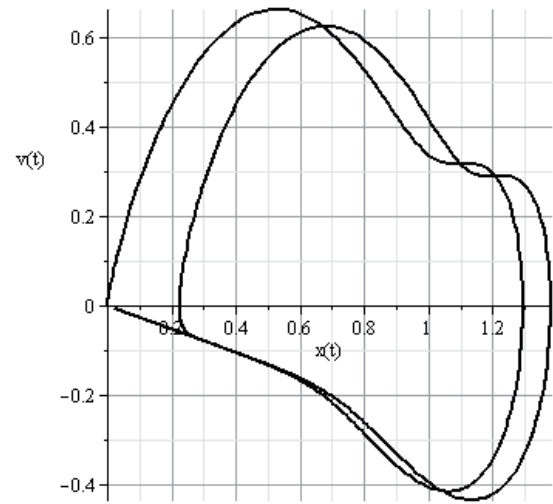
(a)



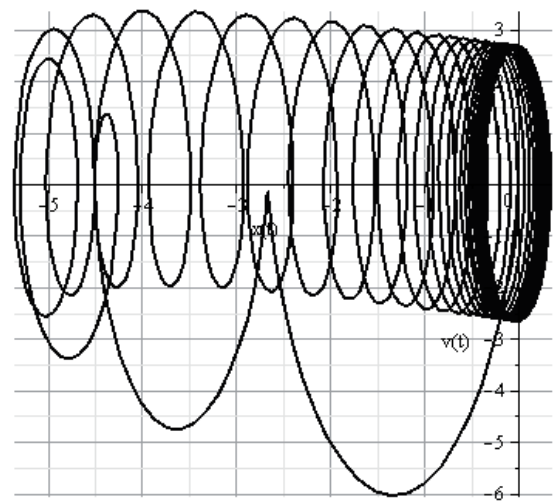
(b)



(c)

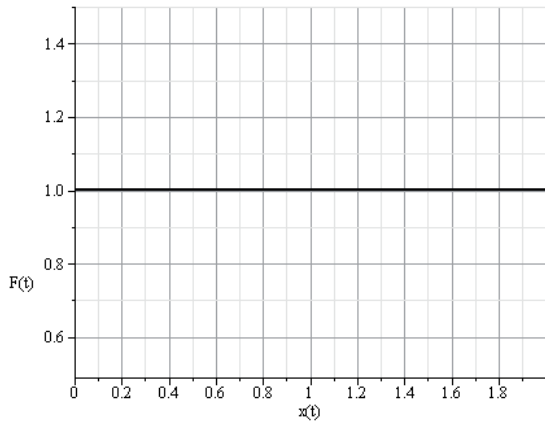


(d)

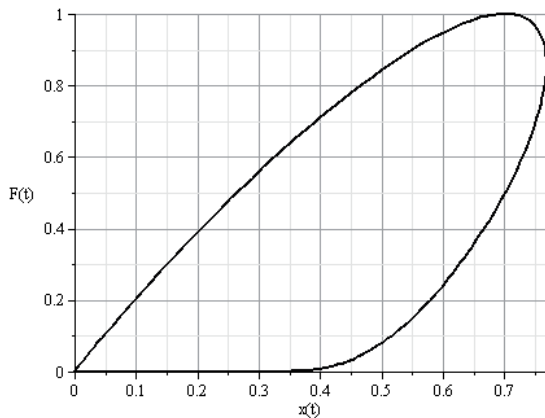


(e)

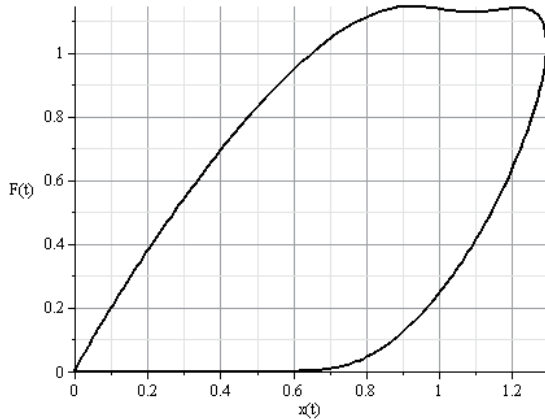
Fig. 2. Displacement vs. velocity response diagrams. Graphs contain relative units. (see text for details)



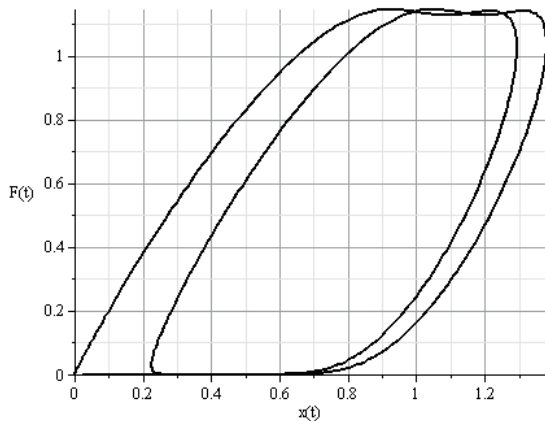
(a)



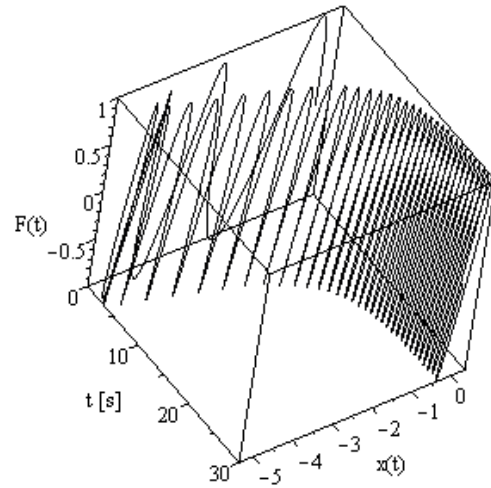
(b)



(c)



(d)



(e)

Fig. 3. Force vs. displacement response diagrams. Graphs contain relative units. (see text for details)

Likewise with the same inputs and characteristic parameters it was obtained force versus displacement diagrams presented in Fig.3.

Qualitative analysis of the results reveals a stabilized evolution for every transient input. Also, for an almost harmonic excitation the system provides a shortly transient state followed by a stabilized regime during the analysis time until stop. Quasi-static flowing regime under constant external excitation put into the evidence a regular evolution towards a final stable state.

It had to be mentioned that computational analysis on numerical models were performed in respect with unitary values of the characteristic parameters in order to produce a qualitative point-of-view about model capability.

#### 4. CONCLUSION

Concluding remarks of this analysis frames and justify the initial hypothesis according to this unitary numerical model is able to assure a great flexibility and high robustness in simulation of the large domain of classical linear rheological models in respect with elastic and viscous behaviour. Qualitative studies briefly presented in this paper reveal a good



stability under different types of inputs, besides enough convergence to obtain each time the final solution.

Future researches will regard the non-linear characteristics including both elastic and viscous components. Main applications on mechanical vibration and shock protective technical solution analysis will be primary taken into account and a harmonization between numerical model and instrumental data will be the next real step to finalize this research.

## 5. REFERENCES

- [1] Bratu, P. *Elastic Structures Analysis. Behaviour under Static and Dynamic Actions*, Impuls Publishing House, 2011.
- [2] Bratu, P. *Theoretical Mechanics*, Impuls Publishing House, 2006.
- [3] Bratu P. *Structural requirements imposed to vibration systems*, Intl. Journal of Acoustics and Vibration, **5**, 2, 2001.
- [4] Bratu, P. Méthodes expérimentales pour la détermination des caractéristiques élastiques et dissipatives aus systèmes antivibratiles en caoutchouc, *The Proceedings of the International Conference on the Theory of Machines and Mechanisms*, 137–139, Liberec, Czech Republic, Aug. 31 – Sept. 2, 2004.
- [5] Kihong Shin, Joseph K. Hammond, *Fundamentals of Signal Processing for Sound and Vibration Engineers*, John Wiley & Sons, Ltd, 2008.
- [6] Bendat, J. S. and Piersol, A. G., *Random Data: Analysis and Measurement Procedures*, Third Edition, Wiley-Interscience, 2000.
- [7] Howard B. Wilson, Louis H. Turcotte, David Halpern, *Advanced Mathematics and Mechanics Applications Using Matlab*, CHAPMAN & HALL/CRC, A CRC Press Company, 2003.
- [8] Etienne Balmes, Jean-Michel Leclere, *Viscoelastic Vibration Toolbox For Use*

with MATLAB, User's Guide Version 1.0, 2004.

[9] Piersol, A.G., Paez, T.L. *Harris' Shock and Vibration Handbook*, Sixth Edition, The McGraw-Hill Companies, 2010.

[10] Nastac, S. Theoretical and experimental researches regarding the dynamic behavior of the passive vibration isolation of systems, Chapter 9 in *Research Trends in Mechanics*, vol. II, Eds.: Dinel P., Chiroiu V., Toma I., Ed. Academiei Romane, 2008, pp. 234-262.

## 6. ADDITIONAL DATA

Corresponding author:

*Silviu NASTAC*

"Dunarea de Jos" University of Galati  
Engineering Faculty in Braila  
Complex Measurements and Virtual  
Instrumentation Laboratory  
Calea Calarasilor 29,  
810017 Braila  
Romania  
email: snastac@ugal.ro

Authors:

*Aurora POTIRNICHE*

*Adrian LEOPA*

*Carmen DEBELEAC*

*Gigel CAPATANA*

"Dunarea de Jos" University of Galati  
Engineering Faculty in Braila  
Research Center for Mechanics of  
Machines and Technological Equipments  
Calea Calarasilor 29,  
810017 Braila  
Romania

emails:

apotirniche@ugal.ro

adrian.leopa@ugal.ro

cbordea@ugal.ro

gcapatana@ugal.ro

## INVESTIGATION OF THE MEMBRANES PERMEABILITY OF THE FLOW CONTROL DEVICE BASED ON PIEZO ACTUATOR

Rimašauskas, M.; Rimašauskienė, R.

**Abstract:** *Piezoelectric actuators are simple design, small size, and relatively low cost elements, suitable for precision positioning systems. Therefore, actuators of such type were chosen for the design of the flow control device.*

*Flow control membrane of the device consists of two plates with micro pores or notches. One of the plates, depending on the type of the actuator, may carry out a rotary motion. While moving, membrane plates with notches or formed micro pores create a Moiré pattern between them, which depends on the flow throughput parameters.*

*Adjusting piezoelectric actuator's position and the Moiré effect resulted between the membranes, it was created a quick, accurate, and relatively inexpensive flow control device.*

*The created flow control device with piezoelectric actuators and Moiré geometric effect is used in gas, liquid, and light flow control systems, and is characterized by its throughput and precision. Such devices are simple and are suitable particularly for precise dosing of flows. The design of the flow control device is patented protected.*

*Key words: flow control, piezo actuator.*

### 1. INTRODUCTION

The piezoelectric and moiré effects were noticed in the end of the 19<sup>th</sup> century. Over the time, manufacturing technologies of piezoelectric elements advanced and new areas of moiré effect implementation were discovered; they were increasingly introduced in various fields [1, 2].

Literature analysis revealed, that piezoelectric actuators have been used in flow control devices of various structures for a long time [3, 4], but the information about the use of moiré effect in equipment of such type is limited.

Moiré effect is an interference pattern created, for example, between two grids that overlay on each other at a certain angle, or have slightly different mesh sizes. It is an interaction of two rasters. Exposed to the light, the unit transmits or reflects it in this time forming bright and dark areas – moiré pattern [5]. Natural and technological Moiré patterns are observed in various environments [6, 7]. They can be made of light, sound, or other types of waves.

The category of flow control and transmission devices covers a range of products designed for facilitating flow management: carrying measurements, fixing parameters of a stream flowing through pipes or hoses, etc.. They can be used for light, gas, liquid, or semi-solid materials. Flow control and transmission devices can be divided into the following groups: valves, valve acting as flow positioning systems, dispensers, and others. This article analyses high-speed flow control systems based on piezoelectric actuators and moiré interference principles. Moiré effect is created in a flow control membrane between two plates with micro pores or notches. It needs to rotate at a certain angle or to move only one of the plates and moiré pattern changes. In such a way the flow closes, opens, or obtains intermediary positions.

Destination of a piezoelectric actuator in a flow control device is to convert electric power to mechanical energy (by movement or turning). Its operational characteristics (speed and accuracy) influence rotation or movement of membrane plates. As it is known, characteristics of piezoelectric actuators are suitable of the use in micro flow control devices, since they enable getting high speed and resolution, and offer great variety of sizes and relatively low price [8-10].

## 2. SELECTION OF THE PIEZO ACTUATORS

To generate a rotary movement in a membrane of a flow control device many types of the piezoelectric actuators can be used. However, most technological constructions are made using ring or cylindrical piezoceramic elements. Actuators of such shapes produce the lowest number of units, thus generating maximum speed of the flow control and obtaining nanometer scale resolution at the lowest cost of the device. The excitation of one of the electrode sectors of cylinder or ring-shaped actuator generates a linear motion. Dividing electrodes to a larger number of segments and using multiphase excitation allows awakening of traveling wave and getting rotating movement of the ring in contact the output link.

Traveling wave motors work on a basis of frictional interaction of flexural or surface acoustic waves of piezoceramic input link with a driven element, since propagating waves produce elliptical trajectories of input link's surface points [11, 12].

When closed piezoelectric ring is driven at one point at a frequency corresponding to the resonance of this ring, it excites a standing wave only, since vibrations propagate in both directions, symmetrically to the vibration source, and interfere with each other. When two vibration sources are installed on the ring, traveling waves can be obtained by superimposing these waves. Using this superposition principle, we can

generate a traveling wave with a shape corresponding to the standing wave's shape.

The n-th mode of an elastic ring is expressed as:

$$u_s(\varphi, t) = A \cos(k\varphi) \cos(\omega t) \quad (1)$$

while propagating wave is expressed as:

$$u_p(\varphi, t) = A \cos(k\varphi - \omega t) \quad (2)$$

Using a trigonometric relation, equation (2) can be transformed to:

$$u_p(\varphi, t) = A \cos(k\varphi) \cos(\omega t) + A \cos\left(k\varphi - \frac{\omega}{2}\right) \cdot \cos\left(\omega t - \frac{\omega}{2}\right) \quad (3)$$

In this way, a traveling wave can be generated by superimposing two standing waves, whose phases differ by 90 degrees from each other. Generally, the phase difference can be chosen arbitrarily (except 0,  $-\pi$  and  $\pi$ ).

As a flow control device having a single degree of freedom (which can perform a rotating motion) cylindrical piezoelectric actuator was selected and investigated experimentally. It is easy to choose actuators suitable for different constructions, since the variety of them is sufficiently large. Monolithic piezoceramic cylinder has unique characteristics; they can work in a super high vacuum (130 nPa and fewer); depolarization temperature occurs at 500 V voltage in the first working cycle. Depending on the location of electrodes on a piezoceramic cylinder, it can create radial, longitudinal, bending, and travelling wave type vibrations in the output link.

Inner and outer surfaces of the monolithic piezoceramic cylinder are coated with a layer of silver. In case, when voltage is connected to inner and outer elements of a piezoelectric actuator with thin walls, it works in radial or longitudinal vibration mode.

Cylindrical piezoelectric actuator's inner and outer surfaces are covered with silver

and divided into three segments, two of 90° and one 180°. Inner and outer opposing electrodes (180°) are connected to each other; other two electrodes (90°) are connected to the opposite two; and the condenser is connected between them (Fig. 1). Thus, combining piezoelectric cylindrical electrodes formed asymmetrical output unit with travelling wave type oscillations.

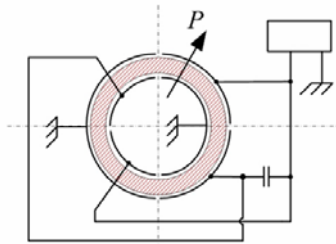


Fig. 1. Connection scheme

Moving the second phase of the harmonics 180° or the first 90° to each other can generate a reverse actuator output.

Traveling wave oscillations are obtained connecting respective electrodes to a multiphase signal generator. If one of the active components of the connector is a hollow of cylindrical shape, then traveling wave is expressed as follows:

$$R = R_0 [1 + \zeta \sin(n_1 \varphi - \lambda t)] \quad (4)$$

where  $\zeta$  - relative amplitude of vibrations;  $n_1$  - wave number, and  $\varphi$  - angular coordinate of available cross-section. In this case, tangential  $\varepsilon_t$  and radial  $\varepsilon_r$  - points on the neutral surface of sphere displacements - are related in such a way:

$$\frac{d\varepsilon_t}{dt} = -\frac{\varepsilon_r d\varphi}{dt} \quad (5)$$

where  $\frac{d\varphi}{dt}$  angular speed of the wave (when  $n_1 = 2$ ); it is equal to the angular harmonic signal. Angular speed of the rotor  $\omega$  depends on mechanical attachment between the components and external value of the moment, but, in any case, it is less

than the effect of frictional interaction between components.

### 3. ANALYSIS OF THE DYNAMIC CHARACTERISTICS OF A CYLINDRICAL PIEZO ACTUATOR

Experiments aimed to find out resonant frequency that would enable achieving the largest output link's shift of piezoelectric actuator (cylinder).

In order to determine these parameters experiments on the experimental stand were carried out. The experimental stand consists of a programmable signal generator, high voltage amplifier, laser doppler vibrometer PolytecTM, analog capture card, and a computer with installed scanning vibrometer software PSV8.8.

Data were collected and processed by specific program in PSV 8.8 graphical environment that allows obtaining the amplitude frequency characteristics of experimental output link.

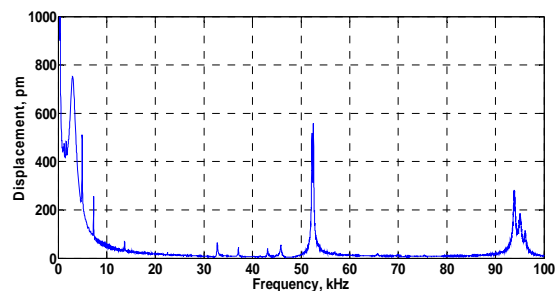


Fig. 2. Displacement's dependence on frequency (voltage  $\pm 100$  V)

With a help of laser vibrometer PolytecTM and computer with specially made PSV 8.8 program, shift's dependence on frequency was found. Measuring the displacement of piezoelectric actuator's output link, the excitation voltage was kept at  $\pm 100$  V, and frequency was 0-100 kHz.

Figure 2 shows that the greatest displacement is achieved at resonant frequencies (52.52 kHz and 93.86 kHz). The experiment confirmed that the output link of piezoelectric cylinder moves in trajectory of ellipses. Figure 3 shows movement trajectories of the output link.

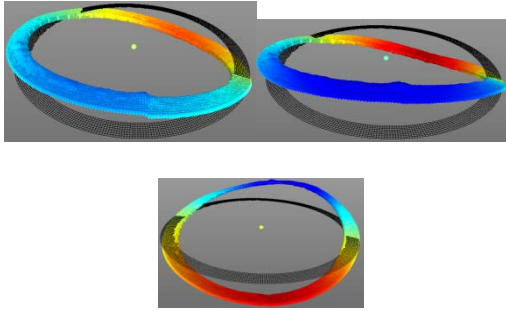


Fig.3. Movement trajectories

The same experimental stand was used for investigation of the resolution of flow control device with piezoelectric actuators (cylinder shape). Displacements of reference point were measured in the following way: a steel ring with a tightly fixed plate with micro pores was fitted on the output link of a piezoelectric cylinder. The same unit was fixed on the steel ring as the starting point. Data was collected and processed by specifically designed program in PSV 8.8 graphical environment, which enables detecting experimental characteristics of reading point's amplitude. After the experiment, the shifts of the reading point were converted into angular degrees of shifting.

The package containing the same number of periods of harmonic signal ( $U_{RMS}=60$  V,  $f=52.52$  kHz or  $f=93.86$  kHz) was used in investigation of the resolution of a flow control device. Shift's dependence on harmonic number of signal cycles in the package is presented in Fig. 4.

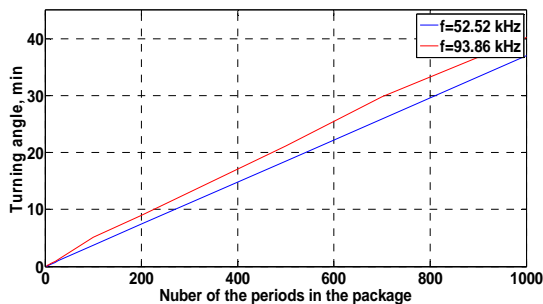


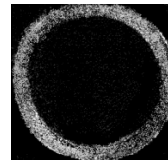
Fig. 4. The dependence of turning angle on the number of periods in the package.

The rotor starts to rotate after forming two harmonic signals whose amplitude  $U_{RMS}=60$  V and frequency  $f=52.52$  kHz or

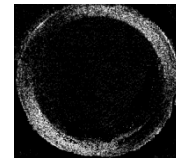
$f=93.86$  kHz for periods of package. The transition process ended after 12ms from the end of the excitation package. After the recalculation of the displacement, in turn, the resolution of 0026', and the in the second case of 0029', was obtained.

Notwithstanding that actuators of such type (generated traveling radial oscillations) are studied very widely, still it is difficult to determine nodal points of its mounting on the surface. Therefore, this problem was solved using an experimental method of holography.

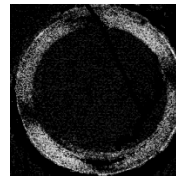
With a help of holographic imaging method the maximum vibration amplitude of actuators output links points was determined..



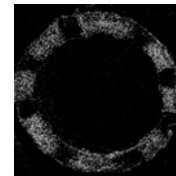
a) frequency 52.52 kHz, voltage 0 V



b) frequency 52.52 kHz, voltage 12 V



c) frequency 52.52 kHz, voltage 50 V



d) frequency 52.52 kHz, voltage 60 V

Fig. 5. Holograms of piezoceramic actuator (cylinder form)

This investigation is needed for construction of flow control device in order to know where to place a steel ring (rotating motion) ensuring minimum friction between links.

After the holography of piezoelectric actuators (cylinder form) at working resonance frequency 52.52kHz and 93.86 kHz, the location of interference bands and holograms at resonant frequency of 52.52 kHz (Fig. 5) were obtained. At the same

time, it was detected that the output piezoelectric actuators link is not deformed when the voltage is 0 V (Fig. 5 a). Increasing excitation voltage to 12 V (Fig. 5 b), two symmetric interference bands appear; the circle repeats to (Fig. 5 c) and so on. The experiment showed that places of shock and abrasion resistant material of supporting elements, where four interfering bands of the output link were obtained, needed to be glued and strengthened with a steel ring in order to obtain lower friction between the output link and the surface of the steel ring so that the ring will not use the entire surface and spin faster and more efficiently.

#### 4. MEMBRANE CONSTRUCTION

In flow control devices of such type, membranes can be made of the plates with different structures, depending on what flow rates and management options are expected. In this article were presented two structures of the membranes:

1. The membrane is made of plates with the same number of notches. In order to obtain maximum throughput and full closure it is necessary to choose an

appropriate ratio  $\frac{\beta_1}{\beta_2}$  between closed and open areas of the plate. Simulations performed showed that the best flow control option is obtained when this ratio is equal to 0.4.

2. The membrane is made of plates with different number of notches. The most important variable is the number of notches. In case where the number of notches differs by one notch, only one interference fringe emerges and the flow runs through one side of a membrane leaving the other side completely closed on that time. The greatest influence is caused by the ratio of closed and open areas' angles  $\beta_1 / \beta_2$ . This parameter was set to 0.3. Only this ratio gives maximum permeability on one side of the membrane and minimum permeability on the other side.

#### 5. RESULTS OF THE SIMULATION

Further simulations were carried out using ANSYS CFX software. First of all the boundary conditions were set. Two identical construction plates were used for the simulation. Water inlet was kept at constant speed - 0.1 m / s, while the outlet was set like a static pressure of 0 Pa. Simulation was carried out without changing boundary conditions, just turning one plate by 0.5 degree. Figure 6 presents the results of the simulation.

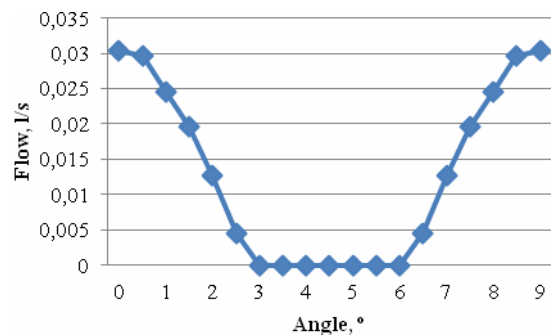


Fig. 6. The dependence between the flow and the turn angle of the plate

It can be seen that when the valve is fully open the flow rate reaches 0.03 l/s. Rotating one of the plate till 3 degrees the flow rate was decreasing and from 3 till 6 degrees the valve was closed. Increasing the angle of rotation til 9° the membrane was opened. And in this point it was completely open and the maximum flow rate was obtained. Further turning repeated opening-closing cycle of the plate.

Analogical simulations were performed with different types of the plates. Boundary conditions remained the same as in the first case. Simulations with plates of different structure showed that maximum flow rate was 0.027 l/s and turning angle did not interfere with it. Although the flow was stable, changing the turning angle altered the place of flow's passage through the membrane. This operation principle might be used for flow control in certain flow control devices.



## 6. CONCLUSIONS

1. After the analysis of industrial piezoelectric actuators it was decided that cylindrical actuator is the best choice for the construction of technological flow control devices. The electrode configuration was selected in order to obtain the travelling wave oscillations in the output link of the cylindrical actuator.
2. The experimental analysis disclosed working characteristics of cylindrical piezoelectrical actuator: resonance frequencies (52.52 kHz and 93.86 kHz) and output link movements of the piezoelectrical actuator.
3. The relationship between plate rotation angle and flow rates was found. When plates are of the same construction, maximum flow rate is 0.03 l / s; when the construction rate is different, the flow rate is 0.027 l / s.

## 7. REFERENCES

1. Lee, K.S. Measurement of stress in aluminum film coated on a flexible substrate by the shadow moiré method. *Applied Optics*, 2008, **47**, 315-318.
2. Liou, N.S. Specimen gratings made from body art paper for in-plane moiré strain analysis. *Polymer Testing*, 2005, **24**, 535-539.
3. Bullough, W.A., Ellam, D.J., Wong, A.P., Tozer, R.C. Computational fluid dynamics in the flow of ERF/MRF in control devices and of oil through piezo-hydraulic valves. *Computers & Structures*, 2008 **86**, 266-280.
4. Suh, H.K., Park, S.W., Lee, C.S. Effect of piezo-driven injection system on the macroscopic and microscopic atomization characteristics of diesel fuel spray. *Fuel*, 2007, **86**, 2833-2845.
5. Li, X.L., Kang, Y.L., Qiu, W., Qin, Q.H., Xiao, X. A study on the digital moiré technique with circular and radial gratings. *Optics and Lasers in Engineering*, 2007, **45**, 783-788.
6. Yin, L.W., Li, M.S., Sunm, D.S., Zou, Z.D., Liu, Y.X., Hao, Z.Y. Features of moiré patterns in HPHT-grown diamond single crystals. *Materials Letters*, 2002, **52**, 187-191.
7. Lee, J.Y., Wang, Y.H., Lai, L.J., Lin, Y.J., Chang, Y.H. Development of an auto-focus system based on the moiré method. *Measurement*, 2011, **44**, 1793-1800.
8. May, F., Dual, J. Focusing of pulses in axially symmetric elastic tubes with fluid filling and piezo actuator by a finite difference simulation and a method of time reversal. *Wave Motion*, 2006, **43**, 311-322.
9. Merry, R., Molengraft, R., Steinbuch, M. Modeling of a walking piezo actuator. *Sensors and Actuators A: Physical*, 2010, **162**, 51-60.
10. Juhas, L., Vujanić, A., Adamović, N., Nagy, L., Borovac, B. A platform for micropositioning based on piezo legs. *Mechatronics*, 2001, **11**, 869-897.
11. Ragulskis, K., Bansevicius, R., Barauskas, R., Kulvietis, G. Vibromotors for Precision Microrobots. Hemisphere Publishing, USA, 1988.
12. Kuribayashi, M., Ueda, S., Mori, E. Excitation Conditions of Flexural Traveling Waves for a Reversible Ultrasonic Linear Motor. *J. Acoust. Soc. Am*, 1985, **77**, 1431-1435.

## 8. ADDITIONAL DATA ABOUT AUTHORS

Rimašauskas Marius, Dr. Lecturer.  
Kaunas University of Technology  
Kęstučio 27, LT -44312 Kaunas, Lithuania  
Phone: +370 614 99258  
E-mail: marius.rimasauskas@ktu.lt

Rimašauskienė Rūta, Dr. Researcher.  
The Szewalski Institute of Fluid-Flow  
Machinery, Polish Academy of Sciences  
Fiszera 14, 80-231 Gdansk, Poland  
Phone: +370 620 70764  
E-mail: rrimas@imp.gda.pl



## FUNCTIONAL REQUIREMENTS AS A COMPANY AND PROCESS MODELING TOOL

Sonk, K. Hermaste, A. Sarkans, M.

**Abstract:** *Using functional requirements as a modeling tool for a company as a whole and using functional requirements to describe a production processes is relatively new approach. For companies with large manufacturing facilities and a large number of different workbenches this kind of representation is especially interesting. It allows to review and reorganize manufacturing process more easily and give alternatives to different workstations that may already exist in some other part of the production. It also enables to assess the production capability of a factory by comparing functional requirements of a product and functions available within a factory or factories. A case study is also included in this paper. It focuses on the production process modeling using functional requirements. To make the modeling easier STEP NC file format is used to create a functional requirements model automatically and enable easier customization of the model.*

*Key words: default company model, STEP NC, functional requirements, automatic model creation, AP238*

### 1. INTRODUCTION

Using different kind of approaches it is possible to model parts of a production process or even the entire process from the customers wishes to the recycling of the product. But few, if any, of these methods try to model the company and the production process as a whole. Mainly because the physical operations, BOMs, company management etc within the same

system makes it too complicated and blurry.

Functional requirements were first used in IT to model a computer program and determining its' functions. It was very effective because it's rarely important how the function is achieved. The research in recent years has been going in the direction of using functional requirements (FR) to model a production process in different fields and more widely. First FR models of any kind of production process were used to determine what kind and, if at all, to use large scale manipulators in different stages of construction [1]. FR models have also been used to help engineers with factory planning [2] and to develop new products as shown in this cases study concerning product packaging [3]. This papers goal is to show how a whole production process and the company can be represented as a FR model using Requirements Management Planning (RMP) tool (developed in ETH Zurich by Inspire workgroup). Further research is required on creating a more detailed model and looking into different kind of file formats that could be used to create the model automatically.

### 2. CREATING UNIVERSAL COMPANY MODEL USING FUNCTIONAL REQUIREMENTS

The basic structure and needs of the company are very similar even if the physical product or the size of the company are very different. This suggests that a universal model can be proposed. This

model can be represented in three different ways as described in [4].

By using RMP tool we can propose a default company model that could be the basis for every company using FR as a method of modeling. This allows us to offer a default model of the company that the model maker has to customize/improve and make it resemble the actual company and its production. This usually means adding new stakeholders and specifying the FR (the needs) of the customer, operator and especially product itself. This is explained more in depth in this paper in section 3.

In the future there can be more specific templates for different industries when there are more models but at the moment a very general model is proposed. These templates can differ in connections between functions or the functions presented. Note: this model can also be used on non-physical products, for example: computer programs.

its' sub-functions. As you can see from Fig 1. we took an example from a laminated floor boards production company. The case study of this company is described in section 3. The customer has the requirement of covering his/her floor. This has a sub-function "to buy the boards". And now we can define with other FR, what these floor boards should be like. Should they be made out of wood, should they have certain dimensions etc. These functional requirements also have properties where we can describe the exact type of wood or maximum length of the floor boards.

The companies' main goal is to earn profit and be sustainable in the long term run. Of course company wants motivated workers, loyal customers, bigger market share and produce good cost efficiently but all of these FR are there to serve "to earn profit". And how does a company earn its' profit? It satisfies the customer needs, which in this case is "to buy floor boards". Only

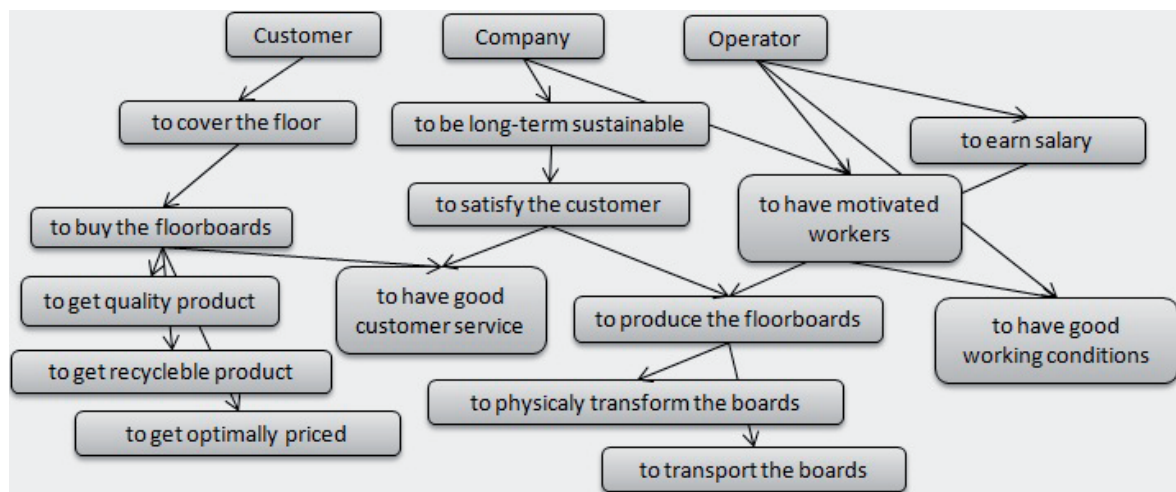


Fig. 1. Simplified model of floorboard production process and of the company using functional requirements.

When making a FR model of a company and its' processes it all starts with the customer. It's the first stakeholder and everything else derives from him/her. Note: the arrows between stakeholders and functions show only who is interested in that function, not hierarchy. Arrows between functions show the function and

now comes in the companies' desire to actually produce the boards. These boards have to have certain physical and esthetic properties that derive from the customer. If it would be possible then company could produce as cheaply as possible. The result would be boards that will break in two weeks, wouldn't fit together etc., but if there are customers willing to pay for that kind of products then all the stakeholders in the model would be satisfied (which is the main goal). But because customer has standards about quality, company must

make investments to guarantee the quality properties i.e. the quality functional requirement actually comes from the customer not from the company. The company is interested in the quality product not directly because it wants to make quality product, but as it wants to satisfy the customers' needs.

Next we add the stakeholder "operator" to the model because we need to physically manufacture the product. Interesting note: the operators' and the companies' basic FR are very similar: they both want to earn (profit/salary). In the operator's case we also have functional requirement "to have good working conditions" which reflects the motivational part of the model. Good working hours, interesting and non-monotonous work, long vacation: all these things can be considered as the motivation and it is quite hard to measure. Difference between different workers also adds difficulty/complexity. But motivation should be sub-functions (secondary) to the "earn salary" because people are more willing to work without some of the good working conditions than people who are willing to work for free.

To earn the salary the operators must participate in the manufacturing of the product. Depending on the complexity of the model we may divide the operators into 5 main groups to make the model more transparent. Different operators for assembly, transport, storing, physical transformation and packaging makes it possible to see the specific FR that are connected to the transport system or what FR are needed for the physical transformation processes. Packaging process itself can be also remodeled using similar techniques that are used in [3]. And now we come to the actual production itself. Different sub-functions that are connected to the operators make up the physical domain of the production. All of the tolerances, machines and materials needed to make the product are added last to the model.

Thus we can propose a universal model for companies as seen on Fig2. It's a simplified version that can be customized to suit different companies' needs. The universal description also contributes to the synergy aspect of the model and synergy deployment as described in [5].

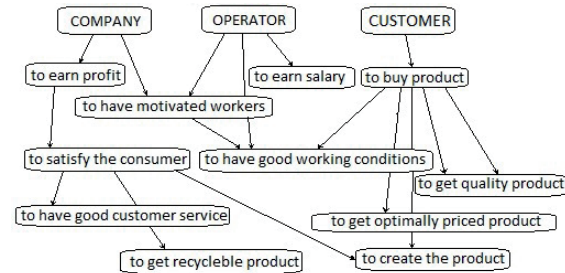


Fig 2. Default company model using functional requirements.

### 3. HOMAG CASE-STUDY

To illustrate and give a more realistic example of the functional requirements used as a modeling tool a case study is presented. HOMAG is a company that develops and builds production and assembly lines for other companies. In this paper we take a case-study of a production line engineered and built for a company that produces laminated floorboards. HOMAG has provided a very detailed process description for the whole production. Starting from where the uncut blanks enter the production line and ending with the packaging and storing of the finished product.

The description of the processes consists of the basic operation(s), specification of the operation and in some cases the dimension/tolerances required. For example, here are two extracts from the process description:

- automatic double-sided longitudinal feeding of raw boards on stacks by means of a fork lift
- control and rejection of boards with waviness > 30 mm

The first extract describes the operation in general: "double-sided longitudinal feeding of raw boards". It also specifies the operation by adding: "automatic" and

"means of a fork lift". The dimensions of the boards are specified at the end of the process description. Because the dimensions of the boards vary and are not important for the process, they are not given here.

For the second extract the basic operations are: "verifying the quality of the boards" and "rejecting boards that doesn't meet the quality requirements". It also specifies the waviness dimension  $>30$  mm. But it doesn't specify how the boards are removed from the line. In this case it is not important because all we need are the functions. Dimensions, tolerances and other physical properties are described later on.

After going over all the process descriptions the next step is to create the functional requirements for each process described. To show how it's done we again take the two extracts from the previous example and convert them into functions.

For the first operation: Function1: to feed raw board stacks

For the second operation: Function 2: to verify the quality of the boards.

Function 3: to reject unqualified boards from the line.

The relationships between functions as shown on fig 1. and fig 2. are just the connections between the functions, they do not show the hierarchy of the model. To better understand the model, each of the major functions have to be looked separately. Using the RMP tool this is done by double clicking on a function to see all of its' connections to other functions and sub-functions. This allows for a better overview of the model.

Now we have production process description that consists of only functions. This means that we don't have any machines or workers or dimensions connected to the process. That enables us to rethink the entire process and make changes in the order of the process, machines used, workers used etc.

In the program we first enter all of the stakeholders who are connected with this

product. There are four types of stakeholders that are part of every model: company, customer, operator and the product itself. Second step is to enter all of the functions and define the relationships between stakeholders and functions.

Each function has a set of properties. These properties are whatever physical we need to describe with that function. For example the function "to feed raw board stacks" can have a property that describes the dimensions of the boards. Additionally we can add the tolerances, type of wood, stack height etc.

Entities can also be connected or added to a process. Entities usually means machines or other physical items connected to the production (transport lines, leaflets, packaging material). If we have decided which kind of machine to use for a process, we can connect it to the function. For example we want floorboards with a certain length and for that we use a band-saw. The function is: to have right measurements for the floorboards. The properties are: length = 1300mm, thickness = 20mm, waviness tolerance  $\pm 30$ mm. The entity is: Powermatic 14" Bandsaw Model PWBS-14CS.

#### **4. AUTOMATIC CREATION OF FUNCTIONAL REQUIREMENTS MODEL**

Because the companies have vast number of variables that vary greatly, the FR model used cannot be 100% universal (even for companies in similar fields). This means that some degree of automation and customization should be introduced when making the company model. This can be done by using STEP NC code (as described later on) or using RFID tags which use could be similar to the processes described in [6]

To make the creation of the FR model easier, efficient and quicker some ideas and concepts are proposed on how an automatic creation of the FR model can be achieved. The idea is to have a semi-

automatic model where the model maker can also use in his/hers engineering know-how as input data. To create the model, we first take a universal company model as shown on fig 3. and then we use the STEP NC file type. It's a protocol that makes the machine code between CAM programs and CNC machines easier to read for humans. And by analyzing the data extracted from the file, we can find out the features that the product has. This in turn allows us to create a FR model automatically.

For example let's take a product that has a hole in it. When using STEP NC file format, this feature is described within the file as shown in Fig 3.

```
#239=ACTION_RESOURCE_TYPE(
'milling cutting tool');
#300=RESOURCE_PROPERTY_RE
PRESENTATION('effective cutting
diameter',
'user defined milling tool',#325,#275);
#328=MACHINING_TOOL('11','use
r defined milling
tool',(#2054,#2055,#2056,
#2057,#2058,#240);
#339=INSTANCED_FEATURE('','to
olpath', 'Plane tolerance feature',
'toolpath',#86910,.F.);
```

Fig. 3. Extract from a STEP NC file

This is just an outtake from a larger file of the command lines that are connected to the cutting of the hole. In this case the hole is made by milling machine. The person who made the STEP NC file has already defined the tool to be used and the tool paths for cutting. Also we have the tolerances for the milling and actually all of the information required for the physical creation of the hole. This in turn means that by recognizing certain features from the file we can automatically look for the entities connected with that process. For example we can automatically add CNC milling machine to the FR model. We also can add the tool used in the process, space occupied by the machine, necessities for milling, storage needed before and after the

milling and also the transportation to and from the machine.

All of the above named entities are all physical. But we need to also add customer, company, operators etc. to the model. This can be done by combining the default FR model with the information from the STEP NC file. Each feature adds a new functional requirement with its' entities which in turn allows us to deduce the persons and sub functions that are connected to that process. For example we have a milling process. Physical properties and entities are added automatically from the file, but the stakeholders are "reverse engineered". Milling requires a machine, machine requires an operator, operator works for the company and the company wants to satisfy the customer. The automatic creation of new functions has to be checked by an engineer because not all of the functions created may not be necessary or can be done in different way. For example, there is more than one way to create a hole. Instead of milling we could use drilling or water jet cutting. This is the place where the engineer can decide which kind of machine to use and what kind of machines already exist in the company.

One way to solve this dilemma is to prompt a window when a feature is recognized and the engineer can choose from different kind of machines. With a product that has hundreds of features this could be very time consuming and stressful so the feature identification should check if there aren't any entities that could do the job. For example if we have a CNC machine, we can perform drilling and milling in the same machine but with different tools. But this is part of further research in this field.

## 5. CONCLUSION

For a more comprehensive overview of the companies' production capabilities a new and different approach is suggested. This paper demonstrates that functional requirements can be successfully used to

model a company and its' production as shown on the HOMAG case study and creating the default company model. The model consists of all the parts and functions of a products' production cycle starting from raw material and finishing with recycling. It also includes all the stakeholders (company, customer, product and operators) within the products life cycle. In addition the model shows the needs, desires and goals of all of these stakeholders making it easier to understand the business model.

STEP NC (and in the future possible other file formats) can be used to create the FR model semi- or completely automatically. This is achieved by using feature recognition and identification parts/lines of file format that is connected to this specific feature. Further research is planned in this area in developing a feature identification for STEP NC files and using FR to describe machines taking part in the processes. One of the future goals is to make the FR model responsive in real time. This can be achieved by using real time monitoring proposed by [7] and using this data to change the physical properties that accompany the functions. For example the length of the raw boards, tolerances for waviness or the power consumption of a milling machine.

## 6. ACKNOWLEDGEMENTS

This research was supported by Estonian Ministry of Education, Research Project SF0140113Bs08, and Estonian Science Foundation (grant F7852). I also wish to extend my special thanks to Inspire workgroup in ETH Zürich and to Archimedes foundation and their international doctoral project "DoRa".

## 7. REFERENCES

[1] Haas. C & Hsieh. T-Y (1994) Determining functional requirements for large scale manipulators, <http://www.sciencedirect.com/science/artic>

[le/pii/0926580594900329](http://www.sciencedirect.com/science/article/pii/S0007850608000668) Accessed: 2011-05-22

[2] Bathelt. J ; Politze. D & Wegener. K (2010), Function Oriented Product Descriptions in Product Development and Factory Planning, *International Conference on Systems Engineering and Engineering Management on the World Congress on Engineering and Computer Science 2010*, San Francisco, USA, ISBN 978-988-17012-0-6, pp 1168—1172

[3] Ten Klooster. R & Lutters. D (2008) Functional requirement specification in the packaging development chain <http://www.sciencedirect.com/science/article/pii/S0007850608000668> Accessed: 2011-04-13

[4] Sonk, K. (2010). Overview of e-manufacturing practices and possibilities. *8th International Symposium "Topical problems in the field of electrical and power engineering. Doctoral school of energy and geotechnology". II* : Pärnu, Estonia, ISBN 978-9985-69-049-9 Lahmets, R. (Ed.). pp 208-211

[5] Hinderus, T. Kaljas, F. Martin, A. Tähemaa, T. Reedik, V. (2010) On synergy deployment in engineering design. Proceeding of the 7th International Conference of DAAAM Baltic Industrial Engineering. Tallinn, Estonia, ISBN 978-9985-59-982-2. pp 84-89

[6] Randmaa, M. Otto, T. Kuusik, A. (2009) RFID Rack Assembly Development for Mobile Platform. Annals of DAAAM for 2009 & Proceedings of the 20th International DAAAM Symposium. Vienna, Austria. ISBN 978-3-901509-70-4. pp 1697-1698

[7] Aruväli, T; Serg, R.; Preden, J.; Otto, T. (2011). In-process determining of the working mode in CNC turning. *Estonian Journal of Engineering*, 17(1), pp. 4 – 16

## STATISTICAL PROCESSING OF ACCELERATED LIFE DATA WITH TWO STRESSES USING MONTE CARLO SIMULATION METHOD

Zaharia, S.M.; Martinescu, I. & Morariu, C.O.

**Abstract:** *This paper presents research about accelerated life data and a simulation of a case study using Monte Carlo method. The statistical processing was realized using the ALTA 7 software. The main objective of this study is to determine the indicators of reliability (Probability density function, Reliability function, Unreliability function, Mean time to failure, Failure rate, and acceleration factor) in normal use for the case study analyzed. The case study is represented by a set of data from accelerated tests with two stresses. Using the previously determined parameters and the accelerated levels, we simulated with the help of ALTA 7 software the values for the times to failure in accelerated conditions.*

*Key words: reliability, ALT, accelerated model, Monte Carlo simulation,*

### 1. INTRODUCTION

Although the technological achievements of the last 50 years can hardly be disputed, there is one weakness in all mankind's devices. That is the possibility of failure. What person has not experienced the frustration of an automobile that fails to start or a malfunction of a household appliance. The introduction of every new device must be accompanied by provision for maintenance, repair parts, and protection against failure. This is certainly apparent to the military, where the life-cycle maintenance costs of systems far exceed the original purchase costs. The problem pervades modern society, from the homeowner who faces the annoyances of

appliance failures, to electric utility companies faced with the potentially disastrous consequences of nuclear reactor failures. The insurance industry would not exist without the possibility of one type of failure or another.

A subject that is so important to many decisions in this world could hardly escape quantitative analysis. The name reliability is given to the field of study that attempts to assign numbers to the propensity of systems to fail. In a more restrictive sense, the term reliability is defined to be the probability that a system performs its mission successfully. Because the mission is often specified in terms of time, reliability is often defined as the probability that a system will operate satisfactorily for a given period of time. Thus reliability may be a function of time. Estimating reliability is essentially a problem in probability modeling. A system consists of a number of components. In the simplest case, each component has two states, operating or failed. When the set of operating components and the set of failed components is specified, it is possible to discern the status of the system. The problem is to compute the probability that the system is operating - the reliability of the system [<sup>1</sup>].

Products are 'born' in the sense that they are manufactured. They enjoy some period of useful service and ultimately 'die' when their service comes to an end, typically by one of the following: product failure, retirement, replacement, or disposal. Also known as life cycle, service life, or useful life, life is defined as the quantity that most



accurately represents how long a product or system lasts. Service life may be defined in terms of total calendar time since fielding, or may be defined exclusively in terms of use-hours (such as flight-hours for aircraft). In some cases, life may even be measured strictly in terms of usage (such as the total mileage on a car), and not on any time measurement. What varies by each case is what constitutes the end of life. At the material and component levels, many of these items are allowed to serve in their capacity until they fail to work, at which time they are usually replaced, either with an identical article or an upgrade. However, high-criticality materials or components are not allowed to run until failure for reasons of safety. Assembly level constituents or higher are usually considered critical, and thus are not allowed to operate until failure either. Instead, they are operated for a fixed interval of time before they are serviced or replaced. Beyond reasons of safety, the service lives of non-critical elements are fixed because their service or replacement follows a set schedule for reasons of economics or convenience [2].

## 2. REVIEW OF ALT TECHNOLOGY

Many of the industrial products produced today for complex technical systems have very high reliability under normal use conditions. The questions then arise of how to make the optimal choice between several types or designs of a device and how to collect information about the corresponding life distributions under normal use conditions. A common way of tackling these problems is to expose the products to sufficient overstress to bring the mean time to failure down to an acceptable level. Thereafter, one tries to "extrapolate" from the information obtained under over stress to normal use conditions. This approach is called Accelerated Life Testing (ALT) or overstress testing. In these tests, reliability practitioners may force the product to fail

more quickly than it would under normal use conditions [3].

The basic propose of ALT is to obtain initial information for issues of quality, reliability, maintainability, supportability, and availability. It is not the final goal. It is accomplished through prediction using the information provided by ALT under laboratory conditions. The most effective ALT of a product design needs to occur under natural (field) conditions. ALT design and the selection of appropriate testing parameters, equipment, and facilities for each method or type of equipment to be tested must be coordinated to provide the test inputs and results that are most beneficial for the quality, reliability, or maintainability problems that the test identifies.

The primary purpose of an ALT is to estimate the life distribution and quantities of interest at a use condition. This estimation involves extrapolation from higher stress levels by using an acceleration model, and thus includes the model error and statistical uncertainty. Sometimes, the model error outweighs the statistical one. The model error may be reduced or eliminated only by better understanding the failure mechanisms and using a more accurate model, whereas the statistical uncertainty can be reduced by carefully selecting a good test plan. A typical test plan is characterized by the stress levels, the number of test units allocated to each level, and their censoring times. The most commonly used ALT in modern manufacturing industry is the constant-stress ALT where stress applied to a sample of units is constant. A typical parametric model of ALT consists of two components: (1) a lifetime distribution that models the time-to-failure at a constant-stress level; and (2) a stress-life model that quantifies the manner in which the lifetime distribution changes a cross different stress levels. There are different types of ALT plans in use, which include subjective, traditional, best traditional, and statistically optimum and compromise plans [4].

In general, the accelerated life testing can be divided into two categories: qualitative ALT and quantitative ALT. Qualitative ALT, such as Highly Accelerated Life Testing (HALT), Highly Accelerated Stress Screening (HASS), torture tests, shake and bake tests, are used primarily to reveal probable failure modes for the product so that product engineers can improve the product design. Quantitative ALT consists of tests designed to quantify the life characteristics of the product, component or system under normal use conditions and thereby provide reliability information [5].

Pursuing the previously stated main purpose of the accelerated life tests, we need a model that relates life to accelerating stress, such as temperature, humidity, and voltage. Such models, usually called acceleration models, can be classified into the following three types: physical models; quasi-physical models; empirical models. Among the most important acceleration models (life-stress) we can mention the following: Arrhenius, Eyring, Inverse Power Law; Life - Thermal Cycling, Life - Voltage, Life - Vibration, Life - Humidity, Life - Temperature – Humidity.

Three basic approaches use ALT technology as shown in figure 1.

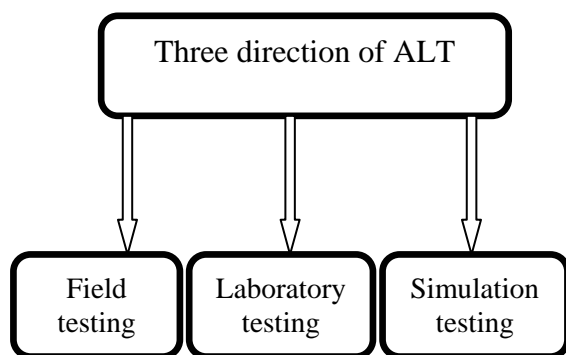


Fig. 1. Three basis direction of ALT

The first approach is special testing with more intensive usage than under a normal use. The second approach is to use accelerated stress testing (AST). For example, if one conducts research upon or

tests the actual car using a simulation of the field input influences with special equipment, then the level of car (or other product) loading is higher than it is normal usage. The third approach relies on using a computer (software) simulation or analytical/statistical methods. Computer simulations have become a useful part of the mathematical modeling of many natural systems in physics and engineering.

### 3. CASE STUDY

Monte Carlo simulation is a powerful tool for modeling: the reliability data of industrial products; the behaviour of some activity, plan or process that involves uncertainty. If you face uncertain or variable market demand, fluctuating costs, variation in a manufacturing you can benefit from using Monte Carlo simulation to understand the impact of uncertainty, and develop plans to mitigate or otherwise cope with risk. Its core idea is to use random samples of parameters or inputs to explore the behaviour of a complex product or process.

In many cases, the life of a product is a function of stress and some other engineering variable, like materials, vendors or operation type. For this type of product, ALTA 7 provides the general log-linear life-stress relationship, which allows you to analyze up to eight stress types and specify an underlying relationship for each stress. ReliaSoft's ALTA 7 software provides an extensive array of tools to help you understand and communicate how a product will perform over time.

A sample with 25 electronic components is subjected to a quantitative accelerated life test in which two stress types are applied to the units. The stress types include temperature and voltage. The time-to-failure data are presented in Table 1. The normal use stress levels are 300 K for temperature and 12 Hz for vibration. The general log-linear life-stress model is used and the Weibull distribution is used as the underlying life distribution for the data set.

Poor accelerated life test plans waste time, effort and money and may not even yield the desired information. Before starting an accelerated life test, it is advisable to have a plan that helps in accurately estimating reliability at operating conditions while minimizing test time and costs. To design the plan for the accelerated life tests of the specimen made out of supple platinum it is necessary to establish the following parameters:

- the acceleration model: temperature – non-thermal (T-NT) model;
- the number of components subjected to accelerated life tests: for accelerated life testing we used 25;
- the distribution law of times to failure used in accelerated life testing: the Weibull distribution was chosen to test the components;
- the stress under normal condition and in accelerated condition: the temperature and vibration in normal testing conditions is 300 K, 12 Hz and the maximum temperature and vibration is 350 K and 18 Hz;
- the accelerated life test plan: for the accelerated life testing of the electronic components we chose 3 levels optimum plan. The test plan was realized using the ALTA software (figure 2).

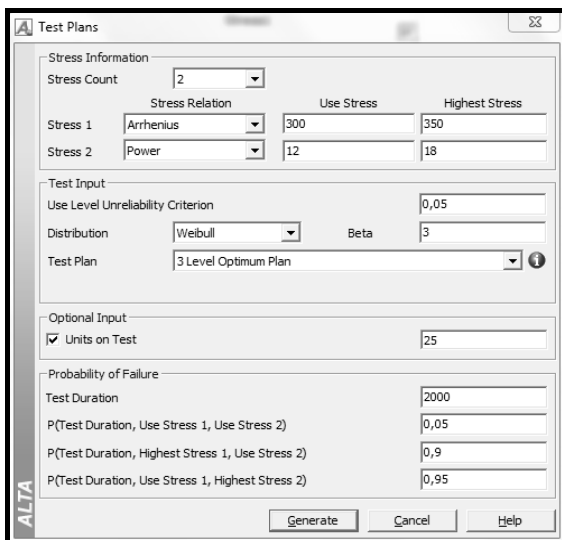


Fig. 2. Design of experiment of ALT

The ALTA 7 software generates an optimum testing report, where the levels of

accelerated life testing and the number of components tested at every accelerated stress level are specified. The testing parameters resulted from the design of the accelerated life testing plan for the specimens made from supple platinum are as follows: 3 levels of testing: 300 K – 15 Hz, 325 K – 12 Hz, 350 K – 18 Hz; the number of tested specimens corresponding to the level of acceleration: 10, 9 and 6 components.

The Monte Carlo simulation window with censoring after a specific number of failures (25) is described in figure 3.

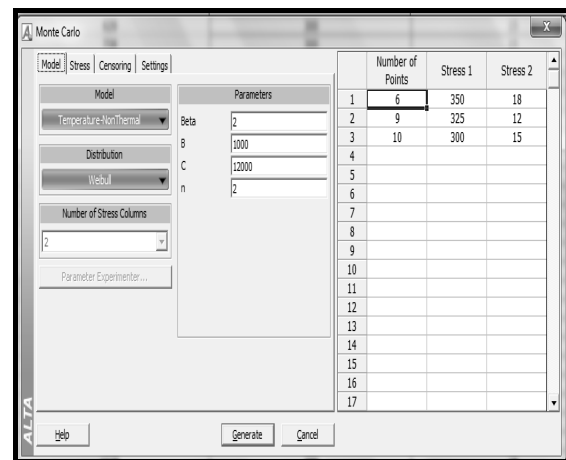


Fig. 3. Monte Carlo simulation

Failure times resulting from Monte Carlo simulation method are described in figure 4.

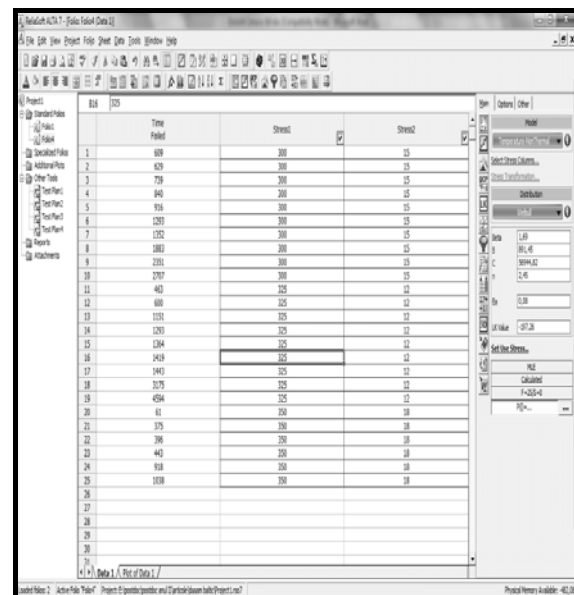


Fig. 4. Time failed vs. Stress 1-2

In figure 5 is described the reliability function (2D) in normal condition (300 K and 12 Hz) for the electronic components.

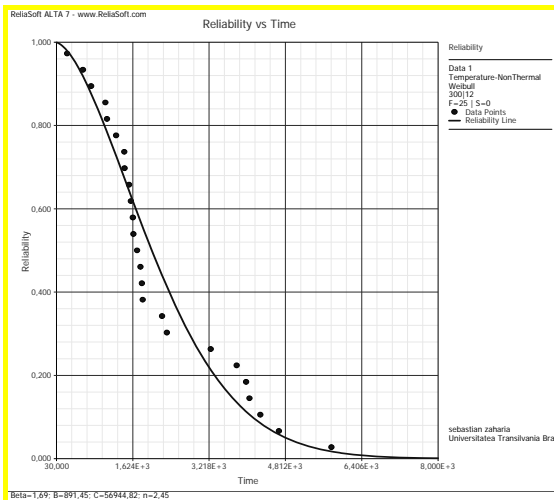


Fig. 5. Reliability function – 2D plot

In figure 6 is represented the reliability function (plot 3D) in normal condition (300 K and 12 Hz) for the electronic components.

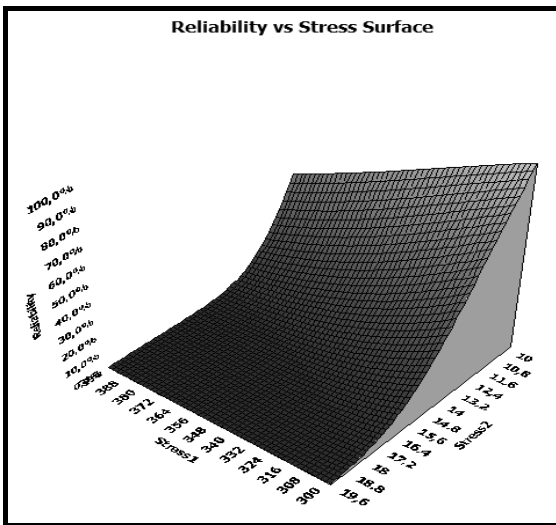


Fig. 6. Reliability function – 3D plot

PDF - a mathematical model that describes the probability of events occurring over time. This function is integrated to obtain the probability that the event time takes a value in a given time interval. In life data analysis, the event in question is a failure, and the pdf (figure 7) is the basis for other important reliability functions, including the reliability function, the failure rate function and the mean life.

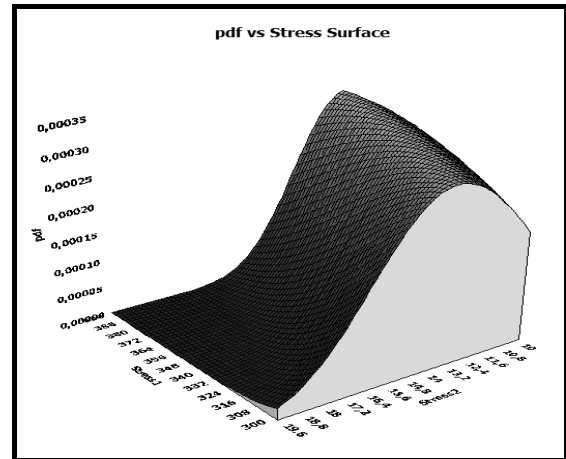


Fig. 7. Probability density function (pdf) – 3D plot

Using the QCP, the mean life at normal pressure (300 K and 12 Hz) is estimated to be 2962 hours as shown in figure 8. The mean life function, such as the mean time to failure (MTTF), is widely used as the measurement of a product's reliability and performance. This value is often calculated by dividing the total operating time of the units tested by the total number of failures encountered. The case study analyzed in this paper, the mean life is determined taking into account only the time of failure (without censored units).

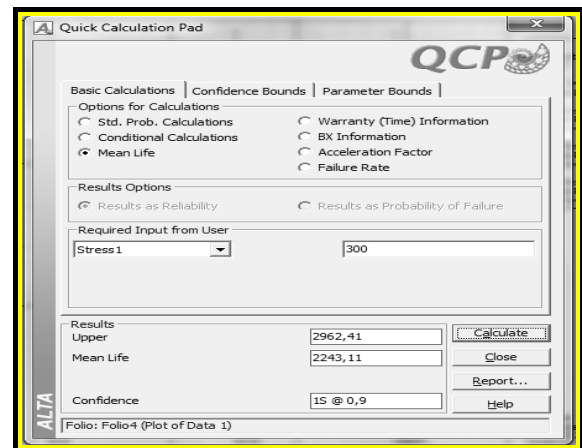


Fig. 8. Mean life at normal stress

BX life represents a time period during which a certain proportion of the population will fail. For example, the B10 life is the time in which 10% of the population will fail. In figure 9 was determined B10 indicator for the case study analyzed in this paper.

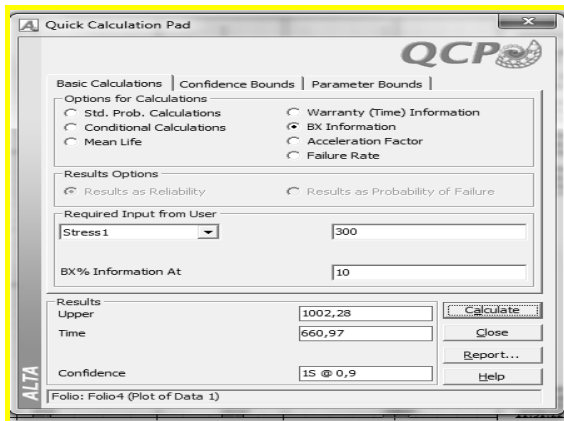


Fig. 9. Determination of parameter B10

#### 4. CONCLUSION

At some industrial products (from the aviation, nuclear and electronic fields), for which a high reliability is estimated, the determination of the life time and of the reliability parameters, under normal stress conditions, implies a long testing period. For this reason we opted for the accelerated life testing methods. These are tests being performed at more intense stress conditions, compared to the normal stress conditions, with the purpose of intensifying the degradation processes and, as an economic result, the shortening of the period and costs related to the testing, while preserving the same failure modes and mechanisms. Accelerated testing is an interdisciplinary field covering topics such as aging characteristics of materials, degradation mechanisms, testing, reliability, statistics, and life assessment. This article provides a case study with two stresses into the field of accelerated testing. Accelerated testing can prove to be a valuable tool for a variety of applications including reliability and life prediction, materials and manufacturing processes selection, and quality control. As further research I will expand the accelerated tests on other components from engineering products using three or more stresses.

#### 5. ACKNOWLEDGEMENT

This paper is supported by the Sectoral Operational Programme Human Resources

Development (SOP HRD), financed from the European Social Fund and by the Romanian Government under the project number POSDRU/89/1.5/S/59323.

#### 6. REFERENCES

1. Klyatis, L. M. *Accelerated reliability and durability testing technology*. Wiley, New Jersey, 2012.
2. Dodson, B., Schwab, H. *Accelerated Testing – A practitioner's Guide to Accelerated and Reliability Testing*. SAE International, Warrendale, 2006.
3. Yang, G. B. *Life Cycle Reliability Engineering*. Wiley, New Jersey, 2007.
4. Elsayed, E. A., Zhang, H. Design of PH-based accelerated life testing plans under multiple – stress - type. *Reliability Engineering and System Safety*, 2007; **92**, 286 – 292.
5. Fard, N., Li, C. Optimal simple step stress accelerated life test design for reliability prediction. *Journal of Statistical Planning and Inference*, 2009; **139**, 1799-1808.

#### 7. DATA ABOUT AUTHORS

**Postdoctoral student ZAHARIA Sebastian Marian**, Transilvania University of Brasov, Technological Engineering and Industrial Management, Address: Colina Universitatii nr. 1, Brasov, Romania.  
Phone: +40-(268) 41.46.90.  
Email: zaharia\_sebastian@unitbv.ro;

**Prof. MARTINESCU Ionel Ph.D.**, Transilvania University of Brasov, Technological Engineering and Industrial Management, Address: Colina Universitatii nr. 1, Brasov, Romania.  
Phone number: +40-(268) 41.46.90.  
Email: ionel\_martinescu@unitbv.ro;

**Asoc. prof. MORARIU Cristin Olimpiu**, Transilvania University of Brasov, Technological Engineering and Industrial Management, Address: Colina Universitatii nr. 1, Brasov, Romania.  
Phone number: +40-(268) 41.46.90.  
Email: c.morariu@unitbv.ro.

## COLLABORATIVE DESIGN PROCESS OF A CONFIGURABLE PRODUCT

Widmaier, T., Kontio, J., Juhanko, J., Piili, H., Kuosmanen, P. & Salminen, A.

**Abstract:** *The demand to fulfil a wider range of customer requirements and the need for customisable products increases constantly. The product life cycle as well as the lead time for product development shortens. Collaborative product development enables faster development of complex products but challenges the communication and the data management. Digital design methods and processes enable the collaborative development and decrease the need for expensive prototyping. In this research, collaborative product development for custom made products is studied. A case study of a configurable bathroom faucet was performed. The digital design for manufacturing using sand casting and laser based additive manufacturing as alternative manufacturing technologies were studied.*

*Key words: configurable product, product development, parameterised modelling, additive manufacturing, laser selective melting.*

### 1. INTRODUCTION

To fulfil a wide variety of customer requirements and to shorten the lead times are important today. To compete with the developing economies European industry has to invest in the product development and in designing high-end and unique products. Modularity and configurability reduce the amount of required components, speed up the production and form a base for customizability.

#### 1.1 Background

Product development projects are usually collaborative. The design can be

decentralised and the communication between different disciplines is challenging. The up-to-date information must be available for all of the participants. Traditionally, prototypes are built for different purposes but it can be time-consuming and expensive. Simulation decreases the need for physical prototypes and speeds up the process. In addition, the design can be optimised with virtual prototypes without manufacturing costs. Digital design can be used to help faster development of products. Computer aided design (CAD) allows fast representations of ideas, makes the collaborative design of complex products and product families possible and enables the creation of documents and files for digital manufacturing. Simulations of virtual prototypes are effectively done by computer aided engineering (CAE) tools. Product data management (PDM) systems attend to store and distribute the huge amount of information created during the development project. To test the collaborative digital design process an electrical bathroom faucet was used as a case study.

Laser based additive manufacturing (LBAM) is a technique in which 3D shaped products are manufactured from fine grained metal powder to solid form by melting the powder layer by layer with a laser beam. The shape of the product is taken directly from a 3D CAD model and the process changes the digital model to a solid metal part[1].

The development of user-friendly software and quick and easy transformation from CAD drawing to finished part have made the LBAM process interesting for

prototyping and modelling. A wide pallet of materials and improved quality of the parts has decreased the gap between end product and parts manufactured with additive manufacturing machines. Nowadays parts are directly manufactured and the method is not just used for manufacturing prototypes and models. Growing trend is towards making parts for small batches and end-use functional parts with long-term consistency [2].

Typical application fields for additive manufacturing are concept models, light weight structures and diverse applications used in mechanical engineering. For turning the LBAM process into production for functional parts with long-term usability, the method needs to be reliable, needs to ensure mechanical properties and geometrical accuracy of the workpiece. Additionally, the process needs to be fast to ensure economical performance [3].

### **1.2 Research problem**

This paper in the field of engineering design discusses designing a configurable product by digital systems in a collaborative product development project. The initial challenge in designing an electric faucet is to involve intuitiveness and user-friendliness. Also, data transfer and communication between the designers with different professional backgrounds need to be studied. The requirements of different manufacturing technologies have to be taken into account in configuring the CAD model. The challenge of a configurable design is to maintain all the requirements with each configuration throughout the design and manufacturing process.

### **1.3 Aim of the research**

The primary targets of the case study were to design a configurable CAD model of an electric bathroom faucet and to study the effect of the selected manufacturing method on the design. In this research configurability was defined as the ability to parametrically modify the design of the model. The secondary target was to design

the CAD model so that the manufacturing documents including files for manufacturing could be produced for each configuration.

### **1.4 Scope of the research**

Requirements and challenges of other fields as well as the whole product development project are reviewed from the engineering design point of view. The development of the faucet is limited to the configurable design of the spout. Existing internal components are used. Requirements set by the selected manufacturing methods on the design are studied but the manufacturing of the product is excluded.

## **2. METHODS**

An existing electrical bathroom faucet was used as a reference. During the design of the configurable faucet the research team used the product development process defined by Ulrich & Eppinger [4].

### **2.1 Product development process**

The process of the faucet development project is divided into five different stages. The phases are planning, concept development, system-level design, detail design and testing and refinement. The planning phase is considered to be performed before project started and is not discussed here.

The process is examined from the engineering design point of view. The focus was defined during the concept development phase. The aim that was set in planning phase was to design a configurable electric bathroom faucet, to build prototypes and to compare the manufacturing techniques from the design and manufacturing points of view. Configurability was defined in the concept development stage as the ability to parametrically edit the size and external shapes of the faucet spout maintaining the original design outlook.

### **Concept development**

The structure and the internal components of the reference electric faucet were



investigated. The components of the reference faucet are shown in Fig. 1.

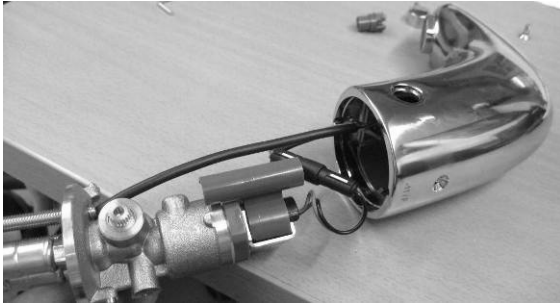


Fig. 1. The spout and the internal components of reference bathroom faucet.

These internal components were decided to be reused in the new faucet design. The components were modelled with Solid Edge software. The team used the CAD documents as a reference in the concept development phase with Rhinoceros [5] as well as in the system level and the detailed design stages with Pro/Engineer Wildfire software. The 3D models were transferred into these systems in STEP format [6].

The use of the existing components set restrictions to the faucet spout design. These components had to fit into the new spout. The positions and the interfaces of the water feed pipe, the thermostat controller, the sensor, and the fitting screw were fixed. Also the thread of the nozzle was fixed. Another requirement for the spout was to design the outlook so it would be intuitive to use. The outlook of each configuration has to guide the user to put the hands into the operation zone where the sensor recognizes the hands and to where the water jet is aimed at.

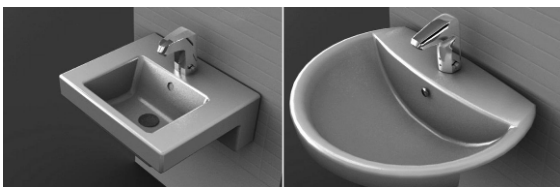


Fig. 2. Proposed concept models created with Rhinoceros software.

The industrial designer of the research team proposed several configuration models and one was selected for the design process. Two examples of the concept models are shown in Fig. 2.

### System-level design

In this case the system-level design can be considered to be divided into two steps: gathering precise information and CAD modelling. The requirements set by the two selected manufacturing methods, sand casting and laser based additive manufacturing (LBAM), were studied. The pattern for sand casting was designed to be manufactured by 3D printing and the core box by NC milling.

The CAD modelling started in Rhinoceros where the surface model of the final outlook was created. The Rhinoceros model was then transferred into Pro/Engineer in STEP format. The modelling had to be started from scratch in Pro/Engineer because the parametric configurability had to be enabled (Fig. 3).

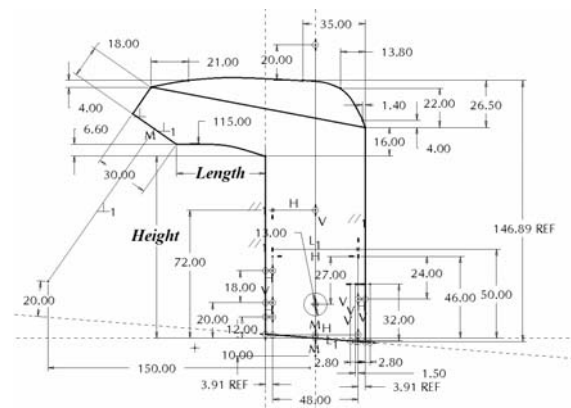


Fig. 3. Parametric model of the chosen concept. *Height* and *Length* can be modified by the design algorithm.

The imported STEP geometry was used as a reference for precise modelling. The profiles were approximated as lines, constant radius arcs and splines with minimal control points. Certain geometric entities were constrained to the STEP geometry. Other entities were first constrained to the STEP geometry to maintain the original design and the constraints were then removed to allow the parametrical editing.

Based on this parametrical solution, a simple CAD model without any internal features was modelled. The demand for ability to modify the size of the spout was set earlier. The size could be edited by changing two parameters: height and

length. To avoid the change of the desired outlook when editing the parameters certain dimensions and geometric entities were set to change relatively to these parameters. If the length of the spout increases, the point where the water jet is aimed at does not increase as much but remains at the hand washing area. Also, a larger spout may look thinner as a smaller one so several dimensions were related to the length parameter with equations to maintain the original outlook with different parameter values.

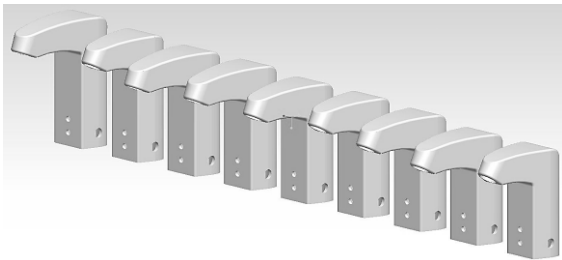


Fig. 4. Different sized instances of the faucet model.

Two types of relations were used. Geometric relations keep entities parallel, perpendicular, tangential, horizontal or vertical to each other. Dimensional relations change the chosen dimensions based on the programmed formula. Setting the geometric relations was straight forward and was done first. The research team discussed which shapes were desired to remain. Formulas for dimensional relations were tested by giving different values for height and length parameters and observing how the outlook was changed. It was examined which dimensions had to be related to the parameters and how much they should change to maintain the desired form. Several dimensions were related to the length parameter linearly. Different sized instances of the model are shown in Fig 4. The external shapes and the parametric solution for configurability were designed for both sand casting and LBAM techniques.

#### Detail design

In detail design the first prototype was made by ZCorp binder jetting machine.

The purpose of the prototype was to make discussion and the design of internal features easier, to see the design physically and to test sand casting. It was binder jetted into two halves to see the internal space and to avoid using cores in possible casting tests.

The research team decided to build two separate CAD models, one for casting and one for LBAM to optimise the model for both methods. Required tapers for casting and overhang supports for LBAM set major requirements for the CAD models. The model designed in the system-level served as a master for both models. The CAD models of internal components were used for designing the interfaces and fittings of the spout.

A product model and a billet model were needed for both casting and LBAM. The product model had all machining and was the CAD representation of the final product. The billet model did not have the machining included. It is a model of a billet produced by casting or by LBAM. The cast billet also had extra features, such as offset taper faces and fillets, which did not exist in the product model. The product and the billet features were modelled to the same CAD file and grouped into machined and billet groups. Additionally, a core box and a pattern had to be designed for the cast spout. To design them associatively a CAD model of the core is needed.

### 3. RESULTS

#### 3.1 Design for casting

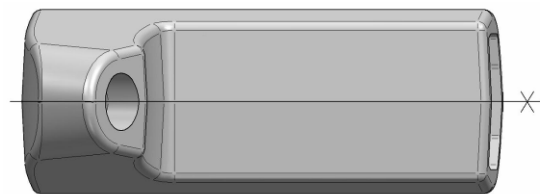


Fig. 5. Joint line of the cast model.

The casting plan was designed collaboratively with casting experts. The joint line is the symmetric plane of the spout (Fig. 5). The casting gutter was designed to be connected to the water feed mount of the spout.

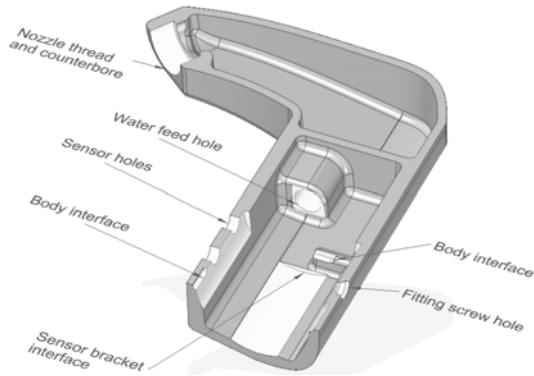


Fig. 6. Machining features of the sand cast spout.

The casting plan set requirements for the tapered surfaces. All taper angles were set to 3°. The external surfaces of the cast billet were offset before tapering in Pro/Engineer to take the required machining allowance and tolerances into account. Only the free hole for the nozzle was designed to be cast but the nozzle thread and all other holes were machining features. The machining features are illustrated in Fig. 6.

### 3.2 Design for laser based additive manufacturing

Manufacturing orientation (i.e. orientation of powder spreading unit) is important in LBAM. Supports were required to be built between the spouts and the platform. Overhang structures, if their building angle is less than 45°, need an additional support structure because powder material is then not any more able to support manufactured parts and droplets are formed to outer surface. The spout was planned to be built in upside down position. This way the orientation was optimal for minimizing overhangs. The only overhang forms to the hollow water chamber. The internal parts of the chamber were wedge-shaped so the restriction on the structure by the building angle was taken into account.

The machining features are illustrated in Fig. 7. The counterbore will be machined after LBAM because the connection with the water feed pipe has to be leak proof. Diameters of holes located perpendicular to the manufacturing direction will not be built precisely because of the bonus-Z

effect, which is the unwanted growth of the part in the z-axis and the part is therefore, out of tolerance. It occurs when the laser energy penetrates beyond the first layer of the part and melts the unsintered powder below the part boundary [7].

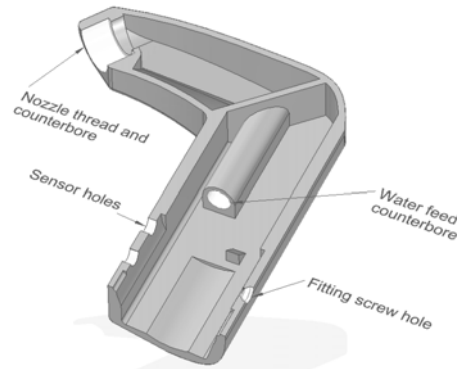


Fig. 7. Machining features of the LBAM spout.

### 3.3 Comparison of the models

Comparison of time spent on design for sand casting and LBAM are represented in Table 1.

	Casting	LBAM
Consulting	11 h	7 h
Configuration model	21 h	14 h
Family instances	2 h	2 h
Tools	7.5 h	
Trail files	5 h	2 h
<b>Total</b>	<b>46.5 h</b>	<b>25 h</b>

Table 1. Time spent in hours on design for sand casting and LBAM.

The time to design the configuration model consists of modelling the configurable product model and the associative billet model. The reason for designing the family instances is to generate and to select customized models from the product family. The associative core, core box and pattern models were included in the tool design. The total time spent on design for casting was 46.5 hours and for LBAM 25 hours.

## 4. CONCLUSION

The current CAD systems are effective in designing complex and configurable products. The used software tools in this research were not the latest versions but

still the utilization of them in a collaborative digital design process was successful.

The import of CAD data in STEP format from Rhinoceros to a parametric model in Pro/Engineer was not successful. The transformation of the geometry to a parametric model needed extra work. The new versions CAD software also from other vendors may provide a solution to this problem.

The design for casting was more time consuming than the design for LBAM. A technique which requires tool design needs more time. In this case the geometry for the casting was more complicated which can be seen in the consulting and configuration model times. Designing the internal geometry of the cast spout as well as planning the casting orientation took their time. The longer time spent on the trial files of the cast model is explained by a bigger amount of parts to be scripted. The geometry of the LBAM spout is simpler. The CAD modelling for the LBAM does not need as much skills because no tools are required but understanding of process limits is required.

## 5. ACKNOWLEDGEMENTS

The faucets were designed and developed in the InnoBusiness project, which is financed by the Technology Development Centre of Finland (TEKES). Oras Company and its personnel are gratefully acknowledged for their contributions and cooperation.

## 6. REFERENCES

- [1] Lehti, A., Taimisto, L., Piili, H., Salminen, A., Nyrhilä, O., *Evaluation of Different Monitoring Methods of Laser Assisted Additive Manufacturing of Stainless Steel*, ECerS XII, June 19-23, 2011, Stockholm, Sweden, 4 p.
- [2] Lehti, A., *Monitoring of stainless steel laser sintering process: comparative study of the suitability of three monitoring*

*methods*, M.Sc. Thesis, Lappeenranta, Finland, 2011, 112 p.

- [3] Lehti, A., Taimisto, L., Piili, H., Nyrhilä, O., Salminen, A., *Correlation between Pyrometer Monitoring and Active Illumination Imaging of Laser Assisted Additive Manufacturing of Stainless Steel*, ICALEO 2011, Orlando, Florida, 10 p.

- [4] Ulrich, K., Eppinger, S. *Product Design and Development*, USA: McGraw-Hill/Irwin, 2004. 366 p. ISBN 0-07-247146-8

- [5] Rhinoceros, Modeling tools for designers, <http://www.rhino3d.com> (09.03.2012)

- [6] ISO 10303. *Automation systems and integration – Product data representation and exchange*, Geneva. International Organization for Standardization. 1994

- [7] Ho, H.C.H., Cheung, W.L., Gibson, I. Effects of graphite powder on the laser sintering behaviour of polycarbonate, *Rapid Prototyping*, 2002, **8**, 233–242, ISSN 1355-2546

## AUTHORS

Aalto University, Department of Engineering Design and Production  
E-mail: [firstname.lastname@aalto.fi](mailto:firstname.lastname@aalto.fi)  
P.O.Box. 14100, 00076 Aalto, Finland

M.Sc. Thomas Widmaier  
M.Sc. Jesse Kontio  
Prof. Jari Juhanko  
Prof. Petri Kuosmanen

Lappeenranta University of Technology  
E-mail: [firstname.lastname@lut.fi](mailto:firstname.lastname@lut.fi)  
P.O.Box 20, 53850 Lappeenranta, Finland

Lic.Sc. Heidi Piili  
Prof. Antti Salminen

## CORRESPONDING ADDRESS

M.Sc. Thomas Widmaier  
Aalto University, Department of Engineering Design and Production  
P.O.Box. 14400, 00076 Aalto, Finland  
Phone: +358 50 5609515  
E-mail: [thomas.widmaier@aalto.fi](mailto:thomas.widmaier@aalto.fi)  
Web: <http://edp.aalto.fi>



## II PRODUCTION ENGINEERING





## RECYCLING OPTIMISATION OF THE ELECTROPHOTOGRAPHIC PRINTS

**Bolanča Mirković I., Majnarić I., & Bolanča S.**

**Abstract:** *The research results of the temperature influence of the offset cylinder in electrophotography with the liquid ElectroInk on the effectiveness of the recycling process of prints have been presented in the paper. By the temperature increase in the domain from 125 – 145<sup>0</sup>C the increase of specks area after pulping appear which then influences their elimination in the flotation process. On the other hand by the increase of temperature the increase of gamut volume of prints appears, i.e. the greater reproduction quality. In the paper the results have been discussed in relation to the principle of electrophotography with the aim of their application in the field of graphic materials development and the ecological sustainability.*

*Key words: recycling, coated paper, electrophotography, image analysis, gamut*

### 1. INTRODUCTION

The digital printing contributes to sustainable development [1]. These printing techniques, in regard to some conventional printing techniques has advantage in fewer influence on environment mainly due to faster make ready and the absence of plate making and its related chemicals, materials, emissions and wastes. The poor deinkability of ink jet and liquid toner electrophotography especially of the former formulations is the biggest environmental challenge of digital printing [2,3].

The recycling of waste paper in relation to the production of virgin paper

influences the consumption of water (25%) and energy (40%), decreases the pollution of the process water (35%) and air (70%), preserves the woods and has the positive economic effect [4].

Deinking is a process for detaching and removing printing inks to improve optical characteristics of pulp and paper using recovered printed material [5]. Deinking plants have several unit operations: pulping, screening, cleaning, washing and/or flotation, dispersion, bleaching, effluent treatment and sludge disposal. Pulping in a deinking plant involves defibering which is accomplished mechanically, and deinking by a combination of chemical, mechanical and thermal action [6]. The most ink detachment is achieved by the addition of chemicals during the defibering operation in the pulper.

Several chemicals are added to the pulper: sodium hydroxide, sodium carbonate, sodium silicate, soaps of fatty acids and surfactants. Bleaching chemicals may be added in the pulper or later in the process, or both [7]. The type and concentration of these chemicals will be a function of the waste paper characteristic to be deinked, the type of separation equipment used to eliminate the contaminants from the pulp slurry and the nature of the end-product [8].

High consistency pulpers used due to the savings in the chemicals, steam, and electrical energy and reduced pulping time [9]. Removal of the detached ink particles then use flotation.

The effectiveness of the deinking

process itself depends on numerous factors. The following ones have to be mentioned: the kind and quantity of chemicals used in different phases of the process as well as the chemical and physical conditions of the system such as pH value, consistency of fiber suspension, defibering time and the hydrodynamic factors of the flotation process [10].

The other influential factors are: the size, shape and the surface properties of the dispersed ink particles, the air volume and the size of the air bubbles have special importance for the effectiveness of deinking flotation. The effectiveness of the process depends on the ability of the printing ink adherence on air bubbles and the strength of this bond in order to prevent their detaching and rebinding to the cellulose fibers [5]. The surfactants stabilize the air bubbles. The surface of the air bubble and the ink is hydrophobic, while the cellulose fibers are hydrophilic.

The main problem of such a complex process is the effectiveness of the printing ink detaching or the toner detaching from the cellulose fibers, removal of the ink particles from the suspension as well as the purification of the waste water. In the described problems, the majority of authors researched the hydrodynamic factors of the process and the influence of chemical and physical conditions of the system on the process effectiveness, while the influence of the conditions in printing process haven't been studied much.

The previous investigations have proved the bad effectiveness of print recycling made in the technique of indirect electrophotography with liquid toner ElectroInk [11]. ElectroInk appears to produce big specks after pulping, which to be difficult to eliminate in a flotation deinking plant. The new generation of ElectroInk produces smaller specks after pulping. Specks which are effectively broken up by dispersion, are floatable in a second flotation loop [12]

The results in this article is a part of the project in which the influence of the conditions in indirect electrophotography (scorotrone, voltage, laser strength, offset cylinder voltage, concentration of the liquid toner etc) on effectiveness of the prints recycling has been researched. Number and area of specks on handsheet made from fibers after pulping and flotation of prints obtained by the change of the working temperature of the offset cylinder at the first transfer of the liquid ElectroInk has been presented.

In order to get the ability - for the prints obtained in the defined conditions of the offset cylinder temperature - to control the print quality and the total information scope on ink (tone, saturation lightness) which is possible to reproduce on the given medium 2D and 3D gamut are presented in the work.

The paper is the contribution to the explanation of the influence of the conditions in electrophotography in the domain of deinkability and it can have the application in the area of the printing materials production and in the design of graphic products taking into consideration the postulates of the sustainable development.

The continuation of our investigations includes the creation of statistical models in the direction of optimisation of the recycling processes of the prints and in the domain of the new graphic material formulation.

## 2. EXPERIMENTAL

¶ The prints made on digital offset machine Turbo Stream HP Indigo were used for analysis. The printing form contained different printing elements: standard CMYK step wedge in the range from 10-100% tone value, standard ISO illustration for the visual control, textual positive and negative microelements, wedges for determination the greyness and the standard wedge with 378 patches for production of ICC profiles and 3D gamut.

ElectroInk of the third generation and the special paper for digital printing, Splendogel EW Soho were used for printing. This paper is coated and it has high brightness grade and its basic characteristics are presented in the table 1.

Parameter	Method	Value
Basis weight	ISO 536	160g/m <sup>2</sup>
Caliper	ISO 534	0,170 mm
Brightness	ISO 2470	93%
Roughness (Bendtsen)	ISO 8791/2-90	57,5ml/min
Water absorption (Coob)	ISO 535	38,49 g/m <sup>2</sup>

Table 1 Characteristics of the paper Splendogel EW Soho

Samples were prepared so that the working temperature of the offset cylinder was changed as follows: 125<sup>0</sup> C, 130<sup>0</sup> C, 135<sup>0</sup> C, 140<sup>0</sup> C and 145<sup>0</sup> C.

For spectrophotometric analysis use X-Rite SwatchBook and ColorShop 2,6 application. From ICC profile with the use of MONACO Platinum program the gamut of prints is established.

For print recycling the method of alkaline chemical deinking flotation was used, which was described in details in the previous work [13]. The handsheets were made using a laboratory sheet former, according to standard method T 205.

For determining ISO brightness of the recycled fibres the spectrophotometer DataColor, Elrepho 450X was used. Specks number and area were assessed with image analysis software Spec\*Scan, Apogee System. This system is utilizing scanner to digitize image. Threshold value (100), white level (75) and black level (65) were chosen after comparing computer images to handsheet.

### 3. RESULTS AND DISCUSSION

As indicator of reproduction quality of prints obtained by the temperature change of the offset cylinder in the process of

indirect electrophotography, two-dimensional and three-dimensional reproduction gamut are shown on fig.1.

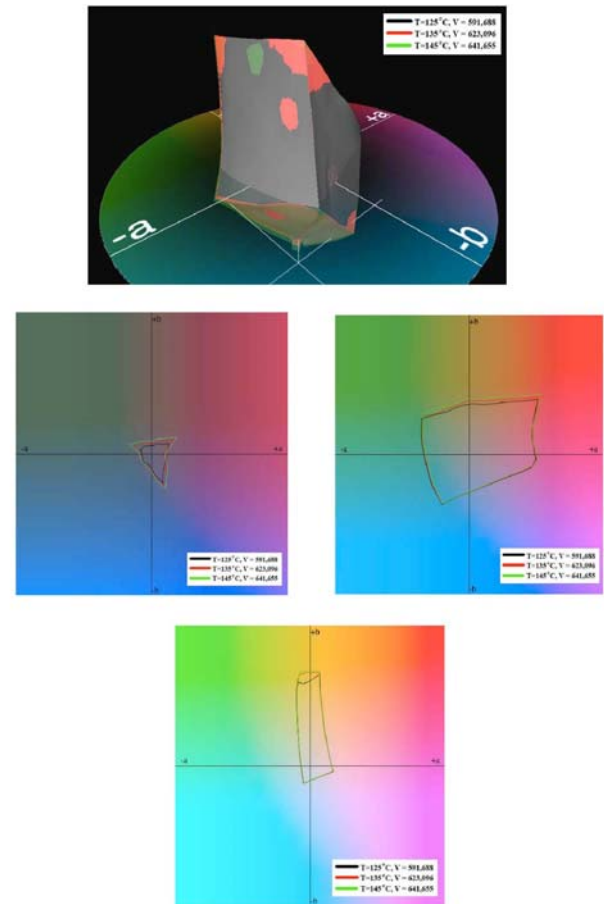


Figure 1. Gamut of print, obtained by using temperature offset cilindre from 125<sup>0</sup> C, 135<sup>0</sup> C and 145<sup>0</sup> in indirect electrophotography printing

The greatest reproduction gamut was achieved at the temperature of 114<sup>0</sup> C and the smallest one at the temperature of 125<sup>0</sup> C.

Sample	V CIE L * a * b * CCU
T=125 <sup>0</sup> C	591.688
T=135 <sup>0</sup> C	623.096
T=145 <sup>0</sup> C	641.655

Table 2. Volumes of gamut V CIE L \* a \* b \* CCU

The gamut increase is not linear with temperature, but it is more expressed in the

lower area from 125<sup>0</sup>C to 135<sup>0</sup>C. The characteristic cross-sections show that the greatest change of tones is in the medium part of gamut. The temperature increase of the offset cylinder influences the increase of the tone values which have high value on +b coordinate, i.e. in yellow tones. At 125<sup>0</sup>C the yellow ink adheres weaker on the printing substrate. Except that, by the increase of the temperature the decrease of the tone colours appear, which have high value on the coordinate -b (green). At the reproduction of the darker tones there are not greater changes.

Figure 2 represents the distribution of the number and area of specks in 26 classes with the size from 0.001-0,006 to <=5 for the handsheet made from the fibers after pulping and after flotation.

Dirt Content Histogram	Dirt Spot Size	Sample Count	Area (sq.mm)
1	>= 5.000	1	10.652
	4.00--5.00	0	
	3.00--4.00	0	
	2.50--3.00	0	
3	2.00--2.50	3	6.624
3	1.50--2.00	3	5.181
7	1.00--1.50	7	8.344
3	0.80--1.00	3	2.656
4	0.60--0.80	4	2.559
11	0.40--0.60	11	5.471
9	0.30--0.40	9	3.163
8	0.25--0.30	8	2.242
6	0.20--0.25	8	1.731
11	0.15--0.20	11	1.935
11	0.10--0.15	11	1.355
4	0.09--0.10	4	0.376
6	0.08--0.09	6	0.504
6	0.07--0.08	8	0.608
18	0.06--0.07	18	1.170
15	0.05--0.06	15	0.817
11	0.04--0.05	11	0.487
19	0.03--0.04	19	0.656
21	0.021--0.03	21	0.522
42	0.013--0.021	42	0.708
109	0.006--0.013	109	1.011
314	0.001--0.006	314	0.978
Totals ->		646	59.751

a) T=125<sup>0</sup> C, after pulping

Dirt Content Histogram	Dirt Spot Size	Sample Count	Area (sq.mm)
	>= 5.000	0	
	4.00--5.00	0	
	3.00--4.00	0	
	2.50--3.00	0	
	2.00--2.50	0	
1	1.50--2.00	1	1.647
3	1.00--1.50	3	3.919
	0.80--1.00	0	
4	0.60--0.80	4	2.862
2	0.40--0.60	2	0.968
2	0.30--0.40	2	0.640
5	0.25--0.30	5	1.367
8	0.20--0.25	8	1.830
4	0.15--0.20	4	0.676
7	0.10--0.15	7	0.875
	0.09--0.10	0	
4	0.08--0.09	4	0.335
2	0.07--0.08	2	0.145
5	0.06--0.07	5	0.332
4	0.05--0.06	4	0.213
2	0.04--0.05	2	0.093
10	0.03--0.04	10	0.357
5	0.021--0.03	5	0.122
13	0.013--0.021	13	0.233
22	0.006--0.013	22	0.195
89	0.001--0.006	89	0.256
Totals ->		192	17.065

b) T=125<sup>0</sup> C, after flotation

Dirt Content Histogram	Dirt Spot Size	Sample Count	Area (sq.mm)
3	>= 5.000	3	22.645
1	4.00--5.00	1	4.434
2	3.00--4.00	2	6.665
1	2.50--3.00	1	2.616
4	2.00--2.50	4	8.629
5	1.50--2.00	5	9.237
7	1.00--1.50	7	8.690
4	0.80--1.00	4	3.396
7	0.60--0.80	7	4.894
18	0.40--0.60	18	8.771
6	0.30--0.40	6	2.065
8	0.25--0.30	8	2.167
5	0.20--0.25	5	1.177
16	0.15--0.20	16	2.740
19	0.10--0.15	19	2.281
3	0.09--0.10	3	0.281
6	0.08--0.09	6	0.496
10	0.07--0.08	10	0.754
9	0.06--0.07	9	0.590
9	0.05--0.06	9	0.487
15	0.04--0.05	15	0.665
24	0.03--0.04	24	0.815
20	0.021--0.03	20	0.516
30	0.013--0.021	30	0.516
90	0.006--0.013	90	0.814
337	0.001--0.006	337	0.970
Totals ->		659	97.312

c) T=135<sup>0</sup> C, after pulping

Dirt Content Histogram	Dirt Spot Size	Sample Count	Area (sq.mm)
	>= 5.000	0	
	4.00--5.00	0	
	3.00--4.00	0	
1	2.50--3.00	1	2.993
	2.00--2.50	0	
1	1.50--2.00	1	1.932
3	0.80--1.00	3	2.597
6	0.60--0.80	6	4.260
4	0.40--0.60	4	1.987
4	0.30--0.40	4	1.355
5	0.25--0.30	5	1.303
2	0.20--0.25	2	0.434
2	0.15--0.20	2	0.371
9	0.10--0.15	9	1.116
1	0.09--0.10	1	0.097
2	0.08--0.09	2	0.163
3	0.07--0.08	3	0.226
4	0.06--0.07	4	0.269
3	0.05--0.06	3	0.163
3	0.04--0.05	3	0.138
5	0.03--0.04	5	0.170
10	0.021--0.03	10	0.254
22	0.013--0.021	22	0.364
44	0.006--0.013	44	0.405
140	0.001--0.006	140	0.332
Totals ->		245	22.104

e) T=135<sup>0</sup> C, after flotation

Dirt Content Histogram	Dirt Spot Size	Sample Count	Area (sq.mm)
4	>= 5.000	4	60.491
4	4.00--5.00	4	17.882
2	3.00--4.00	2	6.493
1	2.50--3.00	1	2.514
1	2.00--2.50	1	2.346
3	1.50--2.00	3	4.884
8	1.00--1.50	8	9.909
7	0.80--1.00	7	6.224
8	0.60--0.80	8	5.584
16	0.40--0.60	16	7.815
8	0.30--0.40	8	2.830
6	0.25--0.30	6	1.665
10	0.20--0.25	10	2.251
6	0.15--0.20	6	1.030
16	0.10--0.15	16	1.849
4	0.09--0.10	4	0.378
7	0.08--0.09	7	0.606
5	0.07--0.08	5	0.389
7	0.06--0.07	7	0.457
13	0.05--0.06	13	0.679
6	0.04--0.05	6	0.258
12	0.03--0.04	12	0.398
23	0.021--0.03	23	0.568
43	0.013--0.021	43	0.715
88	0.006--0.013	88	0.835
333	0.001--0.006	333	0.932
Totals ->		641	139.982

f) T=145<sup>0</sup> C, after pulping

Dirt Content Histogram	Dirt Spot Size	Sample Count	Area (sq.mm)
1	>= 5,000	1	5.317
1	4,00-5,00	1	4.034
1	3,00-4,00	1	3.348
2	2,50-3,00	0	
2	2,00-2,50	2	4.706
2	1,50-2,00	2	3.185
6	1,00-1,50	6	7.658
4	0,80-1,00	4	3.790
5	0,60-0,80	5	3.647
8	0,40-0,60	8	3.651
6	0,30-0,40	6	2.075
5	0,25-0,30	5	1.342
7	0,20-0,25	7	1.624
16	0,15-0,20	16	2.778
11	0,10-0,15	11	1.401
4	0,09-0,10	4	0.389
5	0,08-0,09	5	0.416
3	0,07-0,08	3	0.219
3	0,06-0,07	3	0.197
6	0,05-0,06	6	0.310
12	0,04-0,05	12	0.541
10	0,03-0,04	10	0.358
9	0,021-0,03	9	0.231
19	0,013-0,021	19	0.317
58	0,006-0,013	58	0.530
186	0,001-0,006	186	0.536
Totals ->		390	52.600

g) T= 145<sup>0</sup> C, after flotation

Figure 2. Results of the image analysis of handsheet obtained by the recycling of electrophotographic prints in relation to the temperature of the offset cylinder

The results show that the effectiveness of removing the specks decreases by the increase of the offset cylinder temperature.

On electrophotographic machines with liquid ElectroInk in the fourth phases is the first ink transfer. It is performed over the offset cylinder. By the activation of Pre Transfer Erase (PTE) the process of ink transfer begins. The emanation with PTS neutralizes the photoconductor surface which results in the possibility of discharging the negatively charged ink from the photoconductor on the positively charged transfer cylinder.

Sample	Number of specks removed by flotation [%]	Area of specks decreased by flotation [%]
T=125 <sup>0</sup> C	70,3	71,4
T=130 <sup>0</sup> C	63,7	79,6
T=135 <sup>0</sup> C	62,8	77,3
T=140 <sup>0</sup> C	37,2	58,2
T=145 <sup>0</sup> C	39,2	61,6

Table 3. Flotation effectiveness

In the first transfer the ElectroInk is brought into contact with the heated rubber blanket. At high temperature the Isopar evaporates which results in the change of the physical state of ElectroInk. From the liquid state the ElectroInk changes into the paste state.

The part of Isopar can be regulated in the paste ElectroInk by adjusting the temperature of the offset cylinder.

The second transfer follows, in which the ElectroInk on the transfer cylinder and the paper on the printing cylinder have to be brought in contact. In this contact the Isopar forms a thin oil layer among the pigment particles and the rubber blanket. The toner particles are pressed into the cold paper and the rest of Isopar evaporates completely.

In the contact of the toner particles and the paper there is the attraction by electrostatic forces as well as between molecular Van der Waals ones.

The described principle and the change of temperature in the defined area leads to the increased number and surface of specs in the phases of the pulping prints as it is presented in the table 4.

The results of the speck area in the table 4 and in the figure 1 explain the badly effectiveness of flotation in relation to the temperature of the offset cylinder. In the flotation is effective in the 10 to 100 μm range [14,15].

Sample	Total number of specks >=0.04mm <sup>2</sup>	Total number of specks >=5mm <sup>2</sup>	Area for specks >=5mm <sup>2</sup>
T=125 <sup>0</sup> C	141	1	10,652
T=130 <sup>0</sup> C	148	2	12. 839
T=135 <sup>0</sup> C	158	3	22.645
T=140 <sup>0</sup> C	161	3	30.588
T=145 <sup>0</sup> C	142	4	60.491

Table 4. Number and the area of specks >=5 mm<sup>2</sup> after pulping in dependence on temperature of the offset cylinder

#### 4. CONCLUSIONS

Based on the results of the image analysis of handsheet obtained from the fibres from the pulping process it can be concluded that by the increase of the offset cylinder temperature in the area from 125-145<sup>0</sup>C the number and the surface of specks increase. The increase of the number of great specs was estimated, as well as of those in the area  $\geq 5\text{mm}^2$ . This is the cause of the worse flotation effectiveness which decreases with the increase of temperature from about 70% to 30%.

On the other hand, by the increase of the offset cylinder temperature in the investigated interval the gamut volume increases for about 49.967 space units which points at the greater reproduction quality.

Knowing that the indirect electrophotography printing is a complex process, with six separate, synchronous phases, the needs and characteristics of the graphic material, along with a number of factors in the field of chemical deinking flotation should be considered. In the further research the experimental design will be used and statistical models will be created to obtain information about optimising processes in the direction of environmental sustainability in this area.

#### 5. REFERENCES

- [1] Viluksela P., Pihkola H., Behm K., Wessman H., Pajula T., Changes in sustainability due to technology development in selected printing processes. In: Advances in Printing and Media Technology. Edlunds N., Lovreček M., (Eds.) IARIGAI, Darmstadt, 2008
- [2] Bolanča I., Bolanča Z., Majnarić I., The Influence of the Digital Printing of Packaging on the Characteristics of the Recycled Fibers Proceedings on Internationale Digital Printing Conference, Amsterdam, (2005), 100
- [3] Carre B., Deinkability of ink jet prints: a new challenge to solve, 3<sup>rd</sup> CTP Research Forum Recycled Fibres, Grenoble, 30-31 January 2001
- [4] Recycled paper facts, <http://beterpaper.nimg.com> (29.02.2012.)
- [5] Renner K., Deinkability of printing inks in: Recycled Fiber and Deinking, Götsching L., Pakarinen H., (Eds) Fapet Oy, 2000
- [6] Fabry B., Pulping and ink detachment, 8<sup>th</sup> ATC Deinking, Grenoble, 29-31 May 2007
- [7] Ayala C., Bleaching of deinked pulp, 8<sup>th</sup> CTP/PTS Advanced Deinking Training Course, Grenoble, 2007
- [8] Theander K., Chemistry studies on surfactant properties relevant to flotation deinking, Vetenskap Och Konst, Stockholm, 2003
- [9] Koffinke R.A., High-consistency slushing effective in deinking, contaminant removal, *Pulp and Paper*, 2004, **58**, 58-61
- [10] Lassus A., (2000) Deinking Chemistry, In: Recycled Fiber and Deinking, Götsching L., Pakarinen H., (Eds.), 241-266, Fapet Oy, ISBN 952-5216-07-1, Jyväskylä
- [11] Fisher A., Digital prints-not all of them are deinkable, Ingede Seminar, September, 2008, Vienna
- [12] Ayala, C., Carre B., Recent progress in the deinking of HP-INDIGO prints, PTS/CTP Deinking Symposium, 2006
- [13] Bolanaca Mirkovic I., Bolanca Z., (2005), Optical properties of deinked pulp, *Journal of Imaging Science and Technology*, 49(3) (2005)284-292
- [14] McCool A., Silveri L., Removal of specks and nondispersed ink from a deinking furnish, *Tappi J.*, 1987, **79** (11)75-78
- [15] Moss, C.S., Theory and reality for contaminant removal curves, *Tappi J.* 1997, **80**, (4), 6

#### 6. CORRESPONDING ADDRESS

Assis.Prof.PhD. Ivana Bolanča Mirković  
University of Zagreb, Faculty of Graphic Arts, Getaldićeva 2, 10000 Zagreb, Croatia, [ibolanca@grf.hr](mailto:ibolanca@grf.hr)



## THE IMPACT OF HIGH-SPEED MILLING ON 3D SURFACE ROUGHNESS PARAMETERS

**Brutans, V.; Torims, T.; Kumermanis M.; Rosado Castellano, P.; Torres, R.;  
Gutierrez Rubert S. C.**

**Abstract:** *High-speed machining is a highly effective production method to achieve the following goals: increased machining productivity, enhanced quality of the machined surface, improved machining economy, improved ecological impact of machining. The objective of this research was to study the technological factors which influence the 3D surface roughness parameters in high-speed milling of two different types of die steel. The factors analysed were the feed rate, overlap and strategy. The depth of cut and cutting speed were kept constant. This article is based on the technological experiment performed in the Department of Mechanical and Materials Engineering of the Polytechnic University of Valencia and measurements of the 3D surface topography in the Mechanical Engineering Institute of Riga Technical University.*

Key words: machining, high-speed machining, cutting, milling, 3D roughness, surface quality.

### 1. INTRODUCTION

High-speed milling (HSM) is being increasingly used in various production processes and has particular advantages in die production. However, publicly available scientific publications are not providing in-depth studies on the correlation between HSM and surface topography. In particular, the influence of the technological parameters of high-speed milling on the 3D roughness parameters is currently uncharted territory. In fact, much

research has been conducted into the area of 2D roughness, but 3D roughness measuring methods and equipment is relatively new.

The overall aim of this research is to improve technological processes (provide recommendations) in order to obtain optimal surface roughness.

The research was conducted in cooperation between the Polytechnic University of Valencia and Riga Technical University.

### 2. HIGH-SPEED MILLING

High-speed milling has found its way out of the laboratory and is becoming an industrial practice. However, it is generally considered to be a new manufacturing technology. This method has many benefits



Fig. 1. Gentiger GT-66V-T16B

compared to conventional milling. Very often, high-speed milling is considered solely as a way to improve productivity



resulting from faster cutting speeds than those used conventionally. Seldom is it emphasised that the product quality can be improved as a consequence of increased accuracy and better surface finish [1].

This research has been conducted on a Gentiger GT-66V-T16B high-speed milling machine (see Fig. 1.). The machine is located in the Department of Mechanical and Materials Engineering of the Polytechnic University of Valencia.

The main technical specifications of the machine are shown in Table 1.

Table 1. Technical specifications of the Gentiger GT-66V-T16B

Spindle speed	16,000 rpm
Spindle motor	26 kW
Rapid feed rate	30 m/min
X/Y/Z-axis servo motor	Each 4.7 kW

### 3. MEASURING ROUGHNESS IN 3D

Existing surface roughness standards comprise only two dimensions. However, the real roughness of the surface is three-dimensional (3D). Roughness parameters of the 3D surface are also important in analysing the mechanics of contact surfaces. Problems in the mechanics of contact surfaces arise owing to a lack of accuracy in defining 3D surface roughness characteristics. One of the most important factors in determining 3D characteristics is the number of data points per x and y axes. The number of data points helps us to define the cut-off length. The number of data points has a significant influence on the accuracy of measurement results, measuring time and size of the output data file (especially along the y-axis, where the number of data points is the number of parallel profiles). The number of data points must be optimal. Too few data points lead to inaccurate results and increased distribution amplitude; but too many data points substantially increase measuring time without broadening the range of fundamental information. The aim

is therefore to find the optimal number of data points for each surface processing method [2].

For the practical 3D roughness measuring, Riga Technical University is using the Taylor Hobson Form Talysurf Intra 50 measuring device with TalyMap Expert data software.

The technical specifications of Talysurf are listed in Table 2.

Table 2. Technical specifications of the Taylor Hobson Form Talysurf Intra 50

Horizontal Performance	
Traverse length – X Min/Max	0.1 mm to 50 mm
Traverse/ measuring speeds	10 mm/s max / 1 mm/s
Data sampling interval in X	0.5 $\mu$ m
Straightness error (Pt)	0.4 $\mu$ m over 50 mm 0.2 $\mu$ m over any 20 mm
Vertical Performance	
Nominal measuring range (Z)	1 mm
Resolution (Z)	16 nm @ 1 mm range 3 nm @ 0.2 mm range
Range to resolution ratio	65,536:1
Stylus arm length, tip size, force	60 mm arm, 2 $\mu$ m radius conisphere diamond stylus, 1 mN force

The practical advantages of the 3D roughness measuring device are shown in Figs. 2 and 3. Both pictures are of the same machined sample surface in one case (see Fig. 3) with camera (zoom 50x), in other case with 3D roughness measuring device in 2D View (see Fig. 3).

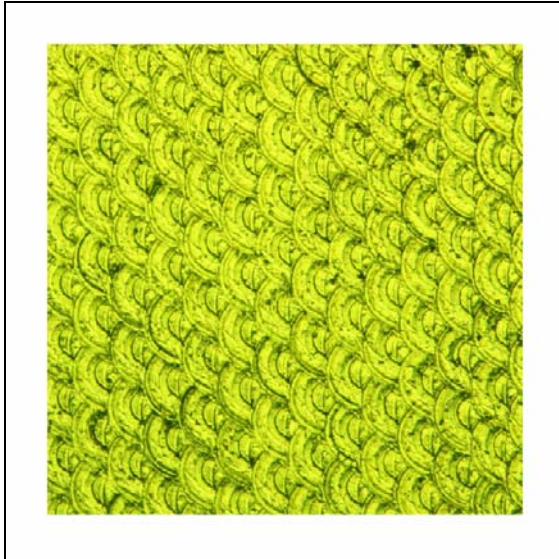


Fig. 2. 2D View from digital camera

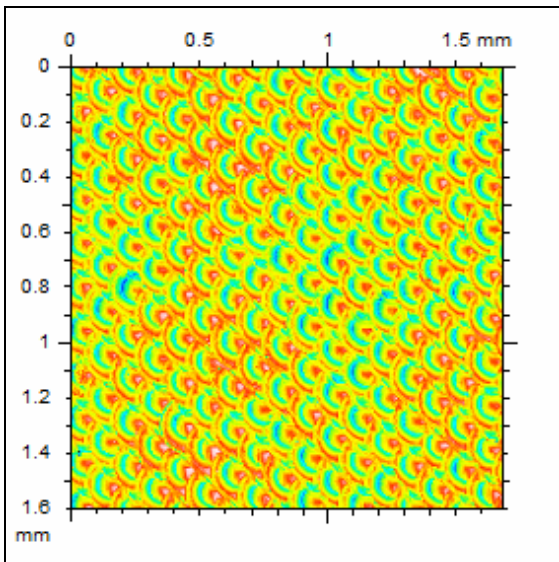


Fig. 3. 2D View from roughness measuring device

#### 4. APPROACH

The experimental research was based on the most popular die steel samples, i.e. 1.2312 (40CrMnMo58-6) and 1.1730 (C45W). Each sample was divided into 16 conditional parts → subsamples (see Fig. 4). Each subsample was machined with a different combination of cutting parameters (feed rate, strategy, pattern and overlap). The depth of cut and cutting speed parameters were kept constant. Also, the same tool was used for all the subsamples.

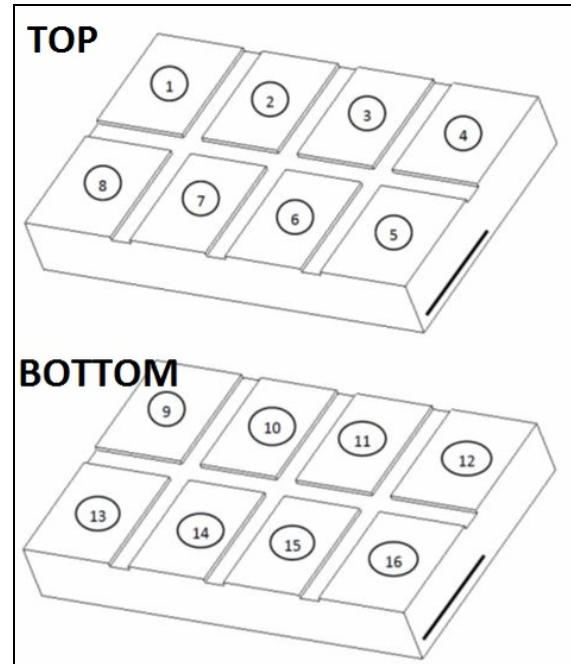


Fig. 4. Subsample numbering

All the cutting conditions and combinations are shown in Table 3.

Table 3. Cutting conditions

Sample	Strategy	Overlap	Feed
1	LP	LO	LF
2	LP	LO	MF
3	LP	LO	HF
4	CP	LO	MF
5	CP	LO	HF
6	LP	HO	HF
7	LP	HO	LF
8	LP	HO	MF
9	CP	HO	LF
10	TLP	LO	MF
11	TLP	LO	HF
12	CP	HO	MF
13	CP	HO	HF
14	TLP	HO	LF
15	TLP	HO	MF
16	TLP	HO	HF
List of abbreviations			
LP	Linear Pattern	HO	High Overlap
CP	Circular Pattern	LF	Low Feed
TL P	Two linear Pattern	MF	Medium Feed
LO	Low Overlap	HF	High Feed

The cutter marked VC2E5BR0400 [VC-2E5B.R4] made by Mitsubishi was

selected for this experiment. The cutter diameter is 8 mm.

## 5. RESULTS

The main findings of this experiment were the identification of major factors and the interaction of factors that affect the surface roughness of machined die steel samples. In order to derive definitive conclusions from this research, we have to collect data from all individually machined subsamples. In this case, we have 32 subsamples with their 2D (example see Fig. 6) and 3D (example see Fig. 5) surface roughness parameters and diagrams.

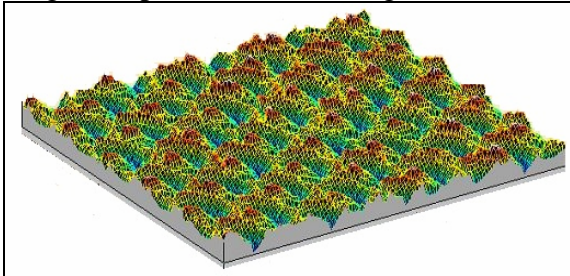


Fig. 5. 3D surface roughness

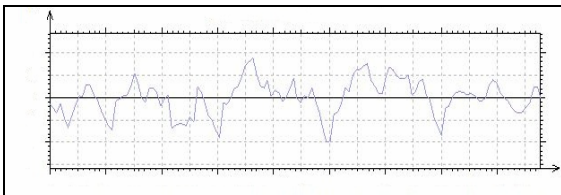


Fig. 6. 2D surface roughness

These results allow us to find the compatibility between the 2D and 3D surface roughness parameters. Analysis of data in ANOVA also provides us with some conclusions.

## 6. CONCLUSION

Initial results of the research outlined above revealed that:

- 1) strategy was the main factor affecting the quality of surface finish.
- 2) the circular pattern strategy provides relatively better surface quality.
- 3) the interaction of strategy and overlap associated with the feed rate had a

direct impact on the 2D and 3D surface roughness.

- 4) higher feed rate provides better surface roughness quality.

Although these are significant conclusions, the research ought to be developed much further. In-depth, comprehensive data analysis will be carried out.

It is important to note that during this research, several non-conventional and unexpected results appeared. These special cases will be further examined.

## 7. REFERENCES

- [1] Kauppinen V., High-speed milling – A New Manufacturing Technology, 4th International DAAAM Conference “Industrial engineering – innovation as competitive edge for SME”, April 2004, Tallinn, pp. 131-134
- [2] Kumermanis M., Rudzitis J., Avisane A. Investigations of 3D Surface Roughness Characteristic's Accuracy // Proceedings of the 11th International Conference of the European Society for Precision Engineering and Nanotechnology, Lake Como, Italy, 23-27 May, 2011, pp. 145-149
- [3] Novakova J., Petrkovska L., Brychta J., Cep R., Ocenasova L., Influence of High Speed Parameters on the Quality of Machined Surface, World Academy of Science, 2009, pp. 274-277
- [4] Vorsari M., Jirapattarasilp K., Kaewkuekool S., The Effect of High-speed Milling on Surface Roughness of Hardened Tool Steel, World Academy of Science, 2011, pp. 469-472

## 8. DATA ABOUT AUTHOR

Valdis Brutans  
Ezermalas street 6k-108  
Riga, Latvia, LV-1006  
Phone: +371-29532998  
E-mail: valdis.brutans@rtu.lv

## RESEARCHES REGARDING THE NOISE AND VIBRATIONS OF METAL TOOTHED WHEEL GEARS AFTER APPLYING A FLUOROPOLYMER DISPERSION OF XYLAN 1052

Caramidaru, V. D.; Vela, I.; Tufoi, M. & Gruescu, C. A.

**Abstract:** *Noise and vibration have a wide spreading in mechanisms. They cause multiple problems that lead to decreasing the lifetime of mechanisms and noisy operation. In the case of the gears, an important source of vibration is placed where toothed wheels are meshing. Shocks appear at the contact between the two homologous flanks, movements as rolling and sliding are generating vibrations as well. Considering that the gear assembling was well done, the vibrations and the noises depend on the processing accuracy of flank contact surfaces, speed and torque. Assuming that a thin layer of shock absorptive material is applied on the flanks, some of the contact energy will be absorbed by it. We investigated comparatively the level of vibrations and noises. The research was made on one step helical gear, including two cylindrical toothed wheels, data being acquired for three differently processed teeth flank. In the first step, the teeth flank is processed only by grinding, after a film dispersion of Xylan 1052 is applied on all flanks. In the last stage, the dispersion layer will be taken down and the teeth will be rectified in order to get two higher precision classes.*

*Key words: teflonized, rectified, grinded, load, Xylan 1052, vibration, noise.*

### 1. INTRODUCTION

While industrial progress is increasing, many technologies are developed for the improving and the optimizing the existing

mechanisms. Thus, in the beginning, the well known gear devices have been manufactured from all kinds of steel and they were improved from many points of view such as: material, production technology, geometry and functionality [3], [4], [5]. All these are leading to various parameters improvement: increasing the rotation speed, torque augmentation, mass decreasing, better corrosion resistance and vibration - noise diminution.

Gears are usually used to transmit torque and speed by a gear ratio. Speaking about gears equipped with cylindrical toothed wheels, in order to have more power transmitted at a higher speed, the material used for wheels fabrication and the teeth flank processing have to be as better as possible. Generally speaking, alloy steels and highly processed surfaces of flanks are used.

A good forward step represents the case of plastic-metal mixture for not so highly-loaded toothed wheels.

By teflonizing the steel wheel, the protection against possible corrosive agents, that can be found in the operation environment, is increased.

We cannot neglect the fact that for an appreciable period of time, such gear equipped with this kind of teflonized toothed wheels can operate with poor lubrication or without lubrication.

Due to the fact that Xylan 1052 is a high-pressure resistant Teflon (PTFE), by adding it on the flank teeth surface, we should obtain a decreasing of vibrations and noise amplitudes.



Therefore, this solution achieved by mixing a steel wheel with a composite-plastic like Xylan 1052, was studied on the test stand as well.

In the last stage, the dispersion layer will be taken down and the teeth flank will be rectified to the corresponding 6 precision class.

The rectification is the machining process of a metal surface (surface smoothing) with an abrasive stone in order to reduce the machining precision class (in our case from 8-grinding to 6-rectifying) and to improve the profile form error and flank alignment error.

## 2. PROBLEM FORMULATION

### 2.1 Vibration generator

In a cylindrical gear, the vibrations are initiated first of all by the teeth gearing. As it is shown in figure 1, the vibrations produced in a gear reducer unit are transmitted through the shafts and the bearings of the housing (casing) whose walls propagate vibrations in the air and lead to the noise appearance. The energy vibrations can be partially transmitted through the shafts both to the driven machine and to the driving one, there dissipating in the air as noise. Vice versa, the gear reducer unit can transmit vibration energy from the driving machine, respectively from the driven one which later it is radiated also as noise through the housing (casing) [3], [4].

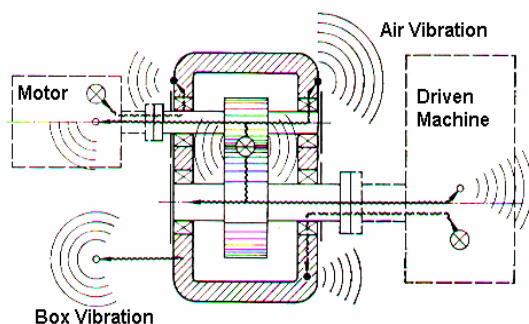


Fig. 1. Gearbox that vibration generator

where:

- × - vibration generator;
- ° - vibration emitter.

In fig. 1, the vibration generators and emitters are theoretically positioned.

Considering that the shafts via ball-bearings transmit better the vibrations produced by the teeth meshing, the accelerometer mounting places were selected over the input bearing A and the output bearing B of the gear (Fig. 3).

### 2.2 Test stand description

The vibration and noise tests were performed on an existent test stand that was specially designed for testing one step gear equipped with two cylindrical toothed wheels [1].

It consists in one 2.5 kW DC motor that drives - via our test gear - an oil pump. This test stand represents a mechanical assembly in an open energetic flux.

As it can be seen in the figure, the triaxial accelerometer was placed above the bearing and the microphone was mounted in the middle of the top surface of gearbox. Vibration and noise measurements were achieved by Bruel & Kjaer PULSE Sound and Vibration Analyzer hardware platform, including FFT & CPB Analysis dedicated software type 7700.

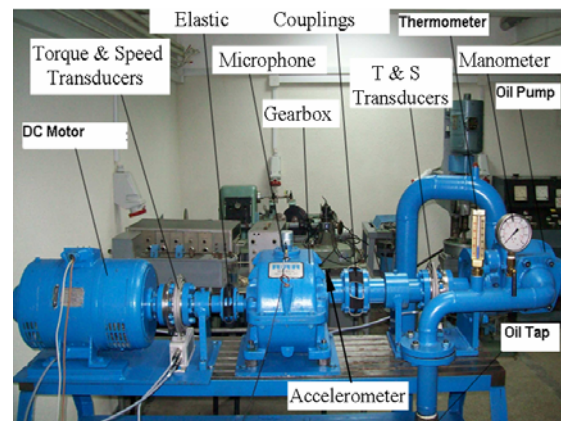


Fig. 2. Test stand

It is able to get signal from the transducers on four channels. The first three channels have been used for the accelerometer and the fourth one was dedicated to the microphone.

Speed produce noise and for the noise amplitude detection, a high performance microphone has been used.

The HBM T10F/FS torque flange extends the range covered to greater accuracy, higher speeds and smaller outside diameters. It is based on a modified T10F measuring body and also it uses the shear stress principle of measurement. The measuring body and the torque introduction part are made of one piece. The patented, compact measuring body geometry increases the measurement precision. The low weight relieves the load on the bearing. Lower mass moments of inertia result in lower dynamic moments when accelerating and braking. Because there are no bearings or slip-rings, there are no maintenance costs involved with the torque and magnetic speed measuring system. Thanks to the modular structure there is a large number of mechatronic variants, making possible the correct torque flange choosing for particular application.

The MP60 is a single channel amplifier for incremental transducers and HBM torque flanges with frequency output, 0.05 accuracy class.

### 2.3 Xylan 1052 coated toothed wheels characteristics

We expect that gear mesh frequency to be the dominant source of vibration and noise and not the natural frequency of gear. That is true in the case of misalignments and when wrong assembling occurs. Also, as many sub-assemblies are into the mechanical device, many natural frequencies could appear and they have a variation of amplitudes depending on the excitation frequency and on the excitation frequency amplitude [2].

By fluoropolymer dispersion process, the geometrical forms such as: profile form error, profile angle error, longitudinal form error, total alignment error, radial run-out, they could be worse than in the case of rectification.

For experimental tests, two toothed wheels have been used, with the following characteristics according to the table 1:

Characteristics	Pinion	Wheel
Pressure angle ( $\alpha$ )	20°	20°
Helix angle ( $\beta$ )	11°	11°
Centre distance (a)	125(mm)	125(mm)
Normal module ( $m_n$ )	4(mm)	4(mm)
Frontal module ( $m_t$ )	4.07(mm)	4.07(mm)
Tooth number ( $z_{1/2}$ )	17	43
Tip diameters ( $d_{a1/2}$ )	80.04(mm)	185.54(mm)
Pitch diameters ( $d_{1/2}$ )	69.27(mm)	175.22(mm)
Root diameters ( $d_{f1/2}$ )	61.47(mm)	166.9(mm)
Base diameters ( $d_{b1/2}$ )	64.95(mm)	164.29(mm)
Tooth heights ( $h_{1/2}$ )	9.28(mm)	9.32(mm)
Tip/root tooth heights	5.38/3.9	5.16/4.16
Tooth heights on cord	5.57(mm)	5.23(mm)
Gear backlash	0.15/0.27	0.15/0.27

Table 1. Pinion and wheel characteristics

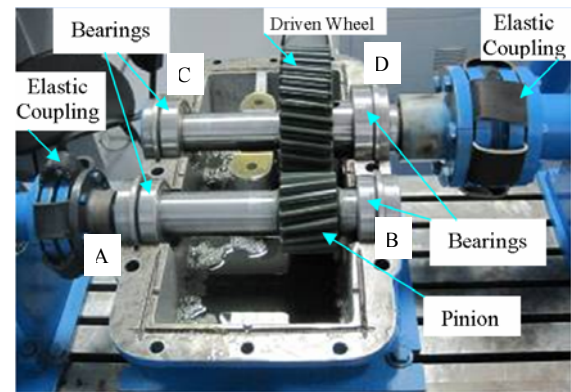


Fig. 3. The mounting position of the pinion and gear wheel

In fig. 3, both toothed wheels are visible and also their mounting position. The Xylan 1052 coating color is specifically dark green as in the above picture.

### 3. EXPERIMENTAL RESEARCH

During measurements, highly vibration amplitudes would appear due to natural entire assembly frequencies and its harmonics materializes in vibration amplitude amplification, leading to resonance. Because we wanted to study only the vibration produced by the gears, the analyze FFT (Fast Fourier Transformation) was used, recording peaks (amplitudes) of the accelerations and velocities measured at the frequency of engagement, respectively its harmonics [1]. In Fig. 4 a quite high amplitude difference is observed between grinded flanks and teflonized flanks near the resonance frequency. while not so much difference between teflonized and rectified flanks is seen.

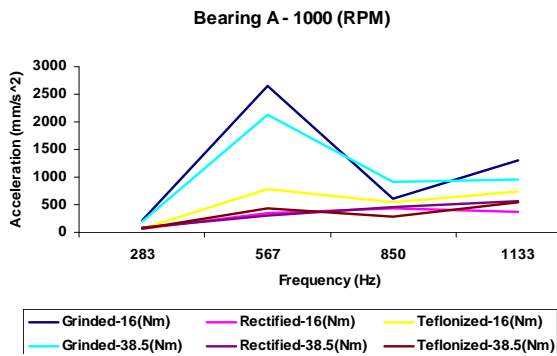


Fig. 4 The acceleration variant depending on the A bearing frequency at a rotation speed of 1000 rpm and a constant load moment

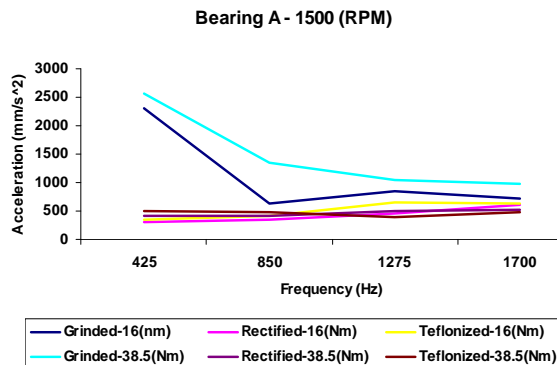


Fig. 5. The acceleration variant depending on the A bearing frequency at a rotation speed of 1500 rpm and a constant load moment

At the gear output, the characteristic shapes evolution is almost the same as in the case of the bearing A. Here, on bearing D instead, between grinded and teflonized flanks there is appreciatively an equal difference of the vibration amplitude, as in between teflonized and rectified flanks.

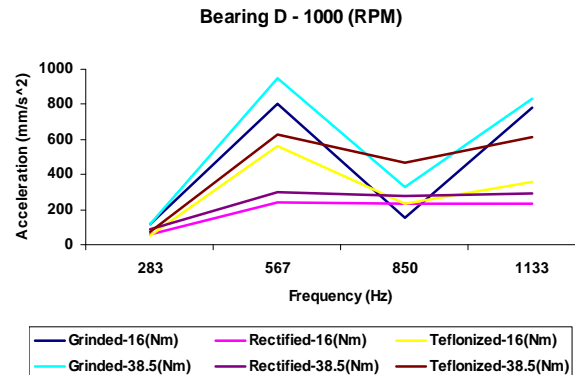


Fig. 6. The acceleration variant depending on the D bearing frequency at a rotation speed of 1000 rpm and a constant load moment

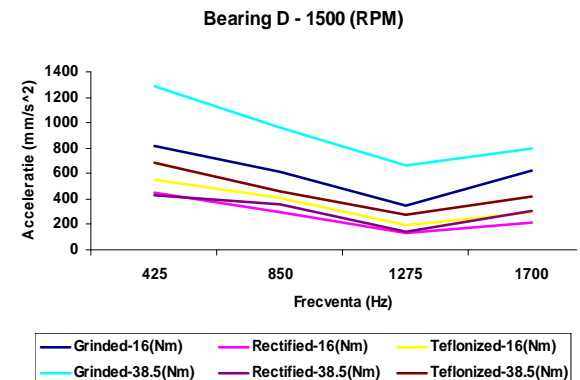


Fig. 7. The acceleration variant depending on the D bearing frequency at a rotation speed of 1500 rpm and a constant load moment

On the same bearing D (Fig. 7), but at the 1500 (RPM) rotation speed, it is noted an important decrease of vibration amplitudes in about of the natural frequency second harmonic and an increasing in proximity of the main harmonic.

The noise amplitudes evolution is drawn in the fig. 8. For all four cases, the noise is increasing on average in the same time with the increment of rotation speed and torque.



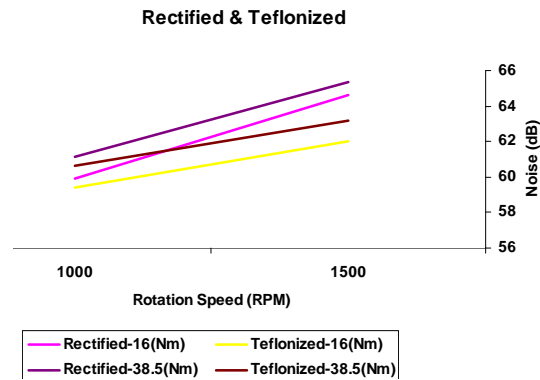


Fig. 8. The noise variant depending on the rotation speed at constant load moments

#### 4. CONCLUSIONS

Increasing the precision class to 6, vibration and noise are significantly diminished at all frequencies taken as references in research. It is notable that the amplitudes of the vibration and the noise are decreasing in the case of a thin Xylan 1052 layer applied only on the grinded flank surfaces as well.

Relatively, comparing the vibration and noise amplitude values in the both cases of teflonized flanks and rectified flanks, they are quite the same. These are easy visible even if amplitude values are enlarged by device natural frequency and its harmonics excitation.

Concluding, the research purpose has been achieved, meaning, when there are imposed high conditions of vibration and noise we can choose the teflonizing of the flanks gears as the this process is easier and cheaper than the rectification.

#### 5. ACKNOWLEDGEMENTS

Special thanks to Mr. Zoltan Korca from "Reductoare Resita SA" for the design and execution of the test stand. We also thank SC Technicoat ROMANIA SRL Campina for filling the tooth flanks of the gears with fluoropolymer dispersion of Xylan 1052.

#### 6. REFERENCES

- (1) Caramidaru, V.D.; Vela, I.; Tufoi, M. & Gruescu, C.A. (2011). *The Influence of the Number of Teflon-Coated Layers Over the Vibrations and Noises to Gear Units Wheel cylindrical Gears*, Annals of DAAAM for 2011 & Proceedings of the 22nd International DAAAM Symposium, ISBN 978-3-901509-83-4, ISSN 1726-9679, Published by DAAAM International, Vienna, Austria 2011, vol. **22**, no. 1, pp 1125-1126.
- (2) Mituletu, I.C.; Vela, I.; Caramidaru, V.D. *Load Torque and Speed Rotation Influence on the Vibration and the Noise of One Step Helical Gear Equipped with Teflonized Cylindrical Toothed Wheels*, "Eftimie Murgu" University of Resita Engineering Faculty, Robotica & Management International Journal, ISSN 1453-2069, June 2011, vol. **16**, no. 1.
- (3) Korca, Z. I. *Cercetari privind reducerea vibratiilor in functionarea reductoarelor cu roti dintate cilindrice*, Teza de Doctorat, Universitatea "Eftimie Murgu" Resita, Facultatea de Inginerie, 2009.
- (4) Korca, Z.; Vela, I. *Design and Execution of a Test Rig for Studying the Vibrations of a Gearbox*, Analele Universitatii "Eftimie Murgu" Resita, Fascicola Inginerie, ISSN 1453-7397, 2008, Nr. **1**, pp. 134-140.
- (5) Bratu, M.; Ropota, I.; Vasile, O.; Dumitrescu, O.; Munteanu, M. *Reserch on the absorbing properties of some new types of composite materials*, Romanian Journal of Materials, ISSN 1583-3186, 2011, vol. **41** (2), pp. 147-154.

#### 7. ADDITIONAL DATA ABOUT THE AUTHOR

Virgil Dan Caramidaru / Eftimie Murgu University of Resita Engineering Faculty, Piata Traian Vuia, no. 1-4, 320085, Resita, Romania / [v.caramidaru@uem.ro](mailto:v.caramidaru@uem.ro) / 0040746035353

## THE CALCULATIONS OF NUTDRIVERS ELECTRICITY CONSUMPTION WHEN ASSEMBLING FIXED THREADED JOINTS

Grinevich I.; Mozga N.

**Abstract:** *In given article the nut driver's electric power consumption studies depending on the corresponding fixed threaded joint's assembly time are made. So far there are no recommendations from the tool manufactures for nut driver's optimal operating modes (the conclusion is made based on the attached instructions which provide instrument manufacturers), when evaluating this aspect taking into account the electrical power consumption and assembly time for different types of fixed threaded joints (wood, metal, plastic, etc.) and also taking into account obtainable tightening moments.*

**Keywords:** *fixed threaded joints, electric power, power consumption calculations, assembly time, optimization, optimal operating modes.*

### 1. INTRODUCTION

In nowadays automated manufacturing the question concerning electric power consumption reduction is of great interest, and it leaves its impact on the final product cost. One of the options for reducing consumption of electric power is an efficient nut driver – screwdriver's use. Further is offered the example of calculations of electric motor's power consumption in order to determine the optimal operating mode when assembling fixed threaded joints.

In the literature [3, 5, 12, 13] is described the power estimation addition from the beginning of speed and load torque, but there is no information about the energy dependence from the set speed. This is due to the fact that the electric motor is usually

used at a constant or slowly changing mode. In quickly changing regime it is not possible to measure the power using the traditional methods (using a wattmeter). Using an electric motor in short-term regimes, it is needed to calculate power for each mode separately. The engine parameters are examined only in the range that they can achieve and it is not considered possibilities to extend this range. This is done because it requires additional investments in order to develop a new equipment.

Knowing what power the electric motor develops and each regime's time it is possible to determine the electric power consumption. Fixed threaded joint's assembly time consists of a rotor head's run-time, screwing time, tightening time and reaction time till the start button is released (ratchet mechanism's operating mode).

In the literature sources [8] are given the run-time and acceleration time formulas, but the impact on overall power consumption depending on this time is not viewed. This is due to the fact that the electric motor is usually operated several tenths of minutes, minutes or even hours and on the total energy consumption's background acceleration time impact is very small. By running the nut driver often with large initial set speed for a short period of time until a few seconds, the run-time energy consumption can take up to 80% of total electric power consumption throughout all operating period.

## 2. ASSEMBLY TIME DETERMINATION

The assembly period of thread connections, using an electric motor, depends on such parameters as acceleration of the electric motor  $\varepsilon$ , inertia of the electric motor's rotor  $J_{ROT}$ , inertia of other rotating parts of the system  $J_L$ , rotation rate of the electric motor and other parameters.

In order to determine the assembly period, first of all it is necessary to calculate acceleration of the rotor head  $\varepsilon$  (1) at the time when the motor is being switched on till the moment when the constant set revolutions are achieved [4].

$$\varepsilon = 10^4 \cdot \frac{M_H}{J_{ROT} + J_L} \quad (1)$$

where:  $M_H$  – momentum developed by a motor when it is being stopped (the maximum momentum the motor can develop).

The time period  $t_{iesk}$ , when gathering rotations is done can be calculated according to the formula (2):

$$t_{iesk} = \frac{\omega}{\varepsilon} \quad (2)$$

where:  $\omega$  – angular rate until which the rotations are gathered,  $s^{-1}$ .

In order to determine the screwing period  $t_{skr}$  (6), first of all it is necessary to determine the number of rotations  $n_{iesk}$  completed by the rotor head during the time of run-out (3) and the number of rotations needed  $n_{kop}$  to conduct assembly (5). It should be taken into account that the electric motor and rotor head have different rotation rates. The rotation ratio between the electric motor and rotor head is determined by the gear ratio  $A$ .

$$n_{iesk} = \frac{\varphi}{360 \cdot A} \quad (3)$$

where:  $\varphi$  – revolution angle done by the electric motor during the run-out period.

The revolution angle  $\varphi$  can be determined according to the formula (4):

$$\varphi = \frac{\varepsilon \cdot t_{iesk}^2 \cdot 90}{\pi} \quad (4)$$

$$n_{kop} = \frac{l}{p} \quad (5)$$

where:  $l$  – screwing length, mm.

$p$  – thread pitch, mm.

$$t_{skr} = \frac{(n_{kop} - n_{iesk}) \cdot 60}{n} \quad (6)$$

where:  $n$  – revolutions per minute of a rotor head,  $min^{-1}$ .

The reaction period  $t_r$  values are determined experimentally. The normal value of the reaction period from the results of 10 measurements with the respective rotation ratio was used in calculations.

## 3. THE CALCULATIONS OF ELECTRICITY CONSUMPTION

Estimating the electric power consumption, it will be calculated in 3 stages for the time period when:

- 1) the motor's run-out takes place,
- 2) screwing with constant initial rotations takes place,
- 3) fastening is completed but the run button is not released yet.

The fastening period will not be taken into account provided that it is too small in comparison to the overall assembly period and has hardly any effect on the final result.

The equivalent circuit (Fig. 1) of the equipment consists of the accumulator's battery, whose electromotive force of voltage  $U_{BAT}$ , inner resistance  $R_{BATT}$  of the accumulator's battery, resistor  $R_E$  where the voltage for determination of the electric power is measured, transistor's resistance  $R_D$ , rotor coil resistance of the

motor  $R_R$  and the comparator's resistance  $R_{COMP}$ , which is equal to zero at the run time, inductance of the motor's rotor coil  $L$ , which is not taken into account in the calculations, acting in the opposite directions of the electric current flow and its value  $E$  is proportional to the motor's rotations.

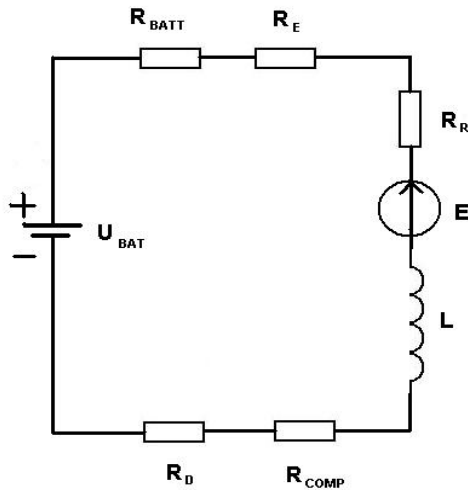


Figure 1. Equivalent circuitry of equipment

In order to calculate the energy consumption during the run-out period, first of all it is necessary to determine the current intensity. The run-out's initial current value  $I_{STALL}$  is provided in the motor's data sheet. The current intensity  $I_{START2}$  at the end of the run-out can be calculated according to the formula (7):

$$I_{START2} = \frac{U_{BAT} - E}{R_{BATT} + R_E + R_R + R_{COMP} + R_D}. \quad (7)$$

The electromotive force  $E$  is proportional to the motor's rotations  $n$ . It can be calculated according to the formula (8) [10, 12]:

$$E = \frac{n}{k_n}. \quad (8)$$

where:  $k_n$  – electric motor speed coefficient,  $\text{min}^{-1}/\text{V}$ .

Now it is possible to calculate the normal current  $I_{START\_VID}$  during the run-out period. Having assumed that the current

decreases linearly during the run-out period, it can be calculated according to the formula (9):

$$I_{START\_VID} = \frac{I_{STALL} + I_{START2}}{2}. \quad (9)$$

Being aware of the current value, it is possible to calculate the power  $P_1$  developed during the run-out period according to the formula (10).

$$P_1 = U \cdot I = I_{START\_VID} \cdot (U_{BAT} - I_{START\_VID} \cdot R_{BATT}). \quad (10)$$

Every accumulator's battery has inner resistance, on which the voltage drop, that is proportional to the current, occurs. It should be taken into account when calculating the power provided that the battery's voltage can drop in half or even more with large consumable electric power that would have a large impact on the final result, not considering the correct voltage value.

Battery internal resistance  $R_{BAT}$  can be determined by the formula (11), firstly measuring battery voltage without load  $U_0$ , then it is necessary to connect the load and measure the battery voltage  $U_{sl}$  and consumed current  $I_{sl}$ .

$$R_{BAT} = \frac{U_0 - U_{sl}}{I_{sl}}. \quad (11)$$

During the screwing period with a constant rate, when the pulse-width modulator is in operation, the pulse range is equal with the  $I_{START2}$  value and it remains unchanged until the fastening period. In order to calculate the normal current value, the fill coefficient  $D$  should be known. It can be determined according to the formula (12) [1, 2, 6, 11]:

$$D = \frac{\tau}{T}. \quad (12)$$

where:  $\tau$  – pulse-width, s.

$T$  – pulse recurrence period, s.  
 $\tau$  and  $T$  can be determined with an Oscillograph, see Fig. 2.

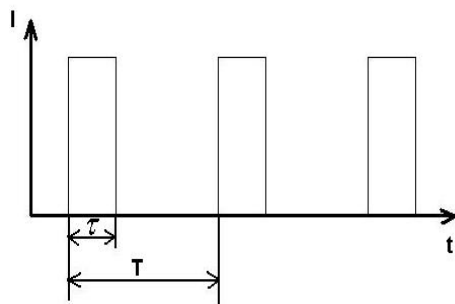


Figure 2. Impulses of the current

The normal current value  $I_{PULSE\_AV}$  in the pulse mode can be calculated according to the formula (13):

$$I_{PULSE\_AV} = I_{START2} \cdot D. \quad (13)$$

Then the power  $P_2$  during the screwing period at a constant rate can be established according to the following formula (14):

$$P_2 = I_{PULSE\_AV} \cdot (U_{BAT} - I_{START2} \cdot R_{BATT}) \quad (14)$$

There are 2 cases distinguished in calculation of the electric current during the reaction period, when the nut is already fastened with the set momentum but the run button is not released yet, when:

-the electric motor is unable to develop the required momentum with the set rotations and, in order to do fastening with the set momentum, a comparator engages. This situation is characteristic to low revolutions of the rotor head ( $300 \text{ min}^{-1}$ ,  $500 \text{ min}^{-1}$ ).

-the electric motor is able to develop the set momentum and the comparator does not engage.

In case the comparator engages, the pulse modulator stops working and the transistor is opened completely with no interruption. The electric current value in the beginning of the reaction period is equal to the  $I_{START2}$  current value, which decreases gradually. When the comparator engages,

full voltage and the required electric current, which is proportional to the motor's revolutions, is delivered, but the rotor head has already stopped and the set momentum acts on the motor. The electric current decrease is justified by the fact that the electric motor starts gathering revolutions when full voltage of the battery is connected. If the electric current drops down to a certain level, the comparator would switch off and revolutions of the electric motor would decrease.

The power  $P_{3\_COMP}$ , in the events when the comparator is in operation, can be calculated according to the formula (15):

$$P_{3\_COMP} = I_{START2} \cdot (U_{BAT} - I_{START2} \cdot R_{BATT}) \quad (15)$$

To calculate the power  $P_3$  during the reaction period, when the comparator does not engage, first of all it is necessary to calculate the speed until which the motor's rotations  $n_{SL}$  decreased (16) [6, 10], changing the electric current value  $I_3$ .

$$n_{SL} = k_n \cdot (E - \frac{R_R M}{k_m}). \quad (16)$$

where:  $k_m$  – electric motor moment constant,  $\text{mNm/A}$ .

$M$  – moment, which loads the electric motor,  $\text{mNm}$ .

The moment constant  $k_m$  is provided in the motor's data sheet. Taking into account that there are transmission gear-wheels between the motor and rotor head, the momentum  $M$  [7, 9], which works on the motor, can be calculated according to the formula (17):

$$M = \frac{M_{ROT}}{A \cdot eff}. \quad (17)$$

where:  $M_{ROT}$  – momentum, working on the rotor head,  $\text{mNm}$ .

$A$  – ratio between rotations of the electric motor and rotor head,

eff – efficiency of transmission gear-wheels.

Being aware of the set rotation rate until which the revolutions of the electric motor decreases, the consumable electric current value  $I_3$  can be calculated according to the formula (18):

$$I_3 = \frac{E - \frac{n_{SL}}{k_n}}{R_{BATT} + R_E + R_R + R_{COMP} + R_D} \cdot D. \quad (18)$$

In the formula (18), the value E should be taken with the set rotations, when the electric motor is not loaded.

The power  $P_3$ , when the comparator is not in operation, can be determined according to the formula (19):

$$P_3 = I_3 \cdot (U_{BAT} - I_3 \cdot R_{BATT}). \quad (19)$$

In order to calculate the electric power consumption during the assembly period, it is necessary to know separate parts of the assembly period, the time, when building of the electric motor's rotations  $t_{iesk}$  takes place, the time  $t_{skr}$ , when the nut is screwed with the set initial rotations and the reaction period  $t_r$ .

The time period, when fastening  $t_{piev}$  of a nut takes place is not taken into account in calculations of the electric power consumption, since it is very short and has practically no effect on the result.

The electric power E for the assembly period can be calculated according to the formula (20). The electric power  $E_{COMP}$  needed to reach the momentum, when the comparator engages, can be calculated according to the formula (21).

$$E = P_1 \cdot t_{iesk} + P_2 \cdot t_{skr} + P_3 \cdot t_r. \quad (20)$$

$$E_{COMP} = P_1 \cdot t_{iesk} + P_2 \cdot t_{skr} + P_{3\_COMP} \cdot t_r. \quad (21)$$

The graphic depiction of the obtained values using Bosch GSR 14.4 VE-2 is showed in Figure 3. and Figure 4.

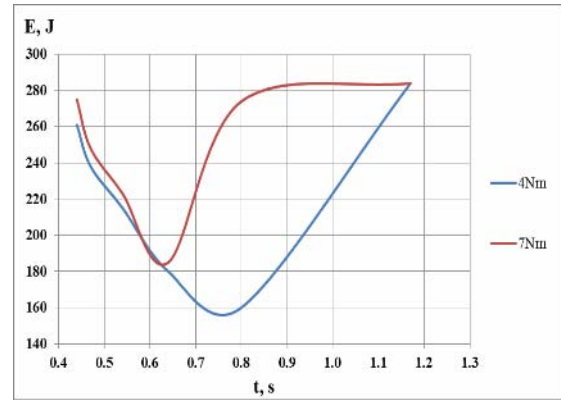


Figure 3. Theoretically determined nut driver's power consumption depending on the time of assembly and tightening torque for the bolt M6x35

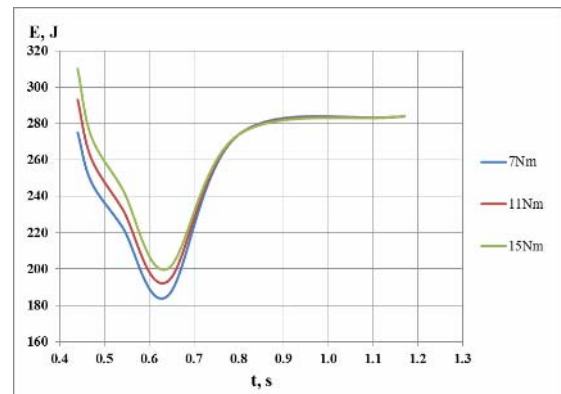


Figure 4. Theoretically determined nut driver's power consumption depending on the time of assembly and tightening torque for the bolt M8x40

## 4. CONCLUSIONS

The theoretical estimates of the fastening period and the consumed electric power were conducted, taking into account the rapidly changing processes of the nut driver in obtaining the rigid thread connections: run-out period, set rotations, reaction period.

It is proved that the nut driver – screwdriver has such operational modes that permit performing of the electric power optimization depending on the assembly period (using pulse-width modulator (PWM) in screwdrivers). The most economical mode of a screwdriver is at such minimum set rotations requiring no additional electric power (involving of the

comparator), providing fastening of a nut with the corresponding moment.

From the obtained graphs it is obvious that when making a fixed threaded joint at low rotational speed consumable energy does not depend on the selected torque. It is explained in such a way that when comparator is turned on, the current is close to the maximum. For the bolt M6 assembly mode is optimal at  $500 \text{ min}^{-1}$  (0,75 s), this is due to the fact that it is possible to reach the tightening torque of 4 Nm without comparator start.

The optimal operational modes according to the electric energy consumption providing the necessary fastening moment of the fixed threaded connections, are showed in Figure 3. and Figure 4.:

- 1) For the bolt M6x35 at 4 Nm and  $500 \text{ min}^{-1}$  and 0,75 s of assembly time;
- 2) For the bolt M6x35 at 7 Nm and  $700 \text{ min}^{-1}$  and 0,63 s of assembly time;
- 3) For the bolt M8x40 at 7 Nm, 11 Nm, 15 Nm and  $700 \text{ min}^{-1}$  and 0,63 s of assembly time.

Taking into account that in the computerized assembly usually using the maximum rotations of a rotor head of the nut driver (because nut drivers don't have rotation regulation options), performing optimization of the energy consumption after the assembly period, approximately from 25%-30% decreasing is obtained.

Despite the fact that simplified formulas (that are intended for electric motors with linear curves) were used for nut driver's electric consumption calculations in which were not taken into account such electric motor's parameters as inductance of rotor coils  $L$ , rotor losses (for rotors with magnetic inducement these losses are not essential), the rotor coils resistance dependence on the temperature, losses of electric power depending on frequency, they allow us to approximately determine the optimal operating mode for the nut driver if taking into account electric power consumption, assembly time and necessary tightening moments for the different types of fixed threaded joints.

## ACKNOWLEDGEMENTS

This work has been supported by the European Social Fund within the Project Nr.2009/0201/1DP/1.1.1.2.0/09/APIA/VI AA/112 "Nanotechnological research of the mechanical element surface and internal structure in mechanical engineering".

## REFERENCES

- 1) <http://www.potomacelectric.com/Downloads/Tutorials/BRUSH%20MOTORS/DC%20brush%20motor%20theory.pdf>
- 2) <http://dl.sumdu.edu.ua/e-pub/EAUSU/5/gl5tel.htm>
- 3) <http://lancet.mit.edu/motors/motors3.html>
- 4) [http://www.btipnow.com/library/white\\_papers/MOSFET%20Power%20Losses%20Calculation%20Using%20the%20Data-Sheet%20Parameters.pdf](http://www.btipnow.com/library/white_papers/MOSFET%20Power%20Losses%20Calculation%20Using%20the%20Data-Sheet%20Parameters.pdf)
- 5) [http://www.me.mtu.edu/~wjendres/ProductRealization1Course/DC\\_Motor\\_Calculations.pdf](http://www.me.mtu.edu/~wjendres/ProductRealization1Course/DC_Motor_Calculations.pdf)
- 6) [http://www.20sim.com/webhelp/toolboxes/mechatronics\\_toolbox/servo\\_motor\\_editor/theory/torque\\_speed\\_plot/general\\_model.htm](http://www.20sim.com/webhelp/toolboxes/mechatronics_toolbox/servo_motor_editor/theory/torque_speed_plot/general_model.htm)
- 7) [http://www.mabuchimotor.co.jp/cgi-bin/catalog/e\\_catalog.cgi?CAT\\_ID=rs\\_755vcwc](http://www.mabuchimotor.co.jp/cgi-bin/catalog/e_catalog.cgi?CAT_ID=rs_755vcwc)
- 8) [https://downloads.maxonmotor.com/Katalog\\_neu/eshop/Downloads/allgemeine\\_informationen/Das\\_wichtigste\\_ueber\\_maxon\\_motoren/newpdf\\_11/DC-Das\\_wichtigste\\_ueber\\_maxonmotoren\\_11\\_EN\\_036.pdf](https://downloads.maxonmotor.com/Katalog_neu/eshop/Downloads/allgemeine_informationen/Das_wichtigste_ueber_maxon_motoren/newpdf_11/DC-Das_wichtigste_ueber_maxonmotoren_11_EN_036.pdf)
- 9) [http://imed.narod.ru/el\\_mech/motor\\_dc.htm](http://imed.narod.ru/el_mech/motor_dc.htm)
- 10) [http://www.electromate.com/db\\_support/attachments/PWM%20technical%20information.pdf](http://www.electromate.com/db_support/attachments/PWM%20technical%20information.pdf)
- 11) <http://www.mech.utah.edu/~me3200/labs/torquespeed.pdf>
- 12) <http://www.micromo.com/how-to-select-a-dc-motor.aspx>
- 13) <http://www.micromo.com/motor-calculations.aspx>



## AN EXPERIMENTAL STUDY OF THE CUTTING FORCES IN THE METAL CUTTING PROCESS

V.Gutakovskis, G.Bunga, G.Pikurs, V.Brutāns, A.Ratkus

**Abstract:** *From the invention of turning machine some engineers are trying to increase the turning productivity. The increase of productivity is following after the breakout in instrumental area, such as the hard alloy instrument and resistance to wear cutting surfaces. The potential of cutting speed has a certain limit. New steel types and cutting tool surfaces types allows significantly increase cutting and turning speeds, but with this increase from the recommended by 20 % the solidity of the instrument decreases by 50 %. For the most operation types the productivity increase begins from the feeding increase. On the average feeding increase by 20 %, the self cost decreases by 15 % when manufacturing the detail in large numbers.*

*Key words: Key words: Metal cutting, cutting forces, FEM analysis.*

### 1. INTRODUCTION

From the invention of turning machine some engineers are trying to increase the turning productivity. The increase of productivity is following after the breakout in instrumental area, such as the hard alloy instrument and resistance to wear cutting surfaces [1]. The potential of cutting speed has a certain limit. New steel marks and cutting surfaces types allows significantly increase cutting and turning speeds, but with this increase from the recommended by 20 % the solidity of the instrument decreases by 50 %. For the most operation types the productivity increase begins from the feeding increase. On the average feeding increase by 20 %, the self cost

decreases by 15 % when manufacturing the detail in large numbers [2, 3]. Turning with high feeding ( or high feed turning ), is one of the most actual problems in the increasing of manufacturing volume but there are some problems one of them is the cutting forces increasement and larger metal removal rate, which decrease the cutting tool life significantly. Increasing of manufacturing volume, going together with the cutting instrument technology and material evolution, such as the invention of the carbide cutting materials and wear resistant coatings such as TiC and Ti(C,N) (Figure 1 a, b). Each of these coating has its own properties and functions in the metal cutting process (Figure 2). Together with this evolution of the cutting tool geometry and machining parameters dependencies are researched. Traditionally for the decreasing the machining time of one part, the cutting depth was increased, decreasing by this way the machining procession. Nowadays the wear resistance of the cutting tools increasing and it is mostly used one or two machining operations (medium and fine finishing). Another way to increase the productivity is the increasing of cutting speed. However the potential is not endless. New cutting tool materials allow us to increase the cutting speed by 20%, but the cutting tool stiffness will decrease by 50 %. The cutting process involves the removal of metal in the form of chips from the workpiece by the action of the cutting tool, which later is coupled to the machine structure through different elastic elements. Normally, any small vibration caused by occasional disturbances, such as

inhomogeneity of the work material and the runout and misalignment of the workpiece, would be damped out by the structure of the cutting system. Sometimes, however, the disturbances are maintained and the system becomes unstable, so that the relative periodic displacement between the tool and the workpiece may build up to large amplitude. This relative periodic motion between the cutting tool and the workpiece is known as chatter. This chatter depends on the cutting forces in the cutting process. The forces acting on the tool are an important aspect of machining. For those concerned with the manufacture of machine tools, knowledge of the forces is needed for estimation of power requirements and for the design of machine tool elements, toolholders and fixtures, adequately rigid and are free from vibration. Cutting forces vary with the tool angles, and accurate measurement of forces is helpful in optimizing tool design and predicting tool life. Scientific analysis of metal cutting also requires knowledge of the forces, and in the last hundred years, many force measurement devices, known as dynamometers, have been developed, capable of measuring tool forces with increasing accuracy. Early methods were based on strain-gage measurement of the elastic deflection of the tool under load. Today, one of the most commonly used dynamometers is a force-platform piezo-electric load cells. For a semi-orthogonal cutting operation in lathe turning, the force components can be measured in three directions, and the force relationships are relatively simple [4,5,6,7].



Fig. 1. Turning insert coating combinations

## 2. METAL CUTTING PROCESS AND CUTTING TOOL DESCRIPTION

In metal cutting the force component is acting on the tool in the direction OX, parallel with the direction of feed, is referred to as the feed force,  $F_f$ . This force acts tangential to the main cutting forces  $F_c$ . To maintain consistency within all machining processes the symbol for this tangential force is frequently written as  $F_t$  rather than  $F_f$ . The third component, acting in the direction OZ, tending to push the tool away from the work in a radial direction, is the smallest of the force components in semi-orthogonal cutting and, for purposes of analysis of cutting forces in simple turning, it is usually ignored. It is of interest that the forces involved in machining are relatively low compared with those in other metal working operations such as forging. For the experimental study of the cutting forces in the metal cutting on the lathe are chosen two types of stainless steel: 420 and 304, also modern cutting tools from SECO, Sumitomo, Kennametal with CVD and PVD coatings, with different type of the chip-breaker geometry, because the chip forming process is also actual question which is necessary to solve in the middle-finish machining operation, because of high chrome and nickel contents in this machined part, what in fact cause problems of the good chip forming process. (Here will be represented only first variant of the cutting forces experimental study using 420 stainless steel and TM4000-coated cutting insert from SECO). These coatings are high wear-resistant, decrease cutting forces and as a result - vibrations in the cutting process (this process was also widely studied [8]). On the figure 2 is shown the modern cutting tool (the toolholder and the cutting insert) and the scheme of the metal cutting process. Each of the metal cutting operations have different grades- chipbreaker and coating combinations for the each machining operation- rough machining, middle machining and fine finishing machining. Cutting inserts for the middle-finishing operations are also called negative inserts

because they are places in the cutting tool under the negative angle (Figure 3). One more important value is the main cutting edge angle „  $\square$  ‐, which using in different machining operations gives us different values of the cutting forces (Figure 4) [9,10].

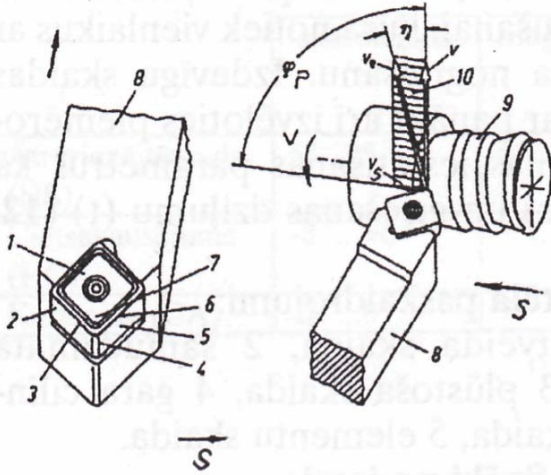


Fig. 2. Cutting tool ( 1 - cutting insert, 2 – secondary plane, 3 - auxiliary cutting edge, 4 - cutting edge nose, 5 - main back surface, 6 - main cutting edge, 7 - chip breaker, 8 - cutting insert holder, 9- machined part, 10 - work plane,  $v$  - cutting speed,  $v_e$  - effective cutting speed,  $\square_p$  – feeding movement angle,  $\eta$  - machining speed angle).

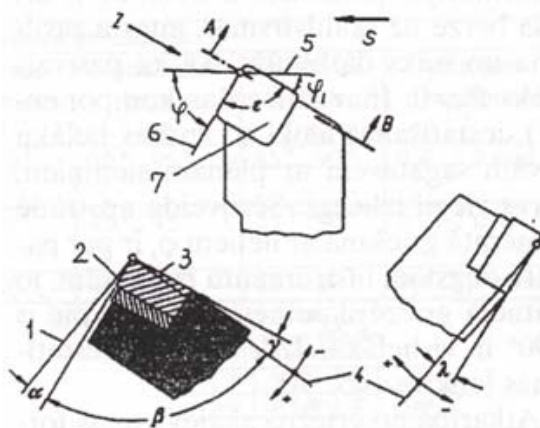


Fig. 3. Negative cutting insert geometry ( 1- tool cutting edge plane, 2- back plane, 3- chip breaker plane, 5- work plane, 6- cutting edge plane, 7- cutting insert,  $\lambda$ - chip breaker plane,  $\alpha$ - back plane angle,  $\beta$ - cutting insert base angle,  $\square$ - main cutting edge angle,  $\lambda$ - cutting edge angle).

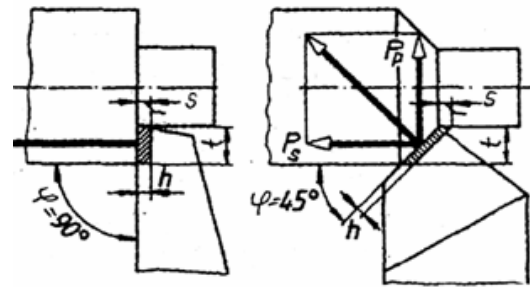


Fig. 4. The dependence of the feeding force  $P_s$  and passive force  $P_p$  from the the main cutting edge angle  $\square$  .

### 3. EXPERIMENTAL PART AND RESULTS

The aim of the experiment is to study the machining parameters, especially cutting force values and machined surface roughness results and also the tool wear. For our tree factor experiment was chosen the 420 stainless steel (12 % Chromium), modern Duratomic coated negative turning insert TNMG 160412-MF4 , TM4000 with cutting edge radius 1,2 mm, lathe 16K20. Experimental machine is shown on figure 5. Machining parameters combinations (table 1) are: feeding - 0,1 mm/Rpm and 0,35 mm/Rpm; cutting depth is 0,5mm; cutting speed 90 m/min., and 112 m/min. The chosen chipbreaker MF4, for medium/finishing turning with TM4000 coating, two holders with cutting angle  $\phi = 90^\circ$  and  $\phi = 60^\circ$ . The main advantage of the MF4 chipbreaker is that the open and highly positive design (up to  $25^\circ$  rake angle) reduces cutting forces. This, in turn gives: low cutting forces - higher cutting speed; increased speed capability - higher productivity; traditional medium - finishing inserts perform well at ordinary speeds, but fail early when the speed is increased. During metal cutting on the lathe three cutting forces take place in this progress. They may vary with tool angles, feed and cutting speed. Figure 6 shows us the component of the force acting in the rake face of the tool, normal to cutting edge, in the direction OY is so called the cutting force  $F_c$  ( $P_p$ ). This is usually the largest

component, and acts at the direction of cutting velocity. The force component acting in the tool in the direction OX, parallel with the direction of feed, is referred to as the feed force  $F_f$  ( $P_s$ ). The third component, acting in OZ direction ( $P_c$ ), pushes the cutting tool away from the work in the radial direction. This is the smallest of the force components. Cutting forces in metal cutting is one of the most actual problems, especially in dry (without cooling) machining process. To study this process we are using dynamometer UDM-600 and computer FEM analysis. The result of the measured cutting force  $P_z$  is shown on the figure 7. Measured mean values of the surface roughness results are shown in the table 2 and best surface roughness result diagram (Fig.8). In our days the computer modelling programs which use Finite Element Method (FEM) analysis, such as ABAQUS, Third Wave Advantage can solve this problem. What in fact was done in cooperation with Helsinki University of technology [11]. The computer modelling metal cutting parameters combination are the same as in the table 1, FEM cutting forces graphics are shown on the figure 9.

Parameter comb. Nr.	1	2	3	4
Feeding, mm/Rpm	0,1	0,35	0,1	0,35
Cutting depth, mm	0,5	0,5	0,5	0,5
Cutting speed, m/min	90	90	112	112
Cutting edge angle	60°	60°	60°	60°
Parameter comb. Nr.	5	6	7	8
Feeding, mm/Rpm	0,1	0,35	0,1	0,35
Cutting depth, mm	0,5	0,5	0,5	0,5
Cutting speed, m/min	90	90	112	112
Cutting edge angle	90°	90°	90°	90°

Table 1. Machining process parameters

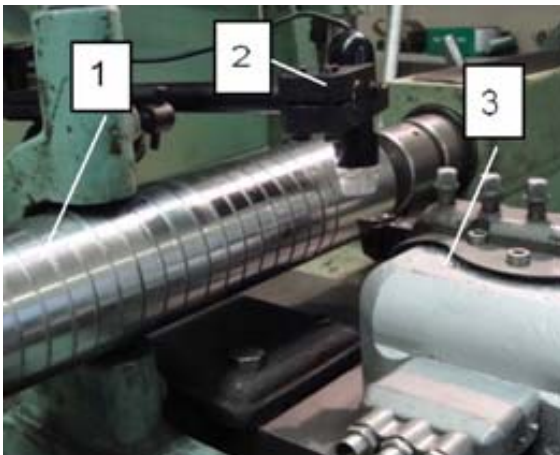


Fig.5 Experimental scheme: 1- machined part; 2 – digital microscope; 3 – UDM – 600 dynamometer

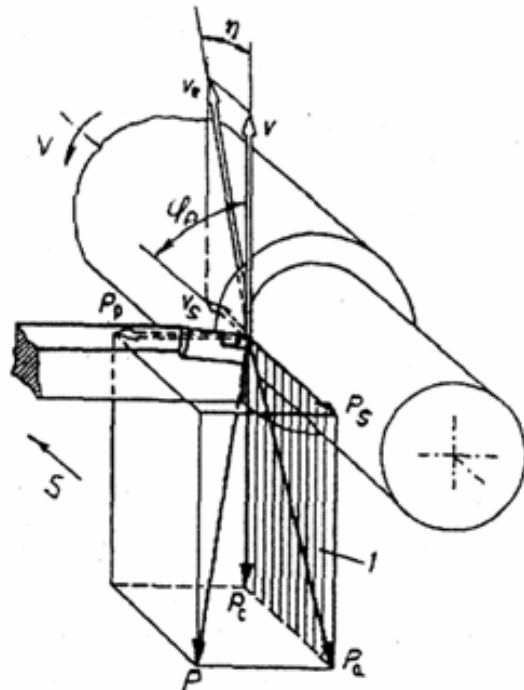


Fig. 6. Cutting forces in the metal cutting process



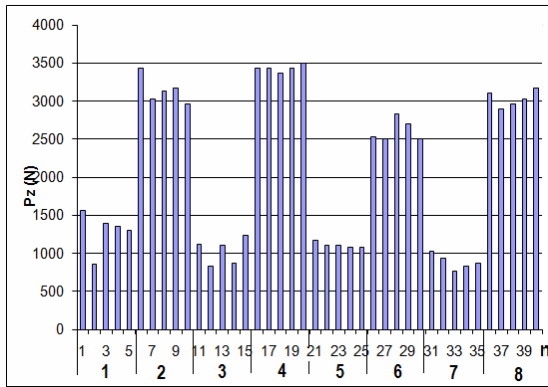


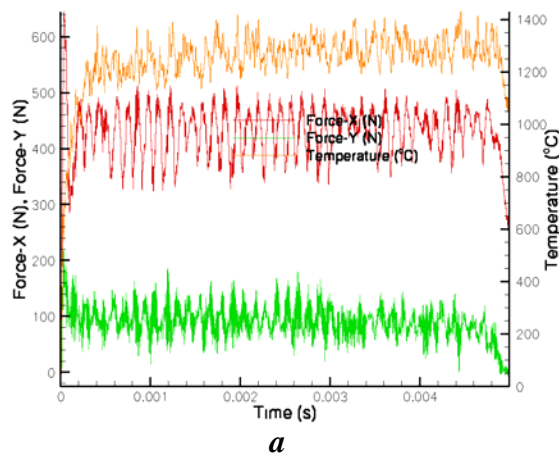
Fig. 7. The result of measured cutting force  $P_z$  during the experiment

Machining block number	Ra, $\mu\text{m}$	Rt, $\mu\text{m}$	Hardness, HB
1	5,92	44,82	262
2	4,57	29,41	275
3	5,04	39	272
4	5,72	40,88	264
5	5,56	47,2	250
6	3,46	21,55	273
7	5,4	41,7	277
8	3,68	35,4	278

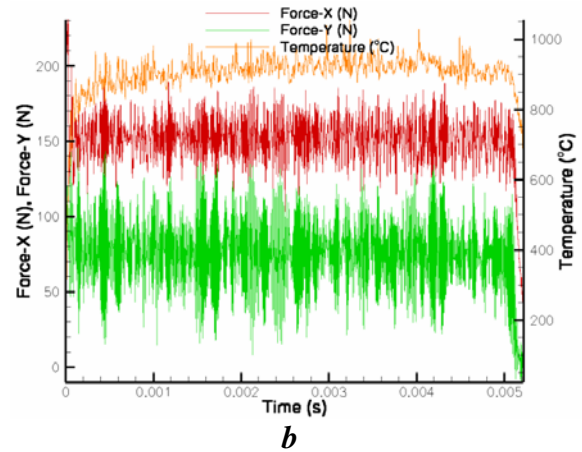
Table 2. Machined surface results



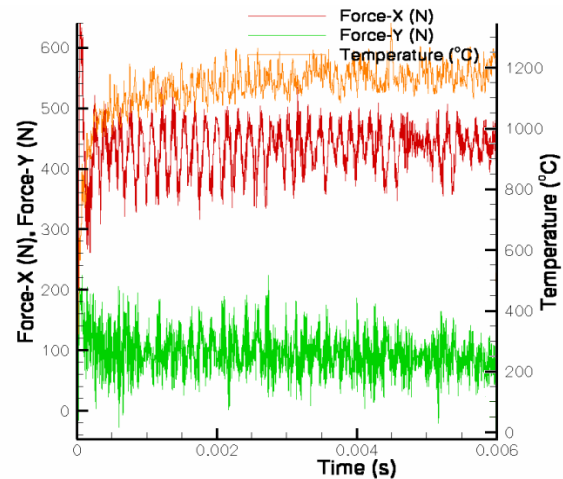
Fig.8. Best surface roughness result diagram.



*a*



*b*



*c*

Fig. 9. Metal cutting forces values results using FEM modelling

## 5. CONCLUSIONS

The experimental results show how machining parameters and technological regimes combinations change machined surface results.

Main conclusion is that in order to obtain better result it is necessary to change the cutting edge angle. However it is not so handy when the different profile surfaces are machined.

In the same time increased cutting speed and decreased feeding are not so important factors because they do not effect seriously machined surface result.

This cutting tool was produced directly for the machining of the stainless steel and in the result we did not see any tool wear.

## 6. ACKNOWLEDGEMENT

*This work has been supported by the European Social Fund within the project «Support for the implementation of doctoral studies at Riga Technical University».*

## 7. REFERENCES

- [1] Bashkov V. M., Kacev P. G. Testing the cutting instrument for durability. M. Machine building 1985.
- [2] Kalpakjan S., Schmid S. R., Manufacturing engineering and technology. Singapore, Jurong. Pearson Prentice Hall. 2006 .
- [3] E.M.Trent, P.K.Wright, Metal Cutting (4-th edition). Boston, Butterworth-Heinemann, 2000.
- [4] Astakhov, V.P., Tribology of Metal Cutting, Elsevier: London, 2006
- [5] Boothroyd G., Knight W. A., Fundamentals of machining and machine tools. Vol. 3, 2006, 573p.
- [6] David A. Stephenson, John S. Agapiou . Metal cutting theory and practice. NY; CRC Press, Taylor&Francis Group, volume 2, 2006, 846 pages.
- [7] Astachov V.P.; Tribology of metal cutting, Elsevier Ltd., 2006, 420 pages.
- [8] Gutakovskis V.; Bunga, G.; Pikurs G.; “Cutting tool vibration in the metal cutting process” Journal of vibroengineering, Volume 13, Issue 4,KTU, Kaunas, Lithuania. 676 - 681 p. 2011
- [9] Bunga, G.; Geriņš, E; “Apstrādes ar atdalīšanu tehnoloģijas”, RTU, Riga, 2007, 83 p.
- [10] Bunga, G.; Geriņš, E; “Inženierizstrāžu materiāli un apstrādājošie sakausējumi” RTU, Riga, 2011, 66 p.
- [11] Bunga, G.; Gutakovskis, V.; Niemi, E.; Laakso, S.; „Finite element method modeling of the stainless steel cutting process using different machining

parameters” Scientific Journal of Riga Technical University, 2009, volume 31, 51-55 p.

## 8. ADDITIONAL DATA ABOUT AUTHORS

**Viktors Gutakovskis**, M.Sc.ing., Riga Technical University, Mechanical Engineering institute, Department of Material Processing Technologies; Address: Ezermalas 6-108, LV 1006, Riga, Latvia.

Phone: +371 7089751, Fax: +371 7089752

E-mail: [VGutakovskis@gmail.com](mailto:VGutakovskis@gmail.com);

**Guntis Pikurs**, M.Sc.ing., Riga Technical University, Mechanical Engineering institute, Department of Material Processing Technologies; Address: Ezermalas 6-108, LV 1006, Riga, Latvia.

Phone: +371 7089751, Fax: +371 7089752

E-mail: [Guntis.Pikurs@rtu.lv](mailto:Guntis.Pikurs@rtu.lv)

**Valdis Brutans**, M.Sc.ing., Riga Technical University, Mechanical Engineering institute, Department of Material Processing Technologies; Address: Ezermalas 6-108, LV 1006, Riga, Latvia.

Phone: +371 7089751, Fax: +371 7089752

E-mail: [Valdis.Brutans@rtu.lv](mailto:Valdis.Brutans@rtu.lv)

**Andris Ratkus**, M.Sc.ing., Riga Technical University, Mechanical Engineering institute, Department of Material Processing Technologies; Address: Ezermalas 6-108, LV 1006, Riga, Latvia.

Phone: +371 7089751, Fax: +371 7089752

E-mail: [Valdis.Brutans@rtu.lv](mailto:Valdis.Brutans@rtu.lv)

**Guntis Bunga**, Asoc. Prof., Dr.Sc.ing., Technical University, Mechanical Engineering institute, Department of Material Processing Technologies;

Address: Ezermalas 6-101, LV 1006, Riga, Latvia.

Phone: +371 7089751, Fax: +371 7089752

E-mail: [Guntis.Bunga@rtu.lv](mailto:Guntis.Bunga@rtu.lv)

## THE DEVELOPMENT OF AN ADDITIONAL FUEL SUPPLY SYSTEM TO AN INTERNAL COMBUSTION ENGINE

Ilves, R.; Küüt. A.; Mikita.V. & Olt. J.

**Abstract:** *The usage of natural resources such as oil is nowadays gaining more and more attention. The Estonian national energy management development plan foresees increasing the percentage of renewable resources in energy consumption by 20 per cent, the percentage of biofuels in transportation fuels by 10 per cent. That is the reason for the increase in using biofuels. Biofuels are used as engine fuels in many countries, however, some problems that hinder using biofuels have not been solved. One of the greatest problems is the cost of biofuels which depends on the raw material, production technologies and quality of the fuel produced. The quality of the fuel is important to ensure the working modes of the engine's subsystems on given conditions as well as the durability guaranteed by the factory. This particular article provides an overview of designing and developing an innovative additional fuel supply system. For doing so, firstly, the problems encountered when using biofuels in engines are discussed, secondly, an overview of a patent research is given. The prototype of an innovative additional fuel supply system is designed, its development stages as well as the problems that need to be tackled are pointed out and discussed.*

*Key words: combustion engine, liquid biofuel, fuel supply system, product development.*

### 1. INTRODUCTION

Biofuels are more and more commonly used in the world due to decreasing fossil

fuel resources. Biofuels can be divided into three: 1) solid fuels; 2) liquid fuels; 3) gas fuels. Gas and liquid fuels are used as engine fuels. Methane produced from biomass is mostly used as gas fuel. Liquid fuels can be divided into plant oils and alcohol. Plant oils include hot and cold-pressed oils and biodiesel; alcohol fuels include biomethanol and bioethanol [1]. There are several problems in using biofuels as engine fuel. Using plant oils as engine fuel may cause excessive sooting and coking of the combustion chamber and injector nozzle [2]. Idle engine operation is aggravated because lots of energy is used for igniting the oil. Major problem consists in the fluidity of fuel at low temperatures. Plant oils are mostly used in compression-ignition engines. Use of alcohol fuels in compression-ignition engines is complicated because alcohol fuels need much more energy for self-ignition than plant oils or diesel fuel [3]. These alcohol fuels are mostly used in spark ignition engines. Their properties cause corrosion and rapid wear of the components of the fuel supply system [4]. Another problem is related to cold-start [5].

In order to use biofuels in spark ignition and compression-ignition engines, the engines with two fuel supply systems have been introduced [6], where main fuel supply system uses standard fuels as engine fuel and additional supply system uses biofuels. In addition to the standard fuel, also biofuel is channelled to the engine cylinder. Problems with combustion and cold-start occurring in case of using biofuels are compensated



with standard fuel [7]. The disadvantage of this system is high cost and complexity of the engine.

The purpose of this present article is to provide an overview of the creation and development of an innovative additional fuel supply system that uses liquid biofuels. The advantage of this new additional fuel supply system is the opportunity to use different biofuels in different engines, by ensuring the durability of fuel supply system and forming of quality air-fuel mixture.

## 2. MATERIAL AND METHODS

The additional fuel supply system was developed based on generally recognized TRIZ methods [8, 9] which in this case consisted of the following main steps:

- 1) identification and definition of the problem;
- 2) searching for typical problem similar to the problem identified;
- 3) analysis of known solutions;
- 4) finding the best solution for the problem in need of solution.

Development of additional fuel supply system requires examination of the problems that emerge when using liquid biofuels and it is also necessary to set the requirements for creating an innovative fuel supply system [10]. The two types of biofuels to be studied include plant oils and bioethanol (max 96.6 %). The aforesaid fuels should be usable in spark ignition engines and compression-ignition engines. Forming of air-fuel mixture by using a single fuel supply system is a complicated process, because in case of plant oils great pressure is used for injection in order to ensure sufficient fuel quantity and forming of quality air-fuel mixture in the cylinder [11]. This is due to great viscosity of plant oils, which at the temperature of 27°C exceeds 30 m<sup>2</sup>/s [12]. Bioethanol has low viscosity (~ 2 m<sup>2</sup>/s). Bioethanol can be injected by means of injectors with low-injection pressure and a large nozzle opening. At the same time the lubricating

properties of bioethanol are significantly worse than those of plant oils [13]. This may cause rapid wear and corrosion of the precise surface finish of the fuel supply systems intended for plant oils. Bioethanol does not mix with standard fuels and plant oils. Therefore they cannot be mixed inside the fuel supply system, in order to avoid return of layered fuel in the fuel tank. Based on these properties the following requirements have been prepared for fuel supply system that describe the properties of devices in demand and less common on the market: 1) can be used with several types of biofuels in one fuel supply system; 2) ensure production of quality air-fuel mixture; 3) fuel supply system can be used in spark ignition engines and compression-ignition engines; 4) ensure durability of the fuel supply system.

The most common biofuel-operated fuel supply systems on the market are either direct or indirect injection standard systems. They are generally intended for one type of biofuel. Pressurised fuel is forced through the injector to the inlet manifold or directly into the cylinder. Main components subject to wear and tear are precise surfaces in injectors and fuel pumps (injector needles, CR injector return valves, plungers). Examples of some fuel supply systems adjusted for biofuels can be found in patent documents EP2208879, US2008202471, WO2009106647, US20090145403, etc.

Based on the aforesaid description, the development of a new fuel supply system requires the reduction of pressure inside the supply system and exact number of junctions. At the same time one has to ensure the highest possible quality of air-fuel mixture in the cylinder. One alternative is to use fuel supply systems equipped with compressed air, where the air flow channelled through venturi nozzle utilises underpressure to suck the fuel into the injector, where the air and fuel are then carburized. The advantage of this system is lack of precise surfaces

and low pressure in the fuel supply system. In order to allow using the fuel supply system both in spark ignition and compression-ignition engines, it has been placed in the engine inlet manifold.

Fuel supply system has been developed on experimental basis, i.e. an initial test device has been built and it has been improved and modified to solve the problems emerging in the course of testing.

### 3. RESULTS AND DISCUSSION

Main parts of fuel supply systems subject to wear and tear include precise surfaces, wear and tear of which causes forming of low-quality air-fuel mixture or reduction of fuel delivery, which in turn determine the power characteristics of the engine. In order to use biofuels, it is recommended to use fuel supply system that has as few precise surfaces as possible. One option is to use pulverizing injectors that operate on the venturi jet principle (see Figure 1).

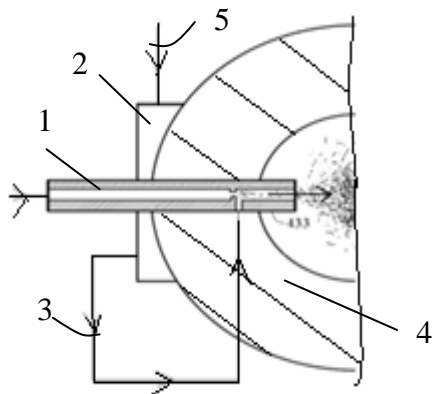


Fig. 1. Basic scheme of the fuel supply system.

Air flow is drawn through injector 1, creating underpressure in the fuel supply line 3 at the end of the injector when passing through the jet opening. Due to underpressure the fuel will be sucked through the fuel supply line into the injector, where the fuel is carburized. In casing 4 of fuel supply system the resulting air-fuel mixture is mixed with air again and drawn into the cylinder. Fuel inlet manifold has at least two

injectors that ensure sufficient productivity of the fuel supply system at different engine modes. The function of fuel inlet regulator 2 is to adjust the quantity of fuel feed from the tank. Irrespective of the viscosity and density of fuel, the system allows breaking the fuel jet into small parts. Implementation of this concept into an engine fuel supply system represents a complex process. The stages of developing the fuel supply system are listed below.

**Stage I.** Concept realisation and construction of the test device.

**Activities:**

1. Carrying out preliminary study:
  - 1.1. Selection of injectors;
  - 1.2. Checking the injection methods, process modelling.
  - 1.3. Elaboration of the principle of system construction.
2. CAD modelling.
3. Preparation of 3D drawings.
4. Preparation of control programmes for CNC benches.
5. Technological mapping.
6. Processing of the details in CNC.

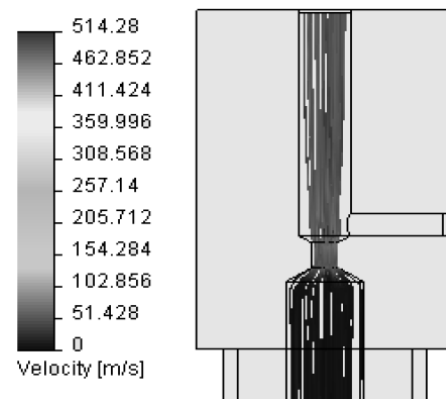


Fig. 2. Process modelling.

**Stage II.** Study of the processes in the fuel supply system

**Activities:**

1. Preparation of simplified test device.
2. Monitoring of processes and making conclusions.
3. Elaboration of enhanced test device



Fig. 3. Simplified test device.

**Stage III.** Study of the operation of improved fuel supply system.

**Activities:**

1. Improving the construction of the test device.
2. Monitoring the operation process of the test device and making conclusions.
3. Elaboration of enhanced construction of prototype devices.



Fig. 4. Improving the construction of the test device.

**Stage III.** Designing the prototype device.

- Activities:**
1. Preparation of improved prototype devices.
  2. Testing and solving any problems that might arise.

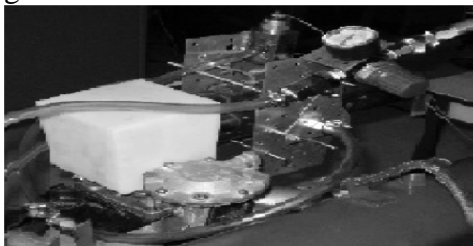


Fig. 5. Prototype devices.

Stage I: The aim is to find a suitable construction for implementing the concept of the fuel supply system. For that purpose the injection quality and productivity of different injectors have been studied in biofuels with varying viscosity. Injectors are placed in the

casing which is positioned in the inlet manifold of the engine. Problems found while testing include condensation of the injected fuel on casing walls and adjustment of fuel quantity. In order to reduce fuel condensation it is necessary to adjust the quantity of injected fuel so as to ensure required engine performance without forming excess air-fuel mixture in the inlet manifold. Air flow regulator is used for adjusting the quantity of injected fuel.

Stage II: Engine testing revealed that the underpressure generated in the inlet manifold was high enough to force the fuel to flow to the manifold through the injectors. This results in uncontrollable engine operation, where the fuel flow to the cylinder increases along with the increasing rotational speed of crankshaft. This problem can be solved by supplementing the system with a fuel doser that channels the fuel to the injectors. Doser consists of fuel distributor, electromagnetic valve and control module. Doser must be placed as close to the injector as possible, in order to reduce the impact of fuel in the fuel supply line during the work mode of the engine, when the doser is in closed position. Dosing effect consists in the operation of pulse-modulated electromagnetic valve at a fixed frequency by changing the signal fill factor. Air flow adjustment is not necessary in case of the above-mentioned solution.

Stage III: Testing the fuel supply system equipped with electronic fuel dosing system revealed excessive forming of air-fuel mixture in the inlet manifold. In order to remove the condensed air-fuel mixture from the system the position of the system casing on the engine has been altered and a return line has been added which allows directing the condensed fuel back to the fuel tank.

Stage IV: Prototype device has been designed in view of the fact that the fuel must flow out of the casing of the fuel supply system at various engine

positions. The reason for that comes from the problem found when testing the device in spark ignition engine. If the cylinder is filled with too rich air-fuel mixture the combustion process will take a long time, which causes backfire in inlet manifold when opening the inlet valve. In case of backfire the condensed fuel ignited in the inlet manifold. To solve the problem it is necessary to supplement the system with a lambda sensor, the signal of which provides a basis for controlling the air-fuel mixture preparation.

As an example of the fuel supply system's work, graphs of carbon monoxide and carbon dioxide have been provided (see figure 6), which have been measured when using the fuel supply system as an additional fuel supply system on a compression ignition engine.

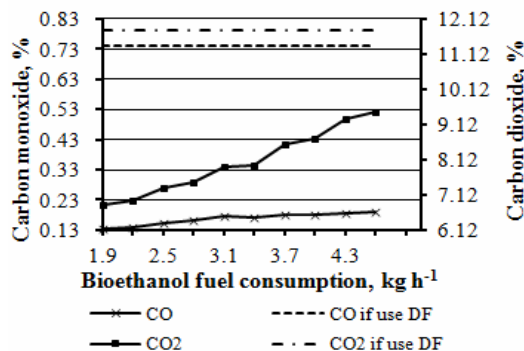


Fig. 6. The carbon monoxide and carbon dioxide in the exhaust gas of a compression ignition engine in relation to the amount of bioethanol fed by the fuel supply system (DF – diesel fuel).

Diesel engine D120 was used as a test engine. The fuel used in the supply system was a 60-per-cent bioethanol. The rotational speed of the crankshaft on engine mode was  $n_e = 1300$  rpm and torque  $T_e = 112$  Nm. During the test, the proportion of diesel fuel was gradually decreased in the air fuel mixture and the amount of bioethanol was increased to ensure the stable engine mode. Using ethanol in the air fuel mixture reduces the amount of carbon monoxide and carbon dioxide in the exhaust fumes. The bioethanol added with the fuel supply

system enabled to replace up to 80 per cent of the diesel fuel on the given mode. This implies that the efficiency of the device is comparable to other electronic additional fuel supply systems.

Using different biofuels in this system did not cause any problems, which means that it has great potential as an additional fuel supply system. The advantage of this solution consists in lack of precise surfaces, which allows using different biofuels without rebuilding the system. Problems may arise from the complex control of the air-fuel mixture forming process.

#### 4. CONCLUSION

There are various development opportunities for fuel supply systems. Dosing the amount of fuel may be considered inaccurate in case of the innovative solution described in the article. Thus it is necessary to continue experimental work for enhancing the system for using it with biofuels. Further development of fuel supply system requires converting the technical solution provided in the article into a multi-point injection system, where fuel is injected into the intake ports just upstream of each cylinder's intake valve. Final improvement would consist in leading the injectors directly into the combustion chamber. Such a technical solution requires highly complex control systems in order to ensure the resistance of the fuel supply system to temperature fluctuations and elevated pressures. The stages indicated in the article represent first steps in developing combined fuel supply system. The developed system allowed using bioethanol in spark ignition engine without the main fuel supply system. It follows that the produced air-fuel mixture had the quality suitable for using in an engine. The purpose of further development is to improve the efficiency of the fuel supply system described in this article.

## 5. REFERENCES

1. Ritslaid, K., Küüt, A., Olt, J. (2010). State of the Art in Bioethanol Production. *Agronomy Research*, **8(1)**, 236 - 254.
2. Knothe, G., Gerpen, J. V., Krahl, J. The Biodiesel Handbook. AOCS Press, USA 2005.
3. Olt, J., Mikita, V., Ilves, R., Küüt, A., Madissoo, M. (2011). Impact of ethanol on the fuel injection pump of diesel engine. 10th International Scientific Conference "Engineering for Rural Development" – 26-27 May 2011, Jelgava, Latvia. 2011, 248 - 253.
4. Ma X.Q., DeCarmine., Xiao T.D. Plasma Spray High Lubricity Nanocomposite Coatings. *Thermal Spray, Advances in Tehnology and Application*. 2004.
5. Irimescu, A. Study of coldstart air–fuel mixture parameters for spark ignition engines fueled with gasoline–isobutanol blends. *International Communications in Heat and Mass Transfer*, Volume 37, November 2010, Pages 1203–1207.
6. Pulkrabek, W. W. Engineering Fundamentals of the Internal Combustion Engine. Prentice Hall, Platteville.
7. Pierre, C., Andrew, S., Gamble, F. MULTI-FUELLING AN ENGINE. 2009. International publication number: WO20091066476. <http://www.wipo.int/patentscope/search/en/detail.jsf?docId=WO2009106647&recNum=52&maxRec=94&office=&prevFilter=&sortOption=&queryString=%28FP%2Fbioethanol%29+&tab=PC+CT+Biblio> (27.02.2012)
8. William Y. Fowlkes. Patenting TRIZ?. 2010.<http://www.triz-journal.com/archives/2010/10/03/>. (27.02.2012).
9. Ulrich, T. K., Eppinger, S. D. Product design and development, Second Edition. Irwin McGraw-Hill, USA, 1995.
10. Pahl, G., Bitz, W., Feldhusen, J. and Grote, K. H. Engineering Design. A System Approach. Third Edition. Springer, Germany, 2007.
11. Puhan, S., Jegan, R., Balasubramanian K., Nagarajan, G. Effect of injection pressure on performance, emission and combustion characteristics of high linolenic linseed oil methyl ester in a DI diesel engine. *Renewable Energy*. Volume 34, May 2009, Pages 1227–1233.
12. Hossain A.K., Davies P.A. Plant oils as fuels for compression ignition engines: A technical review and life-cycle analysis. *Renewable Energy*, Volume 35, January 2010, Pages 1–13.
13. Smith, E.J. Lubricating and additive mixtures for alcohol fuels and their method of preparation. . International publication number: US4595395. <http://www.freepatentsonline.com/4595395.pdf> (27.02.2012)

## 6. ADDITIONAL DATA ABOUT FIRST AUTHOR

Risto Ilves (Phd Student) – Tartu.  
Estonian University of Life Sciences,  
Institute of Technology, 56 Kreutzwaldi  
Street, EE51014, Estonia.  
E-mail: [risto.ilves@emu.ee](mailto:risto.ilves@emu.ee)  
Phone: +37258161529.

## IMPACT OF APPLICATION OF EXCELLENCE MODELS ON ORGANIZATIONAL PERFORMANCE

Kiitam, A. & Tammaru, T.

**Abstract:** *In this paper some issues of adaptation and application of excellence models are outlined. Possible approaches to impact assessment of use of excellence models are considered mainly based on international experience relevant for Estonia. Some conclusions for projects related to quality awards and recognition schemes applying EFQM and adapted excellence models in different sectors are presented.*

*Key words: Excellence models, EFQM, impact assessment, adaptation, sectoral models.*

### 1. INTRODUCTION

Use of excellence models (EM), as one of key tools for promoting quality and excellence in organizations, has become more and more widespread throughout the world in the past two decades. EMs are widely used for self-assessment as well as for external evaluation and recognition. The two most widespread reference models for frameworking different EMs are nowadays the Performance Excellence criteria of Malcolm Baldrige National Quality Award (MBNQA) and the EFQM Excellence Model (EFQM MEM).

Designing different national, regional and sectoral quality awards on the basis of these and other reference models requires consideration of various issues related to complexity, usage and cultural environment of EM to be designed, as well as experience with the former use. Therefore the analysis of experience of use of EMs in order to adapt a new or existing EM is important. In this paper we discuss

some issues related to the impact of use of EMs, in order to consider this impact while implementing and adapting EM to be used in a small country like Estonia.

### 2. IMPACT OF EM I: SOME METHODOLOGICAL ISSUES

When trying to assess the impact of use of EM on the basis of experience of use of EMs in Estonia, one of the major problems is that due to the smallness of the country it is practically impossible to collect such amount of statistically homogeneous data, which permits to reach acceptable statistical confidence for building models and making conclusions about relationships and impacts related to the use of EM (e.g., the number of organizations participating in annual national quality award contest is about 10-15, which for 10 years time interval results in only about 10-25 comparable organizations with appropriate excellence level per award category).

Therefore, it seems appropriate to assume that the influence mechanisms and relationships which have been identified in EM studies abroad can be applied to Estonian organizations as well.

Despite of the fact that this assumption is de facto forced it still seems rather logical due to the universal nature of EMs, grounded by universality of underlying total quality management (TQM) principles for EMs. In a more detailed manner, the assumption that international experience related to EM impact experience can be directly used in Estonia, can be grounded as follows:

1) Despite the complexity and methodological problems with different TQM implementation and EM impact studies (PIMS study, GAO study ea [1]), the overall conclusions seem to hold in similar manner in different reports, including mainstream conclusions concerning usefulness and pay-off of use of TQM and EM;

2) Overall conclusions concerning mechanisms of functioning and impact of different EMs are also rather similar, even in case they are grounding on different reference models like MBNQA or EFQM models.

3) At least on the qualitative level, the analysis of available Estonian data has not indicated any major contradictions with existing relevant EM impact studies.

However, this assumption of applicability of findings from relevant abroad studies concerning business excellence (BE) may introduce some "calibration error" for Estonia, as two types of critical success factors influence when using TQM/EM [2]:

- structural critical factors of excellence or factors required for successful implementation of TQM in any socio-cultural environment, and
- foundation critical factors of excellence or factors needed for the successful implementation of TQM in specific socio-cultural environments.

Therefore it seems appropriate to assume that the general findings about impact of use of EM apply for Estonia, but numerical/quantitative conclusions might need more careful acceptance. In addition to this it is necessary to accept that use of EM cannot guarantee that all decisions will be right (it has been estimated that 20% of Business Excellence programmes in the USA and Europe fail [3]).

### **3. IMPACT OF EM II: THREE DIMENSIONS**

The analysis of impact of use of EM is a rather multifaceted issue. In case of Estonia, when considering the impact of

use of EM in current business and cultural environment at least the following three aspects seem to be relevant for most of organizations:

- 1) excellence level
- 2) financial performance
- 3) sustainability / adaptability to change.

These three impact dimensions can be featured by following aspects and trends.

#### **2.1 Excellence Level**

The excellence level lies in terms of assessment in the very centre of EM. It reflects the maturity level of use of TQM/EM by the organization and is measured via the (total) excellence score resulting from external or self-assessment procedure used. In terms of underlying TQM concepts and values, it is most closely related to customer and employee satisfaction categories of EM, which usually have the highest weight in total score (often about 20-30% of score in MBNQA and EFQM based EMs). Therefore the total impact of EM is based on different studies strongly correlated namely with scores in customer and employee satisfaction categories. According to several studies, this correlation is supported by positive correlations between different categories in case the assessment indicates successful implementation and use of EM (e.g. study by Saunders and Mann for New Zealand organizations indicates that for self-assessment data correlation coefficient equals  $r = 0.94$  for relationship between customer focused results and financial and market results; this corresponds to determination coefficient value  $D = 0.88$  and thus indicates very strong connection) [4]. Provided that issues like satisfaction and happiness seem to have in current organizational cultural environment growing importance for persons/employees, it is expectable that the importance of these categories at least in near future will remain high. It is also important that there exists strong correlation of corresponding scores with



scores of other enabler and result categories.

## 2.2 Financial Performance

The financial performance has been traditionally a very relevant impact issue, first of all for profit-oriented organizations. Therefore the impact of use of EMs on financial performance has been a subject of interest in different studies, starting from traditional question "will quality management pay off?". These studies have used data collected by special surveys, and the general conclusion has been that there exists a positive correlation between the use of TQM and financial performance. The first such major study on an excellence model was conducted by the United States General Accounting Office in 1991 [1]. This led to a report linking improvement performance with quality efforts in the 20 highest scoring Baldrige Award applicants over the years 1988 and 1989. The evidence from this sample suggested that the organizations achieved improved employee relations, better quality, lower costs, greater customer satisfaction, improved market share and improved profitability [3].

A milestone study by Hendricks and Singhal introduced into BE studies use of data which is contrasting financial performance of quality award winners (mainly amongst public traded companies in USA, which means that the reference EM was dominantly MBNQA) against benchmark companies forming the control sample [5]. This approach provides a factual, objective, and statistically valid assessment of impact of use of EM on financial performance. In terms of time scale, this study indicated that appearance of impact of EM use takes considerably long time and the benefits will only be realised in the long run. More specifically, the data indicated that not much will happen during the first five years, which could be considered as a reasonably long period for EM implementation and introduction into organization (prior to

winning the award). The financial performance results during this implementation period don't indicate significant difference against results of benchmark companies (control sample data). The difference will however appear during post-implementation period, which is next five years after winning the award, the award winners outperforming benchmark companies in all financial performance indicators considered: operating income, sales, return on sales, return on assets, total assets, number of employees. With share price performance, award winners outperformed the S&P 500 companies and the control sample of benchmarks. Thus, the overall conclusion is that when EM is implemented effectively, financial performance improves dramatically.

For Estonia, the natural reference model for different EMs is the EFQM Excellence Model (EFQMEM), and this choice has been also implemented in practice. Therefore, in order to find a closer supporting know-how it is appropriate to use EM impact studies which are based on EFQMEM use as reference model and are close enough in space and time. Accordingly, the closest seems to be a study carried out by Centre of Quality Excellence, University of Leicester (funded by EFQM and British Quality Foundation) [6]. This study uses the same methodological approach as above study by Singhal and Hendricks and analyses financial performance of 120 award winning companies which have been using EFQMEM for their excellence efforts. The companies have been awarded at European, national, and in the cases of some countries, regional level (winning a quality award in Europe is generally an indication that a company has effectively implemented the principles of the EFQM Excellence Model). The performance measures used for the study are share value and accounting based measures, which include revenue/sales, costs, operating income, capital expenditure, total

value of assets and number of employees. For each award winning company a comparison company was selected, thus the size of control sample is also 120 and data is paired. To ensure objectivity in collecting data on financial performance, the data collection and analysis efforts has been focused only on publicly traded companies. The data has been analysed over an 11 year time period anchored around the year when a company received its first award.

The overall conclusion from this financial performance data analysis might be the following: when principles of the EFQM EM have been implemented effectively, performance improves in both short and long periods of time. As a numerical excerpt the following numbers indicating how much the award winning companies outperform the comparison companies by an average in time period five years after receiving an award might be presented: higher growth in sales by an average of 77%, higher increases in operating income by an average of 18%, higher increases in capital expenditure over assets by an average of 28%.

### **2.3. Sustainability and Adaptability to Change**

The third dimension of impact of using EM is related to sustainability and adaptability to change. Thus, this dimension is related to an ensemble of features of organizations which are more difficult to measure in quantitative manner but which in current rapidly changing and somewhat anxious business and cultural environment are very vital for survival and development of organizations. These features are related to the ability of organizations to change, their (strategic) agility, innovativeness, flexibility. For Estonian situation amongst the recent survey-type studies which address these issues the most relevant seems to be the Oakland Consulting PLC study [3]. The conclusions of this study seem to be relevant for Estonia first of all because the sample of analysed

organizations is large enough, includes mostly European organizations which business excellence programmes are grounded on the use of EFQM Excellence Model, and considers both private and public organizations (in total 101 public sector and 91 private sector organizations responded in the survey). Brief summary of the conclusions relevant for our purposes can be presented as follows:

- benefit of BE is delivered to several stakeholders: employees, customers and the organization itself;
- organization's ability to react to its changing environment (strategic agility), was found to have a positive relationship with performance;
- BE positively correlates with strategic agility, which in turn correlates with higher levels of performance;
- key sources of advantage for organizations relate to their people;
- for private sector organizations, reputation, brands and the customer base are also important sources of advantage. For public sector organizations, these are also the culture of the organization and the service providers;
- it takes about three years to build the advantages, which gives an indication of how patient an organization must be when implementing BE.

As expectable, the results indicating relationships between excellence level and the above survival/change ability measures are more difficult to quantify than financial performance impact measurement results. However, the positive correlations can sometimes be calculated and tested for significance (e.g., the determination coefficient of model for strategic agility scale vs BE scale is  $D = 0.312$ , and the determination coefficient of model for strategic agility scale vs performance scale equals  $D = 0.585$ ; both  $D$  values were significant at the 0.001 level,  $N = 192$ ).

In total, the findings suggested that organizations which successfully implement BE develop the ability to respond to change, a capability that is

becoming more critical as the pace of change increases. What is more, this capability leads to benefits for many of the organization's stakeholders.

The conclusions of this study are supported also by a recent study for Asian companies of five countries, initiated by Asian Productivity Organization (APO) [7]. Some findings of this APO study relevant for us can be presented as follows:

- companies reported that in addition to the fact that BE had a major impact on their competitiveness and performance, the use of EM was also relevant for long-term competitiveness and sustainability;
- in general only minor changes to the design of the EM frameworks (if any) were needed, but innovation and how it relates to business excellence needs to be more clearly explained to companies;
- time and effort should be put into making the frameworks easier to understand and the value of the frameworks needs to be more clearly communicated;
- BE should not just be marketed as "BE" or "continuous improvement". BE frameworks help companies to improve in a multitude of ways;
- BE has major impact on competitiveness and performance;
- the awards are important, but the prime motivator for the majority of companies is to "improve performance".

#### **4. IMPACT OF EM III: CONCLUSIONS FOR ESTONIA**

Summarizing the above findings from BE studies, for Estonia we can conclude the following:

- 1) The positive impact of use of EMs in different dimensions (excellence, financial performance, sustainability) is practically guaranteed provided that the models are implemented in substantial and appropriate way;
- 2) It takes considerable time while this positive impact will appear (approximately 3...5 years) and the measurement and direct proof of this effect is very difficult;

3) Provided that financial performance and sustainability/agility dimensions of impact are more difficult to measure than direct excellence score which will be registered during external or self-assessment anyway, while there exists rather strong positive correlation between these three impact dimensions, it is appropriate to assess the excellence level growth mostly on the basis of (external) assessment scores (including total score and different enabler and result category scores). However, comparability of scores and reliable assessment here require that assessment procedures and especially the "calibration" training of assessors are made in correct and careful manner. This should also include intensive communication of assessors and their switchover between use of different EMs (while maintaining general similarity of different EMs and scoring principles).

4) In order to enlarge positive impact of use of EMs, it is necessary to use adaptation of models for different sectors and clusters of economy/society. This helps reception of models and promotes their substantiality while keeping assessment schemes economical and unified on basis of same reference model.

#### **5. SOME CONSIDERATIONS FOR ESTONIAN SCHEMES OF USE OF EXCELLENCE MODELS**

On the basis of similarity of impact mechanisms of using EM mentioned above, it is appropriate to use a single reference model for Estonia, and this model should naturally be EFQMEM. The adaptation of this model for different sectoral, cluster and organization's category schemes for different award, recognition and self-assessment purposes should be based on optimal complexity approach while keeping necessary overall BE principles in models. The most important resource for a small country like Estonia for these EM uses is adequate population of qualified and experienced assessors, who can participate in different external

assessment schemes and guarantee adequate level of accuracy of assessments. The assessment should be reliable first of all in terms of total excellence score, which enables also acceptable reflection for other impact dimensions like financial performance and sustainability/agility. Provided that the amount of assessors for a small country is limited while the precision level of assessment cannot be compromised, there is need for minimization of workload for sectoral models while keeping necessary assessment accuracy/precision. Provided that individual score estimates by assessors can be according to normal assessment guidelines taken as independent estimates and assessment consensus can be numerically approximated by statistical average, the two-sigma measurement uncertainty for a team of  $M$  assessors can be estimated as  $U = 2\sigma / \sqrt{M}$ , where standard deviation  $\sigma$  of individual assessment uncertainty may be estimated via testing assignments of assessor calibration training (preferably averaging  $\sigma$  over sufficient sample of corresponding deviation data). For calculation of recommendable size of assessor team then the assumption might be that width of categorization indifference zone equals to half of categorization zone width  $\Delta$  in assessment result presentation (e.g. in excellence model based recognition schemes C2E or R4E [<sup>8</sup>]); this leads to about 95% confidence level in category identification correctness. Correspondingly, such considerations for gaining acceptable measurement uncertainty level for assessment procedure lead to following inequality condition for assessment team size limitation:

$$M \geq (2\sigma / \Delta)^2 .$$

For example, if according to some assessment categorization guidelines  $\Delta = 25$  point on 1000 point scale and  $\sigma = 28$  points, then the size of assessment team should be  $M \geq 5$ , which is quite common in practice.

## 7. REFERENCES

1. G. A. O. *Management Practices: U.S. Companies Improve Performance through Quality Efforts*. Washington D.C., General Accounting Office, 1991.
2. Zairi M., and Alsughayir, A.A. The Adoption of Excellence Models through Cultural and Social Adaptations: An Empirical Study of Critical Success Factors and a Proposed Model. *Total Quality Management & Business Excellence*, 2011, **22**, 641-654.
3. Tanner, J.S. *White Paper: Is Business Excellence of Any Value? Does It Generate and Sustain Organisational Advantage?* Oakland Consulting, 2005.
4. Saunders, M. and Mann, R. Self-assessment in a multi-organisational network. *Int. Journal of Quality & Reliability Management*. 2005, **22**, 554-571
5. Hendricks, K. B. and Singhal, V.R. Does Implementing an Effective TQM Program Actually Improve Operating Performance: Empirical Evidence from Firms That Have Won Quality Awards. *Management Science*, 1997, **44**, 1258-1274.
6. Boulter L., Bendell, T. e.a. *Report on the Impact of the Effective Implementation of Organisational Excellence Strategies on Key Performance Results*. CQE Univ. Leicester, Leicester, 2005.
7. Mann, R.. *Report of the APO Survey on the Impact of Business Excellence/Quality Awards on Enterprises*. Asian Productivity Organization, 2011.
8. Eesti Kvaliteediühing [WWW] <http://www.eaq.ee/edasipurgiva-organisatsiooni-c2e-auhinna-materjalid> (01.03.2012)

## 5. ADDITIONAL DATA ABOUT AUTHORS

Andres Kiitam, PhD, Professor, Dep. of Mechatronics, TUT, phone +372 6203 204 [andres.kiitam@ttu.ee](mailto:andres.kiitam@ttu.ee)  
 Tiia Tammaru, MSc(Eng.), Dep. of Mechatronics, TUT, mob +372 56 636 679 [tiia.tammaru@ttu.ee](mailto:tiia.tammaru@ttu.ee), Ehitajate tee 5, Tallinn, 19086, Estonia

## THE LABORATORY OF DRAWING LESS MANUFACTURING

**Kostal, P.; Delgado Sobrino, D. R. & Velisek, K.**

**Abstract:** *At the end of 2008 our institute - Institute of Production Systems and Applied Mechanics responded to the challenge number.: OPVaV-2008/2.2/01-SORO ASFEU Agency and the Ministry of Education has developed a project called "Laboratory of flexible manufacturing systems with robotic handling for environment without drawing production". The flexible manufacturing system will contain the two CNC controlled machines (milling and lathe machines). These machines will be interconnected by a transport system and operated by industrial robots. This flexible manufacturing system will also include a quality control station including the camera system and shelf storage.*

*In the final phase of this project in year 2012, the flexible production system will be linked with the CAD laboratory of our institute*

*Key words: intelligent manufacturing systems, manufacturing process, control system, drawing less manufacturing.*

### INTRODUCTION

Before 70<sup>th</sup> years of last centuries the mass production respond to basic requirements of market, but after this get started consumer affect the market. The producer must adapt to consumers requests and get started production of some variants of its products. This changeover has significant impact to mass production. Producers who can produce the wild range variants of its product have domination at market.

Today market is characterized by strategy of consumer's individualization. This strategy is oriented to consumer's requests.

Consumers want new products and time has a fundamental task to its satisfaction. The production was broadening, innovation cycle is shortening, and the products have new shape, material and functions.

The production strategy focused to time need change from traditional functional production structure to production by flexible manufacturing cells and lines. Production by flexible cells (FMS) are most important manufacturing philosophy in last years.

This manufacturing concept requires identification of part families and machine groups in order to exploit similarities and achieve economies in the entire manufacturing cycle.

This philosophy is based on similarity:

- ▲ similarity of manufactured parts,
- ▲ similarity of process plans.

Recognize the similarity of manufactured parts allows grouping them to groups by machines required to its manufacturing. By manufacturing of this group of parts we achieve economical effect near to mass production.

### THE GROUP TECHNOLOGY

In design time of manufacturing cell by group technology solve identification of machined parts set. These sets of parts need identical technological devices (usually machine tools). The group technology divides the whole manufacturing process to independent detached manufacturing units – cells. All of them produce the own set of similar parts.

Machine tools from one of cell (dedicated for one set of parts) are not applicable for other set of parts. This machine layout has

advantage in minimal material handling and manipulation.

Setup times for machine tools are very short because the technological process for a given set of part is very similar.

Process planning for a small batch of manufactured parts in manufacturing cell is simple.

This manufacturing philosophy is very effective and process managing is easy. By set of similar parts to group we can achieve unified material flow in manufacturing cell for all manufactured parts included to given group. By proper managing of manufacturing processes is possible to achieve the continuous flow production.

Advances of group technology:

- a reduction in setups,
- a reduction in inventory level,
- a reduction in transportation time of goods,
- an effective control of production,
- reliable delivery time,
- higher management efficiency,
- cost savings in setup time, manpower, tooling, machine tool maintenance and work in process,
- integrating various functional areas by providing sufficient information.

Material flow for parts on classic manufacturing philosophy (without a group technology) is shown at Fig. 1.

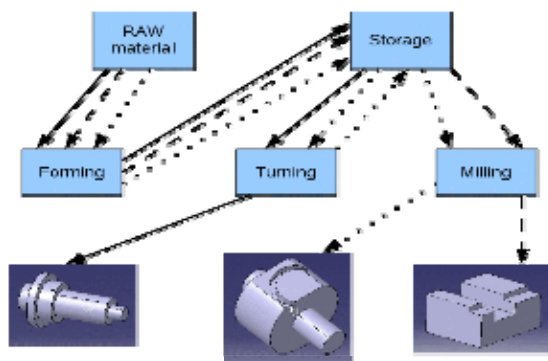


Fig. 1 Material flow in traditional manufacturing

The material flow is very complex. Material handling and manipulation are realized across a whole workshop. Cost for material moving is high and require a lot of time.

After application of group technology and manufacturing cell philosophy the material flow is simple. (Fig. 2)

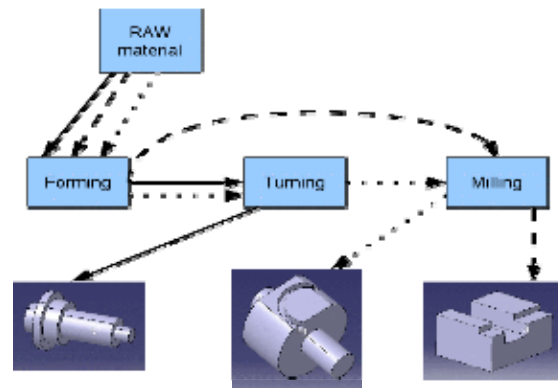


Fig. 2 Material flow in cell manufacturing

Materials are manipulated only inside of manufacturing cells. Material moving time is short and manipulating is effective.

## THE MANUFACTURING SYSTEM DESIGN

The flexible manufacturing system will contain the two CNC controlled machines (milling and lathe machines). These machines will be interconnected by a transport system and operated by industrial robots. This flexible manufacturing system will also include a quality control station including the camera system and shelf storage.

The supplementary devices are used mainly to manipulation with workpieces and tools:

- ▲ workpiece storage and device for workpiece changing,
- ▲ storage, controlling and changing of tools,
- ▲ quality control.

A part of complex automated manufacturing process is an automation of technological process control, automated transportation, handling, feeding, and interchange of workpieces, tools and automated waste cleaner. There are many technological sites existing, which match given requirements. Besides obvious

computer techniques for controlling the manufacturing machines, automatically working bins, loaders, conveyors, manipulators and industrial robots are implemented step by step. As industrial production is growing constantly, besides implementing of the classical automated means, which were mentioned above, manufacturing systems with intelligent control are being installed.

Material flow is an integral part of every production system. Material flow is an integral part of every production system. In this paper we will focused to material flow suggestions possibilities in the flexible manufacturing system. The material flow is determined by several variants of system layout. [4]

The design of manufacturing system is a part of manufacturing process planning. The main determining factors for the manufacturing system design are: the product, the production volume, the used machines, the disposable manpower, the disposable infrastructure and the legislative frame for the specific cases.

The automation of manufacturing and assembly process can be run in the term of the manufacturing profile, material flow or information flow. These basic elements of the manufacturing process are usually automated together in the praxis, but it is not the condition. The task of the manufacturing and assembly process control is to provide the process running in the status of dynamical stability and the replacement in the equilibrium status on the same or acceptable standard by the deviation of the equilibrium status. The process control is characteristic as the process organization in system that provides the achievement of the required final state; assembly or manufacturing process. The utilization of this information for the manufacturing process control could be only then if it is known the noted model of system behavior by means of that it is possible to create the control algorithm and technical system for its realization by defined aim. [5]

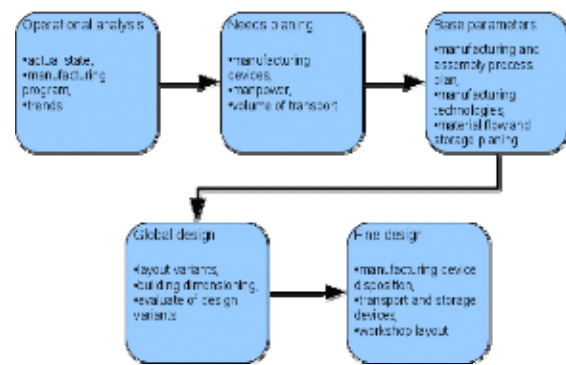


Fig. 3 The general sequence of manufacturing system design.

During detailed inspection, it seems advisable to analyze the technological workplaces that are functional and spatial areas:

- ⤴ Technological area as space where are performed technological operations on workpieces,
- ⤴ Manipulation area as space where are performed manipulations (operational and intermediate operational) with workpieces, tools and waste,
- ⤴ Directing area as space in which are performed controlling operations,
- ⤴ Area of maintenance as space in which is realized set up, maintenance, servicing etc.

## THE LABORATORY LAYOUT

At the Fig. 4 is showed the final variant of flexible manufacturing system layout. This system contains two machining centers (milling and turning), assembly station, shelf storage with the manipulator and industrial robot on the rail. This final variant of a flexible manufacturing system is extended by a transport system in a closed loop, quality control station and by a robotized assembly station.



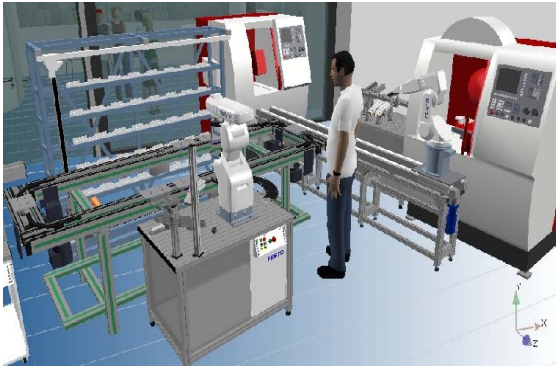


Fig. 4 The flexible manufacturing system visualization

In the process of material flow planning, it is necessary to consider the fact that the aim of the plan is not the transport and storage of material as these activities are expensive and do not improve the material value. Current systems for handling, transport and storage provide a great number of possibilities for the application of expensive and complex systems. The optimal design should contain minimum storages, transport and handling. Hence, the suitable way before the elaboration of detailed system solution is to reduce mentioned activities to a minimum. [5]

All features of manufacturing system must be planned considering mutual interactions and verified by a simulation model before the system realization.

From the point of view of manufacturing and material flow, it is talking about mutual connections and formation of material chain. The main aim is the mutual coordination of all material flows and assurance of the efficiency of material flow between individual segments of a chain. [5]

We want to produce (simulate production) various components of shaft, flange, bracket and box shape in this system. Each component made will represent piece production that means only one piece of this component will be made. Variability (dimensions and shape versions for each component) will be relatively wide. Planning and management of the production process in FMS must be adapted to that fact.

The whole process starting with design up to storage of final component must run automatically without human intervention. That means, material in the FMS storage system will be automatically taken out of store, transported to individual machines according to program, put in operating area by a handling device (industrial robot). Machine will execute individual technological operations to reach final properties (shape and dimension) of the component. Simple components can be worked by one machine only but in case of more complicated parts, the component will have to be handled in the machine (e.g. turned to another position) or relocated to another machine so that other necessary technological operations can be realized (sometimes this relocation between individual machines needs to be repeated several times). [6]

## CONCLUSION

Flexible manufacturing cells allows manufacturing the small numbers of part from huge range of types and achieve good economical effects near by large batch or mass production. The manufacturing cells structure has connected the machines and save the production time, space and production costs too.

Functions of machines are coordinated and the material flow can be quick Manufacturing process of components, parts or final products usually are not realized at one workplace. The manufacturing logistics solve tasks about organization of material and information flow in manufacturing. The importance of manipulating and transport devices are underlain fact that more than 50% time needed to manufacturing are spent by manipulation and transport and automation level of these processes are smaller than automation level of technological processes.

Our main aim of project is building of laboratory, in which will be located flexible manufacturing system consisting of at least two production machines with

NC control (milling machines, lathe). These machines will be linked with transport system and they will be served by industrial robots. Within this flexible manufacturing system will be also station for quality control with camera systems and rack warehouse.

After termination of the project our Institute will have a fully functional prototype of a flexible manufacturing system with robotic operation of individual production facilities, which will be integrated with CAx laboratories.

## REFERENCES

- [1] Hrušková, Erika - Holubek, Radovan: Increasing of effectiveness of manufacturing and directing technical level. In: Proceedings in Manufacturing Systems. - ISSN 2067-9238. - Vol. 5, No 4 (2010), s. 203-208
- [2] Košťál, Peter - Mudriková, Andrea: Material flow in flexible manufacturing and assembly. Computing and Solutions in Manufacturing Engineering, September 25-27, 2008, Brasov, Romania. In: Academic Journal of Manufacturing Engineering. - ISSN 1583-7904. - Supplement, Issue 1 (2008), s. 185-191
- [3] P. Košťál, P. Kerak, and I. Kiss, "Development of new generation production machines and systems - The Intelligent fixture at flexible manufacturing," *Annals of faculty Engineering Hunedoara – International Journal of Engineering*, vol. IX, no. 1, 2011.
- [4] R. Ruzarovsky, S. Horvath, and K. Velisek, "Designing of automated manufacturing and assembly systems," in *ANNALS OF DAAAM FOR 2008 & PROCEEDINGS OF THE 19TH INTERNATIONAL DAAAM SYMPOSIUM*, VIENNA UNIV TECHNOLOGY, KARLSPLATZ 13, WIEN, A-1040, AUSTRIA, 2008, pp. 1201-1202.
- [5] Mudriková, Andrea - Hrušková, Erika - Horváth, Štefan: Areas in flexible manufacturing-assembly cell. - článok vyšiel v časopise: *Annals of Faculty of Engineering Hunedoara - Journal of Engineering*, ISSN 1584-2673, Tome VI, Fascicule 3, 2008, str. 123-127. In: *Scientific Buletin*. - ISSN 1224-3264. - Vol. XXII (2008), s. 293-298
- [6] Mudriková, Andrea - Charbulová, Marcela: Intelligent Assembly Systems. In: *AMO Conference*. - ISSN 1313-4264. - Vol. 3. 9. International Conference Advanced Materials and Operations : *Scientific Reports. Project CII-BG-0203-02-0809 CEEPES*. Bulgaria, Kranevo 24-28 June 2009 (2009). - Sofia : Technical University of Sofia, s. 591-595

## ADDITIONAL DATA ABOUT AUTHORS

Corresponding Author: Peter Košťál, Faculty of Material Science and Technology, Slovak University of Technology, Paulínska 16, 91724 Trnava, Slovak Republic, e-mail peter.kostal@stuba.sk

## ACKNOWLEDGMENT

This article was created with the support of the OP Research and development for the project **Laboratory of flexible manufacturing systems with robotized manipulation supported by no drawing production** ITMS 26220220055, co-financing from the resources of European Regional Development Fund.



Support research activities in Slovakia/ Project is co-financing from resources EU



## QUALITY OF MANAGEMENT PRACTICES AND APPLICATION OF COMPLEX AUTOMATED SYSTEMS

Kristjuhan, K.; Metsla, E. & Ling, H.

**Abstract:** *This study plugs an important gap in empirical evidence of a relationship between quality of management practices and application of complex automated systems. A pilot study was conducted in Estonian companies which apply robot welding. Evidence of a strong correlation between quality of management practices and effectiveness in utilizing this complex technology was shown. The study also presented a novel survey instrument for studying company's management and technological capabilities.*

*Key words: management practices, quality of management, technological capabilities, complex automated systems, methodology.*

### 1. INTRODUCTION

Management innovation theory suggests that companies which do not possess strong management practices are not capable of economically beneficially utilizing complex technological systems [1]. Also, quality authorities, such as Mizuno [2] and Kondo [3], have argued that applying automated systems presupposes excellently planned and coordinated processes, superb information flow, and standardized and disciplined operations. Such processes and operations would premiss high quality of management at the middle and frontline levels of an organization which are supported by clear direction from the top management. However, empirical evidence of a relationship between the quality of management practices and ability to utilize complex automated systems has been lacking.

Recent research in Estonia has indicated that quality of management in companies in Estonia is relatively low both in general at company level as well as at operational production management level [4, 5]. Yet, a number of Estonian manufacturers have invested in complex technology over recent years, resulting in their overall assessment of their technological capability as satisfactory [5]. The same patterns are evident in the 2011 Estonian machine building sectorial study which states that the majority of Estonian machine building companies lack formal management practices both at company level and at operational production management level [6]. Regardless, nearly half of the companies participating in the study attested to having revamped their manufacturing processes by greater automation and implementation of novel technologies, such as laser cutters, welding robots and 3D measuring equipment [6].

This paper argues that, in accordance with theoretical perspectives, there exists a strong positive correlation between a company's quality of management practices and its capability to utilize complex automated equipment, such as a welding robot.

The paper is structured in the following way: introduction, theoretical framework, method, results, and conclusions and discussion.

### 2. THEORETICAL FRAMEWORK

#### 2.1 Management Practices

A number of studies have been carried out over the past half a century to identify what

is it that managers do in their daily work. The majority of such studies have been in the form of an observation of managers' work. Also interviews with managers and document reviews have been used.

An exception to the above described line of research was Henri Fayol, who was a top manager himself as well as a scholar. Fayol was one of the first to propose a comprehensive theory of management. He posited that there were five principal functions of management: planning, organizing, coordinating, leading and controlling [7]. Later management scholars have often reduced the five functions to four by removing coordination (e.g. see Daft [8]).

Other oft cited management scholars have been Mintzberg and Kotter. Both of them conducted original studies into what managers do. Mintzberg observed activities of five top managers over a five day period and proposed 10 roles of managers based on the observations [9]. Kotter observed work of 15 top managers (for more than 600 hours in total) and additionally collected information from different documented sources in organizations [10]. The limitations of these studies were that, first, the number of managers observed was very small. Second, both scholars only directly observed top managers of organizations. Quality scholars, such as Mizuno [2] and Kondo [3], have argued that, in fact, the most important level of management in terms of delivering quality products and services to customers is the frontline management. Several studies cited in Carroll and Gillen [11] have shown that managers at all levels of an organization participate in planning, coordinating, controlling, and problem solving. Finally, later empirical research has failed to confirm some of their conclusions, e.g. distinct existence of Mintzberg's ten managerial roles has not been confirmed [11].

Fayol's model of management functions has stood the test of time [11]. A number of scholarly works have applied these

functions directly in empirical research or based research models on them. For example, the „PRINCESS“ factors study by Mahoney, Jerdee, and Carroll cited in Carroll and Gillen [11] extended Fayol's five functions to eight factors of planning, representing, investigating, negotiating, coordinating, evaluating, supervising, and staffing. The study investigated time allocation of managers on the listed factors. Another indication of a theory's descriptiveness of a phenomenon is if independent studies of the same phenomenon reach similar results. An independent study by Luthans and Lockwood in 1984, cited in Luthans, Rosenkrantz and Hennessey [12], applied an observation method to measure behavioral frequency of managerial activities. The study identified 12 categories of managerial activities (hereinafter called management practices): planning/coordinating, staffing, training/developing, decision making/problem solving, processing paper work, exchanging routine information, monitoring/controlling performance, motivating/reinforcing, disciplining/punishing, interacting with outsiders, managing conflict, and socializing/politicking [12]. The Luthans and Lockwood management practices can be easily conceptually related to Fayol functions with the exception of socializing/politicking. The latter practice encompasses nonwork-related chit chat and gaming [12] and thus was not the object of Fayol's studies. The results of the authors' conceptualization of this relationship have been provided in Table 1.

Luthans and Lockwood management practices have been successfully operationalized by Luthans and his colleagues in later research as well as by other scholars. Some examples include Asllani and Luthans' study of knowledge managers [13], and O'Driscoll, Humphries and Larsen's study of links between performance of managerial activities and perceived managerial effectiveness [14].

Fayol functions	Luthans and Lockwood practices
Planning Coordinating	Planning/coordinating Exchanging routine information Interacting with others Decision making/ problem solving
Organizing	Staffing Processing paperwork
Leading	Training/developing motivating/reinforcing Disciplining/punishing Managing conflict
Controlling	Monitoring/controlling performance
-	Socializing/politicking

Table 1. Comparison of Fayol functions and Luthans and Lockwood management practices (authors' conceptualization)

In this study the Luthans and Lockwood management practices and detailed descriptions of activities have been operationalized to define management practices, quality of which is measured in relation to the company's technological performance.

## 2.2 Quality of Management Practices

While classical economics and its related organization theories, such as the industrial organization, tend to downplay the role of managers in a company's performance, management scholars are determined that managerial activities have a significant role in a company's results [15]. Yet, due to the complexity of defining management and the large variety of factors influencing company performance, investigations into how management relates to company performance are scarce.

Horovitz and Thietart made an early attempt to find relations between classical managerial functions of organizing, planning and controlling, and firm performance by controlling for company size and industry sector [16]. Good

managerial practices were related to good performance in this study.

Bloom and van Reenen used a complex survey instrument to collect data on company practices and compare these to company performance in the form of accounts and the stock market data [17]. Also this study found that better management practices were associated with better company performance, including higher productivity, profitability, and survival. However, the survey instrument was not theoretically based.

Svirina measured the efficiency of Fayol's functions and company performance (e.g. profitability, financial stability, and market share) [18]. One of the results of the study suggested that spending time and money on performing motivational functions is more effective than an equal distribution of resources.

In this study we define quality of management practices as level of application (both in scope and depth) of management practices in a company. The general structure of the study is depicted on Figure 1.



Fig. 1. Quality of management and performance (authors' conceptualization)

## 2.3 Quality of Management Practices and Application of Complex Technology

While early research has shown that higher quality of management is associated with better performance of a company, management innovation scholars posit that application of complex technological systems outright presupposes strong management practices [1, 19]. Yet, again, empirical evidence is hard to come across. A study by Wang, Klein and Jiang

discussed implementation of Enterprise Resource Planning (ERP) in Taiwan [20]. The limitation of this study was that a self-report instrument was administrated to companies' project managers directly responsible for the technology project. Thus partiality bias could not be ruled out. Another study by Bloom, Sadun, and Van Reenen, conducted on panel data, suggested that US companies were more productive in using IT partially due to their higher management and organizational capital compared to, for example, UK companies [21].

This study provides empirical evidence of a relationship between quality of management practices and application of complex technology by uniquely focusing on highly complex industrial technology – a welding robot.



Fig. 2. Hypothesized relationship between quality of management and technological capability

In accordance with theoretical perspectives, the hypothesis is that there exists a strong positive correlation between a company's quality of management practices and its capability to utilize a complex automated equipment. (See an illustration of this relationship in Figure 2.)

### 3. METHOD

A pilot study was carried out among Estonian manufacturers which applied robot welding. A novel online survey instrument was used. An additional aim

was to assess the workability of the survey instrument.

Quality of management was measured via management practices and activities as defined by Luthans and Lockwood [12]. Eight out of the 12 Luthans and Lockwood management practices were operationalized: planning/coordinating, staffing, training/developing, decision making/problem solving, exchanging routine information, monitoring/controlling performance, motivating/reinforcing and managing conflict. These practices were selected due to their apparent positive effect on operational performance. Four practices (processing paperwork, disciplining/punishing, interacting with others and socializing/politicking) were excluded due to their apparent neutral or negative effect on operational performance. A sample question might have sounded, „Please assess the level of decision-making and problem-solving in your company“, followed by a detailed description of the activities in this management practice. Respondents were asked to mark one out of five levels of quality of the management practice ranging from „There are no such activities present in our company“ to „Such activities are regular and documented. Results are publicly displayed on walls (information boards) for everyone to see“. Planning/coordinating was divided into long-term or strategic (defined by a time period longer than 1 year) planning and short-term (defined by time period shorter than 1 year) planning. Thereby the total number of quality of management practices questions was nine.

In addition, respondents were requested to specify which of three management levels - top management, middle-management and/or frontline management - were actively practicing these management activities to see whether any of the management levels had a specific effect on the company's technological capability.

Company's technological capability was measured by a single right first time [22] (also referred to as „first-time-right“)

measure of the robot welding. Respondents were also able to mark one or more probable causes in a provided list, if right first time was less than 100% in their company.

The pilot instrument was administered via a freeware Kwik Surveys online application. Links to the survey instrument were sent to one top or middle manager in each company (e.g. General Manager, Quality Manager or Production Manager). Five manufacturing companies in Estonia which possessed in-house robot welding were selected for the pilot study (2-digit EMTAK 2008 codes 25, 28 and 31).

Analysis of the results of the survey was conducted in a following manner. First, linear correlation coefficient was determined between total quality of management (measured as sum of category responses) and the technological capability measure. Next, an analysis of variance (ANOVA) was utilized in order to determine whether (1) different management levels or (2) general variables, such as company size, capital ownership or tenure of full implementation of robot welding provided statistically significant dependencies to company's technological capability. Last, frequency analysis was carried out among determinants of right first time parameter. In addition, it was assessed whether the respondents found the survey instrument easy to fill in, or should changes be made to it in future studies.

#### 4. RESULTS

Correlation coefficient of .74 suggests that there is a significant positive dependency between the quality of management practices and technological capability. Thus an assumption can be made that higher level of management quality allows predicting presence of company's higher technological capabilities.

Results of ANOVA suggest that there is no reason to support the initial hypothesis about the company's management levels

impact to its technological capabilities. In the frame of the nine management practices asked from the respondents there is no evidence about statistically significant dependencies at significance level .05 ( $F(3,1)=9.55$ ;  $F(3,1)=2.57$ ;  $F(3,1)=.81$ ;  $F(3,1)=8.73$ ;  $F(3,1)=2.24$ ;  $F(3,1)=2.72$ ;  $F(3,1)=.23$ ;  $F(3,1)=4.20$ ;  $F(3,1)=4.20$ ).

In addition, there was no reason to support the hypothesis about the existence of statistically significant dependencies between company's size, capital ownership and tenure of full implementation of robot welding with technological capability at significance level .05 ( $F(3,1)=3.27$ ).

The most frequent responses for causes of poor right first time were missing jigs (3), poor quality of material (2) and missing a competent operator for the robot (2).

Respondents found the survey instrument easy to use. More nominal range options for or the actual right first time measure could be asked in next studies for a better defined correlation.

#### 5. CONCLUSIONS AND DISCUSSION

The study provided evidence that there is a strong positive correlation between a company's quality of management practices and capability to apply complex automated systems. To test the hypothesis further, a full-scale study should be conducted among respective companies. This would also allow to further studies of dependencies between technological capability and management levels.

#### 6. REFERENCES

1. Mol, M. J., and Birkinshaw, J. The sources of management innovation: When firms introduce new management practices. *Jour of Bus Resch*, 2009, **62**, 1269-1280.
2. Mizuno, S. *Company-wide Total Quality Control*. Asian Productivity Organization, Tokyo, 1988.
3. Kondo, Y. *Companywide Quality Control: Its Background and*



- Development*. 3A Corporation, Tokyo, 1999.
4. Vadi, M. et al. *Eesti juhtimisvaldkonna uuring*. EAS, Tallinn, 2011.
  5. Gans, K., and Kokla, M. *Tootmisjuhtimise operatiivtasandi uuring*. EAS, Tallinn, 2011.
  6. Varblane, U. et al. *Eesti masinatööstuse sektoruuring*. EAS, Tallinn, EAS, 2011.
  7. Fayol, H. *General and Industrial Management*. Pitman, London, 1949.
  8. Daft, R. *Understanding Management*. The Dryden Press, Fort Worth, 1995.
  9. Mintzberg, H. *Managerial Work: Analysis from Observation*. *Management Science*, 1971, **18**, B-97-B-110.
  10. Kotter, J.P. *The General Managers*. The Free Press, New York, 1982.
  11. Carroll, S.J. and Gillen, D. J. Are the Classical Management Functions Useful in Describing Managerial Work? *Acad of Mngt Rev*, 1987, **12**, 38-51.
  12. Luthans, F., Rosenkrantz, S.A. and Hennessey, H.W. What Do Successful Managers Really Do? An Observation Study of Managerial Activities. *The Jour of App Beh Sci*, 1985, **21**, 255-270.
  13. Asllani, A. and Luthans, F., What knowledge managers really do: an empirical and comparative analysis. *Jour of Know Man.*, 2003, **7**, 53-66.
  14. O'Driscoll, M.P., Humphries, M. and Larsen, H.H. Managerial activities, competence and effectiveness: manager and subordinate perceptions. *The Int Jour of HR Mngt*, 1991, **2:3**, 313-326.
  15. Holcomb, T.R. Holmes, M. R, Jr. and Conelly B.L. Making the most of what you have: managerial ability as a source of resource value creation. *Strat Mngt Jour.*, 2009, **30**, 457-485.
  16. Horovitz, J.H. and Thietart, R.A. Strategy, Management Design and Firm Performance. *Strat Mngt Jour.*, 1982, **3**, 67-76.
  17. Bloom, N. and Van Reenen, J. Measuring and Explaining Management Practices Across Firms and Countries. *The Quar Jour of Econ*, 2007, **CXXII**, 1351-1408.
  18. Svirina, A. Measuring Managerial Efficiency: A Balanced Approach. *Gl Jour of Bus Resch*, 2010, **4**, 97-104.
  19. Kelley D.J. O'Connor, G.C., Neck, H. and Peters, L. Building an organizational capability for radical innovation: The direct managerial role. *Jour of Eng and Tech Mngt*, 2011, **28**, 249-267.
  20. Wang, E. G., Klein, G. and Jiang, J. J. ERP Misfit: Country of Origin and Organizational Factors. *Journal Of Management Information Systems*, 2006, **23**, 263-292.
  21. Bloom, N., Sadun, R. and Van Reenen, J. It ain't what you do, it's the way that you do IT: Investigating the productivity miracle using multinationals. Working paper. <http://www.cepr.org/meets/wkcn/6/6644/papers/Van%20Reenen%20paper.pdf> (31.01.2012).
  22. Loveridge, K. Non-financial performance indicators. In *The Blackwell Encyclopedia of Management* (Cooper, C. L., ed.). Blackwell Publishing, [http://www.blackwellreference.com/subscriber/tocnode?id=g9780631233176\\_chunk\\_g978140511828621\\_ss6-1](http://www.blackwellreference.com/subscriber/tocnode?id=g9780631233176_chunk_g978140511828621_ss6-1) (29.02.2012).

## 7. CORRESPONDING ADDRESS

MSc., MBA Kadri Kristjuhan  
TSEBA  
Tallinn University of Technology  
Akadeemia Road 3, 12618 Tallinn, Estonia  
Phone: +372 512 0927  
E-mail: kadri.kristjuhan@gmail.com

## INTEROPERABILITY BETWEEN DIFFERENT INTEREST GROUPS PRACTICE PORTAL CASE STUDY

Lemmik, R.; Karjust, K.

**Abstract:** *Interoperability is a property referring to the ability of diverse systems and organizations to work together (inter-operate). To achieve interoperability between different organizations or interest groups, one possible way is to build specific web portals where structured information can be easily published and consumed. Current work describes the solution where traineeship mediation process was organized through Practice Portal in TUT Faculty of Mechanical engineering. There are different Interest groups associated with the portal: Students – publish their traineeship requests and join traineeship events; Companies – publish their traineeship offerings and organize traineeship events; Lecturers – represent students or companies in certain situations; Curators – collect the information and manage traineeship.*

*To meet the needs of those interest groups the development project was launched to specify all traineeship processes in TUT Faculty of Mechanical engineering and according to those processes build specific web portal. Current paper focuses to the following aspects during this project: Analysis – how to find out all requirements; Design – how to structure requirements from IT solution viewpoint; Develop – how to find proper technical architecture; Implement – how to go live and involve all interest groups to use the solution.*

*Key words: interoperability, CRM, diverse system, practice portal, database*

### 1. INTRODUCTION

Web technologies offer the opportunity for our colleges and universities to move from having a historic focus on processes to being information- and communications-based institutions [1].

The customer is rightfully the center of the university information model. Unlike many commercial enterprises, with simple client provider relationships, universities have a complex set of relationships with a wide variety of constituents. In fact, the term customer is misleading in a university context. We are using customer to mean the full community of individuals who have a relationship with our institution. Institutionally we tend to think in terms of separate categories for each of these relationships and separate institutional departments to service them [1,2].

#### 1.1. Customer Relationship Management

CRM is both a business strategy and a set of discrete software tools and technologies, with the goal of reducing costs, increasing revenue, identifying new opportunities and channels for expansion, and improving customer value, satisfaction, profitability, and retention. CRM focuses on automating and improving the institutional processes associated with managing customer relationships in the areas of recruitment, communication management and marketing. CRM takes a very customer-centric view of the entire customer life cycle, which means that a CRM business strategy places the customer at the center of the organization's universe. From the

perspective of the customer, a CRM business strategy allows interaction with the college or university from a single entity that has a complete understanding of their unique status [1].

## 1.2. Web Portals

The World Wide Web continues to be the preminent application on the Internet because it has regularly reinvented itself. In fact, for most people, the World Wide Web has become synonymous with the Internet. With the introduction of Web portals, the Web is in the process of reinventing itself once again. Portals are not a fad or a new name for something that we've been doing all along. They will turn the Web from an institution-centric repository of information and applications to a dynamic user-centric collection of everything useful to a particular person in a particular role. Instead of a single home page that

proclaims identically to all who visit how grand the institution is, portals will give nearly every user a customized, unique Web page [1].

## 1.3. Practice Portal in TUT

The Practice Portal project was launched in Tallinn University of Technology (TUT) Faculty of Mechanical engineering to cover traineeship recruitment and communication management processes. Compared to the current CRM and Web portal solutions on the market the requirements were more or less specific so the best way was to build its own portal solution. Traineeship recruitment process presented in Fig.1 compared to the regular employee recruitment process contains some specific tasks related with the assignments where university side curator or lecturer is involved to coordinate the recruitment process and to provide approvals.

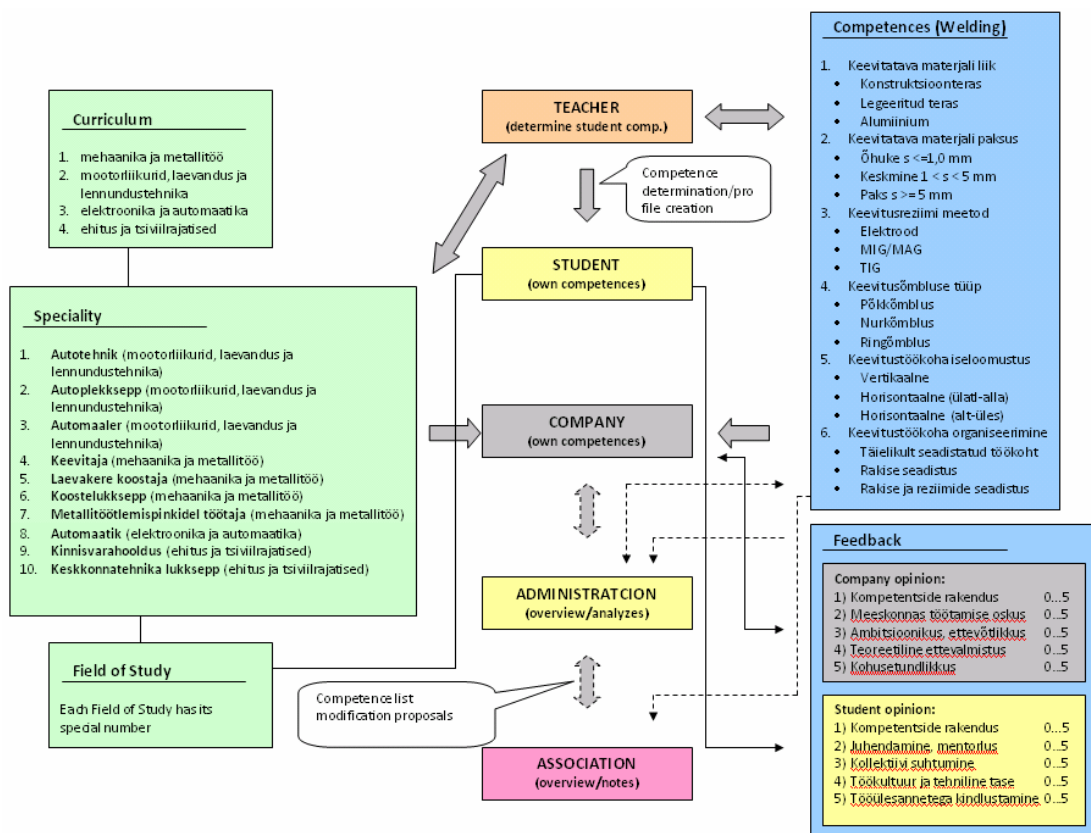


Fig.1. Traineeship recruitment process

## 2. ANALYSIS

A business process is a set of one or more linked procedures or activities which collectively realize a business objective or policy goal, normally within the context of an organizational structure defining functional roles and relationships [3].

Current chapter describes main business requirements from analysis perspective which are base for portal business logic and user interface design.

### 2.1. Users and roles

All users need to be registered, anonymous access to the portal isn't allowed. After registration user fills the profile data and curator approves it. User profile contains names, contact information, additional information and curricula association. Users can be in following roles:

#### Student

- Modify profile data
- Post traineeship requests
- Apply for traineeship
- Join to event

#### Lecturer

- Modify profile data
- On behalf of company post traineeship offerings
- On behalf of student post traineeship request
- Approve traineeship applications
- Post events
- Approve event participation

#### Company

- Modify profile data
- Post traineeship offerings
- Approve traineeship applications
- Approve events

#### Curator

- Modify profile data
- Approve profiles
- Post traineeship documents

- Manage portal main data

### 2.2. Traineeship requests

Traineeship requests will be published by students containing general information and structured data. Companies can find through portal the student requests matching their offerings. With the request student can apply for traineeship or lecturer can assign students request for traineeship. All traineeship applications need to be approved mutually by student, company and lecturer.

### 2.3. Traineeship offerings

Traineeship offerings will be published by companies containing general information and structured data. Students can find through portal the offerings matching their requests. Students can apply for traineeship offering or lecturer can assign students request. All traineeship applications need to be approved mutually by student, company and lecturer.

### 2.4. Feedback

Every traineeship case ends with the feedback given mutually by student and company. Feedback contains questionnaire and competence ratings. Curricula related current competences are associated with student profile and required competences are associated with traineeship offering. Feedback combines both competence lists.

### 2.5. Events

Events will be organized by lecturer and company co-operation, example company visitations. Published event contains main information and structured data and it will be approved by company. Events are shown in event calendar where students can find interesting events and join to them. All event participations need to be approved by lecturer

## 2.6. Documents

Traineeship associated documents can be uploaded to portal by curator. Documents are associated with meta-data containing general information and structured data to publish specific grouping and sequence.

## 3. DESIGN

Feature Driven Development (FDD) is an agile and adaptive approach for developing systems. The FDD approach does not cover the entire software development process, but rather focuses on the design and building phases. However, it has been designed to work with the other activities of a software development project and does not require any specific process model to be used. The FDD approach embodies iterative development with the best practices found to be effective in industry. It emphasizes quality aspects throughout the process and includes frequent and tangible deliveries, along with accurate monitoring of the progress of the project [4].

Current chapter describes business logic and user interface design principles of the Practice Portal presented in Fig.2.

## 3.1. User interface

Portal has multi-language, web-based user interface. It contains following sections:

- Language selection
- Logged in user info
- Dynamic main menu
- Tabbed main page
- Footer with contact and disclaimer

## 3.2. Navigation logic

Portal navigation mainly contains list-card type logic where chosen list is opened from main menu item. According to the role rights it is possible to open current and add new cards from list. Card opens always in view mode and according to the user rights it is possible to edit and delete it. All Lists and Cards are shown as tabbed pages where tabs contain additional info related with the active card. From related info list it is possible to open once again related info card and so on. It is everywhere possible to use NAVIGATE button to move one logical level back, it's like intelligent Back button. Current action info is shown on left corner of the main page

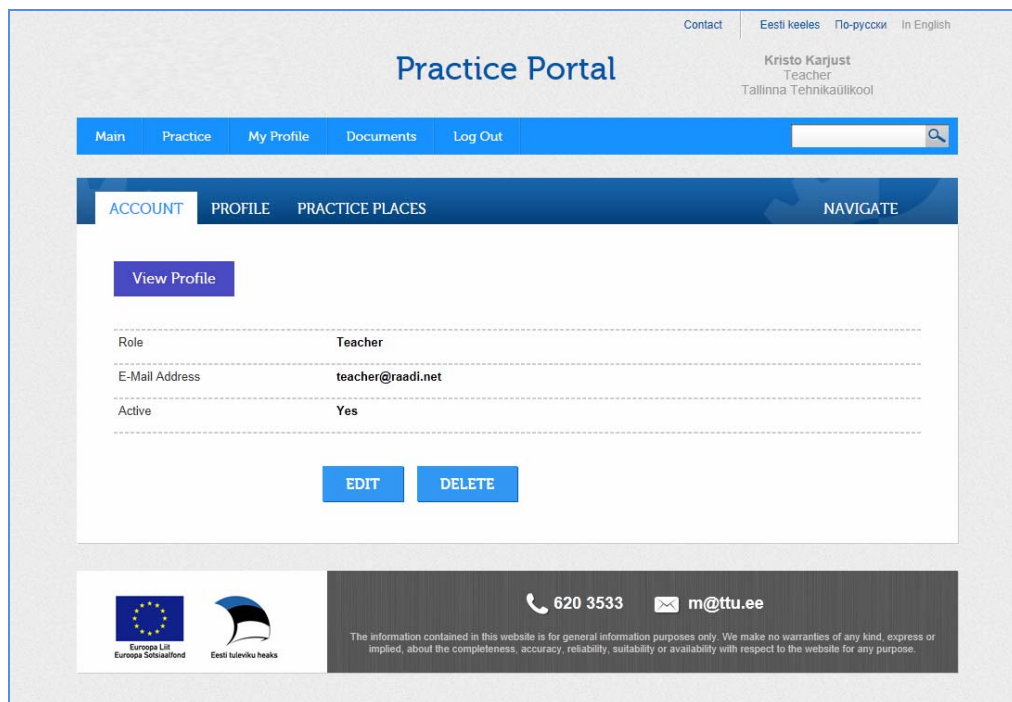


Fig.2. Practice Portal user interface

#### 4. DEVELOPMENT

At the most basic level, the Web works off a client / server architecture. Simply stated, that means that both a central server and a client application are responsible for some amount of processing, presented in Fig.3. Almost all of the work of Web applications takes place on the server. The Web server is responsible for communicating with the browser [5].

##### 4.1. PHP programming language

PHP belongs to a class of languages known as middleware. These languages work closely with the Web server to interpret the requests made from the World Wide Web, process these requests, interact with other programs on the server to fulfill the requests, and then indicate to the Web server exactly what to serve to the client's browser [5].

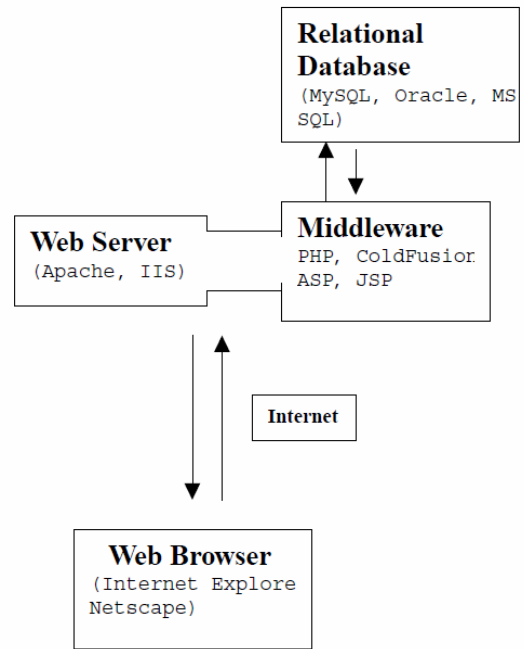


Fig.3. Architecture of Web applications [5]

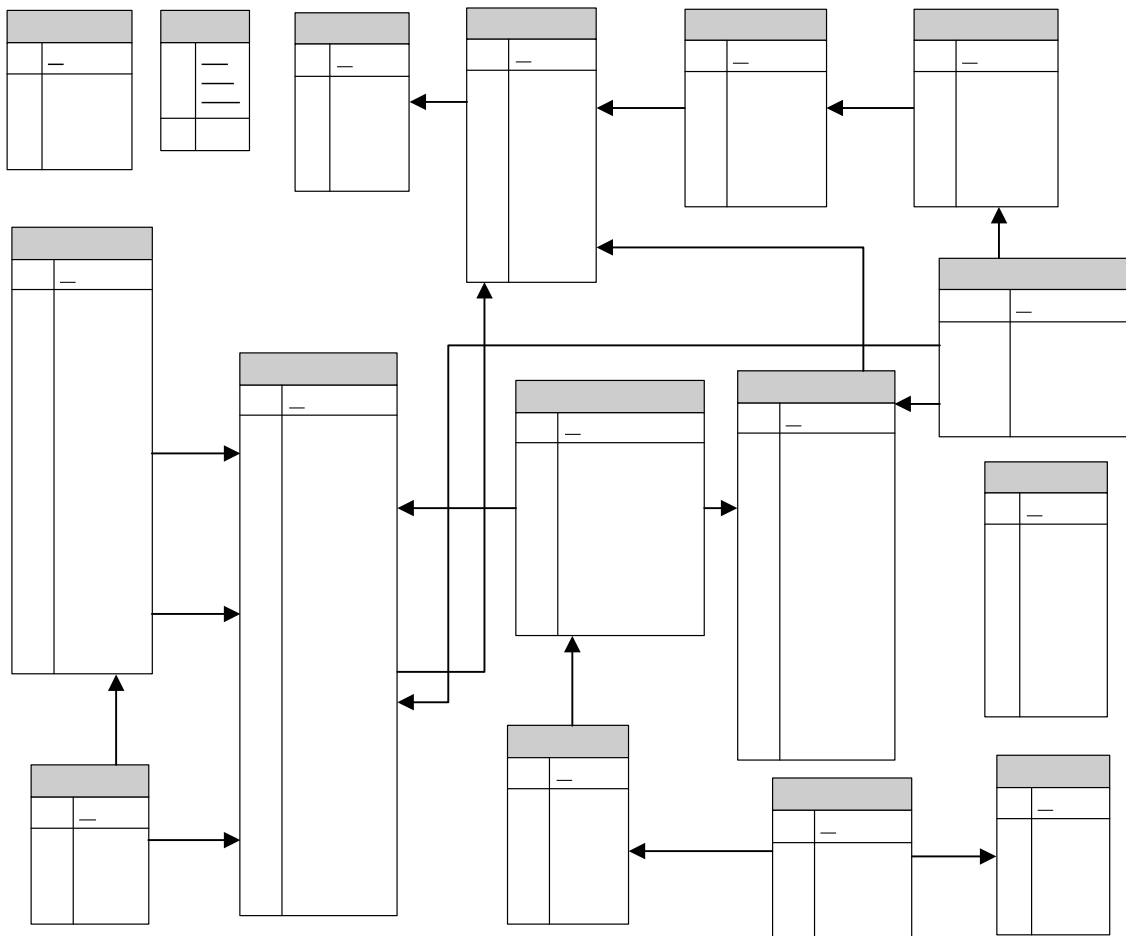


Fig.4. Practice Portal data model

## 4.2. MySQL database

Relational database management systems (RDBMSes) provide a great way to store and access complex information. All the major databases make use of the Structured Query Language (SQL). Some of the more popular commercial RDBMSes are Oracle, Sybase, Informix, Microsoft's SQL Server, and IBM's DB2. In addition to MySQL, there are now two major open-source relational databases. Postgres has been the major alternative to MySQL in the open-source arena for some time. For a while, Borland released its Interbase product under an open-source license and allowed free download and use [5].

## 4.3. Practice Portal architecture

In current project PHP and MySQL have been chosen as widespread open-source, freeware and cross-platform components for architectural base.

PHP programming code in current project has been structured as modular as possible which allows easily to expand and improve the application. All kind of hardcoding is avoided i.e. all multi-language captions and user role rights are stored in database and can be easily modified by end-user.

Data model in MySQL database, presented in Fig.4 is designed as normalized relational structure without unnecessary data redundancy. By using table triggers the data integrity is guaranteed.

Multi-language functionality is currently limited with three languages: Estonian, Russian and English. All user interface texts, messages and captions in three languages are stored in translations table. For main data translations, data tables contain three name\_xx fields for texts in different languages.

## 5. CONCLUSION

The project described in current paper was successful in general. The problems were

solved during project and can be avoided next time by using experience from current project. Next steps will be to expand the usage of this portal over the whole university and to co-operate with other similar projects to integrate and consolidate this kind of web portals.

## 6. REFERENCES

1. Richard N. Katz and Associates. Web Portals and Higher Education: Technologies to Make IT Personal. Jossey-Bass, 2002
2. Karjust, K. Küttner, R.; Pääsuke, K. Adaptive web based quotation generic module for SME's. Küttner, R. (Toim.). In *Proceedings of the 7th international conference of DAAAM Baltic industrial engineering, 22-24th April 2010, Tallinn, Estonia*. Tallinn: Tallinn University of Technology, 2010, 375-380
3. Workflow Management Coalition, The Workflow Management Coalition Specification: Terminology & Glossary, WfMC-TC-1011 v3.0, February 1999. [http://www.wfmc.org/standards/docs/TC-1011\\_term\\_glossary\\_v3.pdf](http://www.wfmc.org/standards/docs/TC-1011_term_glossary_v3.pdf) (effective link on 1 March 2012).
4. Pekka Abrahamsson, Outi Salo & Jussi Ronkainen. Agile software development methods – Review and analysis. VTT Publications, 2002
5. Brad Bulger, Jay Greenspan & David Wall. MySQL/PHP Database Applications, Second Edition. Wiley Publishing, 2004

## 7. CORRESPONDING AUTHORS

PhD student Rivo Lemmik,  
Ass. Prof. Kristo Karjust

Department of Machinery,  
Tallinn University of Technology,  
Ehitajate tee 5, Tallinn,  
19086, Estonia.  
E-mail: [rivo@raadi.net](mailto:rivo@raadi.net)



## IDENTIFICATION OF PARAMETERS CHARACTERIZING THE NONLINEAR BEHAVIOR OF VISCOUS-ELASTIC SYSTEMS ON DYNAMIC LOADINGS

**Adrian Leopa, Silviu Nastac, Carmen Debeleac, Gigel Capatana, Aurora Potarniche**

**Abstract:** *There are situations when certain mechanical systems or buildings may be damaged or destroyed in case of external dynamic loadings from human activities or due to natural hazard (seism). A measure to counteract these negative consequences is including in the mechanical system or to exposed dynamic loadings construction, of some systems for isolation and damping oscillatory movements, such as viscous-elastic systems. These viscous-elastic systems, by prolonged exposure to atmospheric factors and claims arising from anthropogenic environment, change their specific operating parameters leading in certain situations to uncontrolled movements that cannot be anticipated. This situation corresponds to behaviour nonlinear of viscous-elastic system, elastic and damping forces having nonlinear expressions. This paper aims to identify parameters capable of indicating the point from which the viscous-elastic system has a changed behaviour as a nonlinear kind.*

*Keywords: dynamic, viscous-elastic, nonlinear, antivibration, shock.*

### 1. SYSTEMS FOR ISOLATING THE MACHINE FOUNDATION

Worldwide, efforts have been intensified to control and mitigate the vibration of both the technological machinery and equipments and that of buildings and bridges. Due to the heavy and varied demand regime, to which passive control systems are subjected, they suffer, in time, degradation that can lead to quantitative changes of the dynamic

response of heavy industrial machinery that work with impulsive action, [1]. The degradation occurring in the dynamic isolation systems determines the change of the expressions of stiffness and damping forces from linear mathematical relationships into nonlinear dependence. It has experimentally been found that this nonlinear behaviour of vibration isolation systems leads to generating oscillatory movements that sometimes exceed the limit levels required by standards in the field. For this reason, the central objective of this paper is to: theoretical quantify quantitatively the nonlinearity degree of passive control systems, through determining the parameters of influence (control) able to characterize not only the cause but also the effect of nonlinear behaviour. Taking this into consideration, a methodology can be developed, based on experimental measurements, able to evaluate in time, the changes in the dynamic behaviour (response) of shock and vibration generating equipment, according to the change in the characteristics of viscous-elastic systems installed under the foundation of the equipment. The avoidance of the appreciation errors in applying this methodology requires its implementation right from the moment of putting into service of the dynamic isolation system of a viscous-elastic type. The evaluation of the isolators' degradation is achieved through periodic experimental determinations in order to determine the influence parameters and to analyses them comparatively with their initial values.

Internationally there is a modern identification technique and a quantification of the damages of an antiseismic devices bridge of hydraulic dissipater type. This algorithm was successfully applied for the quantification of the structural integrity of the bridge *Vincent Thomas* - Los Angeles.

## 2. ANALYSIS OF DYNAMIC BEHAVIOR OF MECHANICAL SYSTEMS MODELED AS RIGID WITH VISCOUS-ELASTIC TRIORTOGONALE LINKS

The identification and quantification of parameters able to characterize the nonlinear behaviour of viscous-elastic systems for dynamic isolation of mechanical structures, involves at a theoretical level, the development of a physical and mathematical model that can accurately characterise dynamically the behaviour of the impulsively loaded system. That is why a physical model is proposed with a very general nature, namely that of solid rigid leaning on four viscous-elastic triortogonal supports (fig. 1), [2].

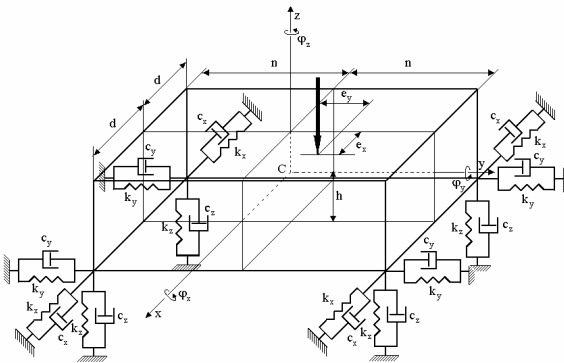


Fig. 1 The physical model

The rigid movements depending on the generalized coordinates are defined as follows:

- $X$  - lateral forced vibration (sliding);
- $Y$  - forced longitudinal vibration (forward);
- $Z$  - forced vertical vibration (leaping);
- $\phi_x$  - forced vibration pitch (galloping);
- $\phi_y$  - forced vibration roll (swinging);

$\phi_z$  - forced vibration turning (return).

This model corresponds to technological equipment such as forging hammers, screw presses, etc., in which rigid solid corresponds to the foundation of machinery. It is considered that the two coordinated planes of symmetry are XOZ and YOZ, in which there are the following terms:

$$\begin{cases} \sum k_{iy}x_i = 0; \sum k_{iz}x_i = 0; \\ \sum k_{iy}x_iy_i = 0; \sum k_{iy}x_iz_i = 0; \\ \sum k_{ix}y_i = 0; \sum k_{iz}y_i = 0; \\ \sum k_{iz}y_iz_i = 0; \sum k_{ix}y_iz_i = 0; \end{cases} \quad (1)$$

and

$$\begin{cases} \sum c_{iy}x_i = 0; c_{iz}x_i = 0; \\ \sum c_{iy}x_iy_i = 0; \sum c_{iy}x_iz_i = 0; \\ \sum c_{ix}y_i = 0; \sum c_{iz}y_i = 0; \\ \sum c_{iz}y_iz_i = 0; \sum c_{ix}y_iz_i = 0; \end{cases} \quad (2)$$

where:

$k_{ix}$ ,  $k_{iy}$ ,  $k_{iz}$  are stiffness coefficients of the bearings after three directions,  $c_{ix}$ ,  $c_{iy}$ ,  $c_{iz}$  are viscous damping coefficients after the three directions,  $x_i$ ,  $y_i$ ,  $z_i$  are rigid motions.

The equations of forced vibration characterizing the foundation behaviour in steady state are in relation (3):

$$\begin{cases} m\ddot{X} + 4c_x\dot{X} - 4hc_x\dot{\phi}_y + 4k_xX - 4hk_x\phi_y = 0 \\ m\ddot{Y} + 4c_y\dot{Y} + 4c_yh\dot{\phi}_x + 4k_yY + 4k_yh\phi_x = 0 \\ m\ddot{Z} + 4c_z\dot{Z} + 4k_zZ = -F_z \\ J_x\ddot{\phi}_x + 4hc_y\dot{Y} + 4(c_yh^2 + c_zn^2)\dot{\phi}_x + \\ + 4hk_yY + 4(k_yh^2 + k_zn^2)\phi_x = -e_yF_z \\ J_y\ddot{\phi}_y - 4hc_x\dot{X} + 4(c_xd^2 + c_zh^2)\dot{\phi}_y - \\ - 4hk_xX + 4(k_zd^2 + k_xh^2)\phi_y = e_xF_z \\ J_z\ddot{\phi}_z + 4(c_xn^2 + 2c_yd^2)\dot{\phi}_z + \\ + 4(k_xn^2 + 2k_yd^2)\phi_z = 0 \end{cases} \quad (3)$$

where  $m$  is foundation mass,  $k$  is rigidity of the viscous-elastic element,  $c$  is damping of the viscous-elastic elements,  $J$  is inertia moments of the foundation block.

The main elastic axes of elastic bearing are parallel to the reference axes.

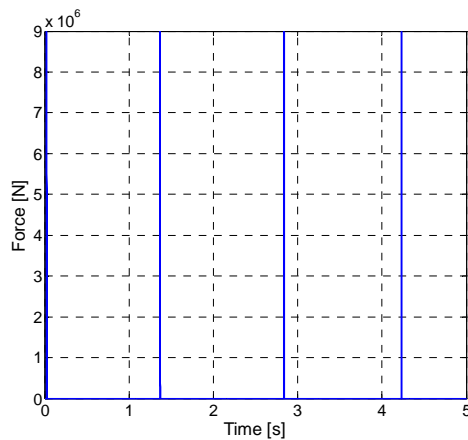
In this case, the movements represented by the variation of coordinates corresponding to the six degrees of freedom, may be decoupled as follows:

- coupled translational motion along the axis X and rotation around axis Y ( $X, \varphi_y$ );
- coupled translational movement along the Y axis and rotation around the X axis ( $Y, \varphi_x$ );
- translational movement along the Z axis independent of the other ways;
- rotation around Z axis ( $\varphi_z$ ) independent of the other ways.

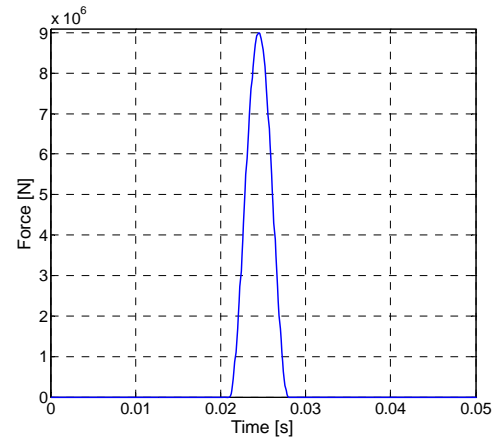
Next only the translation movement along the Z axis will be analyzed.

### 3. CHARACTERIZATION OF FORCE APPLICATION

System excitation is considered as impulsive force  $F_z$  eccentrically applied on the axis OZ. This model is specific for technological equipment to which the technology force is impulsively applied in the vertical direction during the working process. The machine-foundation system is considered, stressed by a disruptive force four-pulse train haversine type (fig. 2 a), the time between applying two consecutive pulses being close but uneven, [5]. Haversine impulse type (fig. 2 b) has the following characteristics: amplitude of  $9 \cdot 10^6$  N, frequency 7.1 Hz and  $\varphi = 3/7\pi$ .



a. Four-pulse train



b. Detail

Fig. 2 Haversine type excitation function

### 4. THE HYPOTHESES FOR CALCULATION

In order to reveal the influence of the nonlinear nature of antivibration system parameters (stiffness and damping) on the dynamic performance of the isolated system, a number of parameters characteristic to vibration are investigated in the following situations:

- elastic and damping forces have linear expressions;
- elastic force in the OZ direction has a nonlinear expression;

$$F_{ez} = k_z(1 + \text{sgn}(\dot{z}) \cdot \beta_1 \cdot z + \beta_2 \cdot z^2) \cdot z,$$

$$\beta_1 = 5 \cdot 10^2 \text{ 1/m}^2; \beta_2 = 2 \cdot 10^6 \text{ 1/m}^2,$$

and viscous forces in the direction OZ have linear expression.

The equation of motion is then like relation (4):

$$m\ddot{Z} + 4c_z\dot{Z} + 4k_zZ = -F_z \quad (4)$$

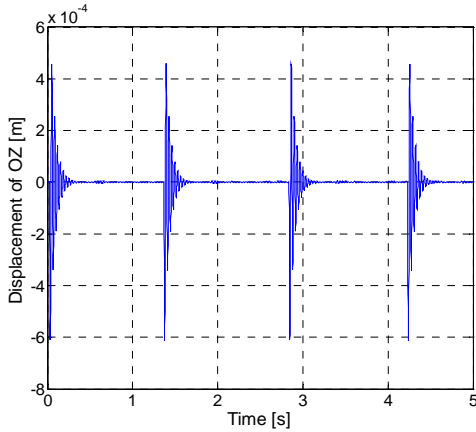
where:  $m$  is foundation mass,  $k_z$  is rigidity of the viscous-elastic element on OZ direction,  $c_z$  is damping of the viscous-elastic elements on OZ direction,  $Z$  displacement on OZ direction and  $F_z$  is excitation force.

Graphical representations were performed using Matlab, [4] and [6].

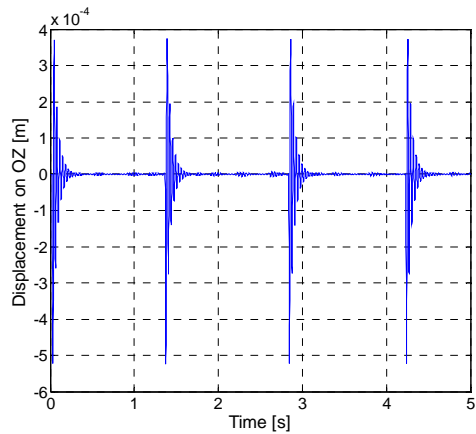
## 5. FORCED LEAP VIBRATION

*A. The response in time of the motion on the OZ axis*

The representation in time of the movement on OZ axis, highlights its amplitude decrease for nonlinear elastic force, to a value of  $3.8 \cdot 10^{-4}$  m compared with  $4.5 \cdot 10^{-4}$  m in the linear case, fig. 3.



a.  $F_{ez}$  = linear function;  $F_{vz}$  = linear function

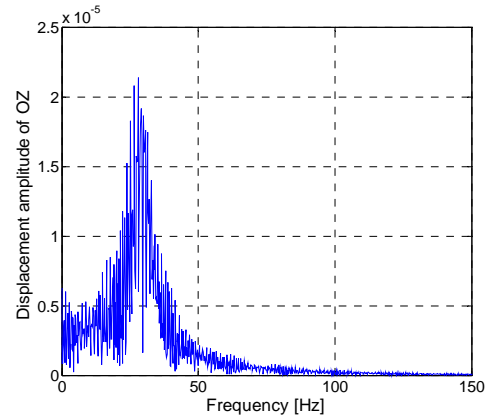


b.  $F_{ez} = k_z(1 + \text{sgn}(\dot{z}) \cdot \beta_1 \cdot z + \beta_2 \cdot z^2) \cdot z$

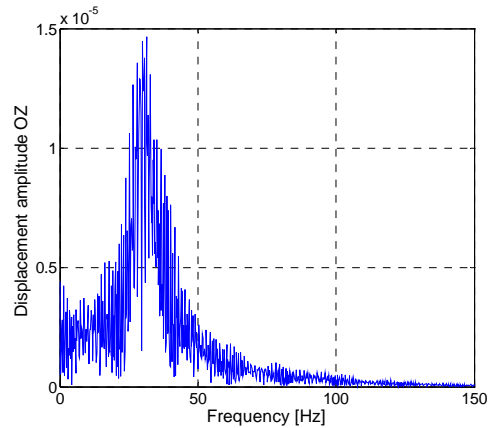
Fig. 3 Movement on OZ axis

*B. The response in frequency of movement on OZ axis*

The frequency responses of the displacement of the system in the OZ direction for the two considered cases are similar in values of dominant frequency spectral components, fig. 4.



a.  $F_{ez}$  = linear function;  $F_{vz}$  = linear function

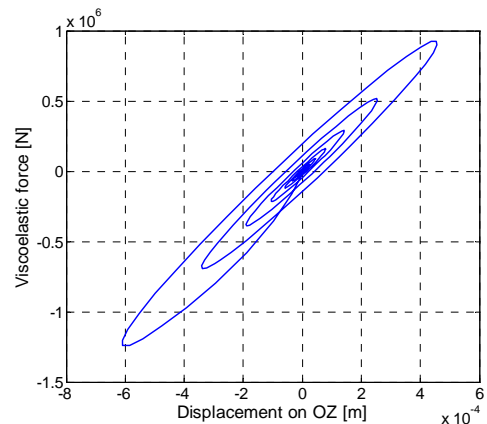


b.  $F_{ez} = k_z(1 + \text{sgn}(\dot{z}) \cdot \beta_1 \cdot z + \beta_2 \cdot z^2) \cdot z$

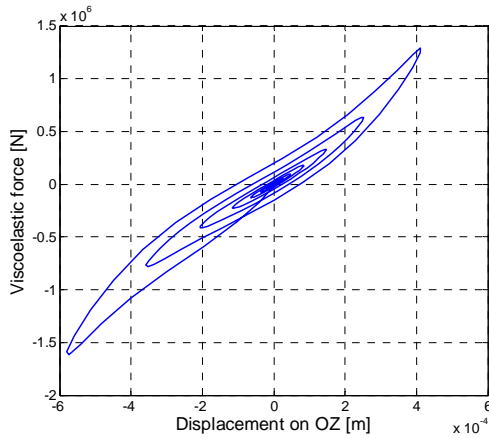
Fig. 4 Frequency spectrum

*C. Energy dissipated by viscous friction*

The value of dissipated energy through viscous friction in one period of movement, decreases slightly in the nonlinear case  $W=930,76$  J compared to the linear one  $W=934,79$  J, the difference being explained by reducing the movement on axis OZ, fig. 5.



$F_{ez}$  = linear function;  $F_{vz}$  = linear function;  $W=934,79$  J



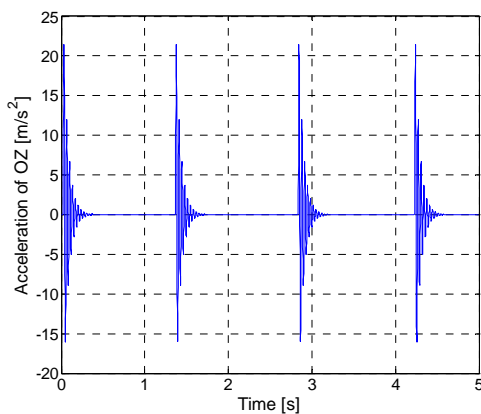
b.  $F_{ez} = k_z(1 + \text{sgn}(\dot{z}) \cdot \beta_1 \cdot z + \beta_2 \cdot z^2) \cdot z$ ;  
 $W=930,76 \text{ J}$

Fig. 5 The hysteresis loop

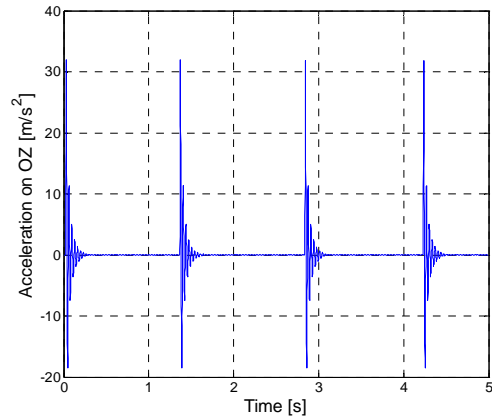
In the nonlinear case, hysteresis curve changes its shape, its median curve being the stiffness characteristic of the isolation systems.

*E. Response in time of acceleration on OZ direction*

From the representation in time of the system acceleration on the OZ direction one can observe a significant increase in amplitude for the nonlinear case to the value  $32 \text{ m/s}^2$  in comparison with  $22 \text{ m/s}^2$  value in the linear case, fig. 6. The explanation of the change of the linear behaviour of viscous-elastic systems into a nonlinear one is the modification of the structural integrity because of their wear or due to external agents such as temperature, humidity and others.



a.  $F_{ez} = \text{linear function}$ ;  $F_{vz} = \text{linear function}$

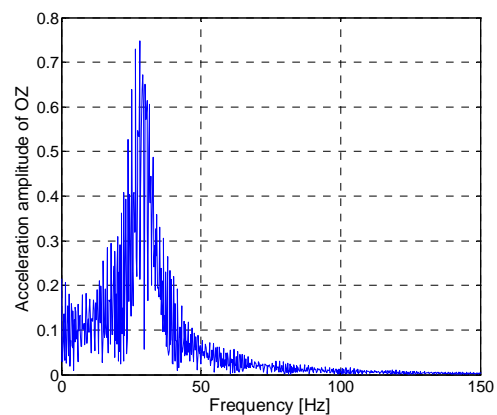


b.  $F_{ez} = k_z(1 + \text{sgn}(\dot{z}) \cdot \beta_1 \cdot z + \beta_2 \cdot z^2) \cdot z$   
 Fig. 6 Acceleration on OZ axis

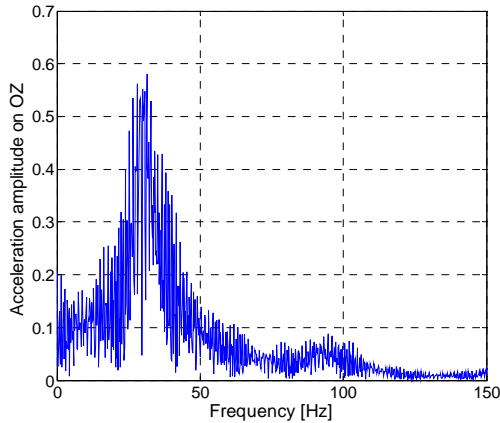
This phenomenon increases the harm degree of the vibrations from the technological equipment towards the environment. The nonlinear behaviour of viscous-elastic systems, according to their structural changes, should be closely monitored over time through certain specific parameters, due to the chaotic motion that may occur during the operation of industrial equipment.

*F. Frequency response of acceleration in the OZ direction*

This representation identifies, for the nonlinear case, the two significant areas of spectral components with central values in  $32.8 \text{ Hz}$  and  $103.4 \text{ Hz}$ , compared to the linear case in which the dominant area is centered on the value of  $28 \text{ Hz}$ , fig. 7.



a.  $F_{ez} = \text{linear function}$ ;  $F_{vz} = \text{linear function}$



b.  $F_{ez} = k_z(1 + \text{sgn}(\dot{z}) \cdot \beta_1 \cdot z + \beta_2 \cdot z^2) \cdot z$

Fig. 7 Frequency spectrum of acceleration on the OZ axis

## 6. CONCLUSION

Moulding the foundations of the machines as rigid with six degrees of freedom leaning on viscous-elastic triortogonal systems, presents a character of generality, this model can thus be simplified according to the characteristics of the equipment or of the dynamic isolation systems.

From the analysis of the results the following aspects can be highlighted:

- among the cinematic parameters of the system vibration disturbed by impulsive forces, the variation of acceleration is the most sensitive in order to highlight the presence of nonlinearity in the viscous-elastic system
- the presence of elastic and/or dissipative nonlinear forces leads to super-harmonic and sub-harmonic vibrations, which increases the possibility of the resonance phenomenon
- the energy dissipated by viscous friction decreases for nonlinear vibration, which means that the industrial vibration propagated have a greater amount of energy that they transmit to the environment.

In this way, this paper has established and characterized a series of cinematic parameters, the displacement, acceleration and energy dissipated by hysteresis, which

through monitoring in time can characterize the degree of nonlinearity of dynamic isolation systems, and consequently the degree of degradation of their viscous-elastic links, [3].

## ACKNOWLEDGMENTS

This work was supported by UEFISCDI (CNCSIS-UEFISCSU), project number PN II-RU-PD code 597/2010.

## 7. REFERENCES

- [1] Bratu, P., - *Sisteme elastice de rezemare pentru masini si utilaje*, Editura Tehnica, Bucuresti, (1990);
- [2] Bratu, P., - *Vibratii neliniare*, Editura IMPULS, Bucuresti, 2001;
- [3] Gafițeanu, M., Crețu, Sp., Drăgan, B. *Diagnosticarea vibroacustică a mașinilor și utilajelor*, Editura Tehnică, București, 1989;
- [4] Gilat, A., *MATLAB: An Introduction with Applications 2nd Edition*, Wiley edition, 2004;
- [5] Harris, C.M., Piersol A.G. *Shock And Vibration Handbook*, McGraw Hill Book Co, 2002;
- [6] Hatch, M., *Vibration Simulation Using MATLAB and ANSYS* - Chapman & Hall/CRC, 2001;

## 8. ADDITIONAL DATA ABOUT AUTHORS

Authors:

Lecturer Dr. Eng Adrian Leopa  
 Lecturer Dr. Eng Silviu Nastac  
 Lecturer Dr. Eng. Carmen Debeleac  
 Asist. PhD. Dr. Eng. Gigel Capatana  
 Asist. PhD. Dr. Eng. Aurora Potarniche

Affiliation: Engineering Faculty of Braila/  
 "Dunarea de Jos" University of Galati.

Address: Calea Calarasilor nr. 29, Braila,  
 postal code 810017, ROMANIA

Contact data:

leopa.adrian@ugal.ro

## INCREASING THE EFFICIENCY OF EXTERNAL TURNING BY USING THE MULTIPLE LAYER CONSTRUCTION OF THE CUTTING TOOL HOLDER

Madisoo, M.; Maksarov V.; Olt, J.

**Abstract:** *The treatment of complex products from hard materials is accompanied by loss of stability of the cutting process, which leads to oscillations, causing an increase in the wear of cutting tools, reducing the longevity of the machine actuators, which ultimately affects the quality and accuracy of processing responsible products. The aim of the work is to investigate the effect of the multiple layers cutting tool holder construction. The different layers are made from plastically deformed steel. The different plates have a anisotropic structure and have different mechanical properties. This construction is considered as a method to improve the effectivity of the cutting tool and helps to reduce the oscillations in the finishing turning. We hereby propose a method for the construction of the multilayer damper instrument holder together with a mathematical model suitable for processing hard materials.*

*Key words: chatter vibrations, metal cutting, turning tool holder, multiple layer construction.*

### 1. INTRODUCTION

Today tool holders are available in a large variety of forms to suit the specific machining requirements. The material properties of the tool holder have a large influence on both the surface quality and dimensional accuracy of the machined workpiece, and on the life of the cutting tool. The material properties of the workpiece and various other factors, can lead to excessive vibrations in the tool

shaft, which in turn causes undesirable chattering. By the use of passive damping elements, integrated on the tool shaft, the dynamic behavior of the tool can be optimized. From the standpoint of dynamic stability we assume that the "tool" is the weakest subsystem of the turning process. The impact of periodical external forces causing an oscillatory process with a frequency equal to the exciting forces or complex periodic processes caused by nonlinear properties of the system, having its own damped and forced oscillations of parametrically excited oscillations and self-oscillation system can violate the stability of the technological system. The intensity of the forced vibrations is particularly great in the resonant region, which is not allowed in metal cutting machines as an operating method for finishing. One aspect of improving the dynamic stability of the subsystem "tool" is the creation of damped tools with increased resistance, with elastic and damping elements that do not change their appearance. It is important for the damped instruments to be characterized by its adaptation to the variable tolerances, load balancing between the cutting edges, as well as to prevent breakage of the cutting edge. [1]

One of the most effective means available to ensure the stability of the partial subsystem "tool" for finishing turned parts is the creation of damped instrument equipped with a multilayer cutting tool holder construction with anisotropic properties.



## 2. METHODS

The chatter vibration system can be represented by the block diagram shown in (Fig. 1.), where the parameters of the dynamic cutting process are shown in the Laplace domain.

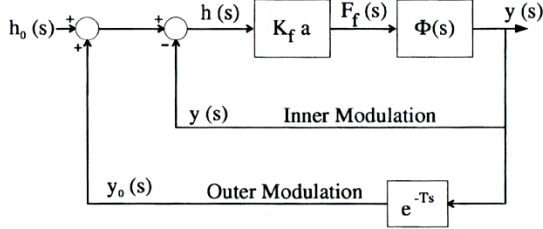


Fig. 1. Block diagram of chatter dynamics. [2]

Input to the system is the desired chip thickness  $h_0$ , and the output of the feedback system is the current vibration  $y(t)$  left on the inner surface. In the Laplace domain,  $y(s) = \mathcal{L}y(t)$ , and the vibration imprinted on the outer surface during the previous revolution is  $e^{-sT}y(s) = \mathcal{L}y(t-T)$ , where  $T$  is the spindle period. The dynamic chip thickness in the Laplace domain is

$$\begin{aligned} h(s) &= h_0 - y(s) + e^{-sT}y(s) \\ &= h_0 + (e^{-sT} - 1)y(s), \end{aligned} \quad (1)$$

which produces a dynamic cutting force of

$$F_f(s) = K_f a h(s). \quad (2)$$

The cutting force excites the structure and produces the current vibrations

$$y(s) = F_f(s)\Phi(s) = K_f a h(s)\Phi(s), \quad (3)$$

Where the transfer function of the single degree of workpiece structure is

$$\Phi(s) = \frac{y(s)}{F_f(s)} = \frac{\omega_n^2}{k_y(s^2 + 2\zeta\omega_n s + \omega_n^2)} \quad (4)$$

Substituting  $y(s)$  into  $h(s)$  yields

$$h(s) = h_0 + (e^{-sT} - 1)K_f a h(s)\Phi(s), \quad (5)$$

and the resulting transfer function between the dynamic and reference chip loads becomes

$$\frac{h(s)}{h_0(s)} = \frac{1}{1 + (1 - e^{-sT})K_f a \Phi(s)}. \quad (6)$$

The stability of this closed-loop transfer function is determined by the roots ( $s$ ) of its characteristic equation, that is,

$$1 + (1 - e^{-sT})K_f a \Phi(s) = 0. \quad (7)$$

Let the root of the characteristic equation be  $s = \sigma + j\omega_c$ . If the real part of the root is positive ( $\sigma > 0$ ), the time domain solution will have an exponential term with positive power (*i.e.*,  $e^{+|\sigma|t}$ ). The chatter vibrations will grow indefinitely, and the system will be unstable. A negative real root ( $\sigma < 0$ ) will suppress the vibrations with time (*i.e.*,  $e^{-|\sigma|t}$ ), and the system is stable with chatter vibration-free cutting. When the real part is zero ( $s = j\omega_c$ ), the system is critically stable, and the workpiece oscillates with constant vibration amplitude at chatter frequency  $\omega_c$ . The chatter vibration frequency does not equal the natural frequency of the structure, since the characteristic equation of the dynamic cutting process has additional terms beyond the structure's transfer function. The chatter vibration frequency is still close to the natural mode of the structure. For critical borderline stability analysis ( $s = j\omega_c$ ), the characteristic function becomes

$$1 + (1 - e^{-j\omega_c T})K_f a_{lim} \Phi(j\omega_c) = 0, \quad (8)$$

Where  $a_{lim}$  is the maximum axial depth of cut for chatter vibration-free machining. The transfer function can be partitioned into real and imaginary parts (*i.e.*,  $\Phi(j\omega_c) = G + jH$ ). Rearranging the characteristic equation with real and complex parts yields

$$\begin{aligned} \{1 + K_f a_{lim}[G(1 - \cos\omega_c T) - \\ H\sin\omega_c T]\} + j\{K_f a_{lim}[G\sin\omega_c T + H(1 - \\ \cos\omega_c T)]\} = 0 \end{aligned} \quad (9)$$

Both real and imaginary parts of the characteristic equation must be zero. If the imaginary part is considered first, then

$$G\sin\omega_c T + H(1 - \cos\omega_c T) = 0 \quad (10)$$

$$\text{and } \tan\psi = \frac{H(\omega_c)}{G(\omega_c)} = \frac{\sin\omega_c T}{\cos\omega_c T - 1} \quad (11)$$

where  $\psi$  is the phase shift of the structure's transfer function. Using the trigonometric identity  $\cos\omega_c T = \cos^2(\omega_c T/2) - \sin^2(\omega_c T/2)$  and  $\sin\omega_c T = 2\sin(\omega_c T/2)\cos(\omega_c T/2)$  we have

$$\begin{aligned} \tan\psi = \frac{\cos(\omega_c T/2)}{-\sin(\omega_c T/2)} = \\ \tan[(\omega_c T/2 - (3\pi)/2)] \quad \text{and} \end{aligned}$$

$$\omega_c T = 3\pi + 2\psi \rightarrow \psi = \tan^{-1} \frac{H}{G}. \quad (12)$$

The spindle speed ( $n[rev/s]$ ) and the chatter vibration frequency ( $\omega_c$ ) have a relationship that affects the dynamic chip thickness. Let us assume that the chatter vibration frequency is  $\omega_c[rad/s]$  or  $f_c[Hz]$ . The number of vibration waves left on the surface of the workpiece is

$$f_c[Hz] \cdot T[s] = \frac{f_c}{n} = k + \frac{\epsilon}{2\pi}, \quad (13)$$

where  $k$  is the integer number of waves and  $\epsilon/2\pi$  is the fractional wave generated. The angle  $\epsilon$  represents the phase difference between the inner and outer modulations. If the spindle and vibration frequencies have an integer ratio, the phase difference between the inner and outer waves on the chip surface will be zero or  $2\pi$ ; hence the chip thickness will be constant despite the presence of vibrations (Fig. 2.). In this case, the inner ( $y(t)$ ) and outer ( $y(t-T)$ ) waves are parallel to each other.

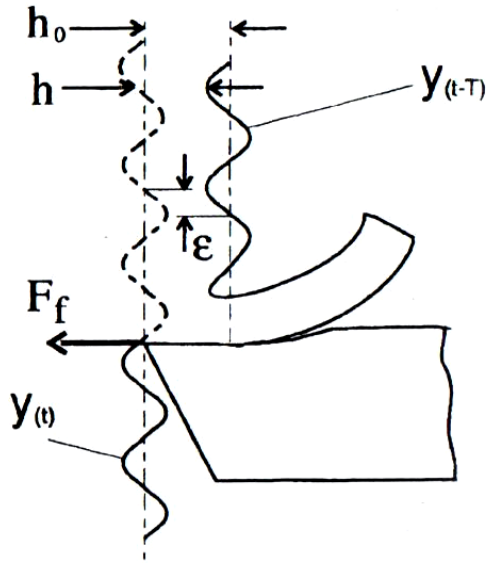


Fig. 2. Wave generation. [2]

If the phase angle is not zero, the chip thickness changes continuously. Consider  $k$  integer number of full vibration cycles and phase shift

$$2\pi f_c T = 2k\pi + \epsilon, \quad (14)$$

Where the phase shift between the inner and outer waves is  $\epsilon = 3\pi + 2\psi$ . The corresponding spindle period ( $T[s]$ ) and speed ( $n[rev/min]$ ) is found to be

$$T = \frac{2k\pi + \epsilon}{2\pi f_c} \rightarrow n \frac{60}{T}. \quad (15)$$

The critical axial depth of cut can be found by equating the real part of the characteristic equation to zero:

$$a_{lim} = \frac{-1}{2K_f G(\omega_c)}. \quad (16)$$

Since the depth of cut is a physical quantity, the solution is valid only for negative values of the real part of the transfer function ( $G(\omega_c)$ ). The chatter vibrations may occur at any frequency where  $G(\omega_c)$  is negative. If  $a_{lim}$  is selected using the minimum value of  $G(\omega_c)$ , the avoidance of chatter is guaranteed at any spindle speed. The expression indicates that the axial depth of cut is inversely proportional to the flexibility of the structure and to the cutting constant of the workpiece material. The harder the work material is, the larger the cutting constant  $K_f$  will be, thus reducing the axial depth of cut. Similarly, flexible machine tool or workpiece structures will also reduce the axial depth of cut or the productivity. [2, 3, 4]

### 3. THE MULTIPLE LAYER CUTTING TOOL HOLDER CONSTRUCTION

The peculiarity of the process of turning tool fitted with the proposed method is to reduce the level of self-oscillations arising in the process of cutting. It is achieved through the orderly disorientation of alternate plates with anisotropic material textures that form the multilayer holder. This construction enables effectively dissipate the energy of the vibrational waves at the boundaries of the transition points between the holder different plates. This method allows to significantly increase the resistance of the tools cutting edge and helps to expand technology opportunities for effective choice of cutting conditions to ensure compliance with the requirements for the dimensional and geometric accuracy, which will in turn contribute the quality of the workpiece. To achieve this goal we have resolved following tasks:

1. Developed a method to construct an instrument equipped with a multilayer anisotropic structure;
2. Investigated the anisotropic properties of the holder plates material;
3. Developed a dynamic model of the technological systems in accordance with the rheological characteristics of chip forming to assess the stability of cutting process using dampening tool.

The cutting tool holder replacement plates are made of steel 45, which consists of many crystalline grains oriented randomly and the material structure is generally isotropic. The anisotropic structure of the material is achieved with pressure treatment. The plastic deformation caused by cold rolling has been made without creating an uneven surface, the resulting micro-structural changes in the material will lead to a change in the direction of macro-fibers which form the material texture. [5]

The proposed cutting tool holder is made from a package of layers assembled together parallel in different planes (Fig. 3).

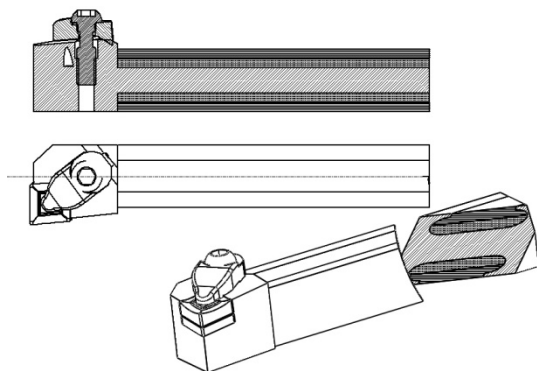


Fig. 3. The assembly of the cutting tool holder

To the bearing holders surface plates are cut from sheet metal with a longitudinal, transverse and vertical orientation of the planes which are relative to the direction of rolling and placed into the holder so that the plates of different structural orientation

form the desired texture of the holder. When oscillations arising in the process of machining characteristics the behavior of the tool holder for small deformations are considered in the form of Hooke's law, taking into account the internal friction in the holder material and that the resistances friction in the joints between the plates is fixed. Caused by the presence of inelastic effects in the texture of the material the internal friction is associated with the movement of dislocations witch cause irreversible hysteresis energy losses within the metal cutter holder during the mechanical vibrations. Line charts of stress - strain do not match for loading and unloading of the tool holder as a result of incomplete elasticity of the metals, but they form a hysteresis loop. It covers an area characterizes the energy dissipated per cycle of loading. Internal friction associated with the static hysteresis, does not depend on the frequency of oscillation when the shape and area of its loop is not connected with the temporary relaxation processes but strongly depend on the amplitude and properties of the material holder. [6] To achieve the maximum damping effect of the deformed plates texture the disorientation of two adjacent plates must be maximized. Then the vibration waves, when passing the interface changes their direction, resulting in the dissipation of energy fluctuations. For small values of disorientated deformed plate textures the energy dissipation is negligible. Therefore in the proposed technical solution the plates in the holder are oriented so that the tangential component of the cutting force transition from one plate to another is carried out so that the deformation texture of the plates was varied by  $90 \pm 10^\circ$  relative to the original holder's core. Under the action of cutting forces in the upper holder having predominantly the maximum tensile stress, and in the lower, supporting, compressive stresses. Therefore, in order to stabilize the strength of the various zones and increase the durability and reliability of the holder,

additional conditions on the orientation of the texture of the deformed plates in the assembly of the holder is needed with respect to the cutting forces. It is known that the maximum tensile stress resistance of the rolled metal is in the longitudinal direction, and the minimum - in a vertical direction relative to the rolling direction. On the contrary the maximum compressive stress resistance has rolled metal in the vertical direction and the minimum in the longitudinal direction. The resistance of the metal in the transverse direction and the tensile and compressive stresses have intermediate values. In this regard the rolling direction in the base plate is oriented parallel to the tangential component of the cutting force. The top plate is oriented parallel to the rolling direction of the radial component of the cutting force, and the plane perpendicular to the rolling mill is the tangential component of the cutting force. The direction of rolling in the middle of the plate is oriented parallel to the action of the axial component of the cutting force. The so called "elastic anisotropy", can greatly change the state of stress in the elastic region and also affects beyond the elastic limit. It has a strong influence on the stress concentration. In general, the larger the anisotropy of the characteristics of elasticity, the greater the stress concentration factor varies depending on the orientation of the force relative to the axes of symmetry, the greater the maximum concentration ratio is the greater is its value for the same isotropic sample. [7]

#### 4. RESULTS AND DISCUSSIONS

The experimental studies to determine the effect of reducing the level of oscillation when using the tool holder equipped with a multi-layer construction and studies on the wear of the inserted cutting tools and the quality improvements of the treated surface showed that the wear of the cutting part of the cutters top plate, by a multi-layer

holder could be less than the equivalent tool. According to test results, that the tool is equipped with multi-layer holder as compared to an analog cutter improves the quality of treatment. The most intense alteration is observed when changing the cutting speed. Practical issues related to the control selection of the cutting process, are depending on the requirements of dimensional and geometric accuracy of machined surfaces [8] which can be solved using an instrument equipped with a multi-layer holder. According to the results of experimental studies using a fractional experiment obtained the functional dependence of the actual margin of accuracy of the machined surface of the cutting. The functional dependence of the actual margin of accuracy in roundness  $\varphi_{06}$  (17), ovality  $\varphi_{Nk}$  (18) and cone  $\varphi_k$  (19) are obtained as the ratio of tolerance to process parts to the field of geometrical deviations of the form of dispersion as a function of cutting speed, depth of cut and feed by using an instrument equipped with multilayer construction.

$$\varphi_{06} = 6,2 \cdot 10^6 \cdot \frac{t^{0.29} \cdot s^{0.22}}{v^{2.14}} \quad (17)$$

$$\varphi_{Nk} = 83,09 \cdot 10^6 \cdot \frac{t^{0.0541}}{s^{0.041} \cdot v^{2.14}} \quad (18)$$

$$\varphi_k = 61,31 \cdot \frac{1}{t^{0.088} \cdot s^{0.258} \cdot v^{0.74}} \quad (19)$$

The calculated values  $\varphi = f(v, s, t)$  of the functions allow you to predict the actual value of the stock on the accuracy of the deviations of geometric shapes, machined surfaces, depending on the set of the cutting tool equipped with the use of multi-layer holder, as well as provide an opportunity to make a comparative analysis of the dependence of the actual margin of accuracy of the cutting conditions for finish turning cutting tools equipped with a multi-layer holder and tools counterpart. The actual margin of accuracy in the processing with the proposed cutter holder design is higher than when operating with an analog cutter on the same cutting conditions.

## CONCLUSION

The developed method for increasing the stability of the cutting process by finishing turning is based on the use of anisotropic properties of plastically deformed structural steel and the effects of dissipation of vibrational waves in the transition section between the disorientated plates which form texture of the tool holder. Based on the studied physical properties of anisotropic rolled steel the tool holder with a multi-layer construction was created. First experimental research examining the influence of the damping properties of the holder to the tool wear, the parameters of cutting and quality of the machined surface were carried out. Future work is planned to be made on experimental studies to investigate the influence of different parameters to the dimensional and geometric accuracy of the machined surfaces. It is important to obtain the functional dependence of the efficiency of selected cutting parameters, depending on the requirements of dimensional and geometric accuracy of machined surface using an instrument equipped on multi layer holder.

## REFERENCES

- [1] Stephenson, David A. John S. *Metal cutting theory and practice*” 2<sup>nd</sup>. ed. Taylor & Francis Group, LLC, 2006.
- [2] Yusuf A. *Metal cutting mechanics. Machine tool vibrations, and cnc*. Cambridge University Press, New York, 2006.
- [3] Elyasberg M. E. *Self-oscillations of machine tools. Theory and practice*. St. Petersburg. Univ. OKBS, 1993.
- [4] Murashkin S.L. *Applied Nonlinear mechanics tools*. L. Mashinostroenije, 1977. (in Russian)
- [5] Callister W. D. *Fundamentals of Materials Science and Engineering*. United States, Wiley, 2007.
- [6] Miklyaev P. G. Friedman J. B. *The anisotropy of mechanical properties of metals*. Moscow, Metallurgiya, 1988.
- [7] Vlado A. Lubarda. *Elastoplasticity theory*. CRC Press, 2002 387 p
- [8] Maksarov, V.V., Olt, J., Leemet, T. *Increase in the stability of technological system with control of the process of cutting*. INTERNATIONAL SCIENCE CONFERENCE OF MATERIAL SCIENCE AND MANUFACTURING TECHNOLOGY, 26-27 June 2008, Prague, Czech Republic, pp. 1-5.

## ADDITIONAL DATA ABOUT AUTHORS

- 1) Marten Madissoo, MSc. Ph. D. Student.  
Jüri Olt, Professor  
Viacheslav Maksarov, Professor
- 2) Increasing the efficiency of external turning by using the multiple layer construction of the tool holder.
- 3) Marten Madissoo, MSc. Ph. D. Student  
Postal Address: Estonian University of Life Sciences Kreutzwaldi 1 Tartu 51014, Estonia. E-mail: marten.madissoomu.ee  
Phone 55617070  
Jüri Olt, Professor and head of the department for agriculture and production techniques. Postal Address: Estonian University of Life Sciences Kreutzwaldi 1 Tartu 51014, Estonia. E-mail: jyri.olt@emu.ee  
Phone 5081671  
Viacheslav Maksarov, Professor and head of the department of mechanical engineering of the National Mineral Resources University "Mining University". Sankt–Peterburg, Russia
- 4) Corresponding Author: Marten Madissoo

## OPTIMAL CONDITIONS FOR VALUATION OF WOOD WASTE BY BRIQUETTING

Menind A.; Križan, P.; Šooš, L.; Matúš, M.; & Kers, J.

**Abstract:** In this paper some important processing parameters of wood waste briquetting are discussed. Firstly, the characteristics of input material (size of the milled product, humidity etc.) were analyzed and then different pre-treatment methods (shredding, disintegrator milling, drying) were used. Final briquette quality depends on basic material composition and optimal technological parameters. The most important parameters affecting the briquette quality are fraction size, pressing temperature, compacting pressure and material humidity. This final briquette quality was evaluated by measuring briquette density and mechanical strength according to known European Standards for solid high-grade biofuels.

*Key words:* material moisture content, fraction size, disintegration, pressing temperature, compacting pressure, wood briquette

### 1. INTRODUCTION

In the boiler plants of EU countries a wide range of various wood-based bio fuels are burned. Wood fuels can be divided into two major groups: non-refined wood fuels (traditional firewood, compressed forest residue, wood chips, sawdust) and refined wood fuels (briquettes, pellets, wood powder).

Alternative fuels like biomass are making breakthrough in energy sector for production of green energy [1].

Fibre hemp and energy sunflower both have potential as raw material for biomass briquetting [2].

In previous studies the recycling technology for production of refuse derived fuel (RDF) was described [3]. Various types of wastes (wood, carton, paper, plastic and textile) were processed by two-shaft and single-shaft shredders to obtain the output product (1–2 mm), which was suitable for briquetting process [4].

It was demonstrated that before briquetting of the waste pre-conditioning of the material would be necessary because lower moisture content improves strength and quality of the briquette [4].

Material composition has great influence on the final quality of produced briquettes (on the density and strength of the briquettes) [5]. Therefore it is strongly recommended to mix municipal waste with organic binder (paper, wood, sawdust) before briquetting [5].

The Slovak University of Technology in Bratislava has laboratory of disintegrating machines and briquetting equipment, which was used for briquetting of wood waste. Similar experiments were made in Research and Testing Laboratory of Materials Recycling of Tallinn University of Technology and briquetting laboratory of Institute of Technology in Estonian University of Life Sciences in Tartu.

In this contribution several briquetting experiments with different type of wood waste from different sources were made.

### 2. EXPERIMENTAL STUDY

#### 2.1 Material and process parameters to be studied

Final briquette quality can be influenced by many parameters. Five of them are having

most significant effect to briquette properties. These parameters are material type, pressing temperature, compacting pressure, fraction largeness and material moisture content.

**Material type**

All the technological parameters of briquetting process are depending on material type. When wood sawdust is processed the following important physical parameters (temperature, pressure, moisture content, fraction size etc.) are having different values when straw, grass, rattan or wood crust briquettes are produced. Every type of material has its own specific nature as calorific value, ash content, humidity, chemical and trace elements content.

Wood contains (see Table 1) lignin which helps to bind the saw dust particles together into the briquette. Lignin acts also as stabilizer of cellulose molecules in cell wall. The more lignin the material contains the more of it can be released to produce briquettes with higher quality. The higher concentration of lignin assures better briquette strength.

	<b>Spruce</b>	<b>Pine</b>	<b>Beech</b>	<b>Oak</b>
Component	[%]	[%]	[%]	[%]
Cellulose	45.6	43.2	39.2	38
Hemi cellulose	27.6	28.0	35.3	29
Lignin	26.9	26.6	20.9	25

Table 1. Approximate chemical composition of European wood

**Compacting pressure**

This is the most important factor influencing the compression strength of briquettes. The strength of briquettes increases with applying higher compacting pressure of briquettes. Briquettes manufactured by using higher compacting pressure are having fewer tendencies to absorb atmospheric humidity during the long term storage [6].

**Pressing temperature**

This factor has significant effect on the quality and strength of briquettes. It determines the lignin excretion by cellular structures of wood. Lignin is released under certain pressing temperature, which has to be unconditionally reached to assure best briquette quality.

**Fraction size**

It affects compacting process of wood saw dust. For larger input fractions of wood need more energy for compacting. Despite of bigger compacting pressure the briquettes have lower homogeneity and compression strength [7]. Size reduction of wood scrap enables to produce briquettes with better quality. Decreasing the fraction size of wood saw dust increases the adhesion strength between the particles [8-9]. Fraction size has also very high influence on briquetting process. For the briquetting of coarser fraction the higher compacting power is needed and briquettes are having lower homogeneity and stability [3]. With increasing the fraction size, the binding forces inside the material are decreasing which results in faster decay by burning (briquette burns faster and that is a disadvantage). The enlargement of fraction size raises the compacting pressure and decreases briquette quality. Smaller fraction size is also an advantage in the drying process [5].

**Material moisture content**

Is also important parameter which has great influence on lignin plasticisation process. Recent compressing technologies are enabling to compact material having relative moisture lower than 18% [10]. When the moisture content of the material is very high, the vaporization of surplus water tears the briquette into pieces. When the moisture content of the material is very low (less than 10%) then the higher pressures should be used to obtain briquettes with higher quality. This is expensive and uneconomic in the point of view of production technology [4].



## 2.2 Mechanical parameters of briquettes

Briquettes must be consistent or otherwise cracks, scratches could appear and fine elements would separate and that is/would be not acceptable. Briquettes with higher density have longer burning time. Standard Ö-Norm M 7135 defines briquette density value for group HP (wood briquettes) and for group RP (crust briquettes) more than 1,12 kg/dm<sup>3</sup> (g/cm<sup>3</sup>), and for other briquettes this value must be more than 1 kg/dm<sup>3</sup> (g/cm<sup>3</sup>). Standard DIN 51731 defines interval of briquettes density values from 1 to 1.4 g/cm<sup>3</sup>.

Standard DIN 52182 (additional standard DIN 51731) also describes testing method for briquette density. The density of the briquette is calculated by formula (1) as:

$$\rho_N = \frac{m_N}{V_N}, \quad (1)$$

where  $V_N$  is the briquette volume and  $m_N$  is briquette weight [7].

The compression strength of briquettes in cylindrical shape is determined by cleft failure [7-8].

## 3. RESULTS AND DISCUSSION

### 3.1 Technological tests with briquettes

The briquettes were made from various particle size of milled wood saw dust materials. For samples manufacturing the briquetting press developed in Slovak University of Technology in Bratislava was used. In Fig. 1 manufactured briquettes from different fractions of pinewood sawdust are presented. By manufacturing briquettes from smaller fraction size of wood particles the visible quality of briquettes was improved.

Then, several tests to estimate the influence of compacting pressure to briquette quality were performed.

The results are presented in the Fig. 2. Briquettes from the same type of material (wood sawdust) with same fraction size with same moisture content were

experimentally manufactured at same pressing temperature by changing only one parameter - compacting pressure. As it follows from Fig. 2 the briquettes manufactured at lower pressures fall to pieces. Briquettes produced at higher pressures are consistent and compact.

### 3.2. Evaluation of the physical parameters in briquetting process

The influence of two important parameters - pressing temperature and compacting pressure to the density of briquettes was determined in following experiments. Four different types of wooden raw materials were used for briquetting. Two samples were from the group of softwoods (pine and spruce) and two samples from the group of hardwoods (beech and oak). Pressing temperature was changed from 85°C to 115°C. The compacting pressure was changed from 61 MPa to 191 MPa. In the briquetting experiments the size of sawdust particle was ~2 mm. All raw materials were dried to achieve same material moisture content 10%. In the experiments the research was focused on determining the differences between various materials behavior throughout the compacting process according to the final briquette density.

From previous and subsequent results it is clear how important parameter is the type of material to be used in the compacting process – briquetting. Among the other significant quantifiable parameter that are also important, the pressing temperature and material moisture content, which have the greatest influence. Pressing temperature is not a direct parameter of the pressed material but significantly influences some material properties, changing and influencing also the material structure and chemical composition during the compacting process.

As it follows from the Figs 3-6 Briquettes from materials with higher lignin and cellulose contents – softwoods (pine,



Briquettes from pine wood with fraction size > 4 mm

Briquettes from pine wood with fraction size < 4 mm

Briquettes from pine wood with fraction size < 2 mm

Briquettes from pine wood with fraction size < 1 mm

Briquettes from pine wood with fraction size < 0.5 mm

spruce) have evidently higher density than pressure for pressing briquette with same

Figure 1. Pressed briquettes from different fraction size of pine wood

briquettes from hardwoods (oak, beech). As it can be seen on curves represented in Figs 3-6 briquettes density is increasing with increase of pressing temperature and compacting pressure. By lower temperatures we need higher compacting

quality, and vice versa. To use higher compacting temperature is better than higher pressure from lignin plasticization point of view.



31 MPa

63 MPa

159 MPa

191 MPa

254 MPa

Figure 2. The effect of the compacting pressure to briquette quality

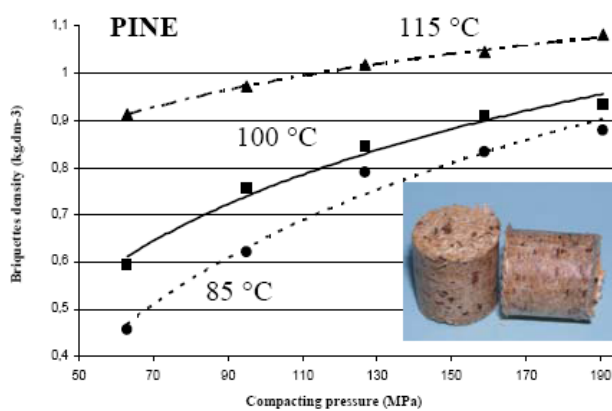


Fig. 3 Dependence of briquettes density ( $\text{kg}/\text{dm}^3$ ) from pine sawdust from compacting pressure (MPa) by various pressing temperatures ( $w_f=10\%$ ;  $L=2\text{mm}$ ).

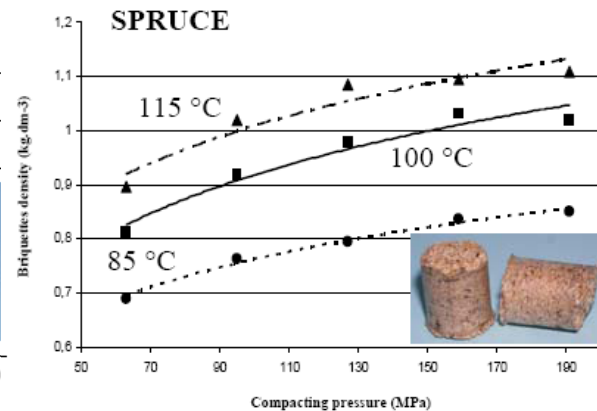


Fig. 4 Dependence of briquettes density ( $\text{kg}/\text{dm}^3$ ) from spruce sawdust from compacting pressure (MPa) by various pressing temperatures ( $w_f=10\%$ ;  $L=2\text{mm}$ ).

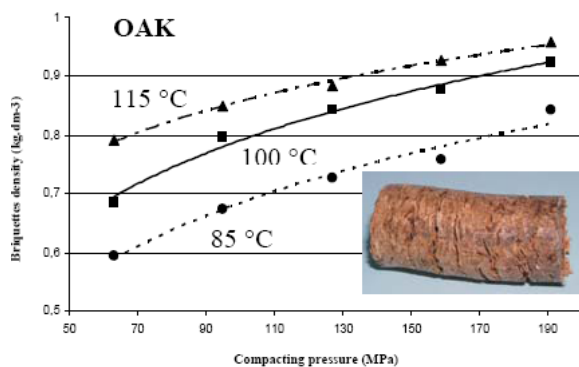
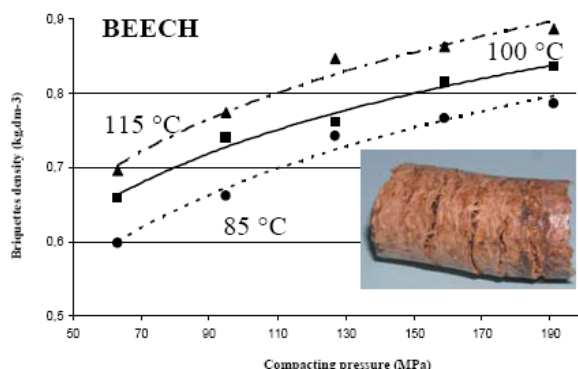


Fig. 5 Dependence of briquettes density ( $\text{kg/dm}^3$ ) from oak sawdust from compacting pressure (MPa) by various pressing temperatures ( $w_f=10\%$ ;  $L=2\text{mm}$ ).

Fig. 6 Dependence of briquettes density ( $\text{kg/dm}^3$ ) from beech sawdust from compacting pressure (MPa) by various pressing temperatures ( $w_f=10\%$ ;  $L=2\text{mm}$ ).



Therefore it is recommended for designing of wood briquetting and compacting machines to include heating section into machine construction.

#### 4. CONCLUSION

The main aim of the experiment was to detect and identify the effect rate of monitored parameters on the final briquettes quality evaluated by briquettes density. By the individual steps it was demonstrated that the most significant effect on briquettes quality has pressing temperature and then material moisture and mutual interaction of these two parameters.

The results our hypothesis that compacting pressure, which may seem to be a parameter having the biggest effect on the Therefore it is very important to know the optimal parameter values which influence final briquette quality for various types of materials.

#### 5. REFERENCES

1. Paist, A., Kask U, Kask L, et al., Potential of biomass fuels to substitute for oil shale in energy balance in Estonian energy sector, Proceedings of Estonian Academy of Science Engineering, 22, 1, (2005), pp. 369-379
2. Alaru, M., Kukk, L., Olt, J., Menind, A., Lauka, R., Vollmer, E., Astover, A., Lignin content and briquette quality of different fibre hemp plant types and energy sunflower, Field Crops Research, 124, (2011), pp. 332-339
3. Kers, J.; Križan, P.; Letko, M.; Šooš, L.; Kask, Ü. & Gregor, A. Mechanical recycling of compounded polymeric waste and evaluation of briquetting parameters, In Proceedings of the 7th international conference of DAAAM Baltic Industrial Engineering 22-24th April (2010), Tallinn University of Technology Press, pp. 468 - 473.
4. Kers, J., Kulu, P., Aruniit, A., Laurmaa, V., Križan, P., Šooš, L., and Kask, Ü., Determination of physical, mechanical and burning characteristics of polymeric waste material briquettes, Proceedings of Estonian Academy of Science Engineering, 16, 4, (2010), pp. 307-316.
5. Križan, P., Matuš, M., Šooš, L., Kers, J., Peetsalu, P., Kask, Ü., Menind, A. Briquetting of municipal wastes by different technologies for quality and properties evaluation. (2011), Agronomy Research, 19, pp. 115 - 123.
6. Križan, P., Šooš L., Matuš, M., Svátek, M., Vukelić, D., Evaluation of measured data from research of parameters impact on final briquettes density, Journal of Applied Mathematics, 3, 3, (2010), pp. 69-76

7. Grover, P.D., Mishra S.K., Biomass Briquetting: Technology and Practices; Food and Agriculture Organization of the United Nations; Bangkok, April 1997.
8. Rizki, M., Tamai, Y., Koda, K., Kojima, Y. and Terazawa, M., Wood Density Variations of Tropical Wood Species: Implications to the Physical Properties of Sawdust as Substrate for Mushroom Cultivation in Wood Research Journal; Journal of Indonesian Wood Research Society, **1**, 1, 2010
9. Nielsen, N.P.K., Gardnerb, D.J.1, Fuel, C.F., Effect of extractives and storage on the pelletizing process of sawdust; Publisher: Elsevier Ltd, Volume 89, Issue 1, January 2010, pp 94-98
10. W. E. Hillis and A. N. Rozsa, High temperature and chemical effects on wood stability; Wood Science and Technology, Volume 19, Number 1, pp. 57-66

## 6. ADDITIONAL DATA ABOUT AUTHORS

### **Andres Menind, MSc.**

PhD student  
 Institute of Technology,  
 Estonian University of Life Sciences,  
 Estonia,  
 Kreuzwaldi 56, 51014 Tartu, Estonia  
 Phone: +372 5185072  
 E-mail: [andres.menind@emu.ee](mailto:andres.menind@emu.ee)

**P. Križan**, PhD. Head of the Institute of Manufacturing Systems, Environmental Technology and Quality Management, Slovak University of Technology in Bratislava, Nám. Slobody 17, 812 31 Bratislava, Slovak Republic, tel.: +421 2 572 96 537, e-mail: [peter.krizan@stuba.sk](mailto:peter.krizan@stuba.sk)

### **L. Šooš, PhD.**

Dean of Faculty of Mechanics  
 Slovak University of Technology in Bratislava,  
 Nám. Slobody 17, 812 31 Bratislava,

Slovak Republic,  
 tel.: +421 905538777  
 e-mail: [lubomir.soos@stuba.sk](mailto:lubomir.soos@stuba.sk)

### **M. Matúš, MSc.**

PhD Student  
 Institute of Manufacturing Systems,  
 Environmental Technology and Quality Management,  
 Slovak University of Technology in Bratislava,  
 Nám. Slobody 17, 812 31 Bratislava,  
 Slovak Republic,  
 tel.: +421 2 572 96 537,  
 e-mail: [milos.matus@stuba.sk](mailto:milos.matus@stuba.sk)

### **Jaan Kers, PhD.**

Professor  
 Chair of Woodworking  
 Department of Polymer Materials  
 Tallinn University of Technology  
 Teaduspargi 5, 12618, Tallinn, Estonia  
 Phone: +372 620 2909  
 Fax: +372 620 2903  
 E-mail: [jaan.kers@ttu.ee](mailto:jaan.kers@ttu.ee)

## INCREASING THE LIFETIME OF FORMING TOOLS

**Bílik, J.; Pompurová, A. & Ridzoň, M.**

**Abstract:** *The paper presents an analysis of the causes of exclusion forming tools for hot forming from activities as well as analysis of factors affecting their life. These basic factors such as material of tool, tools design, production method, the method of heat treatment, thermal and mechanical stress of tool and conditions of forming. The paper also presents some options for increasing the life of forming tools for hot forming. These include the possibility of boriding, duplex treatment (plasma nitriding and PVD coating) and work hardening of surface layers.*

*Keywords: Life of die, die wear, surface layers work hardening, dies production*

### 1. INTRODUCTION

The issue of lifetime of die is difficult due to the amount of factors that may affect the life of die. Improving processes, technologies of production, heat treatment and surface treatment gradually leads to solving the life of die. Currently in the life of the die is mainly about economic efficiency of production, i.e. is necessary in view of the number of such procedure of production die to choose the forgings produced have achieved the best economic effect. In some cases, the choice of the procedure and renovation of the dies leading to the maximum basic life and overall life may not lead to maximum economic effect. It depends on the type of forging and, in particular, from type of production. The arrival of major car manufacturers in Slovakia there was pressure on suppliers from the point of view of reducing production costs. In the production of

formed part and therefore also an important item in the cost of production of forgings entering is also the price of forming tool. Therefore, solving the problem of life is currently forming tools in the present.

### 2. CAUSES OF REMOVAL OF THE DIE FROM THE ACTIVITY

Among the causes of removal the die of the activities at the disposal of certain operating conditions include:

- Wear abrasion cavity dies – dies are the most seen in those parts of dies, where there is the largest movement of material during forging to (Fig. 1). Wear depending on conditions in the field of forming material and the surface of the tool may be in the nature of the contact abrasive and adhesive character of wear. Abrasive wear is caused mainly forging on oxide particles (splatter), or hard foreign particles from the environment or the structure of the hard phase forming material. Adhesive wear is caused by adhesive forces of the meeting between contact surfaces of die and forming material.

- Bruising exposed parts of die – bruising, in particular die for disembarking the parts of the cavity. Exposed locations to drop from the standpoint of bruising are shown in Fig. 1. Studies have shown that the depth of the cavity power hammer dies after forged about 1000 forgings changed to 0.8 to 1.1 mm when the average number of 4 to 6 strokes is necessary to forged one forging is deformation 0.0005 to 0.0003 %. Studies on the changes of the

dimensions of the cavity further has shown that most are changing dimensions of cavities in the early stages of using dies (600 to 1000 forgings to forged). Then followed by a phase of relative stabilization of the dimensions and, therefore, it is appropriate to propose the optimal forging, which can increase the lifetime of the tolerance that 30 to 40%.

- Formation of networks of fatigue cracks due to thermal fatigue and the scorching the surface layer – after the formation of fatigue cracks, the effect seems itself more intense tan, as it creates the conditions for pulling out larger particles of the material surface. Occur while the leaking material to crack difficult if the collection of forgings resulting in the disposal of the die. On Fig. 1 are the sections where the reflected surface of the tan dies. In small transient radii to drop on them quite pretty much tearing of thermal fatigue cracks. Therefore, e.g. from R3 to R6 radii zoom in some cases can lead to an increase in life span 2 to 3 times.

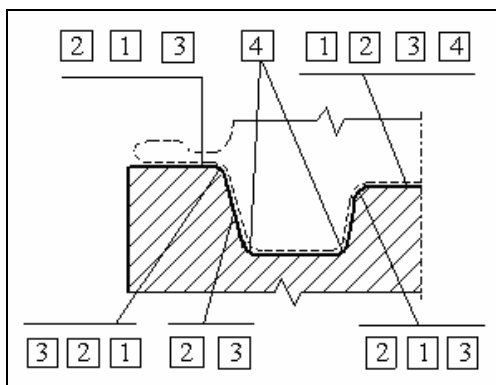


Fig. 1 Ways of die cavity wear in die forging with flash; 1 – bruising, 2 – abrasion wear, 3 – scorch, 4 – fatigue [1]

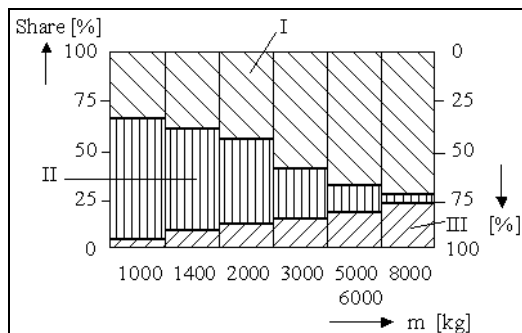


Fig. 2 The predominant types of wear of power hammer dies [1]; I – bruising, II – abrasion, III – scorch

On Fig. 2 are the predominant types of wear of power hammer dies depending on the weight of falling parts. On Fig. 3 are the predominant wear types of dies for presses. Fig. 3 shows that the bruising in the die for press plays a smaller role than die for power hammers, rising significantly affect scorch, increasing the impact of attrition, especially in small presses and there are also reasons for exclusion due to die cracking.

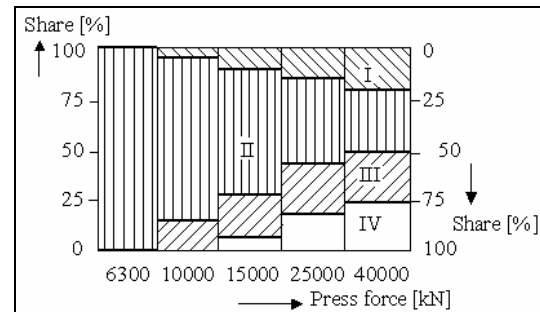


Fig. 3 The predominant wear types of dies for presses depending on the strength of the press [1]; I – bruising, II - abrasion, III – scorch, IV - crack

In some cases it is also due to the emergence of deep cracks in the discarded prematurely die that arise more frequently in the dies for presses and are called thermal cracking. The cause of their formation is the tensions arising from the pressure of forged, sudden changes in temperature and irreversible deformation of the material associated with the cyclical changes of temperatures. Thus has greater thermal expansion and the bigger is the material of the instrument by the cavity to the accumulation of tension rather that may lead to the emergence of deep cracks and premature discarding dies from the activity. Among the reasons for the early disposal of the dies from the activities may include incorrect heat treatment dies (e.g., failure to comply with the prescribed procedure of heat treatment,

hardness, failure to comply with the bursting of the dies in heat treatment etc.), defects in the materials of the dies, incorrect handling of die (in particular the wrong pre-heating dies before forging), errors in the construction of dies.

### **3. FACTORS AFFECTING THE LIFE OF THE DIES**

The main factors affecting the life of the dies may include material of die, design of die, method of die manufacturing, method of heat treatment and quality of the die, thermal and mechanical stresses in the die forging, forging conditions. The material for the production of dies are places certain requirements and conditions of the type of hardware. The material is very important factor influencing life of dies, is paid too much attention but in view of the limited scope of the contribution is not possible given all the factors sufficient space. In the selection of suitable steel for dies, it is necessary to take into account the quantity of the produced forgings, shape and dimension of forging, the size and type of forging machine and its operating conditions for the forgings, the possibility of carrying out proper heat treatment dies. In the construction of dies must be respected the principle of guaranteeing the proper functioning of the dies and its sufficient durability life. Regards compliance with size transition radii and taper to comply with the shape and dimensions of the die and flash space, and compliance with surface roughness, etc. Design principles are to some extent the norm but also the experience and knowledge of the constructor plays an important role. Currently, aid for the construction of the dies provide computer programs intended for simulation of forging processes (e.g. FORGE 2, FORGE 3, FORMFEM, FORM 2D, SUPERFORM, SUPERFORGE, DEFORM), which allow to optimize the forging process.

Method of production of dies (machining, forming and casting) also affects the life of dies. From this point of view, the best way of forming dies appeared. Production of dies by forming is more limited in terms of size and shape and size of the cavity itself dies [3]. Therefore, attention is drawn to the possibility of additional improvements to the surface layer. The method of heat treatment and quality of currently manufactured die crucially affects their life. Therefore, it is necessary to pay attention to the heat treatment. Heat treatment of materials of dies most frequently includes:

- normalizing – especially if they were forged die blocks,
- soft annealing, before production of dies from conventional machining, or before production,
- the production forming dies (by pressing, shooting),
- stress relieving
- hardening of the manufacture or die, respectively before production of the cavity itself (using the methods of cultivation to enable machining of hardened materials)
- tempering the hardness required (usually 46 to 48 HRC)

Thermal and mechanical stresses of the die in the process of forging also significantly affect their life in. The cyclic heat and mechanical stress is causing by the thermal and mechanical fatigue and, consequently, the emergence of a network of fine surface fatigue cracks. On the thermal fatigue affecting the mechanical and physical properties of the die materials, the nature of the macrostructure in cross-section dies, mechanical and chemical and thermal treatment the surface of the die cavity, the operating conditions of the work dies. The hardware conditions that affect the life of dies can be included methods of preforming of forming material, size, power forging machine, forging temperature level, the method of heating the material, method of removing scale,



the method of preheating the die, the die height of the working temperature (frequency and duration of forging cycle) method and type of lubrication, cooling, and another dies, the mode of operation and treatment die, method of storage and recovery (renovation) die. Determination of the proportion of the various factors on the life of the die and the respect of the production and technological parameters of the resulting in the manufacture of dies as well as in the manufacture of forgings is quite difficult, and therefore also the lifetime of dies for the same forgings may vary considerably.

#### 4. SOME OF THE OPTIONS TO INCREASE THE LIFE OF DIES

The surface layer is crucially affects the base and also the overall life of the dies. Among the methods of work hardening surface layers applicable for dies can be included:

- chemical-thermal treatment, i.e. nitriding, boriding,
  - ion implantation
  - PVD coating and PAPVD,
  - duplex treatment - plasma nitriding and PVD coating,
  - mechanical hardening of surface layers produced by machining cavities such as dynamic shot peening prior to heat treatment (achieving finer in granulometry martensitic structure in the surface layer) or after heat treatment (increase in fatigue strength, etc.) [1, 2].
- In the article specified only some of the listed methods increasing life of dies. Boriding is the saturation of the surface of steel with boron to increase wear resistance to abrasive friction, sliding friction and friction at elevated temperatures. Typical boriding layer consists of borides FeB and Fe<sub>2</sub>B and is shown schematically in Fig. 4 [5].

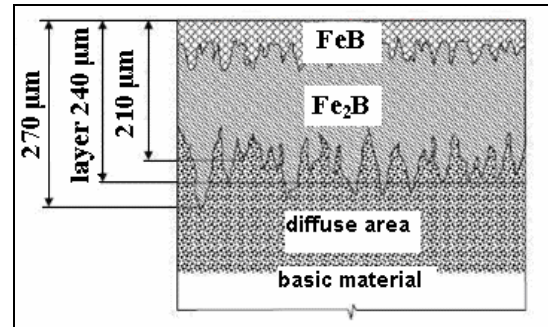


Fig. 4 Schematic representation of two-phases boriding layer [5]

Boriding process is carried out routinely in the temperature range 800 to 1050°C. Boriding layer thickness is usually in the range of 0.1 to 0.3 mm and boriding time 3-6 hours. Carbon and alloying elements slow the growth layers of borides. The application process is boriding of tools for cold and hot molds for pressure casting of non-ferrous metals, the beams to pull wires, rods, etc. Microhardness of borides FeB reaches 1900 to 2100 HV. Alloying elements W, Mo, Mn, Cr slightly increased hardness. Boride Fe<sub>2</sub>B a microhardness of about 1650 HV hardness Fe<sub>2</sub>B alloying elements affect. The borid FeB is stable when heating to 800°C and borid Fe<sub>2</sub>B is stable to 1000°C. Duplex treatment lies in the fact that after the standard of heat treatment of plasma nitriding of die place under conditions that ensure the creation of diffusion layers without nitriding surface layer of nitride. This is followed by deposition or PVD CrN coatings PAPVD, TiCrN, TiN/TiCN (Cr/CrN) x 3 and (CrN/TiN) x 3 Duplex treatment was successfully applied to smaller die used i.e. the fittings on automatic forging machines type Hatebur. In the case of processing dies, depending on the type of coating, reached the increase of life from 1.3 to 1.5 times [4]. On Figure 5 is the diagram of the basic life of the die steel 1.2713 (55NiCrMoV6) after application of mechanical reinforcement coating by shot peening.

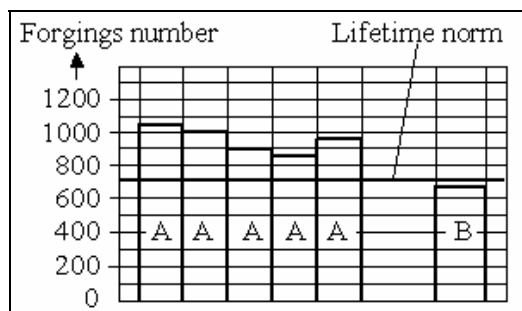


Fig. 5 Diagram of basic life of the die steel 1.2713 (55NiCrMoV6) for forging connecting rods; A – shot peening, B – normally produced (average life) [1]

In the face of the forging process is necessary to maximize the life of shall in particular:

- observance of the correct temperature of heating of forged material and preheating of dies,
- to vote by minimizing the possibility of heating formation of oxides, i.e. direct electric heating,
- to elect the most suitable ways of minimizing material flow preforming as in the finishing cavity, forging pressure reduction and the elimination of scale,
- to elect the most suitable ways of lubrication and the removal of scale from cavity dies,
- meet as regularly as possible with the hardware cycle by shortening the maximum contact with the die forged so as to avoid excessive overheating of the surface layers,
- the correct choice of forging machine and its technical condition and under.

## 5. CONCLUSION

The aim of this paper is to highlight the factors affecting in particular the basic life of dies as well as some of the options to increase the life of dies. In the paper are specified only some methods of improving the surface layers that can be used to increase the base and the overall life and die or other shaping tools for hot working. A separate chapter of the life of the dies is lining renovation and dies (by reducing the die cavity with a deepening,

surfacing and smaller die also impressed or gun nailing). However, this is not lining and renovation must complement the contribution.

## ACKNOWLEDGEMENTS

Autors are thankful for APVV 0057-07 grant support.

## REFERENCES

1. Bílik, J. *Increasing life of dies by mechanical work hardening of surface layers. Dissertation thesis* MTF STU, Trnava, 2002.
2. Bača, J., Bílik, J., Tittel, V. *Technology of Forming*. STU, Trnava, 2010
3. Polák, K., Hobemägi, A. *Production of cavity dies by forming*. Alfa, Bratislava, 1988.
4. Suchánek, J. a kol. *Increasing life of dies by duplex coating*. In: *Acta Metallurgica Slovaca - Roč. 11, special issue 2. 4<sup>th</sup> International symposium, 4. THER TECH FORM '05. Tále - Nízke Tatry, 5.-8.9.2005 (2005)*. - Košice : Technická univerzita v Košiciach, p. 178-182
5. Hazlinger, M., Moravčík, R.: *Chemical-heat treatment of materials*. Trnava: AlumniPress, 2008

## AUTHORS

Bílik, Jozef, Pompurová, Anna & Ridzoň, Martin  
 Slovak University of Technology  
 Faculty of Materials Science and Technology in Trnava  
 Institute of Production Technologies  
 Bottova 25  
 917 24 Trnava, Slovakia  
[jozef.bilik@stuba.sk](mailto:jozef.bilik@stuba.sk)  
[anna.popurova@stuba.sk](mailto:anna.popurova@stuba.sk)  
[martin.ridzon@stuba.sk](mailto:martin.ridzon@stuba.sk)

## UNCERTAINTY FOCUSED STRENGTH ANALYSIS MODEL

Põdra, P. & Laaneots, R.

**Abstract:** *Strength analysis is a critical phase when developing engineering solutions and determining respective components safe dimensions. Uncertainty based method for strength calculations will be investigated in this study. This concept requires that a calculation model is developed for each particular strength calculation case, where the initial data estimates along with the estimates of their uncertainties are the inputs. This approach allows to better optimise the value of design factor and facilitate a new solid method for engineering analysis, where the correctness of calculation results is assured at the certain predefined confidence level.*

*Key words: machine design, strength analysis, uncertainty, component safety*

### 1. INTRODUCTION

The objective of the strength analysis is often to calculate the value of some component dimension in order to assure the component safe and reliable operation during the whole predefined service life. Each strength analysis, based on statics' or dynamics' strength condition, is performed by the use of a number of influence- or input quantities. And the value of the selected output quantity is calculated using analytical or experimental relationships and input quantities' values. The estimates of the values needed for solving the case are determined based on known data, given in standards, handbooks or other sources. The formula or analysis model, describing the relationship of the output quantity with other quantities, must be developed according to the calculation task in

question. The problem, however, is that the values of input quantities are known only approximately, i.e. with some uncertainty. In order to assure the component performance and safety even at the most critical combination of input quantities' values, certain level of safety must be assumed in the analysis. The needed level of safety is characterised by the required value of the factor of safety, that also known as the design factor. The value of design factor is usually determined based on engineering practice and following statistical guidelines presented in textbooks, handbooks, standards, etc. (Table 1) [1]. They are to be refined, thus, according to the experience of each particular design engineer.

Type of loading	Type of material	
	Ductile	Brittle
Static	2	6
Repeated	8	10
Shock	12	15

Table 1. Recommended values of design factor

Too large value of design factor is followed by the excessive material use. Too small value, however, decreases the strength and endurance of component below the critical level. The well-reasoned and optimum value of design factor provides the product a competitive advantage. Development of the method, based on the analysis of uncertainties of parameters influencing the component strength that allows to design safe products with better optimised material use is therefore highly motivated.

## 2. THEORY

The calculation model used in strength analysis could in general terms be expressed as

$$G(Y, X_1, X_2, \dots, X_i, \dots, X_n) = 0, \quad (1)$$

where  $G$  is the model basic functional relationship,  $Y$  is the output quantity of the model, i.e. the parameter to be calculated and  $X_1, X_2, \dots, X_i, \dots, X_n$  are the input quantities the output quantity is dependent on. The input quantities of the calculation model (1) could also be dependent on other quantities, including constants. The model (1) could therefore appear to be rather complicated, sometimes even to such extent, that it is not possible to formulate it exactly. The functional relationship of the calculation model may be identifiable experimentally or may exist as an algorithm to be evaluated numerically. Thus, the interpretation of the function  $G$  must be larger than that of a purely mathematical function. It is important, that the function  $G$  includes all input quantities that influence the value of the output quantity  $Y$ . If the practical observations indicate, that the present function  $G$  does not model the calculation procedure with needed accuracy, it must be complemented with additional input quantities. Since the values of the input quantities in calculation model (1)  $X_1, X_2, \dots, X_i, \dots, X_n$  are not known exactly, the estimates of the values of these quantities must be used in practice instead. By replacing the quantities in calculation model (1) with respective estimates, the function general form appears

$$y = g(x_1, x_2, \dots, x_i, \dots, x_n) \quad (2)$$

where  $y$  is the estimate (approximation) of the output quantity  $Y$ ,  $g$  is the relationship used in particular calculation formula (mathematical, experimental or other relationship for obtaining the output

quantity) and  $x_1, x_2, \dots, x_i, \dots, x_n$  are the estimates of input quantities' values.

In order to calculate the result with the formula (2), that functional relationship  $g$  must be known. Since the calculation result  $y$  is the estimate (approximation) of  $Y$ , it must be presented together with the data about its uncertainty.

In the case, that all input quantities in functional relationship (2) are uncorrelated, the combined uncertainty of the calculation result  $y$ , following the law of propagation of uncertainty and based on the uncertainties of input quantities' estimates, [2] can be expressed as

$$u(y) = \sqrt{\sum_{i=1}^n \left( \frac{\partial g}{\partial x_i} \right)^2 u^2(x_i)} \quad (3)$$

where  $u(y)$  is the combined uncertainty of the calculation result and  $u(x_i)$  is the standard uncertainty of the input quantity estimate  $x_i$ .

Depending on the predefined confidence level, that combined uncertainty (3) must be multiplied with a coefficient and the expanded uncertainty is expressed as

$$U_p = k \cdot u(y) \quad (4)$$

where  $U_p$  is the expanded uncertainty of the calculation result  $y$  at the confidence level  $p$ , that is associated with coverage probability and  $k$  is the coverage factor, the value of which depends on  $p$ .

$U_p$  characterises the possible limits of the calculation result  $y$  value and the choice of the value of  $k$  depends on the requirements of the coverage probability set forth for that calculation. Coverage probability 100 % is never possible. Determination of the suitable confidence level is a business decision – it shows the percentage of the components or products in question that should not fail. Assuming the normal distribution of the quantity  $y$ , the values of selected coverage factors at respective confidence levels [2] are given in Table 2.

Allowed number of failed components out of 10000	Confidence level $p/\%$	Coverage factor $k$
3173	68,27	1
455	95,45	2
27	99,73	3
0	100	$\infty$

Table 2. Values of the coverage factor  $k$

In classical strength calculations the component is considered safe, if the strength condition is fulfilled

$$S = \frac{\sigma_{\text{lim}}}{\sigma_{\text{max}}} \geq [S], \quad (5)$$

where  $S$  and  $[S]$  are the factor of safety and design factor respectively,  $\sigma_{\text{lim}}$  is material limit stress (yield stress  $R_e$  or ultimate stress  $R_m$ ) and  $\sigma_{\text{max}}$  is the maximum value of stress in that component.

In order to determine the optimum design factor  $[S]$  value, several risks and aspects could be considered, such as:

- severity of risks related to the failure of that component and the possibilities of failure processes' early detection;
- uncertainties of the values of loads, geometrical dimensions and material properties;
- simplifications of the calculation model and formulae, etc.

All relevant issues, influencing the component safety, must be taken into account using respective input quantities  $X_i$  with their estimates  $x_i$  (these could be regarded as partial factors of safety) in the calculation models (1) and (2).

In the best case the concept of design factor could be abandoned altogether (taking  $[S] = 1$ ) and the safe estimate of the quantity  $Y$  is the respective limit value  $y_{\text{lim}} = (y + U_p)$  or  $y_{\text{lim}} = (y - U_p)$ . Now the strength condition (5) takes a new shape

$$S = \frac{\sigma_{\text{lim}}}{\sigma_{\text{max}}(y_{\text{lim}})} \geq 1, \quad (6)$$

where  $\sigma_{\text{max}}(y_{\text{lim}})$  is the maximum value of the component stress in the case that the value of the quantity, calculated using (2) is safe  $y_{\text{lim}}$ .

The strength analysis example of the cantilever beam, together with respective uncertainty analysis is presented below.

### 3. RESULTS AND DISCUSSION

The safe value of the diameter of a uniform circular cross-section cantilever beam (Fig. 1) must be calculated. The confidence level (coverage probability) of the calculation result must be 99,73 %, giving the value of the coverage factor  $k = 3$  (Table 2). In that simple case the initial quantities are as follows:

- load of the beam  $F = 3000$  N is acting perpendicular to the beam axis;
- beam is to be manufactured of steel E295 with the limit stress equal to the yield stress, according to EVS-EN 10025-2 [3]  $\sigma_{\text{lim}} = R_e = 285$  MPa, if the thickness of the material is in the limits (16 ... 40) mm;
- distance of the load acting point from the housing wall  $l = 250$  mm.

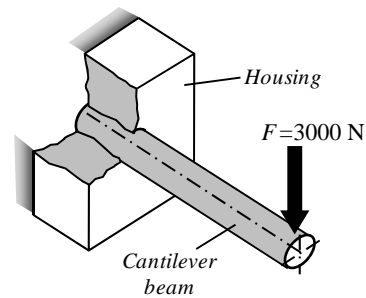


Figure 1. Cantilever beam

Under the influence of  $F$  the beam deforms elastically with the maximum value of the bending moment  $M$

$$M_{\text{max}} = Fl = 3000 \cdot 0,25 = 750 \text{ N} \cdot \text{m}$$

located at the beam attachment area to the housing (Fig. 2).

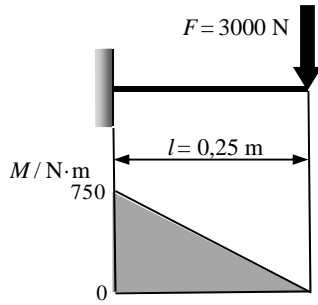


Figure 2. Calculation scheme and bending moment  $M$  diagram of the beam

Mathematical function for the beam diameter calculation is [1]

$$d = \sqrt[3]{\frac{32Fl}{\pi R_e} [S]} = \sqrt[3]{\frac{32Fl}{\pi R_e}}, \quad (7)$$

when taking  $[S] = 1$  and the beam diameter, i.e. the output quantity, value estimate is obtained

$$d = \sqrt[3]{\frac{32 \cdot 3000 \cdot 0,25}{\pi \cdot 285 \cdot 10^6}} = 0,0299 \text{ m} \approx 30 \text{ mm}.$$

This calculation is followed by the uncertainty analysis and the input quantities' standard uncertainties must be determined first, using methods outlined above [2, 4] and formulae (3) and (4), because the input quantities are uncorrelated.

Giving the formula (7) another form

$$d = \left(\frac{32}{\pi}\right)^{1/3} F^{1/3} l^{1/3} R_e^{-1/3}, \quad (8)$$

the combined uncertainty of the beam diameter  $d$  can be calculated according to (3), using the relationship

$$u(d) = \sqrt{\left(\frac{\partial d}{\partial F}\right)^2 u^2(F) + \left(\frac{\partial d}{\partial l}\right)^2 u^2(l) + \left(\frac{\partial d}{\partial R_e}\right)^2 u^2(R_e)}, \quad (9)$$

where the partial derivatives of (8) appear

$$\frac{\partial d}{\partial F} = \frac{1}{3} \left(\frac{32}{\pi}\right)^{1/3} l^{1/3} R_e^{-1/3} F^{-2/3}, \quad (10)$$

$$\frac{\partial d}{\partial l} = \frac{1}{3} \left(\frac{32}{\pi}\right)^{1/3} F^{1/3} R_e^{-1/3} l^{-2/3} \text{ and} \quad (11)$$

$$\frac{\partial d}{\partial R_e} = -\frac{1}{3} \left(\frac{32}{\pi}\right)^{1/3} l^{1/3} F^{1/3} R_e^{-4/3}. \quad (12)$$

There is no data given about the load  $F$  in addition to its value. Since all the values in the deviation range may characterise the load  $F$  with equal probability, its values have a rectangular distribution in the limits of that deviation range. And the standard uncertainty of the load  $F$  estimate is [2]

$$u(F) = \frac{\{F\}}{\sqrt{3}} \quad (13)$$

where  $\{F\}$  is the parameter of the deviation range, expressed as  $(F \pm \{F\})$ .

The distance of the load to the housing wall  $l$  may change in the limits of its tolerance  $T_l$ . Also in this case, the values of the dimension  $l$  follow the rectangular distribution and the standard uncertainty of the dimension  $l = 250$  mm estimate is [2]

$$u(l) = \frac{T_l}{2\sqrt{3}}. \quad (14)$$

The value of the yield stress  $R_e$  is taken from the standard EVS-EN 10025-2 and assuming the rectangular distribution of the  $R_e$  in the deviation range limits, its standard uncertainty is calculated as [2]

$$u(R_e) = \frac{\{R_e\}}{\sqrt{3}}, \quad (15)$$

where  $\{R_e\}$  is the parameter of the deviation range, given as  $(R_e \pm \{R_e\})$ .

The parameter  $\{F\}$  for the load  $F = 3000$  N may have a rough value of  $\{F\} = 500$  N. The reasonable tolerance for the distance  $l = 0,25$  m is considered  $T_l = 10$  mm. The value of  $\{R_e\}$  for  $R_e = 285$  MPa is determined here by the rounding interval

$\{R_e\} = 5$  MPa. The values of the input quantities' standard uncertainties, calculated using the values above and formulae (13), (14) and (15), are given in Table 3.

$u(F)$ , N	$u(l)$ , m	$u(R_e)$ , Pa
290	$2,9 \cdot 10^{-3}$	$2,9 \cdot 10^6$

Table 3. Standard uncertainties of input quantities

Writing the formula (9) in the form

$$u(d) = \sqrt{A + B + C}, \quad (16)$$

its parameters based on (9) will be

$$A = \left( \frac{\partial d}{\partial F} \right)^2 u^2(F), \quad (17)$$

$$B = \left( \frac{\partial d}{\partial l} \right)^2 u^2(l) \text{ and} \quad (18)$$

$$C = \left( \frac{\partial d}{\partial R_e} \right)^2 u^2(R_e). \quad (19)$$

The values of  $A$ ,  $B$  and  $C$ , according to relationships (10), (11) and (12) together with the data in Table 3, are shown in Table 4.

$A$ , $m^2$	$B$ , $m^2$	$C$ , $m^2$
$9,3 \cdot 10^{-7}$	$1,3 \cdot 10^{-8}$	$1,0 \cdot 10^{-8}$

Table 4. Components of the combined uncertainty of the output quantity

The values of the combined uncertainty and expanded uncertainty of the beam diameter  $d$  can be calculated next using formulae (16) and (4) respectively

$$u(d) = \sqrt{9,3 \cdot 10^{-7} + 1,3 \cdot 10^{-8} + 1,0 \cdot 10^{-8}} = \\ = 0,976 \cdot 10^{-3} \text{ m} \approx 0,98 \text{ mm}$$

$$U_{99,73\%} = 3 \cdot 0,98 = 2,9 \approx 3 \text{ mm}.$$

Now the calculation result of the beam diameter is  $d = 30 \text{ mm} \pm 3 \text{ mm}$ . The safe value of the beam is  $d = 33 \text{ mm}$ .

For comparison, another calculation is made, taking the relative uncertainty of all input quantities equal to 15 %. The input quantities standard uncertainties, following the method outlined above, are shown in Table 5 and the respective components of output quantity combined uncertainty are given in Table 6.

$u(F)$ , N	$u(l)$ , m	$u(R_e)$ , Pa
260	$2,2 \cdot 10^{-3}$	$25 \cdot 10^6$

Table 5. Standard uncertainties of input quantities with equal relative uncertainty

$A$ , $m^2$	$B$ , $m^2$	$C$ , $m^2$
$7,5 \cdot 10^{-7}$	$7,7 \cdot 10^{-7}$	$7,7 \cdot 10^{-7}$

Table 6. Components of combined uncertainty of the output quantity with the equal relative uncertainty of input quantities.

Now the combined and expanded uncertainty of the beam diameter were calculated

$$u(d) = \sqrt{7,5 \cdot 10^{-7} + 7,7 \cdot 10^{-7} + 7,7 \cdot 10^{-7}} = \\ = 1,51 \cdot 10^{-3} \text{ m} \approx 1,5 \text{ mm}$$

$$U_{99,73\%} = 3 \cdot 1,5 = 4,5 \approx 5 \text{ mm}.$$

The calculation result in this particular case appears  $d = 30 \text{ mm} \pm 5 \text{ mm}$  with the beam safe diameter equal to  $d = 35 \text{ mm}$ .

The comparison of the combined uncertainties' components according to Table 4 and Table 6 is presented on Fig. 3. It can be seen in the present cases, that if the relative uncertainties of the input quantities are:

- equal, their influence on the value of the output quantity' combined uncertainty is also approximately equal;
- different, their impact on the output quantity combined uncertainty may be considerably different. In this example the uncertainties of yield stress  $R_e$  and distance dimension  $l$  may safely be left out of consideration.



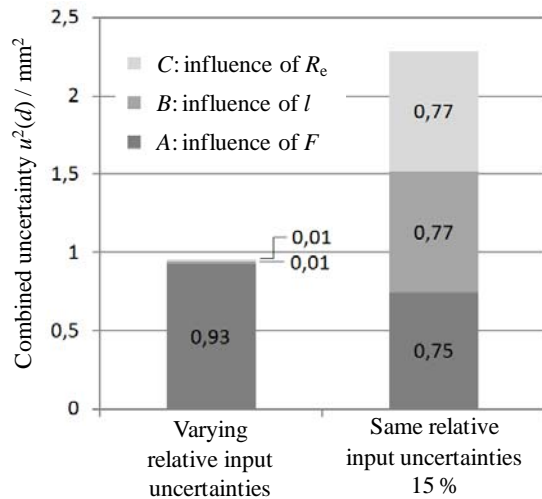


Figure 3. Components of the combined uncertainties

For verification of the uncertainty based calculation results, the beam diameter was also calculated using the classical approach, with the value of design factor  $[S] = 2$  (Table 1) and formula (7)

$$d = \sqrt[3]{\frac{32 \cdot 3000 \cdot 0,25}{\pi \cdot 285 \cdot 10^6}} \cdot 2 = 0,0377 \text{ m} \approx 38 \text{ mm}$$

It can be concluded, that the uncertainty based strength analysis model provides well-reasoned results and in this case allows to justify the use of smaller beam diameter than that calculated by classical method.

#### 4. CONCLUSIONS

The analysis of the calculation model above shows that the approach with partial derivatives may be complicated in terms of mathematics, but this problem could be solved using appropriate computer software and programs.

When using the concept of uncertainty, there is possible to, following the predefined level of confidence, give a better reasoning for the choice of machine components dimensions, loads and material properties.

This method also allows to analyse the influence of different input quantities and respective uncertainties on the values of the calculation result and its uncertainty, especially in the cases of complex engineering calculations involving many parameters, coefficients and physical constants. The use of respective computer programs allows, for instance, to efficiently analyse the need for input quantities standard uncertainties in order to obtain the reasonable value of output quantity' expanded uncertainty, etc.

More sophisticated cases will be analysed in further research.

#### 5. REFERENCES

- [1] Mott, R. L. *Applied Strength of Materials – 4th ed.* Prentice-Hall, 2002.
- [2] Laaneots, R and Mathiesen, O. *An Introduction to Metrology – The second, thoroughly completed edition.* Tallinn: TUT Press, 2011.
- [3] *EVS-EN 10025-2:2005.* Hot rolled products of structural steels – Part 2: Technical delivery conditions for non alloy structural steels. Tallinn: EVS, 2005.
- [4] Raba, K. *Uncertainty Focused Product Improvement Models – Thesis on mechanical and instrumental engineering E46.* Tallinn: TUT Press, 2009.

**Acknowledgements.** This work was supported by Estonian Ministry of Education Research Project No. SF0140091s08.

#### 6. ADDITIONAL DATA

Priit Põdra and Rein Laaneots, Tallinn University of Technology, Dept. of Mechatronics, Ehitajate tee 5, 19086 Tallinn, Estonia. E-mail: priit.podra@ttu.ee; rein.laaneots@ttu.ee

## DEVELOPMENT OF PATTERNLESS SAND MOLD MILLING MACHINE

Pullinen, T.; Sievänen, S.; Schiestl, M.; Kiviluoma, P. & Kuosmanen, P.

**Abstract:** *Casting molds are traditionally produced using a pattern which is a model of the cast product. The manufacturing of the patterns is time consuming.*

*Currently the goal of the manufacturing industry is to minimize the steps from a CAD model to the finished product. Methods to shorten the process have become possible due to technical developments and recently casting molds have been done by milling the sand with industrial robots. However, their structure limits the material removal rates, thus a need for a more effective method still exists. A fast numerically controlled sand milling machine was designed and built as a first step towards a new fast and flexible multi-milling-head patternless molding system.*

*Using the developed machine the casting molds can be machined much faster than with traditional methods.*

*Key words: machining, sand mold, patternless casting, rapid prototyping.*

### 1. INTRODUCTION

#### 1.1 Sand mold background

Sand molds are usually manufactured by using a set of two single-sided pattern plates incorporating the shape of opposing sides or the geometry of the casting. These patterns are used to create the main parts of the mold by filling the space defined by the pattern plate and a casting frame with casting sand. Thus, the shape of the casting is copied as a cavity in-between the two main parts ("cope and drag") of the mold. This conventional method of molding also sets limitation for the shape of the casting.

Starting production of a new casting requires manufacturing new patterns. Purchasing a pattern set may be expensive and take long time. Storing the patterns also takes considerable space.

BMW and Audi have started to use Simtech's patternless casting method. In this method a robot (Fig. 1) mills the mold cavity straight into the sand. Previously these casting molds were made with patterns. Because this new method does not require physical patterns the direct cost and time savings are significant. The total cost of bringing the prototypes to market was close to 40 000 € using the traditional method but using the new method the cost was reduced down to 4000 €. The time used for the whole manufacturing process was reduced from 17 to 5 weeks. The time savings came from not having to produce a physical pattern. Also, the mold could be prepared beforehand. [1]



Fig. 1. Simtech's patternless casting milling robot. [1]

The patternless method allows the cast product to be produced without the limitations caused by using the pattern. The pattern needs to have draught (taper) in order to be easily removable from the sand mold. Without these limitations more

complex castings can be made. This also allows using less material. [2]

There are foundries in Finland that already exploit patternless casting method. These foundries produce single piece and short series medium and heavy size castings At URV (Uudenkaupungin rautavalimo Oy) a conventional 3-axis milling machine is used instead of an industrial robot to mill the sand. This kind of machine does not have the structural limitations of a robot, thus allowing faster material removal rates.

### 1.2 The problem foundries are facing

Finnish and more broadly European foundries are facing increasing difficulties in competing against the foundries of lower cost level countries. As the customer base of foundries and demand structure in Europe change, the service concepts and manufacturing systems have to adapt in order to survive.

Demand of short series castings in Europe is expected to retain. Thus, the importance of agility and flexibility in casting manufacturing is considered to increase. A new breed of ultra-agile jobbing foundries with highly flexible production system is needed. They would be able to respond to small and large series orders extremely fast. Typically, during a high season, customer might have to wait several months to get the ordered castings delivered. An ultra-agile jobbing foundry would be able to take an order, and start the production of the casting immediately and deliver it to the customer in significantly reduced time. The same production method could also be implemented as a lateral production line in an automatic production line foundry. While the rest of the foundry serves the normal large volume orders, this line would be able to react exceedingly fast and be very efficient in producing molds for prototypes and small batches of products.

## 2. PATTERNLESS SAND MOLD MILLING

### 2.1 Casting mold line

A rapid way to create casting molds is needed to build an ultra-agile jobbing foundry. One way to achieve this is to build a casting mold production line where sand filled molding boxes move forwards on a conveyor (Fig. 2). On the conveyor there are three sequential milling stations.

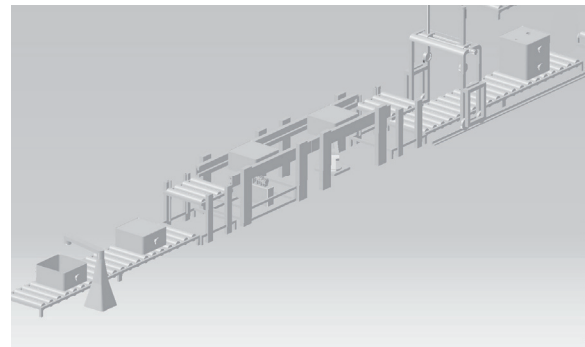


Fig. 2. Casting mold line.

At the first station a numerically controlled multi-tooled sand milling machine does the rough milling of the mold. It removes about 70 % of the removable sand. In the next station a similar machine does the pre-finishing and removes roughly 20 % of the removable sand but it uses much finer tools than the first machine. The last station consists of an industrial robot that does the finest milling and finishes the back-draft (undercut) shapes of the mold. All of these stations have roughly the same processing time, thus there are no bottlenecks on the production line. Our study focuses on the first step of the casting mold line (Fig. 3). If cores are needed they are also manufactured using a multi-tooled sand milling machine for the rough sand removal and they are finished using a robot.

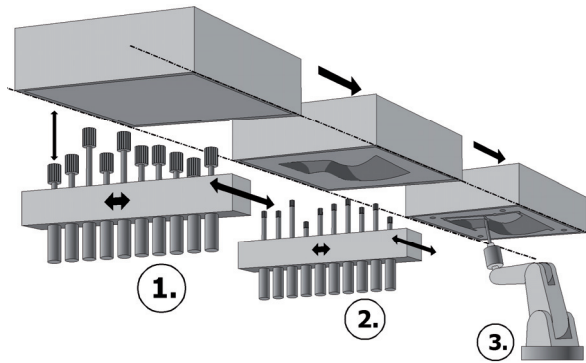


Fig. 3. The three step milling procedure.

## 2.2 Tools

Milling sand can wear the tools down exceedingly fast. The time it takes for a tool to become unusable depends strongly on the material the tool is made from. Using a cutting speed of 30 m/min, cut depth of 1 mm and feed speed of 50 mm/s high-speed steel (HSS) tool could cut continuously for 2 minutes. Carbide tool lasted 8 minutes and polycrystalline diamond (PCD) tool lasted 70 hours in a study conducted in Beijing. The dominant failure modes for the tools were flank wear and micro-tipping. The main wearing comes from abrasion by the SiO<sub>2</sub> particles in the sand. The amount of abrasion is dependent on the sand grain size and the bond strength in the sand block. [3]

However study conducted by the University of the Basque Country reveals that by using carbide tools coated with PVD (TiAlN) in aggressive conditions, tool life of 80 minutes could be achieved. The price of the PCD tools is 8...12 times higher than carbide tools'. The study gives better quality-price ratio to carbide tools, therefore use of carbide tool is recommended. [4]

## 3. RESULTS

### 3.1 Inverted machine design

Creating a numerically controlled three axis sand milling machine suitable for use on a mold production line was the focus of this study. The molding box, which is full of sand, is located over the milling

machine, and the cutting head is located under the mold. With this unique design the removed sand drops straight down from the mold to the base of the milling machine (Fig. 4). This eliminates the need to remove the milled sand from the molding box in the middle of the proposed three step milling line and once the milling of the mold is completed it is immediately ready for casting. This also gives the possibility of automating the machining process, reducing the need for human operators. Therefore the proposed ultra-agile jobbing foundry can produce the castings even faster and more economically.

Another major benefit of the inverted design is that the machining can be made without the use of a through-tool vacuum system, which is seen on many other sand milling solutions. Through-tool vacuum system requires specialized tools, which are more expensive. Removing the vacuum system allows the milling machine to use common end-mills which are more cost efficient.

### 3.2 Protecting the machine

A major problem in sand machining is the need to protect the machine from the abrasive sand grains. In a study conducted by University of Basque Country it was recommended that the milling machine should be equipped with a vacuum system to collect the produced sand. An industrial vacuum cleaner is able to collect sand with grain size of 300...400 μm but grain sizes smaller than 100 μm are volatile and could settle in any part of the machine. Therefore, the need for a precise seal for the moving parts of the machine is required. Also an air filtration system should be implemented to keep a healthy workplace environment. [2]

However, installing a vacuum system is not always economically viable. Therefore the developed machine uses only mechanical seals to protect all the critical components. The machine enclosure is sealed so that no sand can escape during milling.



### 3.3 The milling machine

The first generation prototype machine includes only one cutting head but the machine is designed in a way that it is easy to add more cutting heads which share a common xy-axis but are independently controlled on the z-axis.

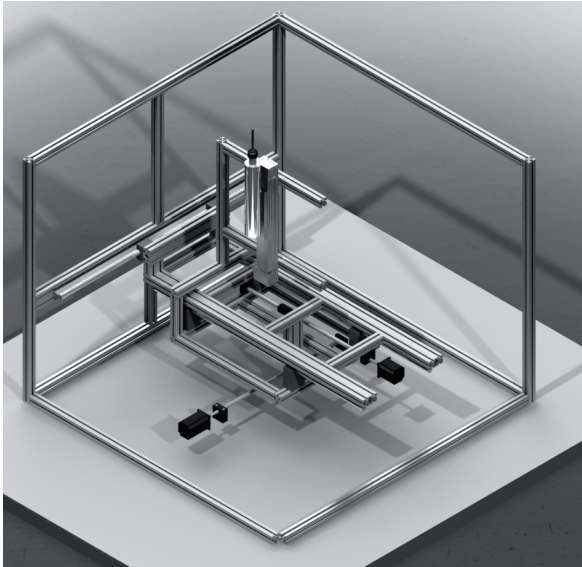


Fig. 4. The sand milling machine with protection and some other parts removed.

The movements of the machine are controlled using three servo motors. X-axis and z-axis are controlled using Granite Devices 300 W BL70-300 and y-axis is controlled using Granite Devices 150 W BL70-150. All of the servos are connected to their own servo controller (VSD-E) and the controllers are connected to a VSDEPI Parallel interface. The VSDEPI is connected to a computer via the printer port. The computer is running Ubuntu based LinuxCNC, which has EMC2 software for controlling the servos (Fig. 5). The EMC2 program is able to read general G-code. All the NC-programs for the milling machine are created with Mastercam CAM-software.

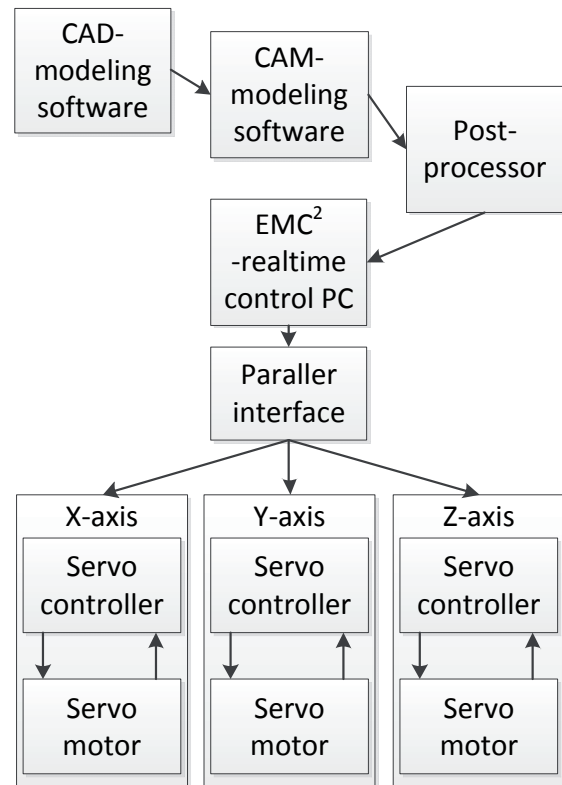


Fig 5. Diagram of the milling machines control system.

The x-axis and the y-axis servo motors are connected to ball-race screws that allow 50 cm of movement. Both of the ball-race screws are under the actual machine protected from the sand using sheet metal covers. The z-axis servo motor is connected to a tooth belt driven linear unit ELGA-TB-G-80-200-0H through a clutch and a 1:10 gearbox (Fig. 6). The linear unit allows 20 cm of movement. This enables the machine to have a working area of 50 cm x 50 cm with maximum cutting depth of 20 cm.

The x-axis guideways are attached to the far sides of the machine's frame. The frame is built using aluminium profile. The guideways are protected by covering them with sheet metal. A holding platform is built for the linear unit carrying the spindle motor on the y-axis guideways. The y-axis guideways are upside down under the x-axis guideways.

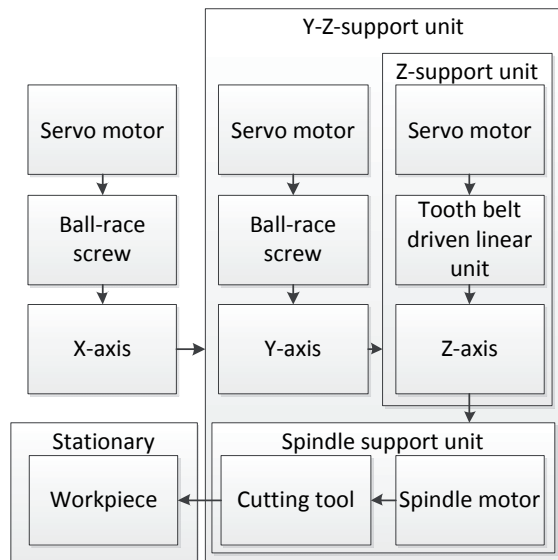


Fig. 6. The mechanical structure of the milling machine.

A 1,5 kW spindle motor is connected straight to the linear unit. The spindle motor has water cooling, which is more resistant to fine sand particles. Speed of the spindle is variable from 0 to 24 000 rpm. Special care in protecting the actuators of machine is taken. Besides using sheet metal covers for directing the sand away from critical components, other methods were also used. The ball screws are extremely vulnerable to sand and thus they are protected using rubber bellows on them. Servos and clutches are protected by using sealed clutch housings. Slight over pressure is applied inside the protecting elements in order to keep the finest dust particles out.

The designed machine is able to create casting molds and maintain working condition despite the fine abrasive sand dust.

#### 4. DISCUSSION

By using the patternless molding technique great savings are achieved in both time and cost. These savings are achieved by reducing the process steps from CAD model to final product. Because of reduced manufacturing steps the possibility of error is also minimized. Customizing the product can be done during mass production and

switching to a completely different product is possible with minimal effort by simply updating the cutting program.

A foundry can use this type of a machine in a prototype or small batch line, allowing them to handle small orders quickly and flexibly.

#### 5. FUTURE DEVELOPMENT

As was stated before, developing the milling machine with a single cutting head is the first step in the process towards a fast multi-spindle machine. Further development is required to produce machines which can be used as a part of an rapid multiple-stage sand molding lines. The milling machines frame is designed so that up to four individual cutting heads can easily be installed on the machine (Fig. 7). Increasing the number of cutting heads will have a major impact on the maximum material removal rates and therefore will greatly increase the processing speed of the molds.

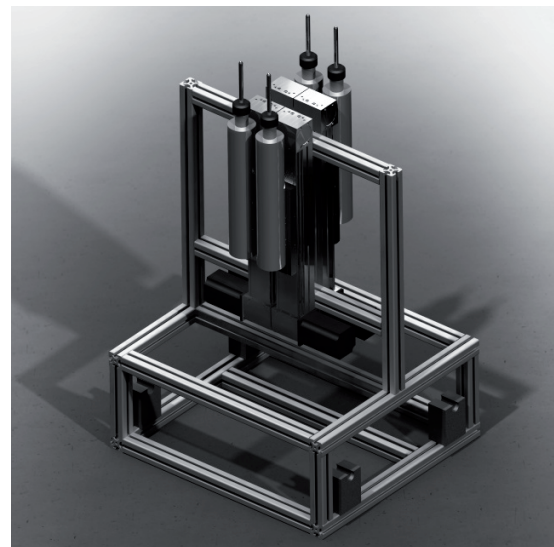


Fig. 7. The Z-support unit with 4 independent cutting heads attached.

However programming such a machine will be much more complicated, compared to a single spindle machine, and requires the use of a specialized CAM-software. During the development process we were unable to find any CAM-software which is

currently able to support such a machine and therefore much development is also required on the software side. One method to get around this limitation is to use a modified postprocessor. However this method can only be implemented when the cutting heads are side by side and the milling is done with straight parallel passes over the mold and therefore is not suitable for use with more efficient toolpaths. The optimal solution is to develop a CAM-software which can be configured to suit any multi-spindle milling machine, thus allowing the production of efficient NC-code directly.

## 6. ACKNOWLEDGEMENTS

The valuable support of laboratory manager Eero Niini and researcher Jari Kostamo are gratefully acknowledged.

## 7. REFERENCES

1. Sirviö, M., *Casting directly from a computer model*, High Technology Finland, 2007, available at: <http://www.htf.fi/direct.aspx?area=htf&prml=591&prm2=article>
2. Rodríguez, A., López de Lacalle, L. N., Calleja, A., Fernández, A., Lamikiz, A. *Maximal reduction of steps for iron casting one-of-a-kind parts*. Journal of Cleaner Production, Vol. 24, pp. 48 – 55, March 2012, ISSN 0959-6526
3. Dong, X., Li, X., Shan, Z. *Rapid Manufacturing of Sand Molds by Direct Milling*, Tsinghua Science and Technology, Volume 14, Number S1, pp. 212-215, June 2009, ISSN 1007-0214
4. López de Lacalle, L. N., Rodríguez, A., Lamikiz, A., Peñafiel, F. J. *Milling of Sand Blocks to Make Casting Moulds*. AIP Conference Proceedings, Vol. 1315, Issue 1, pp. 1065-1067, January 2011, ISSN 0094243X

## 8. CORRESPONDING ADDRESS

Panu Kiviluoma, D.Sc. (Tech.), Post-doc researcher  
Aalto University School of Engineering  
Department of Engineering Design and Production  
P.O.Box 14100, 00076 Aalto, Finland  
Phone: +358 9 470 23558,  
E-mail: [panu.kiviluoma@aalto.fi](mailto:panu.kiviluoma@aalto.fi)  
<http://edp.aalto.fi/en/>

## 9. ADDITIONAL DATA ABOUT AUTHORS

Sievänen, Samuli, B.Sc (Tech)  
Phone:+358 40 7397684  
E-mail: [samuli.sievanen@aalto.fi](mailto:samuli.sievanen@aalto.fi)

Pullinen, Tomi, B.Sc (Tech)  
Phone:+358 40 5209726  
E-mail: [tomi.pullinen@aalto.fi](mailto:tomi.pullinen@aalto.fi)

Schiestl, Markus, B.Sc (Tech)  
Phone:+358 40 5756926  
E-mail: [markus.schiestl@aalto.fi](mailto:markus.schiestl@aalto.fi)

Kuosmanen, Petri, D.Sc. (Tech.), Professor  
Phone:+358 9 470 23544  
E-mail: [petri.kuosmanen@aalto.fi](mailto:petri.kuosmanen@aalto.fi)



## THE TECHNOLOGY FOR LOW-VOLUME MANUFACTURING OF FENDERS FOR AN ADVANCED LIGHT ELECTRIC VEHICLE

Pääsuke, K; Pohlak, M.

**Abstract:** *Modern manufacturing industry is bound to meet the customers requests for increasing customization of products. With conventional technologies, being suited for mass production and using expensive tooling, it is often complicated to fulfill these demands with reasonable price. Several low-volume manufacturing technologies and also Additive Manufacturing technologies will be analyzed and compared in present paper. In the end of the paper a case-study of determining the most-suitable technology for manufacturing fenders for an advanced light plug-in electric vehicle will be presented.*

**Keywords:** *Electric vehicle, Additive Manufacturing, Rapid Prototyping, Vacuum Forming.*

### 1. INTRODUCTION

In the increasing need for customizing products, technologies which are suitable for flexible and low-volume production gain importance. Rapid Prototyping (RP) technologies were first used for prototyping, but several of these have proved to be ready for real production and constituted a new group of manufacturing technologies - Rapid Manufacturing (RM) [1, 2, 3]. According to

Eyers these technologies are: Stereolithography (SLA), Fused Deposition Modelling (FDM) and Selective Laser Sintering (SLS) [4]. The selection of a RP process is mainly based on the speed and costs involved; the quality and accuracy are a secondary priority. If the application is an end-use product, then the requirements are much more stringent: in product design, some of the most important criteria are the product functionality, appearance, shape or geometry and most relate to the material selected by the designer and material properties [4]. In the present paper the potential manufacturing technologies for manufacturing of the fenders of an advanced light plug-in electric vehicle - EXO bike - are analyzed. The manufacturing of the scooters is in the transition-phase from prototype to low-volume production, hence the quantities are small and the developed solutions can change to some degree. As different technologies have different advantages and disadvantages, the selection of the technologies will have a strong effect on the final outcome – is it the mechanical properties or the look itself. In addition, the costs of different technologies can vary greatly.

## 2. EXO BIKE AND ITS FENDERS

EXO bike (Fig. 1) is a state-of-the-art electric scooter. The frame is cut by laser from aluminum sheet and bent afterwards to achieve the structural strength and low weight. The energy is stored in lithium-ion batteries. The scooter weights altogether approximately 40 kg and can drive roughly 60 km. As the design of the scooter is unique there was a need to develop and manufacture inter alia its own fenders. The design of the fenders (Figure 2 and 3) is similar to the scooter itself: edgy, faceted and futuristic. The overall dimensions of the front fender are 470 x 150 x 200 mm and rear fender 430 x 200 x 200 mm. The requirements for the material of the fenders are mostly associated with mechanical properties: it has to withstand vibration and slight impacts, but also atmospheric conditions.



Figure 1. EXO bike.

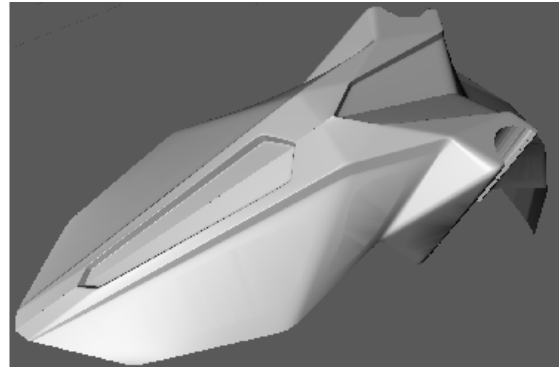


Figure 2. Front fender.

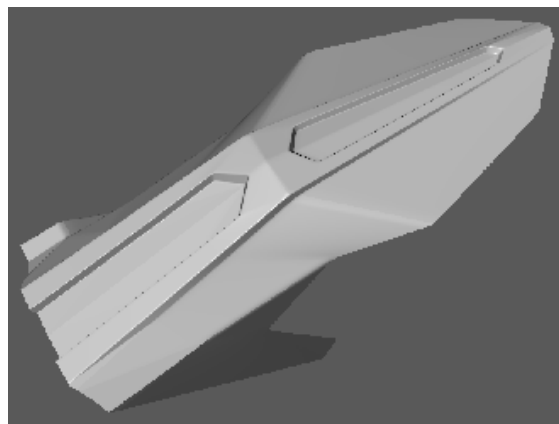


Figure 3. Rear fender.

## 3. POTENTIAL TECHNOLOGIES

In the present chapter the selection of suitable Additive Manufacturing (AM) and low-volume manufacturing technologies will be presented.

### 3.1. RP/RM TECHNOLOGIES

The RP technologies are manufacturing techniques for building objects from a three-dimensional Computer Aided Design (CAD) models. The product to be fabricated is presented as a multilayered CAD model, where successively each layer is converted to a physical layer, then bonded to the preceding layers, until the product is completed [5].

The most popular RP technologies for plastics are SLS, FDM and SLA. Additive Manufacturing derives from the principle the parts are built/manufactured – by adding material, not by removing it, as in most of the machining technologies.

### **3.1.1. Selective Laser Sintering**

In SLS the parts are made from powder, which is spread layer by layer onto the building platform and each layer is sintered by hatching the present cross-section with laser beam. The unsintered powder will support the parts during manufacturing.

### **3.1.2. Stereolithography**

UV-curable photopolymer resin is used in SLA for making the parts. SLA offers the highest accuracy among the AM technologies [6]. In the manufacturing process the resin is spread layer by layer onto the vat and the cross-sections of the part are cured by laser beam. As the resin is liquid, it does not support the parts and supporting structures must be added to ensure the stability and immobility of the parts during manufacturing. In build-process the resin is only partially cured and postcuring is required.

### **3.1.3. Fused Deposition Modelling**

In FDM thermoplastic filament is used to achieve three dimensional complex parts layer by layer. The filament is melted immediately before depositing onto the model. Soluble supports are required for overhanging sections and fragile structures.

## **3.2. Low-volume manufacturing technologies**

There are several technologies, which can be used for production in high- and low-

volume, but also for prototyping. The present paper will focus on three of such technologies, which all are used for manufacturing thin-walled parts from sheet-material. These technologies are: vacuum forming (VF), hydroforming (HF) and Incremental Sheet Forming (ISF).

### **3.2.1. Vacuum Forming**

VF is used for low- to high-volume manufacturing, but also for prototyping depending from machines and also from the durability of the mould [7]. In vacuum forming thin plastic sheet is heated up slightly above glass transition temperature ( $T_g$ ) or near to melting temperature ( $T_m$ ) [8], stretched onto a mould and then formed by applying vacuum between the mould and plastic sheet. Vacuum forming itself is relatively fast and simple, but machining the mold is time-consuming. In prototyping-phase the expenses of mould should be as low as possible as the mould is used only a few times, therefore the moulds in prototyping-phase are often made from lightly machinable material.

The size of the fenders meets the possibilities of vacuum forming. There are several types of materials with different thicknesses, mechanical properties, colours and appearances. If the prototype and mould are suitable, the shift from prototyping to low-volume production takes minimum effort.

### **3.2.2. Incremental Sheet Forming (ISF)**

ISF is considered an emerging sheet metal forming technology [9-12], for prototyping or small- to medium-batch manufacturing. There are two basic types of ISF: forming without support (negative) and forming with

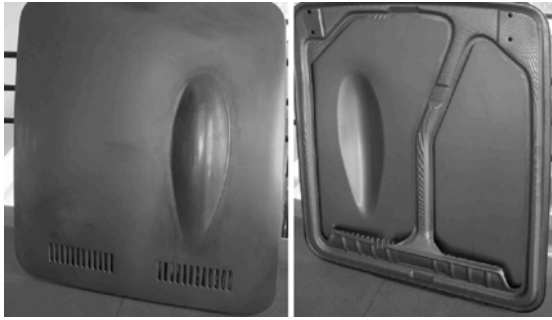


Figure 4. Honda S800 hood made by Amino in small series [13].

support (positive). The process is numerically controlled and capable of producing complex structures. As ISF is usually carried out in conventional CNC milling machines, the process offers high flexibility. ISF has so far interested mostly car-industries (Honda (Figure 4), BMW, Daimler-Chrysler), who see the potential of ISF by manufacturing large body-panels for prototypes and individualized vehicles [13].

### 3.2.3. Hydroforming

Hydroforming has gained interest in latest years due to increasing need of weight reduction of modern vehicles [14]. There are two types of hydroforming: tube hydroforming and sheet hydroforming. The process starts with fastening the sheet-metal between the mould and supporting frame.

The hydraulic fluid in high pressure is directed between the sheet-metal and the frame. The pressurized fluid causes the sheet to expand and form following the mould surface.

Finally, the hydroformed sheet is removed and post-processed (the fastening-edges are cut off etc.) if necessary.

## 4. THE COMPARISON OF THE TECHNOLOGIES

In present chapter the previously described technologies will be compared and analyzed. The diagram of different technologies that were analyzed to produce the fender are depicted in Figure 5.

### 4.1. Additive Manufacturing Technologies

The AM technologies are suitable for manufacturing a few samples, as it is fast and comfortable. As mentioned earlier, the technology imposes almost no restrictions to the design of the part. Therefore it would be possible to manufacture the fenders, which would be optimized in reference to low weight and high mechanical properties. Such optimizations lead often to complex design and constructions, which would be impossible to achieve with conventional technologies.

The hindrance of using AM technologies, in this particular case, are the large dimensions of the fenders. To manufacture the fenders in one piece, the building chamber of the AM system has to be relatively big. This all results in high building-volume and price. The materials offered in AM are usually with limited properties. For example the mechanical properties are slightly lower than

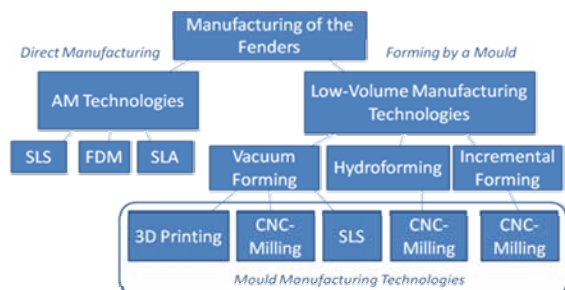


Figure 5. The tree of handled technologies for manufacturing the fenders.

in case of injection moulded parts [15]. As the parts are made layer by layer in AM technologies, the surfaces of parts can be stepped (depending on the position in manufacturing) and the surfaces might need post-processing. The selection of colours is also limited in AM excluding FDM.

#### **4.2. Low-volume manufacturing technologies**

The low-volume manufacturing technologies described earlier require greater human labor. As all of the described technologies use mould, the expenses of manufacturing the mould must be added to the costs.

ISF is performed mostly on CNC milling machines and as the main technology for manufacturing the mould is also machining, it can be executed on the same machine. Although the mould for HF is probably the most expensive and most time consuming to manufacture, the process of HF itself is times quicker than of ISF.

The moulds for VF in prototyping/low-volume manufacturing phase are usually made from easily machinable materials. In addition, it is possible to manufacture the mould also by AM technologies, for example by 3D Printing or SLS.

All of the three technologies require post-processing to cut out the formed part. To achieve the desired colour by ISF and HF, painting is also needed. In addition, none of the technologies enables negative angles for the parts to ensure the removing of the parts from the mould.

### **5. THE MANUFACTURING OF THE FENDERS**

As VF is the cheapest and simplest of the three low-volume manufacturing technologies and as there is first a need for several fenders not just one, VF was chosen for the technology to manufacture the fenders of EXO bike.

The mould was milled from MDF-blank (MDF - medium-density fibreboard) by 3-axis CNC milling machine DYNA 3116 by using a round mill. The mould was post-processed with sandpaper and filler afterwards.

VF was performed on Formech 300 XQ Quartz vacuumforming machine. For the material HIPS (high-impact polystyrene) with thickness of 3 mm was selected.

Although the design and functionality are often verified by obtaining the physical model by some agile technique, in present case the rationality of using a AM technology is arguable. The costs of fenders obtained by VF are comparable to the costs of for example SLS by the same model.

### **6. CONCLUSION**

Several low-volume manufacturing technologies and AM technologies were analyzed regarding the need for manufacturing fenders for an advanced light plug-in electric scooter in low volume. Due to flexibility and low costs vacuum forming was selected for the technology for manufacturing the prototype and the first series. The mould was milled from FDM-material by 3-axis CNC milling machine with round mill. Although AM technologies offer even higher flexibility and they are

used even for real production, these technologies were considered unsuitable for such large parts.

## 7. REFERENCES

1. Ajoku, U.; Hopkinson, N.; Caine, M. Experimental measurement and finite element modelling of the compressive properties of laser sintered Nylon-12. *Materials Science and Engineering: A*, 2006, **428**, 211-216.
2. Zarringhalam, H.; Hopkinson, N.; Kamperman, N.F.; de Vlioger, J.J. Effects of processing on microstructure and properties of SLS Nylon 12. *Materials Science and Engineering: A*, 2006, **435-436**, 172-180.
3. Kruf, W.; van de Vorst, B.; Maalderink, H.; Kamperman, N. Design for Rapid Manufacturing functional SLS parts. *IPROMS*, 2006, 389-394.
4. Eyers, D. R.; Dotchev, K. D. Rapid manufacturing for mass customization. *IPROMS*, 2009, 29-34.
5. Dong, L.; Makradi, A.; Ahzi, S.; Remond, Y. Three-dimensional transient finite element analysis of the selective laser sintering process. *Journal of Materials Processing Technology*, 2009, **209**, 700–706.
6. Melchels, F.P.W.; Feijen, J.; Grijpma, D.W. A review on stereolithography and its applications in biomedical engineering. *Biomaterials*, 2010, **31**, 6121-6130.
7. Harper, C.A. *Handbook of Plastic Processes*. John Wiley & Sons, Timonium, 2006.
8. Schmidt, F.M.; Le Maout, Y.; Monteix, S. Modelling of infrared heating of thermoplastic sheet used in thermoforming process. *Journal of Materials Processing Technology*, 2003, **143-144**, 225-231.
9. Rauch, M.; Hascoet, J.Y.; Hamann J.C.; Plennel, Y. A new approach for toolpath programming in Incremental Sheet Forming. *International Journal of Material Forming*, 2008, 1191-1194.
10. Pohlak, M.; Küttner, R.; Majak, J. Modelling and optimal design of sheet metal RP&M processes. *Rapid Prototyping Journal*, 2005, **11(5)**, 304 - 311.
11. Pohlak, M.; Majak, J.; Küttner, R. Manufacturability and limitations in incremental sheet forming. *Proceedings of the Estonian Academy of Sciences, Engineering*, 2007, **2**, 129 - 139.
12. Pohlak, M.; Majak, J.; Küttner, R. Incremental sheet forming process modelling-limitation analysis. *Journal of Achievements in Materials and Manufacturing Engineering*, 2007, **2**, 67 - 70.
13. Emmens, W.C.; Sebastiani, G.; van den Boogaard A.H. The technology of Incremental Sheet Forming—A brief review of the history. *Journal of Materials Processing Technology*, 2010, **210**, 981–997.
14. Hartl, Ch. Research and advances in fundamentals and industrial applications of hydroforming. *Journal of Materials Processing Technology*, 2005, **167**, 383–392.
15. Gibson, I.; Rosen, D.W.; Strucker, B. *Additive Manufacturing Technologies*. Springer, New York, 2010.

## CONCEPT FOR ONLINE WEB MACHINE TOOL CONTROL BASED ON OPEN SOURCE

Radelja, H., Hasković, D., Šikulec, L., Plančak, M., Kršulja, M. & Car, Z.

**Abstract:** *The direction for the future development of the production process is complete autonomy, artificial intelligence, ability to diagnose errors, self-repair and, most importantly, to minimize impact of human factors. Although technology is not yet mature enough for a complete exclusion of worker from the machining process remote control could enable unmanned operation.*

*The concept offered in this study consists of building a custom WEB application for machine tool control that provides flexibility, operation from any remote location, ensures platform independence and low cost due to use of Open Source Architecture.*

*Key words: remote control, WEB control, CNC machine tool, WEB-based manufacturing, Open Source*

### 1. INTRODUCTION

There have been a number of key changes through the development of machine tools, which have, each for themselves, improved and simplified their use. In particular, one can emphasize the development of the CNC control that proved to be more productive, easier to use, enabled production of more complicated workpieces and made the technology accessible to a wider number of users. Any improvement also means higher productivity, accuracy, efficiency and ultimately, higher profits in manufacturing. One of the prospects of development that are discussed today is the remote control. This type of control is particularly interesting because, thanks to automated

systems that regulate all the parameters of processing, the operator no longer has to be close to the machine tool while operating. From the viewpoint of production economy, if the employee does not have to be by the machine, but instead it can monitor it while on another job, this presents a benefit because worker can perform several tasks at the same time, he can do some other work or monitor several machines simultaneously.

Remote control enables not only monitoring but to completely control the process - in case of error, processing can be stopped, check what caused the error, possibly change the parameter and continue processing.

A number of researches are conducted on remotely controlling the machine tools, with different approaches and solutions for different aspects of the problem [1]. In most cases, it was just a simulation and monitoring processing without the possibility of operating in real time.

One part of the research is focused on supporting the design and planning process over the Web, such as CyberCut [2], Internet Manufacturing [3], which offer solutions for overcoming the problem of physical distance from the R&D teams and technology planning process and offer practical platform for concurrent engineering.

One popular approach to implement remote control is to establish a client - server communication, either by developing their own applications or by using commercial software [4] such as VNC or pcAnywhere, which allows taking control over the system that controls the machine tools



from a remote location. The advantages of this solution are ease of implementation, the use of existing infrastructure, but there are major drawbacks in terms of flexibility, providing real-time control and safety in case of a disconnection.

The solution offered in this study consists of building a custom Web application for machine tool control that provides flexibility, scalability, operation from any remote location, and ensures platform independence and low cost due to use of Open Source Architecture.

## 2. TELECONTROL

Telecontrol is defined as a continuous and direct control of the remote machine [5]. Advantages of telecontrol are already identified and widely present in everyday life, mostly for the purpose of improving the quality of human life. Whether it is the TV remote control device, smart house, a remote support for a service or a product, control of the plant or the remote control of robots that perform hazardous tasks.

The application of telecontrol for the machine tools operation opens up new possibilities to extend the usability and commercialization of a machine.

It enables virtual business between geographically distant subjects [6] through the formation of partnerships and utilization of external resources without the necessity of purchasing the equipment. Allows manufacturers to locate production facilities closer to the customer or the less costly location while highly skilled workers who operate the equipment can be located closer to the R & D department and the administration for better communication and centralization of human resources. It also enables cost reduction because it opens up the possibility of working from home, the parallel execution of some other work or operating multiple machines simultaneously. Therefore, it is not surprising that one of the better-known manufacturers of machining equipment,

OKUMA, for a series of products THINC®-OSP Constant Care [7] offers, free of charge, support that includes remote monitoring and control of devices for diagnostic and service.

There are many web-based collaboration systems [8], mainly for:

- simultaneous design,
- Web-based RP,
- project management,
- Conflict Resolution during collaboration.

Rare for:

- Monitoring workshop machining - Job Shop,
- remote-controlled CNC machining,
- advanced automation facilities,

which are typically limited in functionality, used for monitoring or offline simulation.

That the machine manufacturers noted the need to develop telecontrol is indicated by the fact that most modern equipment has the ability to connect to the Internet, while only ten years before that option had only about 10 % of CNC machines [9].

### 2.1 Control method selection

One of the most important criteria when choosing a method of control is of a financial nature. The goal is to develop a system based on open source, free programs and infrastructure that is flexible, cost-effective but with relatively limited capabilities, or a system with far more advanced functions and capabilities, ready to use "out of the box", for which however, is necessary to provide significant financial resources. The choice will depend on the characteristics of the problem to be solved and of the assessment which method is the most affordable, most reliable, most widespread and most cost-effective.

This concept is based on open source infrastructure, with the intention of researching its capabilities, bearing in mind the comparative advantages of flexibility and platform independence.

There is a large choice of means of communication, the use of the GSM mobile network, local wired and wireless

networks, Bluetooth technology, infrared, radio frequency and others. For the purposes of remote control internet imposes as the most suitable, since it is most widespread and enables global connectivity.

The Enhanced Machine Controller (EMC2) is selected for the control unit of the machine tool, the Open Source CNC controller, based on the RS-274 standard programming language. Its functions are available externally and can be easily implemented in a web application. The control unit was developed as part of the Ubuntu linux distribution, so it is convenient to choose that operating system for machine tool control.

Exclusively free open source applications were used. Apache server and SQL database, and for programming the Web application HTML, Java, PHP, and socket programming.

## **2.2 The security and robustness issues**

The first aspect of network security is data loss and the delivery order of the information packages, which is solved using the TCP protocol. When working with data exchange and remote control there is always the possibility of compromised security, meaning unauthorized access to the data or changing the control instructions causing damage to the computer and equipment. This can be extremely dangerous, because if the system is compromised not only that the machining process can cause material damage, but since it handles sharp tools and fast moving parts it may cause serious injury. Intrusions can be deliberate, but also they can be accidental connections to

an unsecured network. Therefore, it is of utmost importance to adequately protect used network. For wireless networks protection various systems of data encryption are implemented.

In addition, there is a risk of malicious software such as worms, viruses, trojans or spyware. Various antivirus programs are designed to help prevent system infection and suppress possible damage caused by malicious software.

## **3. REMOTE CONTROL CONCEPT**

Today the most popular and most common way of communicating is the internet. It allows users to search, browse, retrieve, disseminate and share information remotely. It truly provides global connectivity and the ability to easily remotely control from any point on Earth [10]. The foundation of the concept of Web telecontrol is based on simplicity and low cost of development and deployment.

Fig. 1 shows a diagram of the developed concept of web control [11]. The concept consists of the developed Web application that is accessed from the computer that is connected to the internet via a TCP/IP protocol. Real time communication with the server is provided using socket programming. Server forwards requests to the EMC2 control unit [12] that is physically connected to the machine tool.

The application of open source provides the flexibility. Since the control unit's functions are available externally for implementation in a Web application, it is possible to directly control the control unit instead of taking the control over the computer on which the control unit is installed.

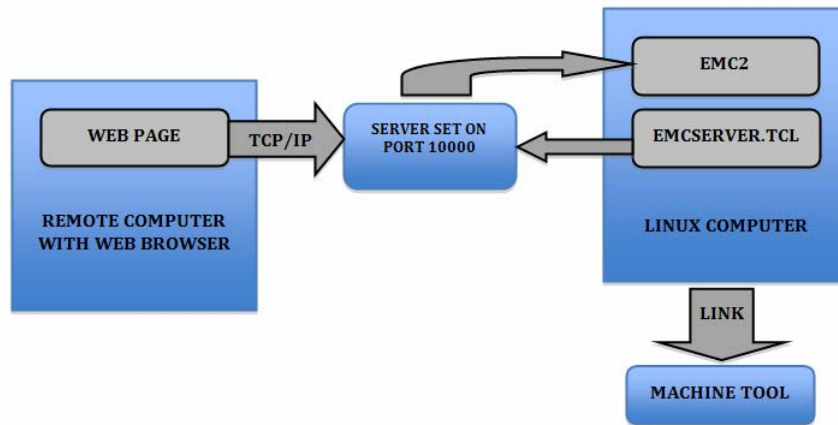


Fig. 1. Schematic representation of WEB control of machine tool

### 3.1 EMC2 control unit

EMC2 is a CNC control unit. It is a free programming solution, which is based on free source code. It is suitable to operate machine tools, machine tools, robots and other automated devices. It can control servo or stepper motors, relays and other devices related to machine tools. The system of stepper engine controlled from Linux PC, which is connected to them through the parallel port, is shown in Fig. 2. These signals are sent to the actuators that drive the engines. It is also possible to control servomotors via interface card or using parallel connectors that are associated with external control units. Script sets the server on port 10000, and after that communication with server is possible. In this way, the Linux computer is configured to expect external commands,

but still remains to define how to establish a link between the website and server set.

### 3.2 Linking web pages to the server

To make a web page able to communicate with the server over the Internet, it must be written in a special programming language; in this case, PHP language was selected. This enables it to send commands in the form of packets of information across an imaginary "pipeline" to server which forwards them to the EMC2 program, and it manages machine. This method of programming data exchange is called socket programming and provides real-time communication between clients and servers. Secured communications, it is necessary to define the function and appearance of Web applications for machine tool control.

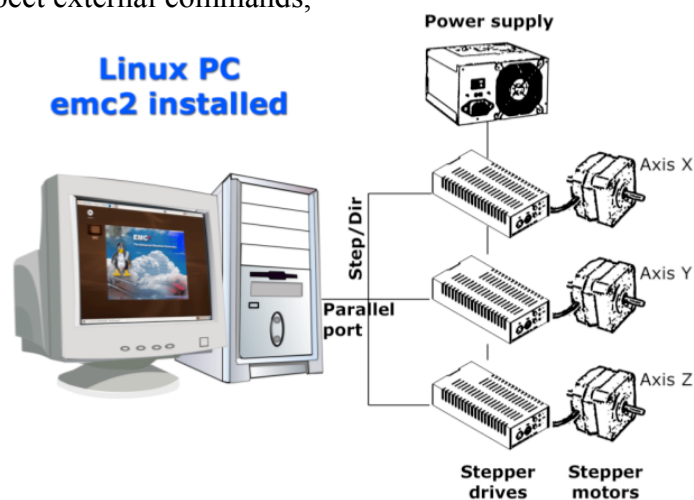


Fig. 2. Scheme of EMC2 control of the 3-axis stepper drive system [12]

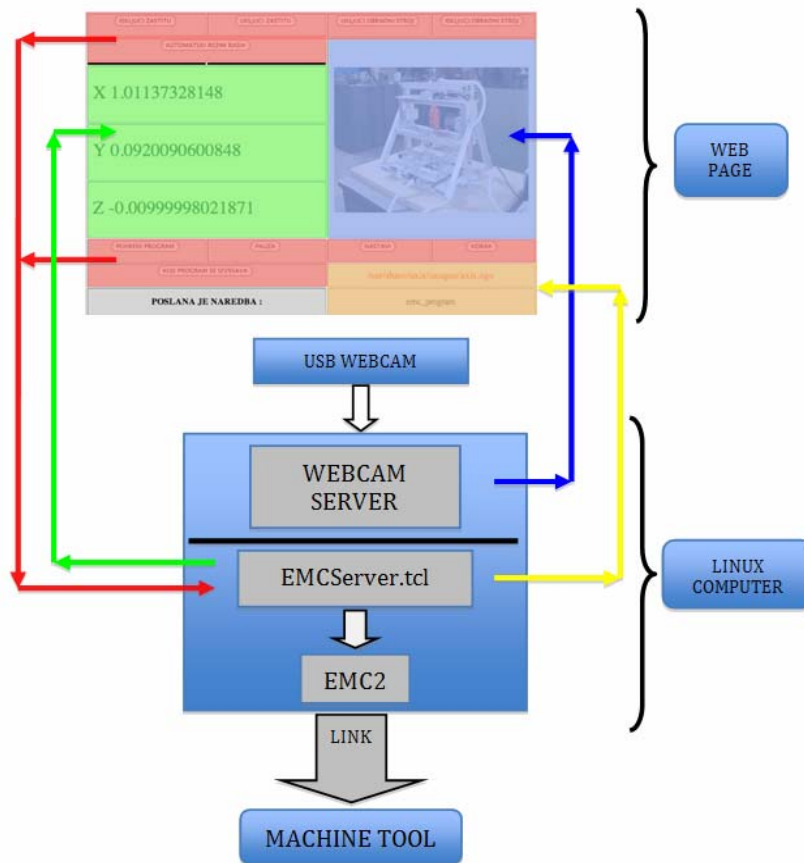


Fig. 3. Web application for machine tool control

To enable the automatic update of web pages JavaScript or JavaScript Timing Events function have been used.

With this function, it is possible to perform a set of instructions in the specified time interval. In this case, command is sent, which gives feedback about position. Update interval is one second.

Due to the physical distance of the user from the machine tool, it is necessary to provide some form of monitoring of machining processes. The best feedback is visual information. For this reason, a web site is capturing live images from Web cameras located near the machine tool pointing towards the workpiece.

With the change of certain parameters, it is possible to change the resolution and image size, number of frames per second and the IP address of the computer on which webcam server is mounted.

The video image is not possible because relationship with a webcam server should be re-established for every update. For that

reason, part of page should be separated from static part in separate frame, which allows viewing HTML document inside another HTML document or Web pages within a frame containing another website. In this case, the static part of the site refers to frames for video display and control buttons, while the coordinates are display is in a separate frame that allows updates.

#### 4. CONCLUSION

The concept of Open Source remote control has been successfully implemented in the example of educational 3-axis milling machine located at the Faculty of Engineering Rijeka, and which can be controlled via the Internet. For demonstration purposes, only basic functions are programmed. On / off machine switch, starting, pausing and stopping the loaded program. This Web application can be easily extended to perform all the functions of the control

unit. Remote control of the machine tool through the web is opening the possibility for online collaboration and renting a machine, therefore one of the directions in which to carry out further research system management tasks and coordination of multiple users, and, ideally, to ensure 24 hour availability of the machine, automatic supply of raw materials and removal of workpieces. For the purposes of online production, it is necessary to develop a virtual model of the machine tool, with the ability to simulate the production process using a remote control. This way user would be able to detect possible faults in selected strategies, cutting data values [<sup>13</sup>] and to train users, to avoid possible errors that could result in damage to the workpiece or machine.

## 5. ACKNOWLEDGEMENTS

The authors would like to acknowledge the support provided by the National CEEPUS Office of Croatia and National CEEPUS Office Serbia, which helped the research through mobility in the frame of the CEEPUS II HR 0108 project.

## 6. REFERENCES

1. Lala, S. P., Onwubolu, G.C.: *Three tiered web-based manufacturing system—Part 1: System development*, Robotics and Comp.-Integrated Man. **23** (2007) 138–151.
2. Ahn, S. H., Sundararajan, V., Smith, Charles, et. al.: *CyberCut: An Internet-based CAD/CAM System* ASME Jour. of Comp. and Inf. Sci. in Eng., Vol.1, **1**, 2001.
3. Tay, F. E. H., Khanal, Y.P., et.al: *Distributed rapid prototyping—a framework for Internet prototyping and manufacturing*. Integrated Manuf Syst 2001;**12** (6):409–15.
4. Lee, R.S., Tsai, J. P., Lee, J. N., et.al: *Collaborative virtual cutting verification and remote robot machining through the Internet*. Proc Inst Mech Eng 2000; 214B:635–44.
5. Angheluta, L., Moldovan, A., Radvan, R.: *The Teleoperation of a Lif Scanning Device* U. P. B. Sci. Bull., Series A, Vol. 73, Issue. 4, 2011.
6. Lan, H., Ding, Y., Hong, J., et.al: *A web-based manufacturing service system for rapid product development* Computers in Industry **54** (2004) 51–67.
7. Felix, C.; *Advantages of Remote Troubleshooting* Production Machining Magazine, Gardner Publications, Ohio 2011-10-2.
8. Wang, L., Orban, P., Cunningham, A., Lang, S.: *Remote real-time CNC machining for web-based manufacturing* Robotics and Computer-Integrated Manufacturing **20** (2004) 563–571.
9. Waurzyniak, P.: *Electronic Intelligence in Manufacturing*, Manufacturing Engineering, Vol. (3), 2001, pp. 44-67.
10. He, H., Wu, Y.: *Web-based virtual operating of CNC milling machine tools* Computers in Industry **60** (2009) 686–697.
11. Hasković, D.; B. Sc. Thesis, University of Rijeka, Faculty of Engineering, 2009.
12. „The EMC Team“: *EMC Handbook*, LinuxCNC.org, 2011. <http://linuxcnc.org> Accessed on: 2011-11-05.
13. Car, Z., Barišić, B., Ikonić, M.: *GA Based CNC Turning Center Exploitation Process Parameters Optimization* Metalurgija. **48** (2009), 1; 47-50.

## 7. ADDITIONAL DATA ABOUT AUTHORS

Assistant **Hrvoje Radelja**, PhD student,  
**Damir Hasković**, MSc,  
 Assistant **Leon Šikulec**, PhD student,  
 Assistant **Marko Kršulja** PhD student and  
 Prof. **Car Zlatan**, PhD, Vice – Dean for  
 business affairs.  
 Faculty of Engineering, Vukovarska 58,  
 51000 Rijeka Croatia E-mail: car@riteh.hr

Prof. **Miroslav Plančak**, PhD,  
 Faculty of Technical Sciences, Trg  
 Dositeja Obradovića 6, Novi Sad, Serbia.  
 E-mail: plancak@uns.ac.rs

## RESEARCH ON BUCKET BORE RENEWAL TECHNOLOGIES

A.Ratkus, *M.sc.ing.*, T.Torims, *Dr.sc.ing.*, Viktors Gutakovskis *M.sc.ing.*

[andriskratkus@inbox.lv](mailto:andriskratkus@inbox.lv), [toms.torims@rtu.lv](mailto:toms.torims@rtu.lv), [vgutakovskis@gmail.com](mailto:vgutakovskis@gmail.com)

**Abstract:** *Novel mobile (in-situ) repair technologies are extensively used for specialized equipment and machinery repairs. The reason for this is the considerable cost reductions and increase in the technological lifespan of the industrial equipment. Such parts as frames, joints or buckets can be renewed to an excellent standard using innovative in-situ technologies.*

*In-situ renovation technology is itself a non-standard operation, even though the techniques used of turning and installation are relatively well studied and developed. Conversely, build-up welding processes can be studied further and potentially substituted by more advanced and economically more attractive, modern surface renovation technologies.*

*Key words: in-situ renovation, build-up welding technology, cladding*

### 1. INTRODUCTION

This paper outlines initial progress of the PhD thesis (literature review) with the aim of developing a comprehensive study of bucket bore renewal technology. The overall aim of this study is to develop an economically justified, backhoe bucket borehole renewal technology, using standard and enhanced technological approaches.

A renewal technology has to meet very high standards, because the output quality must offer operating performance and durability comparable to the new product. Furthermore, surface roughness, shape and

tolerances have to be identical or even superior to manufacturers' requirements. This requires an in-depth, systematic study of the pins and buckets bores, which are the most popular items for renewal. Finally, it has to be possible to provide appropriate grade with suitable in-situ renewal technology.

### 2. RENEWAL TECHNOLOGY

Conventional in-situ drilling and repair technologies are implemented by installing equipment directly on the damaged product using specialized centring devices. The bore central axis is used as a basis for positioning. The damaged layer is then removed mechanically by means of a turning operation. Once this is complete, the renewable surface is covered by a new layer of material using conventional MIG/MAG welding (Fig.1.). This is followed by final operation: turning to the nominal bore size.

Conventional MIG/MAG (GMAW) welding technology is one of the cheapest new layer build-up techniques and is therefore most widely used. Furthermore it is easy to adapt this build-up technology for inner surface (bore) cladding.

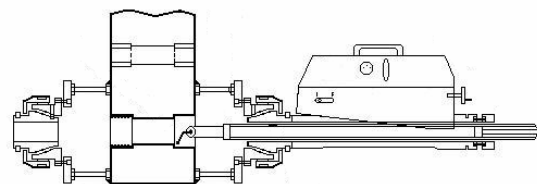


Fig. 1. MIG/MAG (GMAW) build-up welding equipment [6]

### 3. PROBLEM STATEMENT

It is important to note that the new material layer must equal or surpass the operational characteristics of a replacement part. It is therefore important to establish the most suitable technology from the available spectrum. Renewal operations like turning and installation are relatively well studied and developed. For these operations, it is possible to adapt and use a wide range of turning and installation equipment and technologies. Therefore research efforts will mainly focus on the new material layer cladding operation. Moreover there is very little research and limited scope for relatively small bore (60-100 mm) build-up technologies [3]. The results from this research can potentially provide a greater understanding and highlight all the benefits of the analysed renewal technologies.

### 4. MAIN RESEARCH TOPICS

The first step is to establish the frame of reference for build-up cladding, based on the properties and features of the renewal technology. Secondly, a comprehensive literature review/research is required in order to identify as many cladding technologies as possible.

Thirdly, we have to identify and justify the most appropriate surface coating technology.

The following criteria will be used within this comparative study:

- Thickness of build-up layer;
- Potential for in-situ application of the renovation technology;
- Potential for cladding and spraying in all torch positions and directions;
- Bore size limits (min. 60-100 mm);
- Possibility to use technology for inner surfaces;
- Substrate temperature during build-up operation and base material stresses;
- Physical and mechanical properties of build-up layer;

- Costs<sup>1</sup>.

In order to facilitate the technology evaluation process, research will commence with the five most important assessment criteria, cf. Table in Annex.

### 5. COATING TECHNOLOGIES

Designing a suitable surface treatment from a given combination of loads poses certain challenges. Not only is it often difficult to precisely and thoroughly understand the operating conditions of a part, but also a very wide variety of possible materials and materials technology processes have to be considered. Selecting an appropriate technology to produce a certain combination of surface characteristics is a very complex process. It involves systematic correlation of specifications with attainable surface properties. Usually, the selection process includes economic and ecological evaluations [2].

All coating technologies fall into two main groups: coating by conventional welding and surface spraying technologies. In addition, several other technologies exist for creating a new layer of metal, such as poly metal (by HOFMANN [7]) and powder metallurgy. A bush insert can also be used to create new metal layer.

These various technologies all involve different technological processes, power sources, filler materials and results.

#### 5.1. Build-up welding

Build-up welding (Fig. 2.) is a technique where a coating is applied during a fully or partially molten phase. A metallurgical bond between the coating and substrate material is created when both the substrate and coating materials are melted [2].

In principle, every welding technique is appropriate for build-up welding. During

---

<sup>1</sup> Preliminary costs. As the technological equipment is generally an innovation and patented, it is difficult to estimate its costs.



the historical development of welding technology, each welding technique has also been used for build-up welding. Nowadays, due to process characteristics, certain welding processes or variants have become particularly popular [2].

Compared to other deposition techniques, build-up welding generally produces coatings with higher adhesion, due to the metallurgical bond created by partially or fully molten materials. The joint between the coating and substrate is never the weakest area of the compound, as long as adhesion-reducing hard phases, produced by inadequate combinations of coating and substrate material, are prevented. These coatings are therefore particularly suited to applications where the renewed parts are subject to heavy wear. Additionally, they offer high edge strength [2, 5].



Fig. 2. Build-up welding torch [3, 6]

Build-up technologies [1, 2, 5]:

- Submerged arc welding (SAW);
- Shielded metal arc welding (SMAW);
- Gas metal arc welding (GMAW);
- Flux Cored Arc Welding (FCAW);
- Plasma arc welding (PAW);
- Light amplification by stimulated emission of radiation (LASER).

These build-up welding technologies are compared in Table 1.

## 5.2. Thermal spraying

Thermal spraying (Fig. 3.) processes offer coatings for parts using a diverse range of coating materials to enhance wear and corrosion resistance, as well as providing a thermal barrier or producing the desired electrical or magnetic properties, etc. The basic principle and definition of the term

thermal spraying is standardised in DIN EN 657. The material to be sprayed is fed to a source of heat in the form of powder, wire or rod, inside or outside the spray apparatus. Here, it is melted superficially or completely, or heated until it is sufficiently soft. A gas stream accelerates the particles towards the substrate, where they are deposited as a coating [2].

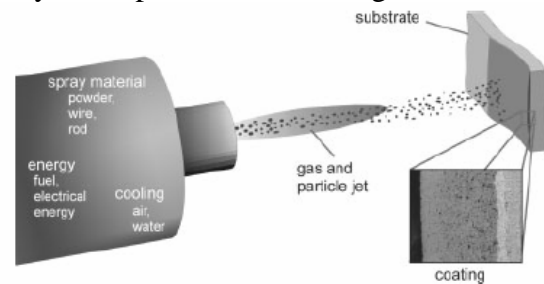


Fig. 3. Principle of thermal spraying [2]

Thermal spraying technologies [1, 2, 4]:

- Plasma spraying;
- Plasma transferred wire arc (PTWA);
- Wire flame spraying;
- High velocity oxy-fuel coating spraying (HVOF);
- Cold spraying;
- Warm spraying;
- Arc spraying;

Table 1. shows a comparison of these spraying technologies.

## 6. CONCLUSIONS

This article illustrates the conclusion of the in-depth literature review, which made it possible to identify the most suitable build-up technology for industrial bucket bore renewal. Clear and understandable evaluation criteria were used and this enabled us to conclude that research should continue in the direction of GMAW, GTAW, PAW and LASER build-up technologies. A comparative table is provided in the Appendix. These four technologies fulfil the initial evaluation criteria and shall be analysed further, including the laboratory experiments and test trials.

## REFERENCES

1. Chattopadhyay R., Advanced Thermally Assisted Surface Engineering Processes, Kluwer Academic Publishers, Hingham, USA, 2004
2. Fr.-W. Bach, A. Laarmann, T. Wenz (eds.), Modern Surface Technology, Wiley-VCH Verlag GmbH & Co. KGaA, Weinheim, 2006
3. Ratkus A. Master's thesis: Research on Bucket Bore Renewal Technologies, Riga, 2011
4. Robert B. Heimann, Plasma-Spray Coating: Principles and Applications, John Wiley & Sons, 2008
5. Welding Handbook, Eighth Edition, Vol. 2. Welding Processes, edited by R. L. O'Brien, American Welding Society, Miami, 1997
6. <http://elsasrl.com/img/download-catalogo-macchine-utensili-portatili/supercombinata-scl-en-informazioni-tecniche.pdf>
7. <http://www.hofmannindia.com/download/e-poly-metal.pdf>

## COMPARISON OF BUCKET BORE RENEWAL TECHNOLOGIES

ASSESSMENT CRITERIA		PERFORMANCE						
TECHNOLOGY	SAW	SMAW	GMAW	FCAW	GTAW	PAW	Build-up by LASER	Plasma spraying
Thickness of build-up layers, mm	5 - 8 mm	2 - 4 mm	0.5 - 8 mm	under to 8 mm	1.6 - 5 mm	1 - 6 mm	2 - 6 mm	up to 2 mm
Potential for on-site application of renovation technology	YES	YES	YES	YES	YES	YES	INSIDE	INSIDE
Cladding and spraying achievable in all torch positions and directions	Standard. - NO	YES	YES - by short circuit material transfer	YES	YES	YES	-	usually only Flat or Horizontal torch pos.
Bore size limits (MIN)	PATENTED	approx. 300 mm	20 mm - 1700 mm	20 mm - 1700 mm	from 40 mm	from 75 mm	-	from 40 mm
Potential to use technology for inner surfaces	Standard. - NO, there are some patents	Difficult	YES	YES	YES	YES	YES	YES
EVALUATION	Shall look forward to patented equipment	Not fit	FIT	FIT, but one must find benefits in comparison with GMAW, wire is expensive	FIT, however benefits and expenses shall be further scrutinised			

## THE IMPACT OF METROLOGY IN INDUSTRIAL SECTOR IN ESTONIA.

Simson, K.; Kübarsepp, T.; Uljas, H. ;Leito, I & Karotamm, L.; Karilaid, M.; Metssalu, M.; Parker, M.

**Abstract:** *The purpose of the survey was to find the impact of metrology on Estonian economy. 450 different enterprises were polled and several interviews were carried out. One of the outcomes was that annual expenditure of 28-40 mln € on metrology produces 2,8 bln € through avoiding unnecessary costs.*

*Key words: metrology, industry, measurements, analysis*

### 1. INTRODUCTION

A well functioning metrological infrastructure is essential for sustainable economy. Reliable measurement results are important in industry (e.g. machinery, electronics), consumer care and protection (food production and inspection), emerging technologies (biotechnology and nanotechnology enterprises) etc. A National Measurement System is an instrument in the hands of government to develop and provide measurement services according to needs in society and in economy. For this reason, it is important for decision-makers to study regularly the operation and functioning of metrological infrastructure.

There are some studies about the role of metrology in some countries but no thorough statistical investigation was found which can be exactly applied for Estonian survey.

In the present paper we briefly describe the methods used in the study. The findings, which are based on statistics from period 2005 to 2009 and polls in 2011 are presented. These findings include metrology related costs, technical situation and needs of enterprises mostly in industrial sector.

### 2. METHODS

The purpose of the study was to find the influence of metrological infrastructure on economy, innovation and sustainability as well to the need for infrastructural development. To achieve the goals, methods were developed for mapping the effectiveness of use of resources and availability of metrological services and its impact on economical growth, quality of life, entrepreneurship and other aspects.

In the study, the use of measurements in several fields was first separately questioned. Mass and related measurements (eg force and torque), dimensional measurements, temperature and humidity, electricity, time, photo- and radiometry, chemical analyses and measurements, water and gas consumption, sound and radioactivity measurements were subject to study. In the next stage, the largest industrial branches were selected based on their annual turnover and exporting capabilities. The aim was to combine the use and future needs for measurements and metrological services in the competitive industrial sector.

The survey based on the data acquired by Statistics Estonia during the years 2005 to 2009 and polls carried out in 2011. The subjects of

survey were selected basing on import and export volumes.

The largest sectors in external trade were:

- Machinery and metal works
- Electrical appliances and electronics
- Chemistry
- Textile
- Foodstuffs
- Furniture
- Power industry
- Plastics
- Wood

Information about sales revenue, value added and trade of sectors was used. In order to exemplify the results of polls, case studies were implemented in different big companies in order to bring out the details and mechanisms between metrology and revenue.

To quantify direct costs on metrology, spending on legal metrology and quality control was used. Additionally, the share of metrology in value added was assessed.

To quantify indirect costs of metrology, the cost of uncertainty was assessed, which is caused by uncertainties of measurement equipment used in trade. In order to assess knowledge about metrology, the development plans of sectors unions were reviewed.

The poll included a pool of 5000 enterprises, from which 450 enterprises were chosen randomly. The multiple-choice questions gathered information about the purpose and significance of the measurements, also needs and volumes of measurements. One of the important aspects was to learn about the relations between measurement accuracy, false measurements and costs through rework, discount and scrapping.

### 3. COSTS

The direct impact of metrology lies in the costs caused by equipment, facility and employees and in the revenue created by metrology tools, like knowledge and avoidance of scrap or excessive production steps. Average annual spending on metrology according to the answered enterprises is 4398€ The measurements are affecting about 80% of enterprises in a significant manner.

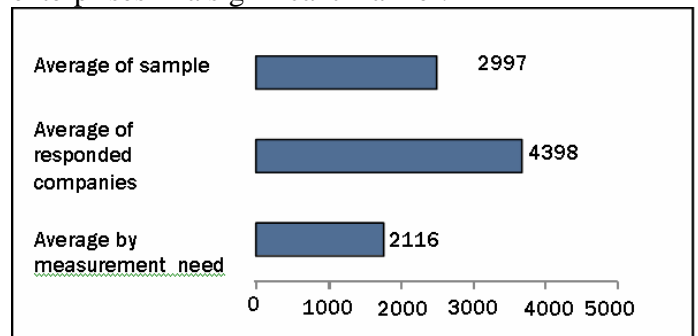


Illustration 1. Annual spending on measurements, €

Over half of enterprises (54%) expressed that failure in measurement or false measurement result affects the ability to sell product or services. The most dependent on measurements are machinery and metal work sectors, furniture production, production of non-metal minerals and agriculture.

About one third (33%) of the respondents said, that they could not sell their product, when it is out of specification. The fraction of 17% of answerers said, that they should do 5-20% discount but only 8% stated, that they do not need to make a discount to sell the product. To summarize, it can be said, that measurements affect at least 79% of the whole revenue produced in Estonia.

Most of the enterprises use measurements for end-product quality control. Very important is the use of metrological tools in process control, raw material control and work environment monitoring.

Especially sensitive to the quality of measurements in Estionia are processes and products in machinery and metal production

sector, furniture production food, printing sector and non-metal mineral production. Also, these sectors can be found in the top of the most exporting industrial sectors in Estonia. The sectors, which produce most of sales revenue and depend highly on metrology, are power production (1,3 bln €), food industry (1 bln €), metal and machinery production (0,85 bln €) and wood industry (0,8 bln €).

The total metrology related expenditure of the enterprises, which took part of the poll, was 1,34 mln €. The most of it, 21%, is spent on chemical analyses, 20% on mass, 19% on temperature, 14% on dimensional and 26% on other types of measurements.

A part of chemical analyses is done for environmental monitoring purposes. It must be brought out, that most of the environment taxes are based on measuring the extent of impact on environment. This includes greenhouse gas, fuel, pollution and many other measurements. The results are the base for applying certain taxes or regulatory obligations on the company.

A good example is the measurement of sulfur levels in ship fuel and its direct impact on transportation cost. This cost causes indirect costs also to the other industrial sectors and operators. The quality of the measurement is therefore very important because of the risk involved.

#### 4. TECHNICAL SITUATION

Metrology is used mainly for quality control purposes including checking of final products as well control of raw materials and process management. In all of the surveyed sectors the most of measurements are conducted for purpose of control of final products. Only 2,7% of the enterprises were not able to specify the purpose of the measurements, which shows, that the knowledge about the role

of measurements and metrology in business processes is well established. In electrical appliances and electronics industry the measurements are conducted moderately in quality control of end products. This shows the diversity of sectors and the difference of needs for metrology.

For products and processes in metal and machinery, furniture, food and print industry accuracy of measurement is essential. These sectors are the most important contributors to foreign trade. For that reason, it is very important to ensure the fulfillment of their needs to not harm the continuity of quality control in those sectors.

Legal metrology affects industry through the measurements taking place in trade and in customs. Mostly the measurements are conducted in the fields of mass, volume, length and different concentration. The direct impact can be expressed to alternative cost which is caused by measurement uncertainty. In that sense measurement uncertainty is used to estimate the possibility of giving or receiving more or less goods, than stated. It could be described as following equation:

$$\text{Uncertainty (\%)} \times \text{cost (€)} = \text{alternative cost of uncertainty (€)}$$

Equation 1

Therefore it is very important to set the optimal legal maximum permissible error limits by the state, so that the risks related to alternative cost of uncertainty for all sides of trade would be as low as possible and in mean time be economically feasible. These regulatory limits set also obligations and additional cost for traders.

Other tools in industrial metrology are mostly aimed to protect the customers from unacceptable quality products. Well established control system helps enterprises to avoid unnecessary costs coming from ill-production, logistics of out-of specification products and warranty costs.

To find out the impact of industrial metrology a magnitude of a mistake in measurements was

estimated which could be acceptable in production, so that the products must not be scrapped. The results of poll showed, that it is allowed to make up to 4% of measurement mistakes. This number must be considered with caution, because every sector has specific features. In addition, some of work-environment measurements, which might have a quite large measurement uncertainty, can affect the aforementioned average estimate significantly.

If the companies' mistake making rate is over 4%, then 33% of the respondents must totally scrap their production. This is a very large amount of products. Additionally, there are quite high costs for rework. Finally, only 9% of answerers said, that it might be possible to sell their products without making any reductions or additional costs.

Another important technological issue of measurement is the time aspect. Measuring of products takes certain amount of time, which can be converted to costs in some more or less direct way. When the metrological tools used in quality control, are in irregular calibration or in verification and, therefore, cannot be used at the moment, the production stops or running of the production possesses a higher risk of producing inadequate products.

Therefore it is important to establish a well functioning metrological infrastructure to minimize the time, during which the measuring and control equipment is out of use. Until now, most of the metrological infrastructure is meeting the needs of industry. The quality of calibration facilities is up to needs- most of the measurement ranges and uncertainty ranges are covered, but in some measurements, eg dimensional, mass, electrical quantities as well chemical analyses, the responsiveness of calibration service is somewhat

problematic. This can be due to several reasons: measurement range, uncertainty and time for service, which can even set higher demands in future.

## **5. NEEDS**

The needs for measurements in industry were studied for the next 3 to 5 years future. In general, the most important was to improve the measurement accuracy and the timeliness of measurements.

The need for achieving more accurate results shows different trends. The companies' tasks are two-fold: fulfill legal requirements and, in order to stay competitive, tighten quality control measures.

The importance of working environment monitoring is constantly growing. In 2007 a survey about chemical analyses was carried out, which showed, that only 11% of enterprises were using measurements for work environment monitoring. In 2011 already 47% of enterprises were measuring working environment parameters. The importance of this marker is much higher, taking into consideration, that in 2007 only medical and food industries were studied, as these are some of the sectors, where environment monitoring regulation requirements are very high.

Needed accuracy of measurements is different in different measurement categories. This is causing some problems of investment planning of metrological infrastructure. Therefore it is very important role of metrological facilities to listen to their customers to be informed about the movements of economy. Rapid changes in economical environment are also causing rapid changes in the needs for measuring capabilities, which can somewhat problematic.

In Estonia, there have been made some significant investments to different R&D enterprises and projects during last years. In such a small country as Estonia, it is important to follow, that the infrastructure is not duplicated and out of work. On the other hand, it is important to provide R&D breakthroughs access to needed measurement equipment at a reasonable cost.



The employees of 64% answered companies and institutions were qualified for current work. On the other hand, 35% enterprises need workers with a better qualification or they need additional training. In addition to industry, also medical and R&D companies expressed a growing need for college-degree specialists, who have a good understanding of measurements in applicable field.

## **5 SUMMARY AND CONCLUSIONS**

The costs on metrology reflect the use of investments very well, although the measuring of the effectiveness is quite difficult. The simplest way to express the effectiveness is through alternative cost. This shows also the undeveloped method for estimation of the effectiveness of metrology- nobody notices metrological infrastructure, when it is well functioning and, therefore normally, it is rather difficult to justify the investments basing on macroeconomics. However, if the infrastructure is performing poorly, it affects dramatically all parties of industry, life quality and sustainability.

This survey is mainly based on polls and statistical information gathered by Statistics Estonia. The objectivity of the reflection of the situation was affected by the scope of 450 answerers. In some branches the subject group was too small to make generalizations of the situation.

The survey showed that metrology affects most of the branches significantly, because measurements are used in quality control mechanisms. As the quality control becomes gradually more important for the enterprises, the importance of measurements is growing. The most metrology-intensive branches are machine and metal industry, furniture production and food industry in Estonia.

It was found, that chemical analyses are the most important measurement type in the production sector, followed by mass

and related measurements. force, torque and weight measurements.

Legal metrology affects industry mostly through trade and environmental taxes. The most important types of measurements in legal metrology are mass and volume measurements and chemical analyses.

The companies stated, that in the next 3-5 years measurement accuracy and timeliness will be more and more important. The importance of accreditation is steady, because it is becoming self-evident. The importance of timeliness shows, that Estonian industry enterprises pursue effectiveness by trying to minimize the downtime caused by maintenance and control.

The working environment measurements are getting more and more important. The difference between 2007 and 2011 is showing dramatically growing interest in acoustics, temperature and other directly working environment related measurements as it is also verified by interviews.

It was found that metrology has the most substantial impact on main industry branches in manufacturing cost optimization. The availability of reliable measurement services is essential for a well-functioning company, industry and whole economy. The annual expenditures on metrology are approximately 28-40 million € facilitating companies to avoid unnecessary additional costs of manufacturing estimated in total 2,8 billion € per year in Estonia. The survey is to be repeated in the future in order to see trends over the years.

The survey indicated that reliable measurements are needed for Estonian industry for quality control, process control and other purposes. The costs carried out by industry are significant and they would grow dramatically, if there would be problems with current service providers. Therefore there is a growing need for a well established metrological infrastructure providing diversity related services.

## 7. REFERENCES

- „Measuring the Impacts of Science: Beyond the economic Dimension”, Benoit Godin and Christian Dore, [http://www.csiic.ca/PDF/Godin\\_Dore\\_Impacts.pdf](http://www.csiic.ca/PDF/Godin_Dore_Impacts.pdf)
- The Impact of Metrology in the economy, industrial companies and quality of life“ [http://cim2010.com/CIM/comunicac/ACruz\\_IPQ\\_The%20Impact%20of%20Metrology.pdf](http://cim2010.com/CIM/comunicac/ACruz_IPQ_The%20Impact%20of%20Metrology.pdf)
- „Economic Impact Report Metrology Investment: Impact on Innovation and Productivity“ <http://www.bis.gov.uk/assets/bispartners/nmo/docs/nms/economic-reviews-august-2010-updates/economic-impact.pdf>
- Keemiliste analüüside ja mõõtmiste hetke- ja arendamisvajadused Eestis. Ivo Leito, Ivari, Kaljurand, Reet Tallo, Kristina Virro. Tartu Ülikool, Bradley Dunbar Associates Estonia OÜ, Tartu, Tallinn 2007.
- Eesti Statistikaamet [www.stat.ee](http://www.stat.ee)

## 8. ADDITIONAL DATA ABOUT AUTHORS

1) Author: Kaarel Simson, R&D specialist, Metrosert AS

2) Title of manuscript ”Metroloogia infrastruktuuri, metroloogia mõjude ning mõõteteenuste hetke- ja arendusvajaduste uuring”

3) Kaarel Simson, R&D specialist, Metrosert AS, Aru 10, Tallinn, Estonia, tel +372 5836 0825, [Kaarel.Simson@metrosert.ee](mailto:Kaarel.Simson@metrosert.ee)

2) Co-authors:

Toomas Kübarsepp, R&D director, Metrosert AS, Aru 10/Tallinn University of Technology, Department of Mechatronics, Ehitajate tee 5, Tallinn, Estonia, tel. +372 681 4815, [tkubarsepp@metrosert.ee](mailto:tkubarsepp@metrosert.ee)

Ivo Leito, Head of Chair of Analytical Chemistry, University of Tartu, Ravila 14a, Tartu, Estonia, tel. +372 518 4176, [ivo.leito@ut.ee](mailto:ivo.leito@ut.ee)

Marikai Karilaid, Partner, BDA Consult OÜ, tel. +372 627 4414, [info@bda.ee](mailto:info@bda.ee)

Harli Uljas, Partner, BDA Consult OÜ, Tatari 64, Tallinn, Estonia, tel. +372 627 4414, [harli@bda.ee](mailto:harli@bda.ee)

Liina Karotamm, Project consultant, BDA Consult OÜ, Tatari 64, Tallinn, Estonia, tel. +372 627 4414, [liina@bda.ee](mailto:liina@bda.ee)

Märt Parker, BDA Consult OÜ, Tatari 64, Tallinn, Estonia, tel. +372 627 4414, [mart@bda.ee](mailto:mart@bda.ee)

Margus Metssalu, tel. +372 627 4414, [margus@asiconsult.ee](mailto:margus@asiconsult.ee)

## INK-JET PRINTING OF PHARMACEUTICALS

**Takala, M.; Helkiö, H.; Sundholm, J.; Genina, N.; Kiviluoma, P.; Widmaier, T.; Sandler, N. & Kuosmanen, P.**

**Abstract:** *Traditional tablet manufacturing process has multiple powder handling and mixing phases. It is time consuming and limits individualized dosing. Furthermore, uniformity of the dose is difficult to achieve. Modern ink-jet printing technology has been successfully applied to polymer electronics and biomaterial applications. It has many advantages that could be utilized in drug manufacturing process, such as faster production cycle with fewer processing steps, precise dosing, on-demand individualized dosing and possibility for on-line quality control. This study examines how well current printer technologies function in printing different types of drug solutions on paper-like substrate. Preliminary tests were carried out with paracetamol and riboflavin-water solutions. The study denoted that printing medicines and bio-polymer coating was possible, the accuracy of dose was very satisfying and personalized dosing was easy to achieve. Further studies with specially manufactured printers are still needed to determine the suitability of the ink-jet printing process in commercial drug manufacturing.*

*Key words: thermal, piezoelectric, print head, paracetamol, riboflavin, personalized dosing.*

### 1 INTRODUCTION

Manufacturing of pills is currently time consuming and often inflexible. That is because the manufacturing process consists of multiple phases, which are

necessary with the technology and methods applied in pharmaceutical industry. Furthermore, the control of the correct dose is done in post-production where random pills are taken to be examined to verify the correct content through statistical methods [1]. Sometimes the amount of the active ingredient in a pill can be very small, which means that the size of the pill has to be increased with added ingredients in order to make it large enough for even picking up from the table. For example, a nitro heart and artery medicine pill has a 0.5 mg active dose of glyceryl trinitrate, whereas the pill itself weights approximately 110 mg. By introducing technology used in printers it could be possible to make the process faster, more accurate, more dynamic and easier to control. Printing technology makes it possible to directly inject active ingredients onto the surface of an edible substrate thus creating drugs that react faster. Compared to a medicine droplet, ink-jet droplet can be up to 20 times smaller [2]. On top of that, new possibilities arise when multiple active ingredients could be injected onto the same surface. MIT has done research concerning the use of a 3D printer in pill manufacturing. Their method included both creating the actual pill and injecting the dose into it [3].

The goal of the present study was to determine if ink-jet techniques can be used in pill manufacturing and how accurate they would actually be. This was done by selecting different manufacturers' low-end printers with different ink-jet technologies and performing a

series of repeated tests and measuring the results.

## 2 METHODS

### 2.1 Printers

The tests were initially intended to perform with two different commercial printers: HP Photosmart B010 (**Fig. 1**) and Epson Stylus SX 425W. The purpose of using two different printers was to test which technology is more suitable for pharmaceutical printing – thermal ink-jet or piezoelectric ink-jet. HP utilizes thermal ink-jet print head and Epson piezoelectric ink-jet print head. However, from the beginning the piezoelectric printer was found to be unable to print any substance. Due to that all of the analysed results are from the thermal ink-jet printer.

The difference in these two technologies is in the way the ink-droplet is formed. Thermal ink-jet uses a heat element – a small resistor – to create heat in order to cause the ink to vaporize and to create a bubble. When the bubble expands it pushes ink out of the nozzle. As the bubble collapses it creates a vacuum, which causes more ink to be pulled from the cartridge into the print head [4] (**Fig. 2**). Piezoelectric printer uses a small crystal at the back of the ink reservoir in each nozzle. Small electrical current is led to the crystal, which causes the crystal to vibrate. When the crystal expands, an ink droplet is forced out of the nozzle and when the crystal contracts, it pulls more ink from the reservoir [5] (**Fig. 3**).



Fig. 1. HP Photosmart B010

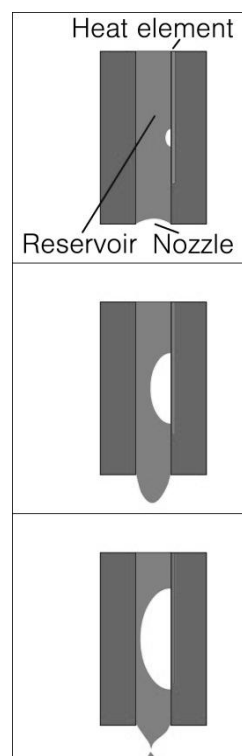


Fig. 2. The principle of bubble jet nozzle [6]

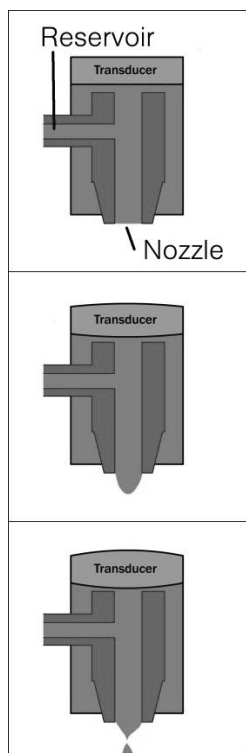


Fig. 3. The principle of piezoelectric nozzle [6]

Tests were made by replacing original ink cartridges with cartridges filled with riboflavin-water-glycerol solution and paracetamol-water-glycerol solution. Small squares were then printed on a standard paper, photo paper and transparent film to determine how well the printers were able to print other liquid than ink. The squares were analysed with a microscope and an UV/VIS-spectrophotometer in order to resolve the amount of pharmaceutical in one printed square and also to find out whether the squares pervaded on the paper or not.

Same test procedure was designed for both types of printers.

## 2.2 Software

A printer firmware is a control software inside the printer. Its task is to interpret the image sent to the printer into a series of signals sent to different actuators such as print head, paper feeders and stepper motors [7].

When printing a coloured image the firmware is given a CMYK-value for every pixel that needs colouring from the printer driver program. CMYK-values

define how the firmware uses cyan, magenta, yellow and black inks to formulate every coloured pixel.

Printer driver is the software that communicates with the printer itself. Its main task is to transform images and texts into a form that the printer understands. Commonly images are presented in RGB colour space when viewed from a computer. By default the printer driver does some colour management to define the best possible CMYK values for the printing device. This leads to situations where, for example, pure RGB yellow is not given as pure CMYK yellow to the printer and thus the printed yellow colour is a composition of ink from multiple ink cartridges.

To be able to print different drug solutions poured into the ink cartridges, the printer is needed to be controlled in a way that guarantees the printed solution contains pure 'cyan', 'magenta', 'yellow' or 'black' drug. For this purpose drug printing software was created (Fig. 4). Its main objective is to produce identical sets of drug doses on a paper substrate, which can then be analysed. Furthermore, it makes it easier to produce different kinds of test samples without the need of writing down every change made to the test. Every parameter of the test can be automatically printed onto the test substrate.

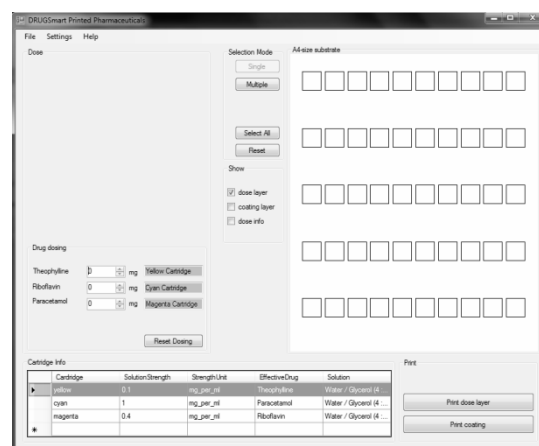


Fig. 4. The user interface of drug printing program.

Another reason for building software is to demonstrate the whole process of printing pharmaceuticals to a substrate in an understandable way. Printing different colours with a common graphic program is not very informative. The ability to change the actual effective drug and drug dosing instead of different colours and colour hues gives way better impression of the process.

The concentration of the dose is proportional to the colour intensity. If the printer is set to use only yellow cartridge, the colour intensity is the Y-value of the CMYK-values. When low Y-value is set for a certain area the printer jets droplets in large intervals but when high Y-value is set the jet interval is much lower and the surface is visually more constant.

There are few parameters that are needed to resolve, before it is possible to print the needed amounts of riboflavin or paracetamol on a substrate. A common ink droplet ranges from few to ten picoliters. But what is unknown is the amount of solution the printer jets in one square and how linearly the solution consumption rise when printing test pages with identical squares of the drug solution but different drug concentration. The exact amount of drug solution printed on the substrate will be calculated with the help of UV/VIS-spectrophotometer. When multiple test sheets are analysed the results can be parameterized for the printing software and the used printer model. Then known amounts of active pharmaceutical ingredient can be printed on a substrate from the software.

### 2.3 Testing method

A series of test samples were printed with the software and HP Photosmart B010 printer. The yellow ink cartridge was filled with the drug solution and other cartridges were left empty. Riboflavin sodium phosphate (RSP) (riboflavin 5'-monophosphate sodium salt, Ph. Eur., Fluka Analytical, Sigma-Aldrich, France)

was used as water soluble active pharmaceutical ingredient (API) of orange colour. Glycerol (85%) was used as moisturizer and viscosity modifier. Purified water was used as a solvent. Printing was done on two different substrates: usual copy paper and photocopy paper (**Fig. 5**). Different printing quality settings were used to analyse visually the linearity of the colour hue when increasing the colour intensity from 10 to 100.

### 2.4 Content analysis

Visual analysis was performed with Olympus BH-2 microscope. Further analysis was performed in water by using UV-VIS spectrophotometer (Perkin Elmer, Lambda 25, Germany). Each printed area was cut out, put into 1.5 ml of purified water, mixed and incubated for 1 to 3 h. The absorbance values of the solutions were measured at 267 nm. Seven areas were used for each concentration printed. In addition, blank copy and photocopy paper samples were used as reference material.

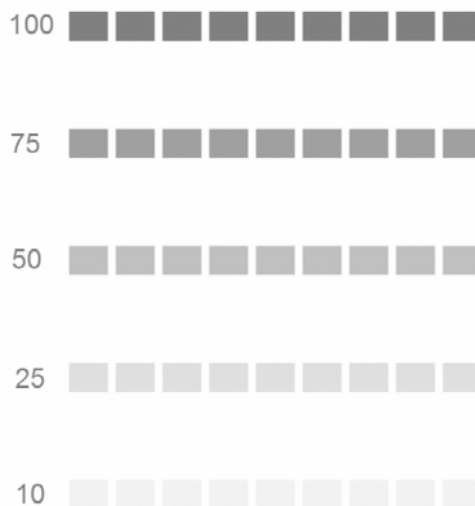


Fig. 5. Printed RSP on photocopy paper. Concentrations printed: 10, 25, 50, 75 and 100.

## 3 RESULTS

The visual analysis of the prints with the Olympus BH-2 microscope showed a clear difference in colour between 10, 25

and 50 colour intensities but no visual difference in colour between 50, 75 and 100 colour intensities. **Fig. 6** shows the print quality with two different quality settings and two different dose intensities. The doses are printed on a transparent film and the pictures are taken from one corner of the printed squares.

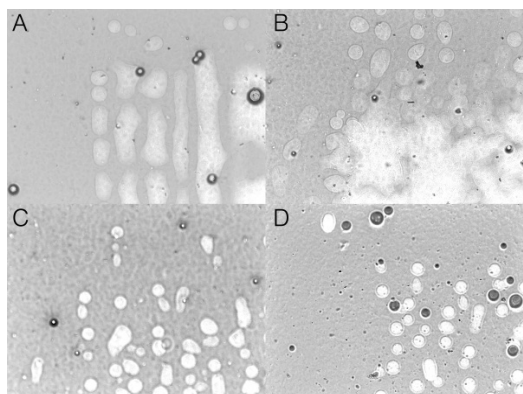


Fig. 6. Microscope images of different samples of riboflavin-water-glycerol printed on an overhead film. (A): 100 per cent dose with normal print quality. (B): 100 per cent dose with best printing quality. (C): 25 per cent dose with normal print quality. (D): 25 per cent dose with best printing quality.

The content of API in the copy and photocopy paper was similar (**Fig. 7**). The content analysis confirmed the results obtained by visual observation of the intensity of colour in the printed areas. There was no linear correlation between the expected printed amount and actual content.

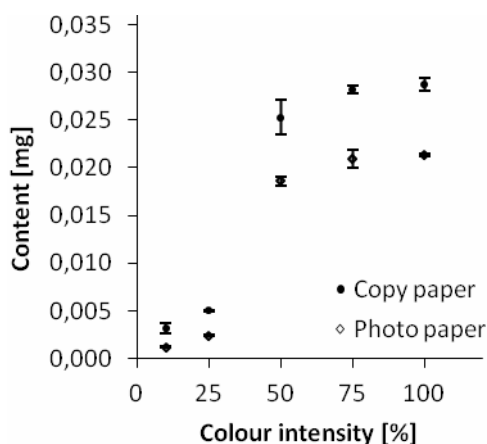


Fig. 7. The content analysis of RSP printed areas. Data are presented as mean  $\pm$  SD (n = 7).

The results with the UV/VIS-spectrophotometer support initial visual analysis. The printer does not increase the amount of printed solution linearly when using 'normal print quality'-setting.

The low standard deviation of the tests clearly showed that the solution concentration was constant through the different tests. This makes the dosing very accurate after the printer and the software are calibrated.

#### 4 DISCUSSION

Initially piezoelectric based printers were thought to work better due to not-so-complicated liquid dynamics. They enable the viscosity to be higher and accommodate other than water-based solutions [5]. However, Epson failed to print anything. Sometimes the solution did not even eject the cartridge into the print head assembly. There are multiple possibilities why they do not function but one major issue could be liquid viscosity. If the viscosity is too high, the pharmaceutical ink is not able to flow through the printer head. Then, if the viscosity is too low, the pharmaceutical ink will go through the print head even when it is not supposed to do so. There is no undisputed information why it is so difficult to print with piezoelectric printers. Therefore, more studies about liquid viscosity and surface tension needs to be made.

Even though thermal ink-jet proved to be applicable technique for printing pharmaceuticals, commercial ink-jet printers are not applicable straight out of the box due to their fault sensitivity. Test printer tended to malfunction, because the drugs dried up so easily on the print head. It would also be vital to get to the firmware of the printer because it is important to know that the printer prints just the required amount of pharmaceuticals. Also the reactions in the solution caused by the thermal element should be considered.



The tests proved that the amount of printed pharmaceutical did not correspond to the amount it was supposed to print with 'normal print quality'-setting. There are few possible reasons for this: the printer still does some colour corrections for the CMYK values or the viscosity of the solution makes the solution either jet in an uncontrollable way or prevents the solution to jet altogether. Also the used 'normal print quality' prints a row of squares in one sweep whereas using best quality results in multiple sweeps per row. Visual analysis indicated clearly that a single sweep gave poor linearity of the different doses. Using 'best printing quality' results in a significant improvement of the linearity between the different dose concentrations.

The tests proved that there is a lot of potential in pharmaceutical printing and it can change the way drugs are manufactured and delivered in the future. One possible scenario could, for example, be that instead of making pills, the drug companies could deliver different ready-to-use formulations of their drug, which could then be printed on demand in the local pharmacy.

Although more research has to be made in order to fully determine the possibilities of drug printing, this research gave insight of some of the challenges that need to be faced before making printable drugs as an alternative solution to pill manufacturing.

## 5 REFERENCES

- [1] Sandler, N., Määttänen, A., Ihalainen, P., Kronberg, L., Meierjohann, A., Viitala, T., Peltonen, J. 2011. *Inkjet Printing of Drug Substances and Use of Porous Substrates-Towards Individualized Dosing*. Journal of Pharmaceutical Sciences Volume 100, Issue 8 (2011-08-01), pp. 3386-3395. ISSN 1520-6017
- [2] University Of Leeds News. 2010. *New research into safer drugs puts pills through the printer*. Available: <http://www.engineering.leeds.ac.uk/faculty/news/2010/safer-drugs-puts-pills-through-the-printer.shtml> . (10. 3. 2012)
- [3] MIT Tech Talk. 1997. *Medicines are 'printed' into pills*. Available: <http://web.mit.edu/press/1997/pills-0416.html> . (10.3. 2012)
- [4] Magdassi, S. 2010. *Chemistry of inkjet inks*. World Scientific. ISBN: 978-981-281-821-8.
- [5] Wijshoff, H. 2010. *The dynamics of the piezo inkjet printhead operation*. Physics Reports vol. 49 pp. 77-177.
- [6] Tyson, J. 2001. *How inkjet printer works*. Available: <http://computer.howstuffworks.com/inkjet-printer.htm>. (1.3.2012).
- [7] Sen, A.K., Darabi, J. 2007. *Droplet ejection performance of a monolithic thermal inkjet print head*. Journal of micromechanics and microengineering Vol. 17. DOI:10.1088/0960-1317/17/8/002

## 6 CORRESPONDING ADDRESS

Panu Kiviluoma, D.Sc. (Tech.), Post-doc researcher  
Aalto University School of Engineering  
Department of Engineering Design and Production  
P.O.Box 14100, 00076 Aalto, Finland  
Phone: +358 9 470 23558,  
E-mail: [panu.kiviluoma@aalto.fi](mailto:panu.kiviluoma@aalto.fi)  
<http://edp.aalto.fi/en/>

## 7 ADDITIONAL DATA ABOUT AUTHORS

Takala, Marko, B.Sc (Tech)  
E-mail: [marko.takala@aalto.fi](mailto:marko.takala@aalto.fi)

Helkiö, Henri, B.Sc (Tech)  
E-mail: [henri.helkio@aalto.fi](mailto:henri.helkio@aalto.fi)

Sundholm, Joni, B.Sc (Tech)  
E-mail: [joni.sundholm@aalto.fi](mailto:joni.sundholm@aalto.fi)

Widmaier, Thomas, M.Sc (Tech)  
E-mail: [thomas.widmaier@aalto.fi](mailto:thomas.widmaier@aalto.fi)

Kuosmanen, Petri, D.Sc. (Tech.), Prof.  
E-mail: [petri.kuosmanen@aalto.fi](mailto:petri.kuosmanen@aalto.fi)

Niklas Sandler, PhD (Pharm.), Prof.  
[niklas.sandler@abo.fi](mailto:niklas.sandler@abo.fi) \*

Natalja Genina, PhD (Pharm.)  
[natalja.genina@abo.com](mailto:natalja.genina@abo.com) \*

\* Pharmaceutical Sciences  
Department of Biosciences  
Åbo Akademi University  
Tykistökatu 6A  
FI-20520 Turku, Finland

## DIAGNOSTICS OF DRUM TYPE WOOD SHREDDER MACHINES

Zarins, M., Torims, T. & Vilcans, J.

**Abstract:** *This paper investigates diagnostic methods and proposes modern service technologies for wood-processing equipment. The aim of this study is to ensure systematic, research-based wood-processing services and continuous, no-failure operation of facilities. We describe the working principle of a particular industrial, drum-type wood shredder and discuss the problems that occurred during operation, including potential excess engine load or construction imperfections. Cutting regime calculations are provided, along with a description of actual improvements and a comparison of cutting regimes before and after improvements. The intended result of this research is a monitoring unit which, with help of a few modifications, can be used on any drum-type wood processing equipment.*

*Key words:* List 4-5 keywords. (wood-processing facilities, drum-type wood shredder).

### 1. INTRODUCTION

This paper is based on the dissertation and research conducted during its preparation. It is the first paper on the subject, describing the problem of the dissertation, the attainable target and a reflection on the research process at the present stage.

Given the current complex economic situation, employers are obliged to optimize their manufacturing processes and reduce the prime cost of an item, in a bid to survive and remain profitable. One means of saving is in manufacturing facility maintenance and repair.

It is possible to reduce expenditure on spare parts and avoid sudden stoppages by

modelling a modern, thought-out, research and diagnostics based manufacturing facility service. A diagnostics model of the junction condition can be developed by performing a series of cyclic measurements and analyzing the results. In this way, the precise moment can be identified when expenditure on complementary parts resources is timely but not destructive.

The present research has been conducted in cooperation with Latvijas Finieris, Ltd, which is the leading secondary wood processing company in Latvia and has a very large number of manufacturing facilities at its disposal.

All of these require constant maintenance and repair, which usually results in major financial outlays. Added to this, sudden stoppages of manufacturing facilities for unscheduled repairs generate significant losses.

The focus of the current research is investigation and analysis of a waste wood shredder machine. At the present research stage, the setup has been carefully studied, its working principle and analysis have been conducted. The main problems and their probable causes have been identified. The work accomplished so far provides a basis for further study, for choosing measuring instruments and the appropriate methodology, as well as for developing a common service system.

### 2. FIELD OF APPLICATION

The object of the study is a drum-type wood shredding machine designed to process large amounts of waste wood into woodchips. We expect that results will be unified and applicable to any kind of drum-type wood shredder diagnostic system and service technology elaboration.

### 3. PROBLEM STATEMENTS

At this moment we have defined several problems related to setup of the operation process.

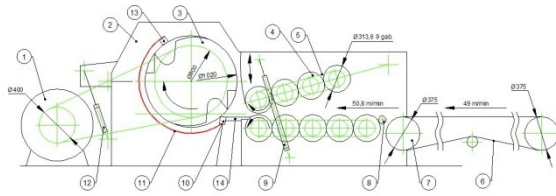


Fig. 1. Shredder setup RAUTE TR 1020 – 1300 V kinematic scheme

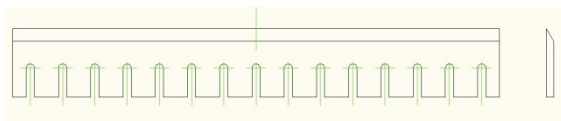


Fig. 2. Blade sketch

Mostly these are connected with high dynamic loads, which occur in junctions during shredder machine operation.

The following problems in particular have been identified: (fig. 1., 10) corpus squirm; posterior counter knife deformation (fig. 1., 13); stowage of forward lead-in plate (fig. 1., 14) fixation screws and working blade wear (fig. 2).

Mainly, the impact initiated by the blade at the moment when the wood chip is chopped from the whole chipping mass is such that the load is delivered to the first supporting blade. The load is large enough to squirm the counter knife casing, see fig. 3.

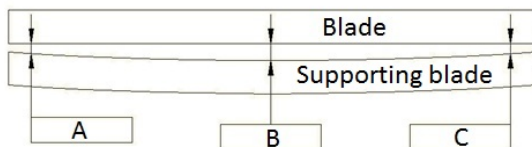


Fig. 3. Deformation of supporting blade.

When regulating the machine, a gap of 0.4-0.7 mm must be set between the blade and the supporting blade. After the said supporting blade casing deformation, it becomes impossible to restore the necessary gap. In particular, if the gap is set in the middle, the edges of blade go into

the rotating blades operation zone; but if the regulation is performed at the edges, the middle gap becomes too large for the supposed standard. Engaging the squirmed supporting blade in the cutting process leads to increased loads in the working area and the wood chip quality decreases.

A load increase is induced not only by the blade-supporting blade gap, but also by normal blade wear which is inevitable. At this moment it is a common practice to use re-sharpened blades after a two-week working cycle. This service model is accepted and implemented without any theoretical background, there are no experimental results to affirm or refute the necessity of the described service cycle model.

Increasing cyclic loads in the shredder working area also increases load on the main engine. As a result there have been a number of cases of main engine overload and even fires.

### 4. RESEARCH COURSE

#### 4.1. Data output

A summary of the working process describing parameters was required in order to undertake any kind of analysis and calculations. Some of these parameters have been partially changed in order to find precise values, and direct measurements have been performed. The main parameters and discrepancies between factory data and real setup working parameters can be seen in Table 1.

Parameter	Factory data	Actual data
Rotor diameter (mm)	1020	1020
Feed roll diameter (mm)	313.6	313.6
Rotor revolutions (rpm)	493	556
Supply speed (m/min)	50	44
Number of blades	2	3
Input hatch dimensions (mm)	1310x375	1310x375

Main engine power (kW)	200	200
Main engine revolutions (rpm)	1000	1000

Table 1. Shredder machine main parameters

#### 4.2. Cutting process characteristic calculations

Further calculations that characterize the cutting process describe parameters and their real value compared with those announced by the manufacturer.

The difference is expressed in percentage form relating to the initial value, in order to evaluate the significance of discrepancies.

- Cutting speed

Cutting speed depends on the rotor diameter and revolution count. The rotor diameter remains constant while revolution count was altered therefore, cutting speed  $v$  is:

$$v = \frac{\pi \cdot D \cdot n}{100} \quad (1)$$

where:

D – rotor diameter

n – rotor revolution count per minute

$$v_{original} = \frac{\pi \cdot 1020 \cdot 493}{1000} = 1580m/min$$

$$v_{real} = \frac{\pi \cdot 1020 \cdot 556}{1000} = 1782m/min$$

We can easily see that increasing the rotor revolution count leads to a cutting speed increase of approx. 12%.

- Supply speed on the teeth

Supply speed on the teeth depends on supply speed in one minute, rotor revolutions and the number of teeth in the rotor.

$$S_z = \frac{S_m}{n \cdot z} \quad (2)$$

where:

$S_m$  – supply speed in one minute

$z$  – number of teeth

$$S_{zoriginal} = \frac{50}{493 \cdot 2} = 0,051m/z \rightarrow 51mm/z$$

$$S_{zreal} = \frac{44}{556 \cdot 3} = 0,026m/z \rightarrow 26mm/z$$

By setting more teeth in rotor, the revolution count has increased by 13%, supply speed has reduced by 12% and feed on the individual teeth has reduced by 51%. Accordingly, mean length of manufactured wood chip has reduced. At the same time, the aforementioned alterations have reduced the overall load on the shredder.

#### 4.3. Shredder vibration forecast

The main cause of vibration in the working process is the floating/variable load, which occurs because of the cyclic entrance of blades into the working area.

The oscillation frequency is constant and can be easily obtained by equation 3. The variable value is the oscillation amplitude, depending on the amount of in-coming shredding material at a precise moment and condition of blades. The amount of supplied material is the time variable and hardly prognosable value because the amount depends on working modes of other related setups. It is not necessary to estimate described oscillations individually. But knife wear provokes regular amplitude raise, which include also oscillations caused by the amount of crumble mass alterations.

$$F = \frac{z \cdot n}{60} \rightarrow \frac{3 \cdot 556}{60} = 27.8Hz \quad (3)$$

where:

$z$  – number of rotor teeth

$n$  – rotor revolution count

As seen from the calculations, the basic oscillation/ vibration frequency is 27.8 Hz. This specific amplitude will be the main factor by which to draw conclusions about the condition of the blade and supporting blade.

## 5. METHOD USED, STATUS AND RESULTS

Currently measurements are being taken at regular intervals to reflect changes in the blade and supporting blade interaction during working process. This is achieved by measuring the gap between the blade and supporting blade at three points, once a day (figure 4, points A, B, C). These readings show both the progress of supporting blade deflection and total wear on the blade and supporting blade. As the in-situ experimental process is currently in the initial stage, the amount of gathered data is insufficient to give a statistically reliable description of wear progress or to develop a mathematical model that describes this process.

Up-to-date results relate to shredding machine working principle research and analysis, defining actual working characteristics and calculations. At this point, the main constructive improvements for the shredding machine have been defined, mentioning that further study can not take place without these improvements. The most problematic and important junction points have been defined, which require new service technology consisting of regular junction condition follow-up and a diagnostic-based maintenance system.

## 6. FURTHER RESEARCH

The next stage is to summarize blade and supporting blade interaction measurement data and place sensors under the supporting blade (figure 4). By setting up load sensors, it will be possible to follow-up and analyze over time the effect of increasing loads on the supporting blade.

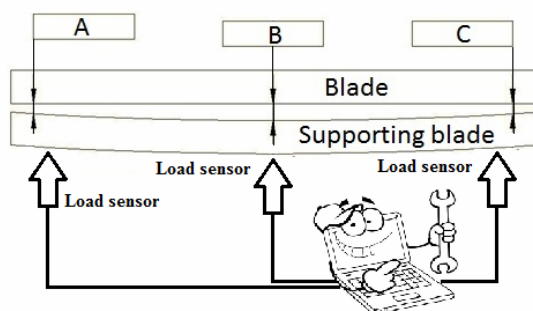


Figure 4. Measurement scheme

Following this, we shall define the relationship between the blade and supporting blade reciprocal wear condition and load sensor data, which in future will make it possible to perform indirect blade-supporting blade monitoring, based on load sensor measurement data. As a result of research, it is planned to develop a programme that will automatically signal when there is a need for facility maintenance or terminate operation of the facility, if necessary.

## 11. REFERENCES

1. Bershinsky A. L., Rezanie drevesini, Vishaia shkola, Minsk, 1975
2. Tuherms H., Kokapstrādes instrumenti, Zvaigzne, Riga, 1985
3. Holmberg, K., Helle, A. & Halme, J., Prognostics for Industrial Machinery Availability, presented at the International Seminar on Maintenance, Condition Monitoring and Diagnostics, Oulu (FI), 28-29th September 2005
4. Kalpakjian S. and Schmid, S. R., Manufacturing Engineering and Technology, Pearson Education Ltd., London, 2006
5. Measurement and control tools [WWW], <http://www.ge-mcs.com/en/bently-nevada-sensors-and-transducers.html>. (22.02.2012)

## 7. CORRESPONDENCE ADDRESS

MSc.ing. Marcis Zarins  
 RTU, Faculty of Transport and Mechanical Engineering, Department of Material Processing Technology,  
 Ezermalas 6, LV-1006 Riga, Latvia  
 Phone: +37126113009  
 E-mail: marciszarins@gmail.com

## MICRO-MACHINING PROCESS AND ITS EFFECTIVENESS

Zawada-Tomkiewicz A.

**Abstract:** *Industrial applications require functional surfaces with a highly defined microtexture. So, the engineered surfaces are additionally finished with the use of a wide range of finishing processes. The paper develops a multi-scale wavelet decomposition of surface image topography to characterize the various stages of finishing process. When modelling the changes in the components of the image, time to achieve the desired quality of the final surface was determined for each variety of finishing process.*

**Key words:** *machined surface, wavelet decomposition, surface image.*

### 1. INTRODUCTION

The abrasive process works by forcing the grains into the surface of the workpiece in such a way that each grain cuts away and simultaneously deforms a small amount of work material. The abrasive grain acts like a miniature cutting tool, when hard grains remove and displace work material by micro-cutting.

The combined shape of grains characterised by their density determines the geometry and morphology of the surface finish. Abrasion process is stochastic in nature because the movement and the geometric properties of grains are characterized by large statistical variability. In the paper the belt grinding process was described where four different cases of finishing were applied. Considerations were based on the machined surface images taken in time. In the paper, the 2D wavelet decomposition was used for the machined surface image description. Wavelet decomposition separated the

components responsible for roughness and micro-roughness. Analysis of energy distribution in components enabled the evaluation of micro-smoothing process in relation to the cutting time.

### 2. MODEL OF MICRO-MACHINING

Grains have a natural roundness of edges and in precision cutting applications when the thickness of the cut layer is comparable to the cutting edge radius, the ploughing or rubbing action can be substantial. Oxley in [1] explained the basics of the process of material removal for a simple case of cutting. At the same time his research showed that, although in practice tools with more geometrically complex shapes are used in material processing, the cutting mechanism for all of them is the same.

A rounded cutting edge affects significantly both the forces and temperatures during cutting, especially at chip thicknesses at or below the cutting edge radius.

When the thickness of the cut layer is smaller than the thickness below which it is unable to form a chip, the tool's active part elastically and plastically deforms the surface of the part. The diagram (Fig.1) shows a field of forces on the grain rounding. It is clear that if the thickness of cut is less than the minimum thickness (Figure 1, point 1), then the tangential force on the rounding may only have a sense consistent with the direction of the flow of the work material around the rounding [2]. Between point 1 and 2 there must be a point 3 (Figure 2) of cut layer separation for which the thickness of cut is the minimum thickness.



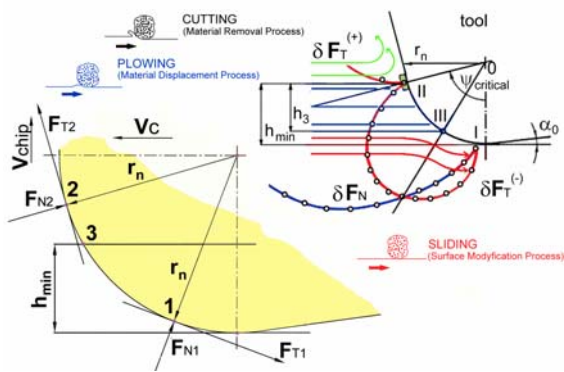


Fig. 1. Force field acting on the rounding of a cutting edge

Cutting and plowing are the most fundamental interactions in grinding, which modify the workpiece surface directly and dominate the material removal efficiency. Although the grain geometry may vary the grain tip can still be considered to include the nose radius. The nose radius typically reflects the sharpness of the grain and how aggressively the material can be removed.

## 2. EXPERIMENTAL PROCEDURE

Experiment concerns a belt grinding operation with a tool consisting of the geometrically calibrated abrasive grains of silicon carbide adhered to a polymer strip. The finishing film is applied on the rotating workpiece with a defined pressure and axial oscillations. This technique removes a depth of cut to  $4 \mu\text{m}$ . In order to assure a comparability of the results, in all the cases only one kind of finishing film was used, i.e. IMFF 9 A/O 1/2" [3].

Four different parameters were applied for micro-smoothing. There was used micro-smoothing, micro-smoothing with axial oscillations, micro-smoothing with buffing compound and micro-smoothing with axial oscillations and buffing compound. Each finishing was run independently. The quality of machined surface was evaluated every 30 seconds and the images of machined surface were taken with the use of optical system (field of view –  $1 \text{ mm}^2$ , depth of field –  $100 \mu\text{m}$ , resolution –  $0.8 \mu\text{m}/\text{pixel}$ ).

Metallic workpiece of C45 steel was prepared in a form of disc with a front face prepared by the grinding process. Then the finishing process was applied to smooth the machined surface. The finishing film and machined surface images are combined together in Fig. 2.

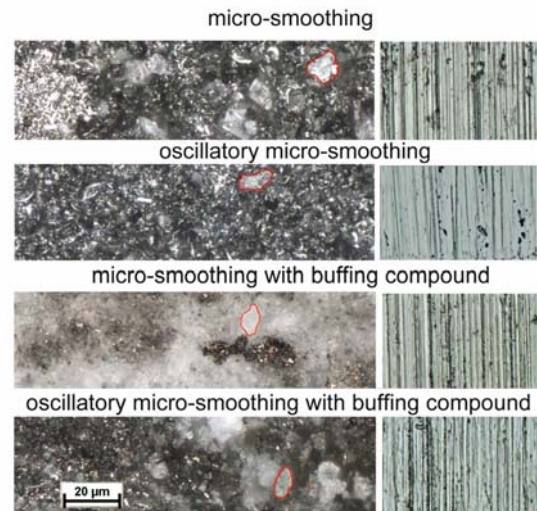


Fig. 2. Image of abrasive paper and machined surface (finishing time – 2.5 min) taken by Nikon Eclipse MA200

## 3. RESULTS AND DISCUSSION

The quality of machined surface was evaluated with the use of CCI 6000. Surface roughness area parameters were measured in five different regions located along the workpiece radius.

A global analyse of the surface topography before and after the belt grinding operation revealed that the belt grinding operation was able to delete the surface topography of the grinding operation. An observation of surface images shows a decrease in the magnitude of the marks. Moreover, the smoothing process deletes completely the “ravines” obtained by the previous operation if the cutting time is sufficiently long.

After the belt grinding operation, analysis was conducted so as to characterize the influence of the process on the surface topography (Fig.3). Measured values of surface roughness parameters were combined together with the surface parameters obtained for a longer time of

cutting considered as sufficiently long (reference surface). The parameters as a function of time were modelled using the model presented in Fig. 3.

The predicted finishing time was different for each of the finishing process. For surface roughness Sa parameter, the finishing time was several minutes for smoothing and smoothing with axial oscillations, seventeen minutes for the other cases of finishing. For surface roughness Sz parameter, the predicted time was two or three time greater.

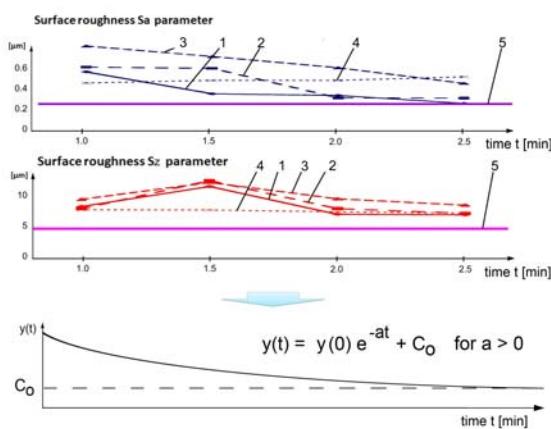


Fig. 3. Surface roughness area parameters in a function of finishing time: 1 - micro-smoothing, 2 - micro-smoothing with axial oscillations, 3 - micro-smoothing with buffing compound, 4 - micro-smoothing with axial oscillations and buffing compound, 5 – reference surface

Machined surface images were analysed to distinguish the difference between the components – energy content in relation to the vertical, horizontal and diagonal details [4]. The algorithm for energy counting consisted of three steps (Fig. 3). First the image was pre-processed. From the image the form was removed and the image was levelled. The second step in the algorithm was the wavelet decomposition. The decomposition enabled to obtain ten independent components (the 1<sup>st</sup> level – LH, HL, HH, the 2<sup>nd</sup> level - LH, HL, HH, the 3<sup>rd</sup> level – LL, LH, HL, HH). The third step in image processing algorithm embraced the energy computing for each of the component.

Figure 4 presents the total energy distribution. Each curve represents the

results for the particular finishing operation and is a result of summing up the energy of the components in time.

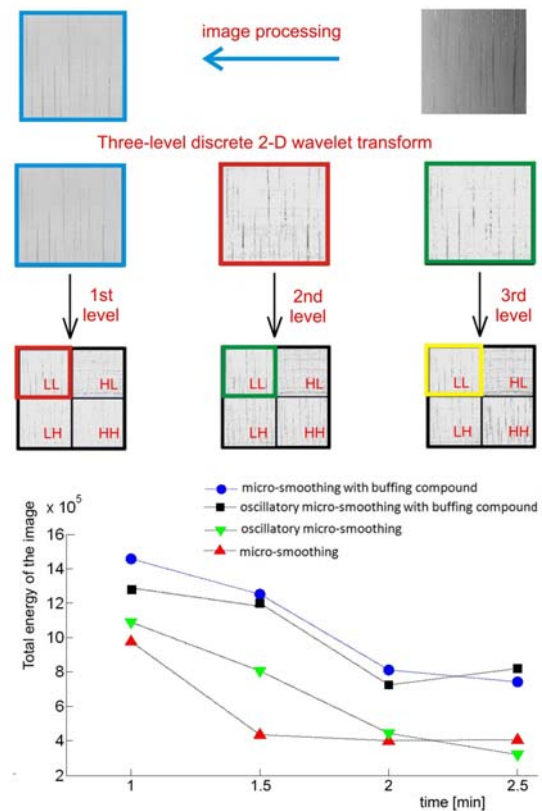


Fig. 4. Wavelet decomposition of machined surface image and total energy of machined surface image distributed along the cutting time

The energy of machined surface image presented as a function of time shows how the micro-smoothing deletes the grinding ridges (Fig. 4). In each case the energy is smaller with the time of cutting. If one tries to judge the progress of finishing basing on a machined surface image one can see two different classes of micro-smoothing parameters.

The first class concerns oscillations. The finishing process supported with oscillations run in the same way – each stage of 30 seconds of finishing results in progress of machined surface quality (the energy is smaller). The second class concerns the buffing compound. The application of buffing compound makes the cutting being very difficult because the grains and the free space between grains are sealed up (Fig. 2). In this way the

minimal thickness of cut for grains is not achieved and the material is plastically deformed instead of cut.

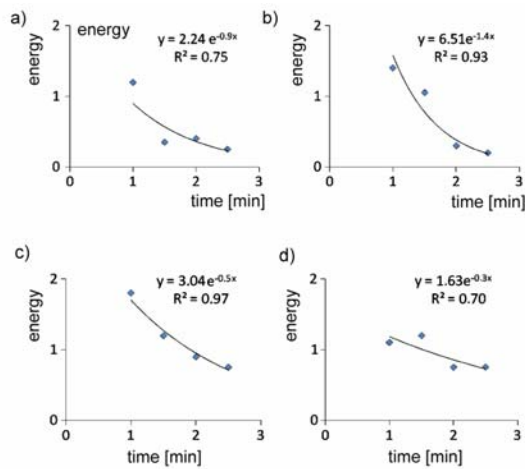


Fig. 5. Total energy of the approximation component of machined surface image in a function of time: a - micro-smoothing, b - micro-smoothing with axial oscillations, c - micro-smoothing with buffing compound, d - micro-smoothing with axial oscillations and buffing compound

In each case (Fig. 5) after the first stage of finishing the decrease in energy is small. The energy analysis of the approximation component confirmed the conclusions for the decrease of surface roughness parameters in time. The considerations concerning the other components also discourage for application of buffing compound in micro-smoothing processes. Additionally the analysis of all the components indicate the preferred order of operations. First it is preferable to use the micro-smoothing operation, then apply the oscillations for the process and finally switch off the oscillations for the final finish of the surface.

## 5. CONCLUSIONS

The micro-smoothing operation was applied for relatively soft C45 steel after the process of grinding. The desired machined surface was expected to be very smooth.

The quality of the surface was described with the machined surface image, which was pre-processed and analysed with the use of two-dimensional Discrete Wavelet Transform. The components of the wavelet decomposition were considered in relation to their being able to evaluate the process parameters and machined surface.

Energy of the machined surface image as a whole was correlated with the roughness parameters. Both the image and surface parameters decreased with the cutting time. It signifies the beneficial influence of the micro-smoothing on the vertical roughness parameters and the possibility of image application in the evaluation of surface roughness.

## 6. REFERENCES

- [1] Oxley P.L.B., The Mechanics of Machining: An Analytical Approach to Assessing Machinability, Ellis Horwood, England, 1989.
- [2] Storch B., Zawada-Tomkiewicz A., Distribution of unit forces on the tool edge rounding in the case of finishing Turning, Int J Adv Manuf Technol. on-line access
- [3] Zawada-Tomkiewicz A., Ściegienka R.: Monitoring of a micro-smoothing process with the use of machined surface images. Metrol. Meas. Syst., 3/2011, 419-428
- [4] Zawada-Tomkiewicz A., El Mansori M., Multi-scale analysis of surface topography after the belt grinding process, Proceedings of 13th International Conference on Metrology and Properties of Engineering Surfaces, pp. 269-273, London 2011

*Corresponding address: Anna Zawada-Tomkiewicz, PhD, TU Koszalin, Poland  
Phone: +4894 3478451, Fax: +4894 3426753, E-mail: anna.zawada-tomkiewicz@tu.koszalin.pl*



### III MECHATRONICS AND SYSTEM ENGINEERING



## OPTIMAL GAP DISTANCE BETWEEN ROTORS OF MINI QUADROTOR HELICOPTER

Aleksandrov, D.; Penkov, I.

**Abstract:** *This paper describes comparison between virtual simulation of rotors for flying platforms (mini UAV - Unmanned Aerial Vehicle) and real experiments. During virtual simulation there were conducted similar to real experiments with the use of scanned rotors (with 3D scanner) and same environment conditions. In quadrotor helicopter (quadrocopter) air flows that are going out from rotors and affecting each other were simulated with CFD (Computational Fluid Dynamics) software. Analysis of several helicopters that have different distances between rotors on different angular velocities were compared.*

*Optimal gap distance between rotors is determined, when helicopter mass is minimum and rotors are creating maximum lifting force (minimum impact of air flows to each other).*

*Key words: UAV, helicopter, rotor, quadrocopter, lifting force, CFD.*

### 1. INTRODUCTION

At first the idea of unmanned aerial vehicles (UAV) started as hobby but in the last decades it found a huge potential both in military <sup>[1]</sup> and civil spheres. UAVs are capable of carrying out work conditions where the surrounding environment is dangerous or not available to human. There is a wide range of applications performed by UAVs, such as police <sup>[2]</sup>, rescue <sup>[3]</sup> and firefighter needs <sup>[4]</sup>, research, cinematography and other spheres. UAVs have exclusive capabilities like hovering, vertical takeoff and landing, limited launching spaces and good maneuvering.

They have generated great interest in industrial and academic circles <sup>[5]</sup>. A thorough research was conducted in stability and controllability spheres. Those UAVs are not using innovative power sources and energy saving issue is very important.

This paper illustrates comparison between virtual simulation of rotors for flying platforms (mini UAV) and real experiments. For real experiments it was built a testing device for measurement of real rotor angular velocity, lifting force and energy consumption of motor.

During virtual simulation with CFD calculation there were conducted equivalent experiments where scanned with 3D scanner rotors and same environment conditions <sup>[6]</sup> were used.

With CFD software the air flows that are going out from rotors and affecting each other in quadrotor helicopter (quadrocopter) were simulated <sup>[7]</sup> and lifting force was determined. Helicopters with different distances between rotors on different angular velocities were compared. Optimal gap distance between rotors is determined when helicopter mass is minimum and rotors are creating maximum lifting force - air flows affect each other the minimally.

### 2. COMPARISON OF REAL AND VIRTUAL EXPERIMENTS

#### 2.1 Real Experiments

In real experiments a brushless motor Robbie 2827-34 with rotors 10 x 4.5 in (rotor length is 10 inches and the pitch is 4.5 inches per revolution) and 8 x 4.5 in



was used. For motor control it was used a brushless motor controller Mikrokopter BL-CTRL 1.2 and it was operated through RS232 port directly from PC (using UM232R USB Serial UART Development Module by FTDI).

A previously calibrated strain gauge sensor PS-08844244 was used for force determination. Rotor rotation speed was measured with optical laser tachometer Omron CT6. Altogether were made measurements for 10 rotor angular velocities for each rotor size.

### 2.2 Virtual Experiments

Virtual experiments for lifting force determination were conducted with CFD software SolidWorks Flow Simulation 2012 [8]. The real rotors were previously scanned with 3D scanner, then imported in SolidWorks as point cloud data and created working models. After this rotor lifting force was determined on different rotor rotation speed [9][10].

### 2.3 Results

Figure 1 illustrates force (produced by 10 x 4.5 in rotor) dependency on rotor rotation speed. A measured force graph was created with the real experiments data and CFD force graph with PC calculation.

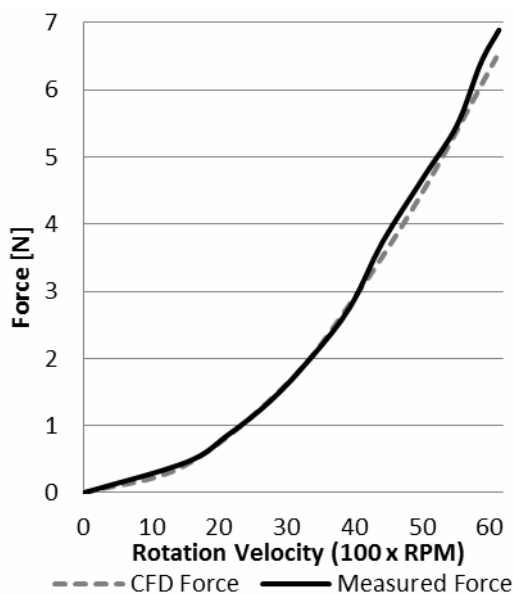


Fig. 1. Lifting force dependency on rotor rotation speed for 10 in rotor.

Both methods give approximately similar result (maximum error is about 3 %). This means that we can use CFD method for similar future analysis and calculation of impact of flows from different rotors on each other.

## 3. GAP DISTANCE OPTIMIZATION

### 3.1 Principle

Gap distance optimization was made with the use of CFD software on simplified quadrotor helicopter model with scanned models of 10 in rotors. Separate calculations for different rotation speeds 1500, 3000, 4000 and 5000 rpm were done. For each angular velocity distance range between rotors changed from 5 to 140 mm (Fig. 2).

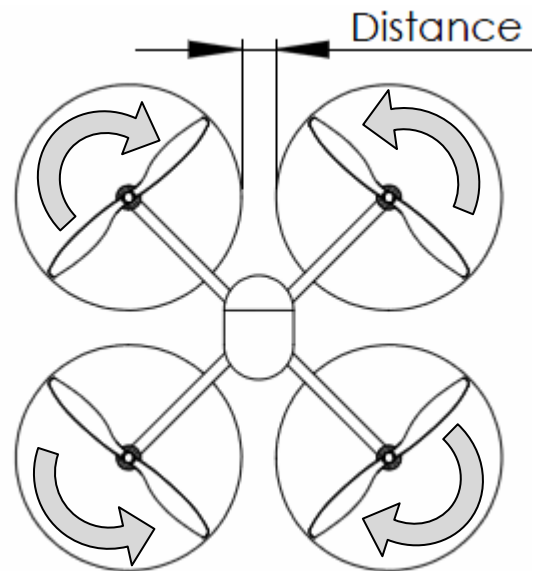


Fig. 2. A simplified model of quadrotor helicopter for CFD analysis that shows the direction of rotor rotation.

### 3.2 Results

Figure 3 illustrates lifting force dependency on distance between rotors. A graph shows that force increases on distances from 5 to 35 mm and this growth is around 15 %. From distance of 70 mm lifting force is decreasing by around 2 % and then stabilizing. This level corresponds to same values we had in real experiments (Fig. 1).

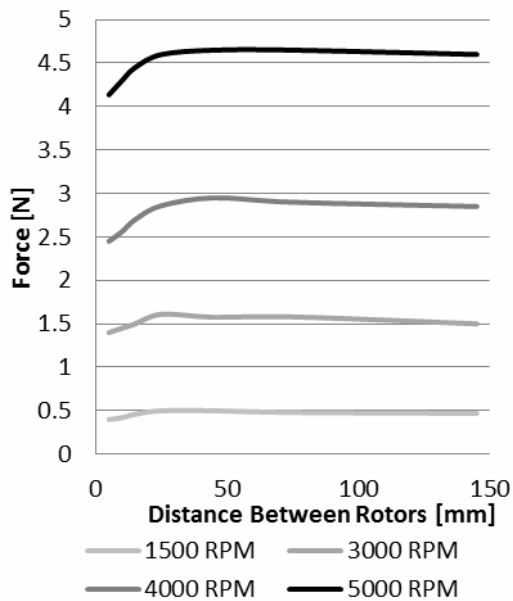


Fig. 3. Lifting force dependency on distance between rotors for different angular velocities.

Figure 4 shows air flow velocities and their directions of quadrotor helicopter when distance between rotors is 10 mm (front and top views).

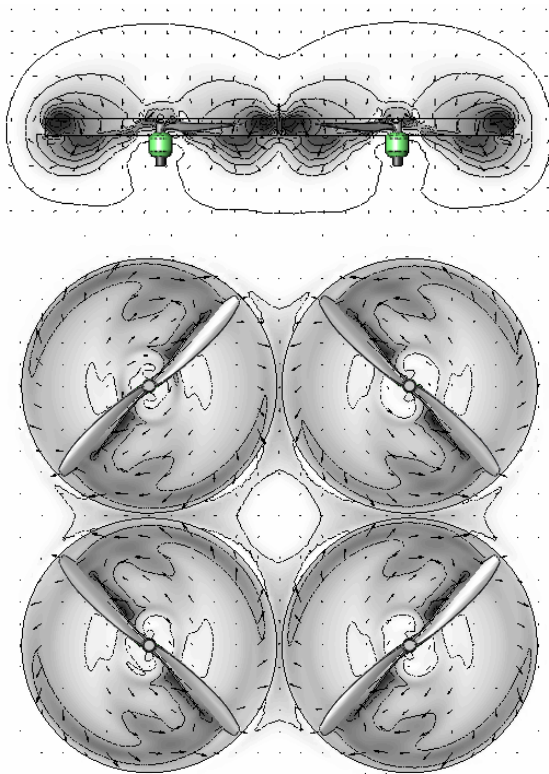


Fig. 4. Air velocity distribution near rotors, distance between rotors is 10 mm, velocity range 0 – 13 m/s.

Near rotating rotor endings appear small turbulent areas where air flow is twisting upwards. In the space between rotors there is a place, where air flows are running into each other and gathered flow goes upwards. This stream particularly compensates lifting force.

Figure 5 illustrates quadrotor helicopter air flow velocities and their directions when distance between rotors is 140 mm. At this distance the influence of air flows from rotors is insufficient and each rotor works as if it stayed separately.

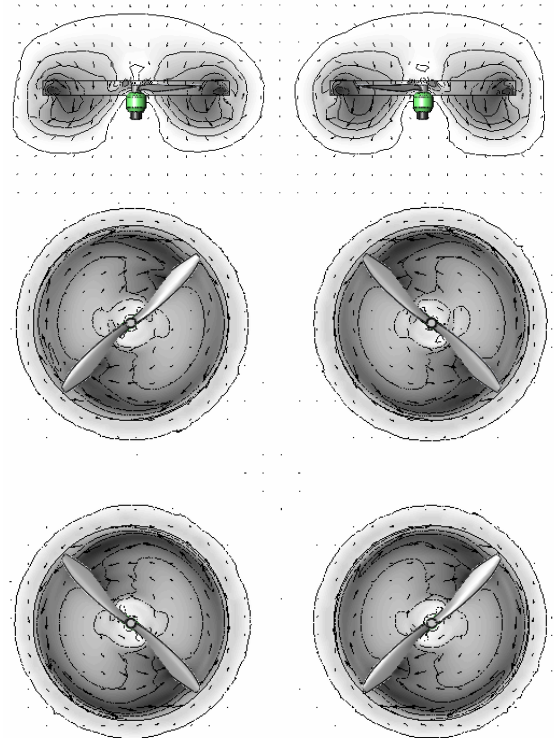


Fig. 5. Air velocity distribution near rotors, distance between rotors is 140 mm, velocity range 0 – 13 m/s.

### 3.3 Optimization

For optimization with use of MATLAB software the artificial neural network was built. Figure 6 shows surface of compliance of neural network, which allows to find produced lifting force at concrete rotor rotation speed and distance between rotors. With neural network it is possible to find optimal distance (where produced force is maximum) on certain rotor angular velocity.

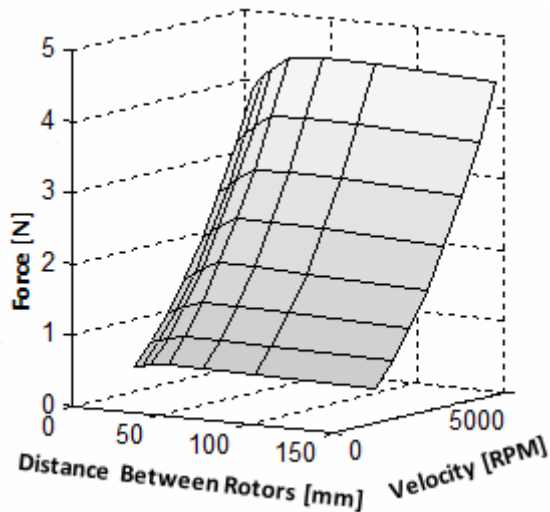


Fig. 6. A surface of compliance of neural network.

For example, distance between rotors of quadrotor helicopter with mass 1150 g (rotor rotation speed in hovering 4000 rpm) must be optimized. Mass of 1 mm central cross section 0.25 grams will be also taken into account. Optimal distance is 32.65 mm. On figure 7 a lifting force parameter shows what force is produced by rotor on certain distance between rotors. A reduced force graph shows lifting force minus weight (in Newton) of lengthened central cross. The difference in motor energy consumption between optimal distance and 140 mm gap is about 20 %.

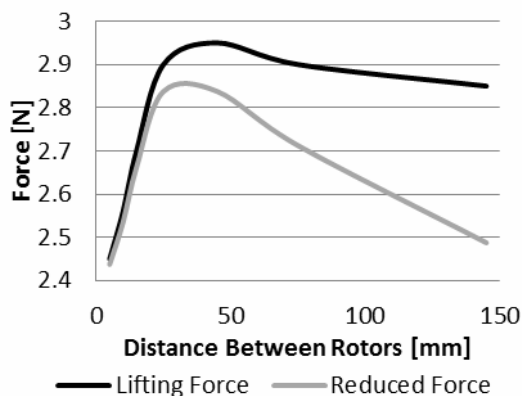


Fig. 7. Optimal distance between rotors for working angular velocity 4000 RPM.

#### 4. CONCLUSION

This paper describes comparison between virtual simulation of rotors for flying

platforms and real experiments and shows that results are trustworthy. With the CFD software there were simulated air flows that are going from rotors and how they affect each other on quadrotor helicopter and their influence on produced lifting force. Optimal gap distance between rotors can be determined with artificial neural network, when helicopter mass is minimum and rotors are creating maximum lifting force.

#### 5. FUTURE RESEARCH

Since CFD calculation does not allow to measure power consumption, next step will be to conduct real experiments of influence of gap distance between rotors on lifting force. With CFD it is impossible to measure how motor power changes with variation of distance between rotors, because crossing air flows can create additional loads on motor. These parameters will be controlled next.

#### 6. REFERENCES

- [1] Girard, A. R., Howell, A. S., Hedrick, J.K. Border patrol and surveillance missions using multiple unmanned air vehicles, In *Proceedings of the 43rd IEEE decision and control* (Tilbury, D.), Atlantis, Bahamas, December 14–17, 2004, 620–625.
- [2] Coifman, B., McCord, M., Mishalani, R. G., Iswalt, M., Ji, Y. Roadway traffic monitoring from an unmanned aerial vehicle, *IEE Proc. Intell. Transp. Syst.*, 2006, **153** (1), 11-20.
- [3] Ryan, A., Hedrick, J. K. A mode-switching path planner for UAV-assisted search and rescue. In *Proceedings of the 44th IEEE conference on decision and control* (Dawn, M.), Seville, Spain, December 12-15, 2005, 1471-1476.
- [4] Casbeer, D. W., Kingston, D. B., Beard, R. W., McLain, T. W. Cooperative forest fire surveillance using a team of small unmanned air vehicles. *Int. J. Syst. Sci.*, 2006, **37** (6), 351–360.

- [5] Peng, K., Cai, G., Chen, B. M., Dong, M., Luma, K. Y., Lee, T. H. Design and implementation of an autonomous flight control law for a UAV helicopter. *Automatica*, 2009, **45**, 2333-2338.
- [6] Aleksandrov, D., Penkov, I., In *11th Int. Symp. „Topical Problems in the Field of Electrical and Power Engineering“* (Zakis, J.), Pärnu, Estonia, January 16-21, 2012, 259 – 262.
- [7] Pounds, P., Mahony, R., Corke, P., Modelling and control of a large quadrotor robot. *Control Engineering Practice*, 2010, **18 (7)**, 691-699.
- [8] Hines, J. *SolidWorks Flo Simulation*, Dassault Systems, Concord, 2011.
- [9] Yongjie, S., Qijun, Z., Feng, F., Guohua, X., A New Single-blade Based Hybrid CFD Method for Hovering and

Forward-flight Rotor Computation. *Chi. Jour. of Aeronautics*, 2011, **24**, 127-135.

- [10] Pape, A., L., Beaumier, P., Numerical optimization of helicopter rotor aerodynamic performance in hover. *Aerospace Sci. and Techn.*, 2005, **9**, 191–201.

## 7. ABOUT AUTHORS

Corresponding author: Ph. D. Candidate Dmitri Aleksandrov, Doctoral student. Peterburi tee 46 – 314, 11415, Tallinn, Estonia, dmitri.aleksandrov@gmail.com, (+372) 58 194 349.

Co-author: Igor Penkov, Docent. Ehitajate tee 5 – V417, 19086, Tallinn, Estonia, igor.penkov@ttu.ee, (+372) 620 3306.

## MACHINERY UTILIZATION MONITORING AND PAUSE IDENTIFICATION PROTOTYPE MODEL DESIGN

Aruväli, T.; Serg, R. & Otto, T.

**Abstract:** *Pauses in manufacturing machinery work cause loss in factory efficiency and productivity. Detection of machinery utilization and pauses identification can give additional information for production planning and increase manufacturing efficiency. Information about machinery utilization can be processed offline to analyse past situations, but it can be also used for real time decisions. Using wireless sensors and Labview programming environment, prototype for machinery status and pauses identification was designed and introduced. Based on the prototype, proposals for industrial machinery utilization monitoring have been given.*

*Key words: wireless sensor network, production planning, real time feedback, condition monitoring, machinery utilization analysis.*

### 1. INTRODUCTION

Manufacturing enterprises main component for success is efficiency in work flow that creates the bases for high productivity. Machinery high level power and speed capability is only one indicator of workstation productivity. The other and even more important indicator is a human activity and knowledge in arranging, planning and running a workstation. Production systems have been changed over the time and every system has its typical requirements for the machinery and production environment. In the early twentieth century Henry Ford introduced mass production that was dominating as main production system over half of

century. It was inflexible, as all the produced items were similar, batch sizes were huge and items were produced to stock. Setup of production line could take months and even years [1]. But now, in modern manufacturing system, flexibility is needed. Key words of modern manufacturing systems are small batch size, flexibility, shortened production cycles, reduced work-in-progress, make-to-order and almost instantaneous delivery [2].

Thus, fast and informative feedback is needed from shop floor to fulfil modern manufacturing system requirements. Need for technology based real time wireless sensor network (WSN) monitoring system, employed by embedded computers, is getting more critical than ever before.

Machinery monitoring is in wide range researched in last years. Working modes are studied by implementing acoustic and vibration signal analysis on lathe [3]. On lathe also bearing condition is monitored using vibration signals [4]. Not only lathe, but also end-milling [5] and drilling [6] are monitored.

Even Smart Machine program has been introduced as manufacturing control system that helps in process planning, tool condition monitoring and health and maintenance [7].

Real time monitoring has multiple usages in different levels. It gives certainty to managing director, tools for better planning for production manager and fast feedback for machining quality to operator.

Modern monitoring is wireless that enables faster and cheaper installation and more flexible usage [8].

Essential is to collect the data from all the workbenches to one database to make it cognitive and simple to use. Modern machines often have database for utilization information preinstalled, but holding the information in separate machines does not give the centralised overview and contribution for productivity rise is poor.

National Instrument (NI) nodes, gateway and Labview programming environment are tools for designing wireless sensor network for monitoring. These tools have also been used in master’s study program for teaching sample real time condition monitoring system [9] and in development of broaching process monitoring system [10].

This paper introduces machinery monitoring importance and set up structure. Furthermore, it describes the design of sample NI and Labview based utilization monitoring model set up and its benefits.

## 2. MONITORING STRUCTURE

Machinery monitoring is beneficial for both: machineries and human competence. Efficiency in production depends on workstations productivity. Productivity is concerned as the effective and efficient utilization of resources (inputs) in producing goods (output) [11]. Preconditions for productivity are technological capabilities and human competences. Machinery monitoring can develop both preconditions (fig. 1). It helps to maintenance machines in optimised schedule, avoid inappropriate machining modes and change tools at right time. In the same time it gives information for better production and human resources planning.

Monitoring is part of modern performance improvement cycle (fig. 2). It is cooperation between operator and manager. Manager analysis results and operator comments and makes

improvement decisions that are implemented by operator.

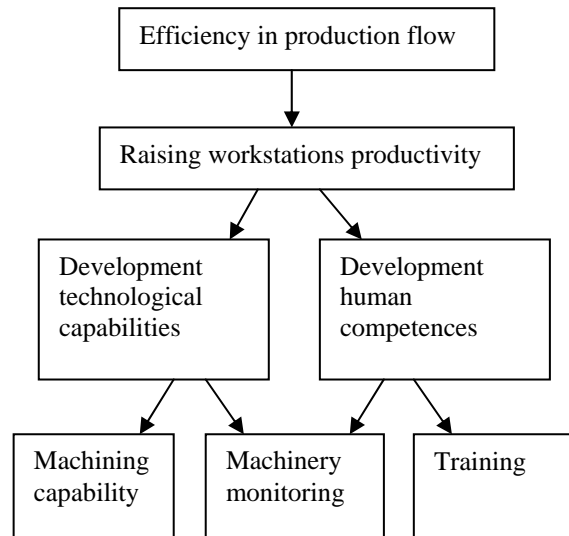


Fig. 1. Efficiency tree in production flow

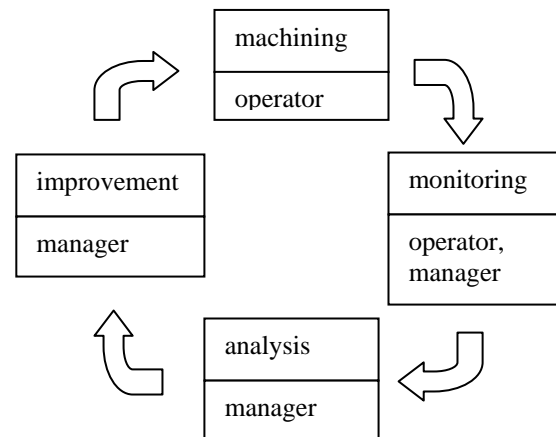


Fig. 2. Monitoring cycle

Monitoring system set up is complicated process with multiple activities that require different engineering knowledge. It requires interdisciplinary cooperation between mechanical engineers (ME), automation engineers (Aut) and information technology engineers (IT). For every activity many decisions have to be done first to develop energy efficient, user friendly and accurate system (fig. 3).



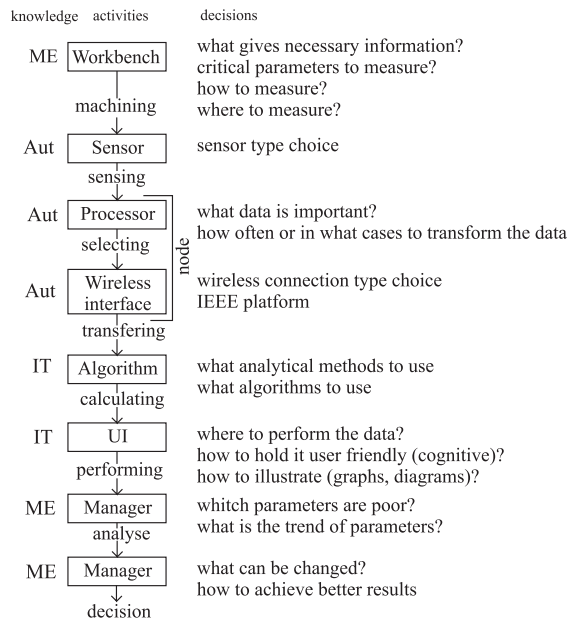


Fig. 3. Main activities and interdisciplinary knowledge in monitoring structure

### 3. UTILIZATION MONITORING AND PAUSE IDENTIFICATION

#### 3.1 Monitoring importance

Utilization rate of machine tools indicates the rate of useful, productive time of machine tools compared with overall working time (workload). In one shift work, utilization rate of machine tools between 75-85% is considered effective [12].

Average small or medium size enterprise (SME) does not have exact and organised overview about utilization rate, setup times, lead time, failure rate and other unplanned pauses. The important is not only utilization rate, but also pause investigation. Pauses in machining can be caused in several reasons as jig setup, work piece setup, planned maintenance, failure in machining, preparation of CAM program, coffee breaks, missing drawing or work order and other operator based reasons.

Investigation of pause reasons helps to find out shortcomings in production planning and in work orders. Awareness of reasons enables to take knowledge based and planned steps for smoother and more efficient production.

Machinery utilization analysis helps to diminish disharmony between same type of workbenches by balancing the usage of them. Furthermore, it helps to plan resources for new orders. Utilization monitoring with pause identification gives multiple information for analysis (fig. 4).

Information displayed (monitoring)

- ↳ Questions (analysis)
  - ↳ Action (improvement)
1. At what time period workbench is utilized
    - ↳ Do we have resources for more orders?
      - ↳ Sales office regulation
    - ↳ Are we working extra hours?
      - ↳ Changing the number of shifts
  2. What is utilization rate
    - ↳ What is productivity level?
      - ↳ Designing better jigs
    - ↳ Comparison of productivity between operators
      - ↳ Operators training
  3. What are rate of setup time, idle time, lead time and time of failures
    - ↳ Analysis of operator work organisation
      - ↳ Rising/diminishing operator extra tasks
    - ↳ Analysis of workbench condition (failures rate)
      - ↳ Planning maintenance
    - ↳ Analysis of production management organisation
      - ↳ Improving of production drawings, work orders flow and material availability
    - ↳ Analysis of production system efficiency
      - ↳ Reorganising production system

Fig. 4. Utilization monitoring and pause identification analysis with improvement decisions

Machinery utilization analysis gives efficiency in company level. But it can be applied also in supply chain and cluster level. Giving out production information from a company expects high level trust of network organisations.

#### 3.2 Sample prototype model design

Shop floor machinery utilization monitoring sample model was designed and programmed for presenting machinery utilization monitoring for students and production managers. Goal of the sample model is to teach effectively monitoring opportunities for students and to introduce benefits of monitoring system to production managers to popularise its usage.

To achieve all the goals, sample model has to be simple and easy to follow. It has to present utilization and pausing information in cognitive user interface (UI). Furthermore, design of workbenches has to



create the feeling of shop floor to be more realistic.

Sample monitoring model kit includes 3 lathe models with micro motor and WSN node, gateway and processor with UI screen (fig. 5). Lathe model was chosen as the most typical workbench for mechanical engineer.

Models had to have the shape and properties similar with a real lathe to carry along the feeling of real shop floor. In the same time their design and electrical wiring must be visible for students. Based on these requirements PMMA sheet plastic was chosen as models structure material. PMMA is easy to process and light weight material, moreover different colours can be used. Front and back sides were created from black PMMA to carry along the feeling of always a little oily machinery. Top, right and left sides were created from clear PMMA to show wiring inside the lathe. Base was open for more curious students and for possible later improvements.

Lathe model body consists WSN node, micro motor, batteries for micro motor, switch for lathe control, relay and wiring between components.

NI graphical programming environment LabWiev was used to create the program for monitoring, to design UI for presenting utilization information in real time and also in historical view.

Graphical program as virtual instrument (fig. 6) has been built to collect the utilization information from lathe models. Real time information about state of all lathes is presented graphically in user interface main view (fig. 7). There is an activity indicator light for every workbench and this is lit when motor is working. As the monitoring system has two direction communication, additionally, remote control switch was added to the lathe to enable remote control of motor. In UI the second indicator was added to show if the workbench has remote control enabled. When remote control is enabled, lathe motor can be turned on and off from the

remote computer in office or in more advanced system over the Internet.

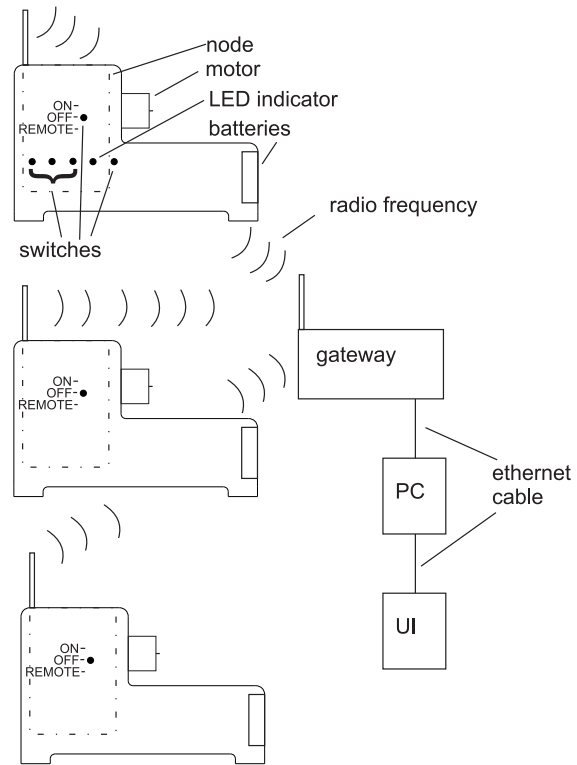


Fig. 5. Monitoring model kit structure

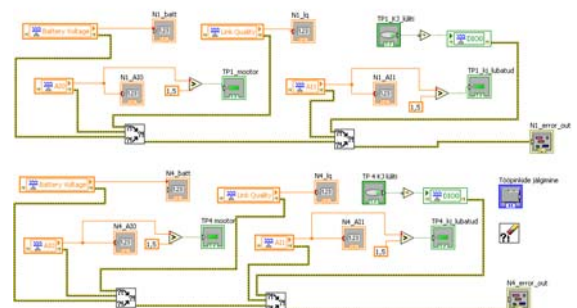


Fig. 6. Virtual instrument graphical program in Labview for lathes 1 and 4.

One of the lathe was equipped with 3 extra switches to determine the reason of pause in lathe working. Switches were named “Planned maintenance”, Fault” and “No order” that should be switched by operator correspondingly if the pause is caused by planned maintenance, fault in machining/unplanned maintenance or operator is lack of work order, drawing or material. The reason of pause is indicated in UI panel (Fig. 8) and saved to the database.

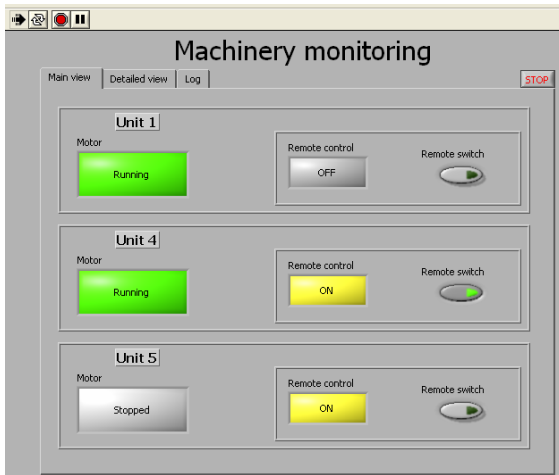


Fig. 7. UI, main view: workbenches utilization and remote control information

UI page 3 has detailed view of battery energy and radio frequency quality information (Fig. 9). UI page 4 has historical view graphical presentation of lathe utilization and pausing information (Fig. 10).

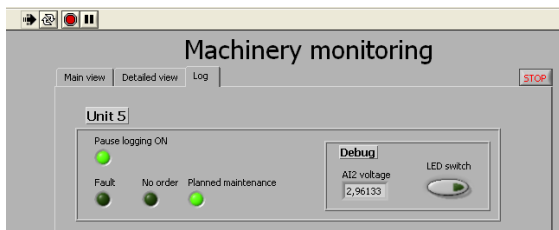


Fig. 8. UI, Investigation of pauses

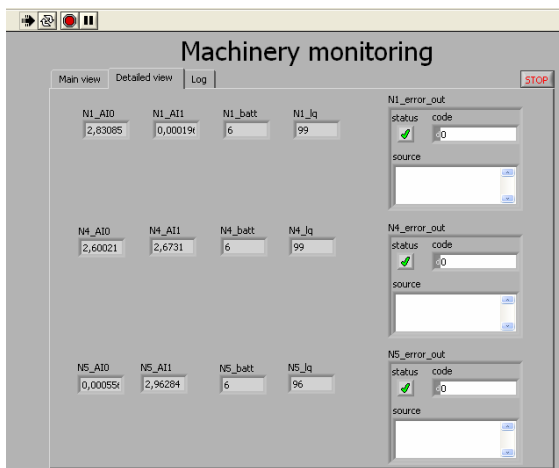


Fig. 9. UI, detailed view: battery energy and radio frequency quality information

Designed utilization monitoring model was presented to master students and a production company management.

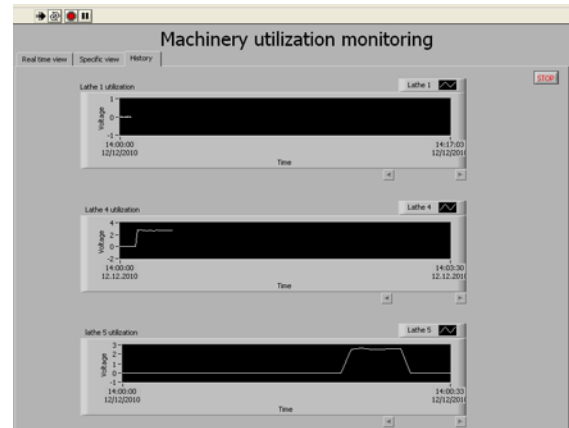


Fig. 10. UI, historical view: graphical presentation of workbenches utilization and pausing reason information

#### 4. FEEDBACK AND DISCUSSION

Machinery utilization monitoring prototype was introduced to mechanical engineering master students, who were surprised that utilization monitoring is not widely used in manufacturing companies. It shows, that for master students, monitoring is one part of manufacturing and they are minded to use it in their further career.

Prototype was also introduced to a manufacturing company management. Compared with students, they were a little more discredited, but they decided to set up a prototype monitoring system to their shop floor cooperation with Tallinn University of Technology. It can be concluded that developed prototype model act as planned and it convinces company managers and students in its beneficial influence in real production. Furthermore, thanks for the model, monitoring system will be set up to the manufacturing company.

In sample model the state of the machine can be determined by measuring certain voltages. NI WSN node analogue voltage input channels were used for that purpose. In practical application it is unadvised to use shorter than 1 second sample times for NI WSN nodes, so AC signal measurement requires more complex measuring front-end schematics. There are industrially produced signal converters available and

suitable for measuring currents and voltages in real production environment.

NI hardware and software are easier to use than typical WSN node (Berkeley node), as NI equipment is preinstalled and programming environment is graphical. Advantage in Berkeley nodes usage is lower price and wider opportunities in programming. For data collection and presentation, separate program must be used to achieve compact, well comparable and cognitive UI.

Next step in utilization monitoring is to set up monitoring system in shop floor and design advanced UI that can be used over the Internet.

## 5. ACKNOWLEDGEMENT

This research was supported by Estonian Ministry of Education, Research Project SF0140113Bs08 and Estonian Science Foundation (grant F7852).

## 6. REFERENCES

1. Womack, J. P., Jones, D. T. & Roos, D. The machine that changed the world. Simon & Schuster, 2007.
2. Viswanadham, N. & Srinivasa Raghavan N. R. Flexibility in Manufacturing enterprises. In *Sādhanā*, 1997, **22**, 135-163.
3. Aruväli, T., Serg, R., Preden, J. & Otto, T. In-process determining of the working mode in CNC turning. In *Est. J. of Eng.*, 2011, **17**, 4-16.
4. Saravanan, S., Yadava, G. S. & Rao, P. V. Condition monitoring studies on spindle bearing of the lathe. In *Int. J. Adv. Manuf. Technol.*, 2006, **28**, 993-1005.
5. Wright, P., Dornfeld, D. and Ota, N. Condition monitoring in end-milling using wireless sensor networks (WSNs). *Trans. NAMRI/SME*, 2008, **36**.
6. Shin, B.; Kim, G.; Choi, J.; Jeon, B.; Lee, H.; Cho M.; Han, J. and Park, D. A Web-based machining process monitoring system for E-manufacturing

implementation. In *J. Zhejiang Univ. SCIENCE A*, 2006, **7**, 1467-1473.

7. Atluru, S., Huang, S. H. & Snyder, J. P. A smart machine supervisory system framework. In *Int. J. Adv. Manuf. Technol.*, 2012, **58**, 563-572.
8. Aruväli, T., Serg, R., Preden, J. & Otto, T. Smart dust applications in production environment. In *7<sup>th</sup> Int. DAAAM Baltic Conf. Indust. Eng.*, 2010, 572-577.
9. Hiiemaa, M. and Tamre, M. Using wireless sensor network components in practical assignments of master's study mechatronics course. In *10<sup>th</sup> Int. Symp. "Topical problems in the field of el. and power eng"*, 2011, 193-196.
10. Shi, D., Axinte, D. A. & Gindy, N. N. Development of an online machining process monitoring system: a case study of the broaching process. In *Int. J. Adv. Manuf. Technol.*, 2007, **34**, 34-46.
11. Riives, J., Otto, T. & Lõun, K. Methods for enhancing productivity and work efficiency in the workshop. In *J. of Machine Eng.*, 2007, **7**, 86-95
12. Lõun, K., Riives, J. & Otto, T. Evaluation of the operation expedience of technological resources in a manufacturing network. In *Est. J. of Eng.*, 2011, **17**, 51-65.

## 7. ADDITIONAL DATA ABOUT AUTHORS

Tanel Aruväli, Dep. of Machinery, tanel.aruvali@ttu.ee

Risto Serg, Research Laboratory for Proactive Technologies, Dep of Computer Control, risto.serg@dcc.ttu.ee

Tauno Otto, Dep. of Machinery, tauno@staff.ttu.ee

All authors are with Tallinn University of Technology, Ehitajate tee 5, 19086 Tallinn, Estonia.

## DEVELOPMENT OF MOVEMENT ALGORITHMS FOR A ROBOT MANIPULATOR

Aryassov, G.; Zhigailov, S. ; Zinovjev, E.

**Abstract:** *In this paper an alternative approach to solving the inverse problem of kinematics is observed. In comparative analysis ways for determining link's rotatory angles using classical and alternative approaches will be observed. It will allow to determine advantages of using the alternative approach proposed in this article. On the basis of the obtained results we can define ways for optimizing the algorithm for solving the inverse problem of kinematics in future.*

*Key words: manipulator, algorithm, trajectory, the inverse problem*

### 1. INTRODUCTION

Commonly during the design of a manipulator only required characteristics of technological process and manipulator's productivity are known. Thus, when modifying a manipulator and choosing the number of its links, their optimal length and characteristics of electrical drives, appears the necessity to solve the inverse problem of kinematics.

Nowadays the inverse problem of kinematics is used in the variety of different areas of life. Among them are war industry, technological industry, cinematograph etc. Because of the theoretical and practical difficulties of the inverse kinematics there is a big area for explorations and making optimizations [2]. In the first approach, the solution of the inverse problem is based on a method of approximations [3]. We have randomly determined these approximations from the equation of motion of the first link's movement at time ( $t=0$ ). According to the

determined equation of motion of the grip, the kinematical characteristics of all links at subsequent times are found.

The second approach is based on a geometrical method. The main idea is to identify the extreme possible positions of links from the determined equation of motion of grip. These extreme positions of links are obtained by replacement of the initial system with a simplified model. Derived algorithm allows to provide sufficient accuracy for a motion of the grip by determined trajectory. The developed algorithm allows to consider manipulator with different number of links and to simulate continuity, smoothness and the minimal time of link's (grip's) motion by determined trajectory. The 3D mathematical model generated in MATLAB is proposed for simulation of manipulator's movement as a graphical solution of inverse problem of kinematics.

### 2. INVERSE KINEMATICS

The main problem of the inverse kinematics is to find connected parameters  $\theta_i = [\theta_1 \theta_2 \theta_3 \dots \theta_n]$  of manipulator, providing set orientations of grip using known positional matrix  $T_6^0$  and orientation of grip of 6-link manipulator (Fig.1) [4]. So, we have:

$$R_6^0 = B^{-1} R_{instr}^{abs} H^{-1} \begin{bmatrix} n_x & s_x & a_x & \rho_x \\ n_y & s_y & a_y & \rho_y \\ n_z & s_z & a_z & \rho_z \\ 0 & 0 & 0 & 1 \end{bmatrix} \quad (1)$$

where: H-matrix of position in coordinates system of grip, B-matrix of position in absolute coordinate system and  $R_{instr}^{abs}$  - matrix of position of an instrument in absolute coordinate system,  $n$  - vector of normal,  $s$  - vector of orientation,  $a$  - vector of axis of rotation.

## 2.1 Classical approach to inverse kinematics

Let us see link frame assignment of robot "Fanuc S-500" [5].

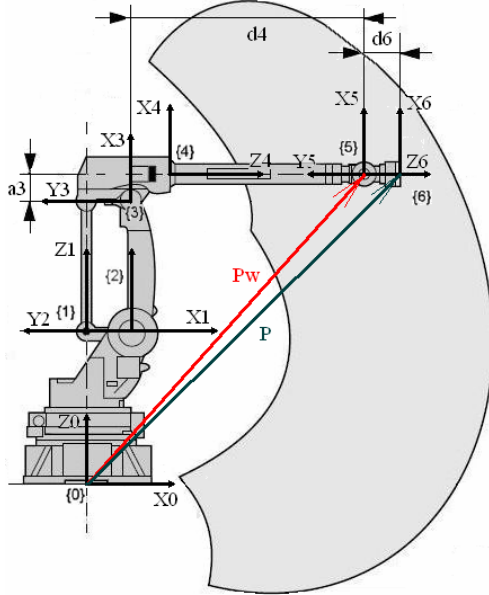


Fig. 1. Link frame assignment

From Fig.1 and initial conditions of inverse kinematics we know vector  $P$  (the grip's position) and matrix of grip's position and orientation  $R_6^0 = [n \ s \ a]$ , we can find the wrist position [1]

$$(P_w): P_w = P - d_6 \cdot a. \quad (2)$$

It is now possible to find the inverse kinematics for  $\theta_1$ ,  $\theta_2$  and  $\theta_3$ . Considering Fig. 2 it is easy to see that

$$\theta_1 = \arctan(P_{wy}, P_{wx}). \quad (3)$$

Once  $\theta_1$  is known the problem reduces to solving a planar structure. Looking to Fig. 2 it is possible to successively write

$$P_{wx1} = \sqrt{(P_{wx}^2 + P_{wy}^2)} \quad (4)$$

$$P_{wz1} = P_{wz} - d_1 \quad (5)$$

$$P_{wx1'} = P_{wx1} - a_1 \quad (6)$$

$$P_{wy1'} = P_{wy1} \quad (7)$$

$$P_{wz1'} = P_{wz1} \quad (8)$$

$$P_{wx1'} = -a_2 s_2 + a_x c_{23'} \quad (9)$$

$$P_{wz1'} = a_2 c_2 + a_x s_{23'}, \quad (10)$$

where coefficients  $c_2 = \cos \theta_2$ ,  $s_2 = \sin \theta_2$ ,  $c_{23'} = \cos(\theta_2 + \theta_3)$ ,  $s_{23'} = \sin(\theta_2 + \theta_3)$ ,  $a_1, a_2, a_3, d_1, d_4, d_6$  - distances from dimension sheet of robot,  $a_x$  - vector connecting points {3} and {5},  $P_{wx}, P_{wy}, P_{wz}$  are dimensions in coordinate system  $Ox_0y_0z_0$ ,  $P_{wx1}, P_{wy1}, P_{wz1}$  in coordinate system  $Ox_1y_1z_1$ ,  $P_{wx1'}, P_{wy1'}, P_{wz1'}$  in coordinate system  $Ox_1'y_1'z_1'$  in Fig. 2.

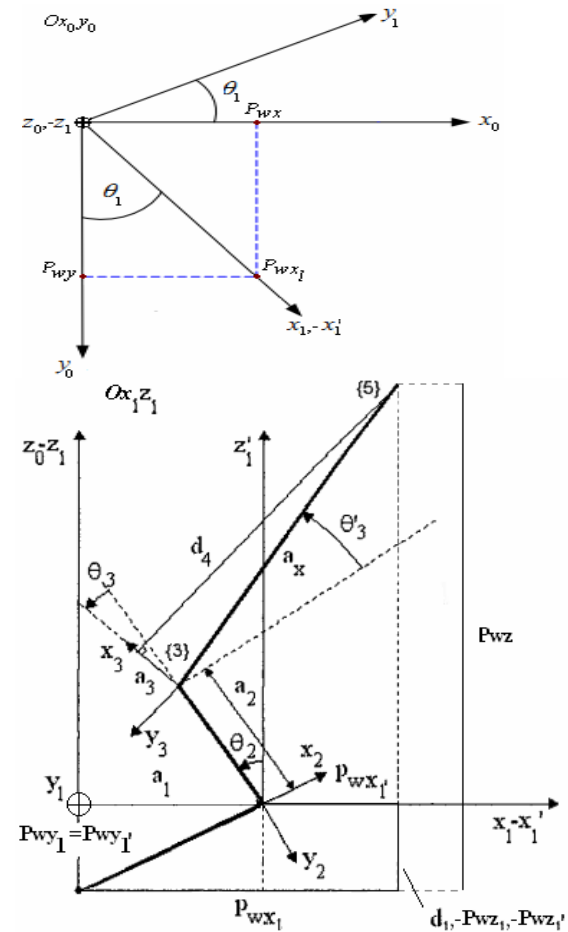


Fig. 2. Anthropomorphic structure

Squaring and summing Eq. (9) and Eq. (10) results in

$$P_{wxl'}^2 + P_{wzl'}^2 = a_2^2 + a_x^2 + a_2 a_x s_{3'} . \quad (11)$$

It gives

$$s_{3'} = \frac{P_{wxl'}^2 + P_{wzl'}^2 - a_2^2 - a_x^2}{2a_2 a_x} . \quad (12)$$

Setting

$$c_{3'} = \pm \sqrt{1 - s_{3'}^2} \quad (13)$$

the solution for  $\theta'_{3'}$  will be

$$\theta_{3'} = \arctan(s_{3'}, c_{3'}) \quad (14)$$

$$\theta_3 = \theta_{3'} - \arctan \frac{a_3}{d_4} . \quad (15)$$

Now using  $\theta'_{3'}$  in Eq. (9) and Eq. (10) results in a system with 2 equations with  $s_2$  and  $c_2$  unknowns

$$P_{wxl'} = -a_2 c_2 + a_x (c_2 c_{3'} - s_2 s_{3'}) \quad (16)$$

$$P_{wzl'} = a_2 s_2 + a_x (s_2 c_{3'} + s_3 c_2) . \quad (17)$$

Solving for  $s_2$  and  $c_2$  gives

$$s_2 = \frac{-(a_2 + a_x s_{3'}) P_{wxl'} + a_x c_{3'} P_{wzl'}}{a_2^2 + a_x^2 + 2a_2 a_x s_{3'}} \quad (18)$$

$$c_2 = \frac{(a_2 + a_x s_{3'}) P_{wzl'} + a_x c_{3'} P_{wxl'}}{a_2^2 + a_x^2 + 2a_2 a_x s_{3'}} . \quad (19)$$

And the solution for  $\theta_2$  will be

$$\theta_2 = \arctan(s_2, c_2) . \quad (20)$$

To find the required joint angles  $\theta_4$ ,  $\theta_5$  and  $\theta_6$  we simply take advantage of the special configuration of the last 3 joints, getting matrix of rotation

$$R_6^3 = (R_3^0)^{-1} \cdot R_6^0 = (R_3^0)^T \cdot R_6^0 , \quad (21)$$

which gives

$$R_6^3 = \begin{pmatrix} r_{11} & r_{12} & r_{13} \\ r_{21} & r_{22} & r_{23} \\ r_{31} & r_{32} & r_{33} \end{pmatrix} \quad (22)$$

$$r_{11} = -c_1 s_{23} a_{11} - s_1 s_{23} a_{21} + c_{23} a_{31}$$

$$r_{13} = -c_1 s_{23} a_{13} - s_1 s_{23} a_{23} + c_{23} a_{33}$$

$$r_{33} = s_1 a_{13} - c_1 a_{23}$$

$$r_{21} = -c_1 c_{23} a_{11} - s_1 c_{23} a_{21} - s_{23} a_{31}$$

$$r_{31} = s_1 a_{11} - c_1 a_{21}$$

$$r_{12} = -c_1 s_{23} a_{12} - s_1 s_{23} a_{22} + c_{23} a_{32}$$

$$r_{23} = -c_1 c_{23} a_{13} - s_1 c_{23} a_{23} - c_{23} a_{33}$$

$$r_{22} = -c_1 c_{23} a_{12} - s_1 c_{23} a_{22} - s_{23} a_{32}$$

$$r_{32} = s_1 a_{12} - c_1 a_{22} ,$$

where  $a_{11} \dots a_{33}$  are elements of matrix  $R_6^0$ .

It is now possible to use the previous result for the ZYZ Euler angles to obtain the solutions for  $\theta_4$ ,  $\theta_5$  and  $\theta_6$ .

For  $\theta_5 \in [0, \pi]$  the solution is

$$\theta_4 = \arctan(r_{33}, r_{13}) \quad (23)$$

$$\theta_5 = \arctan\left(\sqrt{r_{13}^2 + r_{33}^2}, -r_{23}\right) \quad (24)$$

$$\theta_6 = \arctan(-r_{22}, r_{21}) . \quad (25)$$

For  $\theta_5 \in [-\pi, 0]$  the solution is

$$\theta_4 = \arctan(-r_{33}, -r_{13}) \quad (26)$$

$$\theta_5 = \arctan\left(-\sqrt{r_{13}^2 + r_{33}^2}, r_{23}\right) \quad (27)$$

$$\theta_6 = \arctan(r_{22}, -r_{21}) . \quad (28)$$

## 2.2 Alternative approach to inverse kinematics

For solution of the inverse kinematics the following functions were developed: «of6», «rotate\_time», «rotate\_d», «time\_angles». Algorithm of their use is shown in the block-scheme Fig. 6.

### 2.2.1 Function «of6»

$$c_2 = b_1 - b_2. \quad (30)$$

Function «of6» is the fundamental function of algorithm for solution of inverse kinematics.

Let us observe movement of manipulator using the system of links  $OABC$  in plane  $xz$  Fig. 3.

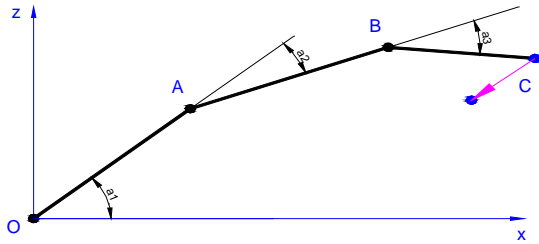


Fig. 3. Input data

We can divide all cycle of «of6» function into few steps:

- 1) Function «of6» gets input data with parameters of manipulators links; number of observing link; coordinates of the start point of observing link and the grip's point of manipulator in this time.
- 2) Function determines the external possible positions of observing link and the maximal angle of its rotation  $b_3$  by control of reaching the point of manipulator's grip (point can be out of reach – too close or too far).
- 3) Function determines angles  $b_1, b_2, c_1$  taking into consideration the maximal possible angle of rotation  $b_3$ .

If observing link is not the last Fig. 4 → function repeats to all remaining links with changed initial coordinates to  $x'z'$  etc. As example angles can be found from Eq. (29)

$$c_1 = b_1 + \frac{2}{3b_2}, \quad (29)$$

where  $2/3$  is exemplifying numerical coefficient for gradation of angles  $c_1, b_1, b_2$ . If observing link is the last Fig. 5 → we can not use previous equation for angles got from the previous link and there is only one solution

Thus, function «of6» determines angles of rotation of manipulator for initial plane  $xz$ .

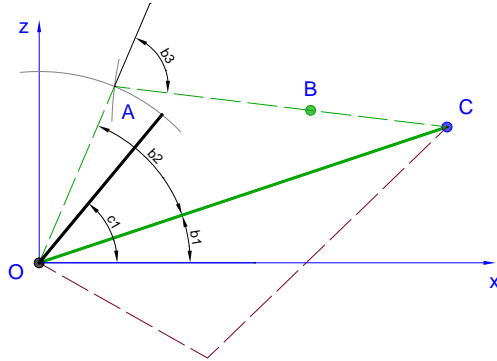


Fig. 4. Solution for every link (except the last one)

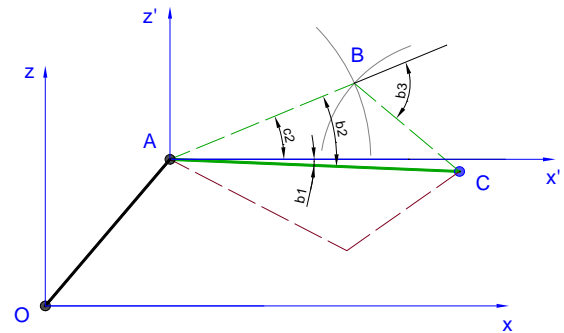


Fig. 5. Solution for the last link

Finally, the obtained results in function «of6» are controlled by main program Fig. 6. After that the optimal variations of angles rotations are defined.

### 2.2.2 Function «rotate\_time»

Function «rotate\_time» finds the minimal time for rotation of every link in 2 required positions for some moment of time.

Trajectory of manipulator consists of 3 mechanical characteristics of links motion: acceleration, inhibition, displacement with constant velocity.

Obviously, the minimal time of rotation of manipulator can be reached by having the highest possible velocity and acceleration of every link. Developing algorithm of function «rotate\_time» permits to find the



weakest (slowest) links of manipulator. Analyzing that and changing mechanical characteristics of the weakest links, we obtain the optimized solutions.

### 2.2.3 Function «rotate\_d»

Function «rotate\_d» gets input data from function «rotate\_time» and finds velocities and accelerations of links and selects the maximal time of movement for every link between two calculated positions. Moreover function «rotate\_d» provides continuous movement of all the links of manipulator.

### 2.2.4 Function «time\_angles»

It is the last basic functions of algorithm. It gives visualization for movement of manipulator and its link in every moment.

### 2.2.5 Simulation program for movement of manipulator

Simulation program for movement of manipulator is algorithm allows to determine velocities and accelerations of grip's point in dependence on time moment by preliminarily selected trajectory. Currently there are 6 trajectories for manipulators movement demonstration. In Fig. 6 you can see full algorithm for alternative solution of inverse kinematics.

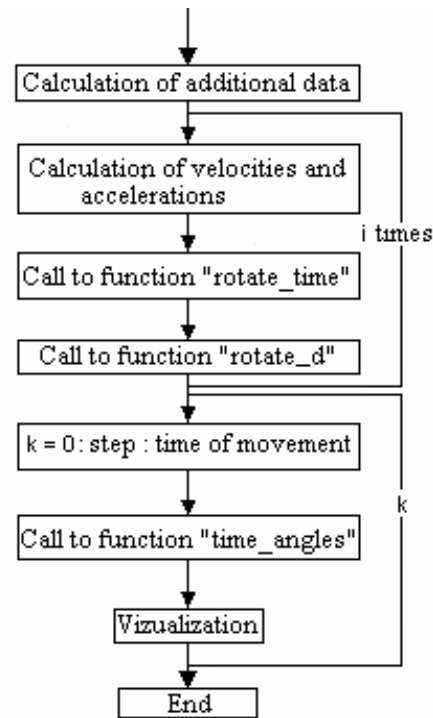
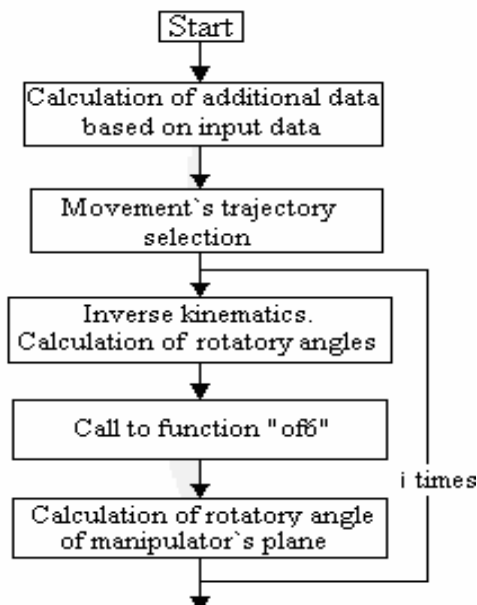


Fig. 6. Common algorithm for alternative solution of the inverse problem of kinematics

All required data for simulation is in massive  $data\{k\}(i,1:7)$ , where 1-7 are parameters of link's angles, velocities, accelerations etc.

In Fig. 7 and Fig. 8 there are few simulated positions of manipulator for some trajectories in 3D space created in MATLAB. The base of manipulator and its rotation around axis z is not depicted, but it was calculated together with other links.

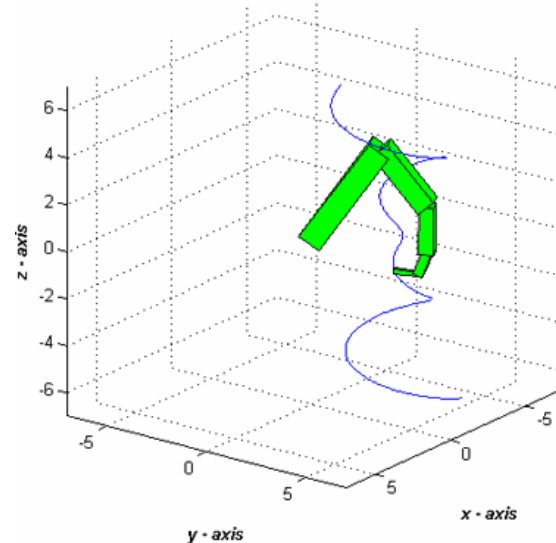


Fig. 7. Visualization of manipulator's "Fanuc S-500" movement (1)

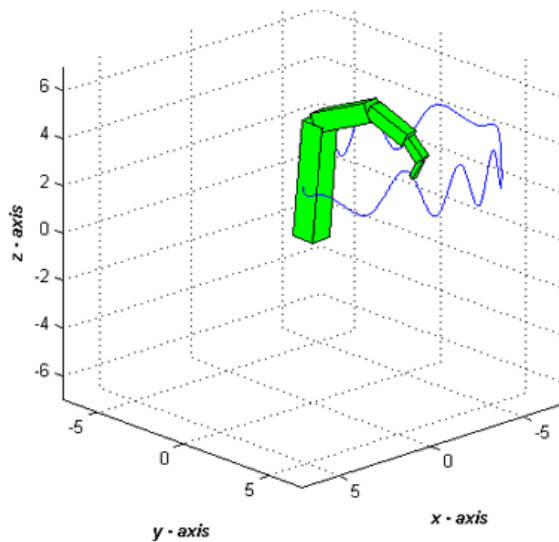


Fig. 8. Visualization of manipulator's "Fanuc S-500" movement (2)

### 3. ADVANTAGES OF ALTERNATIVE APPROACH

From description of classical and alternative approaches we can emit few important advantages of alternative approach :

- Possibility to optimize velocities and accelerations of manipulator's links in dependance of parameters of links (length, weight, power of driving motors etc) to get the minimal possible time for every task
- Possibilities in more simple correction of rotatory angles to complete some complicated tasks (reach of point placed behind an mechanical barrier etc)
- Possibility to work out common algorithm of manipulator's movement to solve both inverse and direct kinematics

### 4. CONCLUSION

Analyzing the main principles of alternative approach for inverse kinematics solution, we got some possible advantages to be compared to classical approach. It defines the main directions of development of proposed algorithm. To the next tasks for manipulator's movement algorithm

optimization we can relate calculation of additional trajectories and working out the most flexible mathematical solutions for calculation angles, velocities and accelerations for n-link manipulators. Well-modernized alternative approach can find its usage in different areas of life saving time of technological cycles, making economy in its usage of electric power, making solution for more and more complicated practical tasks.

### 5. REFERENCES

- [1] Norberto Pires, J. *Industrial robots programming.*, Springer, London, 2007
- [2] Sciavicco, L., Siciliano, B. *Modelling and Control of Robot Manipulators.*, Springer, London, 2004
- [3] Vukobratovic, M., Stokic, D. *Scientific Fundamentals of Robotics 2. Control of Manipulation Robots.*, Springer-Verlag, Berlin, 1982
- [4] Vukobratovic, M., Stokic, D. *Scientific Fundamentals of Robotics 3. Kinematics and Trajectory Synthesis of Manipulation Robots*, Springer-Verlag, Berlin, 1986
- [5] Official site of the "FANUC robotics America Corporation", <http://www.fanurobotics.com>

Gennady Aryassov, Ass.Professor, Tallinn University of Technology, Department of Mechatronics, Ehitajate tee 5, Tallinn, [gennadi.arjassov@ttu.ee](mailto:gennadi.arjassov@ttu.ee)

Sergei Zhigailov, Doctoral student, Tallinn University of Technology, Department of Mechatronics, Ehitajate tee 5, Tallinn, [sergsil@gmail.com](mailto:sergsil@gmail.com)

Jevgeni Zinovjev, Bachelor of Science, Swedbank AS, IT engineer, Liivalaia 8, Tallinn, Estonia, [jzinovjev@gmail.com](mailto:jzinovjev@gmail.com)

## PRODUCTION MACHINERY UTILIZATION MONITORING BASED ON ACOUSTIC AND VIBRATION SIGNAL ANALYSIS

Astapov, S.; Preden, J. S.; Aruväli, T. & Gordon, B.

**Abstract:** *Real-time monitoring of machinery and systems at the shop floor is essential for many tasks in the manufacturing context. One of the potential application areas of machinery and system monitoring is machine utilization monitoring, which provides the source data for planning. Optimal schedule planning is a critical step in maximizing the efficiency of a manufacturing facility. The paper considers a set of signal processing and analysis procedures that enable machinery monitoring by employing audio and acceleration sensors which can be easily installed. Testing results of the proposed system show good quality of machine state identification.*

*Key words: machinery monitoring, acoustic signal processing, vibration signal processing, process state classification*

### 1. INTRODUCTION

Machinery monitoring in the shop floor is useful from several perspectives. Machinery monitoring can provide information for both machine utilization optimization and preventive & predictive maintenance purposes. Monitoring machine utilization will allow for increasing the efficiency of the production facility. Predictive maintenance will decrease the number of accidental failures, thereby increasing machine utilization and efficiency.

One of the solutions for machinery monitoring is the use of wireless sensor networks technology [1], which makes it possible to apply the monitoring equipment

to the monitored devices with minimum expense.

Most recent research articles handle acoustic and vibration monitoring in order to inspect a work piece and cutting tool quality [2] or machinery working mode [3], however discarding the basic feedback about machinery utilization. Higher level comprehensive information about working modes has improved the process mostly theoretically so far. On the other hand raw, filter free information about machinery activity can give faster, more practical and efficient results in shop floor. It is also important to achieve objective feedback as the data can be corrupted if handled by several workers, each with his or her own understanding of the process.

Actually, most modern machinery already has built in automatic utilization detection and data acquisition and storage capabilities. But the problem is that every single machine collects only its own data and the analysis of this scattered data is inefficient and time consuming. Furthermore, after restarting, the data stored in production machinery often disappears. Thus organized machinery utilization feedback for the entire shop floor accumulated in one application would be a useful tool for production planning in a company (on a bigger scale also in a supply chain or cluster).

This paper introduces and compares several signal processing and classification methods applied to acoustic and vibration signals in order to detect Computer Numerical Control (CNC) machinery utilization.

## 2. SIGNAL PROCESSING METHODS

Digital Signal Processing (DSP) aims to extract information from (typically periodic) signals relevant for a specific application [4]. For the task of shop floor machinery monitoring a scheme of DSP presented in Fig. 1. is applied, which combines the means of signal processing and classification of the signal's parameters.

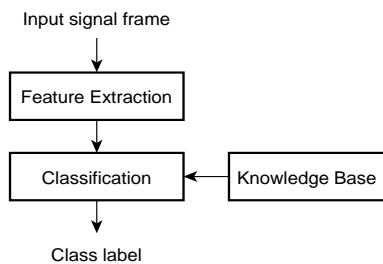


Fig. 1. Signal processing system

The system operates frame-by-frame, processing sections (frames of length  $N$ ) of the digitized signal from a memory buffer. For every processed signal frame the system then outputs a class label, which specifies the estimated state of the monitored machine.

The first step of DSP is the feature extraction (FE) procedure, which derives the signal parameters, relevant in the identification of specific machinery operation states. The resulting set of features is much shorter than the raw signal frame and does not contain redundant signal information which is relevant in a resource constrained system. The vector of extracted features is then analyzed by a classification algorithm, which estimates the most probable class label (corresponding to a process state) by applying a pre-defined knowledge base of the monitored process. This knowledge base is derived from a training signal, which contains relevant machine operation states, providing references for the classification algorithm.

### 2.1 Feature Extraction Methods

In the paper two FE methods are considered, both of which derive the

parameters of the signal in the frequency domain.

The first method is an analytical one and is based on effective frequency interval selection. The simplified scheme of the method, which we will call Spectral means, is presented in Fig. 2. The incoming signal frame is transformed by applying the Fast Fourier Transform (FFT), which decomposes the temporal signal into a set of its frequency components, called a frequency spectrum (we apply one specific application of the FFT [5]). The most distinguishable frequency intervals of the signal pattern are specified during system analysis and at run time the mean values of those intervals are calculated and concatenated into the feature vector.

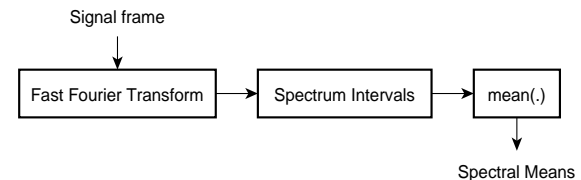


Fig. 2. Feature extraction of spectral means

The second method (Fig. 3.) is a popular feature representation of audio signals [6], called Mel-Frequency Cepstral Coefficients (MFCC). The frequency power spectrum, which is a squared absolute frequency spectrum, is scaled to the mel-scale and the cepstral coefficients are calculated by applying a Discrete Cosine Transform (DCT).

The mel-scale is given by

$$Mel(f) = 2595 \log_{10} \left( 1 + \frac{f}{700} \right), \quad (1)$$

where  $f$  is the linear frequency in Hz. It models the human sound perception and is almost linear up to 1 kHz and logarithmic thereafter, imitating the increasing deficiency of human perception of the higher frequencies. The cepstral coefficients of the resulting mel energies provide information about the harmonic frequencies present in the power spectrum.

In this paper we apply the implementation of MFCC by Ellis [7]. The mel-scaled

energies and the cepstral coefficients are concatenated to form the feature vector.

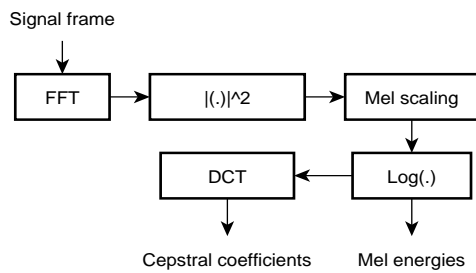


Fig. 3. MFCC feature extraction

## 2.2 Classification Methods

Two conceptually different classification methods are chosen for comparison: correlation-based and a fuzzy algorithm.

The knowledge base of the correlation-based classifier consists of  $C$  reference vectors, at least one per class. The algorithm makes its class estimate by calculating the correlation between the incoming feature vector and each of the  $C$  reference vectors. The reference vector corresponding to the maximal correlation determines the class label. The algorithm is very simple, but not very robust nor noise tolerant.

The fuzzy classification algorithm is more sophisticated and robust. For its decision-making it uses a rule base which is derived from a large number of reference feature vectors [8], thus accounting for the variance in process dynamics. The inference mechanism is based on the principals of fuzzy logic. It calculates the degrees of membership of the unknown feature vector to the feature subspaces corresponding to different classes. The feature subspace of the highest membership value defines the winning class.

## 3. TEST SIGNAL ACQUISITION

### 3.1 Experiment Setup

The experiments took place at the shop floor of a small size manufacturing facility during common operational conditions, i.e. full staff and standard machinery operation cycles. Two pieces of manufacturing

equipment were chosen for testing: the two degree of freedom Vytex 200 watts CNC laser cutting machine LST4896 and the three degree of freedom AXYZ CNC-router 6020.

During the experiment the laser was cutting small rectangular pieces of a 1 mm polystyrene sheet. The cutting proceeded row-wise with the carriage returning the laser head to the beginning of the previous row with one piece position lower from it. The laser cutting process consists of the following states:

- 1) Laser is idle.
- 2) Laser is cutting.

The CNC-router during signal acquisition was cutting a sheet of 21 mm plywood. During the whole process of cutting several shapes from the plywood the spindle did not stop spinning, thus the procedure is regarded as a continuous working cycle. The router possesses several operation states:

- 1) Router is idle.
- 2) Compressed air supply enabled.
- 3) In addition to 2): vacuum pump enabled.
- 4) In addition to 3): dust collector enabled.
- 5) In addition to 4): cutting process.

In total two types of signals were analyzed during the cutting experiments: the acoustic signal acquired by a microphone and a vibration signal acquired using an acceleration sensor. Both types of signals were acquired in parallel to each other and thus correspond to the same events.

### 3.2 Acoustic Signal Acquisition

Audio signals were measured using a Shure SM58 microphone and converted to digital form using a Roland Edirol UA-25EX audio signal processor at 44.1 kHz sampling rate in mono channel mode, saved in a 16-bit Waveform Audio File (WAV) format. Thus the audio signal is normalized to a scale of  $[-1, 1]$ .

In both the laser and router cases the microphone was placed beside and directed towards the apparatus approximately 1.2 m

above the floor. Thus no direct contact was made between the sensor and the machine.

### 3.3 Acceleration Signal Acquisition

Vibration measurements were made with an analog dual-axis accelerometer ADXL311 with a sensitivity of  $\pm 2g$ ,  $0g$  bias of 1.5 V and sensitivity of 174 mV/  $g$  at the operating voltage of  $V_{DD} = 3$  V. The signals were digitized at a sampling frequency of 1 kHz using an Agilent U2354A data acquisition device.

For the laser test the accelerometer was firmly attached on top of the x-axis carriage. The x axis was then pointed perpendicular to the movement of the carriage and the y axis – parallel to it. During the routing experiment the transducer was attached to the spindle parallel to the Earth surface with x and y axis pointed along the first two degrees of freedom of the carriage.

As in both cases the sensor is placed parallel to the ground, the gravitational component is not present in the axis's readings and the  $0g$  bias is easily subtracted from the signal. Signal analysis was performed on just one axis – the one that shows greater deviation of the signal during different process stages.

## 4. SIGNAL PROCESSING AND CLASSIFICATION RESULTS

Signal processing starts with an analysis step where it is determined whether the events of interest are at all distinguishable in the signal and if they are, their corresponding time intervals are specified. The analysis is performed by examining the signals in the frequency domain using spectrograms (i.e. three-dimensional plots of successively lined up signal frame spectra). Class labels are assigned to all the distinguishable process states of interest. Sample datasets are generated for reference and testing. After the datasets have been generated, analysis and testing ensues.

### 4.1 Signal Analysis, Processing and Reference Class Label Assignment

For signal processing a frame size of 16384 samples for audio signals is chosen, which corresponds to 0.372 s at the sampling frequency of 44.1 kHz and 256 samples for the acceleration signals which corresponds to 0.256 s at the 1 kHz sampling frequency. Every signal is analyzed by its amplitude and shape in the time domain and by its spectral pattern in the frequency domain. A plot of the laser audio signal and its spectrogram is presented as an example in Fig. 4. As it can be seen, the idle time intervals (0-10, 104-107, 201-204, 298-304 s) and the cutting cycle intervals (10-104, 107-201, 204-298 s) are well separable and thus identifiable.

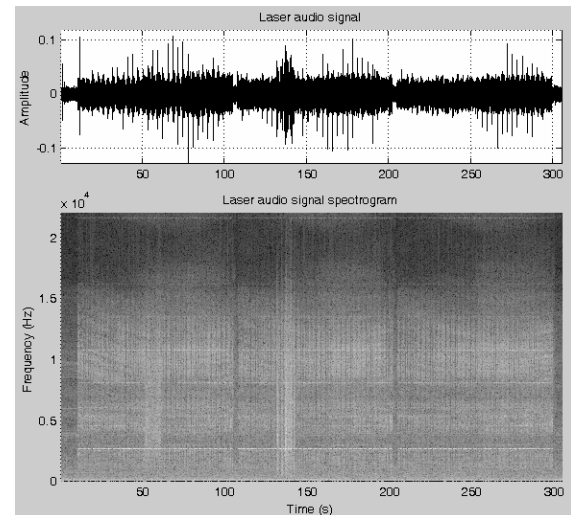


Fig. 4. Laser audio signal and spectrogram

The identification of both states of laser operation described in Section 3.1 is thus possible. Class labels are assigned accordingly: class 1 to state 1) and class 2 to state 2). For the acceleration signal analysis the y axis (the one parallel to the carriage movement) is chosen. The vibration levels are very low in case of this machine, thus the identification is based more on the carriage movement. Class labels are assigned as for the audio signal. For the router all five modes of operation can be identified using the audio signal, the assigned class labels are identical to the mode of operation indexes (Section 3.1).

The acceleration sensor is able to differentiate only the fifth state (cutting) from all the others. As the sensor is placed on the spindle, it detects only its vibration; all other vibrations seem to be well dampened. Thus two class labels are assigned: class 1 to states 1) - 4) and class 2 to state 5).

#### 4.2 Classification Results

The knowledge base of the correlation-based classifier consists of reference feature vectors, one per class. Each vector is derived by taking the average values of 20 successive vectors from the signal dataset, belonging to the same class. The rule base of the fuzzy controller is trained on half of the dataset feature vectors. For both classification methods whole datasets are used for classification accuracy testing. The classification accuracy is estimated in the percentage of correctly classified frames, i.e. the ratio between the number of frames with estimated class labels concurring with the reference and the total number of frames in the signal.

The classification accuracy for the correlation-based classifier is presented in Table 1. The majority of the estimates is above 95%, the average being 91.7%, which is an excellent result considering low robustness of the classification algorithm. For the laser experiment the results are however ambiguous, since the laser is not cutting the material continuously and stops emission during the transition from one cut piece to the other. This results in some frames during the cutting stage being classified as non-operation, which is ultimately correct. Therefore the actual classification quality is higher, than estimated by the ratio metric.

	Sp. means	MFCC
Laser audio	92,68	97,56
Laser accel.	91,80	65,80
Router audio	91,76	95,72
Router accel.	98,39	99,85

Table 1. Correlation classifier results (%)

The classification results for the fuzzy classification algorithm are listed in Table 2. As expected, the accuracy is higher than for the correlation classifier with the average value being 93.1%. The results for the laser experiment are similar to the previous case, with the ratios being even lower, signifying a greater sensitivity of the algorithm to the process dynamics. These ambiguous results are presented in the upper subplot of Fig. 5.

	Sp. means	MFCC
Laser audio	89,02	98,05
Laser accel.	73,40	87,65
Router audio	98,68	98,72
Router accel.	99,85	99,49

Table 2. Fuzzy classifier results (%)

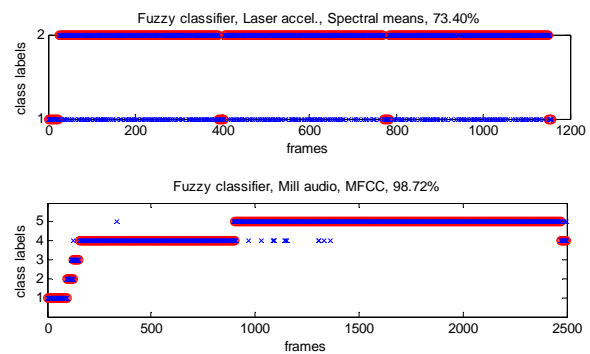


Fig. 5. Signal classification result example plots: circles denote reference and crosses denote estimated class labels

#### 4.3 General Quality Assessments

The set of experiments with the test data can be considered successful. High machine state identification accuracy was achieved for almost all test signals. The fuzzy classification algorithm shows better performance as was expected. However the correlation-based algorithm is likely to produce more erroneous results with increased background noise. Both feature extraction algorithms have proven to be applicable. The increase in the number of classes does not affect classification quality (lower plot of Fig. 5.) if the classes are well enough separable.



## 5. FURTHER RESEARCH

The experiments were conducted using only one measurement point per signal type. An obvious direction for future research is multipoint measurements and the development of methods that would enable cooperation and complementation of several monitoring system procedures for more concise and robust decision-making. The methods should be also evaluated in the presence of greater background noise.

From the aspect of production planning, knowing the reason behind the pauses in production is important. Therefore the automatic methods of interruption cause estimation are worthy of research.

## 6. CONCLUSION

Several signal processing and classification methods applicable for a manufacturing machinery monitoring system were evaluated in the paper. The combinations of these methods were tested on signals acquired by acoustic and acceleration sensors at the shop floor of an industrial facility under common operation conditions. Two machines were considered for the experiments – a laser cutting machine and a CNC-router. Testing results have shown that the proposed system is capable of identifying the operation states of these machines with high efficiency.

## 7. ACKNOWLEDGEMENT

The work presented in this paper was partially supported by Innovative Manufacturing Engineering Systems Competence Centre IMECC that is co-financed by Enterprise Estonia and European Union Regional Development Fund (project EU30006), by Artemis JU Project Simple (grant agreement number 100261), Research Project SF0140113Bs08 and Estonian Science Foundation (grant F7852).

## 8. REFERENCES

1. Wright, P.; Dornfeld, D. and Ota, N. Condition monitoring in end-milling using

wireless sensor networks (WSNs). *Trans. NAMRI/SME*, 2008, **36**.

2. Guo, Y.B. and Ammula, S.C., Real-time acoustic emission monitoring for surface damage in hard machining, *Int. Jour. of Machine Tools and Manufacture*, 2005, **45**, 1622-1627.

3. Aruväli, T.; Preden, J.; Serg, R.; Otto, T., In-process determining of the working mode in CNC turning, *Est. Jour. of Eng.*, 2011, **17**, 4 – 16.

4. Vaseghi, S. V. *Multimedia signal processing: Theory and applications in speech, music and communications*. John Wiley & Sons Ltd., UK, 2007.

5. Frigo, M. and Johnson, S. G. FFTW: an adaptive software architecture for the FFT. *IEEE Int. Conf. on Ac., Sp. and Sig. Proc.*, 1998, **3**, 1381-1384.

6. Peeters, G. A large set of audio features for sound description (similarity and classification) in the CUIDADO project. *CUIDADO I.S.T. Project Report*, 2004.

7. Ellis, D. PLP and RASTA (and MFCC, and inversion) in Matlab using melfcc.m and invmelfcc.m. *labrosa.ee.columbia.edu*, Last upd. Aug. 2010, Last vis. May 2011. <http://labrosa.ee.columbia.edu/matlab/rasta/mat/>

8. Riid, A. and Rüstern, E. An Integrated Approach for the Identification of Compact, Interpretable and Accurate Fuzzy Rule-Based Classifiers from Data. *15th IEEE Int. Conf. on Intell. Engin. Sys.*, 2011, 101-107.

## 9. ADDITIONAL DATA ABOUT

### AUTHORS

Sergei Astapov, Research Laboratory for Proactive Technologies, Dep. of Computer Control, sergei.astapov@dcc.ttu.ee

Jürjo Preden, Research Laboratory for Proactive Technologies, Dep. of Computer Control, jurgo.preden@ttu.ee

Tanel Aruväli, Dep. of Machinery, tanelaruväli@hotmail.ee

Boris Gordon, Dep. of Computer Control, borsi.gordon@dcc.ttu.ee

All authors are with Tallinn University of Technology, Ehitajate tee 5, 19086 Tallinn, Estonia.

## MICRO/NANOROBOTICS IN TECHNOLOGICAL MICRO/ NANOPROCESSING AND MICRO/NANOSYSTEMS ENGINEERING

Gheorghe, Gh. I. & Badita, L. L.

**Abstract:** *Micro/nanorobotics applications make it to expand in several areas. Some of the most important applications are nanopositioning and nanomanipulation. Technologies /micro-nanotechnologies for nanomanipulation include observation, setting in motion, measurement, system's design and manufacture, calibration and control.*

*We are using a Hexapod positioning system, Micro-Movement F-206, for positioning the samples studied with an atomic force microscope. The connection between these two systems is done with a finger device that allows nanopositioning of samples. This system is used for characterizations and determinations of tribological parameters of surfaces containing different materials. We determined roughness surfaces of some femoral heads from hip prostheses realized by steel, CoCrMo, steel coated with TiN; polycrystalline diamond compact surfaces COMPAX 1321; steel-component material of different mechanical parts.*

*Key words: Micro/nanorobotics, micro/nanopositioning, micro/nanoprocessing, micro/nanosystems engineering*

### 1. INTRODUCTION

On the nano-scale basis, technology has shifted to a more powerful and intelligent control of material structure, suggesting the feasibility of achieving the control of the molecular structure of matter atom by atom.

Nanorobotics deals with the study of nanometer scale robotics and include robots that are nanometer-size and large

robots able to manipulate objects with nanometer dimensions. Nanorobotics [1] integrates various disciplines, including nanofabrication processes used to produce nanoactuators, nanosensors and nanometer scale physical modeling. In this field are also included manipulation technologies, like nano-scale assembly of units, biological cells and molecules manipulation and types of robots used to perform these tasks.

Materials science, biotechnology, biomedical sciences, engineering sciences, electronics and mechanical stimulation will benefit from nanorobotics developments [2]. With the ability to position and orient nanoscale objects, nanorobotic manipulation is a promising way to enable the assembly of nanosystems, construction and characterization [3] of micro/nanoelectromechanical systems (MEMS/NEMS). Materials characterization is important when we want to determine features of different surfaces that are used in many areas. Tribological parameters help to this type of characterization, mainly for worn surfaces. There are techniques with complex mechanisms that allow to obtain these parameters and to observe all the surface characteristics.

### 2. MANIPULATION METHODS

The most common ways to achieve nanometer scale setting in motion are the electrostatic, electromagnetic and piezoelectric. For nanorobotics manipulation the actuators, generating large movements and forces, are the most suitable for such applications.

Electrostatic charge is based on the accumulation of free electrons in a material, which can exert an attractive force on opposite charged objects or a repulsive force on similar charged objects. Very low power consumption associated with electrostatic devices determines moving highly efficient implementation. Electromagnetic fields appear by the movement of electric current through a conductive material. Attractive or repulsive forces are generated adjacent to the conductor and proportional to current flow. Focusing and accumulating these forces, the movement will be created. Piezoelectric movement appears after dimensional changes generated in certain crystalline materials subjected to an electric field or an electrical charge. In this way structures can be achieved, which collect and focus the force of dimensional changes and uses them to create movement. At the micro-scale, piezoelectric materials were used in linear transport devices and most nanomanipulators use piezoelectric actuators. Thermal movement produced by thermal expansion amplification refers to the tendency of matter to change in volume in response to a change in temperature.

### 3. NANOROBOTIC SYSTEMS FOR NANOMANIPULATION

Technologies for nanomanipulation [4] include observation, setting in motion, measurement, system's design and manufacture, calibration and control, the results dissemination and man-machine interface. The basic requirements for a nanorobotic 3D system for nanomanipulation include nanometric scale positioning resolution, a large workspace, sufficient freedom degrees and orientation's control of multiple effectors for complex operations. Nanomanipulation was made possible by scanning tunneling microscopy (STM), atomic force microscopy (AFM) and other types of microscopes appearance to scan

the sample [5]. Nanorobotic manipulators (NRMs) have 3D positioning capacity, orientation's control and systems employed in real-time observation that can be integrated with microscopes to scan the sample.

STM can be applied to particles with the size of atoms. A standard STM is not suitable for complex manipulation and cannot be used in 3D space because of its limitation in 2D positioning.

AFM manipulation involves the movement of an object by tapping it with a tip. A typical manipulation occurs as follows: the image of a particle in non-contact mode, then oscillations remove and the sweep of the tip over the particle that is in contact with the surface. The mechanical pushing can exert more powerful forces on objects and so, it can be applied to manipulate larger objects. 1D and 3D objects can be manipulated on a 2D substrate.

A nanorobotic manipulation system with 16 degrees of freedom (DOFs) is shown in Fig. 1a, which can be equipped with three or four AFM tips as effectors both for manipulation and measurement.

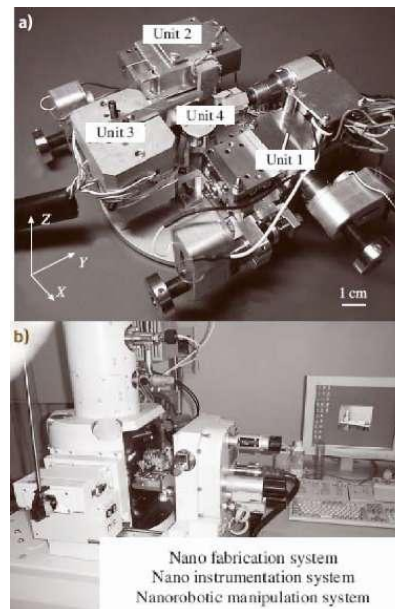


Fig. 1. Nanorobotic system. (a) Nanorobotic manipulators. (b) System set-up.

The main functions of this nanorobotic manipulation system are nanomanipulation, nanoinstrumentation,

nanofabrication and nanoassembly. Measurements of four semiconductor samples are probably the most complex manipulation that can perform this system because it is necessary to stimulate four independent samples by four manipulators. If all four samples are used together, many and various applications are possible for manipulators.

A nanolaboratory shown in Fig. 1b integrates a nanorobotic system for nanomanipulation with an analytical system and a nanofabrication system. It is a complex system, taking into account that it can be applied for nanomaterials manipulation, nanogroups manufacturing, nanodevices assembling and in situ properties analysis of such materials, groups and devices.

#### 4. TECHNIQUES AND MECHATRONIC SYSTEMS USED FOR CHARACTERIZATION OF MATERIALS SURFACE

Wear processes occurring inside different systems are often impossible to see with the naked eye. A methodology of ascending degrees of resolution was established using macroscopic (resolution millimetres), microscopic (resolution microns) and nanoscale (resolution nanometers) measurements.

Characterization of worn surfaces and determination of its tribological parameters can be achieved by noncontact surface measurements using atomic force microscope, confocal microscope, scanning interferometer or triangular laser.

At INCDMTM, characterizations and determinations of tribological parameters for surfaces containing different materials are realized using an atomic force microscope (Microscope Probe NTEGRA - Fig 2) working in the noncontact mode. Working principle of AFM is to measure the interaction force between tip and sample surface using special measuring heads, made of a cantilever with a pointed end.



Fig. 2. Atomic Force Microscope NTEGRA Probe NanoLaboratory: 1 – base unit; 2 – measuring head; 3 – vibration isolation system; 4 – optical viewing system.

The samples are positioned on the base unit of AFM using a robotic nanomanipulator that has more DOFs including rotation for control of orientation and thus, can be used to manipulate 0D objects (spherically symmetric) to 3D objects in space [6].

A Hexapod positioning system for Micro-Movement, F-206 [7], being produced by Physics Instruments (PI) GmbH & Co KG, Karlsruhe, Germany, is used in this experiment and is integrated at INCDMTM, within MEMS/NEMS laboratory. This 6-axis positioning system consists of an attachment position system (Fig. 3a) and a control unit (Fig. 3b).

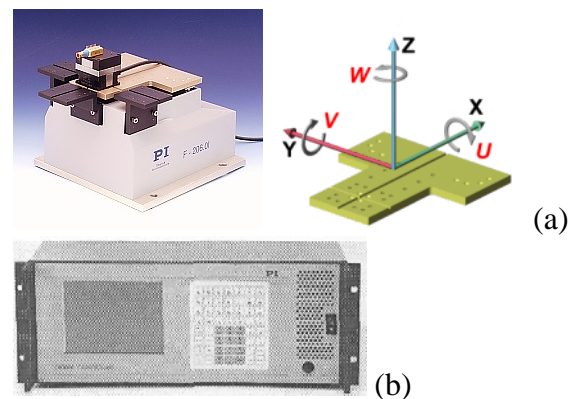


Fig. 3. F-206 alignment and positioning system with six axes: (a) hexapod positioning system – all commands and operations are using (X, Y, Z and U, V, W) coordinates. Travel range: X = -8 to +5.7 mm, Y = ±5.7 mm, Z = ±6.7 mm, U = ±5.7°, V = ±6.6°, W = ±5.5°; (b) control unit.

A keyboard and a monitor for the control unit may be used to control F-206 system directly or, typically, the control unit can be controlled by a PC. System's mechanics uses a parallel - cinematic positioning system, containing 6 linear actuators with screw actuators and optical encryption systems. The system provides 6 DOFs and a minimal increase of movement of 0.1  $\mu\text{m}$ . Workspace boundaries are not parallel to the axes, but it cannot overcome a rectangular solid which is given by the limits of movement X, Y and Z. The control unit is equipped with integrated software to define a pivot point anywhere inside or outside workspace of F-206 system. Rotation around this pivot point may be ordered for any combination of the 3 rotation axes.

All orders for positioning "F-206 platform" are given in orthogonal coordinates and converted by command system in F-206 specific actuator positions and speeds before making the action.

The connection between NTEGRA Atomic Force Microscope and the Hexapod positioning system for Micro-Movement F-206 is done with a finger device (gripper) that allows nanopositioning of samples used. A scheme of the obtained complex system used to characterize and analyze the studied surfaces is presented in Fig. 4.

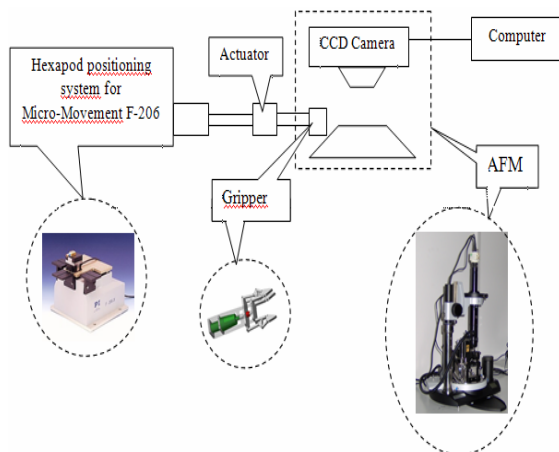


Fig. 4. Complex mechatronic system made up of NTEGRA Atomic Force Microscope and F-206 alignment and positioning system with six axes.

## 5. EXPERIMENTAL RESULTS CONCERNING TRIBOLOGICAL CHARACTERIZATION OF DIFFERENT MATERIALS SURFACES

In our institute were carried out characterizations and determinations of tribological parameters (like surface roughness) of different surfaces: areas of the femoral heads of hip prostheses CoCrMo (Fig. 5), femoral heads of hip prostheses TiN (Fig. 6), femoral heads of hip prostheses Ti6Al4V (Fig. 7), polycrystalline compact diamond COMPAX 1321, steel – component material of different mechanical parts.

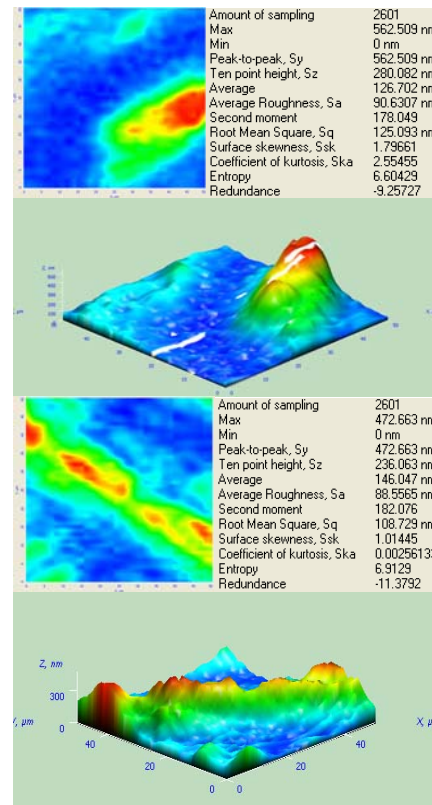


Fig. 5. Tribological characterization of CoCrMo surfaces using NTEGRA AFM

Femoral heads surfaces and component parts made of steel, titanium alloys or CoCrMo alloys, generally, deteriorate due to the pressures produced by mechanical movements of the systems it is part of.



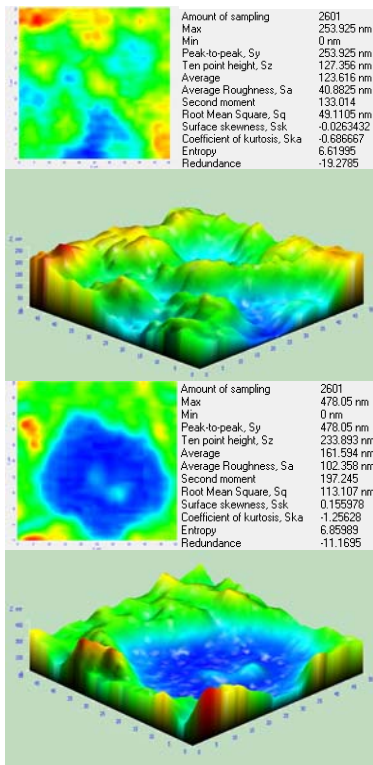


Fig. 6. Tribological characterization of TiN surfaces using NTEGRA AFM

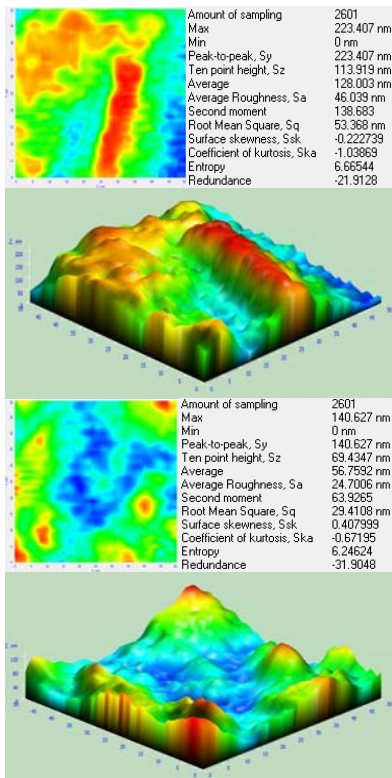


Fig. 7. Tribological characterization of Ti6Al4V surfaces using NTEGRA AFM

As it is shown in the examples presented, roughness has different values (in different

parts of the same femoral head) depending on the movements of the body that uses the prostheses.

Besides the hip prostheses surfaces characterization, were also characterized several polycrystalline compact diamond COMPAX 1321 surfaces. This material can be used as an active part of a lathe tool for processing metallic/non-metallic materials. Tribological parameters obtained can be seen in Fig. 8, together with the 3D image of the worn surface.

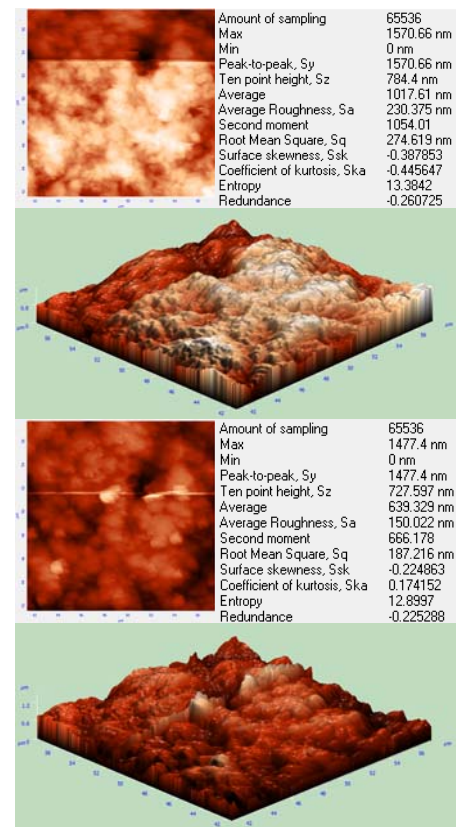


Fig. 8. Tribological characterization of polycrystalline compact diamond COMPAX 1321 surfaces using NTEGRA AFM

## 6. CONCLUSION

In order to obtain a clear characterization of realized parts surfaces or the coatings from the femoral head of a hip prosthesis the study of its topography and roughness determination are useful. Such a study can be made by different techniques and different systems. AFM was used because its images display high quality and dense

nanocrystalline structure of prepared thin films. NTEGRA Probe Microscope has been connected with a Hexapod positioning system for Micro-Movement F-206 in order to obtain a complex positioning of the sample, followed by surface characterization and determination of few tribological parameters.

INCDMTM Bucharest, Romania, by its MEMS/NEMS Laboratory, will develop in the future, micro/nanorobotic systems/micro/nanosystems for micro/ nanomanipulation and micro/ nanopositioning, micro/ nanotechnological micro/ nano-platforms for European modernization and qualifications of micro/ nanoindustries and micro/ nanoengineering.

## 7. REFERENCES

- [1] Gheorghe, I. Gh. *Intelligent MicroNanoRobotics*, Ed. CEFIN, Bucharest, 2010.
- [2] Gheorghe, I. Gh., Palade, D. D., Moldovanu, A., Ciobota, D., Pacioga, A. *Advanced micro-technologies through rapid prototyping by selective laser sintering*, Ed. CEFIN, Bucharest, 2010.
- [3] Vlad, S., Cristea, M., Ciobanu, C., Macocinschi, D., Filip, D., Nistor, A., Gradinaru, L. M. Characterization of some soft polyesterurethane films. *J. Optoelectron. Adv. Mater.*, 2010, **12**, 2278-2287.
- [4] Avouris, Ph. Manipulation of Matter at the Atomic and Molecular Levels, *Acc. Chem. Res.*, 1995, **28**, 95-102.
- [5] Baur, C., Gazen, B. C., Koel, B., Ramachasran, T. R., Requicha, A. A., Zini, L. Robotic Nanomanipulation with a Scanning Probe Microscope in a Networked Computing Environment. *J. Vac. Sci. Technol.*, 1997, **B15**, 1577-1580.
- [6] Gheorghe, Gh. I., Badita, L. L. *Advanced micro and nanotechnologies in mechatronics*, Ed. CEFIN, Bucharest 2009.
- [7] Gheorghe, Gh. I. *Integrated intelligent MicroNano-Technologies*, Ed. CEFIN, Bucharest, 2010.

## 8. ADDITIONAL DATA ABOUT AUTHORS

Authors: Prof. univ. dr. eng. Gheorghe Ion Gheorghe; PhD student phys. Liliana-Laura Badita  
Manuscript "Micro/nanorobotics in technological micro/nanoprocessing and micro/nanosystems engineering"  
National Institute of Research and Development in Mechatronics and Measurement Technique (INCDMTM)  
6-8 Sos. Pantelimon, District 2, Bucharest, Romania  
Phone +40 21 252.30.68/69  
Fax +40 21 252.34.37  
E-mail: [cefin@cefin.ro](mailto:cefin@cefin.ro)  
[www.cefin.ro](http://www.cefin.ro)

Corresponding Author: Liliana-Laura Badita, [badita\\_l@yahoo.com](mailto:badita_l@yahoo.com)



## MICRO-TECHNOLOGIES AND SPECIAL MATERIALS FOR THE DEVELOPMENT OF MECHATRONIC MICRO-NANO SYSTEMS FOR ULTRA PRECISE MEASUREMENT PROCESSES

Gheorghe, Gh. I. & Despa, V.

**Abstract:** *This scientific work deals with new technologies that apply laser micro-sintering of special materials with structures based on nickel, titanium and cobalt, for new high precision linear and angular mechatronic micro-displacements micro-nano-systems.*

*Scientific work is based on experiments and tests of laboratory micro-technology and micro-nano-systems used in the advanced areas of micro-engineering and micro-medicine.*

*Key words: advanced micro-technology, mechatronic micro-nano-systems; micro-sintering; micro-engineering.*

### 1. INTRODUCTION

Currently, are known and applied various advanced micro-technologies using conventional operating principles and especially advanced unconventional operating principles.

Of these, the most advanced and effective is the advanced micro-technology of selective laser sintering based on the new principles of integrated design - 3D design - execution of micron layers made from nano-grained powders, successively deposited and solidified.

Selective Laser Sintering - SSL - is a family of methods that can build a solid body from various types of material - plastic, metal, ceramic - very rare methods or physical, mechanical and biocompatibility properties, made from special powder material by solidification, by exposure of successive layers of powder

under the action of various powers laser beams.

Through this micro-technology, parts, subassemblies and assemblies are obtained, with any geometric complexity of mechatronic micro-nano-systems for ultra-precise measurement processes.

Selective laser sintering advanced micro-technology for metal micro-powders was implemented and used in INCDMTM Bucharest in advanced research for high-tech micro-engineering, micro-medicine fields, and so on.

### 2. SELECTIVE LASER MICRO-SINTERING

Selective laser micro-sintering is based on the intelligent mechatronic equipment type EOSINT M 270 and the rapid prototyping process based on three-dimensional CAD data and micro-powders of various alloys, and bronze-based alloy, martensitic steel, stainless steel, super alloy cobalt-chromium, titanium alloy and so on.

The intelligent mechatronic equipment type EOSINT M 270 (Fig. 1) with the schematic diagram shown below (Fig. 2) represents the technical and technological infrastructure of the advanced micro-technology and laser sintering.

Micro-powder metallic materials as used in the selective laser sintering technology, have special physical and micro-mechanical qualities, have properties of biocompatibility and corrosion resistance and are suitable for biomedical, aerospace, mechatronics, robotics, and automotive industry and so on.

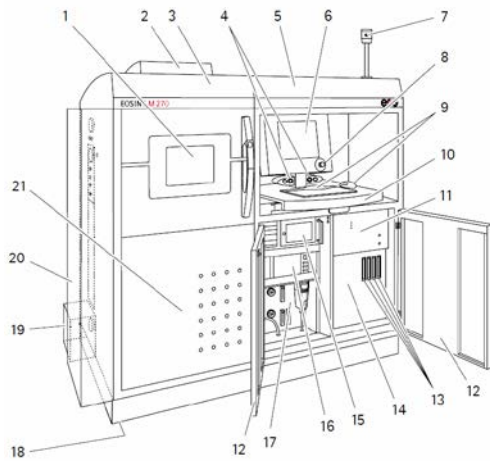


Fig. 1 EOSINT M 270

Legend:

1. Processing room
2. Scanner lid
3. Left hood of the optical system  
(Only for EOS service personnel)
4. Xtended installation mode only:  
release key
4. Right hood of the optical system  
(Only for EOS service personnel)
6. Screen
7. Xtended installation mode only:  
Signal light
8. Emergency stop button
9. Keyboard and mouse
10. Operating table (pivot)
11. Laser
12. Front door
13. Xtended installation mode only:  
Protective gas shift indicator
14. Xtended mode installation:  
Shielding gas control unit
15. Process computer
16. Final stage engine
17. Air maintenance unit
18. Anti-state carpet connection
19. Cable shielding
20. Control cabinet
21. Front cover  
(Only for EOS service personnel)

Selective laser sintering processes is based mainly on the experience gained in the design of intelligent steno-lithographic

equipment and expanding technological research on some other group of materials with mechanical and technological properties closer to the needs of MEMS and NEMS constructions and functional assemblies.

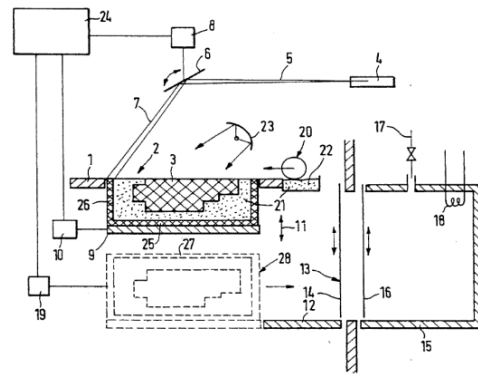


Fig. 2 Schematic diagram

Legend:

1. Horizontal work section
2. Active surface of the working board
3. Section through piece
4. Laser generator
5. Focused laser beam
6. Beam deflection device
7. deflected laser beam
8. controller
9. base plate work
10. Adjuster
11. Direction indicator
12. Board receivers
13. Opening
14. Watertight door
15. Container for disposal
16. Container door seal
17. Inert gas supply means
18. Heating
19. Download device
20. Powder coating applicator
21. Powdery material
22. Powder supply
23. Radiator heating
24. Central control device
25. Fixing layer powder device
- 26 to 28. Container

In the rapid prototyping project, we have succeeded in demonstrating that a thin

layer (of approx. 18  $\mu\text{m}$ ) of certain mixtures of powders under the action of the laser beam can reach locally, based on duration of exposure, the melting temperature of the transition of the powder layer to liquid state. Based on the physical properties of powders, immediately after the laser action has ceased, almost always local solidification is attained, obtaining a compact layer, placed on the direction of molecular chains, surrounded by a volume of powders exposed to laser light.

The explanation of solidification is essentially based on the same mechanism of stereo-lithographic procedures, installing chemical bonds forming linear molecular chains, or three-dimensional trees.

For these states, state transitions, which imply a significant local heating device, can be accelerated by initializations and controlled by inhibitory substances and the energy can be obtained by concentrated heat sources in the working place, laser radiation, and so on.

All these sources must be adapted and adjusted on the fly, so as to give additional heat to reach the melting temperature which provides favourable thermal and kinetic conditions and development process by establishing molecular chains and partial crystalline structure, with the transition from liquid to the solid state, strengthened, that marks the sintering process.

In terms of energy, industrial powders / micro-powders, with a wide range of melting temperatures, require a different heat input from the concentrated source of energy. Choosing the activation energy required is possible by selecting fast heating regimes under dynamic sintering process.

The diversity of these regions has attracted finally the „selective sintering” denomination. In conclusion, this phase is better than the earlier period when stereo-lithography technology and equipment were researched, designed and approved, by the following elements of technical progress, as follows:

- stereo-lithography processes are limited to use acrylic or epoxy photo-polymers which could be generate a small range of products;
- selective laser sintering processes are based on a lot of material such as plastics, ceramics and metal powders, which will result in even more products at a higher layer of performance, i.e. with physic-mechanical properties closed to the requirements of used equipment parts.

### 3. SPECIAL MATERIALS AND TYPES OF SINTERING

Due to fundamental and applicative research conducted it was concluded that the sintering mechanism explanation is more complex because it is different from conventional sintering due to the flowing features, as follows:

- selective sintering is initiated prior to making powders, although powders are pressed by roller compaction (Fig. 3);

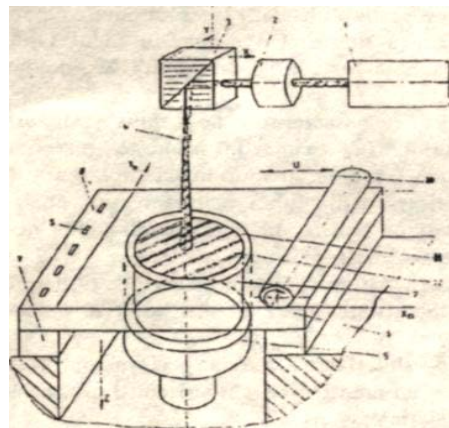


Fig. 3 Roller compaction

- the variety of powders with different melting temperatures pretends power laser devices with continuous emission for melting. Therefore, instead of He-Cd lasers, are adopted higher power CO<sub>2</sub> lasers;
- the universal character of SLS equipment, resulting from the initial set of materials that can be processed with a CO<sub>2</sub> laser facility. Because of its selectivity, the device can provide power emission.

In continuous regime, at the level of automated regulations, that provide:

- low intensity when melting wax;
- higher intensities for melting metal powders;

Sintering achieves high performance when using a powder mixture consisting of two groups of material;

Types of particles used in selective laser sintering technology in the laboratories of INCDMTM Bucharest, Romania, are mainly as follows:

- a. metal powders, category A:
  - o EOS CobaltChrome MP1
  - o EOS CobaltChrome SP2
  - o MaragingSteel EOS MS1
  - o StainlessSteel EOS GP1
  - o StainlessSteel EOS PH1
- b. metal powders, category B:
  - o EOS Titanium Ti64
  - o EOS Titanium TiCP

Geometric peculiarities of metallic powders are shown in Figure 4.

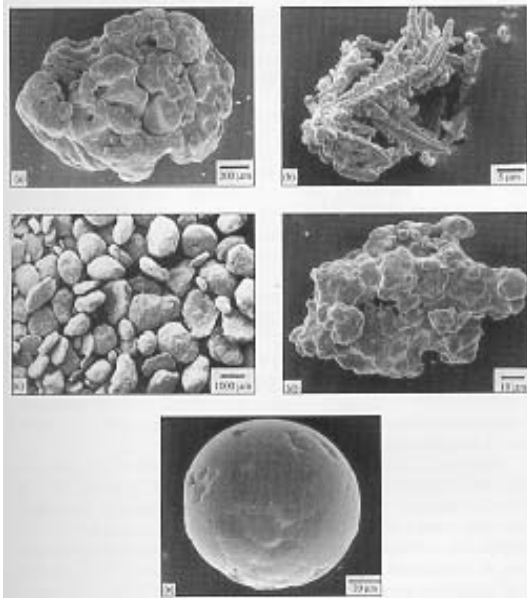


Fig.4 Geometric peculiarities of powders

#### 4. EXAMPLES OF INDUSTRIAL APPLICATIONS OBTAINED IN THE LABORATORY OF INCDMTM

Biomedical applications obtained are based on DICOM files to build a bone structure and is subjected to FEM analysis (Fig. 5 and Fig. 6).

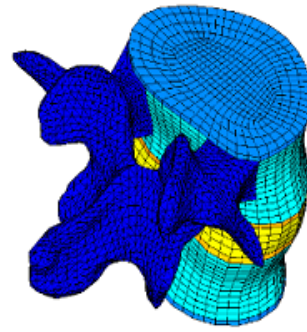


Fig.5 and Fig. 6

Applications obtained in the field of high accuracy are based on the CAD software and specialized software for rapid prototyping, as follows:

- o SolidWorks 2009 SP3.0,
- RapidWorks 2.3.1,
- NextEngineHD
- o PR-EOS Tools
- o EOS PSW offline
- o EOSTYLE,

that represents a specialized element – micro-motor gas turbine, shown in Fig. 7.



Fig. 7 Micro-motor gas turbine

Applications obtained for the aerospace field are based on the piece made from



EOS CobaltChrome MP1, are shown in Figure 8.

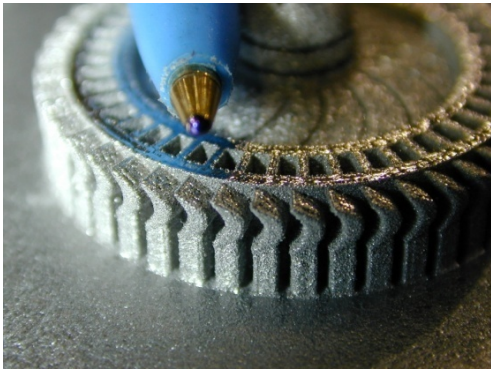


Fig. 8 EOS CobaltChrome MP1

Applications obtained for the field of finite implant elements in the laboratory of INCDMTM are shown in Figure 9,



Fig. 9 Implant elements

whose pre-execution phase, which is prior to physical execution, is the 3D design shown in Figure 10

The applications obtained in new concepts and developed by INCDMTM in the rapid prototyping laboratory, are shown in Figures 11 and 12.

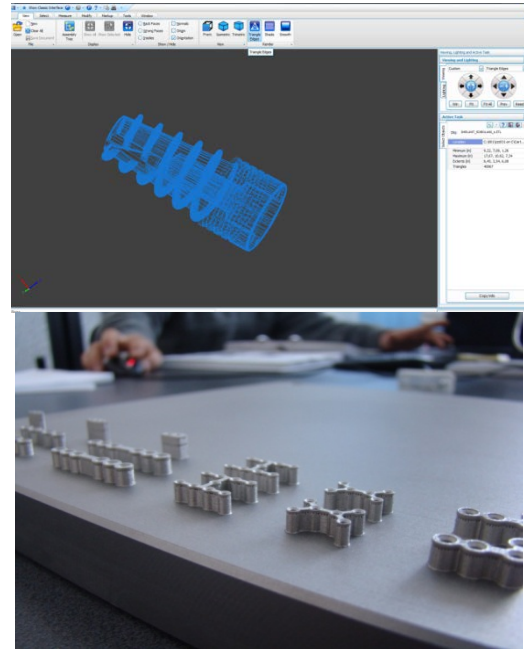
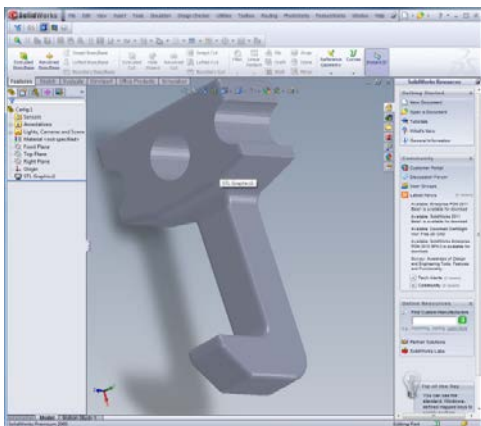


Fig. 11 and Fig. 12

In all applications obtained in the laboratory of INCDMTM and presented above, schematic representation of the data stream are shown in Fig. 13.

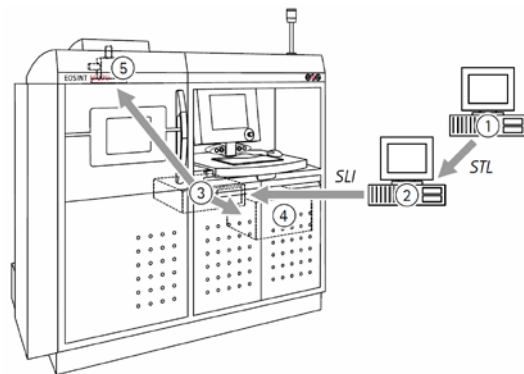


Fig. 13 Schematic of data stream.

Legend:

- 1 CAD data generation
- 2 Data preparation
- 3 Process computer
- 4 Laser
- 5 Scanner

## 5. CONCLUSION

New perspectives for the development of selective laser sintering technology, concern, immediately:

- o development of the triad: engineer-clinician - IT specialist;

- design of new advanced research technologies and biomedical devices, implants, 3D scanning, CT scan, MRI scan, DICOM handling, 3D design, e-Manufacturing (Rapid Prototyping, Rapid Manufacturing, Rapid Tooling),etc.;
- creation of a centre of excellence in research for new technologies related to CT and MRI medical imaging, 3D geometric modelling of osteo-articular structures, FEM mechanical and parameterization analysis (Finite Element Method -), Computer assisted surgery and Micro-surgical and orthopaedic corrective methods quantitative assessment.

## 6. REFERENCES

- [1] M. Shellabear: Trends and Prospects for e-Manufacturing using Laser-Sintering, PR 24th Seminar, Tokyo, June 2003.
- [2] Shellabear M., Lenz J., Junior V.: e-Manufacturing with Laser-Sintering - to Series Production and Beyond, Lane, Erlangen, September 2004
- [3] Thomas, W., Wolf,: Marks' Standard Handbook for Mechanical Engineers, Section 13.5 "Surface Texture Designation, Production, and Control", 2009
- [4] Yan, M., Gu, P., Huang, X., Zhang, X.: Analysis of Accuracy machine for rapid prototyping of quality components, Proceedings-of-SPIE, The-International-

Society-for-Optical- Engineering, V3517, 1998

## 7. ADDITIONAL DATA ABOUT AUTHORS

Authors: Prof. univ. dr. eng. Gheorghe Ion Gheorghe; PhD student eng. Veronica Despa

Manuscript "Micro-technologies and special materials for the development of mechatronic micro-nano systems for ultraprecise measurement processes"

National Institute of Research and Development in Mechatronics and Measurement Technique (INCDMTM)  
6-8 Sos. Pantelimon, District 2, Bucharest, Romania

Phone +40 21 252.30.68/69

Fax +40 21 252.34.37

E-mail: [cefin@cefin.ro](mailto:cefin@cefin.ro)

[www.cefin.ro](http://www.cefin.ro)

Valahia University of Targoviste

Blvd Carol I, Nr. 2, 130024, Targoviste, Dambovita, ROMANIA

Tel. +40/245/206101

Fax. +40/245/217692

Email: [rectorat@valahia.ro](mailto:rectorat@valahia.ro)

Corresponding Author: Gheorghe Ion Gheorghe, [geocefin@yahoo.com](mailto:geocefin@yahoo.com).

## **ADAPTRONIC MICROTECHNOLOGIES REGARDING MECHATRONIC NANOMETRIC MICRO-NANOSYSTEMS FOR MICRO-NANODISPLACEMENTS AND MICRO- NANOPOSITIONING**

**Gheorghe, I. Gh.; Istrateanu, S.**

**Abstract:** *This paper summarizes by the new mechatronic concepts and adaptronic microtechnologies and based on the results of laboratory experiments on physical models and virtual models, development of mechatronic nanometric micro-nanosystems for micro-nanodisplacements and micro-nanopositioning applicable in metrology laboratories.*

*Key words: adaptronic microtechnologies; nanometric micro-nanosystems; micro-nanodisplacements; micro-nanopositioning*

### **1. INTRODUCTION**

Intelligent mechatronic microtechnologies have contributed to the creation, development and implementation of highly precise mechatronic and nanometric micro-nanosystems with different type of technical and technological applicative functions and also of metrological type for micro-nanodisplacements and micro-nanopositioning.

In their conceptual and constructive evolution, highly precise mechatronic and nanometric systems and microsystems integrates principles and solutions based on new scientific discoveries, which become obsolete at some point and therefore require replacement or upgrading.

By using values engineering for highly precise mechatronic and nanometric systems and micro-nanosystems analysis it is concluded that technical and technological possibilities of replacing or upgrading obsolete components with new components based on latest scientific

knowledge and discoveries, thus contributing to creation and development of adaptronics, as new technology to modernize intelligent mechatronic and micro-nanomechatronic products.

Moreover, adaptronic technology has emerged as a result of support and further development of high-tech advanced mechatronics field (and micro-nanomechatronics), which is even advanced multidisciplinary and interdisciplinary domain providing new concepts and new solutions for mechatronic and micro-nanomechatronics, presently, and for the integronic and micro-integronics one in the future.

Adaptronics with mechatronics (and micro-nanomechatronics) form an important part of nanoscience and nanotechnology.

### **2. TRENDS IN ADAPTRONICS FIELD**

The development of high intelligence products using intelligent integrated micro-nanotechnologies characterizes the foundation of the technical, technological and scientific potential for achievement new high-tech products with high added value and hybrid concept specific to mechatronics and integronics, studying the dynamics of the masses, electrons displacement and the information flow.

New high intelligence products structure includes mix-hybrid integrated and multifunctional models, such as:

- Systems and micro-nanosystems for tasks programming that generate desired displacements/ movements and their



sequences according to the requirements/ conclusions provided, evidenced by micro-nanocontrollers and micro-nanoprocessors;

- sequences and motion systems and micro-nanosystems, comparing the functional parameters of the movement with the required parameters, with the implementation of compensations and appropriate corrections, using Proportional - Integrator - Derivative (PID) control algorithm;
- power amplifier systems and micro-nanosystems that amplifies the signal in accordance with the requirements of actuators and sensors;
- actuators systems and micro-nanosystems, that transfer the parametric signal in input signal according to the requirements of information process;
- systems and micro-nanosystems of micro-nanomechanisms and micro-nanomechanics transmissions, that realizes adaptation of actuators parameters to the requirements of the processing technology;
- architectural sensorial systems and micro-nanosystems informing and processing information flows related to technological processes parameters and that send appropriate signals to motion systems;
- systems and micro-nanosystems specific to signals training that include filters, amplifiers, etc., which processes signals in accordance with the requirements for entry into motion controllers;
- and other systems and micro-nanosystems.

Structure of new products with high intelligence is influenced by scientific progresses in the mechatronics and integronics fields, especially in the adaptronics.

A first future trend of adaptronics is towards design, development and maturation of "intelligent machine", which possesses sensorial properties with planning capacity, pattern recognition,

navigation, learning and intelligence, in this regard, understanding the ability to achieve a purpose or to have a desired behavior under uncertainty - uncertainty sources are represented by the occurrence of unexpected and contingent events and by incomplete and insufficient information to decide what to do).

Integrated adaptronics in "intelligent machine" allows interaction of the machine with the environment, through input quantities - information, energy, material, displacement, s.o. and by the output quantities - information, energy, actions, effects, s.o.

Architecture of adaptronics to an intelligent machine includes, as systems or subsystems, as follows:

- perception intelligent systems and subsystems, with the role of collecting, storing, processing and distribution of information on the machine's state and the machine operating environment;
- knowledge intelligent systems and subsystems with the role of assessment of information collected by perception subsystems and action planning tools;
- execution intelligent systems and subsystems with the role of responsibility for carrying out the machine actions, based on interactions from the other subsystems;
- intelligent self-healing systems and subsystems with the role of keeping the machine in good working conditions and to ensure intermittent monitoring of machine behavior, to prevent any damages or seize them immediately they appear;
- energy conversion systems and subsystems with quantitative assurance role and form of energy needed for other subsystems to have a well-functioning.

Adaptronics integrated in "intelligent machine" makes possible development of its integrated functions such as: perception, knowledge and execution. Another trend of adaptronics is conception and design, which considers the whole chain,

kinematically intelligent – informational with its entire complex and compact structure and its interconnection through data bases, speed of processing, decision and execution.

Adaptronics creative valences have already started to be confirmed in many mechatronic and integronics products in education, research and intelligent manufacturing fields, highlighting a new development of high intelligence products to a science of integration processes and highly integrated systems, similar to human anatomy.

The development of adaptronics field trends, in systematization perspective, is based on European 2020 and European 2030 strategies, which provide the most dynamic economy in the world, based on intelligent knowledge and able to ensure a continued economic growth.

On this line, adaptronics with mechatronics and integrons will be the new fundamental scientific basis for stimulating transdisciplinarity, interdisciplinarity and creativity.

### **3. ADAPTRONIC MICRO-TECHNOLOGIES – SUPPORT FOR NEW MECHATRONIC NANOMETRIC MICRO-NANOSYSTEMS FOR MICRO-NANO-DISPLACEMENTS AND MICRO-NANOPOSITIONING**

In the adaptronic microtechnology are many processes and intelligent technology systems designed by computer simulations, optimization and verification of the discussed solutions, alignment with international norms and standards and organological integrations to detail level, to ensure the overall performances of new mechatronic nanometric micro-nanosystems required by the applications submitted by the theme of design and technological procedure.

Adaptronic microtechnologies impose conditions through the research theme, such as:

- micro-nanodimensions and mass;
- micro-nanotrajectories of micro-nanodisplacements;
- micro-nanoworking space;
- micro-nanodeformations admitted to structure and frequency;

Adaptronic analysis regarding kinematics and structure of mechatronic nanometric micro-nanosystems, comprises the following:

- calculation of direct kinematics by the expression of position vector of the characteristic point and the transformation matrix (transfer);
- calculation of inverse kinematics by determining the reverse position given in the working space, based on the set of parameters specific to the structure of fundamental micro-nanomechanisms;
- speeds/ accelerations analysis by calculation and simulation of speed and acceleration of characteristic point or all degrees of freedom;
- evaluating the ensemble, from the following points of view:
  - developed working space has to be subject to design requirements and conditions;
  - rotation and translation couplings has to intervene in the calculation of stiffness;
  - speed and maximum acceleration of characteristic point has to be drawn indirectly from the design conditions that refer to the final trajectory;
- dynamic analysis to determine design parameters of the structure by:
  - inverse dynamics;
  - analysis of structure deformation;
- dynamic performances evaluation by:
  - maximum moment that should be as small as possible in accordance with the principle of low cost;
  - total mass, which must be as small as possible in accordance with the principle of low cost;
  - sufficient load capacity;
  - maximum deflection of the structure, which must be less than the

- allowable deflection imposed by the design conditions;
- evaluation of structure's deformation, from the final stage of detailed design of the structure
- detailed design of the structure, subject to constraints, which refer to:
  - total deformation value should be much lower than the admissible one;
  - natural frequency must be higher than admissible frequency;
  - determination of sensitivity of each element from the structure;
- final evaluation of the structure for:
  - total mass, which must be the minimum possible;
  - maximum deformation, which must be less than the allowable limit;
  - minimum natural frequency for a given trajectory must be greater than permitted one;
- in the case of failure to attain performance imposed by research topic, the cycle of the steps specified is repeated until completion values satisfying the conditions.

Adaptronic microtechnologies involved in future strategy of nanometric mechatronic and integronic micro-nanosystems will involve in the following key vectors:

- research of issues related to multirobot mechatronics micro-nanosystems, regarding planning of motion and orientation, regarding human-robot and robot-robot communication, regarding the distribution of intelligence in a large group of robots;
- research of complex control algorithms implementation to a robot / micro-nanorobot;
- research / design of intelligent micro-factories model, based on an operator, a network of processing modules with multiple levels of control, micro-nanorobots and surveillance micro-nanoinstruments;
- research of group assembly planning and management;

- research of forces distribution simulation between multiple robots that cooperate in the manipulation process;
- research of specific tasks simulation of micro-objects;
- research of some computer stations adaptable for micro-nanoassemblies;
- research of flexible microrobots using new principles of operation;
- research of micro-nanoassemblies using micro-nanorobots;
- research of micro-nanomanipulation micro-nanosystems for atomic force microscopes;
- research on intelligent materials and structured materials in thin layers;
- research on mechatronization and integronization of automobile;
- s.o.

#### 4. EXAMPLES OF ADAPTRONIC MICROTECHNOLOGIES FOR THE DEVELOPMENT OF INTELLIGENT MECHATRONIC TECHNOLOGICAL PLATFORMS

By applying adaptronic microtechnologies and adaptronic concept have been made realized, conceptual and constructive-functional:

- Mechatronics – integronics technological platform for measurement and multiparametric metrological inspection (fig.1)

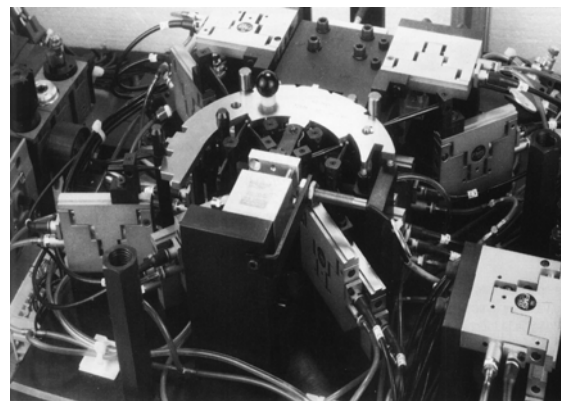


Fig. 1: Mechatronics – integronics technological platform for measurement

and multiparametric metrological inspection

- Mechatronics – adaptronics technological platform with evaluation micro-nanosystems for accelerometers, digital devices and rotating microactuators (fig.2)

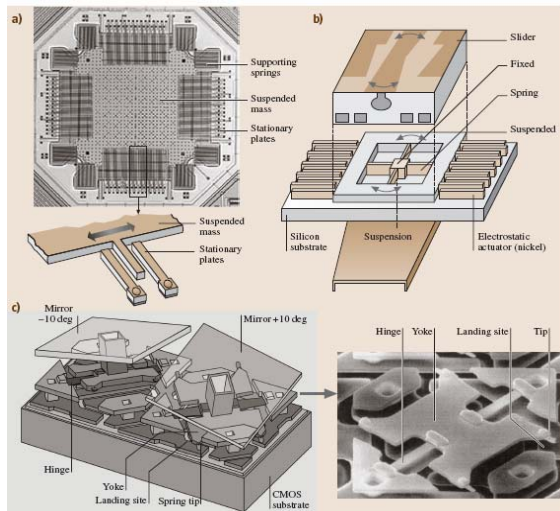


Fig. 2: Mechatronics – adaptronics technological platform with evaluation micro-nanosystems for accelerometers, digital devices and rotating microactuators

- Mechatronics – adaptronics technological platform for measuring and evaluating intelligent manufacturing process (fig.3)



Fig. 3: Mechatronics – adaptronics technological platform for measuring and evaluating intelligent manufacturing process

- Mechatronics – adaptronics technological platform for tribological measurement and evaluation (fig.4)

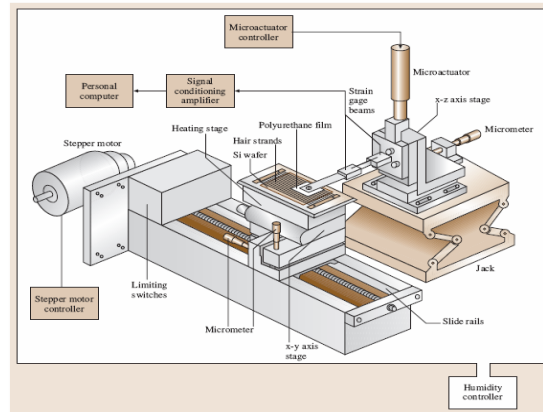


Fig. 4: Mechatronics – adaptronics technological platform for tribological measurement and evaluation

- Mechatronics – adaptronics technological platform with hexapod robots (fig.5)



Fig. 5: Mechatronics – adaptronics technological platform with hexapod robots

## 5. EXPERIMENTATION OF ADAPTRONICS IN MECHATRONIC MICRO-NANO-SYSTEMS FOR MICRO-NANO-DISPLACEMENTS

In INCDMTM laboratories were tested nanometric mechatronic micro-nano-systems for micro-nano-displacements and micro-nano-positioning which aim to

integrate the adaptronic micro-parts of much higher performance with new operating principles for:

- increasing the range of work, in the micro-nanometer field of hexapod robotic micro-systems;
- increasing opportunities for handling and manipulation of the hexapod micro-robotic system with atomic force microscope;
- integration of the "finger grip system" in the hexapod micro-robotic platform for the modernization of the power of atomic force microscope;
- modernizing the characterization of thin film structures, on the mechatronics technology platform with atomic force microscope – hexapod micro-robot;
- widening of the mechatronic technology platform with atomic force microscope – micro-robotic hexapod with new mechatronic, structural and functional development micro-nano-systems, meant to increase opportunities for characterization, measurement, evaluation and integration;
- integration of sensoric and actuator sub-systems, new operating principles and metrological parameters superior in micro-robot hexapod structure, field of action and development work in adaptronic mechatronic technology platform;
- development of an atomic force microscope technology platform – hexapod micro-robot, with many other functions:

- measurement, positioning and calibrating;
- 3-D topographic exploration
- use of laser measurement and exploration of surface micro-geometry;
- highly precise metrological comparison;
- Integration of software measurement and calibration;
- medical micro-nano-devices testing;
- dynamic and static testing;
- tribological and micro-nano-tribological characterization;
- etc.

## 6. CONCLUSIONS

The development of adaptronic concepts and micro-technologies, although at the begin, define key drivers of support, development and especially capitalization of the high-tech advanced fields of mechatronics and integronics, and in the future, the maturation and development of the triad: mechatronics - integronics - adaptronics, that will contribute substantially to the intelligent manufacturing strategy, to intelligent economics and to the intelligent society.

Adaptronics will ensure in the future, on one hand the modernization of the fields of mecahtronics and integronics by replacing obsolete parts with new parts with scientific solutions based on recent scientific findings, and on the other hand, by the hybrid integrative development of mechatronics and integronics by adaptronic association of new intelligent functions, new innovative solutions and new intelligent knowledge.

The triad: mechatronics - integronics - adaptronics, will be in the future, the scientific and technological pole of excellence with competitive and ever-generative capability.

## 7. REFERENCES

- [1] Drexler, E.. et. al. "Nanosystems: Molecular Machinery, Manufacturing and Computation", John Wiley & Sons, New York, 1992;
- [2] Fisher, U, Alcock, S.J. and Turner, A.P.F. Biosensors& Bioelectronics, 1995, **23**, 10;
- [3] Freitas Robert A., Nanomedicine, vol 1-4, (1998, 2004), [www.foresight.org/Nanomedicine/NanoMedTOC.html](http://www.foresight.org/Nanomedicine/NanoMedTOC.html));
- [4] Gheorghe Ion Gheorghe, Liliana Badita, Micro si nanotehnologii avansate in mecatronica, Ed. CEFIN, 2009;
- [5] Gheorghe Ion Gheorghe. Microingineria inteligentă, Ed. CEFIN, 2009.

## **9. ADDITIONAL DATA ABOUT AUTHORS**

Authors: Prof. univ. dr. eng. Gheorghe Ion Gheorghe; PhD student eng. Simona Istriteanu

Manuscript “Adaptronic microtechnologies regarding mechatronic nanometric micro-nanosystems for micro-nanodisplacements and micro-nanopositioning“

National Institute of Research and Development in Mechatronics and Measurement Technique (INCDMTM) 6-8 Sos. Pantelimon, District 2, Bucharest, Romania

Phone +40 21 252.30.68/69

Fax +40 21 252.34.37

E-mail: [cefin@cefin.ro](mailto:cefin@cefin.ro)

[www.cefin.ro](http://www.cefin.ro)

## LOW SPEED MOTION FEEDBACK FOR THE UNMANNED GROUND VEHICLE

Hiiemaa, M. & Tamre, M.

**Abstract:** *In low speed operation, data from wheel encoders of the Unmanned Ground Vehicle (UGV) suffer greatly from approximation errors, which reduces the quality of closed-loop control. Because encoder events are more rare in low speed operations, practically all events should be regarded including their time of occurrence to extract maximum amount of motion information out of them. Hardware-specific properties of a single-pole magnetic encoder are reflected in encoder simulations to evaluate M/T method's attractiveness while operating at very low angular velocity.*

*Key words: encoder, motion feedback, low speed, uncertainty, transitional noise*

### 1. INTRODUCTION

Remotely controllable Electric Unmanned Ground Vehicles (UGV-s) have several applications, which require precision control driving. Research project [1] was initiated in TUT Dept. of Mechatronics to develop a mobile platform for a wide range of applications from simple all-terrain transportation to counter IED (counter Improvised Explosive Devices) operations.

On a relatively flat and hard terrain, where motion parameters like jerk, acceleration and velocity must strictly be kept within limits, Intelligent Motion Control Layer (IMCL) which has been described further in a previous studies [2], show satisfactory simulation results. IMCL on-board electronics was designed to simulate few simple motion scenarios

every sampling interval (originally 0.1 s) to find the best fitting "mode change" points from default scenario, while handling input data delays, approximation (quantization) noise and rejecting disturbance. Having set the constraining limits for the motion parameters, user can send velocity or position change commands to the vehicle using one simple joystick of the control station, without accidentally violating those limits. Such limits vary according to the nature of a particular operation.

When sampling interval was shortened (down to 0.01 s), there was an immediate need to virtually increase wheel encoder resolution to cope with the approximation noise [3]. Placing the encoder right to the motor shaft (before 12:1 gearbox) improved the SNR.

Because only pulse count data within the fixed intervals was fed into IMCL simulation model, very low SNR was produced at low speed operation. In velocity, acceleration and jerk calculations the noise component was increasingly dominant. This necessitated choosing more advanced encoder signal analysis. Digital filtering method was discarded in this development stage because it might mask some fast movements (caused by backlash or vibration) from IMCL analysis.

More advanced M/T method (M register divided to T register method) significantly improves encoder input angular velocity estimation accuracy and requires only minor functionality from additional hardware [4]. Another method, which considers only the time difference of the occurrence of the last two events, in



most cases suffers more from differential and transitional noise and therefore is not used. As velocity increases, the M/T method outperforms the aforementioned one, because the velocity feedback calculation of M/T method includes wider span of time and usually a greater number of encoder events. Current study is primarily aimed at comparing previously used method and M/T method, provided that magnetic encoder with its hardware-specific drawbacks is used (instead of optical) as feedback solution for IMCL of the UGV.

## 2. HARDWARE

### 2.1 Interface of Encoder

Quadrature incremental encoder interface with signals "A" and "B" is found the most suitable for transmitting asynchronously occurring events (transitions) from extremely low frequency to the highest frequency used. Zero signal "Z" is not essential as magnetic encoders, presented in current study, have additional interfaces like (SSI, PWM) to transmit also absolute values but using these are not expected in this study [5].

### 2.2 Single Pole Magnetic Encoder

Compared to optical encoder, magnetic encoder is less sensitive to harsh environment conditions like low temperature, mechanical shock, vibration, dust, mist and even magnet displacement. Magnetic encoder can also be produced cheaper and in smaller package, compared to its optical or other technology using counterparts with the same resolution [6]. As seen in Fig. 1., magnetic encoder can be made very compact due to its simplicity.

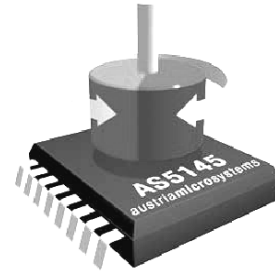


Fig. 1. Magnetic rotary encoder

Magnetic encoders, although emulating the same quadrature output interface as optical encoders, have different concept of operation. Instead on having many slits on code-wheel, these encoders use DSP-s to convert Hall-sensor signals to quadrature encoder output.

Because Hall-effect sensors, operational amplifiers and ADCs pick up noise, encoder output suffers from transitional noise. For example Austriamicrosystems AS5145 has 0.03 degrees RMS (1 sigma) x1 (68.27% of readings) in "slow mode" while the resolution of the encoder is 0.088 degrees (12-bit). Hysteresis of 0.35 degrees (4 steps) has been introduced to the AS5145 to eliminate flickering of A, B signals when the magnet is stationary but this does not solve the main problem. Hysteresis, when not regarded in IMCL, would even detect false disturbance at velocity direction change.

There is also a rated constant data propagation delay of 384  $\mu$ s in "slow mode" operation due to limited internal sampling rate (typically 2.61 kHz). This delay is short compared to the sampling interval (0.01 s) and does not influence low speed motion feedback noticeably.

Integral uncertainty (maximum error with respect to the best line fit) reaches its maximum ( $\pm 0.5$  degrees) about every 128 pulses. Because we are investigating low rotational velocity mostly below 8 pulses per sample interval this influences the signal less than 1/32 of a degree (about  $\pm 0.031$  degrees). Maximum deviation, therefore, caused by integral

uncertainty in 12 rpm or below, could be considered insignificant (4.2%).

Contrary to the integral uncertainty, differential uncertainty consisting mostly of transitional noise, causes higher uncertainty at lower angular velocities. AS5145 has rated transitional noise 0.03 degrees (0.34 steps) RMS in "slow mode". This is dominant factor of uncertainty when velocity must be extracted from encoder signals below 12 rpm. While quantization error (originally below 1 step) can be reduced by MT method, there is no such remedy for transitional noise. Without using MT method, approximation noise and transitional noise would both contribute to the increased uncertainty.

### 2.3 Multi-Pole Magnetic Encoder

Using linear magnetic encoder with multi-pole magnetic ring was proposed in [3]. It permits using hollow shaft and may provide increased resolution compared to the single pole solution. Still, it would be more difficult to evaluate and model it without having the physical hardware set-up with actual encoder chip and magnet ring installed. As low-speed measurement relies on accurate positioning, significantly higher dynamic non-linearity combined with mechanical imperfections of the magnet ring are expected to cause hard-to-predict deviation from the simulation results.

### 2.4 Low Speed Feedback Usage

Four-wheel drive, complemented by accurate torque control of each wheel, is necessary when driving on extremely difficult terrain like wet soil or thick snow. Wheel spin-up may not only cause instability when suddenly finding good grip. It may also damage soft terrain, dig in and make further efforts to advance difficult if not impossible. Keeping all four wheels in sync would be desirable most of the time – especially when ending a drive. This leaves some space inside wheel tracks to build up speed later. Straight motion on the UGV requires less space to build up the

velocity because there is no problematic skid action.

Turning from stalled state should be avoided on soft terrain. Zero radius turns have the highest risk of digging in because all wheels have inefficient directions of movement. Within skid action wheels do not efficiently grab the wet soil to clean the path for the wheels and pull the entire vehicle to a new angle. In such conditions it is essential to have stable, low-speed control of the vehicle.

Aforementioned and other similar driving techniques are not universal but accurate low-speed encoder input with minimal data analysis would reveal the necessity of using one or another. When soft or slippery terrain is combined with steep slopes, there is a need for changing UGV stance as well to distribute the centre of gravity, change clearance. This can be done by leg servos.

Each wheel of the UGV is equipped with electromechanical disc brake. This type of brake is not suitable for high torque dynamic braking but it is sufficient for parking. Low-speed feedback of encoders allows IMCL to choose the best point in time to apply the parking brake at zero speed.

Low speed operation is also necessary when UGV is driving on a hard and uneven terrain because acceleration peaks from servo wheels propagate through torsion springs to the chassis and may damage delicate payload. Depending on the exact profile of the terrain and stance of the UGV, such peaks are not always detected by wheel encoders or leg encoders (measuring torsion spring flexion). 3-axes acceleration sensor is placed to the payload area to monitor that. Still, fast and accurate angular velocity feedback from the wheels also limit swing action by keeping angular velocity well constrained and stable.

## 3. SIMULATION

Quadrature encoder signals "A" and "B" are not analysed separately because only

one-directional movement is simulated and hysteresis (built into the magnetic encoder) prevents false appearance of direction change, which could otherwise be caused by the transitional Gaussian noise (top centre of Fig. 2).

Velocity angle signal was generated when low constant angular jerk was applied to the stationary encoder shaft.



Angular velocity of the UGV wheel reaches approximately 1 rpm in 3 seconds, which is much below everyday usage and are considered as worst case. Motor shaft, through 12:1 gearbox, reaches 12 rpm. As encoder resolution is 12-bit (4096 ppr), 12 rpm causes about 8 events per interval at 100 Hz IMCL sampling rate. Simulation plot (Fig. 3), therefore, mostly describes situations, where up to 8 events per interval occur within time span of 3 seconds.

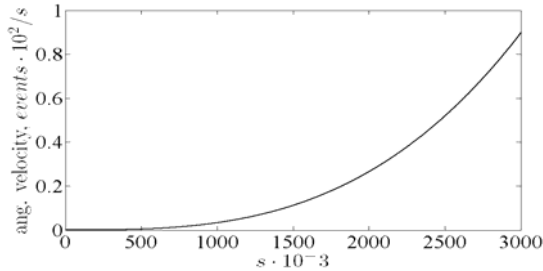


Fig. 3. Angular velocity plot (ideal)

The following plot (in Fig. 4) illustrates event-counting method (events per sample interval) with approximation noise only.

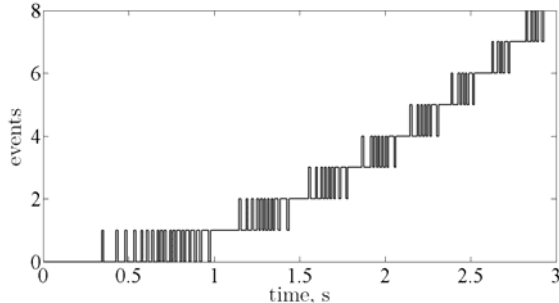


Fig. 4. Event count plot

Fig. 5 illustrates event counting method after adding transition noise of the encoder with 4-step hysteresis.

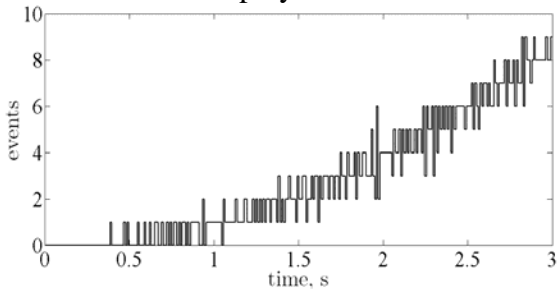


Fig. 5. Event counts with transitional noise

Simple event counting method left intervals up to 0.3 s (Fig. 6.) between events discarded.

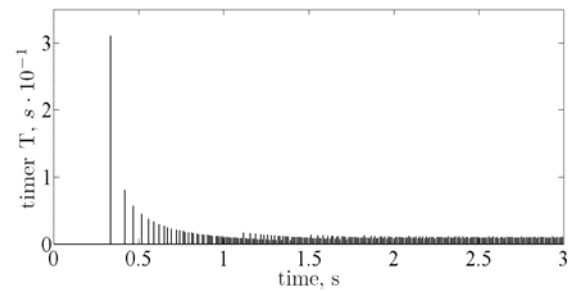


Fig. 6. High freq. timer captured values

Virtual timer (1 MHz) captures those intervals. Event count register (M) is divided to the captured time (T) and normalised (Fig. 2). Such non-integer values describe angular velocity more accurately. Without transitional noise, the plot is shown in Fig. 7.

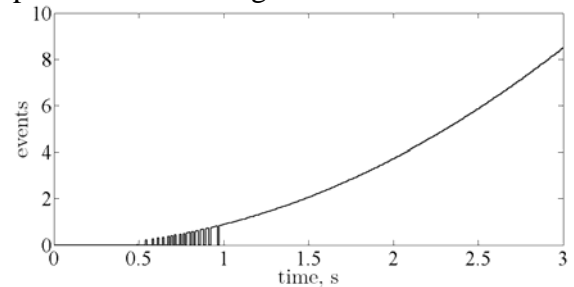


Fig. 7. Angular velocity with M/T

Here sample intervals without a single event are considered as zero velocity, causing the velocity signal to pulsate at ultra low velocity range. That range is far below the everyday use of the UGV control and may be filtered out on demand, without the cost of losing valuable response time.

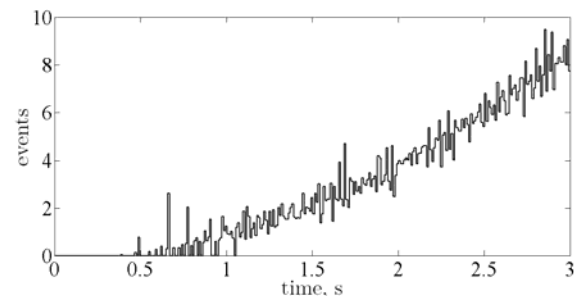


Fig. 8. Ang. velocity with M/T and noise

As noise level of the velocity signal is noticeably reduced (in Fig. 8), M/T method proves to be beneficial even in the presence of such transitional noise as in the investigated magnetic encoder.

#### 4. CONCLUSION

Harsh environment vs. the need for compact design makes single-pole magnetic encoders optimal choice for UGV wheel motion feedback. Because such devices have typically much higher noise than their optical counterparts, simulation was created, where the critical properties of one particular magnetic encoder were investigated. Comparison of event counting and M/T method was performed with and without transitional noise, proving the M/T method useful in either case.

Simulation plots also revealed that transitional noise (provided the same proposed acquisition schema is used) is not picked up by the signal analysis at ultra-low velocities. In case the hardware vibration proves to exceed transitional noise extensively, complementary hysteresis could be introduced to the microcontroller software with minor effort. This and other mechanical imperfections like backlash influence to the IMCL control quality are likely to be investigated in our future studies.

Studies related to the UGV control are continuing in the Department of Mechatronics [7]. Simulation results for single-pole magnetic encoder were promising enough to implement the solution in hardware.

#### 5. REFERENCES

[1] Tallinn University of Technology, Dept. of Mechatronics, "Universal Ground Vehicle", Research proj. L523, 2005-2008.

[2] Hiiemaa, M; Tamre, M. Semi-Autonomous Motion Control Layer for UGV-type Robot. In *Recent Advances in Mechatronics 2008-2009* (Brezina, T. and Jablonski, R., eds.), Springer, 2009, 1, 203-207.

[3] Hiiemaa, M; Tamre, M. Practical Issues in Utilizing Intelligent Motion Control Layer in UGV-type Robots, In *8-th Int. Symp. Topical Problems in the Field of Electrical and Power Engineering*. 2010, 190-192.

[4] Hachiya, K.; Ohmae, T. Digital Speed Control System for a Motor Using Two Speed Detection Methods of and Incremental Encoder. In *Power Electr. and Applications, 2007 Europ. Conf.*, 2007. 1-10

[5] austriamicrosystems AG, AS5145 (12-Bit Programmable Magnetic Rotary Encoder) Datasheet Revision. 1.12. 2008. 1-36

[6] Shuanghui, H.; Yong, L; Minghui, H. Study on a Novel Absolute Magnetic Encoder. In *Proc. of the 2008 IEEE*. 2008. 1773-1776.

[7] Tallinn University of Technology, Department of Mechatronics, "Proactivity and Behavioural Models of Mechatronic and Production Systems", Research project SF0140113Bs08, 2008-2013.

## **6. ADDITIONAL DATA ABOUT AUTHORS**

Hiiemaa, Mairo. Ehitajate tee 5, Tallinn  
19086, [maido.hiiemaa@ttu.ee](mailto:maido.hiiemaa@ttu.ee);

Tamre, Mart. Ehitajate tee 5, Tallinn  
19086 [mart@staff.ttu.ee](mailto:mart@staff.ttu.ee)



## COMPARISON OF AERIAL IMAGERY AND SATELLITE IMAGERY FOR AUTONOMOUS VEHICLE PATH PLANNING

Robert Hudjakov & Mart Tamre

***Abstract:** The focus of our research is to improve navigation capabilities of an off-road unmanned ground vehicle (UGV) by improving its perception range. We train an ortophoto classifier by using data gathered by UGV and then extrapolate the data into wider area by using aerial imagery from unmanned aerial vehicles (UAV). The current progress report analyses feasibility of using satellite images instead of or together with aerial imagery and discusses an optimization technique that executes classifier as needed by path planner saving processing resources and time.*

***Keywords:** UGV, UAV, cost map, path planning.*

### 1. INTRODUCTION

There are battery powered off-road multi-purpose UGV platforms developed in Tallinn University of Technology [1] objectives of which contains driving to target GPS coordinate, executing a task and returning to base. By fusing the on-board sensors of an UGV with overhead imagery we can increase the effective perception range of the UGV helping to reduce the time and energy requirements for executing said mission. In addition we can plan a path to objective ahead of time and predict the feasibility of the mission with current battery charge.

Our proposed system consists of classifier, cost map generator and path planner. The

system uses previously gathered UGV data and aerial imagery as an input and produces a long haul path for UGV, the prior knowledge and aerial imagery is used to train an image classifier that is then used for cost map generation and path planning. We intent to repeat the cycle of data gathering, classifier training, cost map generation and path planning after the mission is dispatched in order to keep the system flexible and to be able to consider new kinds of obstacles after they have been discovered by UGV.

In this article we are analyzing the possibility of using satellite imagery together with or instead of aerial imagery. There are two explicit scenarios that we cover: whether it is possible to replace aerial imagery with lower quality satellite imagery and is it possible to switch over from aerial imagery to satellite imagery when UAV goes offline? The aerial imagery is preferred over satellite imagery for it has higher resolution and it can be gathered ahead or during the mission ensuring its freshness.

In addition we describe an optimization technique that increases the performance of aerial imagery evaluation by combining cost map generation and path planning steps. The advantages are twofold. First we benefit from reduced processing requirements allowing cheaper and more mobile hardware (in terms of power requirements). Secondly it allows us to generate path faster which in turn allows us regenerate the updated path to

objective more often.

## 2. AERIAL IMAGERY VS. SATELLITE IMAGERY

Thus far we have done all our experiments with aerial imagery and we have estimated that we get comparable results with satellite imagery, this time we decided to put the hypothesis to a bench. For the experiment we chose identical area to our aerial data set from Google maps database [2] [3] [4] [5], up-scaled the satellite imagery to identical resolution of aerial imagery and hand classified it (Illustration 1).

It must be noted, however, that the satellite imagery has about 4x lower resolution, was taken during different time of the day, different time of the year and different year. The aerial data set was acquired during a summer time when grass was green and multiple construction projects were ongoing so there was a lot of construction debris. The satellite imagery was acquired a year later during spring when grass was not up yet and there was little debris from construction projects left.

Our processing pipeline consists of three distinct steps: image classification, cost map generation and path planning. For image classification we pick patterns from aerial imagery and feed them into a classifier that outputs a feature vector. For the classification we use two approaches that are described in finer detail in our previous publication [5]: with method A we try to detect all features that are present on input pattern and with method B we try to detect to which category belongs the pixel in the middle of input pattern. The outputs of method A are independent meaning that the input pattern may contain multiple features that we are looking for (houses, roads, etc) while the outputs of method B are dependent - the center pixel may belong to only one category.

The objectives of this experiment are twofold:

- We want to verify that our classifier can get comparable classification rates with satellite imagery.
- We want to verify the feasibility of cross usage of a trained classifier e.g. we want to see if a classifier that has been trained on aerial imagery is usable on satellite imagery and vice versa.

### Method A

Method A is based on the idea that a convolutional artificial neural network is capable of extracting distinct features from input pattern and linear classifier layer can then be trained to report presence of objects in input pattern. In layman's terms each classifier output is trained to answer simple questions such as "Is there a house in input pattern?", "Is there a tree in input pattern" or "Is there some grass in input pattern?". All the classifier outputs are independent, there can be multiple features simultaneously present in the input pattern.

For the experiment we used a classifier that is based on convolutional neural network and had three 29x29 neuron inputs for a 29x29pixel pattern with three color channels. The second hidden layer had six 13x13 neuron feature maps that were connected to all inputs using 5x5 neuron kernel and the third layer had fifty 5x5 neuron feature maps that were connected to all second layer feature maps using 5x5 neuron kernels. The final hidden layer consisted of a linear classifier with 100 neurons in it and the output layer had 4 neurons for four feature categories: houses, roads, grass and debris. The specific classifier configuration was chosen because we have reported multiple experiments with it in the past [2] [3] [4].

For the experiment we generated two data sets - one from aerial imagery and another from satellite imagery. Next we randomized the internal parameters of our classifier and trained it on aerial data set. Finally we tested the trained classifier on both aerial test set

and satellite test set. The same operation was repeated with a classifier trained on satellite data set and the results were saved into Table 1.

data set. Not only the color of the grass was different on the data sets, but also the sharp texture of grass on aerial imagery was replaced with botched texture of mud on

**Table 1**

	Aerial imagery classifier	Satellite imagery classifier
Aerial data set	Correctly classified: 97,9% Rates of good classification: Houses, rate=99,4% Roads, rate=99,7% Grass, rate=99,8% Debris, rate=98,8%	Correctly classified: 11,2% Rates of good classification: Houses, rate=83% Roads, rate=78% Grass, rate=42% Debris, rate=50%
Satellite data set	Correctly classified: 9,4% Rates of good classification: Houses, rate=48% Roads, rate=87% Grass, rate=41% Debris, rate=48%	Correctly classified: 98,9% Rates of good classification: Houses, rate=99,7% Roads, rate=99,8% Grass, rate=99,9% Debris, rate=99,6%

As seen from above table the classifier is usable both with aerial imagery and satellite imagery - the classification rate in both cases is well over 90%. The cross use, however, is limited. The classifier that was trained on lower quality satellite imagery was capable of detecting houses on higher quality aerial imagery but the reverse did not hold.

satellite imagery (Illustration 1). Similarly the aerial imagery had a lot of debris but satellite imagery had next to none and hence the cross use of classifiers for debris detection is not reliable.

The roads were similar on both data sets and the classifier could detect the roads on both - this is important results because having a



**Illustration 1: Path planning using classifier with high uncertainty levels. Cost map (left) and planned path (right).**

Because on one imagery the grass was up and green while on other imagery it had not yet grown, the classifier trained on one data set can not be used to detect grass on other

classifier that can detect roads is better than not having a classifier making our system usable even in unfavorable conditions.



**Illustration 2: Grass on aerial imagery vs. mud on satellite imagery**

Our cost map generation algorithm is built to cope with classifier uncertainties and is capable of producing output even when classifier is only capable of detecting some of the features. By feeding the classifier trained on aerial imagery with satellite imagery we receive a cost map where everything besides roads are marked as unknown terrain and during navigation the roads are preferred.

The following illustration (illustration 2) shows the path planning capability of our system with classifier that has been trained with aerial imagery using satellite imagery. Despite on the overall the classifier could only correctly classify 9,4% of patterns, it could find roads with relatively high certainty and thus can be used for path planning.

The results are better with the classifier that is trained on satellite imagery and used on aerial imagery (Illustration 3). Both the roads

and the buildings are clearly detected and since our proposition is to re-train the classifier while UGV is moving (using freshly gathered data) the classifier trained on satellite imagery has good starting values. To validate that claim we took a classifier that has been trained on satellite imagery and trained it for one single epoch on aerial imagery. The classification rate for all items went up from 11,2% to 66% and in detail the classification rate for houses went from 83% to 98%, for roads from 78% to 96%, for grass from 42% to 88% and for debris it went from 50% to 79%. We saw a similar increase after we took a classifier that had been trained on aerial imagery and used it on satellite imagery. After one epoch of training the total classification rate went up from 9,4% to 54%.

### **Method B**

Method B will train the classifier to detect



**Illustration 3: Comparison of cost maps: satellite classifier on satellite imagery (left) vs. satellite classifier on aerial imagery (right). Darker areas have lower traversal cost than lighter areas.**

the category of a single pixel in input image, particularly the pixel from the center of the pattern. The classifier will then answer the question “Into which category belongs the pixel in the center of this pattern?”. The categories are exclusive and thus the classifier outputs are dependent.

The experiment setup was identical to method A: we generated two data sets and trained a classifier on each of them. The classifier were then tested and cross tested on the data sets and results are in the Table2.

**Table 2**

	Aerial imagery classifier	Satellite imagery classifier
Aerial data set	Correctly classified: 88% Rates of good classification: Houses, rate=97,87% Roads, rate=97,07% Grass, rate=94,13% Debris, rate=97,93%	Correctly classified: 20,4% Rates of good classification: Houses, rate=66,4% Roads, rate=67,57% Grass, rate=76,23% Debris, rate=52%
Satellite data set	Correctly classified: 12,7% Rates of good classification: Houses, rate=55,73% Roads, rate=77,77% Grass, rate=48,67% Debris, rate=57,93%	Correctly classified: 89,9% Rates of good classification: Houses, rate=97,37% Roads, rate=96,93% Grass, rate=96,33% Debris, rate=98,63%

The results are very similar to those of method A. The classifier can be trained on both aerial data set and satellite data set to a nearly identical classification capability. The effects we observed during cross testing of classifiers using method A also hold for method B: the classifier trained on satellite imagery is better at classifying aerial imagery than the classifier trained on aerial imagery is at classifying satellite imagery. All the combinations of classifiers and data sets are capable of finding roads and since our cost map generator is built to deal with uncertainties of classifier we can use them for at least preliminary path planning. The conclusions from comparing the satellite data to aerial imagery:

- Classifier trained on the aerial imagery works well on the the aerial imagery
- Classifier trained on the satellite imagery works well on the satellite imagery
- The classifier trained on lower quality imagery also works well on higher quality imagery but the reverse does not hold.
- The classifier that has been trained on satellite imagery is a good starting

point for re-training on aerial imagery. Reverse also holds true; the classifier that has been trained on aerial imagery is a god starting point for re-training on satellite imagery.

- When using a trained classifier on a different imagery we must take into account the changes in nature - where there is grass on summer there is mud on spring and snow in winter. Each has different color and texture.

Because the roads are easily distinguishable it is better to use non-matching classifier on terrain where roads are present than not to use overhead imagery at all.



### 3. INTEGRATION OF COST MAP GENERATION AND PATH PLANNING

The cost map is a grid on nodes; each node has a cost associated with it. For generating the cost map we divide an aerial photo into a grid of 29x29 pixel patterns and feed the patterns to our classifier which outputs feature vectors for the patterns. The pattern size is determined by the size of classifier input layer; to enhance the cost map resolution we use overlapping patterns. The feature vectors are mapped into a probability vectors using a threshold vector. For cost calculation the probability vectors are multiplied with a weight vector and a constant bias is added [4] [5].

$$\text{cost} = \sum_i d(f_i, t_i) \cdot W_i + c_u$$

where

- F is classifier output vector,
- T is threshold vector,
- d is the transformation function that maps classifier output to probability [5],
- W is the weight vector,
- $c_u$  is constant bias.

It is important to note here that for calculating the cost of each node we need to evaluate the pattern associated with the node using a classifier. The evaluation of the pattern is relatively expensive operation when compared to the cost calculation.

For path planning we use A\* algorithm [6] which is improvement over Dijkstra's algorithm [7] and generates an optimal path from start node to end node. There's an excellent tutorial on A\* algorithm by Patrick Lester:

- 1) Add the starting square (or node) to the open list.
- 2) Repeat the following:
  - a) Look for the lowest F cost square on the open list. We refer to this as the current square.
  - b) Switch it to the closed list.
  - c) For each of the 8 squares adjacent to this current square ...
    - If it /.../ is on the closed list, ignore it. Otherwise do the following.
    - If it isn't on the open list, add it to the open

list. Make the current square the parent of this square. Record the F, G, and H costs of the square.

- If it is on the open list already, check to see if this path to that square is better, using G cost as the measure. A lower G cost means that this is a better path. If so, change the parent of the square to the current square, and recalculate the G and F scores of the square. /.../

d) Stop when you:

- Add the target square to the closed list, in which case the path has been found /.../, or
- Fail to find the target square, and the open list is empty. In this case, there is no path.

3) Save the path. Working backwards from the target square, go from each square to its parent square until you reach the starting square. That is your path. [8]

H is an heuristic value that estimates the cost of moving from current node to end square, G is the cost of moving from start node to current node and  $F = G + H$ . When calculating the cost G for any given neighboring node we add the cost G of current node to value taken from cost map.

Because the A\* algorithm does not necessarily use all nodes in cost map and because the generation of whole cost map is relatively slow process (when compared to path planning stage) we can get significant improvements to our algorithm by combining the path planner and the cost map generation steps.



**Illustration 4:** red line presents the used path and the nodes evaluated by path planner are marked using dark area. Overall there was need to evaluate 7% of the aerial image for the path planning

When we calculated the cost of a node only when it was needed by path planner we can occasionally reduce the combined time of cost map generation and path planning by order of magnitude - especially when the path from start to end point is clear (illustration 1, illustration 2).

However, this optimization technique does not affect the worst case scenario - there are cases where we still need to evaluate the whole imagery for path planning particularly in scenarios where there are no clear pathways to designated target position.



**Illustration 5:** red line presents the used path and the nodes evaluated by path planner are marked using dark area. Overall there was need to evaluate 25% of the aerial image for the path planning.

#### 4. CONCLUSIONS

Our proposed system of extending UGV perception distance by extending UGV local experiences to wider area using aerial imagery works equally well using satellite imagery. We can also use classifier that has been trained for satellite imagery on aerial imagery and using of a classifier that is trained on similar imagery is a good starting point for re-training it for specific imagery in terms of quick results.

By combining the cost map generation and path planning stages we can reduce the total time it takes for cost map generation and

path planning up to 10x. The performance increase comes from executing the classifier on overhead imagery (expensive operation) as needed by path planner. The optimization, however, does not affect the worst case scenario where we still need to generate whole cost map.

#### 5. BIBLIOGRAPHY

- [1] M. Hiiemaa and M. Tamre, "Semi-autonomous Motion Control Layer for UGV-Type Robot," pp. 203-207, 2010.
- [2] R. Hudjakov and M. Tamre, "Aerial Imagery Terrain Classification for Long-Range Autonomous Navigation," *Proc. of International Symposium on Optomechatronic Technologies*, pp. 88-91, 2009.
- [3] R. Hudjakov and M. Tamre, "Aerial Imagery Terrain Classification for Long-Range Autonomous Navigation," *Proc. of the 7th International Conference of DAAAM Baltic Industrial Engineering*, pp. 530-535, 2010.
- [4] R. Hudjakov and M. Tamre, "Ortophoto Analysis for UGV Long-Range Autonomous Navigation," *Estonian Journal of Engineering*, no. 17, p. 17-27, 2011.
- [5] R. Hudjakov and M. Tamre, "Aerial Imagery Based Long-Range Path Planning for Unmanned Ground Vehicle," in *Mechatronic Systems and Materials*, Kaunas, 2011.
- [6] P. E. Hart, N. J. Nilsson and B. Raphael, "Correction to A Formal Basis for the Heuristic Determination of Minimum Cost Paths," *SIGART Bull.*, no. 37, pp. 28--29, December 1972.



- [7] E. W. Dijkstra, "A note on two problems in connexion with graphs," *Numerische Mathematik*, vol. 1, no. 1, pp. 269-271, 1959.
- [8] P. Lester, "A\* Pathfinding for Beginners," 18 July 2005. [Online]. Available: <http://www.policyalmanac.org/games/aStarTutorial.htm>. [Accessed 28 02 2012].

## DYNAMIC LOADING SYSTEM FOR AIR BEARING TESTING

Iruikwu, D.; Isomaa, J-M; Korkkolainen, P.; Kiviluoma, P; Kuosmanen, P.;  
Calonius, O.

### Abstract:

*Reducing friction between moving surfaces helps reducing the overall energy consumption of mechanical machinery in industry. Air bearings offer very low friction between the bearing and its counter surface, but their behaviour under static and especially dynamic loading is difficult to predict.*

*In this paper, a test system for studying the behaviour of bearings under static and dynamic loading is presented. The test system consists of a piezo actuator controlled by computer that is generating the load for a aerostatic thrust bearing. The bearing is loaded against a large circular counter surface. During the tests measurements of the loading force, frequency, air consumption and the air film thickness between the bearing and the counter surface are collected on a PC.*

*Results show that the presented test rig can be used to determine the dynamic characteristics of air bearings.*

*Key words: dynamic loading system, piezo actuator, air bearings, frequency, counter surface.*

### 1. INTRODUCTION

Air bearings are typically used in applications where frictionless and high precision motion is required. Typical examples of high precision application are high precision measurement systems [1][2]. Air bearing application exploiting low friction can be found in laboratory equipment and in devices moving heavy loads on floor. The need to reduce power consumption and improve efficiency of

different machines opens new possibilities for air bearing technology. For example, oil lubricated journal bearings have tendency to transform energy to heat [3]. To meet the requirement of low power consumption, air bearings must be able run without extensive leakage in industrial applications at rough environment under dynamic loading.

The main characteristics of air bearings are load capacity, air gap height and air consumption. These characteristics are typically measured in laboratory conditions. These measurements are based on static loading of the air bearing on a rotating counter surface [4], or a rotating runner [4][5]. Several attempts to model the dynamic behaviour of thrust air bearings have been made [6][7]. In order to experimentally determine the characteristics of air bearing under dynamic load the test setup was developed. Obtaining result of the dynamic response will not only aid in predicting the behaviour of air bearings in typical applications but also help the design of air bearings for new, more robust industrial environments [8].

### 2. METHODS

#### 2.1. Test rig structure

Dynamic loading system is designed to be movable and easy to use in different test setups. This makes it possible to use different types of counter surfaces and different load directions. Considering that the system is built on a 30 mm thick steel base plate that can be fixed to various locations. The basic concept can be seen in Figure 1.

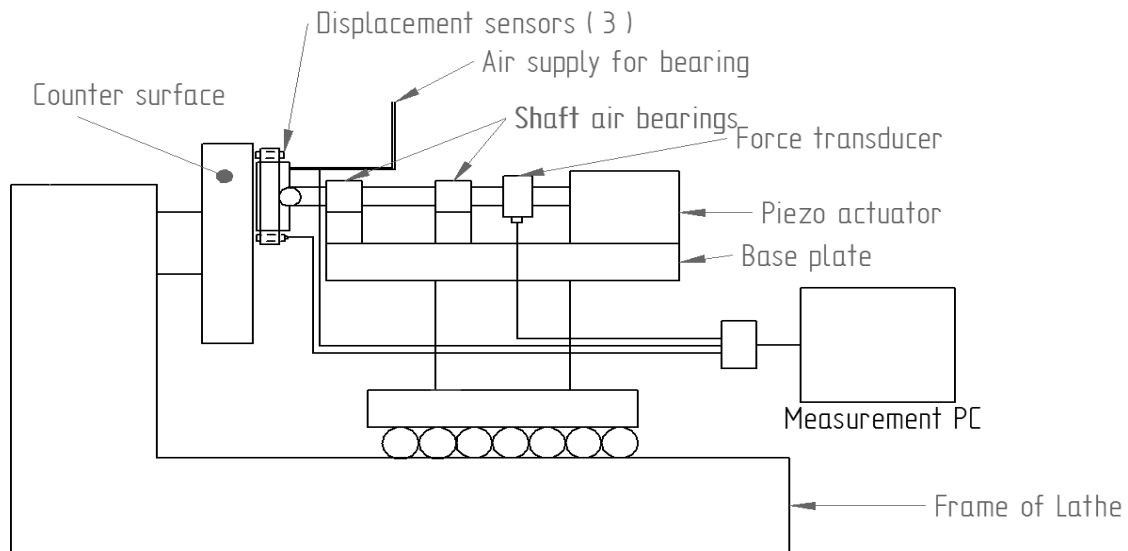


Fig. 1. Schematic of the test rig

The test rig is attached to the large-size lathe (1M65). It was chosen as a base for the test rig because of the rigid structure and precise guide ways. It offers also a simple mechanism to adjust the preload of air bearing.

## 2.2. Loading and load measurement

A piezo actuator was selected for this study because it provides the required load and displacement. The fast piezo actuator makes it possible to load bearing dynamically with different wave forms. The used piezo actuator can provide a load up to 2500 N, which meets the loading requirement. The actuator is designed to provide a displacement of 60  $\mu\text{m}$  at 100 V input. Preload of the air bearing is adjusted with the hand screw of the tool side in the lathe.

The 5 kN force transducer (HBM U2B), that measures the bearing load, is fixed between piezo actuator and 20 mm diameter shaft. Air bearing is fixed to the shaft by a threaded stud and a ball joint. The ball joint ensures the parallelism between air bearing and counter surfaces. The 20 mm diameter shaft is guided by aerostatic bearings (New Way S302001). The whole loading system is fixed on a rigid steel base plate.

## 2.3. Air gap height measurement

The air gap height between the bearing surface and the counter surface is measured with three displacement transducers. Using three displacement transducers allows the measurement of the bearing alignment, as well. The displacement transducers are attached to the bearing via a fixing collar. This same measurement configuration has been used in the previous air bearing studies successfully [4]. Test system needs high precision displacement measurement so eddy current sensors were chosen (MicroEpsilon, 1mm measurement range). Eddy current sensors are very sensitive to the material type, surface quality, geometry and inhomogeneity in the counter surface material. Thus the sensors were calibrated by pushing the bearing against the counter surface with 100 N preload and measuring the actual zero positions of each sensor. During the calibration the air feed for the bearing was disconnected.

Measuring the air gap height with displacement sensors directly attached to the bearing minimizes the errors occurring from the deformation of the test system. The force measurement was placed between the piezo actuator and the shaft, which was supported by nearly frictionless air bearings, to minimize the error generated by friction forces.

## 2.4. Air supply

Air bearings need stable and high quality air feed to work properly. A precision regulator with a gauge (SMC IR1020) was fitted to the air feed line. The system pressure was set to 5.2 bar during the tests. Air consumption in the bearing during the tests is measured using two different flow meters (SMC PFM710, measuring range 0.2...10 l/min and FESTO SFE3, measuring range 5...50 l/min) to ensure wide measuring range. Air quality was guaranteed using a service unit between shop air supply and test system that consisted of a filter (SMC air filter), two separators (mist separator AFM20, micro mist separator AFD20) and pressure regulator (SMC AR20).

## 2.5. Data acquisition

The data coming from the sensors and measurement devices are recorded on a PC. To ensure sufficient resolution and sampling rate in the recording, a 14-bit analogue-to-digital board running at 10 kHz, was used. To avoid aliasing in the recording an analogue low pass filter at 2.5 kHz was used before the data sampling. Average duration of measurements was 10 seconds. Data from each measurement was stored in a PC for analysis. During static loading tests the measurement results were based on the average of each channel. Analyses of the dynamic measurement were based on the synchronous averages of the force, displacement, air consumption and air pressure. When running sweep tests to find resonant frequencies of the system, raw data was used to see the behaviour of the system.

## 2.6 Test Bearing

The test bearing was an aerostatic orifice type air bearing (Nelson Air Corp., FP-C-040) with surface diameter of 100 mm and cylindrical height of 25 mm. The orifice type bearing has 12 equally spaced orifices of 190  $\mu\text{m}$  on a circumference of diameter 63 mm.

The connection of the air bearing to the piezo actuator was made by a linking shaft with diameter of 20 mm and a ball mounting screw on which the air bearing sits. The connecting shaft was axially aligned in position by the aid of two cylindrical air bearings which allows the axial movement of the shaft as it distributes the applied load axially on the counter surface. The rear end of the shaft is fixed to a force transducer which measures the applied load and the transducer is mounted on a Piezo-actuator which produces the required load.

## 2.7 The Counter Surface

A stationary surface fixed firmly to a lathe chuck was used. The counter surface is a large disk of diameter 400 mm with surface roughness of 0.89  $\mu\text{m}$  and 0.76  $\mu\text{m}$  at the radial and circumferential direction respectively.

## 2.8 Test Categories

Three testing categories were used to study the test rigs performance:

- Low frequency dynamic loading (1 Hz)
  - a. Low load (500 N)
  - b. High load (1500 N)
- High frequency dynamic loading (200 Hz)
  - a. Low load (500 N)
  - b. High load (1500 N)
- Frequency sweep dynamic loading (1...400 Hz)
  - a. Low load (500 N)
  - b. High load (1500 N)

These categories were chosen to see how the test rig behaves under relatively low loading in varying frequencies. The higher load level was chosen to be near the test bearings nominal loading level.

## 3. RESULTS

### 3.1 Dynamic measurements at 1 Hz

Dynamic loading was first measured with adjusting the preload to low load (500 N) first and then to high load (1500 N) and by giving the piezo sinusoidal signal of 1 Hz,

so that the amplitude of the force produced by the piezo would be 70 N. Air pressure was 5 bar. The forces and the air gaps can be seen in Figures 2.and 3.

### 3.2 Dynamic measurements at 200 Hz

The frequency of the load was risen up to 200 Hz sinusoidal signal with same amplitude that was in measurements with 1 Hz. Air pressure was 5 bar. The forces and the air gaps can be seen in Figures 4. and 5.

### 3.3 Behaviour of the system through frequency range 1...400 Hz

The behaviour of the whole system was tested by sweeping the frequency of loading force from 1 Hz to 400 Hz keeping the same dynamic loading during the measurement. The force creation and air gap can be seen as a function of frequency in the Fig. 6 and 7.

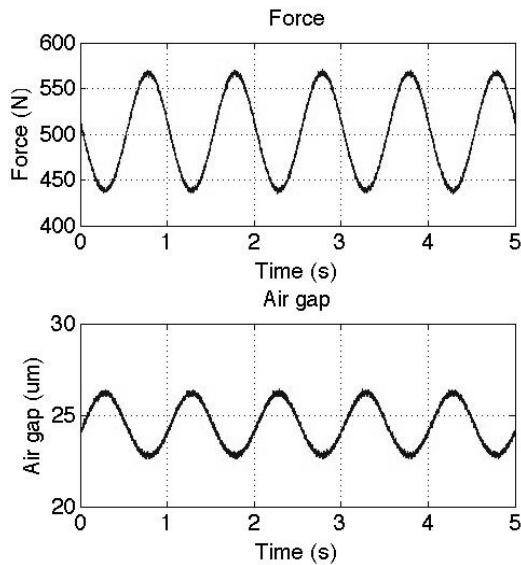


Fig. 2. Force and air gap of dynamic loading at 1 Hz, 500 N preload.

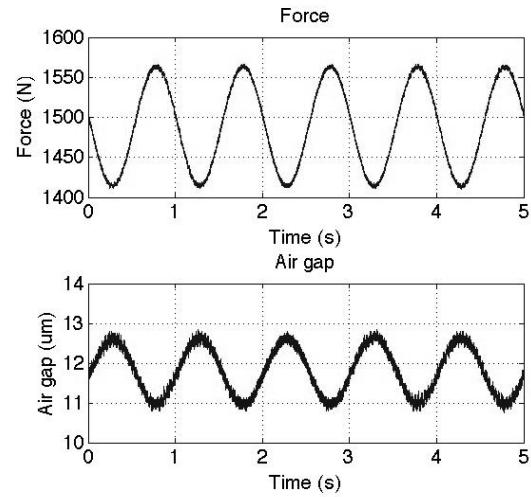


Fig. 3. Force and air gap of dynamic loading at 1 Hz, 1500 N preload.

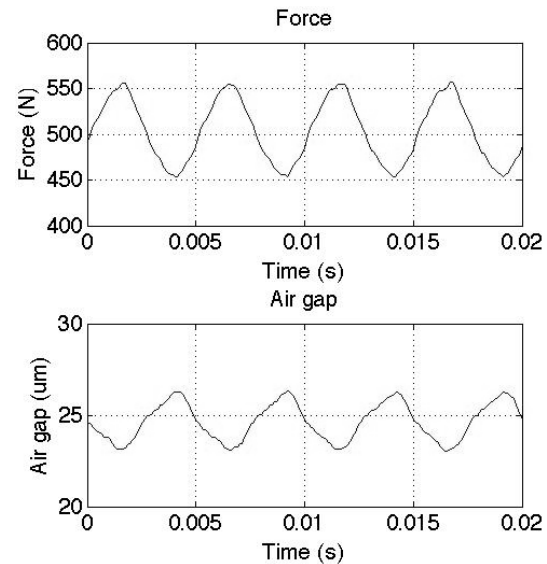


Fig. 4. Force and air gap of dynamic loading at 200 Hz, 500 N preload.

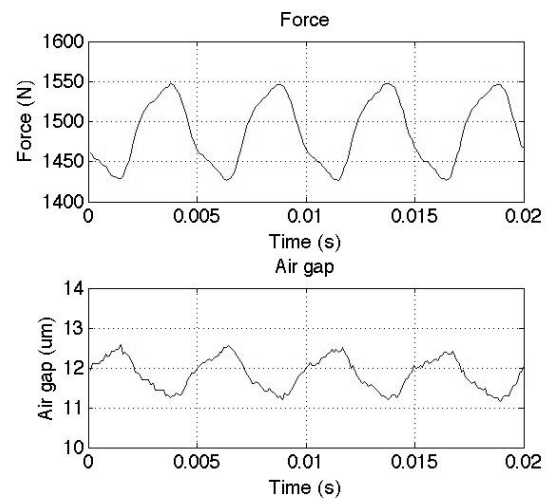


Fig. 5. Force and air gap of dynamic loading at 200 Hz, 1500 N preload.

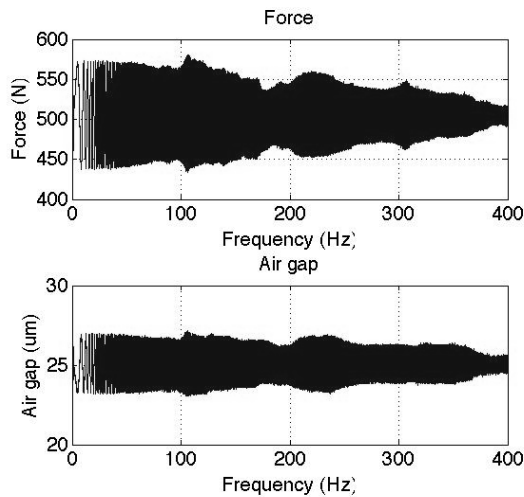


Fig. 6. Force and air gap of frequency sweep 1...400 Hz, 500 N preload.

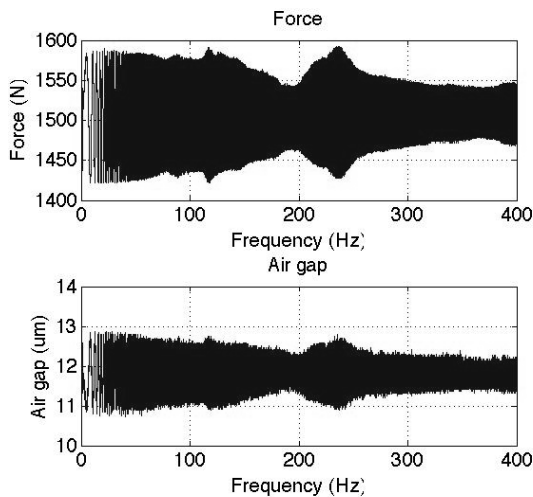


Fig. 7. Force and air gap of frequency sweep 1...400 Hz, 1500 N preload.

#### 4. CONCLUSION

Adding piezo actuator to a air bearing test rig made it possible to run controlled tests with different dynamic loading patterns. By measuring the load, air gap height, air consumption and air pressure it was possible to see the behaviour of the air bearings under various dynamic loads.

During sensor calibration it was noted that the system can keep static loading which might be problematic for piezo actuators. The piezo amplifier's feedback control system was capable to keep the force stationary.

Under low frequency (1 Hz) dynamic loading seen in Figures 2 and 3 the piezo

actuator can produce desired sinusoidal force. Under this low frequency loading the air film thickness change was congruent with the force.

Higher frequency loading (200 Hz), Figures 4 and 5, the force generated by the piezo actuator follows less accurately the sinusoidal input signal. Air film thickness shows same kind of behaviour as the force figure although the response is even more uneven. This is partly caused by the force fluctuation.

The behaviour of the test system can be seen in Figures 6 and 7. The amplitude of dynamic force generated by the piezo actuator falls at the frequency of 180...200 Hz and again after 230 Hz. This is supposed to be caused by the test systems dynamic properties. The air film thickness follows the force variation. Variation in air film thickness has local minimum at the frequency of 180...200 Hz and falls again after 230 Hz respectively.

The system works well under low loading frequencies but under higher frequencies the force amplitude starts to drop. Better understanding about the results and their causes could be accomplished by measuring the piezo actuators movement directly in addition to the air film thickness measurements.

No resonances in the mechanical structure of the system were detected under tests. This gives confidence that the system is suitable for this kind of testing. The structure allows easy change of air bearing and it can be fixed to various test beds. This test system makes it possible to easily run tests with various loads and frequencies so that dynamic properties of air bearings can be measured under well controlled and variable loading conditions. With the built dynamic loading system it is easy to determine if the air bearings are suitable for different environments, like rough industrial circumstances.

## 5. REFERENCES

- [1] Cyber Technology GmbH.  
<http://www.cybertechnologies.com/wp/news/high-precision-measurements>.  
(7.3.2012).
- [2] National University of Singapore.  
<http://www.bioeng.nus.edu.sg/biomechanics/facilities.html>. (7.3.2012).
- [3] Valkonen, A., Juhanko, J., Kuosmanen, P., Martikainen, J. Intelligent Monitoring of Journal Bearings. CIMAC Congress 2010, Bergen, Norway, June 14-17, 2010.
- [4] Calonius, O., Kiviluoma, P., Kuosmanen, P. Large-scale Test rig for assessment of characteristics of flat air bearings running against a rotating counter-face. 56<sup>th</sup> IWK International Scientific Colloquium, Ilmenau, September 12-16, 2011.
- [5] Lee Y., Kim T. Y., Kim C. H., Kim T. H. Thrust bump air foil bearings with variable axial load: Theoretical predictions and experiments. Tribology Transactions, 2011, **54:6**, 902-910.
- [6] Aguirre, G., Al-Bender, F., Van Brussel, H. A multiphysics model for optimizing the design of active aerostatic thrust bearings. Precision Engineering 34, 2010, 507-515.
- [7] Al-Bender, F. On the modelling of the dynamic characteristics or aerostatic bearing films: From stability analysis to active compensation. Precision Engineering 33, 2009, 117-126.
- [8] Calonius, O., Kiviluoma, P., Kuosmanen, P. Air bearings for heavy-

duty industrial applications – effect of bearing type and operating conditions on energy efficiency, The 8th IFK International Conference on Fluid Power, Dresden, March 26 - 28, 2012.

## 6. CORRESPONDING ADDRESS

Panu Kiviluoma, D.Sc. (Tech.), Post-doc researcher  
Aalto University School of Engineering  
Department of Engineering Design and Production  
P.O.Box 14100, 00076 Aalto, Finland  
Phone: +358 9 470 23558,  
E-mail: [panu.kiviluoma@aalto.fi](mailto:panu.kiviluoma@aalto.fi)  
<http://edp.aalto.fi/en/>

## 7. ADDITIONAL DATA ABOUT AUTHORS

Iruikwu Daniel Obiora, B.Sc (Tech)  
Phone:+358 4 035 59795  
E-mail: [daniel.iruikwu@aalto.fi](mailto:daniel.iruikwu@aalto.fi)

Isomaa Matti, B.Sc (Tech)  
Phone:+358 4 055 79912  
E-mail: [matti.isomaa@aalto.fi](mailto:matti.isomaa@aalto.fi)

Korkkolainen Pauli, B.Sc (Tech)  
Phone:+358 4 513 01917  
E-mail: [pauli.korkkolainen@aalto.fi](mailto:pauli.korkkolainen@aalto.fi)

Kuosmanen, Petri, D.Sc. (Tech.), Professor  
Phone:+358 9 470 23544  
E-mail: [petri.kuosmanen@aalto.fi](mailto:petri.kuosmanen@aalto.fi)

Calonius, Olof, D.Sc. (Tech.), Researcher  
Phone:+358 9 470 24573  
E-mail: [olof.calonius@aalto.fi](mailto:olof.calonius@aalto.fi)



## MEASURING TEMPERATURE AND WATER CONTENT IN ROAD STRUCTURES WITH SENSOR EQUIPPED RFID TAGS

Kõrbe, K.; Kuhl, K. & Koppel, O.

**Abstract:** *In northern countries several freeze-thaw cycles may occur per day making it especially significant to monitor temperature and water content in road structures. The way to acquire this data in different layers of road structure is still costly, difficult and time consuming. The data is valuable as an input in choosing upon the suitable design technology. In this article an idea is presented and preliminary tests are carried out to use RFID tags with sensors in road structures to measure continuous data about significant parameters throughout the lifecycle. The results of these tests proved that RFID tags can be read through different layers and depths of road construction materials. The use of gathered data in road performance measurement systems is proposed.*

*Key words: RFID, road infrastructure, data collection.*

### 1. INTRODUCTION

In all northern countries similar special problems with road deterioration due to cold climates occur but vary with variations in temperature, geology and other condition as traffic configuration, road design practices etc. The deterioration of roads can have serious consequences for the safety and comfort of road users and reconstructions cause extra need for financial assets.

In developed countries investments in transportation infrastructure account for a significant part of appropriations to the real sector and adequate data from performance measurement systems is required for making investment decisions and in monitoring executed projects. Radio Frequency Identifi-

cation (RFID) technology is a relatively new technology in road construction field but has widely spread in Intelligent Transportation Systems (ITS). Because of its benefits construction and transportation industries are researching and implementing RFID technology to improve data storage applications and also to develop "smart RFID tags" that are able to sense, monitor, and adapt to their changing environment. RFID has been identified as one of the cornerstones of the upcoming Internet of Things (IoT) and the focus is moving from conventional RFID towards next generation pervasive networked and interconnected systems [14].

Currently pavement and road structure monitoring needs significant personnel time or the use of costly equipment but there is need for this data as an important input in choosing upon the suitable design technology for new projects and in measuring [6]. In this article an idea is presented to use passive and Battery Assisted Passive (BAP) RFIDs with sensors in road structures to measure continuous data about significant parameters throughout the lifecycle of the road. Previous research [8] has indicated readability problems with the use of RFIDs therefore the authors conducted preliminary tests to verify the suitability of the suggested technology.

The estimated lifetime and durability of suggested technologies are more close to lifetime of the road than other low-power wireless technologies such as Wireless Sensor Networks and Active RFID Sensor Tags and therefore do not require intrusion to road structures for data acquisition and maintenance reasons.

## 2. MOTIVATION OF THE RESEARCH

The climate of Estonia, comprising of several freeze-thaw cycles even per day in winter makes it particularly important from the sustainability point to have knowledge about temperature changes and the amount of water moving through pavement and in different layers of the embankment. Cracking of pavements related to low-temperature frost action and freeze-thaw cycles is a well-recognized problem in most northern countries. Premature deterioration of road pavements is related to high frequencies of freeze-thaw cycles, primarily where subgrades are composed of fine-grained, saturated material [5].

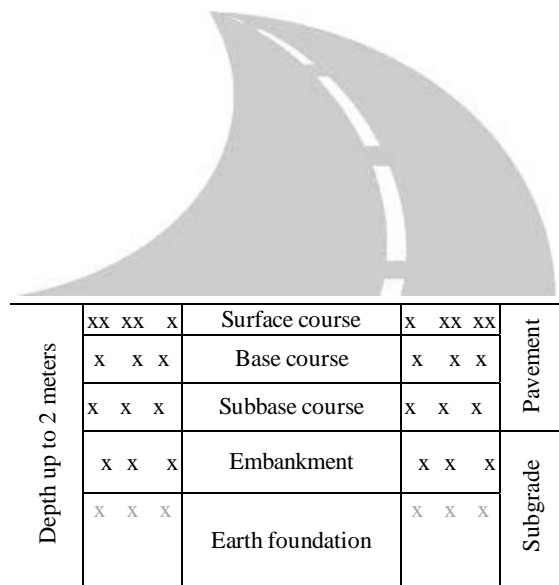


Fig. 1. Road cross section (x mark the planned locations of tag)

Once in a pavement or embankment water plays a primary role in giving shorter service life, service-ability and increasing the need of rehabilitation measures. In order for a road to be sustainable it is necessary to do the following: consolidate well the earthworks, have good sub-base drainage, keep the water-table low, preventing the moisture content of the sub grade increasing, avoid failures due to binder stripping, not to allow water to remain on top of the surface course weakening the surface due to hydraulic pressure. If improperly canalized,

water can also cause soil erosion and a breakdown of pavement edges.

With below 0 °C degrees and freezing the deteriorating effect is even much greater. Cold temperatures in winter are great concern for transportation agencies because due to frost action the phenomena called frost heave occurs, a road will actually "heave up", being the major deterioration of roads especially in case of insufficient drainage.

Therefore it is essential to monitor the above mentioned causes of deterioration in order to avoid design failures and to give support to the road agencies to establish the best requirements for designing and constructing sustainable roads. Authors have chosen to suggest measuring water content and temperature simultaneously in road structures using passive and Battery Assisted Passive (BAP) RFIDs with sensors (see Fig. 1).

## 3. RFID TECHNOLOGY

RFID technology as we know it today dates back to 1970's when Mario Cardullo's and Charles Waltons devices were patented in 1973 succeeding with the marketing of first usable products in 1979. The RFID technology is a means of uniquely identifying an object with a wireless radio link, allowing data to be stored on an RFID tag and retrieved in remote application at a later point of time [1].

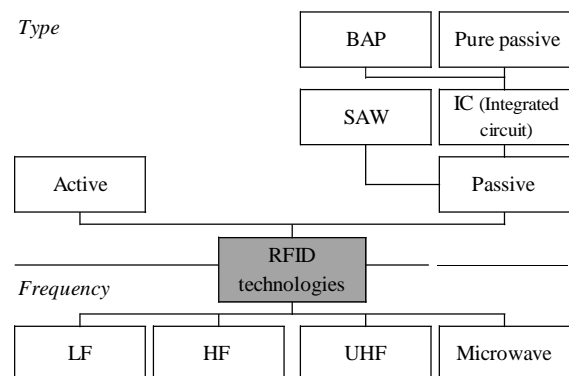


Fig. 2. Typology of RFID technologies

Wireless sensors incorporated in RFID systems are important in several industrial,

consumer and logistics applications. By extending RFID tags to sensing applications the products become smarter and RFID sensor network applications are emerging and moving towards commercialization [9]. Two RFID technologies are available: (SAW) and Integrated Circuit (IC) based. Passive RFID sensor tags may be categorized as Surface Acoustic Wave (SAW), IC Passive and IC BAP. Multiple designs of adding sensors on passive RFID tag exist (see Fig. 2).

These technologies have been successfully used in various applications amongst others also in the construction industry. Due to the progress in integrated circuit technology, it is expected that RFID will play an important role in the global circulation infrastructure. It is expected that more RFID tags will be used in the future as sensory functions come more common-place [12].

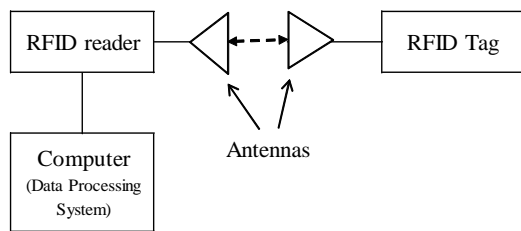


Fig. 3. RFID system generic structure [3]

A typical RFID system includes three components: an antenna or coil, a transceiver (with decoder), and a transponder (RFID tag) electronically programmed with unique information, as illustrated in Fig. 3.

#### 4. SYSTEM DESIGN

##### 4.1 System Architecture

Authors have studied RFID tags with sensory functions because it is considered that the RFID tag can detect some conditions of structures and transfer its information through external reader [10]. With this in mind we are trying to develop a system ((see Fig. 4) to monitor the condition of road structure and establish the impact of water content and temperature change to road deterioration and with the use of RFID tags with sensory functions.

The device may be located in the moving vehicle or placed stationary on the road side. The RFID reading on motion will add certain requirements on the tag and reader antenna orientation, but at the same time reduces cost. Having many metering points with stationary readers will cost more than few, but often by-passing vehicles with the Interrogator on board [5], [8].

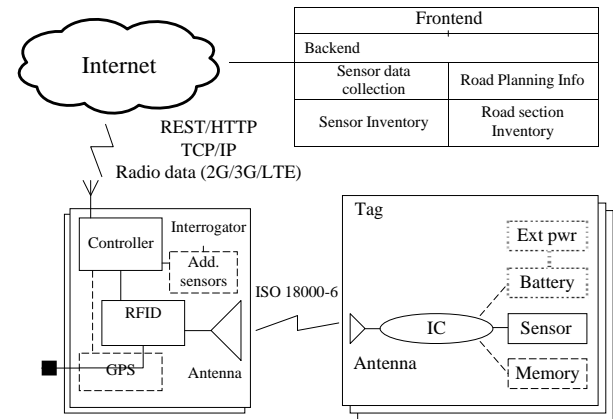


Fig. 4. System architecture

Interrogator processes and enriches the raw sensor tag data. It consists of a RFID reader together with an antenna and data processing system. It may contain the GPS module to add the location coordinates to the sensor reading event to allow reporting in deviations of stored data and field information. Interrogator contains additionally sensors for reading the air temperature, relative humidity, and speed of the Interrogator when in motion.

The data from Interrogator towards the Backend server is transmitted over REST style HTTP(S) interface on top of TCP/IP network to avoid possible data communication network operator restrictions and makes the data transfer operator and media agnostic. For moving units, radio network is necessity. Stationary units may be connected to fixed communication line if available.

Backend server keeps the inventory of installed sensors (location, installation date, depth, layer material) and collects the sensor data (interrogator identifier, sensor identifier, reading location, temperature and water content in road structures, signal strength,

temperature and relative humidity in Air) sent by interrogators. Road section inventory (section name and identifier, owner, maintaining organization, condition, and history) is kept in the same database to allow reporting based on the road sections.

Backend keeps also road planning information (e.g price by the road section) to be able to report on the deviations between the plans and current situation and do the cost calculations of the delta to assist decision modeling of upcoming road construction projects. The reports and online sensor data is displayed and rendered to the graphical format in frontend graphical user interface to be used by the stakeholders. Sensor data is made available to third-parties through public API (Application Programming Interface) using Open Data principles. Correction functions for sensor readings are applied in the backend during the data collection process.

## 4.2 Sensor applications

For IC tags normally sensor tag comprises four major blocks – an analogue sensor, analogue-to-digital converter (ADC), digital controller circuit and RF part with antenna. The BAP tag may contain optionally Non-volatile memory (e.g. FeRAM) for data storage, ultra long-life energy storage (e.g. lithium-polymer, thin film super-capacitor) and renewable power source (e.g. piezoelectric or photovoltaic generator).

It is known that low-cost Capacitive Soil Water Content sensors that are suitable for this type of application are sensitive to soil density, temperature, salinity, and supply voltage (RF signal strength) variations [2], [11]. The calibration method to correct the readings based on geostatistics, sensor clustering and information sharing has been proposed by Zhang [18].

The proportional-to-absolute temperature (PTAT) current generator, directly representing the temperature, delivers a PTAT current and a reference current, keeping the latter's value constant over the temperature range of interest. In the RFID

tag the ADC then processes both currents into the digital data stream, passes to the controller which encodes the result into the response [7], [13]. Also a design without ADC has been proposed by Shenghua [17] to even more reduce the power requirements of the sensor.

The capacitance and time domain reflectometry (TDR) method are two widely used electromagnetic (EM) techniques for soil water content estimation. Both methods make use of the strong dependence of EM signal properties on volumetric water content that stems from the high permittivity of water compared to mineral soil solids, and air. The basic principle of the capacitance method is to incorporate a dielectric medium (e.g. soil) as part of the dielectric of the sensor capacitor [2].

Temperature and Water Content measurement using SAW tags has been shown by L. Reindl [16]. The SAW RFID tag consists of an inter-digital transducer (IDT) and a series of acoustic reflector traps etched into a piezoelectric substrate. The tag reader emits a radio wave pulse to the IDT that is converted piezoelectrically into a nanoscale acoustic wave. The wave travels past the reflectors to produce a unique pattern of reflected pulses. These travel back to the IDT, where they are piezoelectrically converted into an encoded radio wave reply signal to the reader. The SAW chip operates in a purely passive mode and does not require supplementary DC power [15].

## 5. PRELIMINARY TESTS

Authors conducted a preliminary empirical and field study to check whether the UHF IC Passive tag transmittance in dry soil and road construction materials is similar to the expected.

For that we connected ThingMagic Vega UHF RFID reader to RHCP (Right Hand Circular Polarized), 7,5 dBiC Antenna and to a PC with software needed for reading. In another end authors used Confidex Ironside metallic, ALN-9629 "Square" Inlay and Avery Dennison AD-824 RFID tags.

Authors were aware of the fact that the metallic tag performance is suboptimal when placed on non-metallic surface, but we decided to test a tag with average performance in the air, which is approximately 4 meters in the combination with our reader. All the tests were executed in laboratory environment in room temperature. Second set of tests was conducted at a road construction site to get proof that the signal could be read through different materials used in road construction from the depths up to 2 metres. During the experiment we inserted the tag in various depths into the soil going up to 2 meters and took readings leaving the variable air gap between the soil and antenna so that the distance between the antenna and tag was never bigger than 3 meters. The success rate of the reading was as expected and we were able to get readings using all three types of RFID tags.

The results provided solid ground on continuing with testing with varying materials to simulate actual conditions. In the preliminary field trials authors tested the Confidex Ironside metallic RFID tag in soils with various moisture, sand, and gravel. We placed the tags in depths up to 2 meters, leaving the gap between the antenna and the tag so that the distance between the antenna and tag was also never bigger than 3 meters. Authors were able to get readings through all tested materials and are confident to move to the next stage to start preparing field test in road construction site.

## 6. FURTHER RESEARCH

As the results of the preliminary tests that proved RFID tags suitability to get readings from the depth of up to 2 meters in the ground we are can continue with the research and field tests in actual conditions as follows.

- Theoretical and experimental study of radio wave propagation from the air through different layers of road construction materials and back taking into account the possible frequencies of suitable Passive or

BAP RFID technologies, environment temperature and water content deviations.

- Evaluation of existing SAW, IC BAP and IC Passive sensor tags in soil.
- Study on energy harvesting and storage solutions suitable for BAP tags.
- Adding sensors to measure if salt used in winter maintenance percolates into road structures
- Study alternative WSN approach using IEEE 802.15.4 (e.g. Zigbee or 6LoWPAN) based sensor mesh network to gather underground sensor data ignoring the current battery lifetime issue.
- Testing removing the battery altogether and storing energy solely in the super-capacitor, there is now a viable option for achieving long-life operation. By designing the node to operate on 50 % energy capacity, the operational lifetime can be pushed out to 20 years [19].

## 7. CONCLUSIONS

Long term monitoring and feedback from sensor equipped RFIDs helps: reduce maintenance cost, improve longevity, enhance safety, and advance research in pavement design.

Authors have conducted a series of tests in laboratory and field conditions and were able to confirm the RFID tag suitability and readability in different depths up to 2 meters of road structures. Literature review and preliminary tests prove that the technical solution presented in this article is perspective and ready to move to feasibility study phase.

## 8. REFERENCES

1. Berthiaume, F., Donahue, K., Rommel, J. *RFID tag selection report*. Rutgers Center for Innovative Ventures of Emerging Technologies, Piscataway, 2011.
2. Bogena, H. R., Huisman, J. A., *et al.* Evaluation of a low-cost soil water content sensor for wireless network applications. *Journal of Hydrology*, 2007, **344**, 32-42.

3. de la Garza, J., Fedrowitz, W. Implementation of RFID Technology in the VT-VDOT Highway Maintenance Monitoring Program (HMMP). In *Proc. of the Intelligent Computing in Engineering Conference*, Plymouth, 2008, 518-527.
4. Djärf, L., Magnusson, R., Lang, J., Andersson, O. *Road Deterioration and Maintenance Effects for Paved Roads in Cold Climates*. Swedish Road and Transport Research Institute, Stockholm, 1995.
5. Dziadak, K., Sommerville, J., Kumar, B. RFID based 3D buried assets location system. *Journal of Information Technology in Construction*, 2008, **13**, 155-165.
6. Faridazar, F., Lajnef, N. Intelligent Multi-Sensor Measurements to Enhance Pavement Monitoring and Safety. In *Passive Wireless Sensor Tag Workshop*, NASA, Houston, 2011.
7. Kim, S., Kim, H.-S., Kim, H., et al. An EPC Gen 2 compatible passive/semi-active UHF RFID transponder with embedded FeRAM and temperature sensor. In *IEEE ASCC'07*, Jeju, 2007, 135-138.
8. Lee, E.-K., Yoo, Y. M., Park, C. G., Kim, M., Gerla, M. Installation and Evaluation of RFID Readers on Moving Vehicles. In *Proceedings of the sixth ACM international workshop on VehiculAr InterNETworking*, New York, 2009, 99-108.
9. Löfgren, L., Löfving, B., Pettersson, T., Ottosson, B., Rusu, C., et al. Low-power humidity sensor for RFID applications. In *Multi-Material Micro Manufacture* (Dimov, S. and Menz, W, eds.). Whittles Publishing, Cardiff, 2008.
10. Mitrokotsa, A., Douligieris, C. Integrated RFID and Sensor Networks: Architectures and Applications. [http://lasecwww.epfl.ch/~katerina/papers/RFID\\_WSN.pdf](http://lasecwww.epfl.ch/~katerina/papers/RFID_WSN.pdf), accessed 04.03.2012.
11. Mittelbach, H., Casini, F., Lehner, I., Teuling, A. J. and Seneviratne, S. I. Soil moisture monitoring for climate research. *Journal of Geophysical Research*, 2011, **116**.
12. Ogawa, S., Sato, T. Monitoring of Concrete Structures Using Passive Type RFID Tags with Sensory Functions. In *The International Conference on Electrical Engineering*, Okinawa, 2008.
13. Opasjumruskit, K., Thanthipwan, T., Sathusen, O., et al. Self-Powered Wireless Temperature Sensors Exploit RFID Technology. *IEEE Pervasive Computing*, 2006, **1**, 54-61.
14. Pesonen, N., Jaakkola, K., Lamy, J., et al. Smart RFID Tags. [http://www.vtt.fi/files/research/mel/smart\\_rfid\\_tags.pdf](http://www.vtt.fi/files/research/mel/smart_rfid_tags.pdf), accessed 04.03.2012.
15. Pfeiffer, G. H. *Using Radio Frequency Identification technology to measure asphalt cooling*. University of Maryland, College Park, 2010.
16. Reindl, L., Ruppel, C. C. W., Kirmayr, A., et al. Radio-requestable passive SAW water-content sensor. *IEEE Transactions on Microwave Theory and Techniques*, 2001, **4**, 803-808.
17. Shenghua, Z., Nanjian, W. A Novel Ultra Low Power Temperature Sensor for UHF RFID Tag Chip. In *IEEE ASSCC'07*, Jeju, 2007, 464-467.
18. Zhang, R.-b., Guo, J.-j., Zhang, L., et al. A calibration method of detecting soil water content based on the information-sharing in wireless sensor network. *Computers and Electronics in Agriculture*, 2011, **76**, 161-168.

## 9. CORRESPONDING ADDRESS

MSc. Kati Kõrbe,  
TUT, Department of Logistics and Transport, 5 Ehitajate Str., 19086 Tallinn,  
Phone: +372 6 202 608,  
E-mail: [kati.korbe@ttu.ee](mailto:kati.korbe@ttu.ee).

## 10. ADDITIONAL DATA ABOUT AUTHORS

Mr. Kristjan Kuhi, Senior Engineer, Ericsson Eesti AS, 9 Järvevana Str., 11314 Tallinn, [kristjan.kuhi@ericsson.com](mailto:kristjan.kuhi@ericsson.com).

Professor Ott Koppel, PhD, TUT, Department of Logistics and Transport, 5 Ehitajate Str., 19086 Tallinn, [ott.koppel@ttu.ee](mailto:ott.koppel@ttu.ee).

## SINGLE-STAGE ELECTROMAGNETIC ELEVATOR MODELLING IN FEMM SOFTWARE

Lapkovskis, V., Mironovs, V.

**Abstract:** In present paper an electromagnetic elevator (conveying device) designed in Riga Technical University (Latvia) is described. Modelling of single-stage electromagnetic elevator in FEMM software is suggested. Analysis of electromagnetic field distribution created by multi-turn coil used as propulsion mean for conveying of ferromagnetic materials by electromagnetic field is presented. Use of different coil materials and coil dimensions is evaluated.

*Key words: electromagnetic elevator, FEMM software, coil*

### 1. INTRODUCTION

There are many specific industrial applications of electromagnetic fields: sensors, actuators, valves, vibration agitators, particulate filters and a great many other technical applications. Amongst them there is a place for specific application of pulsed electromagnetic field, namely for conveying of ferromagnetic materials in tubes. A millisecond impulse of electromagnetic field is acting as a propulsion mean for moving of ferromagnetic materials inside a tube. Ferromagnetic powders manufacturing industry is one of the end-users of presented approach [1].

Nowadays manufacturers of ferromagnetic powders are using a traditional screw [2], belt conveyors, bucket elevators, chain tubular conveyors [3] or pneumatic conveying systems [4] for powder handling. Due to extensive wear of construction materials, a periodic

maintenance of such conveyors is required. Moreover, powder raw materials are becoming contaminated of wear products (particles). The electromagnetic conveyor can be considered as a solution for certain industrial applications, and especially in powder metallurgy.

One of the most demanding tasks is a conveying of ferromagnetic powders in vertical pipes for further processing. As a possible solution the Powder Materials Laboratory of Riga Technical University has designed a laboratory-scale single-stage electromagnetic system for powder conveying on short distances (up to 5 meters) in pipes [5]. Scheme of laboratory equipment EMC-05 [6] for ferromagnetic powder conveying by impulse electromagnetic fields is shown in Fig. 1. In our laboratory setup a power unit is produced by HBS Bolzenschweiss-Systeme GmbH [7] has been used.

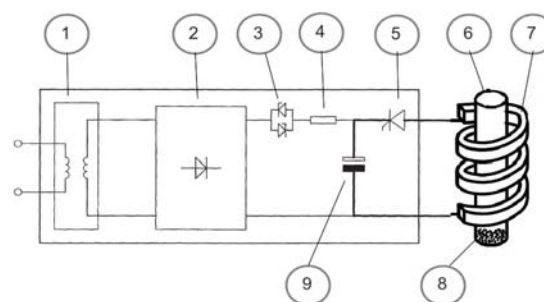


Fig. 1. Schematic of the equipment used for ferromagnetic powders conveying by impulse electromagnetic field.

1 – transformer, 2 – rectifier, 3 – triac (thyristor), 4 – charging resistor, 5 – discharging thyristor, 6 – conveyor tract, 7 – coil, 8 – ferromagnetic powder, 9 – capacitor battery.



Schematically the approach for conveying by electromagnetic fields is shown in Fig. 2.

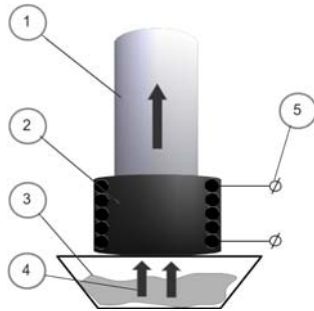


Fig. 2. Schematic ferromagnetic materials conveying in vertical pipe.

1 – pipe (conveyor tract), 2 – electromagnetic coil, 3 – reservoir filled with ferromagnetic powder (iron powder), 4 – gripping of ferromagnetic powder by impulse electromagnetic field applied, 5 – coil connection to the generator of electromagnetic currents (power unit).

Industrial iron powders have iron content 96.5-99.5%. Specifications of iron powders suitable for transportation by electromagnetic field are presented in Table 1.

Particle size range, $\mu\text{m}$	45-200
Fe content in powder (by weight), %	96.5-99.5
Apparent density of powder, $\text{g/cm}^{-3}$	2.3-3.9

Table 1. Iron powders used for conveying by impulse electromagnetic field.

## 2. ELECTROMAGNETIC CONVEYOR MODEL IN FEMM

We have chosen the FEMM - a powerful free software for electromagnetic problems modelling [8], [9]. FEMM is a 2D FEA software package developed by Eng. D. Meeker [10].

There are different models of accelerator

devices where pulsed electromagnetic fields are used [11]. In case of fine particles (or iron powders) the reluctance conveying approach was used [12]. A selected approach is based on the attractive ferromagnetic properties of the transportable material which provoke acceleration. FEMM modelling is realised for the computation of the force on a mass of iron powder at various positions relative to a wound air-cored coil.

For modelling of electromagnetic field distribution a set of wound air-core coils has been used (Table 2.). A cross-sectional view of coil is shown in Fig. 3.

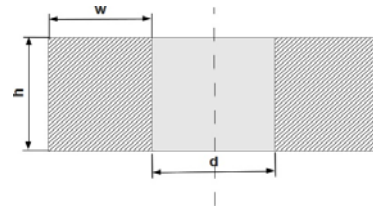


Fig. 3. Coil cross-sectional view.

w – winding thickness, mm; h – winding height, mm; d – coil's internal (wound) diameter, mm

Coil No.	Winding material	w, mm	h, mm	d, mm
Coil(01)	Copper	25	25	50
Coil(02)	Aluminium	25	90	50
Coil(03)	Copper	40	75	50

Table 2. Electromagnetic coils used for modelling in FEMM.

In order to evaluate an electromagnetic lifting force for current model a set of ferromagnetic powder bodies (cylindrical powder fillings) has been defined (Fig. 4., Table 3.)

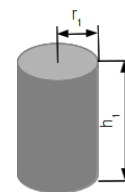


Fig. 4. Powder bodies used for the modelling of electromagnetic elevator.

Label of powder body	$h_1$ , mm	$r_1$ , mm
a	35	25
b	25	25
c	15	25

Table 3. Dimensions of ferromagnetic powder bodies used for modelling.

A schematic of electromagnetic elevator input geometry is shown in Fig. 5. Initially, the powder body is located underneath the coil.

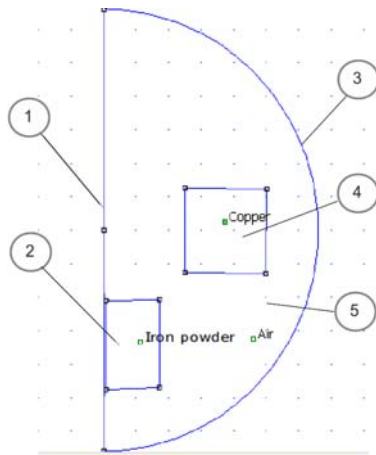


Fig. 5. Electromagnetic elevator: axisymmetric model set-up in FEMM. 1 - symmetry axis, 2 – iron powder, 3 – outer boundary of interior region, 4 – coil cross-section, 5 – interior region (air).

It was established experimentally that for the laboratory device the minimal voltage of impulse current source when it is possible to observe and register a lifting phenomenon of fine ferromagnetic materials is 50 V. Thus, for the FEMM model the similar conditions have been chosen. Coil electrical input parameters [13] for the model are shown in Table 4.

Coil No	Calculated source current density, MA/m <sup>2</sup>	Electrical conductivity of wire material, MS/m
Coil(01)	0.608	59.6
Coil(02)	0.158	35
Coil(03)	0.123	59.6

Table 4. Power source current density, and electrical conductivity of coils.

The following assumptions of FEMM model have been taken into account: steady current (in coil), no eddy currents, simulation for every position (shift) of powder body along the z-axis is calculated for the steady-state conditions. Example of magnetic field density plot for Coil(01) is shown in Fig. 6.

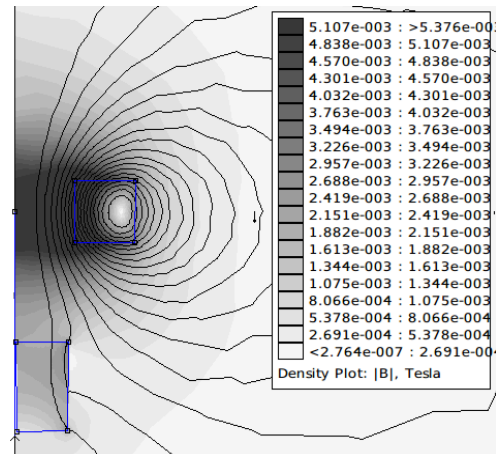


Fig. 6. Magnetic field density plot for Coil(01).

For evaluation of electromagnetic interaction between coil and powder body, a programme written in Lua language [14] has been used. The following actions are performed during an execution of Lua script:

- Shifting a powder body along z-axis,
- Performing a numerical analysis of the model,
- Calculating z-directed component of force for every position of powder body.

### 3. RESULTS

Output results of force vs. distance between powder body and coil centre modelling are presented below in Fig. 7, 8, 9.

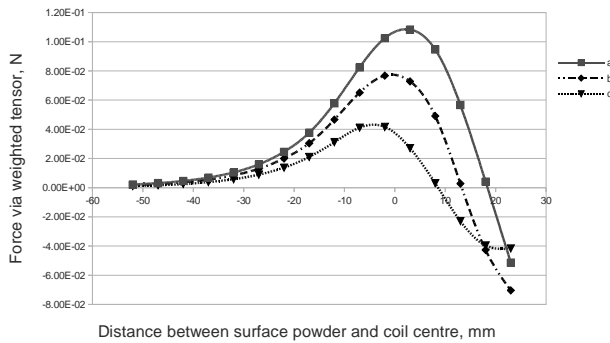


Fig. 7. Force vs. distance between powder body and coil centre modelling output for Coil(01) calculated for powder bodies (a), (b), (c).

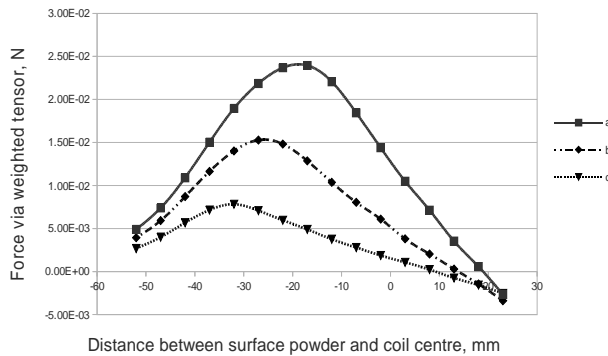


Fig. 8. Force vs. distance between powder body and coil centre modelling output for Coil(02) calculated for powder bodies (a), (b), (c).

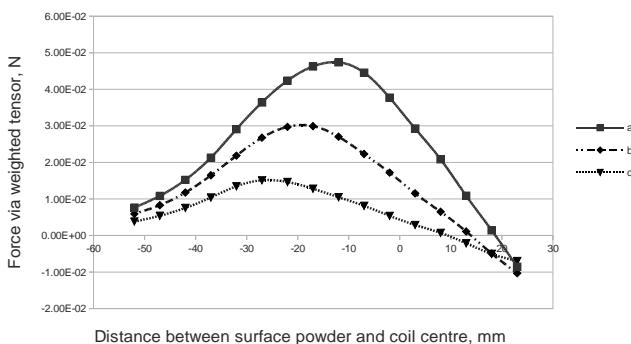


Fig. 9. Force vs. distance between powder body and coil centre modelling output for Coil(03) calculated for powder bodies (a), (b), (c).

It is evident that coil's geometry plays an important role in conveying model. For Coil(02) and Coil(03) the maximum of force is achieved at the entrance of coil wound or in the first half of coil's height. In the same time the highest force values have been shown by Coil(01). In fact, the experiments confirm the effectiveness of Coil(01) [15]. The best simulation results have been shown by coil made of copper wire e.i. Coil(01).

### 4. FURTHER RESEARCH

Further research is necessary for pilot equipment construction, which can be used in real manufacturing facilities. The modelling procedure can help in design of low-energy pilot equipment for conveying of ferromagnetic materials. Meanwhile, it is important to evaluate an influence of electromagnetic impulse fields on powder segregation, especially in case of continuous exploitation. FEMM software will be used for modelling of different mixing equipment based on electromagnetic phenomena [16].

### 5. CONCLUSIONS

The FEMM software is useful instrument for evaluation of different geometries and materials used in design of electromagnetic elevator.

Modelling approach has confirmed a previous research on construction of electromagnetic conveying equipment.

The following modelling is necessary for evaluation of combination of factors influencing on the effectiveness of electromagnetic elevator.

### 6. ADDITIONAL DATA ABOUT AUTHORS

Mr. Vjaceslavs Lapkovskis,  
Researcher.  
Azenes str. 16, lab. 331, LV-1048,  
Riga, Latvia  
[lap911@gmail.com](mailto:lap911@gmail.com)  
[www.lab331.info](http://www.lab331.info)  
Ph. (+371) 29536301

Mr. Viktors Mironovs.  
Dr.hab.Sc.ing.  
Azenes str. 16, lab. 331, LV-1048,  
Riga, Latvia  
[viktors.mironovs@gmail.com](mailto:viktors.mironovs@gmail.com)  
[www.lab331.info](http://www.lab331.info)  
Ph. (+371) 67089270

Corresponding Author:  
Mr. Vjaceslavs Lapkovskis,  
[lap911@gmail.com](mailto:lap911@gmail.com)  
Ph. (+371) 29536301

## 7. ACKNOWLEDGEMENTS



This work has been supported by the European Social Fund within the project "Support for the implementation of doctoral studies at Riga Technical University"

## 8. REFERENCES.

- [1] S. Saito, J. Ohta, and M. Fujinaga, "JIP® Iron Powder Products and Technical Trends in Powder Metallurgy," *jfe-steel.co.jp*, vol. 16, no. 16, 2011.
- [2] A. Kurjak, "The vertical screw conveyor- powder properties and Screw conveyor design (Master Thesis)," Lund Institute of Technology, 2005.
- [3] S. Schmolke, A. Katterfeld, and F. Krause, "Experimental Tests and Design of Tube Chain Conveyors," *wase.urz.uni-magdeburg.de*.
- [4] D. Mills, M. G. Jones, and V. K. Agarwal, *Handbook of Pneumatic Conveying Engineering*. Marcel Dekker, 2004.
- [5] V. Mironov, J. Viba, and V. Lapkovsky, "Electromagnetic transportation of ferromagnetic powders in pipes /in Russian/," *Poroshkovaya metallurgiya*, vol. 33, pp. 53-59, 2010.
- [6] V. Lapkovskis and V. Mironovs, *Laboratory equipment EMC-05. Introduction to conveying of ferromagnetic powders by impulsed electromagnetic field*. 2012.
- [7] HBS, *HBS CD 1501 Power Unit. Operating manual*. 2005, p. 72.
- [8] K. B. Baltzis, "The FEMM Package: A Simple, Fast, and Accurate Open Source Electromagnetic Tool in Science and Engineering," *J. of Engineering Science And Technology Rev.*, pp. 83-89, 2008.
- [9] S. Zurek, "Magnetic core with a coil. 2D magnetostatic with FEMM 4.2," 2008.
- [10] D. Meeker, *Finite element Method Magnetics v4.0, User's Manual*. 2006.
- [11] S. W. Kim, H. K. Jung, and S. Y. Hahn, "An optimal design of capacitor-driven coilgun," *Magnetics, IEEE Transactions on*, vol. 30, no. 2, pp. 207–211, 1994.
- [12] G. W. Slade, "A simple unified physical model for a reluctance accelerator," *Magnetics, IEEE Transactions on*, vol. 41, no. 11, pp. 4270–4276, Nov. 2005.
- [13] D. J. Griffiths, *Introduction to electrodynamics*, vol. 3. prentice Hall New Jersey:, 1999.
- [14] R. Ierusalimschy, L. H. de Figueiredo, and W. Celes, *Lua 5.1 Reference Manual*. Lua. org, 2006, pp. 1-19.
- [15] V. Lapkovsky, V. Mironov, A. Shishkin, and V. Zemchenkov, "Conveying of Ferromagnetic Powder Materials by Pulsed Electromagnetic Field," in *Euro PM2011 – Tools for Improving PM: Modelling & Process Control*, 2011, pp. 253-258.
- [16] V. Mironovs, V. Lapkovskis, and J. Baroniņš, "Method and device for mixing of powder materials," *LR Patent application 14383 A*, 2011.

## 3D FIT GARMENT SIMULATION BASED ON 3D BODY SCANNER ANTHROPOMETRIC DATA

**Olaru, Sabina; Filipescu, Emilia; Filipescu, Elena; Niculescu, Claudia & Salistean, A.**

**Abstract:** *With the increased desire among customers for individualized and customized fashion products, an interest in 3D virtual garment simulation has been growing throughout the world. 3D garment simulation has used for many things, such as virtual fashion shows, online fashion communities, the virtual trying-on of garments, and more. The present paper aims to realize a dress garment simulation on a virtual mannequin obtained by 3D body scanning. The result will be the testing of the 2d designed pattern after the fitting on the virtual mannequin using specialized 3D software.*

*Key words: 3D Body Scanner, Computer Aided Design (CAD), Fit Simulation*

### 1. INTRODUCTION

Advanced and integrated technologies, such as the optical measurement, the electronic signal and data digital processing, the computer software and hardware, propelled the traditional 2D measurement of the anthropometric data towards a new trend – the use of a 3D body scanning technique for the anthropometric data achievement[1].

The 3D Body Scanner used in the clothing sector research promises to revolutionize the way the clothing item will be manufactured and sold. The anthropometric data achieved by scanning have the potential to offer new insights for issues related to clothing dimensioning and fitting.

Virtual garment simulation is the result of a large combination of techniques that have also dramatically evolved during the last

decade. Cloth simulation has however matured enough to introduce its potentials to the garment industry. The main needs to be fulfilled are mostly related to virtual garment prototyping, as well as visualization applications related to and virtual fashion and prototyping [2]. Garment simulation makes it easy for designers, pattern makers and apparel manufacturers to present style decisions, test the fit of a garment and create accurate and visually stunning samples in less time and share them instantly, without expensive sewing and shipping costs.

Flat sketches often are not able to truly explain a designer's vision to the development team or potential buyers.

The present paper shows how efficient is to work with garment simulation, work method which make it possible for users to see the garment from any angle in a static pose or even in motion using a virtual mannequin. The virtual mannequin is obtained from the 3D scanning of the customer body and in the 3D garment simulation it can be tested the fit between the body and the garment. Regarding the results, the designer can change the initial pattern and correct the particular garment according to the customer needs. A pattern is a 2-dimensional representation of a 3-dimensional object; ultimately the garment will be worn by someone, and the pattern maker is responsible for the way that garments fits. Many pattern makers use 3D garment simulation to test their pattern blocks and basic shapes while they are drafting the pattern, to make sure that the balance and slopes of the garment are correct [3,4].

## 2. 3D FIT GARMENT SIMULATION

### 2.1 Virtual mannequin obtained by 3D body scanning

The VITUS Smart XXL scanner (Fig. 1) is based on the most precise optical triangular method with laser, for the 3D image capture, in conformity with EN ISO 20685:2005 3-D scanning methodologies for internationally compatible anthropometric databases.

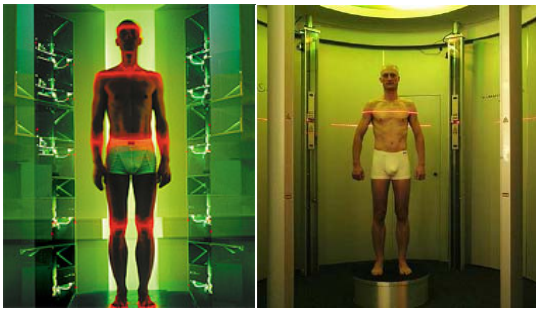


Fig. 1. 3D Body Scanner VITUS Smart XXL

The system combines the efficiency and flexibility of an automate capture of the body sizes, providing the user the possibility to define individual measuring rules perfectly fit to his/her own requests.

The Anthroscan Software allows draw/capture from the virtual body/mannequin some different dimensions, such as: height, lengths, widths, depths, perimeters, diameters, bending angles and distances to a vertical imaginary plan. The system also allows creating plans, conceiving sections, measure distances within sections, as well as open curve lines, as shown in Fig. 2.



Fig. 2. Dimensions of the scanned virtual body

Special soft wares are used to import the virtual mannequin in the 3D fit simulation software. The 3D body obtain by scanning must be cleaned by the overlapped points, defects, unclosed polylines, unclosed surfaces perceived by the software as "holes" and so-called "noise effect".

### 2.2 2D pattern design using the 2D PDS OPTITEX software

The present paper shows one of the ways to realize a garment simulation. In order to obtain a correct fit, the pattern must first be correctly designed in 2D and must be developed to be able to generate, starting from 2D patterns the necessary data to generate the 3D physical model of the garment and execute the simulation.

The 2D dress pattern was designed using the geometrical method, in the PDS OPTITEX CAD software. Using the software you can create the important patterns line, add points and align then vertical. After the pattern is ready, you can add on the pattern the notches, the seam type which can be copied, duplicated or replicated for all the displayed patterns, the dart can be added, edited or cut.

In the final phase, it is necessary to realize pattern verification: the patterns can be measured to be sure are at the correct dimensions or can be joined together for a better verification.

After all the measurement and pattern checking are done, the pattern can be graded for the according grading table. The results of using all the function and according to an algorithm the pattern for the dress garment will be obtained (Fig. 3).

### 2.3 Preparation the 2D dress pattern for the garment simulation

Creating 3D cloth from 2D flat patterns requires additional information which consists of: initial 3D position and mannequin import, stitching information (What goes to what?), define materials and texture (Stretch, Rigidity...), colors, prints, logo's, stitch widths & textures (Shading). The work flow for obtaining the fit



simulation, it is as it can be shown in the figure below: patterns must be created in 2D but also there is the possibility to import 2D patterns from different CAD systems.

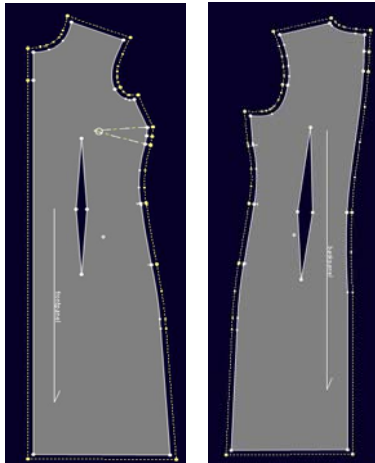


Fig. 3. 2D dress pattern

On the designed/imported 2D patterns must be added the stitches information and then to define the fabric and texture type. Once all these steps are done, the 3D module must be open, where the garment is posing on the virtual mannequin and verify the patterns position one to another and also the pattern position to the mannequin. In the end, the simulation can be done and the result is a visualization of the fit between the garment and the mannequin. Having this result, the designer can modify the initial patterns till it is obtained a perfect fit (Fig. 4).

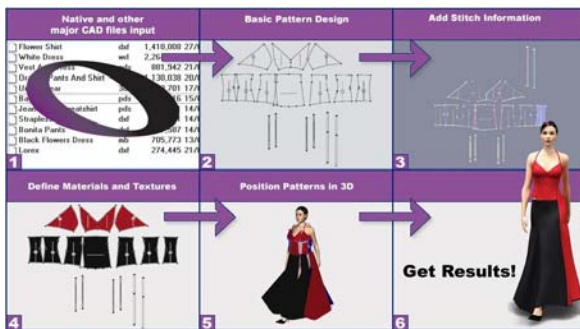


Fig. 4. Simulation steps

OptiTex 3D gives the power to simulate cloth on a variety of body sizes and shapes. The virtual mannequin obtained by 3D body scanning is imported in the

simulation software. In PDS click the 'View' menu, select '3D Windows' and then select 'Model' to open the 3D Viewer window. After selecting the "Model" function a new window will be displayed from where can be loaded the need mannequin. After loading the needed mannequin, in the same window will be displayed the measurement characterization of the mannequin, dimensions according to the real body type for which the dress is being designed (Fig. 5).

Once the model is loaded, the Body Dimensions dialog already has default measurement values for each parameter. For each parameter the model has a default location from which the measurement is taken. If you click on a slider for a parameter, or click inside its associated edit box, you can see the location of the measurement represented by a highlighted blue line.

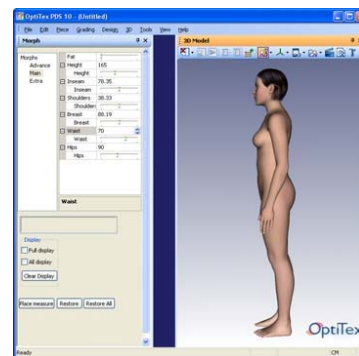


Fig. 5. Mannequin import

For example, if a click is done on the slider for the Waist parameter a blue line appears around the area of the model's waist in the 3D viewer. Often, the placement of these default locations will not be exactly what you want, so the system allows you to modify their placement to any position you like. The key to changing measure placement is in using the measure tools.

The next step is to add the stitches information between the 2D patterns. In order to be able to realize the simulation, the garments must have stitch information added on the segments which will be sewed together. Furthermore we will



present one way which is used for the dress stitching operation (Fig. 6).

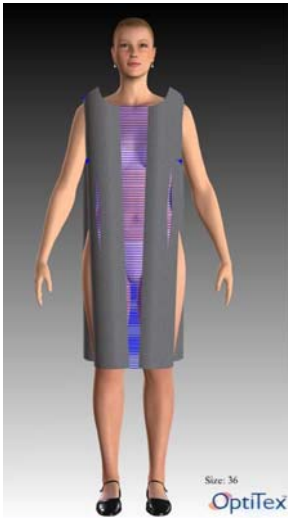


Fig. 6. Dress stitching operation

Method Point to Point - Click on a grading point then on the next point in a clockwise manner, this defines the first “Half” of a stitch. Notice the change of cursor to a double sewing machine. Do not forget that grading points have to be viewed in order to select them. To define a stitch in a counter clockwise manner press the Shift key while selecting the second point (Fig. 6).

After stitching all necessary segments, we are ready to verify the connections and run the simulation.

Position the cloth again by clicking the “Place Cloth”. Now you can see the actual stitching connections in 3D. Stand-alone stitches are not visible at this point. At this point you have either finished stitching correctly, or maybe you are missing some stitches, or some stitches might be reversed (Fig. 7).

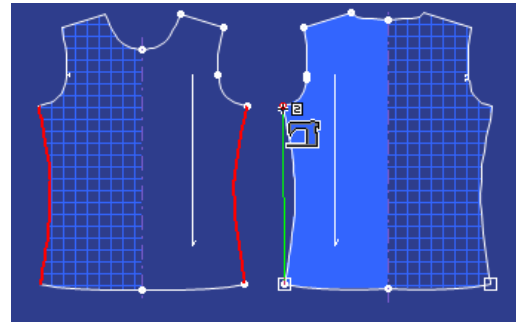
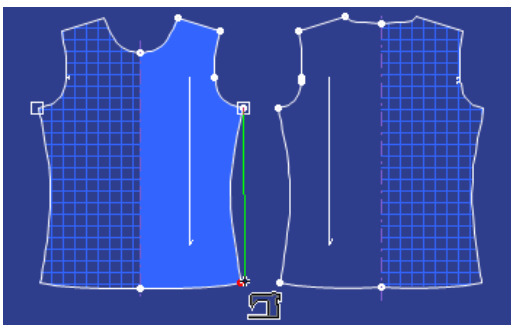


Fig. 7. Pattern position in the simulation

The simulation is now ready to be done. In order to start the simulation press the “Simulate draping” button, and the garment will be fit to the mannequin (figure 8).

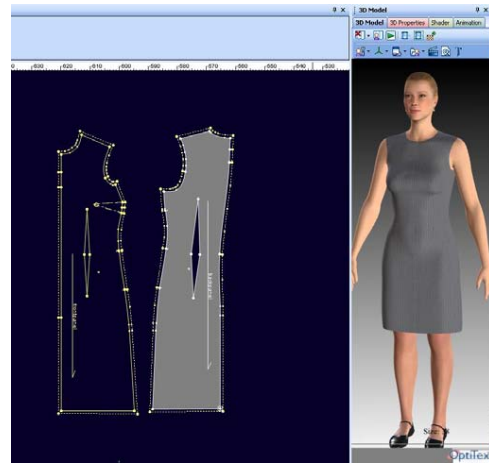


Fig. 8. Draping simulation

A very important fact in the garment simulation is the material mechanical properties and also the texture. In the 3D module there is the option to set the mechanical parameters of the cloth. The mechanical parameters that must be introduced are: bend, stretch, shear, shrinkage, weight, friction and thickness (Fig. 9).

If the garment do not fit properly on the parametric mannequin or the model must be changed, all the modification can be applied on the patterns from the right side and after that re-simulate the new patterns (Fig. 10).

If the model must be changed, or de designer wants to try how it would look a different model using the same mechanical fabric parameters and same mannequin, all it must be done is to apply the model

changes in the left side of the working window, where are displayed the patterns and then re-simulate the garment.



Fig. 9. Cloth simulation

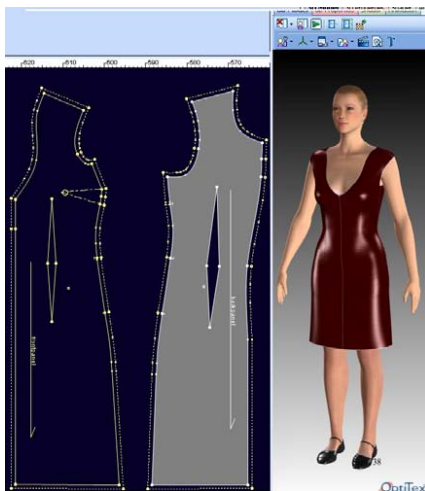


Fig. 10. Modification of the upper side of the pattern

There is an import way how to check the pattern fit on the body, called “tension map”. Using this method it is possible to see where the garment fits correctly and offer a comfort sensation this would be displayed by green areas and blue areas and also can be noticed the places of the garment where it is too tight to the body and will not allow good movement, this will be displayed with red color (Fig. 11). The tension map for the front side of the garment shows that the patters are too loose at the chest line, at the waist line are too tight noticing the red area and at the

bottom are at perfect dimension. The designer should modify the pattern at the chest line and waist line (Fig. 11 a).

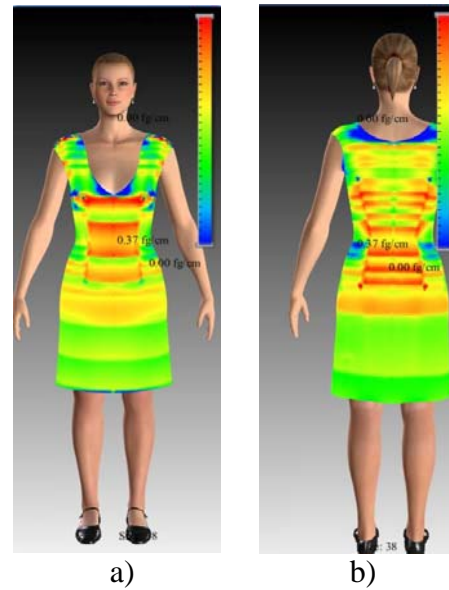


Fig. 11: Tension map

The tension map for the back side of the garment shows that at the shoulders line the patterns are too lose and as the front side tension map shows, the waist line is too tight. The designer should modify the patterns at the shoulders line and waist line (figure 11 b).

### 3. CONCLUSION

With the increased desire among customers for individualized and customized fashion products, an interest in 3D virtual garment simulation has been growing throughout the world. 3D garment simulation has used for many things, such as virtual fashion shows, online fashion communities, the virtual trying-on of garments, and more. The present paper aims to realize a dress garment simulation. The result will be the testing of the 2d designed pattern after the fitting on the virtual mannequin using specialized 3D software.

The present papers shows how efficient is to work with garment simulation, work method which make it possible for users to see the garment from any angle in a static

pose or even in motion using a virtual mannequin. This work is a premier for the Romanian clothing industry.

We can use the customer dimension by 3D body scanning and in the 3D garment simulation it can be tested the fit between the body and the garment. Regarding the results, the designer can change the initial pattern and correct the particular garment according to the customer needs. A pattern is a 2-dimensional representation of a 3-dimensional object; ultimately the garment will be worn by someone, and the pattern maker is responsible for the way that garments fits.

After all the steps are done, and the simulation is performed, using the fit tension map, the designer can know if the garment is a perfect fit or it must be modified. The tension map have 3 different colors: blue if the garment is loose, green if the garment is perfect fit, red if the garment is too tight. For the present paper, the garment should have been modified to the chest line and shoulder lines and also to the waist line.

#### 4. ACKNOWLEDGEMENTS

This work was cofinanced from the European Social Fund through Sectoral Operational Programme Human Resources Development 2007-2013, project number POSDRU/89/1.5/S/56287 „Postdoctoral research programs at the forefront of excellence in Information Society technologies and developing products and innovative processes”, partner Bucharest Academy of Economic Studies – Research Center for “Analysis and Regional Policies”.

#### 5. REFERENCES

1. Diaconu M, Diaconu M, Visileanu E, Niculescu C., Generalized algorithms for automatic design of apparel products, *Industria Textila*, 2010, **61**, 207-2091

2. Niculescu C, Filipescu E., Avadanei M., General aspects concerning the development of a female dimensional typology using 3D body scanning measurements, *Industria Textila*, 2010, **61**, 271-275.

3. Filipescu E., Avadanei M., Clothing structure and pattern design, Ed. Performantica, Iasi, 2005

4. Loghin, C., Ionescu. I., Hanganu, L., and all, Functional Design of Protective Clothing with Intelligent Elements, *Annals of DAAAM for 2009 & Proceedings of the 20th International DAAAM Symposium*, 2009, 435-436.

#### 6. ADDITIONAL DATA ABOUT AUTHORS

Corresponding Author: Dr. Eng. Olaru Sabina, National R&D Institute for Textile and Leather, 16, Lucretiu Patrascanu street, 030508, Bucharest, Romania, [sabina.olaru@certex.ro](mailto:sabina.olaru@certex.ro)

Prof. Dr. Eng. Filipescu Emilia, Faculty of Textile, Leather and Industrial Management, “Gheorghe Asachi” Technical University, 53, Dumitru Mangeron street, 700050, Iasi, Romania, [emfi@tex.tuiasi.ro](mailto:emfi@tex.tuiasi.ro)

Dr. Eng. Filipescu Elena, Faculty of Textile, Leather and Industrial Management, “Gheorghe Asachi” Technical University, 53, Dumitru Mangeron street, 700050, Iasi, Romania, [elena.filipescu@yahoo.com](mailto:elena.filipescu@yahoo.com)

Eng. Niculescu Claudia, National R&D Institute for Textile and Leather, 16, Lucretiu Patrascanu street, 030508, Bucharest, Romania, [claudia.niculescu@certex.ro](mailto:claudia.niculescu@certex.ro)

Eng. Salistean Adrian, National R&D Institute for Textile and Leather, 16, Lucretiu Patrascanu street, 030508, Bucharest, Romania, [adrian.salistean@certex.ro](mailto:adrian.salistean@certex.ro)

## WHEEL MOTION RESISTANCE AND SOIL THRUST TRACTION OF MOBILE ROBOT

**Petritsenko, A.; Sell, R.**

Department of Mechatronics, Tallinn University of Technology, Ehitajate tee 5, 19086  
Tallinn, Estonia

**Abstract:** *The research presented in this paper is focusing on the wheel-terrain interaction of mobile robots. In particular four most common interaction cases are analysed and mathematical relationships in terms of forces are pointed out. The purpose of defining the wheel-terrain interaction forces for different cases are to transfer them into the design library for helping designer in early design process. The design library is a part of early design framework and the mathematical relationships, in addition to other relations, are defined by novel System Engineering description language - SysML. As a result of this study the library consists of mathematical models for most common wheel-terrain interactions of wheeled robots.*

*Key words: mobile robot, motion, terrain, traction, modelling.*

### 1. INTRODUCTION

It is well known, that at beginning of design process of wheeled robot several parameters must be chosen and finally their compliance to the functional and performance requirements verified. Usually verification of chosen parameters, specified in requirements, is carried out by means of simulations of mathematical models with different complexity level or field tests.

At the beginning and during the design process many parameters and mutual interaction must be evaluated, compared

and finally selected for specific robotic applications. One of the crucial sub-systems of mobile robot is a locomotion sub-system. The design and selection of conceptual locomotion system fix many further robot parameters, including key performance and terrainability parameters. In wheeled mobile robot, obviously one of the key components is wheel itself. When selecting wheel parameters (material, coverage, geometry, etc.) it is important to analyse the required terrain capabilities of the robot and performance criteria of passing the obstacles and holes. In addition, designer has to keep the mind open and do not rely only the conventional solution. For example in mobile robotics, many unconventional locomotion solutions are applied to improve the terrainability and flexibility in small scale locomotion end actuator. New solutions and wheel-terrain studies can be found in literature [1], [2] including patented invention from Tallinn University of Technology, Department of Mechatronics [3]. In this paper we are focusing on the detail analyses of wheel-terrain interaction and forces influencing on the different conditions in off-road terrain. The research results are mathematical models formulated into novel engineering description language – SysML (System Modeling Language) [4]. This approach enables to reuse the common cases on later mobile robot design, including early stage simulations and candidate solution evaluation process.

## 2. WHEEL MOTION RESISTANCE

### 2.1 Motion resistance due to wheel-terrain interaction ( $R_R$ )

When a robot moves on paved surfaces and roads it consumes energy to overcome the rolling resistance between the tires and the ground, as well as gravitational and inertial forces. Obstacles are dealt as a specific case and are simulated separately.

Rolling resistance between the tire and the ground is attributed to tire slip, scrubbing in contact patch, deflection of the road surface and energy losses due to tire adhesion on the road and hysteresis. Rolling resistance varies with the type and material of tire tread, velocity of vehicle, and environmental parameters, such as temperature and humidity [5].

There exists four general wheel-terrain interaction cases [6] shown in Fig. 1.

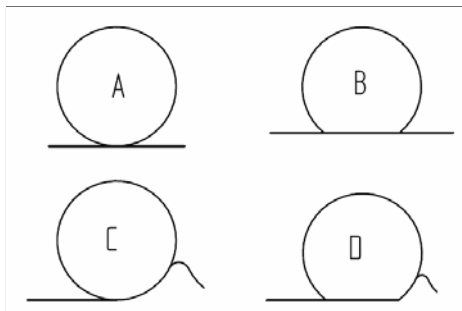


Fig. 1. Possible wheel-terrain interaction cases

Notations for Fig.1

- A) rigid wheel travelling over rigid terrain,
- B) deformable wheel travelling over rigid terrain,
- C) rigid wheel travelling over deformable terrain,
- D) deformable wheel travelling over deformable terrain.

These four different wheel-terrain interaction cases involve different wheel resistance forces involved in mathematical models. Simulation models are generated according to mathematical model. This

allows designer to select different cases according to simulation interest.

#### Case A – rigid wheel travelling over rigid terrain

This model is simplified approach of wheel-terrain interaction. The model assumes that rolling resistance of the tire neglected and wheel-terrain interacts to each other at single contact point. This kind of model suits for metallic wheels or wheels with solid non-metallic tires.

#### Case B – deformable wheel travelling over rigid terrain

In this wheel-terrain interaction case pneumatic tires are usually considered. Deformation of the terrain is generally neglected and it is considered that rolling resistance is caused primarily by the tire hysteresis, i.e. due to deflection of carcass of tire. When tire is rolling the carcass of tire is deflected in the area of ground contact patch and centre of normal pressure shifts in direction of rolling. The shift of centre of normal pressure causes increase of rolling resistance.

Complex relationships between design and operational parameters of tire and its rolling resistance make it difficult to develop an analytical method for predicting of rolling resistance [7]. Determination of rolling resistance, therefore, relies almost on experiments. For modelling purposes, design library is composed consisting of different tire manufacturer's data, where average rolling resistances of pneumatic tires are given. Additionally, design library consists of data, where rolling resistance of tire at different inflation pressure is given as well. In the absence of tire manufacturer's data, the empirical formulas to calculate the rolling resistance of tire are used and given in [8].

#### Case C - rigid wheel travelling over deformable terrain

In this model it is assumed that wheel travelling over off-road terrain is subject to sinkage. Wheel is classified as rigid if

deflection of under static loading is much lower than deformation of soil/terrain. This model fits to metallic wheels, solid non-metallic tires and high-pressure pneumatic tires operating on weak soils. In case of pneumatic tires, the rolling resistance due to tire hysteresis is neglected. The main cause of the motion resistance is due the deformation of the soil. Motion resistance of tire consists then from two major contributions: the compaction resistance and the bulldozing resistance.

#### Compaction resistance

This form of wheel motion resistance can be analyzed considering the mechanics of a rigid wheel rolling into soft terrain. The motion resistance of rigid wheel is produced by vertical work done in making a rut of depth  $z$  as [7]

$$R_c = \frac{\left(\frac{3W}{\sqrt{D}}\right)^{\frac{(2n+2)}{2n+1}}}{(3-n)^{\frac{(2n+2)}{(2n+1)}} (n+1)b^{\frac{1}{(2n+1)}} \left(\frac{k_c}{b} + k_f\right)^{\frac{1}{(2n+1)}}} \quad (1)$$

where  $b$  – width of wheel contact area;  $k_c$ ,  $k_f$  and  $n$  – pressure-sinkage parameters of the specific terrains;  $W$  – vertical force exerted by the tire to the terrain;  $D$  – wheel diameter.

The pressure-sinkage parameters for different soils are found from literature and included to the design library for modeling purposes.

#### Bulldozing resistance

Bulldozing resistance is developed when a substantial soil mass is displaced by a wheel. This type of resistance is very common when a wheel compresses the surface layers of soil and pushes compacted soil fore and aft of the tire [7]. Soil bulldozing phenomenon is apparent in the case of a wide wheel traversing very loose soils and has been estimated to cause a significant increase in total motion resistance for sinkage values greater than 1/6 of the wheel diameter. The bulldozing

resistance on narrow tires is mitigated by the fact that a portion of the soil bulk is pushed to the sides of wheel. The bulldozing resistance can be calculated by implementing the theory of bearing capacity of soils subject to various criteria of failure. The equation to calculate the bulldozing resistance is given in [9] and not repeated here.

#### Case D – deformable wheel travelling over deformable terrain

In this model it is assumed that tire is subject to sinkage and deflection of tire is in same order as deformation of off-road terrain. If the maximum contact pressure that terrain can support is greater than combined inflation pressure of tire and pressure due to the stiffness of the carcass, then the tire flattens at contact patch with the terrain. This model suits best for low to medium pressure pneumatic tires travelling over off-road terrains [7], [8].

The compaction resistance of deformable wheel travelling over deformable terrain is derived in [8] and is

$$R_c = \frac{bp_{gr}^{\frac{(n+1)}{n}}}{(n+1)\left(\frac{k_c}{b} + k_f\right)^{\frac{1}{n}}} \quad (2)$$

where  $p_{gr}$  – average ground pressure which is usually provided by the tire manufacturer for a given inflation pressure and wheel loading. Eq. (2) shows that the compaction resistance of a flexible wheel is solely a function of width of contact patch (minimum width of tire in this case) and geophysical properties of soil. Additional resistance that has to be accounted is rolling resistance due to tire hysteresis as it was pointed out in case B.

#### 2.2 Motion resistance due to slopes ( $R_s$ )

Ground slopes add a component to the motion resistance of wheel which is proportional to the component of parallel to slope.

### 2.3 Aerodynamic motion resistance ( $R_A$ )

Aerodynamic drag is dependent on aerodynamic factor and square of speeds. Aerodynamic drag of wheel can be neglected due to its low influence to wheel motion resistance.

### 2.4 Inertia resistance ( $R_{in}$ )

The generation of inertia forces is closely related to traction forces that are available at wheel-terrain contact surface. Traction is limited by mechanical properties of terrain and loading at wheel/soil interface patch. Thus inertia properties of wheel and robot can be properly evaluated after determination of maximum tractive effort available at wheel-terrain contact patch.

## 3. SOIL THRUST AND TRACTION

Vehicle motion relevant to the terrain is produced through traction ( $F_k$ ). Caused by a physical process of adhesion and deformation, traction develops at the interface of a powered wheel with the ground. The maximum produced traction is limited by the adhesion between wheel and ground [7] and the torque-speed characteristics of vehicle's prime mover and drivetrain which basically determine that maximum torque and power transmitted to the wheel.

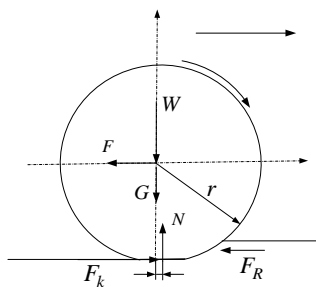


Fig. 2 Forces acting to the driven wheel

For locomotion in soft soils traction is limited by mechanical properties of soil and loading at wheel/soil interface patch. Maximum force that can be sustained by the soil before excessive slippage occurs is

known as soil thrust. The study of mechanics of traction generation provides equations for configuration of a robot's wheel and overall robot geometry. Forces acting on driven wheel generally are shown in Fig.2

#### Case A – rigid wheel travelling over rigid terrain

This model assumes that wheel-terrain interacts to each other at single contact point. Only force acting at wheel-terrain interaction point is frictional force. No slip of tire allowed in this model. Maximum traction developed is proportional to the wheel load and is limited due to Coulomb's friction force

$$F_k = \mu_s (G+W) \quad (3)$$

Where  $\mu_s$  - sliding coefficient of friction, G and W – weight of wheel and load to wheel respectively.

This relationship is well known from classical mechanics of rigid bodies and is the simplest model to evaluate a maximum traction force.

#### Case B – deformable wheel travelling over rigid terrain

When tire is rolling, carcass of tire is deflected in the area of ground contact patch. Deformation of rigid surface is neglected. Due to tire deflection the distance that tire travels when subject to driving torque will be less than in free rolling and longitudinal slip of tire occurs. The traction force developed is given then as simplified function of longitudinal slip of tire as [7].

$$F_k = \mu_p (G+W) \left( 1 - \frac{\mu_p (G+W)}{4C_i i} \right) \quad (4)$$

where  $\mu_p$  - coefficient of adhesion; i – slip of tire;  $C_i$  – longitudinal stiffness of tire.

#### CASE C and D – rigid and flexible wheel travelling over deformable terrain

For rigid and flexible wheel travelling in soft soils traction is limited by mechanical properties of soil and loading at wheel/soil



interface patch. Maximum tractive force  $F$  is limited by the thrust produced by soil, which in turn is proportional to mechanical strength of soil. Data on the stress/strain relationships of disturbed soils, sand, snow, and saturated clays have verified the appropriateness of Janosi-Hanamoto relationship to describe shear stress-strain behavior of unprepared terrain [7],[10] as

$$\tau(\theta) = (c + p(\theta)\tan\phi) \left( 1 - e^{-\frac{j}{K}} \right) \quad (5)$$

where  $c$  and  $\phi$  are modulus of cohesion and angle of internal friction of soil,  $p(\theta)$  – normal pressure distribution in soil as function of contact angle between wheel and soil;  $j$  - the shear displacement and is function of slip velocity;  $K$  - shear deformation parameter, Integration of the Eq. (5) over contact patch area leads to total tractive effort as

$$F_K = \int_0^{\theta_0} \tau(\theta) \cos\theta d\theta \quad (6)$$

Of critical importance to the amount of forward thrust developed at tire-soil interface is geometric shape of the tire, which has to be determined before evaluation of the integral in Eq. (5).

### 3.1 Net traction

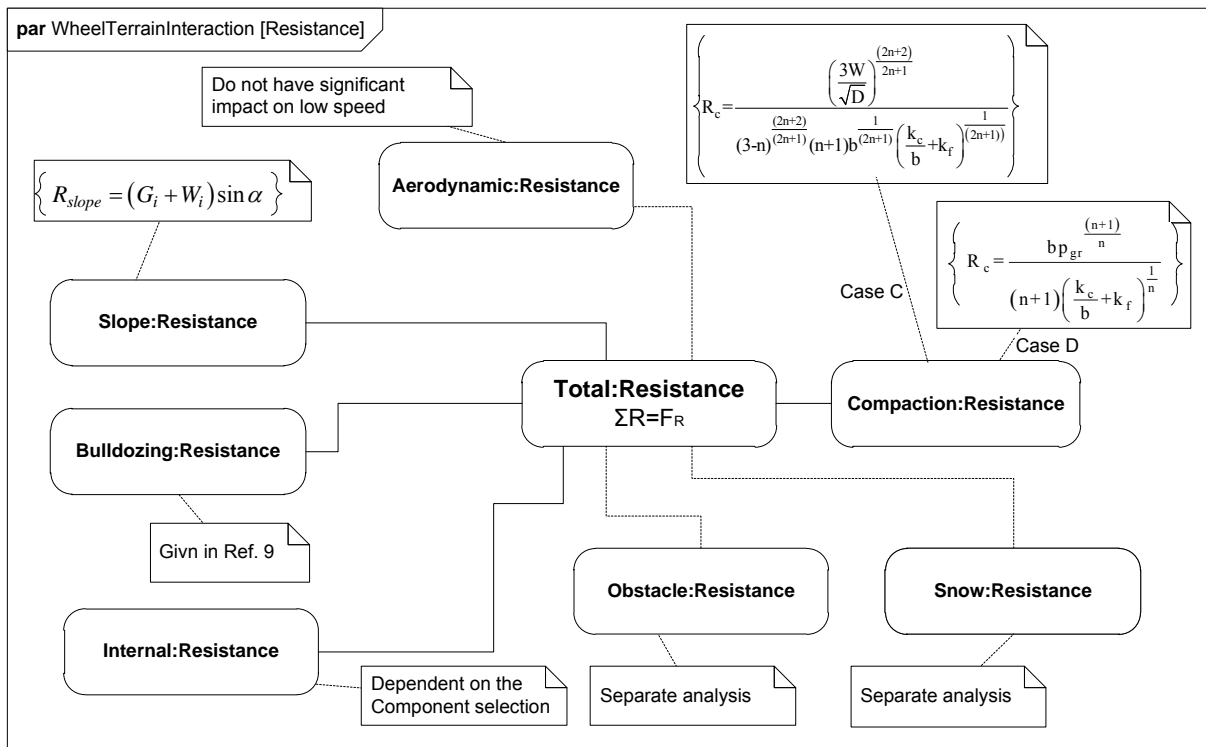
Net traction of the driven wheel shown in Fig. 2 is the force equal to the difference between the tractive effort  $F_K$  developed by the wheels and resisting forces as

$$F = F_K - \sum_{i=1}^n R_i \quad (7)$$

Net traction is available force that can be used to generate acceleration of the wheels and robotics.

## 4. MODEL LIBRARY

The framework supporting early design process is developed during the previous research [11]. One of the key factors of this framework is a design library which consists of unified mathematical models



transferred into the SysML graphical

Fig. 3 Simplified SysML parametric diagram of resistances in wheel-terrain interaction

diagram format. The model design library offers pre-defined models for designer to start fast and efficient early design process on mobile robotic domain. In this paper we have described the wheel-terrain interaction cases which are the ground issue of the wheeled robots and have to have therefore well formulated and verified. The corresponding unified SysML parametric diagram is shown in Fig. 3. where the key factors are highlighted. This graphical representation can be used as a input for the simulations or transferred automatically into the analytical calculations.

## 5. CONCLUSIONS

In this paper the major resistance forces and generation of traction forces in different basic wheel-terrain interaction cases are introduced. The mathematical description of them are generated and transferred into graphical diagram format of SysML. It allows performing efficient and optimal early design stage by offering the necessary simulation models at the beginning of the design stage, when many wheel parameters and wheel-terrain interaction cases must be evaluated, compared and finally selected for specific robotic application.

## 6. ACKNOWLEDGEMENT

This research was supported by funding of the Estonian Science Foundation grant No. 8652

## 7. REFERENCES

1. Zheng, L., et. Al. *A Novel High Adaptability Out-door Mobile Robot with Diameter-variable Wheels*, Proc. of the IEEE Int. Conference on Information and Automation Shenzhen, China, 2011
2. Chengbin Ma, Min Xu & Hao Wang, *Dynamic emulation of road/tyre longitudinal interaction for developing electric vehicle control systems*, Vehicle System Dynamics, 2010, 49:3, 433-447.
3. Sell, R., Kaeeli, M., *Wheel-Leg (Wheg)*, Patent no EE05283B1, 2009
4. OMG SysML - System modeling Language specification, OMG document formal/10-06-02, 2010
5. Gillespie, T., D. *Fundamentals of vehicle dynamics*. Society of Automotive Engineers, Inc, 1992.
6. Iagnemma, K., Dubowsky, S. *Mobile Robots in Rough Terrain*. Springer-Verlag Berlin Heideberg, 2004.
7. Wong, J., Y. *Theory of Ground Vehicles 4<sup>th</sup> Ed.* John Wiley & Sons, Inc; Hoboken, New-Jersey, 2008.
8. Saarilahti M. *Soil interaction models*, In: Haarlaa R, Salo J, University of Helsinki, Pub. 31, 2002.
9. Genta, C. *Introduction to the Mechanics of Space Robots*. Springer, 2011.
10. Ray, L.R., Brande, D.B., Lever, J.H. Estimation of net traction for differential-steered wheeled robots. *J. of Terramechanics*, 2009, **46**, 75-87.
11. Sell R., Coatanea E., Christophe F. *Important aspects of early design in mechatronic*, 6th International Conference of DAAAM Baltic Industrial Engineering, Tallinn, 2008

## 8. ADDITIONAL DATA ABOUT AUTHORS

Raivo Sell, Ph.D, senior researcher, Tallinn University of Technology, Department of Mechatronics, Ehitajate tee 5, Tallinn, raivo.sell@ttu.ee

Andres Petritsenko, Ph.D, researcher, Tallinn University of Technology, Department of Mechatronics, Ehitajate tee 5, Tallinn, andres.petritsenko@ttu.ee

## AUTOMATIC PRODUCTS IDENTIFICATION METHOD

Pölder, A.; Juurma, M; Tamre, M.

**Abstract:** *This paper gives an overview of automatic products identification method which can be used in some respects for standalone or complementary tracing of objects. The method can be applied only in a case when each traceable object has unique visual properties (for example wood). The basis of described work is traceability of raw material in wood supply chain, especially traceability of the saw material in sawmill.*

*The first development in this kind of approach originates from EU- 6th Framework Project Indisputable Key and is developed further at Tallinn University of Technology.*

*Keywords: Identification, traceability, production automation, machine vision, saw material.*

### 1. INTRODUCTION

In today's industry, where the energy efficiency and reducing carbon footprint has main importance alongside with quality of the products, monitoring of products and materials, tracing, inspection and respective control of the production processes are gaining more and more importance. Those processes are more adapted at consumer goods production and for example in metal working industry at the moment. In renewable materials industry like wood or polymer or natural materials industry the principles are only gaining attention recently.

Considering the wood production sector the target to implement the abovementioned principles is to investigate the quantitative measures of performance of the wood supply chain, and

quantification of the potential effects on the performance. Products and materials automatic or semi-automatic traceability should support finding tools and methods for holistic supply chain management, optimization and trade-off analysis by combining product quality and process economy with environmental impact from life cycle perspective, which could provide a new dimension to decision support systems in the industry and would avoid sub-optimization due to its holistic nature. Combining the information flow with the physical flow of material allows to associate objects with information. In order to gain information, a data acquisition infrastructure is needed and the data acquired has to be sensibly selected according to the business needs [1].

To achieve material traceability several technologies can be used, for example RFID or machine vision systems. When the objects are traced on the production line the position specific information can be used for tracing.

### 2. SYSTEM OVERVIEW

Wood supply chain consists of several parts, for example: harvesting, transport, log sorting etc. One important part is to ensure the traceability of saw material inside sawmill.

The marking and reading of the boards starts from sawmill green sorting position where the sawn boards are sorted by quality. Boards are marked and after that the code is verified by the reading system. Next reading position is in the position where the boards are packed for the kilns. After the kilning process the boards are

sent to the final sorting where they are re-sorted. In the final sorter the board end with marked code is removed. To maintain traceability it is necessary to read the code before the board is cut. After that the code is remarked and verified.

The 8x18 Data Matrix ECC200 barcode was used since it has good error correction, high redundancy and high information density. The codes were applied by industrial printer and read by smart camera based vision system.

During the tests it occurred that it is very hard to achieve code readability over 95 % in one reading position on automated lines due to different problems regarding to material surface and marking quality. This means that in a case when there are for example 4 reading positions and the readability in each position is 95 % the overall readability and therefore traceability is about 80 %. Therefore it is necessary to improve the readability.

### 3. QUALITY PARAMETERS

To ensure code quality and improve readability the code quality parameters were introduced [2]. By evaluating the quality parameters automatically it is possible to locate the source of the problems for elimination. This evaluation system can be used in collaboration with reporting system, which can trigger the alarm when the quality decreases for some longer period.

The quality parameters can be used for estimating if the code will be read in following positions. If the code has high quality grade it is not necessary to store any additional information about the code. If the code has low quality there is higher possibility that it is not read in the following positions and it is necessary to store some additional information into database for further matching.

Several dimensions which can be measured from acquired board end image can be used for describing board end and code quality.

Board end mean intensity has strong influence in code readability. When intensity is low the contrast between the code and its background is also low. Another dimension which is used for quality estimation is board end region of interest (ROI) histogram which describes the distribution of pixel intensities. For quality estimation the lookup histogram is generated by using certain amount of images where the board end and image quality is good. Each processed image histogram is compared with lookup histogram and the difference and its standard deviation gives us the estimation about how different it is. Histogram is good for estimating overall board end brightness and its distribution, indicating if the contrast between background and code is sufficient.

To estimate how the pixel intensities are distributed over the board end area the board end was distributed into vertical and horizontal stripes (ROIs). Mean intensity of each stripe is calculated and differences between beside intensities were found. High standard deviation of those differences indicates that there are lots of changes in intensities and therefore the quality is low.

In many cases the marked code has deformed due to board end vibrations during the code marking. To estimate if the vibration is present the code edge coordinates in several rows and their standard deviation is found. If the deviation is high then the code has vibrated and therefore the quality is low.

For deciding if the board end has acceptable quality it is necessary to calculate value which summarizes all the parameters. The total quality estimation can be calculated by summing up all the quality parameters giving each one specific scale. The scales were found experimentally by measuring all the parameters of large scale test reading, the base of decision was the positive reading result. All the described quality parameters do not have strong correlation with

readability and therefore they are used as estimators. [2]

#### 4. HISTOGRAM BASED MATCHING

Quality parameters give the estimation if the code is readable in following positions and approximate estimation why the code is not read. They do not give additional information which could be used for identifying board in following positions.

For that some additional information is needed. It is not reasonable in first approach to measure specific features or defects but to try to evaluate the whole region of interest at once and try to implement something more common and simpler like histogram of board end.

Histogram shape depends on the lighting conditions, size of board end (size of ROI) and changes inside ROI (Fig. 1. and Fig. 2.). If the conditions in between reading positions differ then the histograms are different. Therefore it is necessary to keep the lighting conditions and all the other parameters as similar as possible in each reading position.

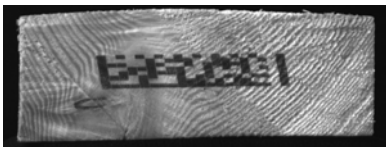


Fig. 1. Marked code on the board end

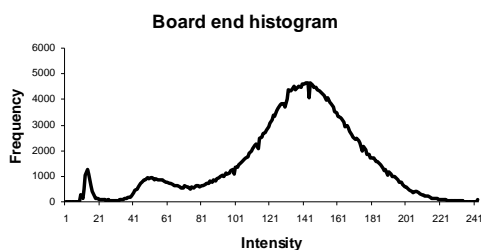


Fig. 2. Board end histogram (peaks starting form left – image background, marked code, board end area)

Each board end histogram is quite unique, especially when there is a marked code which gives a peak on certain range of intensity values.

When using histogram as unique identifier it is necessary to pre-process it due to probable changes in between positions and changes on the board end when it is moving from one position to another. All the histograms have to be made comparable, for example if the board end is darker or lighter than original or the distance from the camera is changed the histograms are not comparable anymore. To compare histograms it is necessary to smooth, rescale and resample the histogram. Rescaling of the re-sampled and shifted histogram ensures that the maximum peak frequency is the same on all the resulting histograms. Re-sampling of histogram compensates board end distance change and rescaling compensates brightness change.

From the test it occurred that histogram is quite sensitive to changes in between different positions: brightness changes, board end size, defocusing and rotation. It appeared that lots of visually quite different board ends had similar histograms and that resulted in mismatches. One downside of histogram based traceability enhancement is that the information gained has no position specific information (for example code location on the board end). That means that two totally different board ends can have similar histogram. That indicates that it is not possible to use histogram alone for improving traceability. [3]

#### 5. LINEAR AVERAGES

Another way to improve the matching of the boards is to use linear averages based matching.

Linear averages on x and y axis direction are the arrays of mean values of each pixel line in the image region of interest (ROI). The positions of different objects on the board end like code or branches are reflected on the directional averages making this method more unique than histogram only [1].

For testing the linear averages method the algorithms for measuring and comparison were created. The measuring algorithm loads image from file, finds board end region of interest and rotates image to ensure that board end wider edge is horizontal. After that the linear averages in x and y direction is calculated (Fig. 3.).

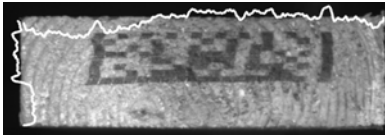


Fig. 3. Linear averages (white plots)

From the averages plots it is possible to aim the location of the code resulting the lower average values and therefore lower part of the plot. After that the results are saved for further processing. The measuring application measures each image and no comparison takes place in this phase.

In the comparison algorithm the simple linear correlation is used for finding the correlation between two comparable data sets. Correlation coefficient close to 1 indicates good match.

Since linear correlation is independent of both origin and scale of the samples it is not necessary to rescale the measured values. That means a small unified change in lighting does not have effect on the comparison results.

The highest correlation coefficient of the results is probably the match if the conditions are acceptable and images of the same board end are similar.

Board end and therefore region of interest has to be rectangular, when the board end is not positioned correctly in front of the vision system it may appear not completely rectangular on the image. When measuring linear averages on those images some parts of board end may be out of ROI or some background can be included into ROI and results are strongly affected.

To evaluate if it is possible to match the images in between the different reading positions it is first necessary to estimate in

what range the correlations coefficients between not matching images are.

In the first test 500 images of marked board ends, acquired from saw line were measured and correlation coefficients between all the measurement results were found (total 124750 comparisons were made). The results show how the correlation coefficients are distributed.

From x axis linear averages correlation coefficients histogram it appeared that most of them are distributed around 0.5 and highest correlation coefficient is 0.94 (Fig. 4.) Note that chart y axis (frequency) indicates the amount of correlation coefficient which falls in defined value range (bin).

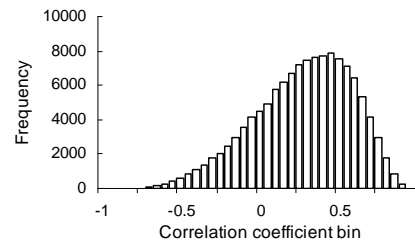


Fig. 4. Histogram of x axis linear averages correlation coefficients

In the y axis case (Fig. 5.) the coefficients are distributed around 0.6 and 355 coefficients (about 0.3 %) are in range from 0.95 to 1.

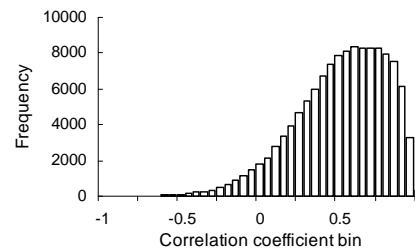


Fig. 5. Histogram of y axis linear averages correlation coefficients

The reason why the peaks is shifted to right is smaller amount of data since board end is rectangular.

In many cases the high correlation coefficient in one direction linear averages does not mean high correlation coefficient in another direction. That means that

indicating the correlation between both, x and y direction should give better result. To do that the x and y direction correlations coefficients are multiplied. In this case histogram peak is around 0 to 0.5 and no close matches exist, no multiplied correlation coefficients fall in the range from 0.9 to 1 (highest is 0.8740). Therefore this parameter seems to be very good candidate for the comparison (Fig. 6.).

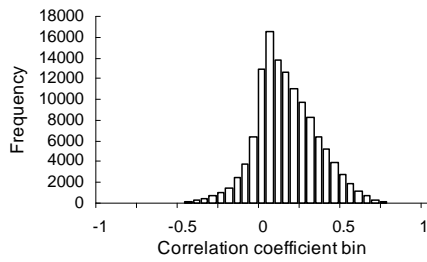


Fig. 6. Histogram of multiplied linear averages correlation coefficients

To evaluate the effect of probable changes in between reading positions several test images were generated (changed image size, changed image brightness, half darkened and added dark dot). Similar test were run as described before only in between modified images and original. It appeared that in a case when the image size was changed the multiplied x and y correlation was below 0.5.

To improve the response of changes on board end size change the data was interpolated. The smaller array is interpolated so that it has the same number of elements as major array and the first and last element value remains the same.

The previous test were run again and now the correlations between each modified image which size or brightness was changed had correlation coefficient (x\*y) over 0.9.

Finally the test with set of 500 images and modified images were run.

In this case the matches between the original and its modifications are more widely distributed; all values above 0.86 belong to randomly selected image and its modifications. The highest correlation

coefficient between other images is 0.85 (Fig. 7. and Fig. 8.).

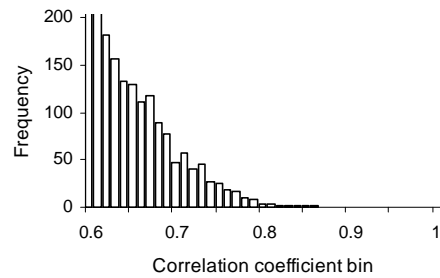


Fig. 7. Histogram of multiplied linear averages correlation coefficients without modified images

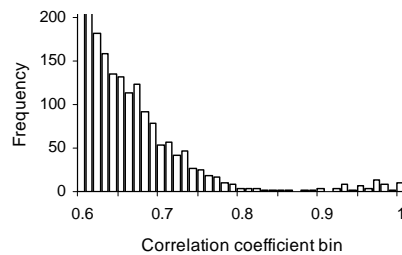


Fig. 8. Histogram of multiplied linear averages correlation coefficients with modified images

According to that it is possible to match the images of board end modifications if the number of comparable objects is small. In real application that can be much more complicated since the number of images is larger and the differences in between comparable positions can vary more. In described tests the comparable images were modified manually and the actual differences in between the positions can be more complex. [1]

## 6. PROBLEMS

When using histogram and linear averages for achieving a traceability of the objects additional comparison algorithm is needed. When reading the code in first position and the same code in second position it is quite easy to match those two readings – the code is exactly the same and that means that only one database query is needed. In a case of histogram and linear averages



reading systems are similar, codes are read and all the parameters are measured and data is saved into database. To match the readings the matching algorithm is needed. Basic idea would be to compare data of each image with all the other data entries and to find correlation between them. The highest correlation is probably the correct match. Depending on the physical distance between two reading positions the amount of processing data can be huge since each data entry must be compared with all the other entries.

One way to reduce the necessary entry comparisons for matching is to classify the data. Choosing the right classifiers and amount of classes is important. Using classes is useless if most of the entries are in same class or if there are lots of classes. Most important thing is to avoid situation when the entries about the same board end fall into the different classes, in this case it is impossible to match them.

One possibility to create classes is to divide all entries into groups simply by some parameter, for example board end brightness. The interval in between maximum and minimum can be divided into several smaller intervals. That raises another problem with the cases when the entry is close to the edge. Due to differences in between positions (lighting position etc) and possible changes on the board end all the parameters can vary in between positions. Therefore it is possible that in one position the entry is placed into one class and in another in another class. One simple way would be to add entries close to the edges to the both classes. That increases amount of time for comparison but reduces the risk of lost match.

Another problem arises when there is no good, outstanding match – one solution would be to consider that entry to be lost. Another approach would be to give several possible matches as a result. Later some of the close matches would be eliminated by other matches and therefore it is possible that finally only the correct match remains.

## 7. CONCLUSIONS

The main scope of this paper is to give an overview of automatic products identification method based on board end traceability in sawmill. The described method is not tested in real application; it is tested in the laboratory using previously acquired data.

Overview of board end quality parameters helps us to understand the main sources of problems and is a base for decision in a case when the marked codes are used in parallel with object uniqueness based traceability system. The board end histogram can be used as second step for estimation since histogram itself is not unique enough for traceability purposes. Final match of objects can be made using linear averages.

The described approach needs further development. Board end finding algorithm must be improved since in many cases it does not work correctly. The quality parameters must be redefined based on larger scale tests. Histogram and linear averages based matching algorithm needs to be improved to gain higher efficiency and processing speed.

## 8. REFERENCES

1. Põlder, A., Juurma, M., Tamre, M. Wood Products Automatic Identification Method Based On Fingerprint Method. In *Mechatronics systems and Materials: Abstracts* (Skiedraute, I. Basukutiene, J., Dragašius, E., eds.). Kaunas University of Technology, 2011, 55.
2. Põlder, A., Abiline, I., Tamre, M., Automatic Visual Code Quality Evaluation For Wood Industry. In *7<sup>th</sup> International Conference Of DAAAM Baltic Industrial Engineering: Proceedings* (Küttner, R., eds.). Tallinn University of Technology, 2010, 554.
3. Põlder, A., Modified fingerprint method for traceability enhancement of marked products. In *Topical Problems*

*in the Field of Electrical and Power Engineering \* Doctoral School of Energy and Geotechnology II: Proceedings* (Lahtmets, R., eds.). Tallinn University of Technology, 2010, 121

## **7. DATA ABOUT THE AUTHOR**

Põlder Ahti, doctoral student,  
Department of Mechatronics, Ehitajate Tee  
5, Tallinn 19086, Estonia,  
[ahti.polder@ttu.ee](mailto:ahti.polder@ttu.ee)  
+372 620 3207

## KINEMATICS AND DYNAMICS OF CONFIGURABLE WHEEL-LEG

Sell, R; Aryassov, G; Petritshenko, A; Kaeeli, M

**Abstract:** *In this paper, the kinematics and dynamics of the configurable wheel-leg is considered. The configurable wheel-leg has been invented by TUT researchers to increase the mobility of the wheeled vehicles, mostly unmanned ground vehicles, on different terrains and to overcome obstacles that are unobtainable to the conventional wheels e.g. climbing on stairs. The paper presents an overview of similar wheels and focuses mostly on the kinematics and dynamics of invented wheel. The result is a mathematical model which can be used for further analysis and simulations.*

*Key words: wheel dynamics, wheel-leg, variable diameter wheel*

### 1. INTRODUCTION

Today's world several different types of mobile robots are in use, both civilian and military domain. Wheeled robots have advantages of good performance when moving on smooth roads. However when obstacle is on the road or robot needs to turn off-road the good performance is gone and different type of locomotion principle have advantages to overcome of the obstacle or move on rough terrain. In rescue robots, it is often case that robot have to run relatively long on smooth terrain but then needs to go up to stairs. It is clear that wheels are not suitable climbing up to stairs. Therefore these robots have usually two locomotion options mounted on the robot. Tracks are mounted with combination of wheel. This solution is not efficient in terms of energy consumption, complexity and stability.

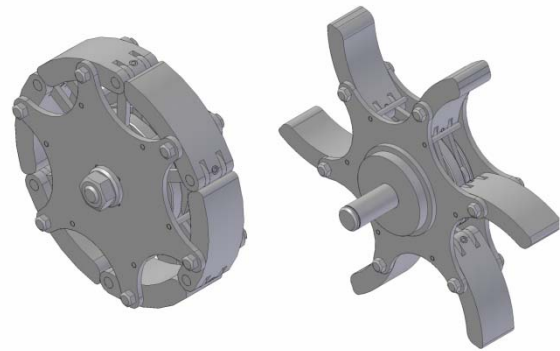


Fig. 1. Wheel-leg (Whieg) in closed and open configuration

In this paper novel patented [1] solution wheel-leg (Whieg), shown in Fig. 1. is introduced. The solution combines the advantages of different locomotion principles by changing the geometry of the end actuator on the fly. By changing the wheel geometry kinematic and dynamic parameters of the wheel-leg are also changed considerably. The study gives essential understanding of kinematic and dynamic properties of the non-conventional rigid wheel-leg and provides necessary information to estimate the minimum torque of wheel-leg actuators. The study is a part of wider research area, which is connected to the study of mobility, maneuverability and trajectory control of wheeled mobile robotics equipped with wheel-legs.

### 2. STATE-OF-ART

Inventing the wheel has been attracted mankind already for thousands of years. Even conventional wheel has been in use without of major modification a long time several inventions have been registered

during last century. The main driving force to invent new versions of wheel is to improve the passability on rough terrains and climb over the obstacles or holes. Several inventions have been developed in Japan [2], in US [3], in Russia [4] and other countries. Several dynamically configurable wheels are also invented very recently, partly driven by space missions where the rover has to be energy efficient and uneven terrain capability on the same time. Zheng et.al have been introduced the diameter-variable wheel [5] for out-door rover which deploys planar polygonal mechanism. Another concept is presented by Xinbo et.al. [6] where wheel is segmented and by expanding the segments the diameter is also extended. Well known application is so called Galileo wheel [7] which uses elastic long scale expandable tracks as a tire. In addition to variable diameter wheel construction several fixed sized but different shape end actuators are developed which can be placed between wheel and leg. Most well-known is a Boston Dynamics RHex robot which uses elastic half-circular wheel-leg as end actuator [8]. All described solutions have their benefits and drawbacks. In next section we are presenting the solution integrating the wheel and leg locomotion principles very tightly by increasing the energy efficiency and construction dimension by offering the wide scale of geometry and dynamic performance change.

### 3. WHEEL-LEG

Wheel-leg is a mechanism, invented by paper authors, that includes good qualities of both wheels and legs. The result of that is a good passing ability in different terrain including stairs and steps. In the smooth terrain the wheel regime is used. When terrain changes to hardly passable the wheel-leg adjusts its configuration by opening the wheel segments so that the passing ability increases drastically. In Fig. 1 two different regime of wheel-leg is

shown, where the change from one regime to other can be done even during the normal operation.

Due to design parameters, the wheel-leg can operate in different mode of operation and change its configuration dynamically (Fig. 1.). When blades of the wheel-leg are closed, it operates nearly as conventional rigid wheel. In case of the blades of the wheel-leg are open, the wheel-leg operates as non-circular wheel and its kinematic and dynamic properties vary within its position.

### 4. KINEMATICS OF WHEEL-LEG

#### 4.1 Kinematics of wheel-leg in the Cartesian reference frame

In Fig. 2 the physical and mathematical model of the fully open variable diameter rigid wheel-leg constrained to move in plane and on the rigid surface. The wheel-leg is modeled as regular hexagon with corners rounded. The rounded corners are represented in Fig. 3 as circles with continuous lines. The sides of the hexagon correspond to the tangencies to the rounded corners of physical model with constant radius.

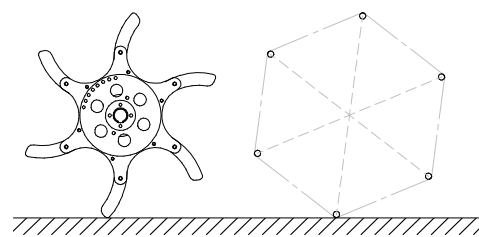


Fig. 2. The physical and mathematical model of wheel-leg

The position of the rigid body in plane is completely defined if it is defined the position of the two points of the rigid body at any instant time of its motion. To define the position of the center of the wheel-leg the two reference frames in Fig. 3 are introduced: ground-fixed reference frame  $Oxy$  and reference frame  $Bx_1y_1$  that moves translatory with respect of the ground-fixed reference frame.

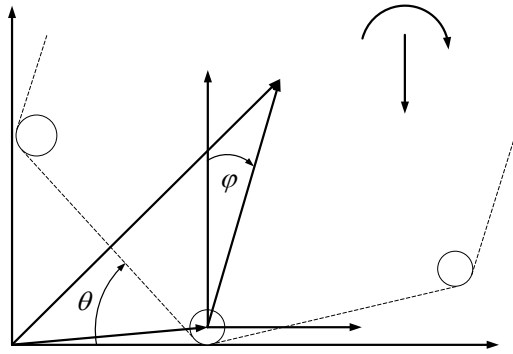


Fig. 3. Rotation of half of the hexagon

The position of the wheel-leg is chosen so that at the beginning of the motion the center of wheel-leg coincides with coordinate axis  $y$  of ground reference frame and angle  $\theta$  of the tangency to the rounded corners of wheel-leg and coordinate axis  $x$  is  $\theta=0$ .

Through the rotation of the  $1/6^{\text{th}}$  of one revolution of the hexagon, the angle  $\theta$  changes from  $\theta$  to  $\pi/3$  that corresponds to the changes of the angle  $\varphi$  from  $-\pi/6$  to  $\pi/6$  measured from the  $y$  coordinate axes. The position vector of the center  $C$  of the hexagon can then be expressed by its components through the generalized coordinate  $\varphi$  as

$$\mathbf{r}_C = \begin{pmatrix} x_0 + r\varphi + l \sin \varphi \\ r + l \cos \varphi \end{pmatrix} \quad (1)$$

where  $x_0$  - the component of the vector  $\mathbf{r}_B$  with respect of the coordinate axis  $Ox$  and corresponds to the initial position of instantaneous center of rotation;  $r$  - the component of the vector  $\mathbf{r}_B$  with respect of the coordinate axis  $Oy$ ;  $l$  - length of the vector  $\mathbf{r}_{BC}$ ;  $\varphi$  - rotation angle of vector  $\mathbf{r}_{BC}$  with respect of reference frame  $Bx_1y_1$ . The first time derivative from the both sides of Eq. (1) yields to velocity expression as

$$\dot{\mathbf{r}}_C = \begin{pmatrix} r\dot{\varphi} + \dot{\varphi}l \cos \varphi \\ -\dot{\varphi}l \sin \varphi \end{pmatrix} \quad (2)$$

where  $\dot{\varphi}$  - the angular velocity vector of the vector  $\mathbf{r}_{BC}$  respect to the reference frame

$Bx_1y_1$ . The second time derivative from the both sides of the Eq. (2) yields to the acceleration of the center  $C$  as

$$\ddot{\mathbf{r}}_C = \begin{pmatrix} r\ddot{\varphi} + \ddot{\varphi}l \cos \varphi - \dot{\varphi}^2 l \sin \varphi \\ -\ddot{\varphi}l \sin \varphi - \dot{\varphi}^2 l \cos \varphi \end{pmatrix} \quad (3)$$

where  $\ddot{\varphi}$  - angular acceleration of the vector  $\mathbf{r}_{BC}$  with respect to the reference frame  $Bx_1y_1$ .

#### 4.2 General kinematics of wheel-leg

In this section the alternative method to establish the kinematic characteristics of the wheel-leg is considered. It is based on the Euler-Savary formulation of the moving and fixed centroids of wheel-leg. This method can have advantages in some cases when wheel-leg moves on the curved or other surfaces in space. To derive the kinematic characteristics of the wheel-leg the Fig. 4 is used.

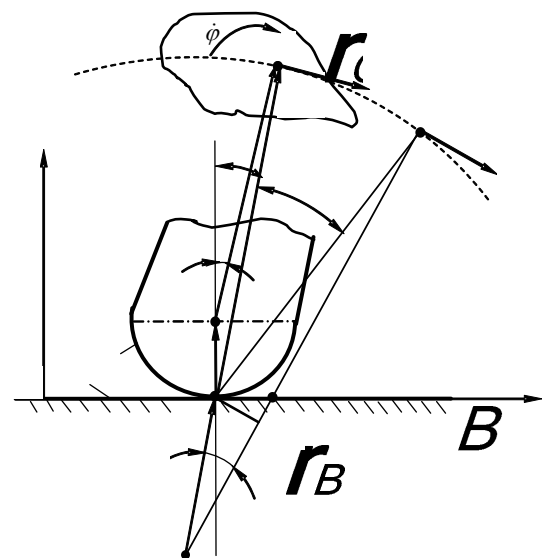


Fig. 4. Rotation of the blade of the wheel-leg.

Let the  $\alpha$ - $\alpha$  will be the trajectory of the center of the wheel-leg, when blade  $L$  rolls on rigid surface. The motion of the blade represents the motion of the moving centroid on fixed centroid with angular velocity  $\dot{\varphi}$ . At the moment, when the blade is in contact with fixed centroid, the vector

$\mathbf{r}_{BC}$ , which connects the center B of the moving centroid  $L$  with center of the wheel-leg, forms the angle  $-\pi/6 \leq \varphi \leq \pi/6$  with respect of the vertical axis  $NN$ . Thus, the rolling time of the wheel blade is  $0 \leq t \leq \pi/3\dot{\varphi}$ .

To find the radius of curvature  $\rho_\alpha$  of the trajectory of the center  $C$  of the wheel-leg, we draw the line from point  $C$  and through instantaneous center of velocity  $C_v$  (in the following for instantaneous center of rotation the notation ICR will be used). The center of the curvature  $K$  of trajectory of the point  $C$  has to lie on this line. The angle between the straight lines  $CC_v$  and  $NN$  is  $\beta$ . The angles  $\beta$  and  $\varphi$  are related to each other according the theorem of sine as follows

$$\sin \beta = \frac{l \sin \varphi}{\sqrt{l^2 \sin^2 \varphi + (l \cos \varphi + r)^2}} \quad (4)$$

Through the very small time interval  $dt$ , when blade  $L$  rolls on the horizontal line, the center  $C$  moves to the position  $C'$  and ICR rolls to the position  $C_v$ . Normal  $C'K$  to the trajectory  $\alpha-\alpha$  has to intersect the ICR of  $C_v$ . From the point  $C_v$  we draw the normal to the line  $CK'$  and denote the angle  $CKC'$  as  $d\alpha$ .

From the angle  $\Delta CKC'$  and  $\Delta KC_vM$  we receive

$$\frac{CC'}{C_vM} = \frac{KC}{KC_v} = \frac{r' + r'_C}{r'} \quad (5)$$

Further

$$CC' \approx CC_v d\gamma = r'_C \cdot d\gamma = r'_C \cdot \dot{\varphi} \cdot dt \quad (6)$$

$$C_vM = C_vC'_v \cos \beta = \dot{\varphi} \cdot r \cdot dt \cdot \cos \beta \quad (7)$$

Substituting the Eq. (6) and (7) to the Eq. (5) we receive the Euler-Savary's equation [9-11] as

$$\frac{r'_C}{r \cos \beta} = \frac{r' + r'_C}{r'} \quad (8)$$

From the Eq. (8) we receive

$$r' = \frac{r'_C r \cos \beta}{(r'_C - r \cos \beta)} \quad (9)$$

and radius of curvature of the trajectory of the center  $C$  according to the Fig. 4 is

$$\rho_\alpha = r'_C + \frac{r'_C r \cos \beta}{(r'_C - r \cos \beta)} \quad (10)$$

where  $\rho_\alpha = CK = r'_C + r$ .

The length of the vector  $\mathbf{r}'_C$  we receive from the vector equation as

$$\mathbf{r}'_C = \mathbf{r} + \mathbf{r}_{BC} \quad (11)$$

The length of the vector  $\mathbf{r}'_C$  through the components of fixed reference frame can be written then in the form

$$r'_C = \sqrt{l^2 \sin^2 \varphi + (r + l \cos \varphi)^2} \quad (12)$$

where  $\varphi = \dot{\varphi}t - \pi/6$ .

Parametrical representation of the trajectory of the center  $C$  according to the Eq. (12) can be written as follows

$$x_C = x_0 + \sqrt{l^2 \sin^2 \varphi + R^2} \sin \beta$$

$$y_C = \sqrt{l^2 \sin^2 \varphi + R^2} \cos \beta \quad (13)$$

$$R = r + l \cos \varphi \quad (14)$$

where  $x_0$  is initial position of the ICR of the  $C_v$ .

The velocity of the center  $C$  becomes then according to the Eq. (12) as

$$v_C = \dot{\varphi} \cdot CC_v = \dot{\varphi} \cdot \sqrt{l^2 \sin^2 \varphi + R^2} \quad (15)$$

Taking the time derivative from the Eq. (15) we receive the tangential acceleration as

$$a_C^\tau = \dot{\varphi}^2 \frac{rl \sin \varphi}{\sqrt{l^2 \sin^2 \varphi + R^2}} \quad (16)$$

where  $\dot{\varphi} = const$ .

Normal acceleration of the point  $C$  taken into account the Eq.(10) and Eq. (15) can be obtained as follows

$$a_C^n = \frac{\dot{\varphi}^2 (l^2 \sin^2 \varphi + R^2)}{r_C' + \frac{r_C' r \cos \beta}{r_C' - r \cos \beta}} \quad (17)$$

where angle  $\beta$  according to the Eq. (4) is defined as

$$\beta = \arcsin \frac{l \sin \varphi}{l^2 \sin^2 \varphi + R^2} \quad (18)$$

Absolute acceleration is defined through Eq. (16) and Eq. (17) as

$$a_C = \sqrt{(a_C^\tau)^2 + (a_C^n)^2} \quad (19)$$

## 5. DYNAMICS OF WHEEL-LEG

To evaluate the maximum torque that can be applied to wheel-leg in motion on rigid surface the Lagrange's equation with undetermined multipliers are introduced [10] in the form

$$\frac{d}{dt} \left( \frac{\partial T}{\partial \dot{q}} \right) - \frac{\partial T}{\partial q} = Q + \lambda \frac{\partial f}{\partial q} \quad (20)$$

where  $T$  – kinetic energy of the wheel-leg,  $Q$  – generalized forces of wheel-leg,  $q$  and  $\dot{q}$  – generalized coordinates and their time derivatives respectively;  $\lambda$  – Lagrangian undetermined multipliers;  $f$  – the equation of constraint.

As the generalized coordinates the translation of the center of the rounded tip B of the blade in the direction of the  $x$  coordinate axis and rotation about this center through the angle  $\varphi$  are chosen. According to the chosen generalized

coordinates the position of center  $C$  can be written as

$$\mathbf{r}_C = (x + l \sin \varphi, r + l \cos \varphi)^T \quad (21)$$

where  $r$  - is constant through the rotation of the point  $C$  with respect to the  $y$ -coordinate axis by angle  $-\pi/6$  to  $\pi/6$ .

Taking the time derivative from the Eq. (21) we receive expression of the kinetic energy as follows

$$T = \frac{1}{2} m(\dot{x}^2 + 2\dot{x}\dot{\varphi}l \cos \varphi + \dot{\varphi}^2 l^2) + \frac{I_z \dot{\varphi}^2}{2} \quad (22)$$

where  $I_z$  – the moment of inertia of the wheel-leg.

The constraint equation  $f$  compliant with generalized coordinates is

$$x - r\varphi - x_0 = 0 \quad (23)$$

where  $x = x_0 + r\varphi$  and  $x_0$  - determines the initial position of ICR. According to Fig. 3 the active forces that do work as weight  $P$  of the wheel-leg and the torque  $M$  are applied to the center of the wheel-leg. Applying the method of virtual work we receive the generalized forces corresponding to the virtual displacement of generalized coordinates as follows

$$Q_x = 0; Q_\varphi = M + Pl \sin \varphi \quad (24)$$

Taking the partial and time derivatives of Eq. (22) and Eq. (23) according to the Eq. (20) we receive Lagrangian system of equation as

$$\begin{aligned} m(\ddot{x} + \ddot{\varphi}l \cos \varphi - \dot{\varphi}^2 l \sin \varphi) &= \lambda \\ m\ddot{x}l \cos \varphi + \ddot{\varphi}(ml^2 + I_C) &= \\ &= M + Pl \sin \varphi - \lambda r \end{aligned} \quad (25)$$

The first equation in Eq. (25) represents the maximum friction force between the surface and the wheel-leg blade that is constituent with constraint equation Eq. (23), i.e motion of wheel-leg without



slipping. From the second equation of the Eq. (25) it is possible to get the expression for the maximum torque that can be applied of the wheel-leg.

The generalized coordinates in Eq. (21) are coupled. Dropping out the term  $x_0$  that represents the initial position of ICR, then the Eq. (25) can be rewritten as

$$\begin{aligned} m\ddot{\varphi}(r+l\cos\varphi) - m\dot{\varphi}^2 l \sin\varphi &= \lambda \\ \ddot{\varphi}(mrl\cos\varphi + ml^2 + I_C) &= \\ = M + Pl\sin\varphi - \lambda r \end{aligned} \quad (26)$$

The Eq. (26) can be solved numerically for both equations to determine the values of the friction forces and applied torques.

## 6. CONCLUSION

In this paper the mathematical formulation of the planar kinematics and dynamics of the wheel-leg is derived. The kinematic properties of wheel-leg were derived by method of rigid body mechanics and by alternative method based on the Euler-Savary formulation of the moving and fixed centroids. The use of Euler-Savary method can have advantageous when wheel-leg moves in curved or other surfaces in space. The Lagrange's equation with undetermined multipliers has been used to establish relationship between the maximum applied torque and the friction force of the wheel-leg. The study of the kinematic and dynamic properties of the wheel-leg has covered only the basic theoretical aspects of the wheel-leg motion in horizontal plane. Thus, to evaluate more capabilities of the wheel-leg the comprehensive analysis of the wheel-leg will be performed in future.

## 7. ACKNOWLEDGEMENT

This research was supported by funding of the Estonian Science Foundation grant No. 8652

## 8. REFERENCES

1. Sell, R., Kaeeli, M., *Wheel-Leg (Wheg)*. Patent no EE05283B1, 2009.
2. Tsunasawa M., *Moving Equipment*, Patent no 23. JP60148780, 1985.
3. Holmes, M., *Vehicle traction assist device*, Patent no US2006131948, 2006.
4. Denisenko, G., *Wheel Propulsion Unit*, Patent no RU280562 C2, 2006
5. Zheng L., et.al, *A Novel High Adaptability Out-door Mobile Robot with Diameter-variable Wheels*. Proc. of the IEEE Int. Conference on Information and Automation Shenzhen, China, 2011.
6. Xinbo C., et. al, *Mechanism principle and dynamics simulation on variable diameter walking wheel*. Second International Conference on Digital Manufacturing & Automation, 2011.
7. Galileo Mobility Capabilities, <http://www.galileomobility.com>
8. Campbell D. and Buehler M., *Stair descent in the simple hexapod 'RHex'*, Proceedings of the IEEE Int. Conference on Robotics & Automation, Taipei, Taiwan, September 14-19, 2003.
9. Angus, R., W. *Theory of Machines Including the Principles of Mechanisms*. NABU Press, 2011.
10. Cleghom, W., L. *Mechanics of Machines*. Oxford University Press, 2005.

Raivo Sell, Ph.D, senior researcher, TUT, Ehitajate tee 5, Tallinn, raivo.sell@ttu.ee

Gennady Aryassov, PhD, Ass. Prof., TUT Ehitajate tee 5, Tallinn, gennadi.arjassov@ttu.ee

Andres Petritshenko, PhD, researcher, TUT Ehitajate tee 5, Tallinn, andres.petritsenko@ttu.ee

Mati Kaeeli, PhD Student, Tallinn TUT Ehitajate tee 5, Tallinn, mati141@gmail.com

## LOCAL AND GLOBAL DESCRIPTORS FOR PLACE RECOGNITION IN ROBOTICS

Shvarts, D. & Tamre, M.

**Abstract:** *The simultaneous auto-localization and mapping of the environment is one of the most pressing problems of robotics. Among the existing SLAM algorithms, place recognition is a must for several cases. As an example, in multirobot SLAM we have several individual maps created by various robots. In order to combine them into one global map we have to identify common places before merging them. In this paper, two methods that were successfully used for performing scene recognition between different images have been compared. We have considered the advantages and limitations of each method regarding our tasks.*

*Key words: local descriptors, global descriptors, GIST, SIFT, SURF.*

### 1. INTRODUCTION

SLAM, standing for Simultaneous Localization and Mapping, tries to locate a mobile robot in its environment and estimate a map of it from sensory information [1]. A wide array of sensors have been used, but nowadays cameras are the preferred ones. At its core, SLAM algorithms apply sequential estimation techniques that estimate a model from noisy data.

In a SLAM framework, the ability of recognizing a previously mapped area is useful in several occasions: for correcting the estimation drift when an area is revisited (a problem known as loop closure) [2]; for relocation in an estimated map (the kidnapped robot problem) [3]; or

for fusing information between multiple robots that are mapping the same area (multi-robot SLAM) [4].

Place recognition in visual SLAM has been usually addressed by constructing a visual vocabulary of local descriptors [2, 3]. Such vocabulary can be expensive to build and store if a robot performs an exploratory trajectory and accumulates new images. While there exists global descriptors in the computer vision literature, they have never been used in SLAM. This paper proposes the comparison of several local and global descriptors for the purpose of place recognition in robotics, both in terms of performance and computational cost.

### 2. LOCAL DESCRIPTORS

In computer vision, local interest points have been used to solve many problems like object recognition, image registration, 3D reconstruction, and more. The usual approach is based on selecting some points in the image and perform a local analysis on these ones. For a successfully work of such methods, a sufficient number of such keypoints have to be detected. In addition, these points should be distinguishable and stable features that can be accurately localized.

A lot of research on the behavior of several types of feature descriptor and detectors has been done. We compared the results of such investigations to select the appropriate feature descriptor and detector for further work. The best feature detector has to meet the following requirements:

- The extracted keypoints have to be rotation and scale invariant.
- Invariance to luminance transformation, at least partly.
- Invariant to blur and noise.

A comparison of six methods that were implemented in OpenCV library was showed in [10]. Five quality and one performance test was done for each kind of descriptor.

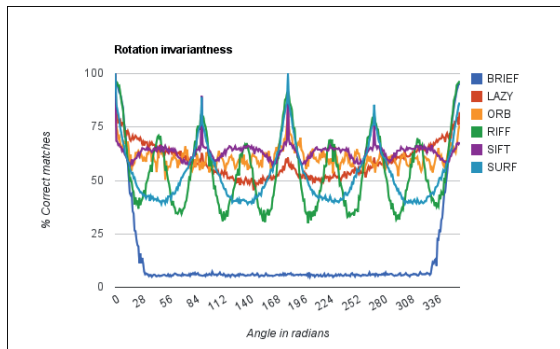


Fig. 1. The result of rotation test for OpenCV's feature detector algorithms.

[Fig. 1] shows that almost all algorithms are partially invariant to rotation except BRIEF, presenting SIFT the best repeatability. Close to SIFT are ORB and SURF feature descriptors.

[Fig. 2] shows the scale invariance performance of different algorithms.

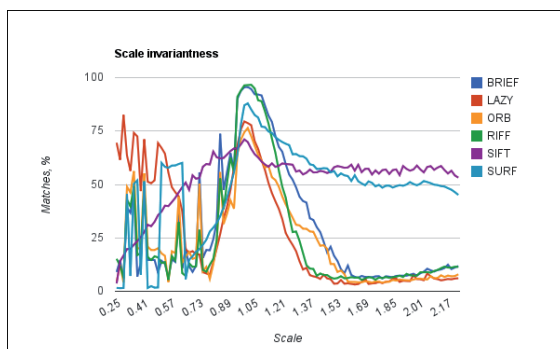


Fig. 2. The Scale test for OpenCV's features detector algorithms.

Again, the most stable results showed SURF and SIFT descriptors.

Almost all the descriptors have a high degree of invariance to brightness change, as shown in [Fig. 3]

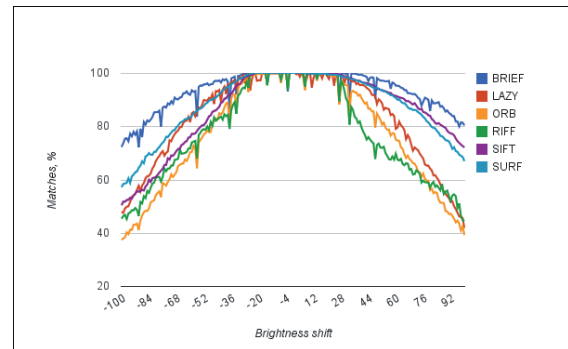


Fig. 3. The result of lighting test for OpenCV's feature detector algorithms.

Based on the materials presented in [10] there are two descriptors that showed the most stable results –SIFT and SURF. It should also be noticed that these algorithms are the slowest among all the tested [Fig. 4].

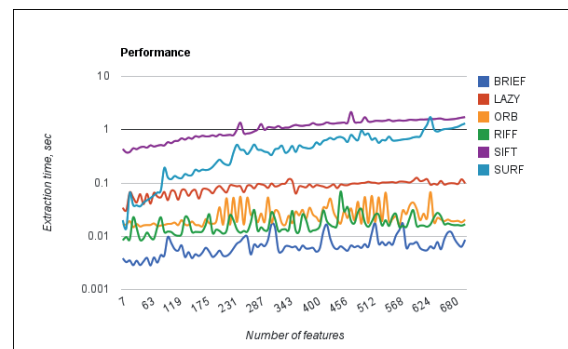


Fig. 4. Speed test of OpenCV's implemented algorithms

The use of these algorithms in real-time applications could be limited due to these computational cost. However, the high quality of the calculated keypoints makes these algorithms irreplaceable for solving many problems in computer vision. A detailed description of those algorithms is not presented here for the sake of brevity. The reader is referred to the original papers [7] and [13] for a deep understanding of both algorithms.

We carried out several additional tests with SIFT and SURF algorithms to determine witch of those has the most suitable performances for our particular purpose. The results are presented in (Fig. 5) and in table 1.

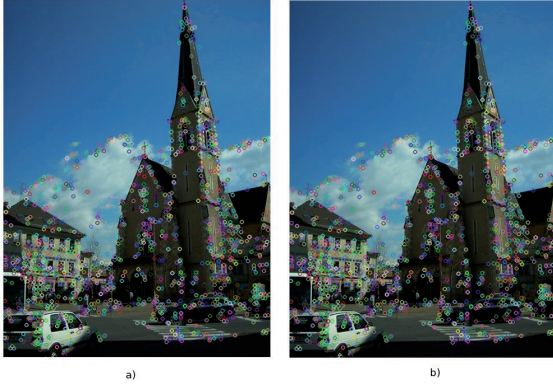


Fig. 5. a) A test-image with extracted keypoints by using SIFT descriptor, b) the same image with extracted keypoints by applying SURF descriptor

	SURF	SIFT
Image size	480x640x3	480x640x3
Number of extracted keypoints	1126 keypoints	1511 points
The execution time	878.86ms	1245.8ms

Table 1. The comparison of two local descriptors.

Both SIFT and SURF descriptors have showed similar results and could apply for solving a issue in SLAM application but with certain limitations. The number of extracted keypoints has played a major role by choosing suitable descriptors for further work.

### 3. GLOBAL DESCRIPTORS

In the previous section we have investigated the properties of different local descriptors. There are several descriptors and we can choose the best one to accomplish specific task. But if we use a local descriptor, the representation of a whole image is restricted to the description of a set of points that was successfully extracted from the image.

In contrast, global descriptors summarize the whole image in a single descriptor, being GIST the most representative [8].

We are going to highlight the major aspects of global descriptors in this chapter.

Investigation in the field of global descriptor is conditional upon that the recognition of the real world scene based on encoding the global configuration, ignoring most of the details and objects information [8]. The abstract description of a scene can be obtained by discrete Fourier transformation of an image:

$$I(f_x, f_y) = \frac{1}{MN} \sum_{x=0}^{M-1} \sum_{y=0}^{N-1} i(x, y) e^{-j2\pi(\frac{fx}{M} + \frac{fy}{N})}$$

$i(x, y)$  is the intensity distribution of the image along a spatial variables  $(x, y)$ ,  $f_x$  and  $f_y$  are the spatial frequency variables. The complex function  $I(f_x, f_y)$  can be decomposed into two terms  $|I(f_x, f_y)| = A(f_x, f_y)$ , the amplitude spectrum of the image, and  $\varphi(f_x, f_y)$  the phase function of Fourier transformation. The phase function represents the information relative to local properties and amplitude spectrum give unlocalized information about to the image structure. The energy spectrum of Fourier transformation  $P(f_x, f_y) = |I(f_x, f_y)|^2$  is a distribution of signal's energy among the different spatial frequencies. The global description of a scene is encoded in this distribution and provides dimensional representation of the image  $i(x, y)$ . It is impossible to operate with such representation of the image in practice, due to the high dimensionality of energy spectrum  $N \times M$ . The standard way for data reduction of matrix of energy spectrum is principal components analysis. It is needed to rearrange the matrix representation in a column vector than PCA extracts a subspace spanned by a subset of a KL functions. The direct implementation of this method is impossible in practice. The reliable calculation of the KL basis function required a number of image samples  $N_l$  more then  $N \times M$ . But in practice we don't have them usually. [8] suggests sampling the function  $A(f_x, f_y)$  as:

$$g_i = \iint A(f_x, f_y)^2 G_i(f_x, f_y) df_x df_y$$

being  $G_i$  are a set of Gaussian functions.

We have tested the MATLAB code (created by author) to examine properties of GIST descriptor and the possibility to use it instead of local descriptors for scene matching.

#### 4. EXPERIMENTAL RESULTS

In this section we examine two different descriptors, global and local. The aim of the experiment is to prove the ability of the descriptors to match two images of the same scene. The way of solving this problem is well understood. The problem consists of estimation of homography between pairs of images. First we have tested the local descriptor. The algorithm is presented below:

**Algorithm:** Local descriptor in problem of matching of two images.

**Input:** Two putative matched images.

1. Extract SIFT features from first and second image. In this section we use SIFT descriptor based on studies in section 3.

2. Estimation of putative correspondences: Find  $k$  nearest-neighbors for each feature. From the feature-matching step we have identified images that have a large number of matches between them. Than we consider  $m$  images that have a largest number of matched points and use RANSAC to select of inliers that are have an impact on calculation of homography.

3. Fundamental matrix estimation: Find geometrically consistent feature matches using RANSAC to solve for the fundamental matrix computation between pairs of images. We just select the image that has a largest number of inlier points.

**Output:** Two matched images.

The better way is presented in [12]. But in our case we have made a simpler experiment. In the next experiment we examine the properties of a GIST descriptors for automatic image matching. As input set we use the same set of images.

During the experiment we calculate the gist descriptor for each image. The best matching is an image with a smaller distance between GIST vectors. The result of two experiments was obvious.

All descriptors are invariant to rotation and scaling. As we said earlier, we don't look at the execution time of methods. We focused more on the properties of methods. Both methods can be successfully applied for the automatic matching of images. But without any additional measurement of performances is obvious that GIST descriptor is faster.

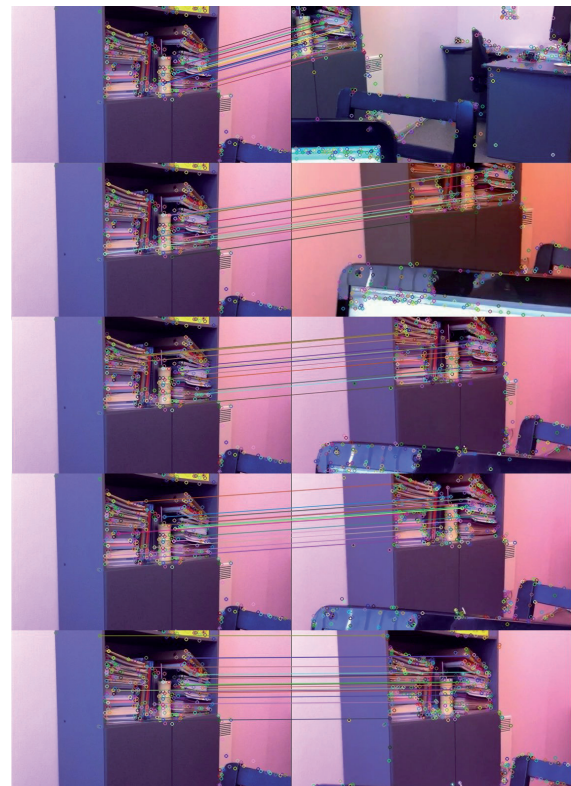


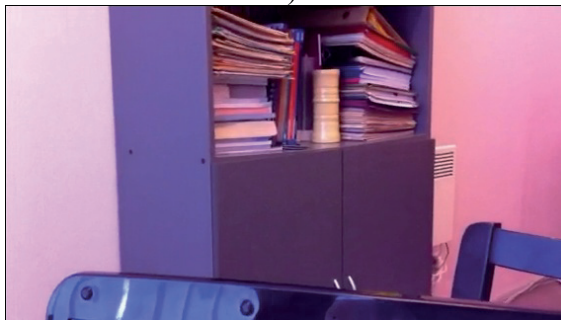
Fig. 6. Dynamic of SIFT descriptor by image matching. In the top image the result of matched points is 44. And we show an increase of numbers of matched points from 44 at the top to 158 points in the bottom image.

We show in the figure 7 the result of the GIST descriptor.





a)



b)

Fig. 7. Image a) is an input image for a GIST descriptor b) output from the GISTtest algorithm.

Finally, we describe an image set. As input for algorithm we choose the first image from the 586 sets of images. The set of images is an image sequence created from the moving camera. The image resolution is 568x320 pixels.

## 5. CONCLUSION

In this paper we have tested different image descriptors, several local and a global one, in order to foresee its possible use in a robotic application. From the several local descriptors that have been evaluated we observe a compromise between speed and performance: SIFT and SURF present the higher invariance to different transformations, but are more expensive to compute than the rest of the local descriptors.

Regarding the global descriptor GIST, we have observed a good performance for scene recognition, a higher compactness and possibly low cost, which indicates a good potential for image matching in robotics. As future work, our aim is to perform a detailed comparison between local and

global descriptors regarding performance and cost.

## 5. REFERENCES

- [1] H. Durrant-Whyte and T. Bailey, "Simultaneous localization and mapping (SLAM): Part I the essential algorithms" Robotics and Automation Magazine, vol. 13, no. 2, pp. 99–110, 2006.
- [2] D. Galvez-Lopez and J. D. Tardos, "Real-time loop detection with bags of binary words" Intelligent Robots and Systems (IROS), 2011 IEEE/RSJ International Conference on, sept. 2011, pp. 51–58.
- [3] B. Williams, G. Klein, and I. Reid, "Real-time SLAM relocalisation" in IEEE 11th International Conference on Computer Vision, 2007, p. 1:8.
- [4] S. Thrun and Y. Liu, "Multi-robot slam with sparse extended information filters" Robotics Research, pp. 254–266, 2005.
- [5] K. Mikolajczyk, T. Tuytelaars, C. Schmi, A. Zisserman, J. Matas, F. Schaffalitzky, T. Kadir, and L. Gool, "A comparison of affine region detectors" International Journal of Computer Vision, vol. 65, no. 1, pp. 43–72, 2005.
- [6] K. Mikolajczyk and C. Schmid, "A performance evaluation of local descriptors" Pattern Analysis and Machine Intelligence, IEEE Transactions on, vol. 27, no. 10, pp. 1615–1630, 2005.
- [7] D. G. Lowe, "Distinctive image features from scale-invariant keypoints" International Journal of Computer Vision, vol. 60, no. 2, pp. 91–110, 2004.
- [8] A. Oliva and A. Torralba, "Modeling the shape of the scene: A holistic representation of the spatial envelope" International Journal of Computer Vision, vol. 42, no. 3, pp. 145–175, 2001.
- [9] B. Williams, M. Cummins, J. Neira, P. Newman, I. Reid, and J. Tardos, "An image-to-map loop closing method for monocular SLAM" in IEEE/RSJ International Conference on Intelligent Robots and Systems, 2008. IROS 2008, 2008, pp. 2053–2059.

[10] *Feature descriptor comparison report*  
<http://computer-vision-talks.com/2011/08/feature-descriptor-comparison-report/>

[11] R. I. Hartley and A. Zisserman, “*Multiple View Geometry in Computer Vision*” ISBN: 0521623049, 2000

[12] M. Brown , D. G. Lowe, “*Recognising Panoramas*”.

[13] Herbert Bay, Andreas Ess, Tinne Tuytelaars, Luc Van Gool, “*SURF: Speeded Up Robust Features*”, *Computer Vision and Image Understanding (CVIU)*, Vol. 110, No. 3, pp. 346--359, 2008



## USING SOFTWARE WITH AI ELEMENTS FOR CONCEPTUAL DESIGN OF MACHINE ELEMENTS

Tiidemann, M.; Kalja, A.; Tiidemann, T.; Tyugu, E.

**Abstract:** *There is usually more than one way to solve a design problem. The actual practice of designing is applying a combination of scientific principles and making decisions based on experimental knowledge. Visualization of calculation results is useful at any stage of the design process. “What is nice to look at, is usually constructively right” – a known Estonian engineer and designer of bridges, prof. Ottomar Maddison, once said. This applies to contemporary design process as well – a lot of elements and parts of drawings are often designed using estimation by sight. On the other hand, designing is often based on approximate calculations like it is usual in the conceptual design.*

*Developing and using problem solvers for design has been a scientific activity in Institute of Cybernetics at Tallinn University of Technology for a long time. Several solver based software environments have been developed. Quite well-known environments from last decades ExpertPRIZ and NUT are simple to learn and they perform automatic calculations in different fields of engineering. A new system CoCoViLa – Compiler Compiler for Visual Languages – has been under development for the last five years.*

*In recent years, the authors have prepared some experimental CAD packages with artificial intelligence features for automatic calculations of machine elements like gear drives, shafts, bearings, belt drives, fits and tolerances. These packages are helpful especially at a conceptual design stage to find standard parameters from tables and to visualize the results. Some examples of using these systems in*

*conceptual design of machine elements are introduced.*

*Key words: mechanical engineering design, AI based CAD software, conceptual design, visualization*

### 1. EXAMPLE OF CALCULATING VALUES FOR CONCEPTUAL DESIGN

Let us have a simplest problem to find approximate parameters of a cogwheel (Fig. 1), if we have initial modulus  $m=3$  mm, diameter of the wheel  $d=140$  mm. The calculus is shown on three ExpertPRIZ windows – left to right (Fig. 2). The language is very close to domain language in mechanical engineering.

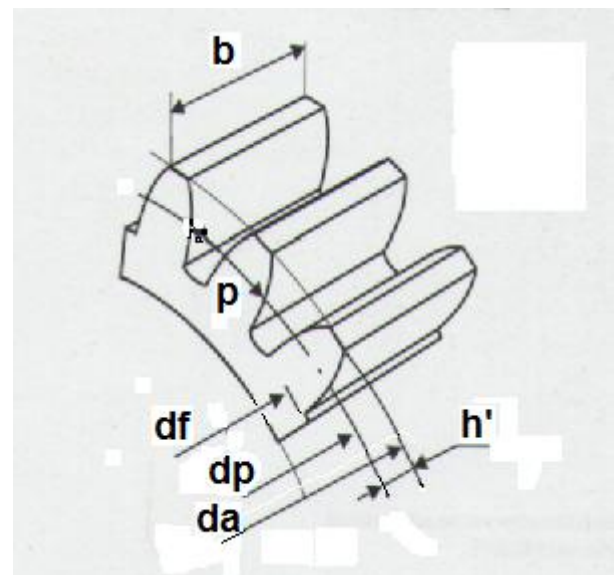


Fig. 1. Elements of gear drive, can be calculated automatically and finding standard values

```

!clear y
d=m*z
da=d+2*m
df=d-2.5*m
m=3
d=140
?z          -> z=45.67

!clear y
d=m*z
da=d+2*m
df=d-2.5*m
m=3
*d=140
z=46
?          -> m=3
          -> z=46
          -> d=138
          -> df=130.5
          -> da=144

!clear y
d=m*z/cos(beta)
da=d+2*m
df=d-2.5*m
m=3
d=140
?          -> m=3
          -> d=140
          -> z=46
          -> df=132.5
          -> da=146
          -> beta=9.7

```

Fig. 2. Example of using ExpertPRIZ for calculating approximate gear parameters.

ExpertPRIZ takes all rows in a workspace as formulas. If we write a command „!clear y”, then the program clears the model from previous actions. Writing all formulas and initial parameters, in a free order, we can ask for a number of teeth ?z. Immediate answer will be: z=45,67.

As the calculated number of teeth it is not an integer value, we take z=46. Continuing the calculation (shown in the next window) we eliminate d (adding \* at the beginning of the row, then the program takes this row as a comment, not a formula). Asking now for all computable values by typing ?, we get them all.

If it is necessary to take already initially d=140, and to calculate a helical gear with a given helix angle beta, we can do this by giving the respective values (shown in the last window). We will get immediately the necessary parameters for conceptual design.

ExpertPRIZ is simple to use in conceptual stage of design. There are designers using it in everyday calculations. Getting an answer, they try to improve it and to find the best solutions in a particular situation. There are examples for using ExpertPRIZ for inventing new devices. In such a case there are no given formulas for calculations, and an inventor must work out the best solutions for a new model. This situation was described in the World Conference TRIZfuture 2005 [3]. Two

examples of inventions (utility models) have been described – Harmonic Chain Drive and Double Rotor Windmill.

We have described elements of program packages that calculate all necessary parameters automatically. Now we can do it together with selecting standard parameters from standard tables, and selecting materials for it. Automatically and very fast.

An effective usage of ExpertPRIZ program packages is for developing and checking student works [1, 2]. The program is very helpful in checking the correctness of calculations, mistakes.

## 2. USING COMPILER COMPILER FOR VISUAL LANGUAGE – COCO-VILA

The latest version of CoCoViLa is suitable for developing visual program packages for designing machine elements. The best results come in this process from cooperation of mechanical engineers and systems programmers. CoCoViLa is based on Java language and can run everywhere where Java is available.

CoCoViLa includes graphical scheme and class editors and a synthesizer. End user works with the scheme editor (Fig.3).

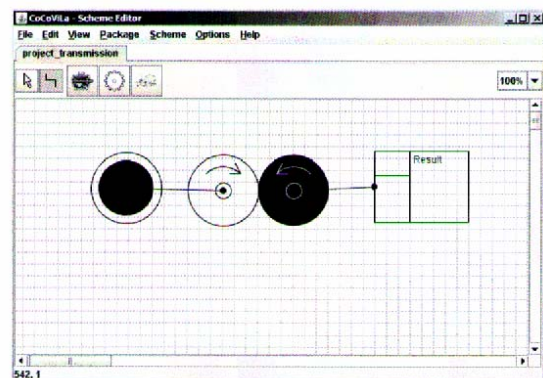


Fig. 3. Scheme editor of gear design package.

By finding a necessary package and loading it one can easily compose a scheme from visual elements. The elements can be connected by means of various relations.

Automatic calculation and immediate synthesis of a new programs happens every time we determinate the input data.

These systems support declarative programming technique, which essentially relies on automatic usage of specifications for program construction. The approach to program development used here is called model-based programming because it essentially uses models in programming. New concepts are defined by specifying their models. Thereafter they can be used for specifying problem conditions, i.e. for giving specifications from which programs can be built. The computer is relied on to get program ready and to run it. These activities can be divided into two separate stages: one is specifying concepts and the other is specifying a problem in terms of given concepts. The characteristic features of this approach are:

- using conceptual and expert knowledge bases actively,
- programming completely in terms of problem domain,
- using a computer in the whole problem solving process, starting from the description of a problem itself and specifications for program construction,
- synthesizing programs automatically.

### 3. EXPERIMENTAL CONCEPTS IN MECHANICAL ENGINEERING DESIGN

We have described the computer workplace of a mechanical engineer, developed specially for conceptual design stage (Fig 4). This supports different stages of mechanical engineering design. The experimental programs in CoCoViLa and related tools are used. There are experimental programs for mechanical transmission, shafts and axes, drives, screw joints, conveyor mechanisms [1-5, 7]. Dimensioning process is easier when using the automatic calculation and finding components of fits and limits, as recommend in ISO standard [6].

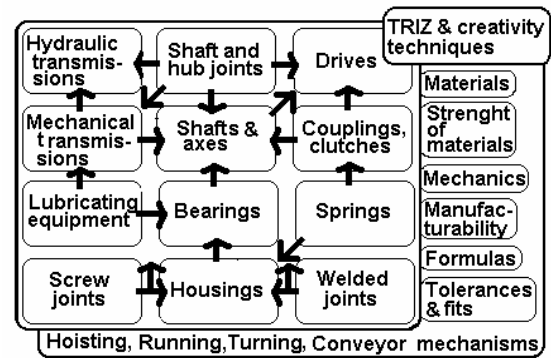


Fig. 4. Workplace of a designer

### 4. PROGRAM PACKAGE FOR DESIGNING GEAR DRIVE IN COCOVILA SOFTWARE SYSTEM.

It was developed together with IT student Merle Viil as programmer. Using this package does not require any special knowledge of Java programming language and specific computer skills. The example was developed for design of gear drive with straight teeth.

Computing algorithm includes data input: necessary parameters of drive, work conditions, efficiency factors etc. The result will be finding necessary motor and getting correct parameters of gear drive. After that the dimensioning of shafts and cogwheels can be done, finding necessary materials for making these machine elements. Up to 60 different parameters are available for design.

The results of calculations can be checked by visualisation of scheme of wheels and shafts in right proportions (Fig 5).

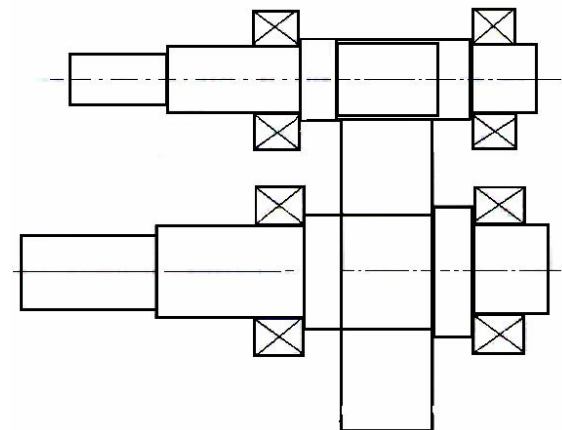


Fig. 5. Visualisation of calculated gear drive dimensions

There are many possibilities to improve package with other variants of gear drive types, as adding arrow teeth for gear package, as an example. In the future, it would be very helpful to have more advanced class editor for the development of packages.

## 5. CONCLUSIONS

- The software packages have considerably increased the effectiveness of work of the designers freeing them from routine calculations, as the examples in fits and tolerances, in gear drive, shafts and axes, bearings etc. show it.
- The end user, using visual programming in CoCoViLa, can put together the kinematic scheme from icons and develop a problem model that will be automatically applied for program construction and calculations.
- The results of calculations can be visualized by drawing schemes and pictures for evaluation of solutions.
- Concentrating efforts on employing personal creative resources could be the challenge of the day. More computer software for innovative thinking for the designers is necessary.

## 6. REFERENCES

1. Kalja, A., Kindel, K., Tiidemann, M., Tiidemann, T. A Multilevel Modelling Environment for Machine Element Design. In *Proceedings OST 01 Symposium on Machine Design*. Tallinn, TUT, 2001, 45-50.
2. Kalja, A., Kindel, K., Tiidemann, M., Tiidemann, T. Dimensioning and tolerancing – some convenient methods. In

*Proceedings of Engineering Graphics BaltGraf-6*. Riga, LTU, 2002. 65-70.

3. Tiidemann, T., Kalja, A., TRIZ and ExpertPRIZ type software in engineering and education. In *Proceedings of TRIZ Future2005*, Graz, University of Leoben, 175-181.
4. Tiidemann, M., Kalja, A., Tiidemann, T. From pencil to CAD and visual programming. In *Engineering Graphics BaltGraf-8: proceedings of the Eighth International Conference* (Annuka, H., ed.). Tallinn University of Technology, Tallinn, 2006, 131 - 136.
5. Kalja, A., Tiidemann, M., Tiidemann, T. Creativity trainings and technical education problems in CAD. In *Proceedings of OST'05 conference*. KTH, Stockholm, 2006, 133-145.
6. Tiidemann, T., Kalja, A. Mõõtahelate ja istude koosarvutamise. Unified Calculation of Dimension Chains and Fits. In: *Tallinna Tehnikakõrgkooli Toimetised 4. Transaction no 4 of Tallinn College of Engineering*. TCE, Tallinn, 2004. 63-65 (In Estonian).
7. Tiidemann, M. *Masinaelementide projekteerimise alused. Fundamentals of the Design of Machine Elements*. Tallinn College of Engineering, Tallinn, 2010, 117 pages. (In Estonian).

## 9. ADDITIONAL DATA ABOUT AUTHORS

Mart Tiidemann, lecturer  
 Tallinn University of Applied Sciences,  
 Pärnu mnt.62, 10135, Tallinn, Estonia  
 mart@tktk.ee  
 Phone: +372 56 462440

## CAMERA GIMBAL PERFORMANCE IMPROVEMENT WITH SPINNING-MASS MECHANICAL GYROSCOPES

Tiimus, K. & Tamre, M.

**Abstract:** This proof-of-concept study was done to research the advantages and disadvantages when combining spinning-mass gyroscopes with an electro-mechanical gyro stabilized camera gimbal mechanism on a small vertical take-off and landing (VTOL) rotorcraft and to show that a method like this has the potential of being used. As spinning-mass gyroscopes conserve angular momentum, they can be used to maintain system orientation and also to eliminate vibrations dispersing through the airframe. The experiment started by attaching a small gyro stabilized gimbal on a miniature VTOL rotorcraft and performing flight tests and logging the data about the base position angles in conjunction with the gimbal mechanisms output shafts position and ability to compensate these rotational movements. After that, 2 spinning-mass gyroscopes were taken from inside missile guidance units and implemented to the system by a special pivoting mechanism. The tests were performed again after upgrading the mechanism. Although the overall take-off weight of the platform increased, the video-image quality, which was the main evaluation method, was significantly improved.

*Key words: VTOL rotorcraft, UAV gimbal, Inertial Measurement Unit, Motion control, Spinning-mass gyroscope*

### 1. INTRODUCTION

Fast developments in the field of small unmanned multi-rotor-configuration rotorcraft have begun to push aside

conventional helicopters due to their simple mechanical build, relatively low cost and secure operation. Being simple to construct and build makes them also very lightweight compared to other VTOL machines. For this reason, multi rotor aerial vehicles are highly maneuverable and stable in non-windy conditions, but very prone to stronger wind gusts, which makes them oscillate and vibrate in a lot of occasions. This may affect the used instrument, especially video cameras with CMOS sensors.

For this reason, a study was performed to see, whether or not combining spinning-mass gyroscopes help to improve the overall performance of a the electro-mechanically gyro stabilized camera gimbal. Spinning mass gyroscopes conserve angular momentum (1) and add synthetic inertia to the system.

$$L = I \cdot \omega \quad (1)$$

By combining mechanical gyroscopes and a positioning gimbal by a specialized mechanism, which takes precession and the rotation of the spinning-mass gyroscopes axes into account, it is possible to eliminate the base motion (in this case VTOL rotocrafts airframe rotational movement (Fig.1)) from affecting the picture.

The obtained result would find many applications where improved gimbal precision and eliminated vibration are crucial like laser illumination, distance measuring, target surveillance and other similar application areas.





Fig. 1. Y6 Multirotor VTOL rotorcraft without gyrostabilised gimbal

## 2. SYSTEM DESCRIPTION

### 2.1. Developed gyrostabilized mechanism

The objective of the study was to find a solution, which improves the performance of a 2-axis electromechanically gyrostabilized camera gimbal [1](2) mounted on a Y6 configuration multi rotor VTOL rotorcraft (Fig. 1). The applicable small gimbal is not roll-stabilized although it can be used in Roll-Pitch configuration if needed.

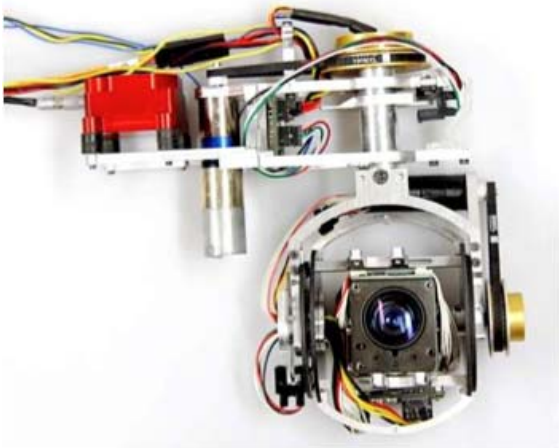


Fig. 2. Electro-mechanically gyrostabilised camera gimbal test platform

The mechanism uses DC planetary gearhead motors with integrated incremental encoders. Absolute position for each axis is retrieved with a binary

code disc and an optical switch. The system uses 3 coordinate systems – ground (0), base (1) = IMU and gimbal (2) (Fig. 4).

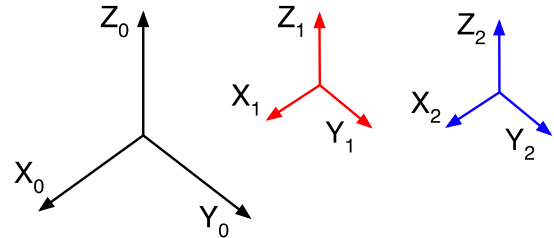


Fig. 3. Coordinate systems: 0 - ground, 1 – base/IMU and 2 – gimbal output

At system startup, the optical switch detects its relative position to zero angle and seeks to according direction until the front is reached (Fig. 5 and 7). At this point the incremental encoders readout is reset [6] and gimbal is ready for operation.



Fig. 4. Tilt mechanism

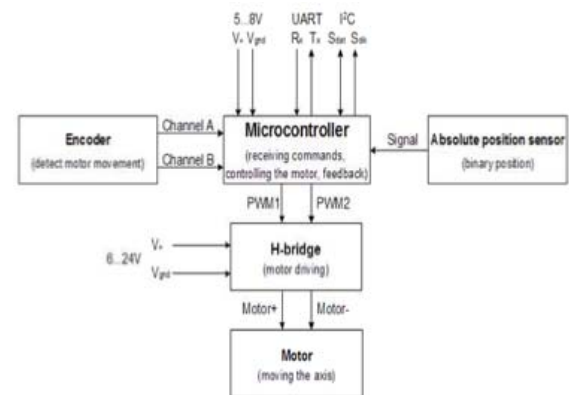


Fig. 5. Block diagram of motor controller

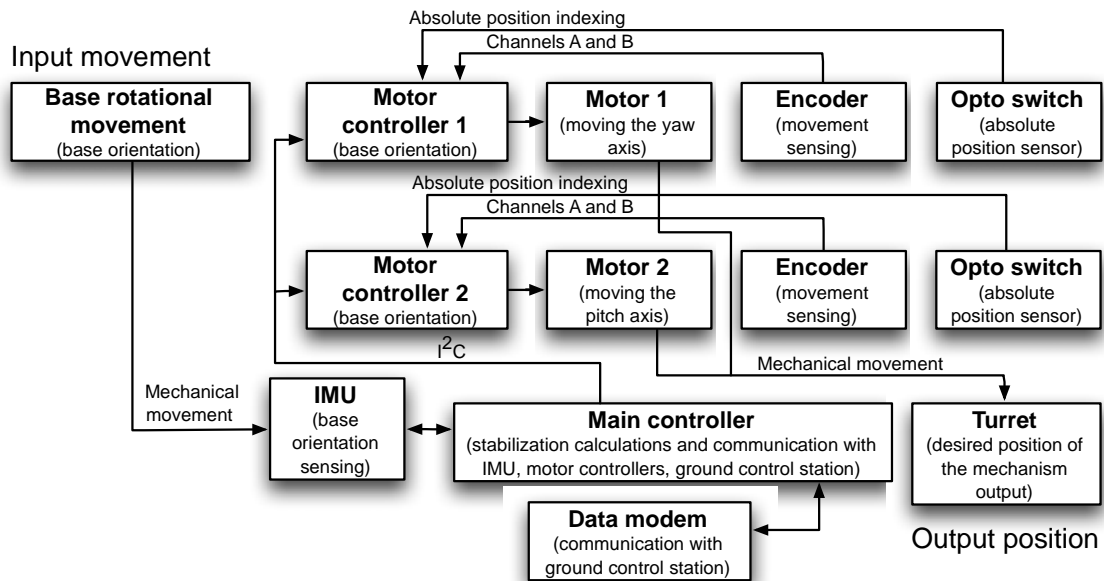


Fig. 6. Block diagram of system processes before implementing spinning-mass gyroscopes

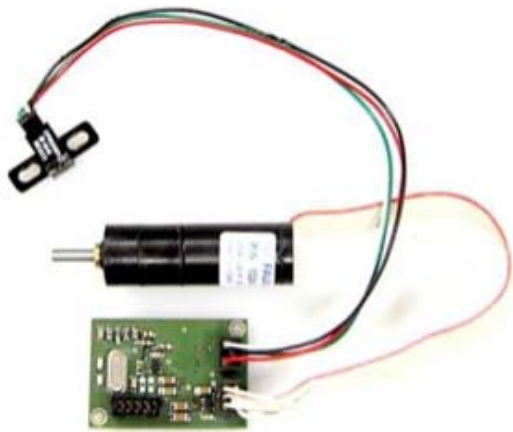


Fig. 7. Tilt actuator: planetary geared DC motor with integrated encoder, controller and absolute positioning sensor (optical switch)

Now the IMU (SBG Systems IG-500A) detects the rotational movement of the base and outputs Euler angles  $\eta = (\varphi, \theta, \psi)$  [5] for yaw, pitch and roll to represent its spatial orientation. This information is processed in the main controller and output to motor controllers by I<sup>2</sup>C bus (Fig.6). The amount needed to compensate for the base movements is calculated and with encoder feedback, the mechanism axes rotate the required amount.

## 2.2. Adding spinning-mass gyroscopes

Spinning mass mounted on a gimbal on a base maintains its orientation based on the principles of angular momentum [3]. The higher the rotating speed and the mass of the spinning body, the higher the applied momentum is needed to deviate the gyroscopes angle of rotation. Coming up with a mechanism that allows to constantly maintain the angle of rotation to the 0-coordinate system or in other words removing the angular base motion [4] is one of the key task for this study.

Precession of the spinning axis occurs when a force is affecting the spinning mass [3]. Although, if the angular speed and/or mass of the spinning wheel is high enough, the axis will hold its position and no deviation occurs.

The mechanical test platform uses two modified spinning-mass gyroscopes (Fig. 8) on 2 DOF-gimbals, so that their rotational axes cross. This mechanism itself is mounted on a separate gimbal, which can pivot in all 3 rotational axes in relation to the base. The electro-mechanically gyro-stabilized servo mechanism is mounted underneath the pivoting point so that the center of mass is



slightly on the lower side thus making gravitation level the system when there is no sideways acceleration occurring. In other cases, the mechanical gyroscopes resist the input force that is caused by accelerating and decelerating the aircraft.

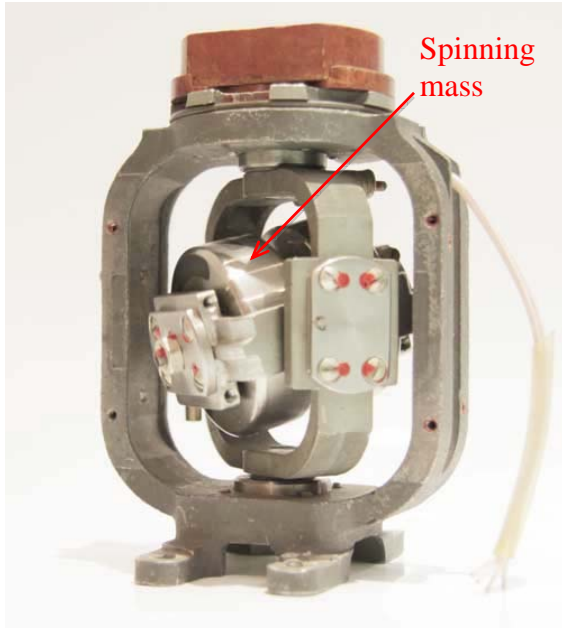


Fig. 8. Spinning-mass gyroscope from a missile guidance system

This implementation adds a fourth coordinate system between the base and the gimbal output (Fig. 9). Coordinate system 1 is now solely the rotorcraft (base), 1A is the spinning-mass mechanical gyroscopes frame and also the IMU, and coordinate system 2 remains the servo-driven output.

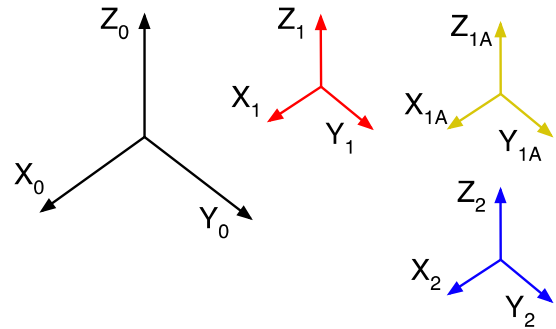


Fig. 10. Coordinate systems: 0 - ground, 1 - base, 1A - , 2 – gimbal output

Because the coordinate system 1A can rotate along with the spinning-mass mechanism, an additional feedback unit is needed on the pan axis to sum up in the final mechanical output of the gimbal. For this application an absolute encoder is needed (Fig. 9), because incremental encoder would also need indexing, which is impossible in this case.

The gyroscopes used in this experiment were removed from a missile guidance system and during testing they were powered up using compressed air.

### 2.3. Multirotor test platform

The base for testing the gyro stabilized mechanism was a custom Y6-configuration multirotor VTOL platform (Fig. 11 & 12). This allowed the gimbal to be mounted in front of the aircraft so that the spinning-mass mechanical gyroscope system

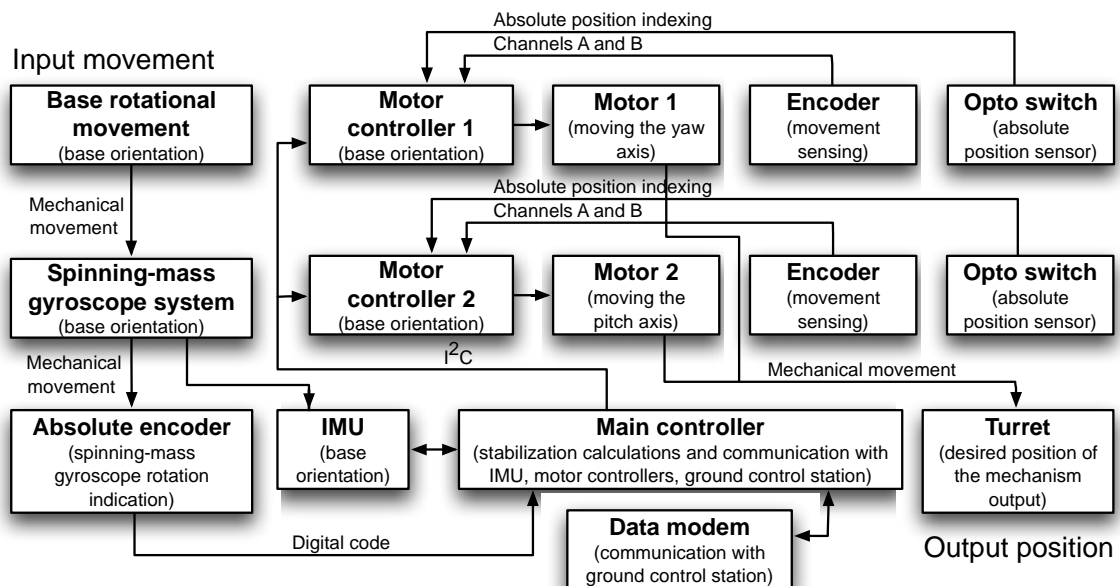


Fig. 9. Block diagram of system processes after implementing spinning-mass gyroscopes

pivoting point is at the same level with aircrafts rotational center (Fig. 13).



Fig. 11. Multirotor VTOL rotorcraft platform with gyrostabilized gimbal

#### 2.4. Results

The aircraft has a standalone flight controller which can also be used to log flight data. When this information was compared with the according data from the gimbal mechanisms IMU unit, it was seen that spinning-mass mechanical gyroscopes greatly reduced the amount of compensation amplitude that was necessary for the camera gimbals output shaft to remain level. Most of the base movements were canceled by the spinning-mass gyrosystem. Another advantage is seen when comparing the pre and after results of a CMOS block camera image. There was no rolling shutter artifact seen in the image, when the mechanical gyroscopes are used. CMOS sensors are

known to be very prone to vibrations and sudden sharp movements.



Fig. 12. Multirotor VTOL rotorcraft in test hangar

### 3. FUTURE DEVELOPMENTS

The proof-of-concept with this system was achieved. Future plans include gathering all the necessary data to develop the methodology and procedures to calculate exact parameters for the spinning-mass gyroscopes. Another important task is to construct customised driving motors for gyroscopes that allow constant and long operation. Finding the correct balance between the spinning masses and their angular velocities allows getting optimum overall mass and saves energy.

### 4. CONCLUSION

The objective of this study was to find a method to take advantage of synthetic inertia provided by spinning-mass

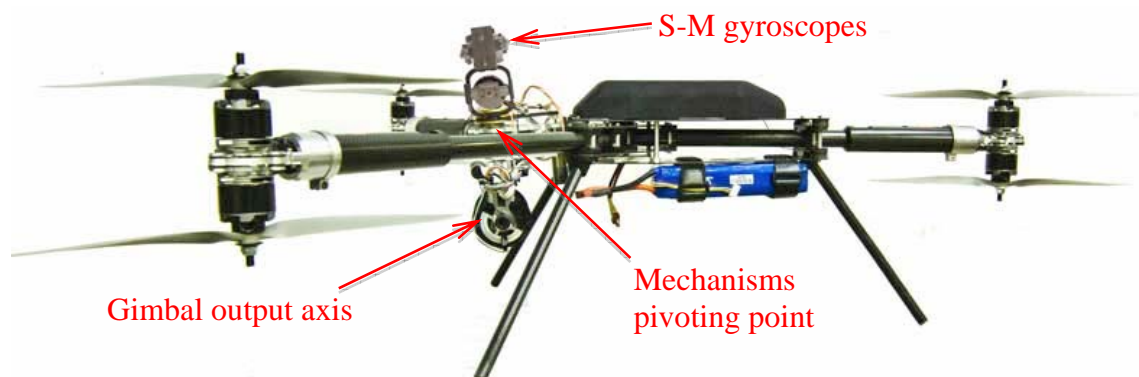


Fig. 13. Test equipment layout on the aircraft

gyroscopes to help in stabilizing a electro-mechanically gyrostabilized camera gimbal. The results were satisfying and the most significant part is the fact that there is no need to void the biggest advantage of multi rotor aircraft, which is being very lightweight and agile, by adding additional mass to the frame of the vehicle to cope in gusty weather conditions. Instead it is possible to modify the gimbal suspension type and use it in conjunction with spinning-mass gyroscopes to keep the gimbal level plus eliminate almost all vibrations. The fact that the gimbal is moving independently from the crafts frame allows to use smaller and lighter servomotors which are used to direct the used instrument to the desired position. This somewhat also compensates the mass of the mechanical gyroscopes. Additional research needs to be done.

## 5. REFERENCES

1. Tiimus, K. & Tamre. M. Camera Gimbal Control System for Unmanned Systems, Tallinn University of Technology, 2010
2. Ghosh, M. Moment of Inertia and Nutation of a Captured Gyroscope, The College of Wooster, 1998
3. Spinning Mass Mechanical Gyroscopes, US Dynamics Corporation, 2006
4. Nettmann, E.F. Comparison of Gyro-Stabilized Camera Mounts for the Motion Picture Industry, Nettmann Systems International, 2011

5. Guinamard, A. IGN-500A AHRS, SBG Systems, 2009
6. Merry, R.J.E., van de Molengraft, M.J.G. & Steinbuch, M. Velocity and acceleration estimation for optical incremental encoders, Eindhoven University of Technology, 2010

## 6. CORRESPONDING ADDRESS

MSc. Kristjan Tiimus  
 Department of Mechatronics, Tallinn  
 University of Technology  
 Ehitajate tee 5, 19086 Tallinn, Estonia  
 Phone: +372 5177186  
 E-mail: kristjan@helicam.ee

## 7. ADDITIONAL DATA ABOUT AUTHORS

- 1) MSc. Kristjan Tiimus, Prof. Mart Tamre
- 2) Title of Manuscript: Camera Gimbal Performance Improvement With Spinning-Mass Mechanical Gyroscopes
- 3) Full Address of all authors:  
 Kristjan Tiimus / MSc. / Department of Mechatronics, Tallinn University of Technology / Ehitajate tee 5, 19086. Tallinn, Estonia / kristjan@helicam.ee / +372 5177186  
 Mart Tamre / Prof. / Department of Mechatronics, Tallinn University of Technology / Ehitajate tee 5, 19086. Tallinn, Estonia / mart@staff.ttu.ee / +372 6203202
- 4) Corresponding Author: Kristjan Tiimus, Tallinn University of Technology, Ehitajate tee 5, 19806, Tallinn, Estonia

## DYNAMIC MOTION ENERGY EFFICIENCY MEASUREMENT OF GROUND VEHICLES

Väljaots, E. & Sell, R.

**Abstract:** *This work is investigating the key parameters of wheeled mobile ground vehicles focusing on the energy efficiency as optimization criteria. For this purpose the self-contained measurement system is being developed for key parameter acquiring. Also simple testing layout is needed for vehicle dynamic motion characterization. The testing results are used for simulation, development and improvement of vehicle platforms in their design stage.*

**Key words:** *mobile robotics, real-time measurement, vehicle dynamics, energy efficiency.*

### 1. INTRODUCTION

Mobile robots have become an ordinary application in civilian and military domain in recent years. Mobile robots can be either remotely controlled, autonomous or combination of these control schema. In general, mobile robot is often also called Unmanned Ground Vehicle (UGV), which is operating on different terrain. UGV's can be constructed in different moving abilities, which depend on tasks needed to perform and working environment. It is possible to construct mobile platforms with optimal performance in means of maximum efficiency for completing given tasks. As mobility needs limited independent power sources, energy management is the key factor to get maximum efficiency to complete tasks. Sufficient motion dynamics with maximum efficiency is one of the most important

construction factors in early design of UGV's. In this paper we are presenting a research about finding the key performance and efficiency measures for outdoor unmanned ground vehicle design. These parameters are used for mathematical model of particular design and simulations on early stage of product development.



Fig. 1. Example of mid-class UGV – UKU, considered as a test platforms.

The research is targeted to the mid-class UGV's and in particularly to the solutions developed in Tallinn University of Technology, Department of Mechatronics (Fig. 1.) [1, 2], and solutions developed in Finland, Aalto University [3] and Oulu University [4]. These solutions are considered as conceptual test platforms as they all have different locomotion solutions. According to these platforms, the efficiency parameters and mathematical models for four different concepts can be developed and also verified on real robots.

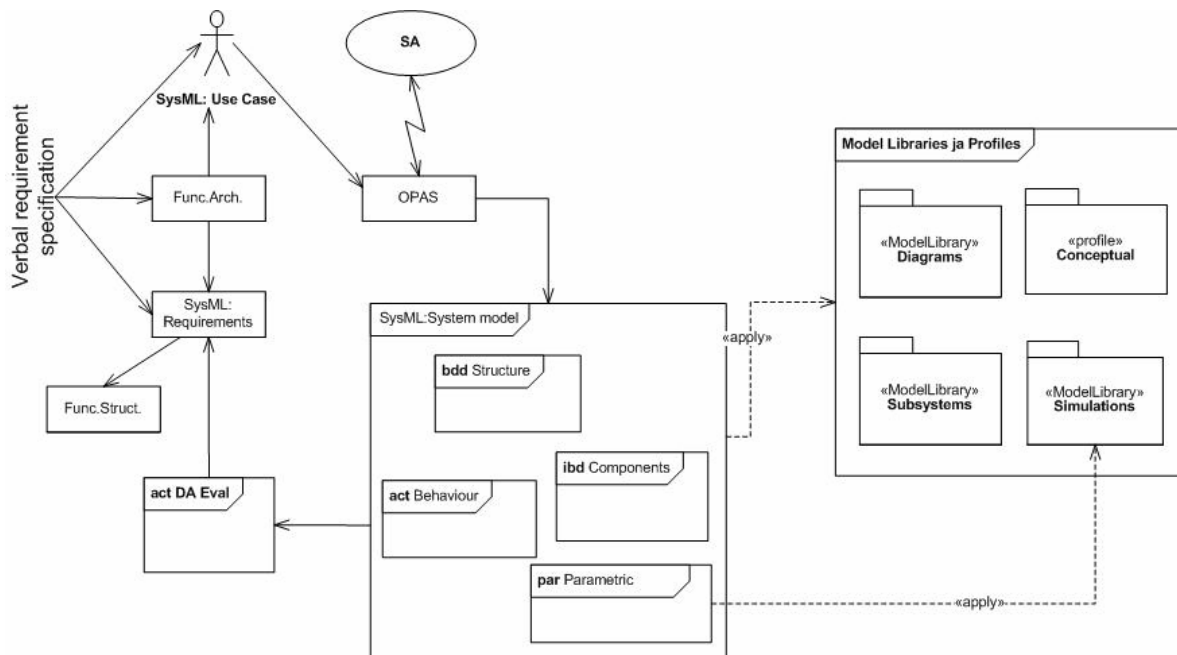


Fig. 2. Conceptual design framework schema supported by SysML.

In addition, this research also provides the measurement methodology described in more detail in research paper [5] and customized measurement device, presented in corresponding author's master thesis [6] to verify the parameters of unified design solutions.

## 2. FRAMEWORK

This work is a part of early design framework research [7] started on 2006 in cooperation of Finnish and German research institutions. The paper is focusing on the topic of different types of vehicles with goal of optimized dynamics and energy efficiency. Determining the optimal key parameters on very beginning of product design stage reduces significantly the product design cost [8] and helps to develop optimal conceptual solution for mobile robot locomotion system.

When a UGV is still in its specification phase, designer and manufacturer wish to perform an early evaluation of the requirements baseline before actually buying the physical hardware. Therefore simulation algorithms and database are needed, which are developed and verified on the different types of vehicles, starting

from conventional cars to hybrid mobile robots. The result of this research plays important role of verifying those mobile robot simulation algorithms and are used to develop autonomous navigation scenarios of robotic platforms. The early design framework is providing tools and methods for conceptual design stage by targeting to qualified and effective result of this stage. The result is a verified and optimal design solution concept reflecting the design requirements and taking into account the different aspects when comparing design candidate solutions. The general concept of the framework is shown in Fig. 2.

## 3. EFFICIENCY AND PERFORMANCE MEASURES

Generally vehicle efficiency can be expressed as a relation between output task and energy consumption [9] as the goal is to save power, but provide sufficient dynamics. Output task is travelled distance, operation time or covered area. Best efficiency cannot be met when operating at fastest velocity or with minimal covered distance, because it yields to high energy consumption. Besides moving mechanism,



there are other factors affecting overall efficiency.

Goal oriented dynamics and efficiency depends on vehicle mechanical movement system and electrical parameters:

- weight,
- power source,
- electric motors,
- transmission,
- rolling resistance;

vehicle piloting algorithms:

- handling,
- navigation planning;

environment:

- traction,
- resistive forces

and also given task.

As performance can be tested and scored, the performance measures for autonomous UGV's can be:

- speed,
- precision,
- style,
- criterion (success/fail),
- score of completed mission goals
- resource efficiency,
- cost efficiency.

UGV optimal performance depends on vehicle properties and piloting system properties [10]. UGV cannot be operated at higher dynamics than its maximum capabilities. Also piloted capability cannot be higher than vehicles maximum. If during test the vehicle capability equals piloted capability, then the robot is operated with optimal performance.

The performance of a system can also be measured by comparing it against some benchmark performance. For piloting capability (handling and navigation planning) the possible standard benchmark can be human performance. Comparable tests can be carried out easily when UGV rides through test autonomously or when radio-controlled by human operator.

In this measurement system, key parameters of wheeled robots focusing on the energy efficiency as design

optimization criteria, important output measures are:

- vehicle weight,
- travelling time,
- travelled distance,
- energy consumption,
- driving direction acceleration,
- traction (wheel slip),
- terrain roughness.

#### 4. UGV ENERGY EFFICIENCY KEY PARAMETERS ACQUIRING

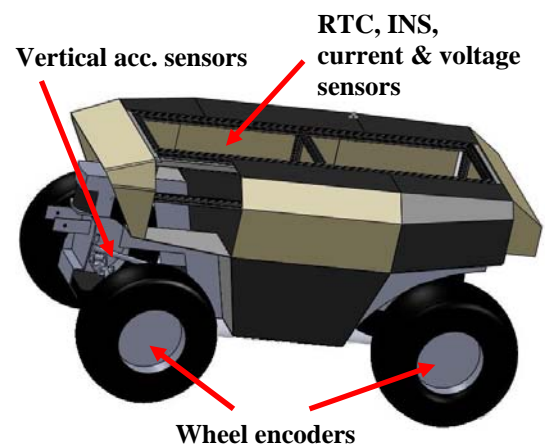


Fig. 3. On-board measurement system

For vehicle classification, it is weighted before testing. Constant weight is important for calculating vehicle energy efficiency as transmissions have different power losses.

Vehicle dynamic motion performance and energy efficiency during real-condition test can be measured using different sensors installed into UGV (Fig. 3) and analyzed with data processor. For this purpose specific measurement system is designed and developed by author.

Travelling time can be measured externally or internally inside vehicle. External system might be infrared laser based timing system installed into start and finish line of track. Better is self-contained system that calculates time with real-time clock (RTC) based on travelled distance using INS and wheel encoders.

The most important measure of dynamical performance is driving direction acceleration that can be measured at

minimum with inertial navigation system (INS) and speed or position can be calculated from integrations. That requires at minimum one-axis MEMS inertial acceleration sensor mounted into vehicle body on longitudinal direction.

Because of INS cumulative error, this is only acceptable on short testing tracks being couple of hundred meters long. This can be easily improved with wheel shaft encoders, which run incremental odometer. As wheel encoders are affected from wheel slipping, they should be mounted only to free wheels. In case of all-wheel drive vehicles, wheels speeds must be compared, but even though wheel slipping is hard to detect. For long tracks, data fusion with GPS enables to keep uncertainty invariable during time.

Important factor for early design and simulation of wheeled robots is sufficient traction planning. Too much traction capability (heavy duty tires or caterpillars) adds considerable rolling resistance and therefore reduces energy efficiency. Wheel slipping can be measured during driving with wheel encoders and detected by comparing free wheel and driving wheel speeds. This is difficult in all-wheel drive vehicles. Problem can be solved using redundant wheel encoders or very precise motor current measurements. Another good possibility is to detect external forces resisting motion while analyzing longitudinal acceleration data [11]. Because in this measurement system longitudinal acceleration is already being detected and measured with INS, this is possible. Wheel slip can be detected if wheel encoder shows higher acceleration than inertial sensor.

For energy efficiency estimation, total current consumption and battery voltage must be measured in battery management system. Total resistive forces are expressed in current consumption and from efficiency point of view, there is no need to know them separately.

Test results are also affected of tracks being used. Driving paths in especially off-

road tracks are difficult to repeat. Therefore testing track terrain on driving trajectory must be classified. In its simplest form, terrain characterization can be carried out when human observers are subjectively scoring the difficulty of the terrain. Advanced terrain measures can also be made with high-resolution 3D lidar. However, quite simple, accurate and cost effective way is to measure terrain profile while driving with vehicle. Therefore terrain parameters must be measured during driving as a vehicle response [12]. Most methods are based on vehicle body vertical acceleration measurements, but more accurate results can be made with MEMS acceleration sensors mounted on vehicles wheels turning axles, which enables to exclude suspension effects (Fig. 4.) [13]. Similar method has shown good results when tested on cars for purpose of pavement roughness analysis in Englo LLC.

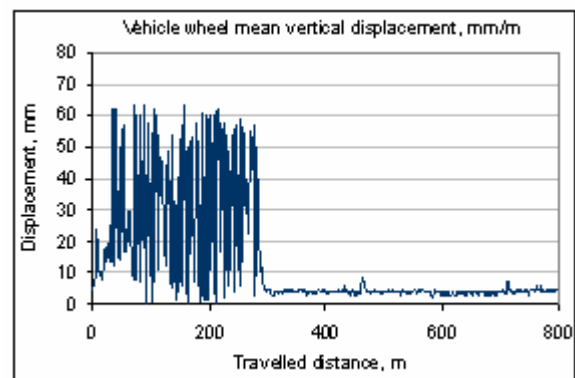


Fig. 4. Terrain profile measurements with light vehicle at speed 10 m/s, driving from rough to smooth concrete pavement.

## 5. TEST METHOD

Simple test is an exam exercise, consisting from a simple task. For comparability, the test should be as elementary as possible. The simplest test is to navigate through straight 200 m long track.

To develop a relation between track conditions and vehicle configuration, different tracks with same length are needed. Higher dynamics can be achieved in smooth concrete pavement road, but



different movement mechanisms are needed in rough land terrain when conditions are hard and track has obstacles. UGV's must be able to provide stable controllability on whatever terrain they may encounter. In real mission conditions UGV might begin an assignment on asphalt but quickly be required to negotiate sand, mud or snow.

As the capability of the different UGV's is different, the test results of the UGV's cannot be straightforwardly compared. Passing through track can be much easier to a tank than lawnmower sized robot. For availability of usable UGV's, it is best to stick in mid-sized robots, like UKU in TUT, which can be compared with other similar light vehicles.

For mechanical and transmission design optimization, piloting capability must be excluded. Conversely, when vehicle design is kept the same, piloting capability can be measured and compared. However, for robot movement optimization in this testing method, piloting effect is kept as low as possible. With different UGV's and vehicles, this is achievable only with human direct- or radio-controlled driving.

Most important performance measures (Fig. 5) that can be acquired in testing are travelling time versus energy consumption. As these are adverse parameters, optimal design improvement solutions can be found between. For wheel and transmission design mapping, it is also useful to measure traction, which enables to detect presence of mud and snow. In parallel, track terrain roughness is measured during driving for complete track characterization. Based on output data, specific energy and "tank-to-wheel" energy efficiency can be calculated to all vehicles on different terrains. If energy consumption is measured and converted into units (MJ) per testing distance, "tank-to-wheel" efficiency can be expressed in units of (km/MJ). If vehicle mass is a constant parameter, specific energy can be expressed in units (MJ/kg).

From key parameters, additional secondary indicators can be found, like effective power etc. Test results will also be compared with simulation results, which enables to evaluate the simulation models.

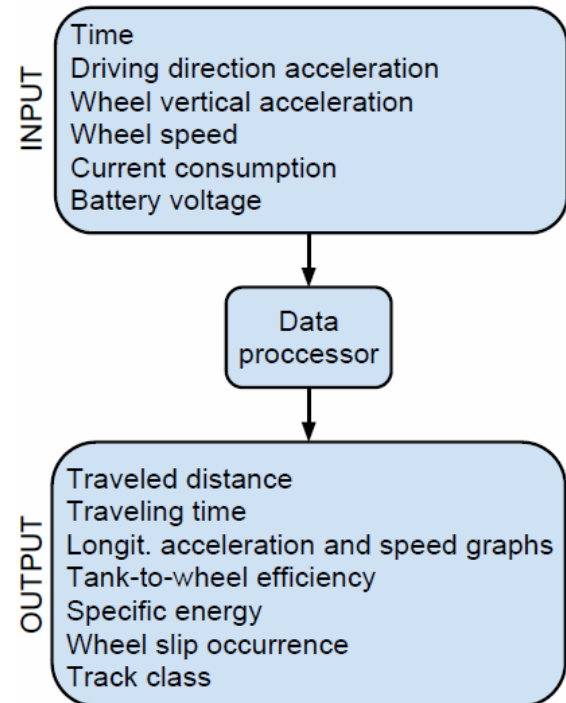


Fig. 5. Measurement system input and output.

As the levels of uncertainty are sensors outputs and their calibration, the data processing algorithms and the interactions of environment and vehicle, driving tests can be carried out with good repeatability when certain important conditions are met. Usually repeatability with (1 – 2) % deviation is achievable on concrete pavement tracks.

## 6. CONCLUSION

The paper summarized mobile robot locomotion system key performance parameters in terms of energy efficiency. Using quite simple measurement system, important parameters from efficiency point of view can be acquired during real-condition tests on different terrain tracks. As vehicle response to track is important, track profile is also recorded. Therefore several UGV's dynamics on different

tracks can be tested and compared. Test data is useful for simulation verification and characterized hardware database for development of energy efficient UGV's.

## 7. ACKNOWLEDGEMENT

This research was supported by funding of the Estonian Science Foundation grant No. 8652 and by Englo LLC.

## 8. REFERENCES

1. Research report of ETF Grant 8652, Tallinn, 2011.
2. Sell, R., Leomar, P. *Universal Navigation Algorithm Planning Platform for Unmanned Systems*. In: Proc. of International Conference Mechatronic Systems and Materials: Vilnius, 2009.
3. Halme, A., Leppänen, I., Suomela, J., Ylönen, S. and Kettunen, I., *WorkPartner: Interactive Human-like Service Robot for Outdoor Applications*, The International Journal of Robotics Research, 2003, **22** (7-8), 627-640.
4. Tikanmäki, A., Röning, J., *Development of Mörri, a high performance and modular outdoor robot*, International Conference on Robotics and Automation, Kobe, Japan, May 12 - 17, 2009, 1441-1446.
5. Väljaots, E., Sell, R., *Measurement Method and Device for Vehicle Dynamics*. In: Proceedings of the 7th International Conference of DAAAM Baltic Industrial Engineering, Tallinn, 2010, 536 - 541.
6. E. Väljaots, *Device for measuring vehicle dynamics*. Tallinn University of Technology, M.Sc. thesis, 2009.
7. Christophe, F., Sell, R., Bernard, A., Coatanea, E., *OPAS: Ontology Processing For Assisted Synthesis*. In: Proc. of the ASME 2009 International Design Engineering Technical Conferences & Design Automation Conference, San Diego, USA, 2009.
8. Sell R., Coatanea E., Christophe F. *Important aspects of early design in mechatronic*, 6th International Conference of DAAAM Baltic Industrial Engineering, Tallinn, 2008
9. Shahab, M. *Energy-Efficient Motion Control of Mobile Robots*. King Fahd University of Petroleum & Minerals, 2009, EE 656, Term 081.
10. van Diggelen, J. Looije, R. Mioch, T. Neerincx, M.A. Smets, N.J.J.M. *A Usage-Centered Evaluation Methodology for Unmanned Ground Vehicles*. 5<sup>th</sup> International Conference on Advances in Computer-Human Interactions, Valencia, Spain, 2012.
11. Iagnemma, K. Ward, C.C. *Classification-Based Wheel Slip Detection and Detector Fusion for Mobile Robots on Outdoor Terrain*. Autonomous Robots Springer, 2009, **26**, 33-46.
12. DuPont, E.M. Moore, C.A. Collins, E.G, Coyle, E. *Frequency Response Method for Terrain Classification in Autonomous Ground Vehicles*. Autonomous Robots, Springer, 2008.
13. Harris, N.K. Gonzalez, A. O'Brien, E.J. McGetrick, P. *Characterization of Pavement Profile Heights Using Accelerometer Readings and Combinatorial Optimization Technique*. Journal of Sound and Vibration, Elsevier, 2010, **329** (5), 497-508.

## 8. ADDITIONAL DATA ABOUT AUTOHORS

M.Sc Eero Väljaots, Ph.D student  
TUT, Department of Mechatronics  
Ehitajate tee 5, 19086 Tallinn, Estonia.  
Phone: +372 56506528  
E-mail: eero.valjaots@gmail.com

Ph.D Raivo Sell, senior researcher  
TUT, Department of Mechatronics  
Ehitajate tee 5, 19086 Tallinn, Estonia.  
Phone: +372 6203201  
E-mail: raivo.sell@ttu.ee

## OPTIMIZING AEROSOL JET® PRINTING OF SILVER INTERCONNECTS ON POLYIMIDE FILM FOR EMBEDDED ELECTRONICS APPLICATIONS

Verheecke, W.; Van Dyck, M.; Vogeler, F.; Voet, A., Valkenaers, H.

**Abstract:** *The Aerosol Jet® Printing (AJP) process is a fine feature sub-micron scale deposition process. The paper discusses the optimization of AJP in order to achieve the desired quality of printed silver ink interconnects on polyimide film for embedded electronics applications. A process window containing the parameters which have influence on the quality aspects of the printed tracks is determined to obtain the optimal quality. Important quality aspects in this research include the geometrical and electrical properties of the printed tracks and also the adhesion of these tracks on the substrate. The geometrical properties are determined by optical image processing and profile analysis. To measure the electrical parameters a micro 4-point probe measuring system is used.*

*Key words: Aerosol Jet® Printing, optimization, interconnects.*

### 1. INTRODUCTION

The production of multifunctional, customized products is getting more and more important these days. Additive Manufacturing (AM) and in particular, the Direct Writing (DW) methods (a subcategory of AM), are very suitable for producing these kind of products. DW techniques have the ability to write or print parts with sub-micron features (e.g. electronic circuits with including conductors, insulators, batteries, antennas, capacitors, etc.) directly from a Computer Aided Design (CAD) file without requiring any pre-processing steps like tooling or

mask preparation. This is because DW technologies deposit a material and building a part layer by layer. The AJP process belongs to the droplet-based DW techniques [1], and is based on a carrier gas that provides kinetic energy for the deposition of a material. In our research AJP is used for printing silver interconnects on polyimide substrates. This paper discusses a quantitative method for determination of the process window consisting a set of parameters which will provide good line quality.

### 2. AEROSOL JET PRINTING PROCESS

#### 2.1 Advantages of AJP technology

The AJP process was originally developed for manufacturing customised micro-electronics. The process is becoming an alternative for thick-film processes and printing processes, such as screen-, stencil- or inkjet printing. This last technology is the closest related to AJP, although AJP allows smaller print resolution, the deposition of material on non-planar substrates and larger nozzle to substrate distance compared to inkjet. Therefore AJP is generally more flexible than other printing processes and is ideal for manufacturing 3D conformal electronics. [2]

Due to its larger viscosity range (0,7 to 2500 mPa.s) AJP allows the deposition of different ink (or ink-like) materials; e.g.: metal-inks, polymer thick film pastes, diluted ceramic powder or epoxies. [3, 4] [5] Those are the reasons why AJP is

becoming a promising technique in the printed electronics industry, with a broad application area including flexible electronics, embedded components (interconnects, resistors, sensors), EMI shielding, flexible displays and solar cells.

## 2.2 Working principle

The principle of aerosol deposition with its process control module (PCM) parameters is shown in Fig. 1. The basic AJP system consists of two important key components: the atomizer and a focussing module in the nozzle. Inks with a viscosity range of 1 to 1000 mPa.s and particle size up to 500 nm can be atomized by a pneumatic atomizer. This type of atomizer uses a high velocity gas stream to generate the aerosol. The aerosol droplets are then transported through the virtual impactor (VI). The ultrasonic atomizer which uses an ultrasonic transducer for generating the aerosol is suited for inks with a viscosity range of 0,7 to 30 mPa.s and small solid particle size of maximum 50 nm. This type of atomizer does not need a VI.

After the aerosol is generated in the atomizer (1) and passes through the VI (2) the print head (3) focuses the aerosol into a concentrated beam by adding a concentric mantle of sheath gas (4) around the aerosol. The focused aerosol stream is directed by the sheath gas to the substrate. By using a sheath gas the aerosolized droplets remain tightly focused over a distance typically from 3 to 5 mm, giving AJP the ability to print over uneven substrates.

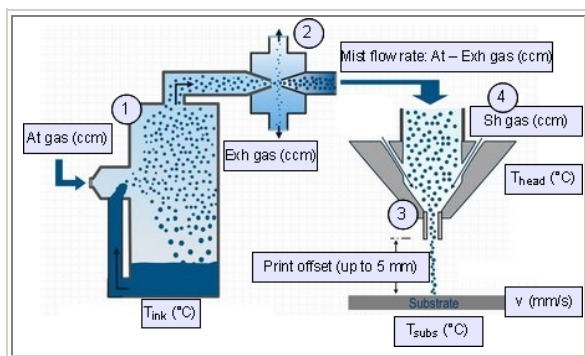


Fig. 1. Aerosol Jet® Printing with pneumatic atomizer [6]

Pre treatment of the substrate include thorough cleaning to reensure a constant wettability of the deposited material over the entire surface.

## 2.3 Influential parameters of the line width

There are a lot of influence factors which will affect the quality of the printed lines. (see Fig. 2.) In particular, the substrate/ink combination, the process settings of the Aerosol Jet system, the number of layers, as well as the relative speed between substrate and print head are relevant to printing quality. [7]

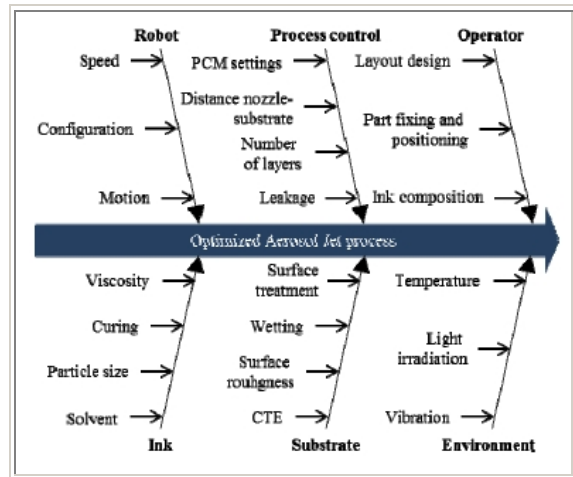


Fig. 2. Factors of influence for the Aerosol Jet® system [7]

The width control of the aerosol beam and thus the line width of the deposited line are controlled by various parameters. The most important PCM parameters are the aerosol gas flow rate, exhaust gas flow rate at the VI, the sheath gas flow rate, the ink temperature and viscosity, the nozzle diameter, the print head temperature and the nozzle to substrate distance (print offset).

The mist flow rate will affect the output rate of material, and thus the line width. The sheath gas flow rate has a smaller influence on the line width. Line width increases with greater print offset. More narrow and higher lines can be obtained by altering the ink formulation (higher viscosity, faster drying, increased

surface tension between ink and substrate) or by altering PCM parameters.

A raise of the ink temperature decreases the output rate thus influences the line width. Increasing print head temperature partially dries the aerosol prior to printing, resulting in narrower printed lines. Excessive drying of the aerosol leads to poor print quality (interruption of the printed line) and could eventually block the nozzle. Slightly reducing the mist flow rate in conjunction with heating the print head results in even narrower printed lines. [8]

#### 2.4 Influence parameters on overspray

Fig: 5. left shows an example of overspray. This phenomenon is usually caused by the smallest droplets in the aerosol. Overspray can be controlled by adjusting some of the AJP settings such as: the atomization gas flow rate, the sheath gas flow rate and the print offset, or by adjusting the ink formulation. [9] To minimize overspray, flow rates (most importantly atomization flow rate) may not be too high.

Excessive overspray occurs when sheath gas flow rate and print head temperature are set too high. Both will cause excessive drying of the aerosol ink, which will also influence the overspray.

An often underestimated influential parameter on the line quality is the cleaning strategy of the substrate. The surface preparation of the substrate affects the surface tension and thus the wettability. A low surface energy substrate will cause less wetting, which results in a bigger contact angle, changing the topography of the printed lines. (See Fig. 3.)

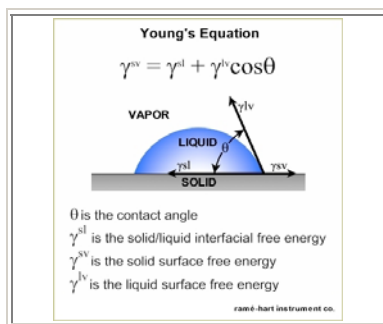


Fig. 3. Contact angle and surface energy [10]

Consistent printing of ink with the Aerosol Jet® System requires a consistent surface, not only because of the proper surface energy of the substrate but also because of the increased possibility for contamination such as oils, fingerprints, dust and atmospheric absorbed materials.

#### 2.5 Post-processing of deposited lines

In a post-processing step the deposited lines are sintered, this is almost always carried out to improve the mechanical and electrical properties of the printed material. [11] The choice of sinter temperature and time is based on the ink and substrate. The conductivity of the CSD-32 ink from Cabot, used for our experiments, in function of the sinter temperature during a sinter time of 30 minutes is examined, the results are shown in Fig. 4 [12].

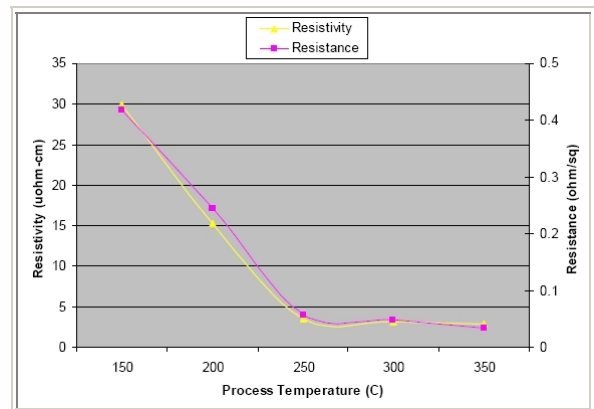


Fig. 4. Electrical properties of Aerosol Jet printed traces on glass, 30min. cure time [12]

### 3. OPTIMIZATION OF AJP FOR SILVER INK

#### 3.1 Preliminary research

As explained in paragraphs 2.3 and 2.4 a lot of influence factors determine the printed line width and quality. It is therefore difficult to determine a proper process window which will provide the desired line width and line quality. A preliminary research was set up to have an overview of the process window consisting parameter combinations. A literature review and information of our

machine supplier (Optomec®) provided a first set of parameters for performing a preliminary research. Good print results were obtained for atomization flow rates (At gas) of 500 to 1000 ccm, mist flow rates of 10 till 25 ccm (atomization minus the exhaust flow rate (Exh gas)), ink temperatures ( $T_{ink}$ ) of 15 to 30 °C, print head temperatures ( $T_{head}$ ) of 20 to 80 °C, print speeds ( $v$ ) of 1 to 20 mm/s, print offset of 1 to 5 mm, temperatures of the substrate ( $T_{subs}$ ) of 60 to 90 °C and sheath gas flow rates (Sh gas) dependant on the setting of the atomization gas. [13]

The used CSD-32 ink consists of silver nanoparticles (size < 60 nm and wt% of 45-55) with a polymer coating, dispersed in a glycol solvent. This ink was printed onto untreated LCD glass plates with a 150  $\mu$ m nozzle diameter. (see Table 1)

For each setting five lines were printed.

At gas (ccm)	Sh gas (ccm)	Mist flow (ccm)
550-800	20-110	20-40
Nozzle ( $\mu$ m)	$T_{subs}$ (°C)	Print offset (mm)
150	80	3
$T_{ink}$ (°C)	$T_{head}$ (°C)	$v$ (mm/s)
22-37	22-37	1-5-10

Table 1. PCM parameters of the preliminary research

For the determination of a rough process window for good line quality, three images of every five lines were taken with the alignment camera and a general quality attribute from 1 to 10 was given to these images. (see Table 2) An example of a few quality attributes are given in Fig. 5.

1	bad, no adhesion
2	bad, big droplets
3	moderate, enough adhesion
4	moderate, less big droplets
5	moderate, overspray
6	moderate, too fluent (wavy)
7	moderate, stains/discontinuous
8	good, soft stains
9	good, too fine
10	good, fine (edge!)

Table 2. General quality attributes

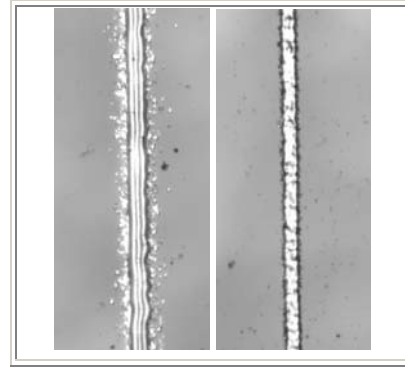


Fig. 5. Examples quality attribute 5-moderate (left) and 10-good (right)

This rough line quality determination gave a first impression of the process window. (see Fig. 6.) Although this process window is quite broad, it provided a good starting point for the set-up of further qualitative analysis and process optimization.

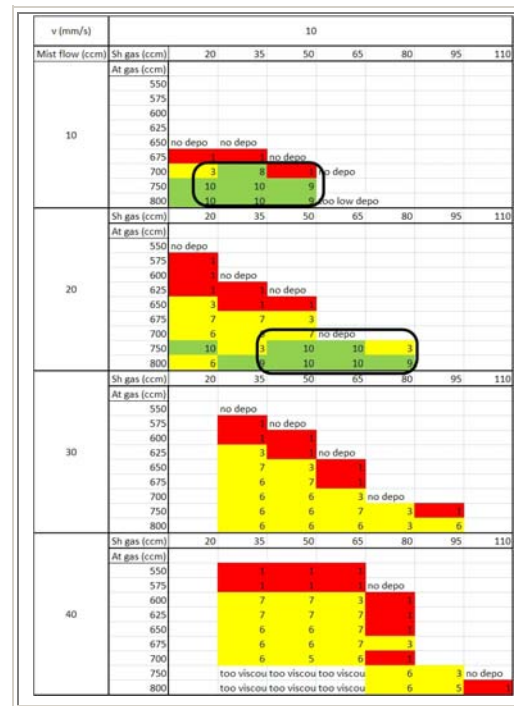


Fig. 6. Rough line quality determination of a broad PCM parameters range

### 3.1 Preliminary tests for resistivity and profile analysis

Besides the determination of line quality, the resistivity and cross section of the printed lines has to be defined for electrical property quantification.



Electrical resistivity measurements were performed with a micro-4-point-probe (M4PP). For these measurements a circuit was designed. (see Fig. 7.)

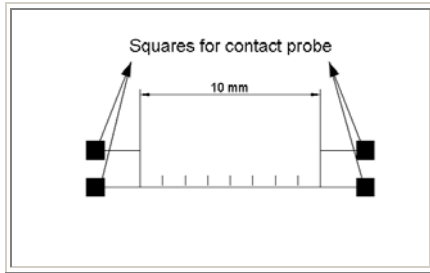


Fig. 7. Circuit for printing and measuring with M4PP

The circuit was printed with CSD-32 ink (also used in the previous tests) on glass which was treated with acetone for 10 min. at 40 °C, and then cleaned with IPA sonication for 5 min.. Because the contact probes of the M4PP damaged the printed silver ink squares, our M4PP system was not suited for measuring these samples. Samples printed on polyimide tape would give better adhesion and resistance measurements could be performed. The set-up PCM parameters for samples printed on polyimide are given in Fig. 8. top. The polyimide tape was attached to a glass plate to provide a flat surface, and was treated with the same cleaning strategy as the previous experiment. Using a micro profile tracker the cross section of the printed lines was measured. (see Fig. 8. bottom) The best sample had a calculated resistivity of 72  $\mu\Omega$ -cm.

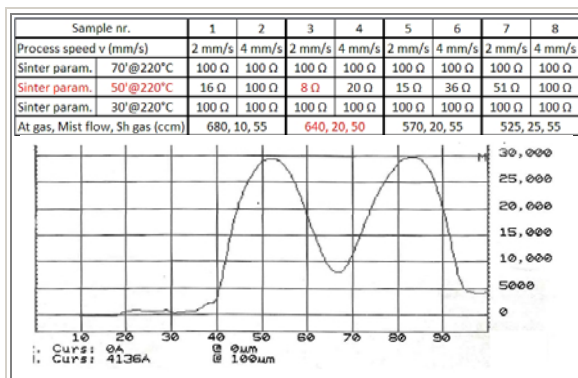


Fig. 8.  $\Omega$ /10mm values per PCM parameter (top); profile of best sample of 8  $\Omega$ /10mm (bottom)

According to Cabot's datasheet the expected resistivity value for this ink is normally ten times less. (see Fig. 4.) The quality analysis using quality attributes 1 to 10 based on pictures taken with the alignment camera appeared to be insufficient for determining a good process window. A more profound analysis was therefore needed.

### 3.1 Quantitative analysis with vision based 2D quality control

The preliminary research using an analysis based on quality attributes gave a broad range of parameter combinations. Therefore succeeding research was needed. This research started from the best PCM parameters selected in the preliminary research and new samples were printed with these settings. Five lines of 10 mm were printed for each PCM setting and every 3 mm an image of  $\pm 0,5 \text{ mm}^2$  was taken along each line. A more profound 2D quality control for quantitative analysis was then set-up.

The line width, the overspray and satellite droplet detection and smoothness of the track were measured on these images. An own-written edge detection algorithm was used to automatically detect zones. (see Fig. 9.)

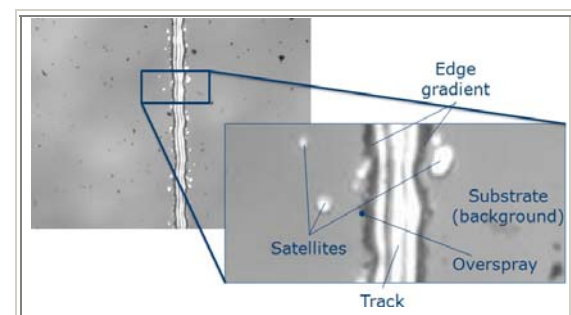


Fig. 9. Different zones of edge detection using maximum gradient greyvalue

Defining the track edges was a first step towards analyzing the track. Based on this data, the line width of the track could be calculated and an analysis of the edge could be made. The different steps consisted of reducing the search zone for the edge, using the gradient of edge as a



start position of search and finding the left and right edge based on maximum gradient principle.(see Fig.10).

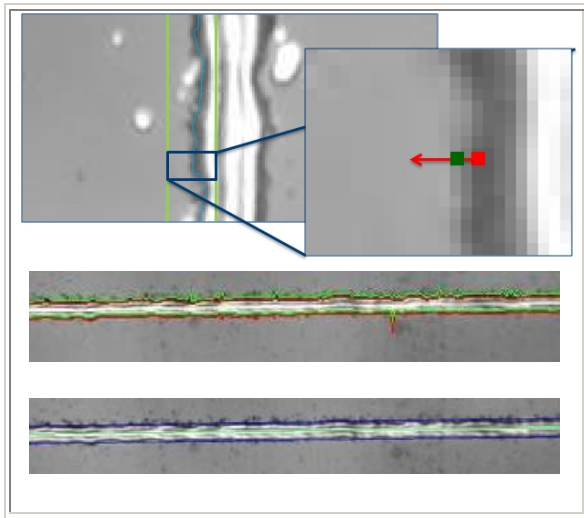


Fig. 10. Gradient of edge (top); samples of edge detection algorithm (bottom)

The line width determination was performed by fitting (Gaussian) a line through the left and right edge. The symmetric line was then calculated and the mean distance left and right to the symmetric line was calculated.

The track edge smoothness was defined by fitting a line through both left and right edge. The smoothness of the edge was calculated by using the shortest distances between edge and fitted line. (equation 1)

$$Es_a = \frac{1}{L} \sum_{i=1}^n |z_i| \quad (1)$$

In equation (1) the shortest distances to the fitted line are represented by  $z$ . The total length of the line is represented by  $L$ . The calculated edge smoothness is represented by  $Es_a$ .

Faulty measurement sometimes occurred but these pictures and extreme data were filtered out manually. An edge detection fault can occur, the bulging effect can influence the line width measurement and the edge determination is sometimes not optimally separated from the overspray zone.

#### 4. DETERMINATION OF THE DETAILED PROCESS WINDOW

For determination of the process window, line width and edge smoothness is used. The line width of the printed lines and relative edge smoothness (the smoothness of the edge divided by the line width in  $\mu\text{m}$ ) are plotted in a 3D scatter graph using the AJP gas flow rates in the X, Y and Z axis. The line width is represented by the size of the sphere were a tenth of the nozzle's diameter is the nominal value and smallest sphere size. The relative edge smoothness is represented by a colour compared to the colour legend. (see Fig. 11.)

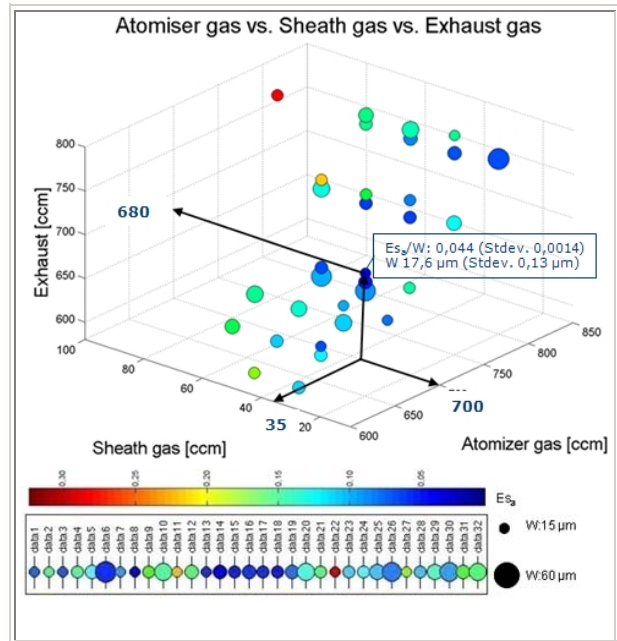


Fig. 11. 3D scatter graph with as best result  $Es_a/W$  of 0,044 (Stdev. 0,0014) and  $W$  of 17,6  $\mu\text{m}$  (Stdev. 0,13  $\mu\text{m}$ )

The results with the smallest line width (17,6 $\mu\text{m}$ ) and best relative edge smoothness (0,044) seemed to be also the best line quality of all the printed silver lines. The PCM parameters were: At gas of 700 ccm, Exh gas of 680 ccm and a Sh gas of 35 ccm. The parameter combination for optimal quality can thereby be selected using this edge detection algorithm for further optimization of the AJP process.

## 5. FUTURE WORK

Further optimization of AJP silver ink lines will be done for better determination of the process window. A profile analysis and resistivity measurement will be done of printed samples with PCM parameters of the optimized zone in the 3D graph.

Future research work concerning the algorithm will be set-up to put more intelligence in the edge determination. Other important quality attributes are track interruption, bulging and zone detection within a track.

## 6. CONCLUSION

After a preliminary research using a rough quality control method based on images, a more profound research was set up to determine the parameter combination for optimal quality. The glass substrate was replaced by polyimide tape to improve attachment and different characteristics of the printed lines were measured and used to setup a quality analysis tool. The line width and smoothness of the edge are measured with the aid of a vision system. Based on these measurements a 3D scatter plot is generated and used for determining a process window where good line quality is achieved, further optimization is still required.

## ACKNOWLEDGEMENTS

The authors acknowledge the support of the IWT in the framework of the EraSME 3DAMEEA project PO7810-EUR-ERA-01

## 7. REFERENCES

[1] Hon, K.K.B., Li, L. and Hutchings, I.M. Direct writing technology—Advances and developments. *Annals of the CIRP-Manufacturing Technology*, 2008, **57**, 601-620.  
[2] Watson, S. Aerosol Jet® Printed Electronics Overview, New Mexico (Albuquerque) USA, [WWW] <http://www.optomec.com> (02.03.2012)

[3] Hedges, M. 3D MID Manufacture via the M3D Process. In *Proceedings of the 8th International Congress Molded Interconnect Devices*, Nuremberg Fuerth, Germany, September 24.-25. 2008.

[4] Akedo, J. Microstructure of ceramic thick film formed by aerosol deposition and its applications to microactuator. *Integr. Ferroelectr.*, 2006, **1**, 55-65.

[5] Brose, M. et al. Aerosol Deposition of Catalytic Ink to Fabricate Fine Pitch Metallizations for Moulded Interconnect Devices (MID). In *Electronic System Integration Technology Conference (ESTC)*, 2010, 1-4.

[6] Folgar, C.E. et al. Solution-based aerosol deposition process for synthesis of multilayer structures. *Materials Letters*, 2011, **65**, 1302-1307.

[7] Goth, C., Putzo, S., Franke, J. Aerosol Jet Printing on Rapid Prototyping Materials for Fine Pitch Electronic Applications. In *Electronic Components and Technology Conference (ECTC)*, 2011, 1211-1216.

[8] King, B.H. et al, Characterizing Aerosol Jet® Multi-Nozzle Process Parameters for Non-Contact Front Side Metallization of Silicon Solar Cells. In: *Photovoltaic Specialists Conference (PVSC)*, 34th IEEE, 2009.

[9] Grunwald, I. et al. Surface biofunctionalization and production of miniaturized sensor structures using aerosol printing technologies. *Biofabrication*, 2010, **2**, 014106.

[10] Contact angle [WWW] <http://www.ramehart.com/contactangle.htm> (02.03.2012)

[11] O'Reilly, M and Leal, J. Jetting Your Way to Fine-pitch 3D Interconnects. In: *Chip Scale Review*[online], September-October 2010, 18-21.

[12] Cabot Printed Electronics Materials, Datasheet CSD-32 Cabot Fine Particle Silver Ink.

[13] Optomec Inc. Aerosol Jet Deposition System Manual, Albuquerque, 2010.

## CONTACT

**Ing. Wesley Verheecke MEng. - Manufacturing Engineering**  
Lessius Mechelen University College | Campus De Nayer  
Faculty of Industrial Engineering Sciences – Manufacturing Engineering (K.U.Leuven Association)  
Jan De Nayerlaan 5 | 2860 Sint-Katelijne-Waver | Belgium  
Tel + 32 15 31 69 44 | Fax + 32 15 31 74 53  
[wesley.verheecke@lessius.eu](mailto:wesley.verheecke@lessius.eu)

## DEVELOPMENT OF TRACKING SYSTEM FOR SATELLITE GROUND STATION

Winter, E.; Dahl, J.; Nordling, K.; Praks, J.; Kiviluoma, P.; Kuosmanen, P.

**Abstract:** *A satellite, in this context, is a man-made object that orbits around the earth. Aalto-1 is the first Finnish satellite and its design follows the popular CubeSat nanosatellite standard. The Aalto-1 is designed to use S-bandwidth which is not typical in small size satellites. To handle the communication with such a small satellite orbiting the earth, a ground station with an accurate tracking antenna is needed.*

*In this paper we present ideas how to design, build and calibrate a low-cost and simple S-band satellite tracking system for educational purpose. The goal was to achieve a tracking accuracy better than one degree.*

*Key words: ground station, S-band, pointing calibration, helix antenna, nanosatellite*

### 1. INTRODUCTION

At this very moment hundreds of satellites in all sizes are orbiting and observing the earth and giving navigation and weather information. Aalto-1 is the first Finnish satellite and its design follows the popular CubeSat nanosatellite standard. The dimensions of the satellite are 340x100x100 mm. One of the main payloads is a spectrometer which takes pictures of the earth in different wavelengths [1]. Because of the large data-packages sent from the spectrometer the satellite needs a high speed wireless connection to the ground station. The Aalto-1 is designed to use S-bandwidth that ranges from 2.4 GHz to 2.5 GHz which is not typical in small size satellites. To

handle the communication with such a small satellite orbiting the earth, a ground station with an accurate tracking antenna is needed, to communicate with the satellite while it passes over the station.

Highly directional antennas are getting more and more popular on satellites because of the need for massive amount of data-transfer [2]. This affects the ground station design so that a highly accurate pointing calibration method is needed. An accurate mechanical structure should also be designed to make this possible. For pointing calibration on S-band frequencies one can use radio objects in the sky e.g. radio galaxies, remains from supernovas or the sun as reference. A problem with highly directional antennas is the side lobes from the antenna which are getting power from surrounding environment. Most of the wireless disturbance around us is in the S-band frequency range and S-band antennas can pick up disturbance from these sources. Another method for calibration is to use an optical device to track the sun. This method can be sensitive for weather and there is inaccuracy caused by the atmosphere. Light scatters and refracts in the atmosphere so that the sun's position is not actually where it is observed. The refractions are zero at zenith and increases to about 0.6 degrees when watching the horizon [3]. Therefore the calibration should be executed when the sun is as high in the sky as possible.

In this paper we present ideas how to design, build and calibrate a low-cost and simple S-band satellite tracking system for educational

purpose. This system consists of an antenna connected to a computer controlled rotating actuator, attached to a mast. The design of the mast has to be lightweight but strong enough to hold the wind load from the antenna. To make the ground station more versatile the mast has to be compatible with different kind of antennas. The goal was to achieve a tracking accuracy less than one degree. To test the accuracy of the ground station, signal strength from several tracked satellites can be measured.

Different pointing accuracy calibration methods are evaluated to see which method would provide the most accurate calibration. The aiming accuracy depends mostly on the mechanical structure where the antenna is attached and on the calibration of the antenna. It is not possible to compensate for the displacement caused by wind load on the mechanical structure since it is a varying load. Therefore the mechanical structure has to be rigid enough not to deform under high wind load. A storm in Finland is defined for wind speeds over 20 m/s [4]. A wind load of 31 m/s was used for a safety margin. Higher wind speeds have been measured in Finland but designing the mechanical structure for higher values is not reasonable since it would add unwanted weight to the structure.

## 2. METHODS

### 2.1 Structure

The ground station consists of an antenna connected to a computer controlled rotating actuator, attached to a mast. The aiming accuracy of the mechanical structure can be improved by making the structure stiff enough to reduce displacement caused by wind load on the antenna. By examining current solutions and their features one could by brainstorming choose between the different features and finally make a design that would suit this project. A three legged design (Fig. 1) was chosen since it is both simple and stable. To ensure adequate

stiffness on the mechanical structure for the ground station a FEM analysis was performed.

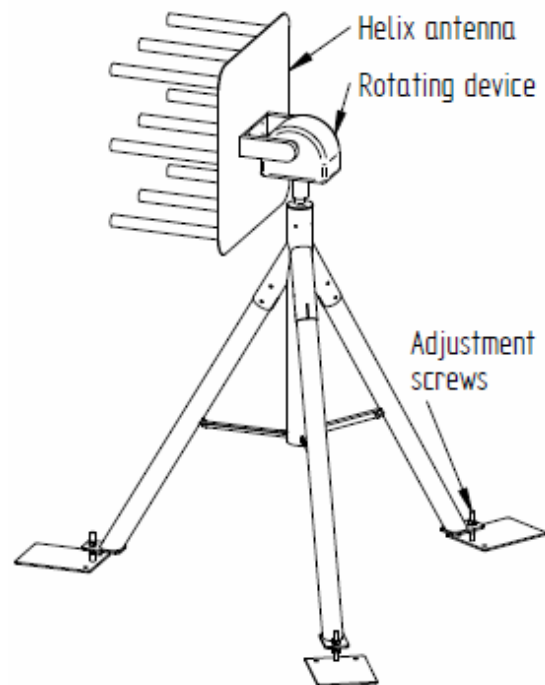


Fig. 1. The mechanical structure of the ground station

The mechanical structure was also designed to be adjustable. This makes it possible to compensate for inaccuracy from small manufacturing errors. All of the legs on the mechanical structure have adjustment screws. This makes it possible to tilt the vertical centre axis of the mechanical structure. Both rotating axes on the rotating device are also adjustable.

The rotating device is an azimuth and elevation rotator. It is possible for the rotator to turn around two axes, the azimuth and elevation axis. Azimuth is the angular measurement for turning along the horizon and elevation is for the height above the horizon. The rotator used in the testing of the calibration had a pointing accuracy of  $\pm 1$  degree.

## 2.2 Calibration

For the calibration part different types of calibration methods were examined to see which one would provide us with the best result and the simplest procedure. Four different kinds of calibration methods were found.

- Using photoresistor and signal measurements from antenna to calculate the position of the sun.
- Using radio objects (active galactic nuclei, supernova remnant).
- Using geostationary satellites.
- Maximising strength of the received signal from tracked object.

All these objects have known positions in the sky and any of these objects can be used as a reference point when calibrating antennas.

Two of the above mentioned calibration methods were disqualified. Geostationary satellites are below the horizon in Finland, and using received signal does not help getting information about how accurate the rotator is. In this paper a proof of concept for the sun tracking calibration system is presented.

The calibration method used involves locating the position of the sun by measuring the brightness with a photoresistor. The schematic of the measuring equipment is illustrated in Figure 2 below. It consists of a photoresistor in a tube with a narrow opening to reduce the spreading angle of the photons from the sun (Fig. 3). The photoresistor is connected to a microcontroller that measures the voltage over the resistor through an analog-to-digital converter. The voltage over the photoresistor changes according to the intensity of the light hitting it. The microcontroller then sends the measurement to a computer on request. The computer stores the received data and plots it in a diagram after the measurements are done. The data contains the values for the intensity of the light and the azimuth and elevation rotation angle of the rotator at that moment. By this method

the brightest spot in the measured area which is expected to be the sun can be located. Measurements from the sun produce data that should match a Gaussian function [5]. When the centre of the sun is found the results can be compared to an online database for the position of the sun at the moment of the measuring. From this the offset of the rotator can be found and adjusted so that it points accurately at the tracked object.

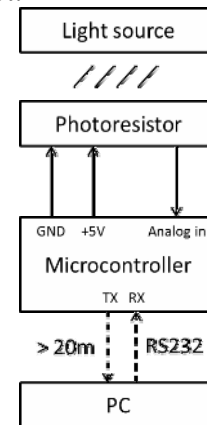


Fig. 2. The principle of the solar locating system

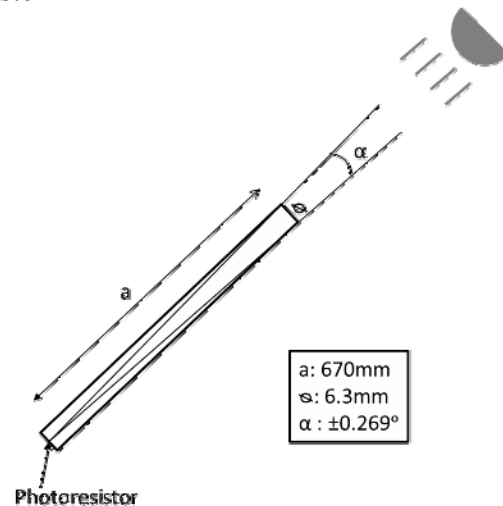


Fig. 3. Attachment of the photoresistor to the calibration tube

The calibration test was done by first determining the position of the sun with the solar locating photoresistor and then by using a helix antenna for getting different kinds of data to compare. With the data

achieved from the two readings a calibration error can be estimated.

Calibration starts by setting the zero point of the rotator to the north or south with the help of a compass. Then the edges of the sun were measured by the photoresistor and the centre position of the sun was calculated. The results were compared to values from Stellarium software [6]. Stellarium is an online software that gives the altitude and azimuth of the sun's position both in units of degrees.

The next step was to check if it is possible to measure the signal strength from radio objects in the sky. Two objects were chosen for this, Cygnus A and Cassiopeia A [7]. Both of these are circumpolar objects in Finland, so they are always above the horizon [8]. It was approximated, based on information gathered from NASA/IPAC extragalactic database [7], that these objects are radiating at 2.4 GHz frequency with enough intensity so that they can be detected with a helix array antenna according to calculations below. Calculations are done for a helix antenna array consisting of 16 helix antennas. This array is the equivalent of a 3m dish antenna. Equation (1) below is used for calculating the brightness needed for observing an object in the sky, as well as for calculating the brightness achieved by the chosen objects.

$$S = \frac{8kk_{\text{sys}}k_s}{\eta\pi D^2(tB)^{0.5}} \quad (1)$$

Where:

$k$  = Boltzmann constant

$k_{\text{sys}}$  = system temperature

$k_s$  = radiometer constant

$t$  = measurement time

$B$  = bandwidth

$\eta$  = efficiency

This gives us approximately minimum

brightness of 172 Jy  $\left(1 \text{ Jy} = 10^{-26} \frac{\text{W}}{\text{m}^2\text{Hz}}\right)$

needed of an object to be observed with our antenna. Cygnus A radiates at 2.7 GHz with 785 Jy and Cassiopeia A with 1495 Jy at 2.8 GHz. This means that the objects are bright enough to be observed by the antenna.

### 3. STATUS AND RESULTS

A FEM analysis of the mechanical structure was made for a worst case scenario with a wind speed of 31 m/s on a 3 m in diameter mesh antenna. An image from the results can be found in Figure 4. The displacement caused by the wind load is so small that the attachment point for the antenna is just 0.04 degrees off-centre during the worst case scenario. The bending of the mechanical structure is therefore almost insignificant under normal weather conditions.

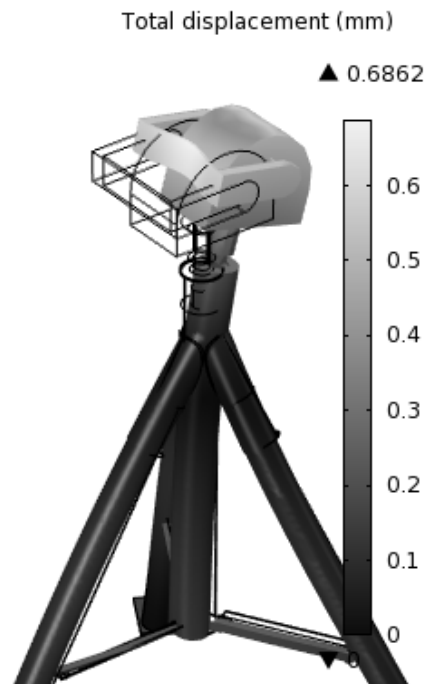


Fig. 4. Results from FEM analysis

The weather in Finland is very demanding in point of view of sun calibration. In winter the sky is cloudy most of the time, which

makes it very hard to use the sun as calibration. Below are the results from measurement of the amount of light hitting the photoresistor at a given turning angle. The equipment used in the testing allowed a  $\pm 0.27$  degree spreading angle of the photons travelling from the sun to the photoresistor. Figures 5 and 6 are presenting measurements from elevation angle and azimuth angle. Figure 5 represents the measurement results in azimuth direction. The maximum value on the fitted function can be found at 46.7 degrees on the rotator. Measurements were done on 1.3.2012 at 11:20 local time GMT +2.

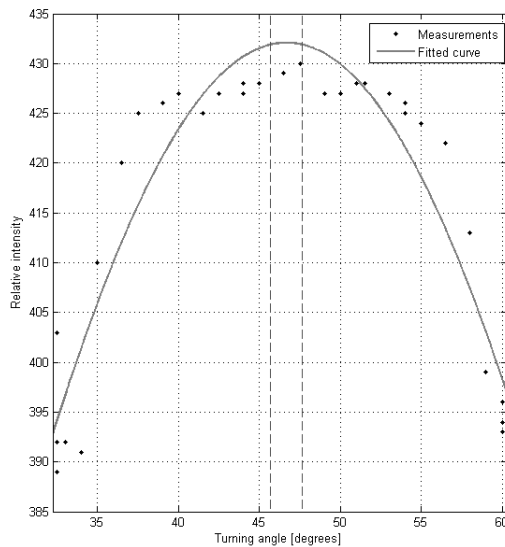


Fig. 5. Azimuth measurements with fitted function

Figure 6 represents the measurement results in elevation direction. The maximum value of the fitted curve can be found at -2.33 degrees, which gives a corresponding value of 357.67 degrees on the rotator. These measurements were done on 11:35 GMT +2.

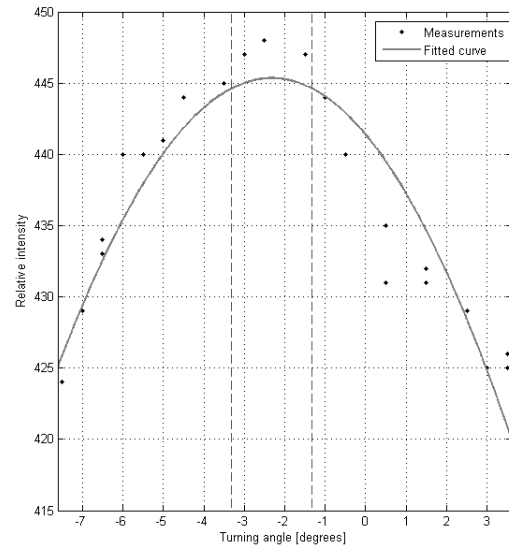


Fig. 6. Elevation measurements with fitted function

#### 4. DISCUSSION

From the measurement values in Figures 5 and 6 one can easily read at which turning angle the light intensity is the strongest. The rotator was not reset to north before the testing so any values of the turning angle are not to be taken into account. The mast which was used for testing was built for VHF/UHF antennas and the beam width on VHF/UHF antennas are huge compared to the S-band antenna beam width. By making the antenna stiffer and by doing more sweeps over the sun the results could be improved. It is also possible to make the measurement equipment more light sensitive by reducing the size of the hole from where light is allowed to pass to the photoresistor.

According to calculations it is not possible to achieve desired pointing accuracy with the equipment used in the tests. The goal was to achieve a pointing accuracy less than  $\pm 1$  degree, which is the same as the accuracy on the rotating device. A more accurate rotating device should be obtained before doing more serious testing but the present testing proves that the concept is valid.



## 5. FURTHER RESEARCH

Next step would be to estimate how accurate the calibration is by measuring sun's position multiple times at different times of the day. One can then compare those results with the actual position of the sun on the Stellarium software and estimate the real pointing accuracy with this calibration method.

For improving the accuracy, the used rotator has to be renewed. The same model used in the test is also available as a high resolution model, which has an accuracy of just  $\pm 0.2$  degrees.

The ground station is intended to be a part of the global educational network for satellite operations (GENSO) which connects ground stations all over the world and enables contact with satellites even when they are not in sight of local ground station. This allows scientist worldwide to access their satellites through this ground station.

## 6. REFERENCES

1. Kestilä, A. et al, Aalto-1, *a Finnish hyperspectral remote-sensing nanosatellite: current progress*, 4th European CubeSat Symposium, 2012
2. Modrzewski, R., *Highly directional patch antenna for CubeSat applications*, 4th European CubeSat Symposium, 2012
3. Allen, C. W., *Astrophysical Quantities*, 3rd ed., Athlone, London, 1976
4. Finnish Meteorological Institute [WWW] <http://en.ilmatieteenlaitos.fi/climate-elements> (14.03.2012)
5. Verma, R., Gregorini, L., Prandoni, I., Orfei, A., *Pointing calibration campaign at 21 GHz with K-band multi-feed receiver*, IRA 441/11, 2011
6. Stellarium, open source planetarium [WWW] <http://www.stellarium.org/> (14.03.2012)

7. NASA/IPAC extragalactic database [WWW] <http://ned.ipac.caltech.edu> (14.03.2012)

8. Karttunen, H., Kröger, P., Oja, H., Poutanen, M., Donner, K.J., *Fundamental Astronomy*, Springer, Helsinki, 2007

## 7. CORRESPONDING ADDRESS

Panu Kiviluoma, D.Sc. (Tech.), Post-doc researcher  
Aalto University School of Engineering  
Department of Engineering Design and Production  
P.O.Box 14100, 00076 Aalto, Finland  
Phone: +358 9 470 23558,  
E-mail: [panu.kiviluoma@aalto.fi](mailto:panu.kiviluoma@aalto.fi)  
<http://edp.aalto.fi/en/>

## 8. ADDITIONAL DATA ABOUT AUTHORS

Winter, Edward, B.Sc. (Tech)  
Phone: +358 50 376 5817  
E-mail: [edward.winter@aalto.fi](mailto:edward.winter@aalto.fi)

Dahl, Johan  
Phone: +358 50 376 7790  
E-mail: [johan.dahl@aalto.fi](mailto:johan.dahl@aalto.fi)

Nordling, Kalle  
Phone: +358 40 563 0865  
E-mail: [kalle.nordling@aalto.fi](mailto:kalle.nordling@aalto.fi)

Kuosmanen, Petri, D.Sc. (Tech.), Professor  
Phone: +358 9 470 23544  
E-mail: [petri.kuosmanen@aalto.fi](mailto:petri.kuosmanen@aalto.fi)

Jaan Praks, M. Sc. University Teacher  
Department of Radio Science and Engineering  
Aalto University School of Electrical Engineering  
Phone: +358 505747975  
E-mail: [jaan.praks@aalto.fi](mailto:jaan.praks@aalto.fi)

